LEABHARLANN CHOLÁISTE NA TRÍONÓIDE, BAILE ÁTHA CLIATH | TRINITY COLLEGE LIBRARY DUBLIN
Ollscoil Átha Cliath | The University of Dublin

Terms and Conditions of Use of Digitised Theses from Trinity College Library Dublin

Copyright statement

All material supplied by Trinity College Library is protected by copyright (under the Copyright and Related Rights Act, 2000 as amended) and other relevant Intellectual Property Rights. By accessing and using a Digitised Thesis from Trinity College Library you acknowledge that all Intellectual Property Rights in any Works supplied are the sole and exclusive property of the copyright and/or other IPR holder. Specific copyright holders may not be explicitly identified. Use of materials from other sources within a thesis should not be construed as a claim over them.

A non-exclusive, non-transferable licence is hereby granted to those using or reproducing, in whole or in part, the material for valid purposes, providing the copyright owners are acknowledged using the normal conventions. Where specific permission to use material is required, this is identified and such permission must be sought from the copyright holder or agency cited.

Liability statement

By using a Digitised Thesis, I accept that Trinity College Dublin bears no legal responsibility for the accuracy, legality or comprehensiveness of materials contained within the thesis, and that Trinity College Dublin accepts no liability for indirect, consequential, or incidental, damages or losses arising from use of the thesis for whatever reason. Information located in a thesis may be subject to specific use constraints, details of which may not be explicitly described. It is the responsibility of potential and actual users to be aware of such constraints and to abide by them. By making use of material from a digitised thesis, you accept these copyright and disclaimer provisions. Where it is brought to the attention of Trinity College Library that there may be a breach of copyright or other restraint, it is the policy to withdraw or take down access to a thesis while the issue is being resolved.

Access Agreement

By using a Digitised Thesis from Trinity College Library you are bound by the following Terms & Conditions. Please read them carefully.

I have read and I understand the following statement: All material supplied via a Digitised Thesis from Trinity College Library is protected by copyright and other intellectual property rights, and duplication or sale of all or part of any of a thesis is not permitted, except that material may be duplicated by you for your research use or for educational purposes in electronic or print form providing the copyright owners are acknowledged using the normal conventions. You must obtain permission for any other use. Electronic or print copies may not be offered, whether for sale or otherwise to anyone. This copy has been supplied on the understanding that it is copyright material and that no quotation from the thesis may be published without proper acknowledgement.

Seismic Analysis of Braced Plan Irregular Structures Using Hybrid Testing and Numerical Modelling

by

Daniel P. McCrum

B.A. B.A.I., MSc., P.G. Dip. Stat., CEng., M.I.E.I.

A thesis submitted to the University of Dublin, Trinity College
in partial satisfaction for the degree of
Doctor of Philosophy

Department of Civil, Structural & Environmental Engineering,
University of Dublin, Trinity College
April 2012

TRINITY COLLEGE
22 OCT 2012
LIBRARY DUBLIN

Thesis 9719

DECLARATION

I declare that this thesis has not been submitted as an exercise for a degree at this or any other university and it is entirely my own work.

I agree to deposit this thesis in the University's open access institutional repository or allow the library to do so on my behalf, subject to Irish Copyright Legislation and Trinity College Library conditions of use and acknowledgement.

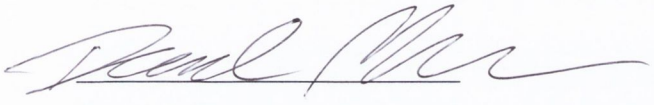

Daniel McCrum

April 2012

SUMMARY

The seismic behaviour of concentrically braced plan irregular structures has been investigated experimentally and numerically. An experimental programme consisting of twenty-four substructured soft-RT hybrid tests of a single-storey concentrically braced frame were undertaken. The hybrid test method combines physical dynamic testing of part of the structure with simultaneous numerical modelling of the rest of the structure. This concept is known as substructuring and allows full-scale cost effective dynamic testing. A structure can be divided into a physical and numerical substructure. The braced plan irregular structures investigated in this thesis have varying levels of torsional stiffness (lateral torsional frequency ratio) and uneven distribution of mass (static eccentricity) in plan resulting in a distribution of the centre of mass away from the centre of resistance of the structure. The consequence of this is a torsional rather than translational seismic response of the structure due to the plan irregularity.

As part of the hybrid test programme, the first (ground) storey concentrically braced frame (physical substructure) as part of a multi-storey braced plan irregular structure was identified as having a highly nonlinear response and was physically tested whilst the remainder of the structure was simultaneously numerically modelling (numerical substructure). In a hybrid test, the displacement command is applied to the physical substructure and the force and displacement feedback from the physical substructure are used to solve the equation of motion for the next target displacement. The physical data from the test provides a more accurate response as compared to a purely numerical model alone could. The physical substructre consists of the part of the structure that typically has a highly nonlinear or rate dependent response that is difficult to computationally model with a high degree of accuracy. The numerical substructure forms the remainder of the structure that has a more predictable response and can be computationally modelled with greater accuracy.

The hybrid tests performed on the physical substructure investigated the seismic response of braced plan irregular structures by variation of some of the important structural parameters affecting the seismic response. Within the experimental programme, the affect of varying realistic but severe levels of static eccentricity and lateral torsional frequency ratio were studied. The Eurocode 8 (CEN, (2004)) accidental eccentricity provision was

applied in design using the torsional effects factor in lateral pushover method of analysis for the braced plan irregular structures. The side of the structure closest to the centre of mass experiences a greater seismic demand and as a result of design to the Eurocode 8 (CEN, (2004)) accidental eccentricity provision the brace sizes are increased on that side (referred to as the stiff side of the structure). The effectiveness of the accidental eccentricity provision was assessed through the experimental programme. The results from the experimental programme were used to validate a purely numerical model of the structure.

To greater understand the seismic response of a braced plan irregular structure, an in-depth numerical parametric investigation of the key parameters affecting the seismic behaviour of braced plan irregular structures was undertaken. Results of this parametric investigation indicated that the static eccentricity and lateral torsional frequency ratio are the most important parameters affecting the seismic response of braced plan irregular structures. Increasing the level of static eccentricity increases the ductility demand on the stiff side and reduces the ductility demand on the flexible side of the structure. Torsionally stiff structures perform better than torsionally flexible structures, with higher levels of ductility demand and interstorey drift observed in the torsionally flexible structures.

The Eurocode 8 (CEN, (2004)) torsional provision is adequate for torsionally stiff structures, and even reduces the ductility demand on the stiff side of the structure for the most torsionally flexible structures at high levels of static eccentricity.

Torsionally flexible structures are subjected to a greater ductility demand (on average 3.75 times) and interstorey drifts as compared to torsionally stiff structures. However, if the level of excitation exceeds the design value, such that the response is more highly nonlinear, the levels of ductility demand become unacceptably high and the level of interstorey drifts exceed Eurocode 8 (CEN, (2004)) limits. It is not recommended that concentrically braced plan irregular structures that are torsionally flexible be allowed in seismic design due to their poor performance in situations where the peak ground accelerations exceed the design peak ground acceleration.

The influence of the plan aspect ratio and bi-directional excitations on the seismic response of concentrically braced plan irregular structures was investigated and observed to have a minimal effect.

ACKNOWLEDGEMENTS

I would sincerely like to thank Prof. Brian Broderick for all his invaluable help as my supervisor. Your relaxed style combined with your expert guidance and advice was ideal.

Most of all, my time during this PhD has been great fun. Without Aoife, John, Will, Andy L, Andy G, Adrian, Alan, Paraic and many others the last three years would have been no fun. Aoife, the last six months with you have been truly great. 'Activities' such as golf, darts, pool, indoor cricket, adventure races, surfing trips and the many evenings in Kennedys have made the last three years fly by. What can I say John, the conference trips to Macedonia and China would have been rubbish without you. Some laugh!

I owe a huge debt to Alan Hunt for proof reading this thesis. Hopefully I can return the favour some day!

I would like to extend my thanks to the technical staff in the department for their ideas, advice and in general, their friendly approach. In particular I would like to show my gratitude to Kevin Ryan and David McAulay. Without your help and hard work I know I would not have finished in time or with as good a thesis.

This thesis is dedicated to my family; Valerie, Sean, Matthew, James, Peter and my close friends.

TABLE OF CONTENTS

DECLARATION ii

SUMMARY iii

ACKNOWLEDGEMENTS v

TABLE OF CONTENTS vi

NOMENCLATURE xi

CHAPTER ONE - Introduction 1

1.1 Motivation 1

1.2 Statement of Problem 1

1.3 Research Objectives 4

1.4 Layout of Thesis 5

CHAPTER TWO – Plan Irregular Structures 7

2.1 Introduction 7

2.2 Irregular Structures 7

2.3 Vertical Irregularity 8

2.3.1 Introduction 8

2.4 Plan Irregularity 10

2.4.1 Single-Storey Models 12

2.4.1.1 Uni-directional Excitation 12

2.4.1.2 Bi-directional Excitation 14

2.4.2 Multi-Storey Models 19

2.4.2.1 Pushover Analysis of Multi-storey Plan Irregular Structures 20

2.4.2.2 Time History Analysis of Plan Irregular Multi-storey Structures 22

2.5 Eurocode 8 Approach to Accidental Eccentricity 28

2.5.1 Seismic Design in Eurocode 8 28

2.5.2 Accidental Eccentricity Design Using Lateral Force Method 30

2.6 Testing of Plan Irregular Structures 31

2.6.1 Previous Test Results 32

2.7 Analysis of Braced Plan Irregular Structures 33

2.8 Passive Control of Plan Irregular Structures 35

2.9 Chapter Overview 36

CHAPTER THREE – Numerical Modelling of Braced Plan Irregular Steel Structures 38

3.1 Introduction 38

3.2 Eurocode 8: Seismic Design of Concentrically Braced Structures 38

3.3 Concentric Bracing Behaviour 40

3.4 OpenSees Computational Platform 44
3.5 OpenSees Modelling of Brace Members 49
3.5.1 Optimal Model Parameters 49
3.5.2 Modelling the Cyclic Response of Brace Members 54
3.5.3 Modelling the 3D Nonlinear Dynamic Response of Braced Frames 57
3.6 Plan Irregular Concentrically Braced Frame Numerical Representation 60
3.6.1 Mass Distribution 60
3.6.2 Lateral Torsional Frequency 62
3.6.3 Plan Aspect Ratio 64
3.6.4 Non-dimensional Slenderness 64
3.6.5 Time Histories 65
3.7 Chapter Overview 67
CHAPTER FOUR - Hybrid Test Method and Validation Test 68
4.1 Introduction 68
4.2 Methods of Dynamic Testing 68
4.2.1 Shake Table Testing 69
4.2.2 Pseudo Dynamic Test Method 69
4.2.3 Continuous Pseudo Dynamic Test Method 71
4.2.4 Substructured Pseudo Dynamic Test Method 72
4.2.5 Real-time Hybrid Test Method 73
4.2.6 Effective Force Test Method 75
4.3 Time Integration Techniques 75
4.3.1 Introduction 75
4.3.2 Explicit Numerical Integration Techniques 76
4.3.2.1 Central Difference Method 76
4.3.2.2 Explicit Newmark Method 77
4.3.3 Implicit Numerical Integration Techniques 78
4.3.3.1 Implicit Newmark Method 79
4.3.3.2 Operator Splitter Method 79
4.3.3.3 Integral Form 82
4.4 Errors in Hybrid Testing 82
4.4.1 Random Errors 84
4.4.2 Systematic Errors 84
4.5 Actuator Delay and Compensation Techniques 85
4.6 Current Implementation of Hybrid Test Method 87
4.6.1 Hybrid Test Facility at Trinity College Dublin 88
4.6.2 OpenFresco Architecture 90
4.6.3 Current Implementation of Event Driven Strategies 93
4.7 Hybrid Test Verification 96

4.7.1 Substructured Portal Frame Test Setup 97
4.7.2 Results from Verification Test 100
4.8 Chapter Overview 104
CHAPTER FIVE – Experimental Programme Set-up 105
5.1 Introduction 105
5.2 Experimental Programme 106
5.3 Experimental Set-up 108
5.3.1 Design of Test Frame 108
5.3.2 Practical Considerations for Experimental Set-up 111
5.4 Instrumentation of Experimental Setup 113
5.5 Numerical Modelling of Experimental Set-up 114
5.5.1 Sensitivity Analysis 115
5.5.2 Final Numerical Model of Test Frame 118
5.6 Hybrid Test Representation 120
5.6.1 Hybrid Test Substructure 121
5.6.2 Hybrid Test Numerical Integration 124
5.7 Chapter Overview 125
CHAPTER SIX – Experimental Results 126
6.1 Introduction 126
6.2 TEST 1 Experimental Results 127
6.2.1 TEST 1A – Cyclic Sawtooth: No Braces 128
6.2.2 TEST 1B – Cyclic Sawtooth: With Braces 128
6.2.3 TEST 1C – 2D Elastic 128
6.2.4 TEST 1D – Elastic 3D: Taiwan Scaled 129
6.2.5 TEST 1E – Inelastic 3D: Taiwan 131
6.2.6 TEST 1F – Inelastic 3D: Taiwan Scaled 2.0 135
6.3 TEST 2 Experimental Results 138
6.3.1 TEST 2A – Cyclic Sawtooth: No Braces 139
6.3.2 TEST 2B – Cyclic Sawtooth: With Braces 139
6.3.3 TEST 2C – 2D Elastic 139
6.3.4 TEST 2D – Elastic 3D: Taiwan Scaled 140
6.3.5 TEST 2E – Inelastic 3D: Taiwan 142
6.3.6 TEST 2F – Inelastic 3D: Taiwan Scaled 2.0 145
6.4 TEST 3 Experimental Results 149
6.4.1 TEST 3A – Cyclic Sawtooth: No Braces 149
6.4.2 TEST 3B – Cyclic Sawtooth: With Braces 149
6.4.3 TEST 3C – 2D Elastic 149
6.4.4 TEST 3D – Elastic 3D: Taiwan Scaled 151

6.4.5 TEST 3E – Inelastic 3D: Taiwan 153
6.4.6 TEST 3F – Inelastic 3D: Taiwan Scaled 2.0 155
6.5 TEST 4 Experimental Results 159
6.5.1 TEST 4A – Cyclic Sawtooth: No Braces 159
6.5.2 TEST 4B — Cyclic Sawtooth: With Braces 159
6.5.3 TEST 4C – 2D Elastic 159
6.5.4 TEST 4D – Elastic 3D: Taiwan Scaled 161
6.5.5 TEST 4E – Inelastic 3D: Taiwan 162
6.5.6 TEST 4F – Inelastic 3D: Taiwan Scaled 2.0 165
6.6 Coupon Tests 169
6.7 Results Discussion 169
6.7.1 Performance of Experimental Procedure 169
6.7.2 Accuracy of Numerical Model 170
6.7.3 Effect of Parameter Variation 177
6.8 Chapter Overview 180
CHAPTER SEVEN – Parametric Study 181
7.1 Introduction 181
7.2 Parametric Study 181
7.3 Numerical Model 182
7.4 Parametric Study Results 183
7.4.1 Base Model 183
7.4.2 Analyses of Base Model Results 187
7.5 Complete Parametric Investigation 192
7.5.1 Static Eccentricity 192
7.5.2 Lateral Torsional Frequency Ratio 200
7.5.3 Plan Aspect Ratio 203
7.5.4 Design for Torsional Effects 206
7.5.5 Over- and Under-designed for Torsional Effects 210
7.5.6 Influence of Bi-directional Excitation 214
7.5.7 Influence of Level of Ground Acceleration 216
7.5.8 Response Attributed to Plan Irregularity and Change in Period of Structure 219
7.6 Results Discussion 223
7.7 Chapter Overview 228
CHAPTER EIGHT - Conclusions 229
8.1 Summary 229
8.2 Conclusions 229
8.3 Recommendations for Further Work 235
References 239

Appendix A1 - Two Dimensional Portal Frame OpenFresco Hybrid Simulation 251

Appendix A2 - Two Dimensional Portal Frame OpenSees Numerical Model..... 255

Appendix B – Test Frame Fabrication Drawings..... 259

Appendix C1 - Two Dimensional Concentrically Braced Frame Hybrid Test Model..... 268

Appendix C2 - Two Dimensional Concentrically Braced Frame OpenSees Model..... 274

Appendix C3 - Three Dimensional Concentrically Braced Frame Hybrid Test Model..... 282

Appendix C4 - Three Dimensional Concentrically Braced Frame OpenSees Model 293

Appendix D1 – Test 1B Results..... 305

Appendix D2 – Test 1C Results..... 310

Appendix D3 – Test 1D Results..... 312

Appendix D4 – Test 1E Results..... 312

Appendix D5 – Test 1F Results..... 314

Appendix D6 – Test 2B Results..... 317

Appendix D7 – Test 2C Results..... 320

Appendix D8 – TEST 2D Results..... 323

Appendix D9 – TEST 2E Results..... 326

Appendix D10 – TEST 2F Results..... 329

Appendix D11 – Test 3B Results..... 332

Appendix D12 – Test 3C Results..... 335

Appendix D13 – TEST 3D Results..... 338

Appendix D14 – TEST 3E Results..... 341

Appendix D15 – TEST 3F Results..... 344

Appendix D16 – Test 4B Results..... 347

Appendix D17 – Test 4C Results..... 350

Appendix D18 – TEST 3D Results..... 353

Appendix D19 – TEST 3E Results..... 356

Appendix D20 – TEST 4F Results..... 359

Appendix E - Three Dimensional Concentrically Braced Frame OpenSees Model..... 362

NOMENCLATURE

The following is a list of the notation used in this thesis.

Latin upper case letters:

Symbol	Definition
A	Width of bay/Cross-sectional area of a member
B	Length of bay
C	Damping matrix
CM	Centre of mass
CR	Centre of resistance/Centre of stiffness
E	Young's modulus
F	Inertia force
F_i	Horizontal force acting on storey i as defined using the lateral force method
FS	Flexible side
F_y	Yield strength of the material
G	Shear modulus
K_E	Elemental stiffness matrix
K_y	Total lateral stiffness of the elements parallel to the y-axis
K_θ	Total torsional stiffness about the centre of resistance
H	Height of a building
I	Second moment of area
I_{xi}	Major axis second moment of area about the centre of mass
I_{yi}	Minor axis second moment of area about the centre of mass
I_y	Minor axis second moment of area
I_z	Major axis second moment of area
J	Torsional constant of section
K^1	Stiffness matrix with stiffness higher than or equal to the tangent stiffness
L	Total length of building/Effective length of a compression member
L_i	Floor dimension perpendicular to the direction of the seismic action
L_e	Distance between the two outermost lateral load resisting elements
L_{max}	Larger plan dimension of structural layout
L_{min}	Smaller plan dimension of structural layout
M	Mass matrix
M_{ai}	Torsional moment applied at storey i about its vertical axis
M_s	Surface wave magnitude
N_{cr}	Elastic buckling load
N_y	Squash load

R	Reduction factor
R_{i+1}	Restoring force vector at $i+1$th time step
$\widetilde{R}_{n+1}$	Predictor restoring force at $(n+1)$ time step is measured when the predictor displacement is applied
$R0$	Control parameters from elastic to plastic branch in material model
S	Soil factor
S_e	Elastic response spectrum
SS	Stiff side
Sv	Relative velocity between the mass and ground in a SDOF system
T	Period of vibration
T_1	Fundamental period of vibration
T_B	Corner period in the response spectrum
T_C	Corner period in the response spectrum
T_D	Corner period in the response spectrum

Latin lower case letters:

Symbol	Definition
a	Acceleration
a_g	Ground acceleration
$a1$ & $a2$	Isotropic hardening parameters governing the increase in compression yield envelope after plastic strain
$a3$ & $a4$	Isotropic hardening parameters governing the increase in tension yield envelope after plastic strain
b	Strain hardening ratio
$cR1$	Control parameters from elastic to plastic branch in material model
$cR2$	Control parameters from elastic to plastic branch in material model
d_r	Design interstorey drift obtained by analysis
e	Eccentricity of the element from the centre of mass
e_{ai}	Accidental eccentricity of storey mass i from its nominal location, applied in the same direction at all floors
e_o	Structural eccentricity
e_{ox}	Structural eccentricity in x-direction
e_s	Static Eccentricity
f_y	Yield strength
h	Storey height
i	Radius of gyration
k_{yi}	Lateral stiffness of each element in the y-direction
m	Mass
n	Number of...

r_k	Stiffness radius of gyration about the centre of resistance
r_m	Mass radius of gyration about the centre of mass
r_x	Square root of the ratio of the torsional stiffness to the lateral stiffness in the y-direction and
l_s	Radius of gyration of the floor mass in plan
q	Behaviour factor
v	Reduction factor
x	Distance from the element under consideration to the CM of the structure measured perpendicularly to the seismic action
x_i	Displacement at the *i*th time step/Distance from the element being considered to the centre of resistance in the x-direction
x_{max}	Maximum value of the relative displacement between the mass and ground in a SDOF system
$\dot{x}_{max}$	Maximum value of the relative velocity between the mass and ground in a SDOF system
$\ddot{x}_{max}$	Maximum value of the relative acceleration between the mass and ground in a SDOF system
$\dot{x}_i$	Velocity at the *i*th time step
$\ddot{x}_i$	Acceleration at the *i*th time step
x'	Predicted displacement
x''	Resulting displacement
$\widetilde{x}_{n+1}$	Predictor displacement at the $i+1$th time step
$\widetilde{\dot{x}}_{n+1}$	Predictor velocity at the *i*th time step
y_i	Distance from the element being considered to the centre of resistance in the y-direction

Greek upper case letters:

Symbol	Definition
Δ	Change in...
Δt	Integration time step
Δt_{max}	Maximum time step
Ω	Ohms
Ω_θ	Lateral torsional frequency ratio
Σ	Sum of...

Greek lower case letters:

Symbol	Definition
α	Hilber integration parameter
α_u	Value by which the horizontal seismic design action is multiplied in order to achieve first plastic action of any member
α_1	Value by which the horizontal seismic design action is multiplied in order to achieve a number of plastic hinges and structural instability
β	Newmark integration parameter
γ	Newmark integration parameter
δ	Torsional effects factor
δt	Response delay
δ_u	Maximum displacement of the structure
δ_y	Yield displacement
ε	Strain
η	Damping correction factor
θ	Angle in degrees
λ	Slenderness of building in plan
$\overline{\lambda}$	Normalised slenderness
μ_δ	Displacement ductility demand
σ	Stress
σ_{cr}	Elastic buckling stress
ω_θ	Uncoupled torsional frequency
ω_n	Natural frequency of the system
ω_y	Uncoupled translational frequency in the y-direction

CHAPTER ONE - Introduction

1.1 Motivation

For millions of people living within the built environment, structural dynamics plays an important, but often hidden role, in their lives. It is the responsibility of structural engineers to ensure the built environment can withstand extreme dynamic actions, such as wind, traffic or earthquake. Structural engineers must understand how the built environment will respond to such dynamic actions. Since commencing the research for this thesis in late 2008, several devastating earthquakes have occurred such as: a Magnitude 6.3 earthquake in L'Aquila, Italy on 6 April 2009; a Magnitude 7.0 earthquake in Port-Au-Prince, Haiti on 12 January 2010; a Magnitude 6.3 earthquake in Christchurch, New Zealand on February 22, 2011 and a Magnitude 8.8 earthquake off the coast of Japan on March 11, 2011. An immediate effect of these earthquakes is numerous fatalities due to structural collapse and falling debris, while in the long-term thousands of individuals are left homeless due to collapsed or unsafe buildings and the resulting slow process of rebuilding. The structural engineering community has the ability to influence the direct consequences of these events by better understanding the seismic response of building structures and aiming to constantly improve their seismic design. Earthquake engineering is devoted to the mitigation of earthquake risk by improving the design of earthquake resistant structures. To this end, the research in this thesis has the fundamental aim to enhance the design of building structures to protect human life during earthquake events.

1.2 Statement of Problem

When an earthquake occurs, a structure moves laterally and/or vertically caused by surface ground motion induced by seismic waves. The lateral motion is typically much greater than the vertical motion, with the ground moving at an acceleration (a_g). Inertial forces (F) are generated in the building as a result of this lateral motion, defined as the product of the mass of the structure (m) multiplied by the acceleration of the structure (a) according to Newton's Second Law ($F = m \times a$). At a fundamental level, the mass, size and configuration of a building structure dictate how the structure will respond to an earthquake event. A stiffer structure has a lower natural period of vibration and will

respond to a given seismic event in a different manner than a more flexible structure with a larger natural period. In essence an earthquake resistant structure has to resist the lateral inertial forces in a safe and reliable manner.

An earthquake engineer has to design a structure to resist the lateral actions applied to it by the earthquake ground motion. In order to achieve this, a lateral load resisting system is needed to resist these lateral forces. Typical methods of achieving increased lateral stiffness are moment resisting frames, shear walls or braced frames as shown in Figure 1.1. The moment resisting frame resists the lateral actions through framing action of rigid connections at the joints. Shear wall systems can be masonry but are typically constructed in reinforced concrete and resist lateral actions through in-plane resistance of the shear wall. The braced frame structures resist lateral actions through axial resistance of the bracing members, either through tension yielding or compressive resistance.

Figure 1.1: (left) Moment resisting frame structure (allstructure.com) (centre) shear wall structure and (right) braced frame structure (www.berkeley.edu)

Concentrically braced frame steel structures have become increasingly popular in seismically vulnerable zones, particularly since the 1994 Northridge (Blakeborough et al., (1997)) and 1995 Kobe earthquakes (Chandler and Pomonis, (1997)). During the Northridge earthquake, many steel moment resisting frame structures suffered brittle beam-to-column connection failure (ASCE, (2000)). Prior to the Northridge earthquake it was thought that moment resisting frame structures performed well during cyclic loading conditions. Concentrically braced steel frame structures have a high lateral stiffness and a good hysteretic response to cyclic loading combined with an efficient use of materials resulting in their increased popularity in earthquake resistant design.

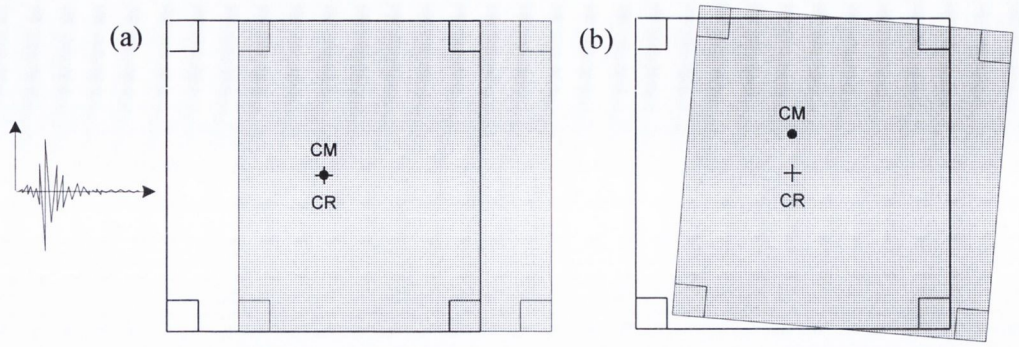

Figure 1.2: (a) Translational seismic response of plan regular structure (b) torsional seismic response of plan irregular structure

The seismic response of building structures dominated by the fundamental mode of vibration generally is purely translational. In terms of seismic design, the response of building structures with a translational dominant response can be predicted with a good degree of accuracy. As shown in Figure 1.2(a), the response of a structure regular in plan is dominated by the fundamental mode resulting in a translational response. Prediction of the seismic behaviour of the structure is somewhat problematic in structures with a torsional rather than translational response during a seismic event. Such structures are said to be 'irregular' structures. Irregularity in building structures can occur in plan or in elevation. Plan irregularity causes a torsional response in plan, and can be the result of an uneven plan distribution of mass or stiffness in the structure. In Figure 1.2(b), the torsional response of a plan irregular structure is shown. The centre of mass (CM) is distributed away from the centre of resistance/stiffness (CR). The uneven distribution of the mass leads to one side of the structure being stiffer than the other. Consequently, a greater dynamic demand occurs on one side of the structure leading to the torsional response. Irregularity in elevation is typically caused by the mass of adjacent floors being significantly different from each other and results in excessive interstorey drifts in a structure. A considerable volume of research has taken place to date on the response of plan irregular reinforced concrete framed and shear wall type structures.

Current code provisions (CEN, (2004)) have largely been based on purely numerical analysis of reinforced concrete framed and shear wall type structures types of structures. Little research exists investigating the seismic response of plan irregular braced structures and much of the research to date investigating plan irregularity in general has proven contradictory. In particular, little experimental validation of the complex response of plan irregular structures has been undertaken to date. Many of the assumptions on the seismic response of plan irregular structures are based on results of purely numerical analyses. The

research presented herein aims to investigate the seismic behaviour of plan irregular concentrically braced steel structures based on numerical analysis validated by experimental data.

1.3 Research Objectives

The fundamental objective of this research is to investigate the seismic response of plan irregular steel braced framed structures. The investigation employs full-scale inelastic hybrid testing combined with numerical modelling of the braced plan irregular structures. The main research objective and areas in existing research identified as lacking are outlined hereafter.

Much of the early research into plan irregularity focused on highly idealised single-storey shear wall type structures. Eurocode 8 (CEN, (2004)) plan irregularity provisions are largely based on the conclusions obtained from these idealised models. More recently the behaviour of more realistic multi-storey framed plan irregular structures has been investigated. This thesis aims to extend the understanding of the response of plan irregular structures by investigating the seismic response of multi-storey plan irregular concentrically braced structures.

Little experimental work has been carried out on plan irregularity and the majority of the research has been undertaken on a purely numerical basis. In particular, to the author's knowledge no such comprehensive experimental study has been performed on plan irregular braced frame structures. This thesis will contribute to the limited existing experimental data on the seismic response of plan irregular structures, and specifically the response of irregular braced frames.

The dynamic testing will comprise of substructured hybrid testing, which tests the critical part of the structure whilst simultaneously numerically modelling the remainder of the structure. A key objective of this study is to achieve the first implementation of the hybrid test method with the Structural Engineering Laboratory at Trinity College Dublin. This implementation will include an assessment of the accuracy and reliability of the developed experimental system when applied to the testing of full-scale braced frame structures.

The hybrid testing procedure implemented in this thesis is a relatively new experimental procedure and few similar seismic tests of this kind have been carried out to date.

Providing seismic test data and observations from the hybrid experiment implemented in this thesis will help to enhance the hybrid test method as an accurate, cost effective method for dynamic testing and analysis of structures.

Using finite element models validated against the experimental results, a parametric investigation of the seismic response of plan irregular braced frame structures will be performed. The parametric study will consist of an examination of the important factors affecting the seismic response of braced plan irregular structures. The significant structural parameters to be investigated will have realistic values relevant to real-world earthquake resistant building design. In particular, the level of static eccentricity and lateral torsional frequency ratio will be investigated in detail. This study will lead to recommendations on the influence of key structural parameters in seismic response and design.

Lastly, the effectiveness of the Eurocode 8 (CEN, (2004)) provision accounting for torsional effects applied to braced plan irregular structures will be assessed. This provision provides a relatively intuitive procedure to account for torsional effects using the lateral pushover method of analysis by increasing the seismic design action on the side of the structure the mass is distributed towards. The effectiveness of this procedure for taking account of torsional effects in seismic design will be investigated using inelastic time history analysis.

1.4 Layout of Thesis

An introduction into the history of research on plan irregular structures is provided in **Chapter Two**. Early research focused mainly on single-storey idealised structures because the response could be easily parameterised allowing researchers to gain insight into plan irregularity. Research into plan irregularity is characterised by its contradictory nature. The lack of experimental validation and minimal research undertaken on plan irregular braced steel framed structures is noted.

Chapter Three discusses the numerical modelling approach implemented in this thesis for a steel braced framed structure with plan irregularity. Experimental studies of concentrically braced steel framed structures are used to validate the numerical modelling approach.

The dynamic test method (hybrid test method) used to investigate the seismic response of a concentrically braced steel framed structure with plan irregularity is detailed in **Chapter Four**. A brief background study of the development of the hybrid test method and important aspects of the experimental procedure are detailed. A simple validation experiment is performed to ensure the test procedure was implemented correctly.

Chapter Five details the experimental set-up. The design of the test structure and physical constraints of the laboratory set-up are described. In **Chapter Six**, the test results from the substructured hybrid test programme on the concentrically braced plan irregular structure are described and observations are detailed. An explanation of the main findings of the experimental programme is given.

In **Chapter Seven** a parametric study of the important structural parameters affecting the seismic response of a plan irregular braced framed structure is presented. The numerical model used in the parameter study is based on the validation numerical model of the experimental results in **Chapter Six**. Results of the parametric study are discussed in detail.

A summary of the conclusions obtained from the work undertaken in the experimental programme and numerical parametric study is presented in **Chapter Eight**.

CHAPTER TWO – Plan Irregular Structures

2.1 Introduction

In this chapter, a brief overview of research into the seismic behaviour of plan irregular structures is presented. Early research focused on the torsional response of plan irregular single-storey structures because the structures could be easily parameterised and their response could be more easily evaluated with reduced computational effort. In more recent years, research has focused on the seismic response of multi-storey structures with more complex models. The Eurocode 8 (CEN, (2004)) provisions for plan irregularity that will be investigated in this thesis will be discussed. Finally, the lack of both analysis and testing of steel brace framed plan irregular structures is highlighted.

2.2 Irregular Structures

Irregularities in building structures refer to the non-uniform response of a structure due to non-uniform distribution of structural properties. There are two types of structural irregularity; vertical (also termed in-elevation) and plan (also termed plan asymmetry). Vertical irregularity typically refers to the uneven distribution of mass along the height of a multi-storey structure or geometrical set-backs changing the floor plan between adjacent floors. During a seismic event, the result can be a soft storey mechanism. Plan irregularity typically refers to the uneven distribution of stiffness or strength in the plan of a structure resulting in a torsional response of the structure when subjected to a seismic excitation. Structures with plan irregularity quite often suffer severe damage in earthquake events because the response of the structure is not only translational, but also torsional (De Stefano and Pintucchi, (2008)). Many plan irregular buildings were damaged in the 1985 Mexico City earthquake (Rosenbleuth and Meli, (1986)). In the Mexico City earthquake, nearly 50% of the collapses could be attributed to plan irregularity (Rutenberg et al., (1992)). The aftermath of the Mexico City earthquake showed that plan irregularity needed to be taken into consideration when providing design guidance. Early research undertaken in Europe into plan irregularity was needed to provide design guidance for the newly developed Eurocodes. The first seismic design Eurocode was published in the mid 1990's and much of the research in the 1980's and early 1990's into plan irregularity was aimed at

providing design guidance for the code. However, currently there is still a lack of agreement on how best to provide design guidance for plan irregular structures. A technical report by the Joint Research Centre (Pinto et al. (2007)) identified the need for research to be integrated into Eurocode 8 (CEN, (2004)) such that design codes would encompass up-to-date technology and knowledge. The design of plan irregular buildings was identified as an area requiring further research by Pinto et al. (2007), who stated that current consensus is lacking in regard to design against natural or accidental torsion. The design for torsion needs to move towards overall drift deformation as opposed to current ductility demands, which should help to prevent the excessive inelastic deformation demands. Other authors recently have also noted the need for further research (De Stefano and Pintucchi, (2008) & Karavasilis et al., (2008)).

2.3 Vertical Irregularity

For completeness, vertical (in-elevation) irregularity will be briefly described to establish the overall context of the research described later.

2.3.1 Introduction

Vertical irregularity results from the uneven distribution of mass, strength or stiffness along the elevation of a building structure. Mass irregularity results from a sudden change in mass between adjacent floors, such as mechanical plant on the roof of a structure. Stiffness irregularity results from a sudden change in stiffness between adjacent floors, such as setbacks in the elevation of a building. Eurocode 8 (CEN, (2004)) states that a building is irregular in elevation if it does not meet the regularity criteria. The criteria are set out in Section 4.2.3.3 of Eurocode 8 (CEN, (2004)) and are summarised as follows:

1. All lateral loading systems such as cores, walls and frames shall run continuously without interruption from foundation to the top of building or, if there are setbacks then to the top of the relevant zone of the building.
2. The lateral stiffness and mass of each floor shall remain constant or else reduce gradually from the base to the top of the building.
3. In framed buildings, the ratio of the actual storey resistance to the resistance required by analysis should not vary disproportionately between adjacent storeys.

4. If setbacks are present in the building then the following criteria are set out in Figure 2.1:
    a. For gradual setbacks preserving axial symmetry, the setback at any floor level shall not exceed 20% of the previous floor plan dimension in the direction of the setback. See Figure 2.1(a) and Figure 2.1(b).
    b. For single setbacks within the lower 15% of the total height of the building structure, the setback shall not be 50% of the previous plan dimension. See Figure 2.1(c).
    c. If symmetry is not preserved in the setbacks, in each face the sum of the setbacks at all storeys shall not exceed 30% of the plan dimension at the ground floor. Individual setbacks shall not exceed 10% of the previous plan dimension. See Figure 2.1(d).

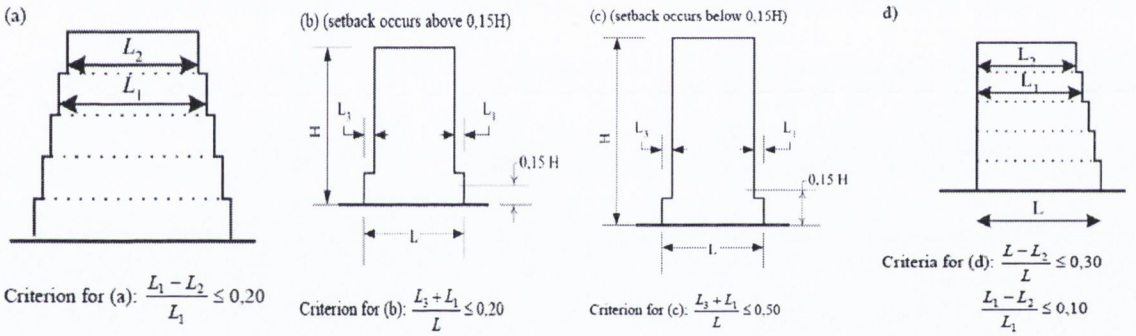

Figure 2.1: Criteria for regularity of buildings with vertical irregularity (setbacks) (CEN, (2004))

If the above criteria are not met the structure is defined as irregular. Consequently, more detailed analysis of the structure must therefore be undertaken to verify interstorey drift, ultimate limit states and damage limitation states.

As a comparison, the Uniform Building Code (ICBO, (1997)) categorises mass irregularity as a floor having an effective mass of 150% of the effective mass of an adjacent floor. A stiffness irregularity is categorised in UBC 1997 (ICBO, (1997)) as a 'soft' storey having a lateral stiffness less than 70% of that of an adjacent floor or less than 80% of that of the next three storeys above. Strength irregularity is categorised as the storey strength being less than 80% of that of the storey above.

The concept of vertical irregularity has been briefly discussed. The remainder of this thesis will be concerned with the torsional response of plan irregular building structures.

2.4 Plan Irregularity

Asymmetric or plan irregular structures are those in which seismic response is not only translational but also torsional, and is a result of stiffness and/or mass eccentricity in the structure. A regular structure may actually be asymmetric if the structure has masonry infill walls or stiffer lateral resisting systems on one side of the structure that have not been taken into consideration in the analysis. In-plan static eccentricity, e_s is defined as the distance between the Centre of Mass (CM) and Centre of Resistance (CR) of the structure at each floor, for example see Figure 2.2. Structures are therefore either Torsionally Balanced (TB) with no static eccentricity, e_s or Torsionally Unbalanced (TU) with a static eccentricity, e_s. Structures with plan irregularity quite often suffer severe damage in earthquake events because the response of the structure is not only translational, but also torsional (De Stefano and Pintucchi, (2008)).

Eurocode 8 (CEN, (2004)) states that a building is irregular in plan if it does not meet the regularity criteria. The criteria are set out in Section 4.2.3.2 of Eurocode 8 (CEN, (2004)) and are summarised as follows:

1. The building shall be approximately symmetric in plan with respect to two orthogonal directions, x and y.
2. The configuration of the plan shall be compact i.e. the limits of the boundary of each floor are marked by a polygonal convex line (any line that is not a tangent to the edges drawn through a polygon meets its boundary exactly twice). If the plan has setbacks, then the plan is still regular if the floor plan area outside a convex polygonal line does not exceed 5% of the area of the total floor plan.
3. The in-plan stiffness of the floor plate shall be much larger than the lateral stiffness of the vertical structural elements.
4. The slenderness $\lambda = L_{max} / L_{min}$ of the building in plan shall not be greater than 4. L_{max} is the larger plan dimension and L_{min} is the smaller plan dimension (see Figure 2.2).

5. At each floor and in each direction (x and y), the structural eccentricity e_o and the torsional radius r must conform to the following conditions;

$$e_{ox} \leq 0.30 \cdot r_x \tag{2.1}$$

$$r_x \geq l_s \tag{2.2}$$

where, e_{ox} is the distance between the centre of mass and centre of stiffness in the x-direction, r_x is the square root of the ratio of the torsional stiffness to the lateral stiffness in the y-direction and l_s is the radius of gyration of the floor mass in plan.

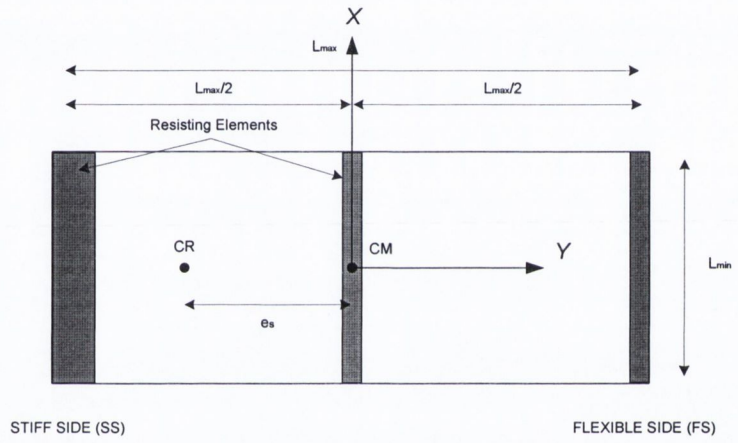

Figure 2.2: Typical configuration of generic plan irregular single-storey model

If the above criteria are not met then in accordance to Eurocode 8 (CEN, (2004)) the structure is defined as plan irregular. Subsequently, analysis of the structure must be undertaken to verify interstorey drift, ultimate limit states and damage limitation states. A brief introduction to the concept of plan irregularity has been provided. The Eurocode 8 (CEN, (2004)) criteria for structural irregularity have been listed. The following sections will describe the approach by the research community to quantifying structural irregularity in single- and multi-storey structures.

2.4.1 Single-Storey Models

2.4.1.1 Uni-directional Excitation

The topic of torsional response of structures subjected to seismic excitation was first addressed by Rosenbleuth, (1957). Since then there has been a substantial amount of research undertaken to greater understand the damage caused to a structure by a torsional response in a seismic event. Figure 2.2 indicates the typical single-storey structural model investigated. In early research simplified single-storey models were used when investigating plan irregular structures because they could easily parameterise and quantify the influence of structural factors on the seismic response (Tso and Bozorgnia, (1986), Hejal and Chopra, (1987), Rutenberg et al., (1992), Correnza et al., (1995), Chandler and Duan, (1997), Goel, (1997), Paulay, (1998), Ghersi and Rossi, (2001)). The relative ease of computation required for these single-storey models and the reduced number of influencing parameters compared to more complex structural systems made the single-storey simplified structures attractive to researchers. Single-storey models were favoured because they allowed the governing parameters to be more easily clarified.

Early research focused mainly on the definition of plan irregularity and the effect of key parameters on the torsional response of plan irregular structures. For example, the effect of parameters such as lateral torsional frequency ratio (Ω_θ), e_s and natural period on the lateral torsional coupling of a single storey model was investigated by Hejal and Chopra, (1987). Sadek and Tso, (1989) perceived that a relatively weak correlation between peak inelastic response and stiffness eccentricity existed, and subsequently proposed using strength eccentricity as a measure of plan irregularity. However, the authors demonstrated that the response of a plan irregular structure cannot be described by a single parameter. Bozorgnia and Tso, (1986) investigated the plan irregular response of a single mass supported by a bilinear hysteretic element and one of their findings was that the uncoupled lateral-to-torsional frequency ratio was not a critical parameter. In a brief literature review by Goel and Chopra, (1990), they indicated that the conclusions of previous research were specific to the system investigated and could not be applied in a general manner.

In the 1990's, the increase in computational power allowed for the analysis of more complex structures. The computation of the seismic response of single-storey structures became more straight forward, however the ability to convert the observations to design procedures was more problematic (Rutenberg and Tso, (2004)). For example, in early

research, the e_s alone could not describe the torsional response of a plan irregular structure. Sadek and Tso, (1989) proposed the use of strength eccentricity as opposed to e_s because in the inelastic range the CR no longer remains constant due to yielding. The lateral torsional frequency ratio Ω_θ, has been widely used to quantify torsional flexibility (this parameter will be described in detail in Chapter Three). [A value of $\Omega_\theta > 1$ means the structure is torsionally stiff, whilst a value of $\Omega_\theta < 1$ means the structure is torsionally flexible]. However, disagreements between researchers initially existed between the actual definition of three possible and legitimate definitions of lateral torsional frequency ratio (Rutenberg and Tso, (2004)). Even simplified single-storey structures, e.g. Figure 2.2, were found to have a large number of parameters for a nonlinear analysis, thus making the response of complex models difficult to summarise. The combination of the complexity of inelastic response and large number of parameters lead to a lack of universally accepted conclusions (De Stefano and Pintucchi, (2008)). It is easy to see why the practising engineering community was reluctant to take on the recommendations made by researchers.

Rutenberg et al., (1992) performed a parametric study on two plan irregular code-designed single-storey structures in order to compare different design codes. The authors found that in the code designed structures the peak ductility demand was lower for the structures designed for plan irregularity compared to their symmetric counterparts due to the higher strength built into the stiff side (SS) member. Larger Ω_θ leads to lower peak ductility demand. For two of the four records used, the peak ductility demand fell for an increase in natural period, while for the other two records, the peak ductility demand increased for an increase in natural period. Peak ductility demand was mostly found in an element on the SS of the structure.

Correnza et al., (1995) performed an inelastic analysis on a torsionally unbalanced plan irregular building model designed to a number of design codes. Correnza et al., (1995) found that considerable additional ductility demand arises in the flexible side (FS) element, which contrasts other researcher's findings. It was noted that code provisions that do not amplify static eccentricity perform poorly, whereas code provisions that do amplify static eccentricity (e.g. EC8-89 Draft (Commission of the Euopean Communities, (1989))) adequately controlled the additional ductility demand.

Chandler et al., (1996) summarise the areas of concern and areas where lack of agreement still existed. In order to resolve the contentious issues, a European Task Group (TG8) was established under the auspices of the European Association for Earthquake Engineering

(EAEE) to study, over a number of years, the seismic torsional effects of stiffness, mass or strength plan irregularity or effects due to vertical irregularities such as setbacks. The work of TG8 lead to the increase in the number of researchers investigating the plan irregular behaviour of structures.

Chandler and Duan, (1997) investigated the performance of a single-story plan irregular structure designed to a number of codes and cite as their reason for undertaking the study that previous considerable research in the area has not lead to universal agreement. The results of the study by Chandler and Duan, (1997) indicated that the SS element is critical to the response of the structure at the SLS and ULS. In EC 8-93 (Communities, 1993) the SS element SLS was observed to be unconservative and also had poor ULS performance. Unlike the SS element, the FS element is generally conservatively designed.

Early research mentioned above has been somewhat contradictory. More recently, investigations into the behaviour of plan irregular single-story structures has moved towards bi-directional excitation of structures as opposed to uni-directional excitation. The next section reviews the study of single-storey plan irregular structures subjected to bi-directional excitation.

2.4.1.2 Bi-directional Excitation

2.4.1.2.1 Comparison Between Uni- and Bi-directional Excited Structures

In any structure, stiffness, mass or strength eccentricity may exist in two orthogonal directions rather than just an idealised single direction. The idealised single-storey models with resisting elements in one direction only may neglect some of the important effects that may influence the inelastic response of the resisting elements. For example, in such uni-directional models, it is assumed that the resisting elements are subjected to uni-directional horizontal forces only (De Stefano and Pintucchi, (2003)). Unlike bi-directional models, typically uni-directional models made no allowance for the gravity loads in the orthogonal direction or the contribution to the torsional response from the stiffness and strength of orthogonal elements. As a result, interaction among bi-directional horizontal and vertical forces in resisting elements is not taken into consideration. More realistic, but still idealised, single-storey structures such as that in Figure 2.3 have been used to investigate

the effect of bi-directional horizontal forces and the interaction between orthogonal resisting elements.

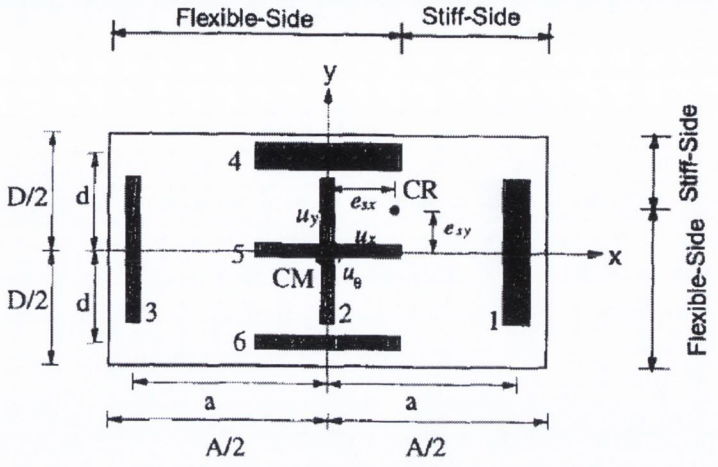

Figure 2.3: Idealised single-storey system with orthogonal resisting elements (Goel, (1997))

An alternative approach proposed by De la Llera and Chopra, (1994, 1995 & 1996) was aimed at conceptually understanding the effects of building plan irregularity rather than performing extensive numerical modelling. Some degree of order was installed in the model characterisation of plan irregular buildings by considering the base shear and torque response histories of different structural configurations (De la Llera and Chopra, (1995)). All combinations of base shear (in both horizontal directions) and the torque applied statistically to cause collapse of each structure investigated provided a base-shear-torque (BST) interaction diagram. The different collapse mechanisms developed in the system were represented in the BST diagrams. Factors controlling the shape of the BST surface and the effect of building response were studied for several structural configurations. The BST interaction diagrams provide most of the information required to describe the inelastic properties of the system and how the structural properties affect the seismic behaviour of the system.

For the purposes of realism, Correnza et al., (1994) included the resisting elements perpendicular to the main direction of the excitation. Correnza et al., (1994) showed that using a uni-directional seismic input for short-period systems gives overly-conservative additional ductility demands compared to a bi-directional seismic event as being resisted by lateral and transverse elements. The ductility demands are found to be accurate for medium- and long-period structures. The authors note that the majority of systems are short-period as opposed to medium- or long-period systems.

Goel, (1997) investigated the seismic response of a plan irregular system using an energy based approach. Goel, (1997) noted that the general conclusion of research to date was that the SS code designed elements were likely to suffer more damage than the FS elements. The FS elements generally had a response similar to the regular symmetric comparison structure. Goel, (1997) noted that the Kobe earthquake (1995) and Mexico City earthquake (1985) indicated otherwise. The sides of buildings facing the streets (FS) in the above mentioned earthquakes suffered greater damage than the sides of the street facing away from the street onto other buildings that were filled with masonry walls (SS). The discrepancy was attributed to previous research not considering structures with large eccentricities in both directions subject to bi-directional excitation. In contrast to existing research, the study indicated that the FS elements could be more vulnerable and the SS responds similarly to the symmetric structure when large eccentricities are taken into account.

Ghersi and Rossi, (2001) studied the influence of bi-directional ground motion on the response of a one-storey structure with plan irregularity. When a symmetric structure is subjected to a ground motion in the orthogonal direction, the response is purely translational. The response to a bi-directional ground motion is translational along the symmetric direction and the rotation of the deck is caused by the orthogonal component. A study of the effect of 30 No. earthquake events on the system was performed. The analyses indicated that the influence of bi-directional excitation on the inelastic response of the structure is minimal as compared to uni-directional excitation. This observation is explained because the orthogonal direction elements almost always remain elastic whereas the elements parallel to the seismic action undergo inelastic deformation similar to uni-directional excitation, so the effect of the bi-directional excitation is minimal.

De Stefano and Pintucchi, (2002) present a more advanced single-storey numerical model in order to overcome some of the simplifications of previous models. The improved model includes the interaction effects in resisting elements between axial forces and bi-directional horizontal forces. The parametric study was undertaken on a torsionally stiff structure and the results indicated that previous structural models that made no allowance for interaction phenomena overestimated the torsional response.

2.4.1.2.2 Inelastic Response of Bi-directional Excited Structures

Some pertinent observations on the inelastic response of bi-directional excited structures were made by De la Llera and Chopra, (1995) and Paulay, (1998). De la Llera and Chopra, (1995) observed that structures subjected to bi-directional ground motion will yield in the orthogonal direction to the main direction of excitation and develop a torsional mechanism when in the inelastic region. Also Paulay, (1998) showed that when a lateral resisting element is in the inelastic region, torsional restraint is lost.

Much of the early research was typically undertaken assuming an idealised bilinear material hysteresis behaviour; however materials such as reinforced concrete cannot be well represented in this manner due to strength deterioration. Therefore, Dutta and Das, (2002) investigated the impact of strength deterioration in a single-storey model by performing bi-directional time history analysis on a plan irregular code-designed structure. For the code-designed mass-eccentric system with strength deterioration, the authors found that the displacement/ductility demands on the FS element of the system showed a nominal increase while the SS element displacement/ductility demands were much larger (in the order of 3 times) than the similar symmetric systems with no strength deterioration.

Dimova and Alashki, (2003) provided an approximate analytical estimation of dynamic effects caused by mass eccentricity on a combined shear wall/reinforced concrete column type structure. It was shown that even a small mass eccentricity resulted in an irregular torsional response and that the draft Eurocode 8 (CEN, (2002)) multimodal analysis underestimated the effects of accidental torsion by up to 21% for 5% eccentricity. Results indicated the application of accidental eccentricities using static application of torsional moments in design in the draft Eurocode 8 (CEN, (2002)) do not adequately describe the dynamic torsional effects. To account for the dynamic effects the authors implemented three-dimensional models in their analysis. Similarly, results from De la Llera and Chopra, (1994) also indicated that considerable differences should be expected between analysis of a mass eccentric system using a fully dynamic analysis with explicitly shifted centre of mass and a static application of torsional moments (e.g. in EC8) (Dimova and Alashki, (2003)).

Stathopoulos and Anagnostopoulos, (2003) performed an assessment on the idealised shear-beam model used in an analysis of single-storey plan irregular buildings. The authors point out that previous research focused on checking the adequacy of code provisions

using a single-storey model with shear-beam load bearing elements. However, Stathopoulos and Anagnostopoulos, (2003) doubted that the results from such analyses can be extrapolated to frame-type structures. The shear-beam model is used to compare mass and stiffness eccentric systems and then form an assessment based on plastic hinge idealisations of single-storey models. Results from the assessment indicated that comparisons between the shear-beam models and more realistic plastic-hinge models showed substantial differences. The authors concluded that the shear-beam model is not adequate for assessing code performance for frame-type buildings. For torsionally stiff single-storey models, the code designed structure performed well. For the torsionally flexible model, the results obtained indicate that an increase in eccentricity results in increased demand on the SS and reduced demand on the FS. Subjecting the model to bi-directional excitation resulted in similar overall behaviour as uni-directional excitation.

The interdependence between strength and stiffness in resisting elements was studied by Tso and Myslimaj, (2003) & Myslimaj and Tso, (2005). Tso and Myslimaj, (2003) offer a design procedure to mitigate torsional damage by providing a desirable distribution of the centre of mass (CM), centre of stiffness (CR) and centre of strength (CV). The optimum arrangement of the CM, CR and CV is to have the CR located on one side of the CM and the CV located on the opposite side of the CM, termed the 'balanced CV-CR location' by the authors. However, the procedure proposed does not provide a unique solution and needs to be carefully evaluated for every structure it is applied to. In this regard, more traditional prescriptive design code approaches are more simplistic and more easily applied. Diaphragm rotation rather than drift or ductility is used as a measure of performance. The reason for this is that drift and ductility measure two very different things; drift relates to protecting the building envelope and ductility relates to control of structural damage (Tso and Myslimaj, (2003)).

Heredia-Zavoni and Machicao-Barrionuevo, (2004) investigated the influence of orthogonal components of ground motion in a linear single-storey bi-asymmetric torsionally stiff and torsionally flexible structure under firm and soft soil conditions. The authors found that the response of the structure was affected by the period of the structure, torsional flexibility and soil conditions. More specifically, for long translational period torsionally stiff structures on soft soil the effect of horizontal components of ground motion was appreciable. Similarly, it was found that for short translational period, torsionally flexible structures on firm soil the affect was also appreciable.

Peruš and Fajfar, (2005) approached the issue of plan irregularity in a general manner by ignoring the influence of design codes. The idea behind this approach is that extensive parametric studies are only valid for providing general conclusions if simple mathematical models are used. The single-storey structure under investigation was torsionally stiff with bilinear hysteretic material behaviour and the structural configurations investigated were mostly mass eccentric. Results indicated that in general for a torsionally stiff structure, the elastic and inelastic responses were similar. The SS response is governed strongly by the effect of several modes of vibration and the influence of the ground motion. The response of the FS of the structure quantitatively depends on the magnitude of the inelastic deformations. If the plastic deformations are small (normalised ductility < 2), the torsional effects in the inelastic structures are slightly higher than the elastic. If levels of normalised ductility exceed 2, torsional effects decrease on the FS. The authors also note that the behaviour of stiffness and strength eccentric systems are very similar. It is important to note that results were strongly influenced by the excitation used. Also, the variations in torsional stiffness and torsional strength were not taken into consideration in the research by Peruš and Fajfar, (2005).

In the above sections, the research history of single-storey models subjected to uni-directional and bi-directional excitation has been detailed. It can be seen that in much of the early research there were inconsistent conclusions and investigations were undertaken in a non-generic manner on a case-by-case basis. More recently, the conclusions based on research undertaken on single-storey models has been more consistent. The research seems to indicate that the SS of the structure is subjected to greater demand in plan irregular structures. It appears that the effect of bi-directional excitation has some effect on the torsional response, but not too substantial (Rutenberg and Tso, (2004)). The effects of bi-directional excitation are reduced if orthogonal elements are introduced to the system. It is evident from the above literature review that a lack of consensus on the structural behaviour of plan irregular single-storey structures exists due to the contradictory conclusions arrived at by researchers. The next question to be addressed is whether any of the conclusions made from single-storey plan irregular models can be extended to more realistic multi-storey models. The next section will detail the research studies undertaken to answer this question.

2.4.2 Multi-Storey Models

The response of single-storey plan irregular models has been described in detail in the previous section. In more recent years, with the increase in computational power and greater availability of three-dimensional non-linear finite element software, research into the seismic response of multi-storey structures has received more attention. The first question proposed by researchers investigating the multi-storey structural response of plan irregular structures was whether the conclusions from single-storey models could be extrapolated to multi-storey structures. Giordano et al., (2008) noted that most research investigating multi-storey framed buildings is concerned with assessing the ability of code provisions to accurately capture the torsional response when assessing limit state conditions (De la Llera and Chopra, (1994), Moghadam and Tso, (2000a), Stathopoulos and Anagnostopoulos, (2005), De Stefano et al., (2006), Kreslin and Fajfar, (2010), Erduran and Ryan, (2011)). However, numerous researchers (Duan and Chandler, (1993), Moghadam and Tso, (1996), Stathopoulos and Anagnostopoulos, (2003), De Stefano et al., (2006)) have noted that many aspects of multi-storey response (e.g. overstrength, participation of higher-order modes or change of dynamic properties) cannot be captured by one-storey models (Ghersi et al., (2007)). This indicates the need for a fresh approach evaluating the complete response of more realistic multi-storey structures with plan irregularity, rather than a simple evaluation of code specifications or reliance on conclusions from single-storey models.

The approach to multi-storey modelling of plan irregular behaviour has been split between lateral pushover analysis methods and time history analysis. The pushover procedure for evaluating the design capacity of a structure is an intuitive method for a designer, who may not be an expert in seismic analysis. In order to capture the torsional behaviour of a plan irregular structure using a pushover analysis, a three-dimensional model is required. However, defining the pushover load shape vector is more complex for a three-dimensional analysis, and several methods of applying the correct load shape vector to a three-dimensional plan irregular structure have been proposed, including Fajfar et al. (2005). Since the mid 1990's, time history analysis has been used to investigate the behaviour of plan irregular multi-storey structures and currently, refined three-dimensional numerical analysis of complex multi-storey structures is possible.

2.4.2.1 Pushover Analysis of Multi-storey Plan Irregular Structures

Many of the structural irregularity studies performed to date on multi-storey structures have been directed at extending the pushover analysis method to plan irregular structures (De Stefano and Pintucchi, (2008)). The pushover method was developed to provide a design procedure for multi-storey structures undergoing translation during seismic excitation. To extend the method to plan irregular structures, the torsional response of the structures also needed to be accounted for. Several methods of applying the pushover forces have been proposed, with the simplest method being that of applying the lateral loads at the CM axis or at an eccentricity (design eccentricity) from the CM axis until the target displacement is reached (Rutenberg and Tso, (2004)). Early research into the pushover method of analysis of plan irregular structures used this simple method (Kilar and Fajfar, (1997)).

Fajfar et al., (2002) extended the pushover method to bi-directionally excited multi-storey plan irregular structures. The results of pushover analysis are combined with elastic dynamic analysis using an improved version of the N2 method (Fajfar and Gaspersic, (1996)). The N2 method had initially been formulated for 2D planar models, but was extended by the authors to 3D models by applying a distribution of the lateral forces along the height of the building at each floor CM (De Stefano and Pintucchi, (2008)). In De Stefano and Pintucchi, (2008) an eight-storey RC walled building was used to demonstrate the suitability of the procedure. Results indicated that the N2 method was conservative but could predict the torsional response of a torsionally stiff structure. Subsequently, Fajfar et al., (2005) improved the method to properly include torsional effects by combining the N2 pushover method with a linear dynamic spectral analysis.

De Stefano and Rutenberg, (1998) and Moghadam and Tso, (2000b) performed pushover analyses on structures with walls and frames. Typically research has focused on either framed or walled structures, or a combination of both. As noted by Rutenberg and Tso, (2004), further research is required on combined structural types because the torsional response is very sensitive to the relative stiffness of the walls and frames. Forming conclusions on the behaviour of structures with combined wall and frame resisting elements based on the behaviour of either walls or frames acting individually is problematic.

Chopra and Goel, (2003) were also concerned with extending the modal pushover analysis procedure for regular structures to plan irregular structures. The results from the proposed modal pushover analysis and nonlinear time history analysis of nine-storey steel framed plan irregular and plan regular structures were compared. Results indicated that the seismic demand for both the torsionally stiff and torsionally flexible structural models gave similar levels of accuracy as that for the plan regular structure when the pushover and inelastic time history result were compared.

Penelis and Kappos, (2005) tried to capture the inelastic torsional response of both single- and multi-storey shear wall type plan irregular structures using a three-dimensional nonlinear static analysis procedure. The load vectors were calculated from a dynamic elastic spectral analysis. The response of the structure is obtained from an equivalent SDOF system which incorporates torsion and translation. The torsion and translation are accounted for by extending previous work that only accounted for translation. The results for the three-dimensional pushover are compared with inelastic time history analysis and they indicate that for the multi-storey structure, the discrepancy between the pushover and time history response is 20%, which is considered satisfactory due to the inherent assumptions in the time three-dimensional nonlinear modelling.

Giordano et al., (2008) performed a three-dimensional pushover analysis of a two-storey masonry building. The results obtained indicated that the FS of the structure receives greater displacement demand, however the results are limited as only one structure was analysed. Similar to previous studies, Ferraioli et al., (2010) assessed the response of a multi-storey framed plan irregular structure using three-dimensional nonlinear pushover analysis and verified the results against nonlinear time history analysis. Good agreement between the results was found for a torsionally stiff structure, but less so for a torsionally flexible structure with high levels of mass eccentricity.

The comparisons of pushover analysis with non-linear time history analysis appear to show reasonable agreement, but only for torsionally stiff structures. The structures analysed in the literature are specific to the individual research. Therefore, it is recommended that whilst undertaking research, inelastic time history analysis should be utilised rather than pushover analysis as the pushover analysis can miss important aspects of the behaviour. It will be shown in the next section how the time history analysis undertaken by some researchers has aimed at understanding the response of more realistic structural forms.

2.4.2.2 Time History Analysis of Plan Irregular Multi-storey Structures

Since the availability of greater computational power in the mid 1990's, inelastic time history analysis of multi-storey structures has become more feasible. As discussed in the previous section, pushover analysis as a method of analysis of plan irregular structures has been popular, but has almost always been validated by inelastic time history analysis. This section will detail the development and conclusions from inelastic time history analyses of plan irregular multi-storey structures. The validity of the extension of design procedures based on single-storey to multi-storey structures will be discussed.

One of the earliest reported time history analyses performed on a plan irregular structure was undertaken by De la Llera and Chopra, (1994) & De la Llera and Chopra, (1996). They studied the inelastic behaviour of a plan irregular multi-storey building that had different plan configurations of resisting planes. De la Llera and Chopra, (1996) developed guidelines to reduce the planwise unbalance that is associated with plan irregular structures. The authors established that it is important to have resisting elements in the orthogonal direction to help reduce the torsional response, and unwanted torsional response can be reduced by changing the strength of some key resisting planes. In general, De la Llera and Chopra, (1996) found that the results for single-storey models and the multi-storey models considered in this study show very similar trends.

Masi et al., (1997) studied the effect of flexible inelastic floor diaphragms on the seismic response of plan irregular multi-storey structures. An extensive parameter study was undertaken with nonlinear analysis of 216 structural variations of a six-by-two bay, two-storey building with varying in-plan locations of shear walls. The analyses indicated that the flexible floor hypothesis resulted in very high ductility demands in certain configurations and the rigid floor hypothesis resulted in a relatively constant response, irrespective of the structural irregularity.

Moghadam and Tso, (2000a) present a procedure to extend the static torsional provision of Eurocode 8 (CEN, (1994)) to plan irregular multi-storey buildings. Based on previous work by the authors, they recommended that a minimal torsional stiffness condition should be stipulated in Eurocode 8 Annex A (CEN, (1994)). The authors propose a simple design criterion for checking minimal torsional stiffness requirements. In order to extend the provisions from the single-storey model to the multi-storey model, a minimum level of torsional stiffness is required. A torsional ratio is proposed as a method to identify

buildings of low torsional stiffness, where a ratio of less than 1.0 would mean the structure is torsionally flexible. The ratio is effectively used as a torsional index. Results indicate that torsionally stiff structures perform well, and torsionally flexible structures do not. If the ratio is greater than 1.0, the static design procedure from Eurocode 8 (CEN, (1994)) can be used.

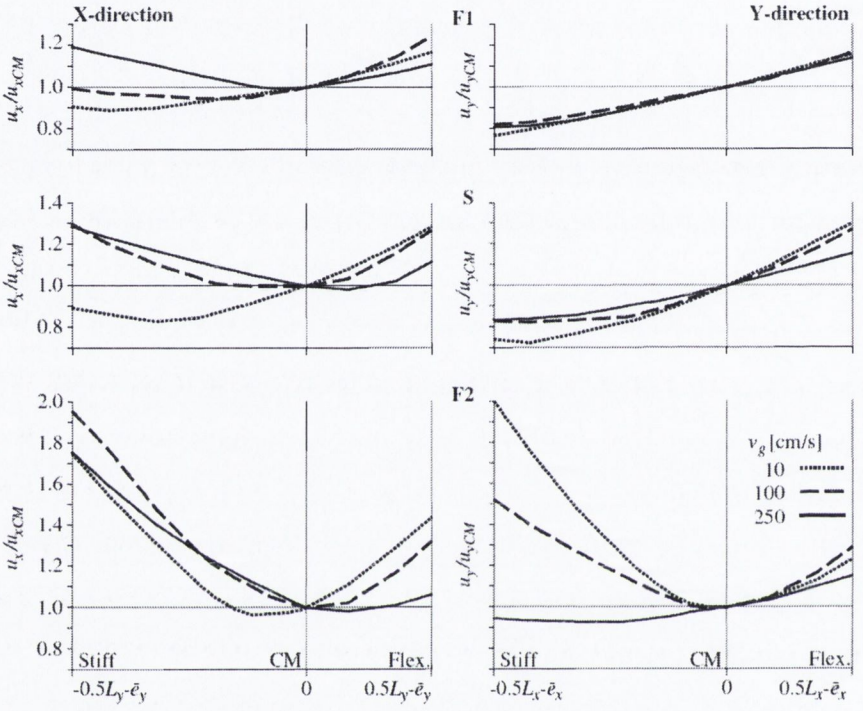

Figure 2.4: Normalised displacements (u/u_{CM}) in the horizontal plane at the top of a building with 15% mass eccentricity (Marusic and Fajfar, (2005))

Marusic and Fajfar, (2005) investigated the seismic response of a mass eccentric five-storey steel framed building designed to Eurocode 3 (CEN, (2005)) and Eurocode 8 (CEN, (2004)) subjected to bi-directional excitation. They found that the intensity of the ground motion influenced the torsional response as it affected the plastic deformation of the structure. For the torsionally stiff structure, the FS displacement demand decreases moderately for increasing plastic deformation and conversely, the SS displacement demand increases for increasing plastic deformations. Results for the three types of structures analysed can be seen in Figure 2.4 (the x-direction is the stronger direction). Building *S* and *F1* are torsionally stiff and Building *F2* is torsionally flexible. Building *S* has moment resisting connections throughout, Building *F1* has moment resisting connections in the planwise corner frames only and pinned elsewhere. Building *F2* has moment resisting connections at the interior connections and pinned connections at perimeter connections.

From Figure 2.4 it can be seen for the torsionally stiff structures (*S* & *F1*) in the weak direction (*y*-direction) the normalised displacements vary almost linearly from the SS to the FS, which implies that only one mode of vibration influences the response. For the torsionally stiff structures (*S* & *F1*) in the strong direction (*x*-direction), the increased curvature of the normalised displacement lines indicates the influence of several modes. As can be seen in Figure 2.4 for the torsionally flexible structure (*F2*) almost all of the displacements are greater than 1, indicating that the torsionally flexible structure performs worse than the symmetric (regular) and torsionally flexible structures. The torsionally stiff and torsionally flexible structures perform quantitatively similar in the elastic and inelastic range. An important observation is that the displacements in the SS of the structure are strongly influenced by the ground excitation used, a point that has also been mentioned by others.

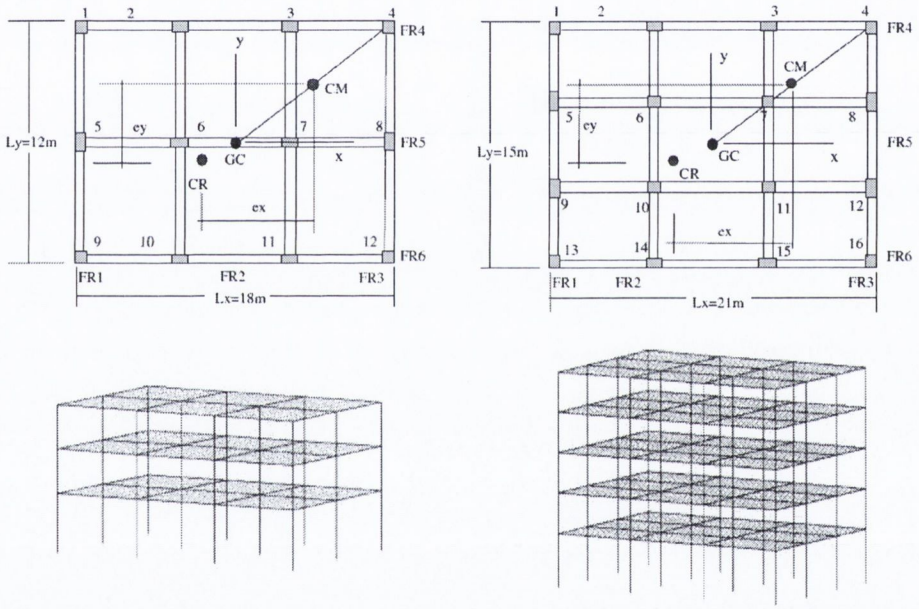

Figure 2.5: Three- and five-storey reinforced concrete structural models (Stathopoulos and Anagnostopoulos, (2005))

Stathopoulos and Anagnostopoulos, (2005) studied the seismic response of three- and five-storey plan irregular code designed RC frame (UBC-97 (UBC, (1997)) & Eurocode 8 (CEN, (1994))) structures (see Figure 2.5) subjected to bi-directional excitation. The study presents one of the first attempts to obtain an inelastic torsional response of more realistic (non-idealised) multi-storey frame type structure.

The results observed by Stathopoulos and Anagnostopoulos, (2005) indicated that in both models the beam ductility demand increased substantially on the FS when the eccentricity

increased, with a less pronounced reduction in the beam ductility observed on the SS. Similarly, damage indices are substantially increased in the FS and decreased in the SS. The results indicate a shortcoming in the design codes, which indicate that increasing the design eccentricity results in a general proportional increase in the stiffness and strength. Thus, the equivalent yield displacement remains approximately constant. However, as described above, the numerical results indicate that as eccentricity increases the FS ductility increases substantially and the SS ductility reduces. This conclusion is contrary to the previous results obtained from one-storey models. The authors therefore state the need for reassessment of the current design code provisions to take account of this contradiction. These results are in contrast to the results obtained by Marusic and Fajfar, (2005), who found the results from their time history analysis of multi-storey models agreed well with those of the previous research on single storey models.

Fernández-Dávila and Cruz, (2006) performed a parametric study on the seismic response of three-dimensional five-storey RC frame type plan irregular structures. The structural models were effectively multi-storey extensions of the idealised single-storey models that have been extensively used previously. The study investigated the effect of the number of resisting planes parallel to the earthquake direction and the influence of elastic parameters. Results were in agreement with previously well-known behaviour observed in single-storey models, in that the SS frame of the structure was subject to greatest local ductility demand.

De Stefano et al., (2006) undertook an investigation to observe the effects of cross-sectional overstrength on the seismic behaviour of multi-storey frame type plan irregular structures. Structural characteristics such as overstrength and higher modes of vibration were believed to not be represented by the simple single-storey models traditionally used. The investigation found that using one-storey models led to the accurate evaluation of multi-storey plan irregular models only when analysed in the elastic region, however when a structure is excited into the nonlinear range, the assumptions of the one-storey models are no longer adequate. The energy dissipative mechanisms in multi-storey structures cannot be represented by one-storey models. The results of the analyses show that ductility demands may become larger at unexpected locations due to overstrength. The ductility demand in the upper floors of the multi-storey structure becomes large on the FS of the structure (50% larger than torsionally balanced structure). This result contradicts most results obtained from single-storey systems in the past and provides further evidence that

results from single-storey structures cannot be universally extended to multi-storey structures.

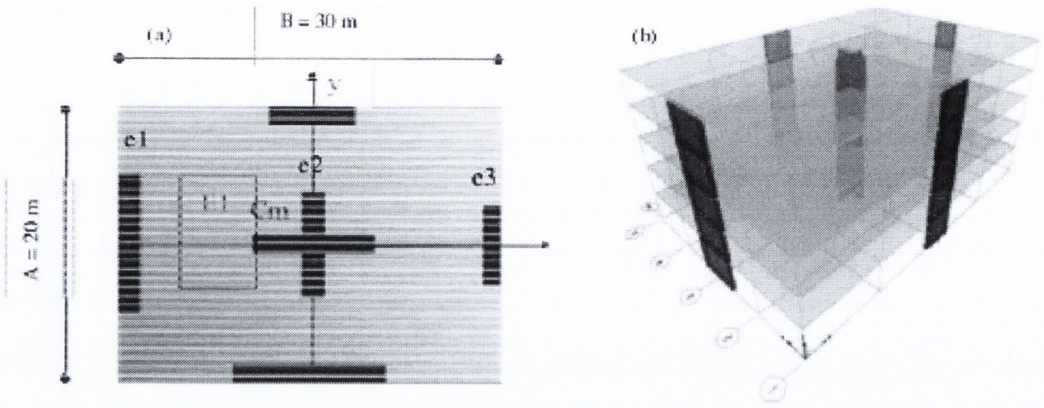

Figure 2.6: Plan and three-dimensional of torsionally unbalanced structure (Aziminejad and Moghadam, (2009))

Aziminejad and Moghadam, (2009) performed a study of the nonlinear response of a series of five-storey plan irregular structures with different strength distributions. The aim of the research was to investigate the effect of the different strength distributions strategies and their effect on the plan irregular response. The typical criteria of; ductility demand, diaphragm rotation, interstorey drift and plastic rotation were used as a measure of damage. The results for interstorey drift and plastic hinge rotation were compared to limits in FEMA 356 (FEMA 356, (2000)). Figure 2.6 displays the plan and three-dimensional views of the plan irregular structure considered in the research. The structure has an idealised resisting element configuration that is not too dissimilar to many of the idealised single-storey models used in previous research. Results indicate that for the torsionally stiff structure studied, models with a smaller strength eccentricity perform better. However, the optimum strength eccentricity that reduces the adverse torsional response depends on the damage criteria used e.g. ductility, interstorey drift or floor rotation. For example, if the damage criterion is set as interstorey drift then the appropriate strength distribution is to have a configuration with a small strength eccentricity. On the other hand, if the damage criterion is set as ductility demand of the SS and FS elements then the appropriate strength distribution is to have a configuration with the centre of strength located between the CM and CR.

It can be seen from the literature review above on the seismic response of plan irregular multi-storey structures that still a definite lack of consensus exists on the expected response of the SS or FS of the structure. Some of the studies mentioned indicate that the SS of the structure is subjected to the greatest demand, whilst other studies indicate the FS to be subjected to greatest demand. Similarly, some research indicates that the results obtained from single-storey models coincide with results from multi-storey structures, whereas other researchers found poor agreement between the results obtained using single-storey and multi-storey models. Aside from the SS and FS response of plan irregular structures, the review of previous research also highlights the importance of stiffness and strength asymmetry. The location of the centre of strength and centre of stiffness are important factors in the torsional response of plan irregular structures. It is clear that further investigation into the seismic response of a variety of structural types is required before any conclusions can be arrived at. Considerations for design codes should be at the front of any researchers mind when tackling this issue.

2.5 Eurocode 8 Approach to Accidental Eccentricity

As has been explained in previous sections, the Eurocode 8 (CEN, (2004)) provisions for plan irregular building structures have been developed based on findings from idealised single-storey models. Two methods have been developed in Eurocode 8 (CEN, (2004)) to account for the accidental eccentricity in plan irregular structures namely; a lateral force method and a modal response spectrum analysis method. The concept of accidental eccentricity has been introduced in Eurococde 8 (CEN, (2004)) to account for uncertainties in the location of the CM. The two methods are described briefly in the following sections.

2.5.1 Seismic Design in Eurocode 8

There are two fundamental design levels in Eurocode 8 (CEN, (2004)); no collapse and damage limitation. The no collapse requirement corresponds to a design seismic action applied to the structure that has a probability of exceedance of 10% in 50 years or a return period 475 years. The damage limitation requirement corresponds to a design seismic action applied to the structure that has a probability of exceedance of 10% in 10 years or a return period 95 years.

There are two design options for the behaviour of a steel structure in Eurocode 8 (CEN, (2004)) namely; dissipative and non-dissipative. Non-dissipative design is used for structures in areas of low seismicity where the structure is expected to behave in the elastic range. If this is not the case, then the structure must be designed to economically resist a seismic action using dissipative behaviour and allowing considerable inelastic deformations to be accommodated. In terms of ultimate limit state, the resistance and energy dissipation capacity assigned to the structure depend on how much of the non-linear response of the structure will be utilised. The level of resistance and energy dissipation capacity utilised in the non-linear response is characterised by the behaviour factor, q and the ductility class chosen by the designer. In terms of damage limitation, serviceability conditions such as drift limitations need to be met.

The basic representation of the seismic action in the code is a reference elastic response spectrum (S_e). The elastic response spectrum (S_e) in terms of acceleration is defined as a function of the period (T), the peak design ground acceleration (a_g), the soil factor (S), the damping correction factor (η) and predefined spectral periods (T_B(s), T_C(s) & T_D(s)) (Elghazouli, (2010)). The soil factor (S), the damping correction factor (η) and predefined spectral periods (T_B(s), T_C(s) & T_D(s)) depend on the soil characteristics taking into account the amplifying effect of soil layers and the seismic characteristics of the proposed design earthquake (higher seismicity areas called Type 1 (surface wave magnitude, $M_s > 5.5$), moderate seismicity areas called Type 2 ($M_s \leq 5.5$) or other defined spectra in the relative National Annex). The elastic spectral accelerations are divided by q to reduce the design forces to avoid the need to perform an inelastic analysis. With respect to design, a simplified equivalent static force approach for regular structures may be adopted (Elghazouli, (2010)). The method can be used if the response of the structure can be reasonably assumed to be dominated by a single mode (typically the fundamental mode).

Two principle methods of design exist; the lateral force method (pushover method) and the time history analysis method. The lateral force method essentially converts the seismic inertia forces to static horizontal pushover forces. The inertia forces are calculated based on the mass, structural period, damping and level of acceleration on an elastic response spectrum. The lateral force method is a static procedure of analysis that does not require complex dynamic calculation. The lateral force method is intuitive and applicable to most design scenarios. The shortcomings of the lateral pushover method of analysis are that the response of the structure needs to be dominated by its fundamental period for the analysis

to be applicable and the analysis does not take into account the effect of higher modes. Inelastic time history overcomes the shortfalls of the lateral force method and allows more complex analysis of structures, such as plan irregular structures. The major drawback to inelastic time history analysis is the computational time and effort required to perform analyses.

The lateral force method of analysis provides the most fundamental approach to designing a structure to resist an earthquake in Eurocode 8 (CEN, (2004)). The application of the lateral force method of design for accidental eccentricity is of interest when dealing with in plan irregularity. Plan irregularity in terms of uneven distribution of mass in plan is essentially accidental eccentricity. In the next section, the design procedure for accidental eccentricity in Eurocode 8 (CEN, (2004)) will be described.

2.5.2 Accidental Eccentricity Design Using Lateral Force Method

As stated in Eurocode 8 (CEN, (2004)) (Section 4.3.3.4.2.7), the results from a pushover analysis may significantly underestimate the deformations in the SS of the structure if accidental torsion effects are not taken into consideration. Hence, a design procedure to take account of accidental torsion effects is incorporated into Eurocode 8 (CEN, (2004)). The uncertainty in the distribution of mass at each floor is taken into account by shifting the CM of each floor by an amount defined as follows:

$$e_{ai} = 0.05L_i \tag{2.3}$$

where e_{ai} is the accidental eccentricity of storey mass i from its nominal location, applied in the same direction at all floors

L_i is the floor dimension perpendicular to the direction of the seismic action

A structure must be regular to allow the application of accidental eccentricity, e_{ai} in design. The criteria for regularity in plan were set out in as mentioned in Section 2.4.1. Eurocode 8 (CEN, (2004)) provides a means of estimating the effect of accidental torsion if it has not been taken into consideration by Equation 2.3 or another more exact means of analysis. The Eurocode 8 (CEN, (2004)) torsional effects factor, δ, applied to the seismic action affects is defined in Equation 2.4;

$$\delta = 1 + 0.6\frac{x}{L_e} \tag{2.4}$$

where x is the distance from the element under consideration to the CM of the structure measured perpendicularly to the seismic action

L_e is the distance between the two outermost lateral load resisting elements

The torsional effects factor, δ is then multiplied by the relevant design lateral pushover action to take account of torsional effects. The criteria for ensuring the structure is not plan irregular, as mentioned in Section 2.4.1, need to be met in order to apply the torsional effects factor, δ in design. The design procedure is quite intuitive for the designer as you are applying a factored action to the side of the structure the mass is distributed towards to better represent the mass distribution towards that side of the structure. The validity of this procedure will be investigated in this thesis by applying the design criteria in Equation 2.4 to a concentrically braced steel structure and subjecting the structure to inelastic time-history analyses and testing regime in order to assess the effectiveness of the design.

Seismic design codes aim to reduce the magnitude of the torsional response of buildings. Penelis and Kappos, (2005) make the point that the code provisions are related to the elastic properties of the building, such as lateral torsional frequency ratio, Ω_θ. However, the same codes promote the design of buildings in the inelastic range by using the 'behaviour factor' q (or 'force reduction factor', R), but at the same time fail to provide explicit guidance on the inelastic torsional response of buildings.

In this thesis, the Eurocode 8 (CEN, (2004)) provision as outlined in Section 4.5.1 will be applied to a plan irregular multi-storey concentrically braced steel structure and the effectiveness of the code provision will be estimated.

2.6 Testing of Plan Irregular Structures

As stated by De Stefano and Pintucchi, (2008) in a review of research on the seismic response of irregular structures since 2002, there is a scarcity of experimental research in the area of structural irregularity. Experimental work is required to reinforce the conclusions that have largely been made based on purely theoretical numerical modelling. Previous experimental work in this area will be discussed briefly in this section.

2.6.1 Previous Test Results

In recent years, there has been a move towards experimental validation of the theoretical research on plan irregular structural response. For example, scale model tests have been undertaken by the European Association for Earthquake Engineering (EAEE) Task Group 8 (TG8) at the University of Bristol Earthquake Engineering Research Centre (Trombetti et al., (2004)). The aim of the research by TG8 were to better understand the behaviour of plan irregular buildings, compare the response of symmetric and asymmetric structures, verify predictive capabilities and assess the code provisions of major seismic codes.

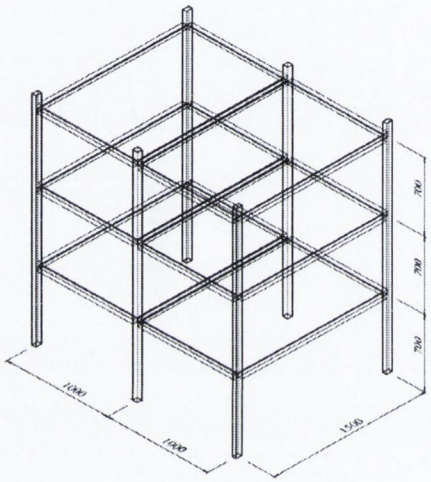

Figure 2.7: Scaled three-dimensional model of steel framed structure tested (Trombetti et al., (2004))

Trombetti et al., (2004) performed scaled (1/5 scale) shake table tests on three-storey symmetric and asymmetric steel framed structures. The structure was a moment resisting frame, as shown in Figure 2.7. The plan irregular structure was compared to a symmetric structure, but neither was designed using a torsional code provision so that the effect of the asymmetry could be quantified. Mass eccentricity of 10% was applied to the plan irregular structure and the results showed a consistent increase in the FS maximum deformations with respect to the deformations at the CR.

One of the most analysed structures ever tested in the field of earthquake engineering was the Seismic PErformance Assessment and Rehabilitation (SPEAR) project undertaken at the European Laboratory for Structural Assessment (ELSA) in Ispra, Italy. As part of the project, a full scale pseudo dynamic (PsD) test on a three-storey irregular reinforced concrete structure was undertaken (Fardis and Negro, 2005). Included in the large volume

of research undertaken on the SPEAR structure were; scaled shake table tests undertaken by Coelho et al., (2005), analytical assessments of the structure performed by Jeong and Elnashai, (2005) and retrofitting solutions proposed by Mola and Negro, (2005). The SPEAR project allowed for the first time a comparative numerical modelling study of a typical existing southern European reinforced concrete structure designed to resist gravity loads only. Results from the test indicated that the FS columns which were located far from the centre of rigidity were damaged more severely than the other columns (Jeong and Elnashai, (2005)).

PsD testing was also performed by Bousias et al., (2007) on a uni-axial eccentric two-storey, one-bay reinforced concrete structure subjected to uni-directional ground motion. The results from the initial test indicated that the FS of the structure sustained large drifts simultaneously in the two transverse directions. Once the initial PsD test was complete on the irregular structure, the columns on the FS of the structure were retrofitted using RC-jacketing and a subsequent test was undertaken.

The lack of experimental validation could seriously hamper code development of seismic provisions for plan irregular structures. It can be seen from the limited number of experiments completed to date that further testing is needed to validate theoretical conclusions made. The proposed plan irregular braced frame structure that is to be investigated in this thesis will be physically tested in order to provide essential experimental data on the seismic response of this class of structure.

2.7 Analysis of Braced Plan Irregular Structures

Within the research undertaken to date into plan irregular structures, very little research on the response of concentrically braced structures exists (notwithstanding the importance of this form of construction in many earthquake regions). Typically, analytical studies have focused on moment resisting frame structures or shear wall structures. The Eurocode 8 (CEN, (2004)) provisions are mainly based on the seismic response of single-storey shear wall type structures. It is important to see if the provisions are applicable to braced steel structures that have a very different inelastic response compared to moment resisting frames or shear wall type structures. This section will briefly detail the different approaches to the modelling of concentric bracing in plan irregular structures.

More recently, some research investigating the seismic behaviour of braced steel structures has been performed; Lignos and Gantes, (2005), Miri and Maramaee, (2009) & Erduran and Ryan, (2011). Lignos and Gantes, (2005) investigated the seismic response of steel braced frame structure with plan stiffness irregularity using modal pushover analysis (MPA). The stiffness irregularity is applied to the building by selecting various locations for the braced frames in the building. The results of the modal pushover analysis indicated that it could predict the response of low-rise buildings well, whereas it underestimated the response of taller structures. The pushover results were validated with nonlinear time history analysis, however the authors note that when a storey mechanism forms between the braces and collapse occurs, MPA is not able to predict this behaviour. The authors were mainly concerned with global response of the structure and did not explicitly mention the SS or FS behaviour or the response of individual bracing members.

Miri and Maramaee, (2009) performed an inelastic time history analysis of the effect of mass eccentricity on the seismic response of a five-storey concentrically braced structure. The study was not very extensive and unsurprisingly the main results indicated that the increase in mass eccentricity resulted in greater storey drifts in the structure.

Erduran and Ryan, (2011) studied the effects of torsion on the behaviour of a peripheral steel braced frame system in a three-dimensional three-storey steel framed structural model. The structure had been designed for 5% eccentricity according to ASCE 7-05 (American Society of Civil Engineers, (2005)). Both elastic response spectrum analysis and pushover analysis were used to capture and evaluate the behaviour of the structure. In general, the observations indicate that the FS of the structure is subjected to greater torsional response due to the dynamic shift in the CR that results from yielding and buckling. In contrast, the SS bracing remains almost elastic. The structure with 5% eccentricity (level of accidental eccentricity in Eurocode 8) experienced significant amplification of the interstorey drifts when subjected to high intensity ground motions. The normalised interstorey drifts for the inelastic response exceeded the interstorey drifts for the elastic response. Unlike previous framed structure research, the interstorey drifts for bi-directional excitations are much greater than those for uni-axial excitation. The authors conclude by saying that a much better response of a braced framed steel structure can be achieved by having the bracing aligned on several lines throughout the building and not just at the periphery of the building. The conclusion is reiterated in separate findings by Ding, (2006) which state that the response of the structure is improved if the bracing is

located closer to the CM of the structure. It would appear from this study that the behaviour of concentrically braced framed structures does not follow the general trends displayed by moment resisting framed structures.

The research to date on braced framed steel structures with plan irregularity has relied solely on analytical studies. To the best of this author's knowledge, no experiments on braced framed steel structures with plan irregularity have been undertaken to date. From the brief summary of the few analytical investigations undertaken to date, it is evident that their conclusions are weak and sometimes contradictory.

2.8 Passive Control of Plan Irregular Structures

A growing area of research in plan irregular structures is aimed at reducing the torsional response of the structure using passive control. The topic of passive control will be briefly discussed in this section to provide an overview of the general trends in plan irregular research, but will not be dealt with further in this thesis. The passive control systems investigated by researchers can be segregated into the following general categories; (1) fluid viscous dampers and their subsequent tuning, (2) other types of damper e.g. tuned mass dampers and (3) base isolation.

Much of the early research into the passive control of plan irregular structures utilised fluid viscous dampers as the control mechanism (Goel, (1998), Lin and Chopra, (2003) & Petti and De Iuliis, (2008)). Fluid viscous dampers had been shown to dampen the vibration response of regular structures, so the aim was to extend this concept to irregular structures. Goel, (1998) showed that it was possible to reduce the edge deformation of a plan irregular structure to similar deformations a symmetric one by using viscous damping.

Other forms of damping studied include the use of tuned mass dampers (Singh et al., (2002) & Wang and Lin, (2005)). Singh et al., (2002) optimised the design of multiple tuned mass dampers and the effectiveness of the optimisation procedure is detailed with several numerical examples. The innovative use of magnetorheological (MR) dampers as control for plan irregular structures was studied by Yoshida et al., (2003). The MR dampers provide semi-active control resulting in all of the responses of the sample building tested being reduced. Li and Li, (2009) also investigated the use of MR dampers for semi-

active control and found the MR dampers to be quite effective at mitigating the torsional response.

Base isolation has been used widely to reduce the response of structural systems to earthquake excitation. Examples of base isolation strategies being applied to plan irregular structures include; Lee, (1980), Tena-Colunga and Gómez-Soberón, (2002), Lee and Ab-Malek, (2010) & Koren and Kilar, (2011). Tena-Colunga and Gómez-Soberón, (2002) found that the effectiveness of the isolator system was reduced by increasing the degree of mass eccentricity. Lee and Ab-Malek, (2010) analysed a base isolation scheme for an L-shaped multi-storey building and observed that base isolation elongated the natural period of the structure helping to eliminate resonance effects at the predominant period of the earthquake. Results indicated that a properly designed base isolation system helped to eliminate the torsional response of the plan irregular structure analysed.

Passive control has been briefly shown to be an effective tool for the reduction of the adverse torsional response of plan irregular structures. Semi-active and active control torsional response of building structures is an area of promising continuing further research.

2.9 Chapter Overview

An overview of research undertaken on plan irregular structures has been presented. The early research focused on simple single-storey structures that could be easily parameterised. The research was extended from linear to nonlinear analysis for single-storey structures. In more recent years, the behaviour of more realistic multi-storey plan irregular structures has been undertaken. From the literature review in this chapter, it is evident that conclusions on the seismic response plan irregular structures are weak and sometimes contradictory. Some research indicates the FS of the structure is subjected to greater demands than the SS of the structure and vice versa. It has been shown that research mainly focused on reinforced concrete structures and some steel moment resisting framed structures, but little research to date has been undertaken on concentrically braced plan irregular structures. Some of the important parameters/aspects of behaviour that have been identified are; the location of the CM and CR, the torsional stiffness/flexiblity of the structure and the level to which the structure is excited in the elastic/inelastic range. The

aim of the research described in this thesis is to better understand the torsional response of plan irregular multi-storey steel braced structures and to assess the applicability of the European design code. This is achieved through the joint use of experimentation and numerical analysis. The next chapter describe the numerical modelling technique given for concentrically braced plan irregular structures.

CHAPTER THREE – Numerical Modelling of Braced Plan Irregular Steel Structures

3.1 Introduction

The previous chapter described the research that has taken place to date on plan irregular structures. In Chapter Two, it has been noted that there is a lack of research into plan irregular concentrically braced steel frame structures. This chapter introduces the characteristics of brace behaviour that affect the earthquake response of such structures, and the proposed computational modelling approach to be used in the investigation of this behaviour. The important factors affecting the plan irregular response of building structures and the modelling of these parameters will be detailed.

3.2 Eurocode 8: Seismic Design of Concentrically Braced Structures

The fundamental aim of this research is to investigate the dynamic behaviour of concentrically braced plan irregular steel structures. As stated in the previous chapter, the design guidance for plan irregular structures in most design standards has been based on highly idealised single-storey structures. In this context, Eurocode 8 (CEN, (2004)) will form the background to which this current research will take place. It is important to understand how Eurocode 8 (CEN, (2004)) deals with the design of concentrically braced steel frames in their own right, prior to their investigation in a plan irregular structure scenario.

Concentrically Braced Frames

Some of the different types of concentrically braced frames commonly used are shown in Figure 3.1. Figure 3.1(a) indicates an X-braced framed structure and Figure 3.1(b) indicates a decoupled diagonally braced framed structure. Both the X-braced and diagonal braced frames rely on dissipative zones in the tension braces only. Figure 3.1(c) indicates an inverted-V braced structure. The capacity of the inverted-V braced structure relies on dissipative zones in the tension and compression diagonals. Figure 3.1(d) indicates a K-braced structure, whose design is not recommended for dissipative design.

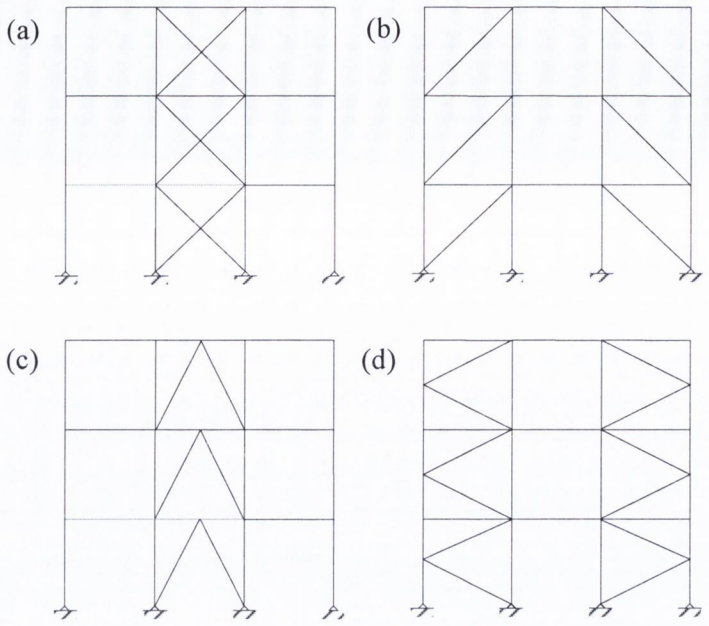

Figure 3.1: Types of concentrically braced frames (a) X-bracing, (b) decoupled diagonal bracing, (c) inverted V-bracing and (d) K-bracing

The behaviour factor, q for the diagonally braced structures in Figure 3.1(a) & (b) in Eurocode 8 (CEN, (2004)) is 4, for both DCM (Ductility Class Medium) and DCH (Ductility Class High). The behaviour factor, q for the inverted-V braced structure in Figure 3.1(c) in Eurocode 8 (CEN, (2004)) has a lower bound of 2.0 for DCM and 2.5 for DCH respectively. This project will only be concerned with the design of X-braced frames and will not deal with the detail of other concentrically braced structural forms.

Eurocode 8 (CEN, (2004)) prescribes conditions in relation to slenderness limits. For X-bracing the non-dimensional slenderness is limited by Eurocode 8 (CEN, (2004)) as follows;

$$1.3 < \bar{\lambda} \leq 2.0 \tag{3.1}$$

The lower limit of 1.3 prevents the bracing members becoming too stocky, which could result in overloading of the columns in the pre-buckling stage. The upper limit of 2.0 prevents the bracing members from being too slender, which could result in a poor hysteretic response. These limits in many cases can be the governing factor in design.

An important point to note is that connection design is only considered conceptually in Eurocode 8 (CEN, (2004)). No specific design procedure for specific connection types is presented in the code; however, preventing damage of the connection by providing sufficient overstrength in the connection is the method adopted. This helps to ensure that the members yield away from the connection. The connection design of the proposed test frame will be discussed in more detail in Chapter Five.

Serviceability Limit State

The serviceability limit state is associated with the damage limitation requirement. The interstorey drift limitations prescribed by the code for buildings having non-structural brittle elements attached to the structure is;

$$d_r v \leq 0.005h \tag{3.2}$$

where;

d_r is the design interstorey drift obtained by analysis

h is the storey height

v is the reduction factor

The factor multiplying the storey height changes depending on the type of structure. For buildings having ductile non-structural elements, the value of this factor is 0.0075. For buildings having non-structural elements fixed to the structure in a way that does not affect the structural deformations, the value of this factor is 0.01.

3.3 Concentric Bracing Behaviour

The aim of a comprehensive numerical model is to capture the important behaviour of brace members whilst remaining sufficiently efficient to be used in everyday analysis. A model is required that can capture the nonlinear cyclic response displayed by a strut undergoing alternative and repeated compression buckling and tensile yielding to significant levels of axial deformation and ductility demand. This section provides a brief introduction to the different analytical methods of replicating the structural behaviour of

bracing members. Examples of experimental studies undertaken on bracing members include; Jain et al., (1978), Black et al., (1980), Popov and Black, (1981), Tremblay et al., (2003), Boutros, (1999) & Goggins, (2004). In particular, testing by Black et al., (1980) has been used extensively by researchers for analytic brace model validation. Researchers have created different types of analytical models based on the observations from experimental data. As stated by Uriz et al., (2008), the three different types of existing analytical models for steel braces are; phenomenological models, physical theory (Ikeda and Mahin, (1984)) and three-dimensional finite element models.

Phenomenological Models aim to imitate the hysteretic behaviour of brace members using physically observed axial force-deformation curves (Longo et al., (2008)). The phenomenological models are computationally very efficient; however, numerous empirical parameters need to be inputted into the models. If the empirical data for a particular specimen does not exist, then other models are needed. Therefore, phenomenological models are case specific and not suitable for a generalised solution. As stated by Huang and Mahin, (2010), phenomenological models are typical pin-ended truss members with a prescribed axial force-deformation relationship that mimics the hysteretic response of the brace. Examples of phenomenological models include Zayas et al., (1980), Ikeada et al., (1984) & Khatib et al., (1988).

Physical Theory Models use simplified theoretical formulations based on physical observations to model the hysteretic behaviour of a brace member. Physical theory models are a combination of phenomenological models and the finite element approach (Longo et al., (2008)). Physical theory models use input parameters based on material properties such as yield strength and elastic modulus in conjunction with geometric properties such as cross-sectional area and moment of inertia (Jin and El-Tawil, (2003)). A typical example of a physical theory model is two elastic elements connected by a plastic hinge at the mid-span. In these models, assumptions are being made about the strain distribution across a section (Huang and Mahin, (2010)) and assuming between plastic hinges the element remains elastic. The typical physical theory model only incorporates uni-directional properties resulting in multi-axis stress states and three-dimensional phenomena such as local buckling not represented in the response. Examples of physical theory models of brace members include; Maison and Popov, (1980), Ikeda and Mahin, (1984), Boutros, (1999), Fell et al., (2006), Uriz et al., (2008) & Dicleli and Calik, (2008).

Continuum Finite Element Models explicitly model the geometry and material behaviour of the brace member. The above mentioned models are special types of finite element

models, however, continuum finite element models aim to overcome drawbacks in th above mentioned models by incorporating multi-axis stress states and three-dimension phenomena. Examples of continuum finite element models of brace members include Fe et al., (2006), Kanvinde and Deierlein, (2007), Huang and Mahin, (2008) & (2009). Th models accurately replicate hysteretic behaviour and can include three-dimension phenomena such as local buckling. However, finite element models require considerab computational time and effort when compared to the other forms of analytical model Typically, the continuum finite element models are used for local models consisting of few structural components rather than modelling an entire structure. Even with moder computers, the computational time and effort is too onerous for most design situation Some drawbacks of basic continuum finite element models are the inability to includ material failure, such as fracture, and large deformations as they are not incorporated in th model (Huang and Mahin, (2010)). More complex finite element packages or specificall developed finite element packages can incorporate complex behaviour such as fracture an large deformation. These continuum models tend to be computational very expensive.

The numerical implementation of bracing hysteresis response used in this thesis is base on physical theory and will be discussed in further detail in Sections 3.3 & 3.4.

Hysteretic Behaviour of Steel Braces

A brief overview of the inelastic cyclic behaviour of a brace member can be seen in Figur 3.2. On Branch A of the loading curve from Point 0 to Point 1, the brace is axially loade in compression. Due to initial imperfections in the brace member, the brace axiall shortens and the brace deflects laterally (either in- or out-of plane). At Point 1, th maximum compressive load is reached as the brace buckles. After Point 1 in Branch B o the hysteresis, the brace deflects laterally at mid-span to accommodate increasing axia displacement. A plastic hinge begins to form at mid-span which leads to a reduction i capacity (Elghazouli, (2003)). At Point 2, the maximum compression displacement of tha cycle is reached and load reversal occurs. In Branch C, elastic recovery occurs when th load is reversed. Branch C has a smaller slope than the Branch A due to the residual latera displacement at mid-span following the compression loading phase (Dicleli and Calik (2008)). In Branch D, tensile yielding occurs. By Point 4, the bending moment i effectively zero in the section at mid-span and the brace is essentially straight. Branch represents uniaxial plastic elongation of the brace. At Point 5, the direction of loading i reversed. Elastic unloading occurs in Branch F as the tensile force reduces. From Point 6

the brace is in compression. In Branch G, compressive loading results in a reduced buckling load at Point 7 due to residual deflections in the brace member, i.e. at the end of the initial cycle, the brace member did not straighten completely resulting in a residual displacement which reduces the buckling capacity. In Branch H, the brace response continues as described above from Branch B.

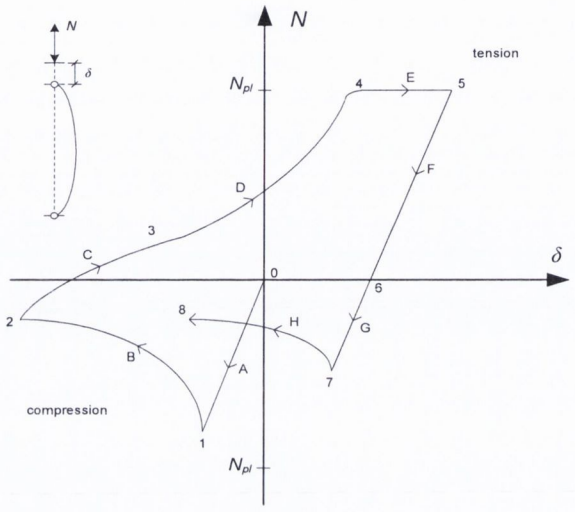

Figure 3.2: Hysteresis zones of axial cyclic response of brace member (Dicleli and Calik, (2008))

Two important effects of cyclic inelastic loading of steel members are the Baushinger effect (Bauschinger, (1886)) and the Growth effect. An accurate material model needs to implement these effects in order to replicate cyclic brace behaviour accurately. The Baushinger effect is named after Johann Baushinger who performed the first measurements of elastic limits under repeated loads and noted that after plastic deformation from loading in one direction, the stress was lower for subsequent loading in the opposite direction (Simsir et al., (2010)). The Baushinger effect can be seen in Figure 3.3, where the tensile yield strength increases at a cost of the reduction in the compressive strength of the brace section. When a specimen is loaded in tension and then reloaded in compression, it is observed that the yield occurs at a reduced stress (Hill, (1998)). McClintock and Argon, (1966) observed that there was some material work hardening as well as softening. It can also be observed in Figure 3.3 that the material modulus of elasticity (stiffness) softens in proportion to the number of loading cycles that have been executed.

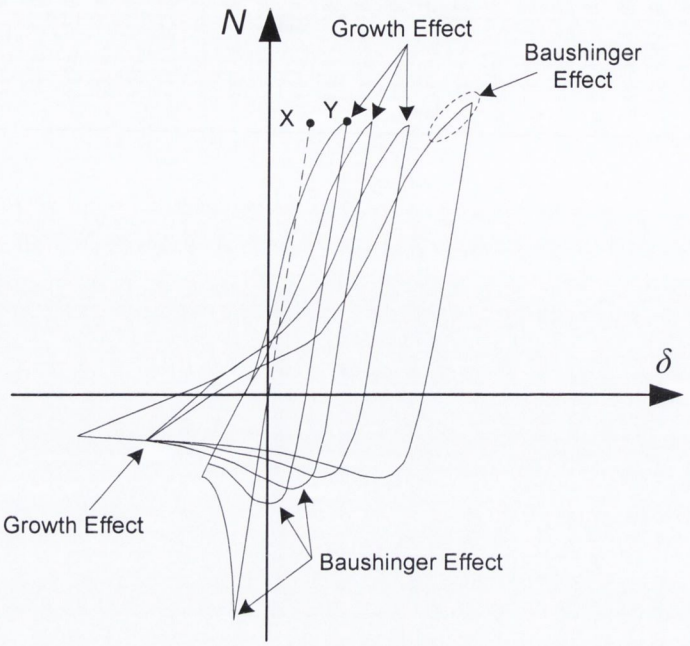

Figure 3.3: Baushinger effect and growth effect (Dicleli and Calik, (2008))

The Growth effect can be seen in the compression unloading and tension loading part of the cycle. During cyclic loading, typically for three cycles, the brace is subjected to the same magnitude of maximum tensile force. However, as can be seen in Figure 3.3, during this phase of unloading and loading, the axial displacement increases. Even though the brace may not have yielded and the brace is subjected to the same load at each cycle, this causes the brace to lengthen (Dicleli and Calik, (2008)). This phenomenon is known as the Growth effect. The reason for the Growth effect is degradation of the axial stiffness during the elastic unloading (Branch C Figure 3.2) and tension loading (Branch D Figure 3.2).

3.4 OpenSees Computational Platform

The computational platform used to model the behaviour of the structural systems in this project is OpenSees (Open System for Earthquake Engineering Simulation) (McKenna et al., (2000)). OpenSees is an open source object oriented framework for finite element analysis. Unlike many commercial finite element packages, OpenSees gives the user control over almost all of the analysis parameters, thus giving the user a greater understanding of their model. It is possible to use OpenSees with a graphic user interface (GUI) called OpenSeesNavigator (Schellenberg and Yang, (2006)), however in this project

a string-based scripting language called Tool Command Language (TCL) (ActiveState, (2010)) is used to call the different methods available in OpenSees.

OpenSees has become increasingly popular amongst the engineering research community as the tool to perform inelastic dynamic analysis. OpenSees provides control for the user of almost every modelling parameter used to perform nonlinear time history analysis. This user controllability is the fundamental reason why researchers use OpenSees rather than other off the shelf finite element software packages in which much of the analyses parameters choices are predefined. OpenSees provides an extensive library of materials/element and it is possible to create an element/material. In the context of this thesis, OpenSees provides the additional benefit of compatibility with the hybrid test procedure being implemented in this thesis, in that the hybrid test software was initially developed to be compatible with OpenSees. The remainder of this section provides a brief description of the computational aspects of OpenSees.

General

The model builder object in OpenSees creates the domain that, as in any finite element software, subdivides the structure into elements, nodes, forces and constraints. The structure of the domain object is shown in Figure 3.4. As shown in Figure 3.4, the model builder objects in OpenSees are; element, node, multiple point constraint, single point constraint, load pattern and time series.

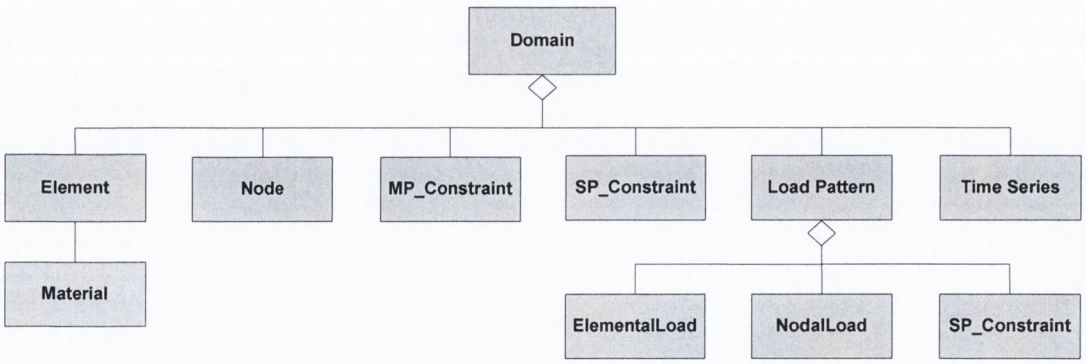

Figure 3.4: Domain object in OpenSees (Mazzoni et al., (2006))

The Domain object is linked to the Analysis and Recorder objects in OpeSees to combine together to perform finite element simulations. Some of the fundamental finite element components of inelastic time history analysis such as; damping, numerical elements, material models, recorders and analysis objects will be discussed herein.

Mass & Damping

The analysis of framed structures used in this thesis models the mass as discrete lumped masses at the nodes. Lumping the masses at the nodes is a structural idealisation and therefore is an approximation of the reality of structural mass distribution.

Rayleigh damping is used in OpenSees to apply damping to the physical system. Rayleigh damping is also referred to as stiffness and mass proportional damping and is widely used in computer programs. The formulation of Rayleigh damping is given below:

$$[\mathrm{C}] = \alpha[\mathrm{M}] + \beta[K] \tag{3.3}$$
$$\xi = \alpha/2\omega + \beta\omega/2$$

where;

C is the damping matrix of the framed structure

M is the mass matrix of the framed structure

K is the stiffness matrix of the framed structure

α & β are the Rayleigh damping parameters

ω is the fundamental period of the structure

ξ is the structural damping

It is apparent from Equation 3.3, if β is ignored, known as alpha damping, the α-parameter is calculated from a known value of damping, ξ ($\alpha = 2\xi\omega$). Alpha damping is good at damping out lower modes of vibration. If α is ignored, known as beta damping, the higher modes of vibration are damped. Alpha damping is the viscous component and beta damping is the stiffness component of damping.

It should be noted that only using alpha damping means that only the first mode of vibration is damped. The second mode of vibration would be damped if the alpha and beta proportional damping was used. The fundamental and second frequency of the structure is approximately 16 and 33 Hz, respectively, for the structure considered. As can be seen in Figure 3.5, the first two frequencies are far enough away from each other that only the fundamental frequency is of importance.

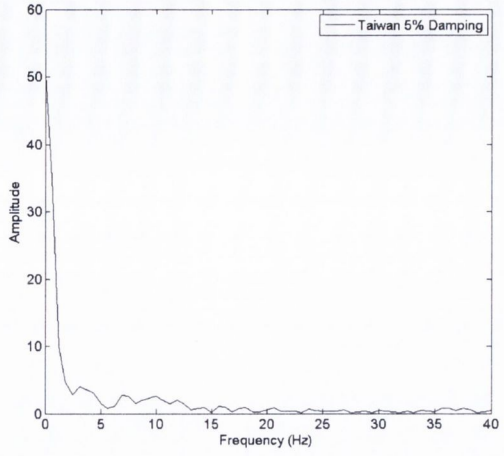

Figure 3.5: Frequency plot of first two frequencies for Taiwan excitation

Numerical Elements and Sections

A structure can be modelled using frame elements or continuum mechanics elements in OpenSees. For the analysis undertaken in this thesis, frame elements are used to model a structure as per the physical theory model representation discussed in Section 3.1. For further details on the capabilities of OpenSees, refer to the user manual (Mazzoni et al., (2006)) or the OpenSees website http://opensees.berkeley.edu/.

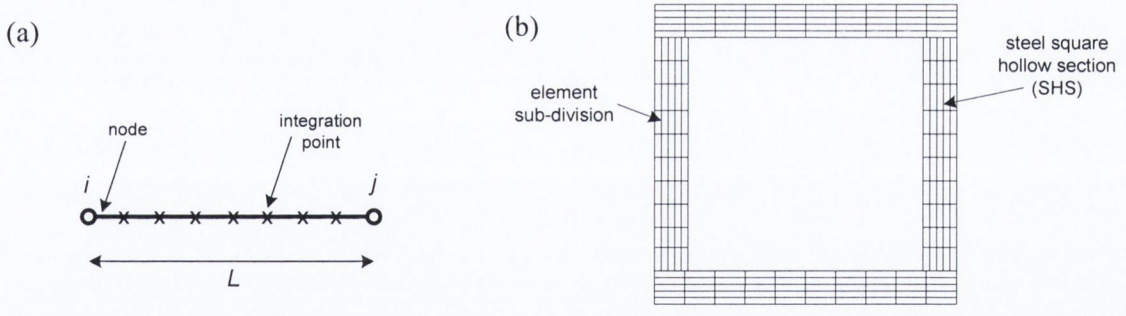

Figure 3.6: (a) OpenSees numerical element and (b) fiber cross-section discretisation of square hollow section

In order to define the properties of a frame element for analysis, a finite element cross-section is specified. The section command creates a stress-strain relationship at integration points along the beam-column element as shown in Figure 3.6(a). The integration points provide locations along an element where the stress and strains are calculated by the Gauss points in the cross section. In Figure 3.6(a), there are 7 No. integration points along the length, L of the element. These elements can be elastic or nonlinear and within the formulation the assumption of plane sections remaining plane is made. The fiber command

used in conjunction with the section command at the location of the integration points is used to discretise the section into smaller regions as shown in Figure 3.6(b). In Figure 3.6(b), the section is divided into 5 No. fiber element cross section subdivisions across the width of each thin walled section and 10 No. fiber element cross section subdivisions along the length of each thin walled section. The Gauss points within the subdivided 'patches' provide the approximation of stress and strain.

Material Models

The list of material models a user can define in OpenSees is extensive. The material models range from the most basic, such as elastic perfectly plastic models to complex reinforced concrete models. The range of material models are too extensive to list here. Refer to Mazzoni et al., (2006) or the OpenSees wiki website (http://opensees.berkeley.edu/wiki) for further details. In terms of this thesis, a comprehensive steel material model is required to adequately replicate the inelastic cyclic response of braced members. The Giuffré-Menegotto-Pinto Material model (Menegotto and Pinto, (1973)) was selected and is detailed in the next section (Section 3.5).

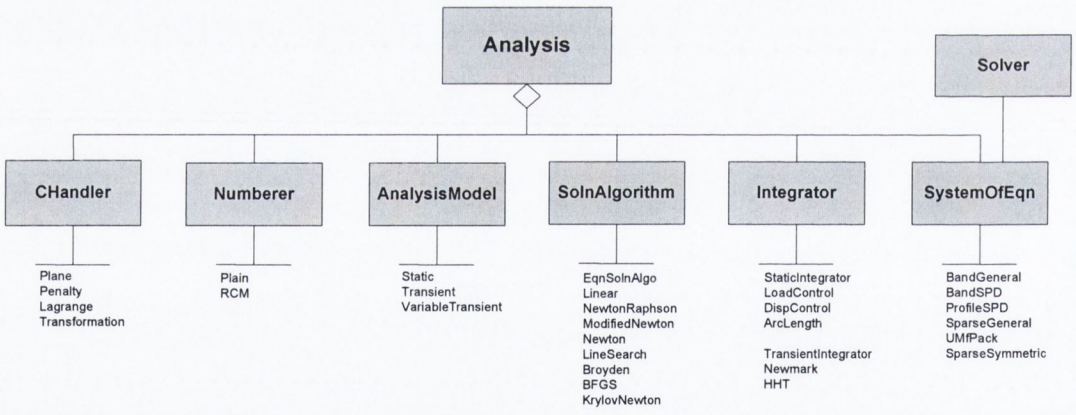

Figure 3.7: Analysis object in OpenSees (Mazzoni et al., (2006))

Analysis Objects

The analysis object moves the model from state time t to a state at time $t+\delta t$. Figure 3.7 illustrates the analysis objects available to the user in OpenSees. As shown in Figure 3.7 the analysis options give the user control over; the method of applying boundary constraints, numbering the degrees of freedom, analysis type, matrix solvers, static and transient numerical integrators and linear system of equation solvers. Most commercial

finite element packages do not offer the user a range of choice when performing an analysis.

Recorders

Recorders are then used to monitor user-defined parameters in the model during an analysis. Recorders include node, element, drift, envelope recorder and display. Nodal recorders record displacement, velocity, acceleration and reaction whereas element recorders record global/local force, stiffness, deformation and stress/strain.

3.5 OpenSees Modelling of Brace Members

This section details the numerical modelling of brace members using OpenSees. The modelling of brace members can be performed in OpenSees using physical theory models, as described in Section 3.3. Firstly, the optimal modelling parameters for the OpenSees physical theory modelling approach and the optimal choice of material model and analysis parameters will be discussed. The proposed numerical model will be validated against experimental results of two-dimensional cyclic tests of brace members and three-dimensional nonlinear dynamic tests of braced frames.

3.5.1 Optimal Model Parameters

Firstly, the modelling parameters that can affect the response of a computational representation of a braced member need to be explored. Using OpenSees, a physical theory model composed of nonlinear beam-column elements to capture inelastic deformations in conjunction with a reasonably sophisticated steel material model was used to represent the brace member response. Physical theory models replicate the cyclic/dynamic behaviour of brace members using two beam-column elements and applying an out-of-plane camber to the mid-span node incorporates the geometric imperfection of a brace member, thus enabling global buckling. The finite element fiber cross-section replicates the material properties of the brace member. The combination of the out-of-plane camber of the frame elements with the fiber cross-sectional representation results in an accurate physical theory model. The important computational factors dictating the numerical response of the brace member include; the number of beam-column elements representing the member, number

of integration points, number of fiber element subdivisions in the cross section and the out-of-plane straightness.

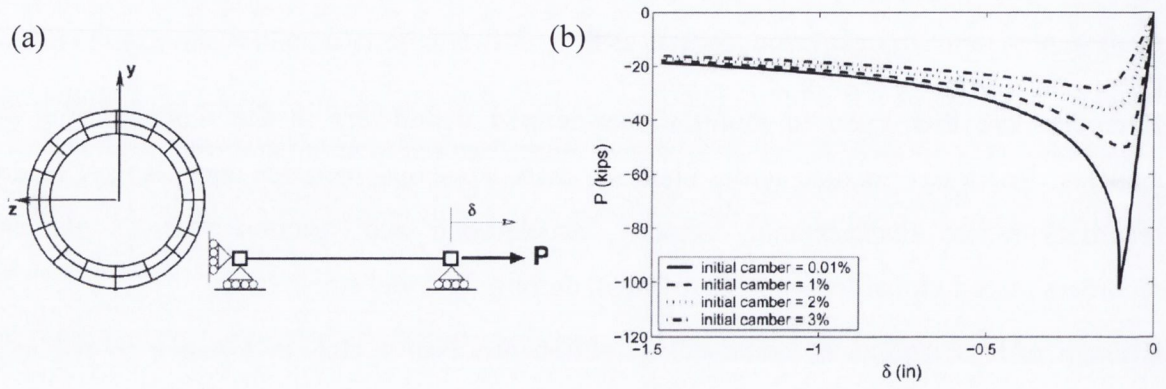

Figure 3.8: (a) Model geometry, loading and section discretisation for parameter study (b) effect of initial imperfection on buckling behaviour of strut (Uriz et al., (2008))

A numerical analysis parametric study was undertaken by Uriz et al., (2008) to verify the optimal numerical modelling parameters for replicating brace member behaviour during cyclic loading. Uriz et al., (2008) performed a series of analyses on the cyclic inelastic buckling of steel braces using OpenSees to investigate the effect of the initial camber, number of elements and level of discretisation of cross-section. The strut model geometry and initial section discretisation are shown in Figure 3.8(a) and an example of the results from the parameter study for level initial imperfect on the buckling behaviour are shown in Figure 3.8(b). It can be seen from Figure 3.7(b) that the level of initial imperfection has a significant effect on the buckling load. From the computational parametric study undertaken by Uriz et al., (2008), the most accurate and efficient OpenSees model for brace members have been identified as follows:

- Nonlinear beam column elements used to represent the brace members
- 2 No. elements to represent each brace member
- 0.1% out-of-plane initial cambre at the mid-length node to induce buckling
- 7 No. integration points along each element
- 5 No. fiber element cross section subdivisions across the width of each thin walled section
- 10 No. fiber element cross section subdivisions along each thin walled section
- A uniaxial steel material model based on the Giuffré-Menegotto-Pinto (Menegotto and Pinto, (1973)) model with isotropic strain hardening

In terms of seismic performance, energy dissipation, initial buckling and xxx are all important responses to model accurately. Say how initial buckling was found to be reasonable accurate. This is based on initial imperfection in brace member.

Steel Material Model

There are two predefined material models available in OpenSees, Steel01 & Steel02. The Steel01 material model constructs a uniaxial steel material with kinematic hardening and optional isotropic hardening described by a nonlinear evolution equation. The Steel02 model constructs a Giuffré-Menegotto-Pinto (Menegotto and Pinto, (1973)) uniaxial steel material model with isotropic strain hardening. The Giuffré-Menegotto-Pinto was used as the material model in analysis because the model allows greater control over the elastic to plastic branches of the material behaviour as compared to the Steel01 model. The Giuffré-Menegotto-Pinto (Menegotto and Pinto, (1973)) material model is defined in OpenSees as follows;

uniaxialMaterial Steel02 $matTag $Fy $E $b $R0 $cR1 $cR2 $a1 $a2 $a3 $a4

where; *matTag* is the unique object integer tag

Fy is the yield strength of the material (N/mm^2)

E is the Young's modulus (N/mm^2)

b is the strain hardening ratio (%)

R0, cR1 & cR2 are parameters controlling the response from the transition region from linear to nonlinear behaviour

a1 & a2 are isotropic hardening parameters governing the increase in compression yield envelope after plastic strain

a3 & a4 are isotropic hardening parameters governing the increase in tension yield envelope after plastic strain

Elastic-plastic Material Response Transition

Within the steel material model, parameters are available to control the transition from the elastic to plastic parts of the material response. The R-value defines how closely the transition from elastic to plastic fits a bilinear transition.

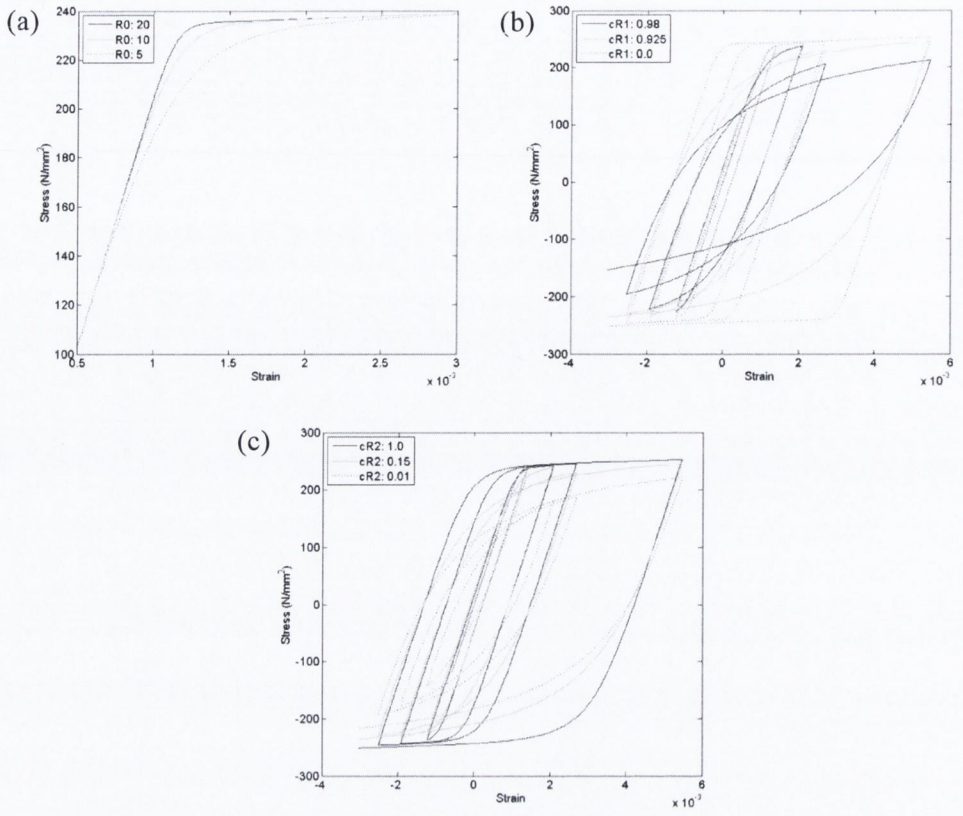

Figure 3.9: Graph of stress vs. strain for Steel02 material model with varying (a) R0 value, (b) cR1 value and (c) cR2 value

As can be seen in Figure 3.8, the R-value governs the transition from the elastic to plastic regions of the stress-strain profile. The larger the *R0* value, the closer the transition is to an idealised bilinear stress-strain transition as can be seen in Figure 3.9(a). Values of *R0* = 20, *cR1* = 0.925 and *cR2* = 0.15 were chosen and are the recommended values in the OpenSees command manual (Mazzoni et al., (2006)). The *cR1* parameter affects the change in stiffness in the material. A value of *cR1* = 0.925 results in a gradual change in stiffness whereas a value of *cR1* = 0.0 results in an abrupt change in stiffness as can be seen in Figure 3.9(b). The *cR2* parameter controls the deterioration in subsequent load cycles. A value of *cR2* = 1.0 results in an idealised uniaxial material response where the inelastic branch of the response has the same outline path for each subsequent loading phase as shown in Figure 3.9(c). A value of cR2 = 0.15 results in a more gradual deterioration in subsequent load cycles as shown in Figure 3.9(c). For a comprehensive review of the modelling parameters for the Giuffré-Menegotto-Pinto Material model (Menegotto and Pinto, (1973)), refer to OpenSees wiki website (http://opensees.berkeley.edu/wiki).

Isotropic Hardening Parameters

Within the steel material model, parameters are available to define the isotropic hardening properties of the material, namely *a1*, *a2*, *a3* & *a4*.

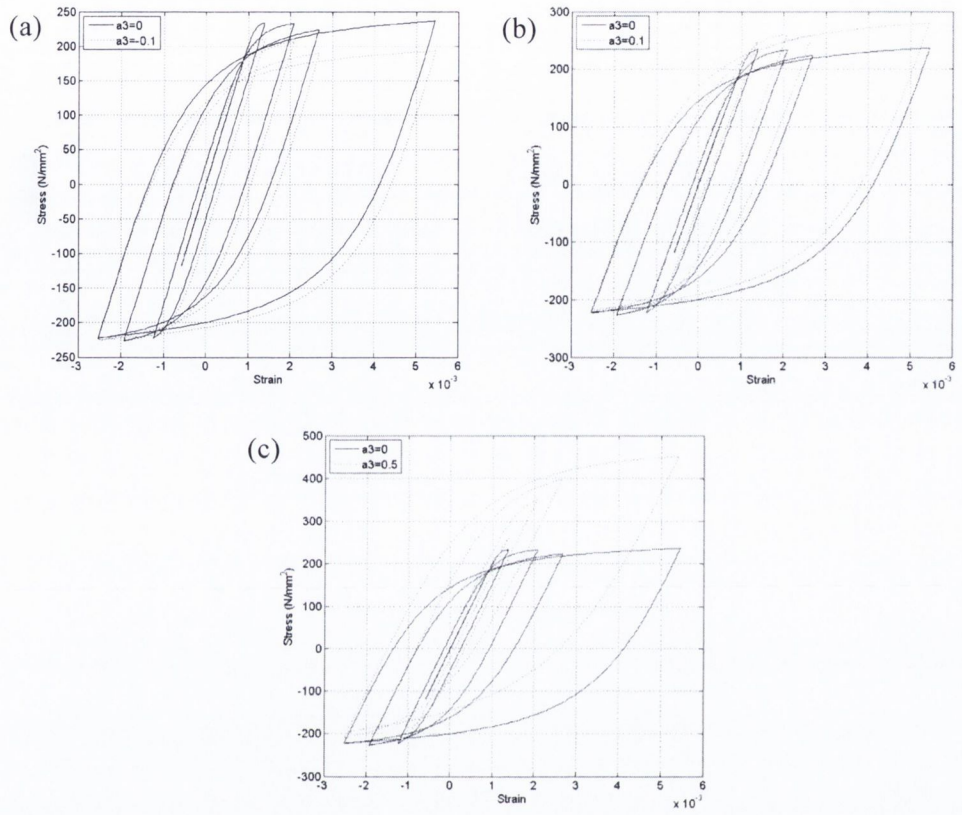

Figure 3.10: Graph of stress vs. strain for Steel02 material model for *a3* parameter variation (a) *a3* = 0 & -0.1, (b) *a3* = 0 & 0.1 & (c) *a3* = 0 & 0.5 (Model has *a1* = 0, *a2* = 1 & *a4* = 1)

A negative *a1* value will result in compressive softening and a positive *a1* value will result in compressive hardening. A large value (e.g. 5) of *a2* will result in the tension and compression branches being similar with slight compressive hardening. A value of 1.0 for *a2* will result in the tension and compression branches being the same. Smaller values of *a2* will result in hardening of the compressive branch of the response. If *a3* is zero, the compressive and tensile branches are the same, as can be seen in Figure 3.10. A negative value of *a3* results in softening of the tension branches (*a3* = -0.1 in Figure 3.10(a)) and a positive value of *a3* results in hardening of the tension branches (*a3* = 0.1 in Figure 3.10(b) & (*a3* = 0.5 in Figure 3.10(c)). A value of *a4* = 1.0 will result in the tension and compression branches being the same. A value of *a4* less than 1 will result in tension hardening. A larger value (e.g. 5) of *a4* results in the tension branches being similar with slight tension hardening. Values of *a1* = 0.0, *a2* = 1.0, *a3* = 0.0 and *a4* = 1.0, were selected for the material model replicating the default values in OpenSees. The selected parameters

gave slight tension and compressive hardening. For a comprehensive review of the modelling parameters for the Giuffré-Menegotto-Pinto material model (Menegotto and Pinto, (1973)), refer to OpenSees wiki website (http://opensees.berkeley.edu/wiki).

Summary

The material model allows definition of the yield strength, Young's modulus and strain hardening ratio. However, more advanced control over the transition from elastic to plastic branches and isotropic hardening properties of the material are available.

3.5.2 Modelling the Cyclic Response of Brace Members

The computational model of the brace member referred to in the previous section was validated against cyclical tests undertaken by Goggins, (2004). The experimental set-up is shown in Figure 3.11(a) and the numerical model of the test set-up is shown in Figure 3.11(b). The model is a two-dimensional model with the stiffener and SHS defined by fiber sections with nonlinear beam column elements. The stiffener plate and SHS brace member are combined in the fiber section between Nodes 1 & 2 and 3 & 4 as shown in Figure 3.11(b). A uniaxial steel material model as defined in the previous section is used. For further details on the experimental setup, cyclic loading, material properties and test results refer to Goggins, (2004), Goggins, (2005) or Goggins, (2006). The two test specimens that were computationally modelled are 1100mm (including end restraint conditions) long 20x20x2.0mm SHS and 40x40x2.5mm SHS specimens respectively. The results of the experiment and numerical model can be seen in Figure 3.12 and Figure 3.13. Load cycles as follows were undertaken on each specimen during the cyclic testing schedule; one cycle of $\pm\delta_y/4$, one cycle of $\pm2\delta_y/4$, one cycle of $\pm3\delta_y/4$, one cycle of $\pm\delta_y$, three cycles of $\pm2\delta_y$ followed by three cycles $\pm(2+2n)\delta_y$, where n = 1, 2, 3....etc.

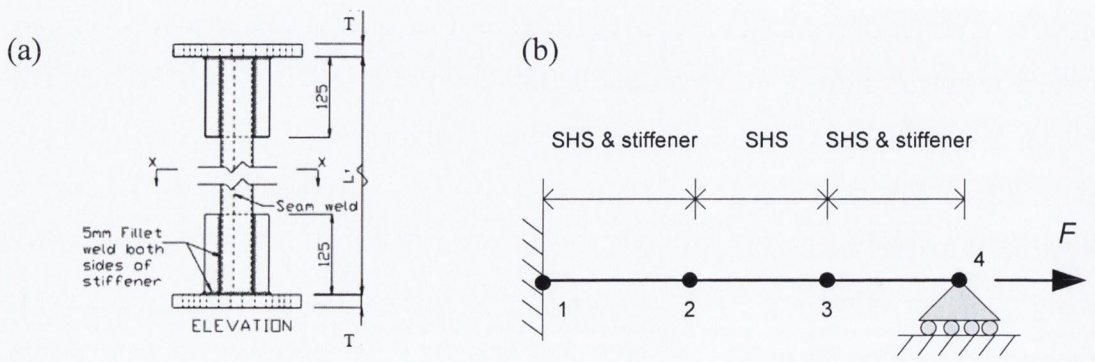

Figure 3.11: (a) Test specimen and (b) numerical model of cyclic experiments (Goggins, (2004))

Figure 3.12 shows the experimental and numerical results for the cyclic test on the 20x20x2mm SHS specimen. From Figure 3.12, it can be seen that the agreement between the experimental results and computational model is good. The evolution of the tensile strength and hysteretic behaviour of the response is well modelled. There is an overestimation of the initial buckling load of 17.7% by the numerical model but in later cycles the buckling capacity is well predicted. The post-buckling phase is softer in the experimental data, resulting in the residual compressive capacity being overestimated in the numerical model. The tensile loading phase and peak tensile capacity is modelled accurately with a 1.6% difference in the peak tensile load. The Baushinger effect (Bauschinger, (1886)) is modelled well, particularly in the buckling phases of the response, as can be seen in Figure 3.12. A negative strain hardening ratio of -1.0% was used in each of the analyses in order to replicate the reduced tensile capacity of the member in subsequent loading phases. With the large number of cycles, it is difficult to see the Growth Effect in Figure 3.12 however; the Growth Effect was modelled accurately. No local buckling was observed during the experimental response of this specimen.

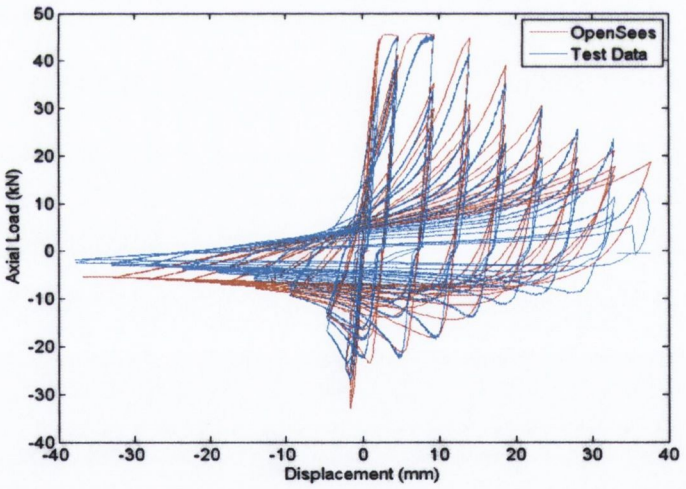

Figure 3.12: Graph of load vs. displacement for 20x20x2mm SHS specimen (test results courtesy of (Goggins, 2004))

Figure 3.13 shows the test and numerical results for the cyclic loading of the 40x40x2.5mm SHS specimen. From Figure 3.13, it can be seen that the response of the test specimen is modelled with reasonable accuracy and shows acceptable agreement. In the test, the member failed by combined overall lateral buckling and local buckling at the plastic hinge locations. There is an overestimation of the peak tensile capacity in the numerical model of 8.9%. There is an overestimation of 3.5% of the initial buckling load in the numerical model. As for the 20x20x2mm SHS, the post-buckling phase is softer in the

experimental data resulting in the residual compressive capacity being overestimated in the numerical model. The point of fracture in this test specimen was not observed in the model, thus leading to an overestimation of the evolution of the tensile strength. The numerical model does not have the capability to model fracture.

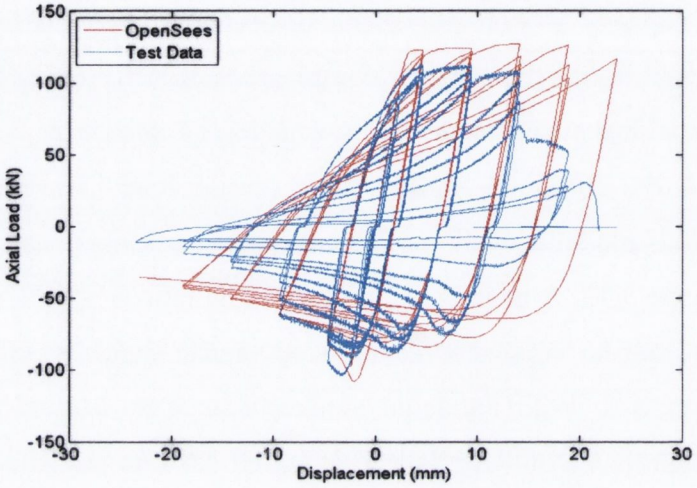

Figure 3.13: Graph of load vs. displacement for 40x40x2.5mm SHS specimen (test results courtesy of (Goggins, 2004))

The results of the analyses in Figure 3.12 and Figure 3.13 indicate the proposed model is capable of predicting the peak resistance with a reasonable level of accuracy. The energy dissipation is modelled successfully in the 20x20x2mm SHS and less well in the 40x40x2.5mm SHS specimen. The stiffness of both test specimens is predicted with reasonable accuracy by the OpenSees model. The model is more accurate for the more slender specimen (Figure 3.12) as compared to the less slender specimen (Figure 3.13) because local buckling occurs in the less slender specimen. The numerical representation of the physical theory using non linear beam-column elements does not take into account local buckling effects. In order to capture local buckling, a solid mechanics approach using continuous finite element model (see Zienkiewicz and Taylor, (2005)) or a unique constitutive model to represent the particular example would be required. The material model used and finite element representation implemented in this model does not have the capability to model fracture in an element. In this context the most accurate physical theory model using non linear beam-column elements for both the 20x20x2mm SHS and 40x40x2.5mm SHS specimen was chosen.

3.5.3 Modelling the 3D Nonlinear Dynamic Response of Braced Frames

In the previous section, the validation of the brace member model was undertaken using static experimental data. The proposed analysis of plan irregular structures requires three-dimensional models to allow for torsional effects and nonlinear time history analysis. The next step is to validate the dynamic analysis of three-dimensional braced steel structures using inelastic time history analysis. Important model parameters such as the boundary conditions, modelling of damping, support excitation and element connectivity need to be verified. The study presented in this section provides a means to create a reliable numerical modelling template in OpenSees for the three-dimensional inelastic time history analysis of braced frame structures subjected to ground motion excitation.

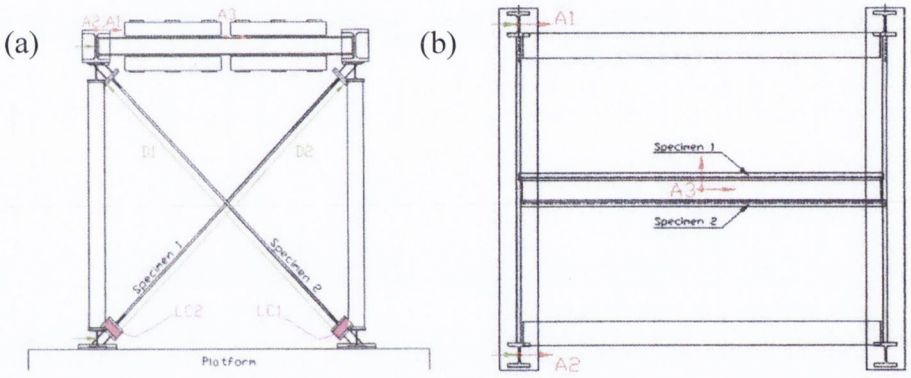

Figure 3.14: Concentrically braced frame test set-up (a) elevation and (b) plan view (masses not shown) (Goggins, (2004))

The concentrically braced test frame in Figure 3.14 was tested by Goggins, (2004) in the Laboratory for Earthquake Engineering of the National Technical University of Athens. The test frame comprises of 4 No. HE 160Mx180 columns, 2 No. 280Mx310 primary beams, 3 No. HE 180Ax171 secondary beams and varying sizes of bracing members. In the series of tests, the bracing members used were as follows; 50x25x2.5mm RHS, 20x20x2.0mm SHS and 40x40x2.5mm SHS. During some of the tests, the bracing members were filled with a concrete mix with a self compacting admixture. OpenSees was used to perform a dynamic time history analysis of the response of this concentrically braced test frame to the ground acceleration record imposed during the test; namely the El Centro record scaled to a peak ground acceleration of 0.81g. The numerical model is a three-dimensional representation of the test structure shown in Figure 3.14.

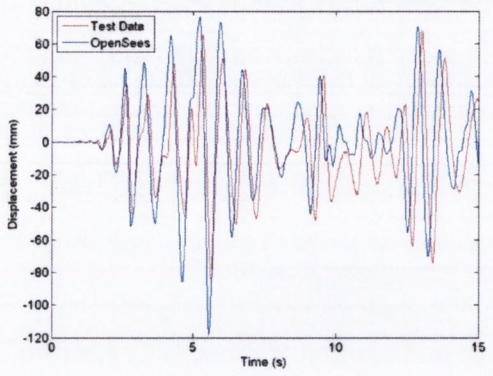

Figure 3.15: Graph of displacement vs. time for 3D inelastic El Centro time history analysis for Node A3

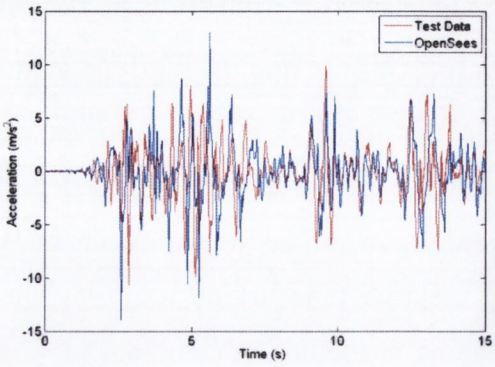

Figure 3.16: Graph of acceleration vs. time for 3D inelastic El Centro time history analysis for Node A3

Figure 3.15 indicates the results of the displacement of Node A3 (as per Figure 3.14) for both the numerical model and test data. The braced specimens in this test were 50x25x2.5mm RHS. From Figure 3.15 it can be seen that the displacement response history of the test structure is quite accurately modelled. The period of the numerical model response matches well with the test data, however the peak displacements are overestimated, particularly around 5 to 6 seconds. The peak difference in the maximum displacement between the numerical model and test results is 29.1%. Similarly in Figure 3.16, the modelled acceleration response is reasonably well matched to the test data; the peak difference in the maximum acceleration between the numerical model and test results being 23.8%. One possible source of inaccuracy in the predictive model is the level of damping used. The peak responses are not predicted with a high degree of accuracy indicating the damping was under-estimated. Overall, the numerical model provided reasonable accuracy in the prediction of the response of the test structure.

From the OpenSees dynamic numerical model of the test structure, the following points to note about the analysis are:

- Geometric detail of the test structure was of great importance in accurately modelling the brace response. For example, explicitly modelling the stub sections that were to represent a pinned connection at the column top and base resulted in a much more accurate model response. Assuming the columns were spanned from the shake table to the beam connection and applying pinned restraints at the nodes did not capture the response of the test specimen accurately.

- In a three dimensional model, out-of-plane camber in the bracing members is required in both axes to account for buckling behaviour in both of the horizontal axes.
- The equal degree of freedom command in OpenSees was used to connect the brace members to the support connections. The equal degree of freedom command applies the same degrees of freedom of a master node to a slave node.
- The zero length element that can be used to connect two nodes at the same location i.e. for the brace end connections, resulted in convergence issues because the stiffness of the zero length element had to be large in order to constrain the connection as required. The zero length element constrains two nodes at the same location by a zero length element with high stiffness.
- The rigid diaphragm command in OpenSees could not be used to model the floor diaphragm. The rigid diaphragm command enforces the same degrees of freedom of all the selected nodes as per a master node. When the rigid diaphragm command was used, the nodes between beams are constrained resulting in very large axial forces in the beam members. The large axial forces resulted in a lack of convergence of the numerical integration due to incompatible element forces. The individual nodes at each floor were assigned adequate nodal fixity to replicate the floor diaphragm response.
- The uniform excitation command was used for the transient analysis. Using the uniform excitation command, the displacements between the support nodes and other non-support nodes is absolute i.e. the support nodes do not displace and are fixed by their constraints.
- The multiple support excitation command can also be used for transient analysis. When using the multiple support excitation, the displacements between the support nodes and other non-support nodes is absolute i.e. the support nodes displace as if they were connected to a moving support. It was observed that for any duplicate nodes connected by a zero length element or equal degree of freedom command a displacement was assigned to the support node, but the duplicate node remained in its approximate location. This resulted in the restraint between the two duplicate nodes not being enforced correctly and resulted in convergence issues during the analysis.

3.6 Plan Irregular Concentrically Braced Frame Numerical Representation

As discussed above, the results of cyclical tests on axial loaded members and the dynamic shake table tests of a concentrically braced frame have been modelled reasonably accurately by the respective OpenSees numerical models. The next step is to progress the numerical model representation of a concentrically braced steel structure to that of a plan irregular concentrically braced steel framed structure. The model will be used for analysis of the effect of variation of key structural parameters within realistic ranges. The following sections will detail the numerical model and specific parameters taken into consideration.

In order to accurately represent torsional seismic response in a plan irregular structure, the computational model needs to be a three-dimensional model. The torsional stiffness of the individual structural elements needs to be included and the three-dimensional representation of the structure is necessary in order to reflect the different demands experienced on each side of the structure. In this section, the important physical properties of a structure that influence its irregular response will be detailed and the numerical representations of these properties will be discussed.

3.6.1 Mass Distribution

As described in Chapter One, asymmetric or plan irregular structures are those in which seismic response is not only translational but also torsional due to stiffness and/or mass eccentricity in the structure. In-plan static eccentricity, e_s is defined as the distance between the Centre of Mass (CM) and Centre of Resistance (CR) of the structure at each floor, as can be seen in Figure 3.17. Structures are therefore either; Torsionally Balanced (TB) with no static eccentricity, e_s or Torsionally Unbalanced (TU) with static eccentricity, e_s. In this research, one of the most important factor affecting the torsional response of the structure is an irregular mass distribution in-plan. Due to the uneven distribution of mass, the structure has a stiffer side (SS) and a more flexible side (FS) as can be seen in Figure 3.17. The SS has the mass distributed towards it and the FS has the mass distributed away from it. The distribution of the mass towards the left hand side of the structure as shown in Figure 3.17 places a greater demand on the structure. Increasing the lateral resistance of this side of the structure results in this side of the structure being stiffer, hence the term stiff side (SS). As discussed in the Chapter Two, researchers refer to the SS of the structure because the structure under investigation has a greater lateral stiffness on one side of the structure as compared to the other. Other researchers investigated the response of in-plan

mass eccentricity only. Typically in these structures, the structure is symmetrically stiff and researchers refer to the SS of the structure as the side of the structure with the mass distributed away from it. The CR has not been altered, but the CM has moved away from the CR.

The concentrically braced steel structure used to investigate plan irregularity is a three-storey, two-by-one bay framed structure as shown in Figure 3.17. The columns are 203 UC 46 columns on every storey and are simply supported in the x-direction. Concentric bracing provides the lateral support at each end frame in the x-direction. The beams are 305x165x40mm UB sections throughout. The structure has a 2.5m high first (ground) storey, a 2.2m high second storey and a 2.2m high third storey, providing typical architectural storey heights. The structure is simplified to only have two bays such that the torsional response can be understood with greater clarity.

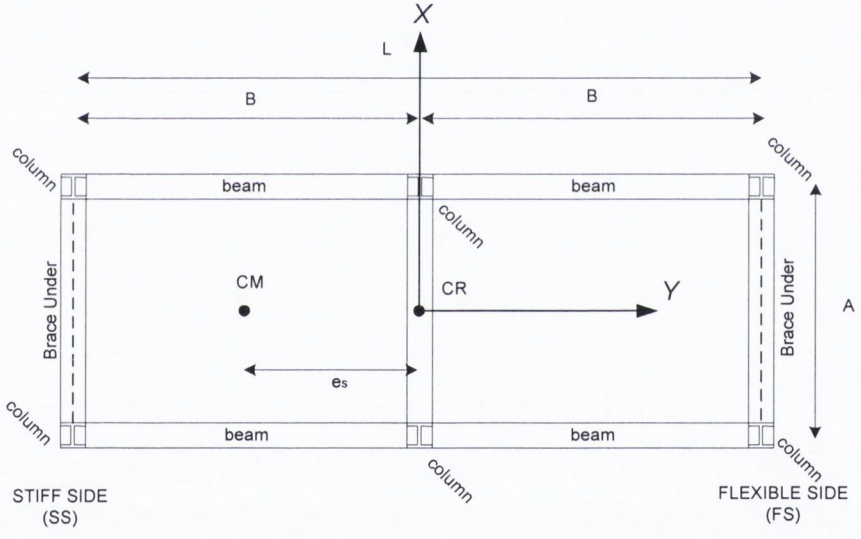

Figure 3.17: Plan view of structure with plan irregularity (lumped masses not shown)

The range of e_s values being considered in this project are shown in Table 3.1. The proposed maximum static eccentricity, e_s is $0.15L$, as any greater level of mass distribution would be very unlikely in a real-world scenario. For the idealised structure shown in Figure 3.17, an e_s of $0.15L$ arises for a mass of 0.533 times the total floor mass at the SS columns and a mass of 0.233 times the total floor mass at the Centre and FS columns of the structure, as indicated in Table 3.1. A value of e_s of $0.15L$ results in a significant shift in mass from the CR and is three times that taken into consideration for the accidental torsion provision in Eurocode 8 (CEN, (2004)).

Table 3.1: Mass eccentricity factors for varying levels of static eccentricity

Static Eccentricity	Mass Factor SS	Mass Factor Centre	Mass Factor FS
0.0L	0.25	0.5	0.25
0.025L	0.367	0.317	0.317
0.05L	0.4	0.3	0.3
0.075L	0.433	0.283	0.283
0.1L	0.467	0.267	0.267
0.125L	0.5	0.25	0.25
0.15L	0.533	0.233	0.233

3.6.2 Lateral Torsional Frequency

One of the most important factors in the torsional response of a plan irregular structure is the lateral torsional frequency ratio, Ω_θ. For $\Omega_\theta < 1$, the structure is considered to be torsionally flexible, and if $\Omega_\theta > 1$, the structure is considered to be torsionally stiff. The calculation of Ω_θ is shown in Equation 3.4;

$$\Omega_\theta = \frac{\omega_\theta}{\omega_y} = \frac{r_k}{r_m} \tag{3.4}$$

where; ω_θ is the uncoupled torsional frequency

ω_y is the uncoupled translational frequency in the y-direction

r_k is the stiffness radius of gyration about the centre of resistance

r_m is the mass radius of gyration about the centre of mass

In order to calculate the lateral torsional frequency ratio, Ω_θ, the stiffness radius of gyration about the centre of resistance, r_k is calculated as follows;

$$r_k = \left(\frac{K_\theta}{K_y}\right)^{0.5} \tag{3.5}$$

where K_y is the total lateral stiffness of the elements parallel to the y-axis and K_θ is the total torsional stiffness about the centre of resistance, defined in the following Equation 3.6;

$$K_\theta = \sum_{i=1}^{n} k_{yi}(x_i - e)^2 + \sum_{i=1}^{n} k_{x_i} y_i^2 \tag{3.6}$$

where; n is the number of elements

k_{yi} is the lateral stiffness of each element in the y-direction

x_i is the distance from the element being considered to the centre of resistance in the x-direction

e is the eccentricity of the element from the centre of mass

y_i is the distance from the element being considered to the centre of resistance in the y-direction

The mass radius of gyration about the centre of mass is calculated as follows;

$$r_m = \sum_{i=1}^{n} \left(\frac{I_{xi}}{m_i}\right)^{0.5} \tag{3.7}$$

where; I_{xi} is the major axis second moment of area about the centre of mass and m is the nodal masses for each element. Equation 3.7 is the same for the mass radius of gyration in the y-direction, however I_{yi} replaces I_{xi} as follows;

$$r_m = \sum_{i=1}^{n} \left(\frac{I_{yi}}{m_i}\right)^{0.5} \tag{3.8}$$

The Ω_θ values that will be studied in this project are 0.75, 0.875, 1.0, 1.125 and 1.25. These levels provide a good distribution of torsionally stiff and torsionally flexible structures while remaining in the realistic range. The value of Ω_θ is varied in the idealised structure by changing the mass applied to the structure resulting in a change in period. The lower bound of Ω_θ of 0.75 required a load factor of almost 2.0 times the gravity load to be applied to the structure. The lower bound of 0.75 therefore dictated the upper bound of 1.25 as an equal amount of Ω_θ for a torsionally stiff structure needed to be checked.

3.6.3 Plan Aspect Ratio

The plan aspect ratio is the ratio between the length (L) and width (A) of the building in plan (see Figure 3.17). It may be expected that a long and slender structure with a high plan aspect ratio experiences a different torsional response during an earthquake event compared to a structure with a lower aspect ratio. The plan aspect ratio will be varied with the following values; 1.0, 1.5, 2.0, 2.5 and 3.0. These values represent plausible building plan dimensions.

3.6.4 Non-dimensional Slenderness

As mentioned in Section 3.2, one of the most important factors influencing the behaviour of bracing members is the non-dimensional slenderness. The buckling of straight compression members is addressed in Eurocode 3 (CEN, (2005)) (or for a good explanation see also Trahair et al., (2008)). It can be shown that the load at which an ideal straight member under axial compression laterally buckles is given by;

$$N_{cr} = \frac{\pi^2 EI}{L^2} \tag{3.9}$$

where; N_{cr} is the elastic buckling load

EI is the flexural rigidity

L is the effective length of the compression member

The elastic buckling load can be written as follows;

$$N_{cr} = \sigma_{cr} A = \frac{\pi^2 EA}{(L/i)^2} \tag{3.10}$$

where; i is the radius of gyration ($i = \sqrt{(I/A)}$)

A is the cross sectional area of the member

σ_{cr} is the elastic buckling stress

From Equation 3.10 it can be seen that the buckling load varies in inverse proportion to the square of the slenderness ratio (L/i). The non-dimensional slenderness ratio can be written as follows;

$$\bar{\lambda} = \sqrt{\frac{N_y}{N_{cr}}} = \sqrt{\frac{f_y}{\sigma_{cr}}} = \frac{L}{i}\sqrt{\frac{f_y}{\pi^2 E}} \tag{3.11}$$

where; f_y is the yield stress of the material and N_y is the squash load ($N_y = Af_y$)

As mentioned previously, for X-bracing the non-dimensional slenderness is limited by the Eurocode 8 (CEN, (2004)) as follows;

$$1.3 < \bar{\lambda} \leq 2.0 \tag{3.12}$$

The lower limit of 1.3 prevents the bracing members becoming too stocky, which could result in overloading of the columns in the pre-buckling stage. The upper limit of 2.0 prevents the bracing members from being too slender, which could result in a poor hysteretic response. As mentioned by Elghazouli, (2003), relatively slender braces may also result in undesirable shock loading on the structure. In many cases, these slenderness values are the controlling parameters of the seismic design. Typically, the tension capacity required for the brace member is less than that provided by a member that is within the limiting value of 2.0 for non-dimensional slenderness. Previous studies such as Goggins, (2004) and Tremblay et al., (2003) as have been undertaken to partly investigate the appropriateness of these non-dimensional slenderness limits.

3.6.5 Time Histories

In order to gain a full accurate understanding of the dynamic seismic response of a structure, a range of earthquake ground motion records need to be applied. In a nonlinear time history analysis, Eurocode 8 (CEN, (2004)) suggests that average value of an action effect from 7 different ground motions should be used for design (See Section 4.3.3.4.3(3) in Eurocode 8 (CEN, (2004))).

Table 3.2 lists the proposed earthquake time histories to be used to investigate the response of the proposed idealised structure. All the earthquake records are taken from the PEER Database (PEER, (2000)). These ground motion records have been chosen to represent different levels of peak ground A/V ratio, which can be used to characterise earthquake records. A/V ratios can be classed as a high ratio (A/V > 1.2), a medium ratio (0.8 > A/V <

1.2) and a low ratio (A/V < 0.8). As can be seen in Table 3.2; the Taiwan, El Centro and Calitri records have Low A/V ratios; the Kobe and Friuli records have Medium A/V ratios and the Spitak and NWCalif records have High A/V ratios.

Table 3.2: Record details and A/V ratio

Record No.	Earthquake Record	Magnitude (Richter Scale)	Distance To Epicentre (km)	Max. Acc. (g)	Max. Velocity (cm/s)	A/V Ratio	A/V Ratio Category
1	Taiwan (1986)	7.3	39	0.153	28.3	0.53	Low
2	El Centro (1940)	7.0	8.3	0.215	30.2	0.69	Low
3	Calitri (1980)	6.5	19	0.177	23.6	0.74	Low
4	Kobe (1995)	6.9	0.6	0.343	38.3	0.89	Medium
5	Friuli (1976)	6.5	37.7	0.315	30.8	1.00	Medium
6	Spitak (1988)	6.8	30	0.119	8.8	1.33	High
7	NWCalif (1951)	5.8	56	0.11	6.1	1.77	High

The intensity of an earthquake is characterised by its peak ground acceleration, velocity and displacement values. However, it is quite common to characterise an earthquake record using the peak ground acceleration only and to use this to calculate the design elastic response spectrum (Eurocode 8 (CEN, (2004))). As noted by Tso et al., (1992) and Broderick, (1994), seismological studies have indicated that peak ground acceleration is associated with high frequency waves and peak velocity is often associated with longer frequency waves. As a result, A/V ratios are higher for ground motion records closer to the earthquake source than ground motion records far from the earthquake source. The ground motion experienced near the earthquake source tends to be more impulsive and of higher frequency and those further from the earthquake source are more periodic and longer duration (Tso et al., (1992)).

The effective duration of a seismic event, which is greater for low A/V records, is also significant in that it determines the energy dissipation requirements imposed on a structure and the degree to which low-cycle fatigue and the deterioration of its resistance will affect the response. Additionally, it is important to include records possessing a range of spectral widths, (i.e. the range of periods over which significant amplification is experienced, being inversely proportional to the A/V ratio) as this determines whether a structure experiences similar response amplification in the linear and nonlinear ranges (Broderick, (1994)).

Table 3.3: Parameter summary table

Parameter	*Range Considered - Minimum Value*	*Range Considered - Maximum Value*
$\overline{\lambda}$	1.3	2.0
e_s	$0.0L$	$0.15L$
Ω_θ	0.75	1.25
PA ratio	1.0	3.0
A/V	0.53	1.77

Table 3.3 summarises the proposed parameter variation under investigation in this research. The maximum and minimum values of each parameter being varied are shown. The proposed hybrid test and subsequent numerical model parameter study (described in following chapters) that will investigate the plan irregular response of a concentrically braced steel structure will be subjected to parameter variations within the limits set out in Table 3.3.

3.7 Chapter Overview

This chapter has described the numerical modelling approach to a plan irregular concentrically braced steel structure. The numerical modelling approach has been built up from parametric studies of the available method in OpenSees along with static and dynamic validation tests. Finally, the structural parameters that are most important to the torsional response of asymmetric irregular structures are described and the applicability to the proposed numerical model approach is detailed. The next chapter details the hybrid test method, together with the modelling procedure described in this chapter, which examines the seismic response of a plan irregular steel concentrically braced structure.

CHAPTER FOUR - Hybrid Test Method and Validation Test

4.1 Introduction

This chapter consists of a literature review describing the development of the hybrid test (HT) method followed by the description of a hybrid test method validation experiment and its results. Firstly, the development of hybrid testing from the fundamental concept of the pseudodynamic (PsD) test method to its current state of development in the form of a real-time hybrid test (RTHT) will be described. In order to see the benefits of hybrid testing, there will be a brief overview of other dynamic test methods available including the relative merits of each test method. Finally, the current implementation of the hybrid test method used in this thesis will be detailed and the experimental results from a validation experiment of a substructured hybrid test will be discussed.

4.2 Methods of Dynamic Testing

As stated by Carrion and Spencer, (2007), when the response of a system is difficult to model numerically e.g. due to nonlinearity or rate dependent behaviour, the most reliable way to verify its response is by testing. Testing is required by some design codes to verify a non-code conforming system. For example in Eurocode 8 (CEN, (2004)), unless there is existing test data, the details of an energy dissipating connection need to be investigated experimentally to verify stable cyclic deformation and energy dissipation to conform to local ductility criteria (see Section 5.11.2.1.3, (CEN, (2004))). Even as computational power is increasing, there is still a fundamental need for testing, either for validation of complex numerical models or to provide accurate input data for a numerical model e.g. material properties.

The main types of structural laboratory testing under dynamic loads are reviewed by Blakeborough et al., (2001). The types of testing are (i) quasi-static testing (ii) shake table testing (iii) pseudo dynamic (PsD) testing and more recently, (iv) real-time hybrid testing (RTHT). Quasi-static testing, such as the static cyclic test method, is typically used to determine structural performance under reversed cyclic loading. The loading rate during the test is very slow, hence the term quasi-static. The main types of dynamic testing above

will be discussed in further detail in the following Sections. Another specific test method worth discussing is the Effective Force Test (EFT) method which is similar in concept to the PsD test method.

4.2.1 Shake Table Testing

A shake table is a rigid table with the structure to be tested mounted on the table. Actuators excite the table to the prescribed dynamic input required. Shake table tests model true dynamic behaviour, however, the shake table test does have some drawbacks. The capacity of the actuators required to perform the test means that the size of the structure that can be tested on the shake table is limited. This drawback typically results in the scaling of the structural systems to be tested. However, it is often difficult to relate the results gained from a scaled model to the full sized model. In particular, size effects do not transfer well for local effects such as crack propagation and local buckling (Carrion and Spencer, (2007)).

The shake table test is truly dynamic; however, there is no control during the running of the test because once the test is set in motion the rate of testing cannot be interfered with unless the test is terminated. Examples of tests exist where the collapse of the structure damaged the shake table itself (e.g. the collapse of an unreinforced masonry building at the LNEC Shake Table Facility, Lisbon, 2005). Other problems include the input excitation not being the same as the resulting table excitation, which can become an issue if the same test as a comparison is to be performed on different shake tables or using the PsD method for example. The cost of shake table tests and the issue of scaling of structural models in order to fit the payload capacity of the shake table are typical constraints.

4.2.2 Pseudo Dynamic Test Method

The concept of the pseudodynamic (PsD) test was first proposed by Hakuno et al., (1969) in which an actuator excitation of a single-degree-of-freedom (SDOF) system was combined with the solution of the equation of motion on an analogue computer. The PsD test method was first formally implemented by Takanashi et al., (1975). The fundamentals of the PsD test can be seen in this test in that the structural stiffness of the test member inputted into the computer model was obtained from the physical experiment of the

structure. The predicted deformations computed by a piecewise linear method were then sent back to the actuator to give the next timestep target displacement for the actuator to apply onto the test system. This procedure was repeated until the end of the test.

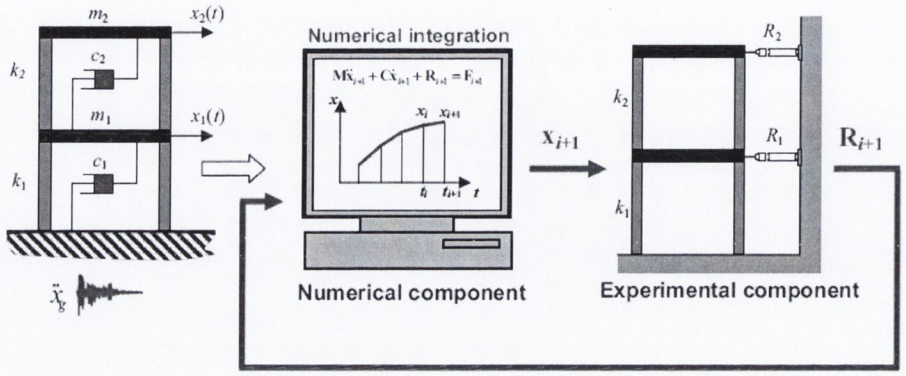

Figure 4.1: Schematic of the hybrid test method (Carrion and Spencer, (2007))

In the PsD test method, it is conventionally assumed that the structure can be represented by lumped masses. At the location of the lumped masses, actuators are provided to apply the dynamic loading to the structure in the form of target displacements. Structural properties such as the inertia and damping are numerically modelled. The equations of motion of the structure are solved by numerical integration. The equation of motion in Equation 4.1 is solved over a series of time steps Δt, i.e. at the *(i+1)th* step of:

$$M\ddot{x}_{i+1} + C\dot{x}_{i+1} + R_{i+1} = F_{i+1} \tag{4.1}$$

in which $\ddot{x}_{i+1}$ is the nodal acceleration vector, $\dot{x}_{i+1}$ is the nodal velocity vector, R_{i+1} is the restoring force vector and F_{i+1} is the external excitation force applied to the system. As per Figure 4.1, if the excitation is an earthquake ground acceleration of $\ddot{x}_g$, then $F_{i+1} = -M\ddot{x}_g$. Figure 4.1 indicates how the displacement x_{i+1} is calculated by the numerical component and sent to the experimental test structure. The displacement command for the current time step for the idealised structure is applied to the structure by the actuators. The measured restoring force, R_{i+1} is then fed back to the numerical model where the displacement for the next target displacement command is calculated. Effectively, the PsD test method is a computational dynamic analysis in which the stiffness term is measured physically (Bonnet, (2006)).

The term pseudo-dynamic implies that the rate of testing is not actually fully dynamic. The slow loading rate of the test structure is required so as not to induce damping or inertia response, because these have already been accounted for numerically (Mahin et al., (1989)). In early investigations into the test method, issues of stability and accuracy of the test method were heavily researched (Shing and Mahin, (1985), Shing and Mahin, (1987) & Takanashi and Nakashima, (1987)). The assumed structural idealisation and numerical representation of the damping along with numerical integration errors raised concerns about the accuracy and stability of the PsD test method. These issues will be dealt with in more detail in Sections 4.2 and 4.3.

The principal benefits of the PsD test method compared to the shake table method are that there are no scaling issues with the PsD test, the cost of a PsD test is lower and the failure mode can be more easily inspected in a PsD test as it is performed at an extended timescale. The disadvantage of the PSD test is that it is not a fully dynamic test and effects such as strain-rate effects cannot be examined (Williams and Blakeborough, (2001)).

4.2.3 Continuous Pseudo Dynamic Test Method

As discussed by Magonette, (2001), the PsD method has the fundamental drawback that the test is undertaken using an expanded timescale and therefore the response of the material being tested must be rate independent. The reason for having an extended timescale is to allow for the time required for numerical integration of the equations of motion and the implementation of the resulting command displacements by the test actuators (Zhang et al., (2005)). The time integration scheme employed therefore needs to be efficient, resulting in explicit integration procedures being typically used in early research; the numerical integration can take place typically in 5-10ms. An implicit method requires iteration in each time-step which results in longer computation time.

Early implementations of PsD testing required a pause phase to allow for the computation of the numerical integration step to be completed, as can be seen in Figure 4.2. During the pause stage of the integration step, there is a certain amount of load relaxation that also leads to inaccuracies. The experiment should preferably be performed in a non-discrete manner to allow smooth loading in order to fully capture the response of the structure. The fundamental idea being that the numerical simulation and the loading of the actuator take

place in unison. The continuous PsD test method was first proposed by Takahashi and Ohi, (1984).

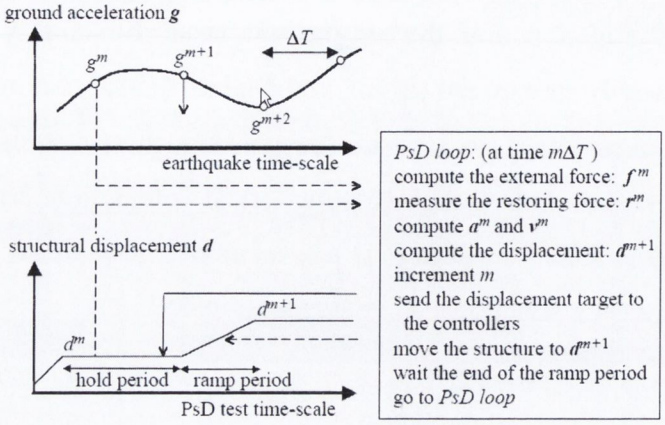

Figure 4.2: Conventional pseudo dynamic method (Magonette, (2001))

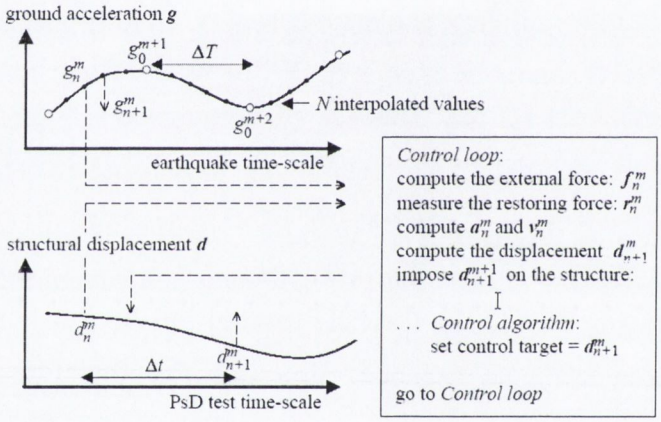

Figure 4.3: Continuous pseudo dynamic method (Magonette, (2001))

The improvement of the continuous pseudo dynamic method was made using a servo-controller to control the movement of the actuator. Figure 4.3 shows how the continuous PsD method differs from the conventional pseudo dynamic method. The control algorithm used by the servo-controller allowed the actuator to follow the target displacement accurately within small time steps preventing the need for the hold period (as shown in Figure 4.2).

4.2.4 Substructured Pseudo Dynamic Test Method

The important feature of substructuring in PsD testing was first introduced by Dermitzakis and Mahin, (1985) and implemented by others; Nakashima et al., (1990), Vannan, (1991), Buchet and Pegon, (1994), Pegon and Pinto, (2000) & Molina et al., (2002). The concept

of substructuring allows the critical part of the structure (typically with a highly nonlinear response) to be physically tested and the rest of the structure to be simultaneously numerically modelled. The force and displacement from the actuator(s) are fed back to the numerical model, where they are used to solve the next time-step command. For example, Figure 4.4 shows a complete knee-braced frame structure and its knee element substructure (Blakeborough et al., (2001)). The critical element, which is the knee element, is physically tested and the remaining structure is modelled numerically.

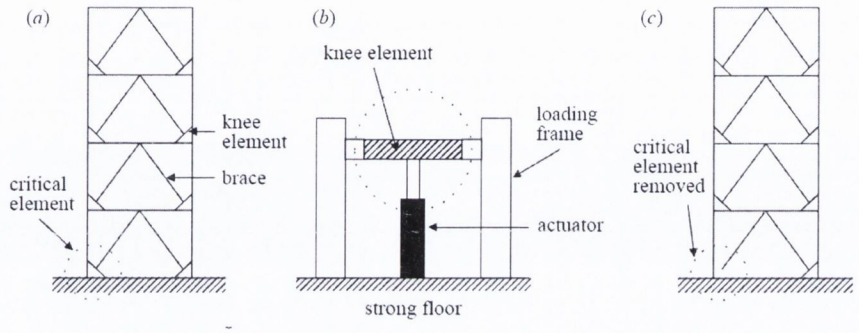

Figure 4.4: Concept of substructuring applied to knee-braced structure. (a) complete structure; (b) physical test of critical element; and (c) numerical model of the rest of the structure (Blakeborough et al., (2001))

The concept of substructuring prevents testing of large, heavy and costly structures. The part of the structure that is difficult to numerically model or whose mechanical response has a critical effect on the dynamic response of the structure is physically tested and the remainder of the structure is simultaneously numerically modelled. The concept of substructuring allows full scale specimens to be tested, thus avoiding scaling issues.

4.2.5 Real-time Hybrid Test Method

The next progression of the continuous PsD method was the real-time PsD method, which for the remainder of this thesis will be referred to as the Real-time Hybrid Test (RTHT) method. Nakashima et al., (1992) present the first system capable of performing a real-time PsD test, termed the fast PsD test. The challenge to overcome when a PsD test is run at a timescale close to or at real-time is that the command for the next time step from the numerical model needs to be computed very quickly. Nakashima et al., (1992) completed a real-time PsD test on a viscous damper. A digital servo-mechanism was used to achieve sufficient actuation accuracy in both displacement and velocity and two memory buffers were used to prevent delay in the actuator command signal. One of the buffers is the main

buffer to receive the regular signal and the other can receive an additional signal for the following step (Nakashima et al., (1992)), thus allowing a continuous command signal, as required. Another method to allow uninterrupted command signals was developed by Nakashima and Masaoka, (1999). An extrapolation-interpolation method is employed in which previous command displacements are used to extrapolate the command displacement to its next value one time step ahead of the current time. This and other techniques enabling RTHT will be discussed in detail in the following sections.

In a RTHT, the damping and inertia response of the test structure are measured in the force feedback and not defined computationally. This is the fundamental difference between RTHT and PsD tests. For structures whose response has velocity dependent characteristics, the RTHT method is especially useful. A RTHT that only tests the critical part of the structure and computationally models the remainder of the structure is known as a substructured-RTHT (S-RTHT). Examples of RTHT that have been undertaken to date include; Darby et al., (1999), Horiuchi et al., (1999), Nakashima and Masaoka, (1999), Blakeborough et al., (2001) & Shing et al., (2004). As noted by Bonnet, (2006) these test arrangements were typically bespoke to the particular laboratory in which they were undertaken.

Some researchers have utilised shake tables to act as the substructure for a RTHT. For example, Reinhorn et al., (2004) used a shake table as the interface to the support structure (i.e. base excitation) and actuators at the interface to the computational substructure. Other researchers who have undertaken hybrid tests using shake tables include Horiuchi et al., (2000), Igarashai et al., (2004), Neild et al., (2005) & Shao et al., (2011). Users of shake tables have seen this development as a positive one because it can address the scaling issues associated with shake table testing.

Another more recent development in hybrid testing is the linking of geographically separate physical testing and numerical modelling facilities via the internet. The internet effectively replaces the laboratory cables that connect the physical substructure to the numerical computation. Another name for this type of testing is online testing. As noted by Elkhoraibi and Mosalam, (2007), other examples of online testing are given by Pinto et al., (2002), Mosqueda, (2003b), Pan et al., (2006) & Takahashi and Fenves, (2006). Tests have been carried out online by The George E. Brown, Jr., Network for Earthquake Engineering Simulation (NEES) in the United States. NEES is a geographically distributed network of research facilities and fast hybrid tests (FHT) can be run at the University of Colorado

either remotely over the internet or else locally from the University of Colorado's facilities. Other online hybrid tests have utilised an event driven strategy to deal with the random execution times that can occur due to internet communication (Stojadinovic et al., (2006)). The NEES system has been the basis for the UK-NEES system linking research laboratories in Bristol, Oxford and Cambridge (Saleem et al., (2008)). The fundamental benefits of online testing are the sharing of test facilities and expertise and the resulting greater collaboration.

4.2.6 Effective Force Test Method

Other experimental procedures have been developed for undertaking real-time testing, such as the Effective Force Test (EFT) method (Dimig et al., (1999), Shield et al., (2001), Zhao et al., (2006), Wu et al., (2007)). The EFT was developed in order to circumvent some of the issues associated with PsD testing. It has been described in a number of papers ((Mahin and Shing (1985), Mahin et al. (1989) & Thewalt and Mahin (1987)) that a PsD test with explicit time-varying forces imposed at each lumped mass to conduct real-time tests could be implemented without the need for computing and imposing required displacements (Dimig et al., (1999)). As stated by Nakashima et al., (1992), the technique is conceptually and physically different from real-time PsD testing because of the lack of a need for displacement control and required integration algorithms. In the EFT method, the force applied to the test structure is a product of the lumped masses and their accelerations, and are therefore independent of structural properties such as stiffness and damping. As noted by Bonnet, (2006), civil engineering structures are often stiff structures subjected to small displacements and high forces to which force control is more suited.

4.3 Time Integration Techniques

4.3.1 Introduction

The equation of motion is a second order differential equation that can be solved using integration in the time domain. Using integration, the loading history is considered to be a series of short-duration impulses, and the solution of the free vibration response of each of these intervals becomes a separate contribution to the overall response of the system (Clough and Penzien, (1993)). Numerical methods replace the need for direct integration.

Numerical integration in the time domain is a step-by-step procedure for solving the equation of motion. The loading and response history are divided into time-steps (Clough and Penzien, (1993)), typically in earthquake response analysis, the lengths of these time intervals or time-steps are those of the time-steps at which an earthquake event has been recorded. The response of the system is calculated based on the initial conditions of the system (displacement and velocity). There are two main types of numerical integration techniques; explicit and implicit. The following sections briefly detail the fundamentals of explicit and implicit numerical integration, describing some of the important numerical integration techniques used in hybrid testing. (For a detailed description of dynamic systems refer to Clough and Penzien, (1993) and for a detailed description of numerical methods refer to (Chapra and Canale, (2006).

4.3.2 Explicit Numerical Integration Techniques

One of the major areas of research into improving the PsD and RTHT methods is the efficiency of the algorithm used for numerical integration. Explicit methods are often used because they are computationally efficient and due to their ease of implementation. One of the drawbacks to explicit methods is that they are conditionally stable, resulting in a limitation on the maximum time step that can be used. The maximum time step is limited by the natural frequency of the system. The limitation is defined as; $\omega_n \Delta t_{max} = 2$, where ω_n is the highest natural frequency of the system and Δt_{max} is the maximum time step. As stated by Shing and Mahin, (1985), the limitation becomes important for structures with higher modes of vibration. The Newmark Explicit and Central Difference Methods (CDM) are two commonly used explicit methods and are briefly described below.

4.3.2.1 Central Difference Method

Many researchers have used the CDM as the integration scheme for PsD and RTHT (Takanashi and Nakashima, (1987), Nakashima et al., (1992), Shing et al., (1996), Nakashima and Masaoka, (1999), Horiuchi et al., (1999), Darby et al., (1999), Algaard, (2001), Zhao et al., (2003), Wu et al., (2005)). The CDM has probably been the most widely used time integration scheme for hybrid testing. The mathematical description of the CDM is given in Equations 4.3, 4.4 & 4.5 below. Firstly, the equation of motion;

$$M\ddot{x}_{i+1} + C\dot{x}_{i+1} + R_{i+1} = F_{i+1} \tag{4.2}$$

Using the CDM the velocity and acceleration are approximated as;

$$\dot{x}_i = \frac{x_{i+1} - x_{i-1}}{2\Delta t},\ \ddot{x}_i = \frac{x_{i+1} - 2x_i + x_{i-1}}{\Delta t^2} \tag{4.3}$$

and it follows that;

$$x_{i+1} = x_i + \Delta t\dot{x}_i + \tfrac{1}{2}\Delta t^2\ddot{x}_i \tag{4.4}$$

$$\dot{x}_{i+1} = \dot{x}_i + \tfrac{1}{2}\Delta t(\ddot{x}_i + \ddot{x}_{i+1}) \tag{4.5}$$

where, x_i is the displacement at the ith time step

$\dot{x}_i$ is the velocity at the ith time step

$\ddot{x}_i$ is the acceleration at the ith time step

Δt is the integration time step

The numerical integration scheme is termed explicit because the new response value for a step is calculated based on the previous step. The method progresses directly from one step to another. From Equation 4.4 it can be seen that the new displacement response is calculated based on the displacement, velocity and acceleration from the previous step.

4.3.2.2 Explicit Newmark Method

The Newmark method (Newmark, (1959)) and subsequent family of modified Newmark methods have proven popular in hybrid testing. The explicit Newmark method has been implemented in the hybrid test in this research project. The mathematical description of Newmark's method in the general form is given as;

$$x_{i+1} = x_i + \Delta t\dot{x}_i + \Delta t^2\left[\left(\frac{1}{2} - \beta\right)\ddot{x}_i + \beta\ddot{x}_{i+1}\right] \tag{4.6}$$

$$\dot{x}_{i+1} = \dot{x}_i + \Delta t[(1-\gamma)\ddot{x}_i + \gamma\ddot{x}_{i+1}] \tag{4.7}$$

where β and γ are the integration parameters. It can be seen that in Equation 4.6 if $\beta \neq 0$ the method requires a measure of the acceleration at the end of the time step, making the method implicit. Letting $\beta = 0$ and $\gamma = \frac{1}{2}$ then the Newmark Method is the same as the Central Difference Method. Letting $\beta = 0$, the prediction of displacement reduces to;

$$x_{i+1} = x_i + \Delta t \dot{x}_i + \left(\frac{\Delta t^2}{2}\right)\ddot{x}_i \tag{4.8}$$

Shing and Mahin, (1985) have shown that error propagation properties of the Newmark method are better than those of the CDM. The explicit Newmark method does not provide numerical dissipation, however Thewalt and Mahin, (1987) have shown that the Newmark system is more reliable and superior to the CDM.

4.3.3 Implicit Numerical Integration Techniques

A numerical integration scheme is termed implicit when the new response value for a step is calculated based on one or more of the current response values as well as previous step values. In general, explicit algorithms have been chosen for PsD testing over implicit integration algorithms because implicit algorithms require iterative correction which could induce undesirable unloading. Another drawback for some implicit integration algorithms is that they require the tangent stiffness of the system being tested, which can be difficult to evaluate during a test (Shing and Manivannan, (1990)). The main drawback to an explicit integration scheme is that it is conditionally stable. On the other hand, implicit integration methods are unconditionally stable (Zhang et al., (2005)). For civil engineering structures, there is generally a large difference between the lowest and highest natural frequencies, and even if only a small number of the lowest natural frequencies are dominant in the dynamic response of the structure, an unconditionally stable scheme may be required so that the structure itself does not govern the time step to be used.

Thewalt and Mahin, (1987) were the first to successfully implement an implicit time integration scheme for PsD testing. The scheme was based on the α-method developed by Hilber et al., (1977) and has proven to be more reliable and superior to explicit schemes (Bursi and Shing, (1996)).

4.3.3.1 Implicit Newmark Method

The implicit Newmark method employs two constants, γ and β, whose values are set such that the scheme is unconditionally stable. The mathematical description of the implicit Newmark method in its general form is given as;

$$x_{i+1} = x_i + \Delta t \dot{x}_i + \Delta t^2 \left[\left(\frac{1}{2} - \beta \right) \ddot{x}_i + \beta \ddot{x}_{i+1} \right] \tag{4.9}$$

$$\dot{x}_{i+1} = \dot{x}_i + \Delta t \left[(1-\gamma) \ddot{x}_i + \gamma \ddot{x}_{i+1} \right] \tag{4.10}$$

The method is most often applied as the Constant Average Acceleration Method (CAAM) with γ = ½ and β = ¼. The CAAM does not produce any numerical damping, unlike the implicit Newmark method which provides numerical damping for $\gamma > 0.5$. Numerical damping is beneficial for improving computational stability; however numerical damping also suppresses the accuracy of the solution.

4.3.3.2 Operator Splitter Method

The two main research directions in hybrid testing in which the implicit schemes have deviated are: (1) using an iterative implicit method; cycling at each time step to match equilibrium (Shing and Manivannan, (1990) & Shing et al., (1991)) or (2) by using the non-iterative, linearly implicit or non-linear explicit operator splitter method (Nakashima et al., (1990) & Combescure and Pegon, (1997)).

A procedure of splitting a numerical integration method into implicit-explicit components was proposed by Hughes et al., (1979). The Operator-Splitter (OS) method for use in PsD testing was first proposed by Nakashima et al., (1990). The OS method prevented the need for an iterative procedure. The method is implicit for the linear part of the response and explicit for the nonlinear part of the response, preventing the need for iteration.

In a similar fashion to the Newmark method, the OS method has had α-damping applied to it, known as the α-OS method (Combescure and Pegon, (1997)). The scheme was developed in order to combine the speed of computation from explicit methods with numerical dissipation. The α-OS method is used in particular in one of the world's leading

research centres on PsD testing at ELSA (European Laboratory for Structural Assessment) in Italy. The mathematical formulation of this scheme is defined as follows;

The *predictor* step

$$\tilde{x}_{n+1} = x_n + \Delta t \dot{x}_n + \frac{\Delta t^2}{2}(1-2\beta)\ddot{x}_n \tag{4.11}$$

$$\tilde{\dot{x}}_{n+1} = \dot{x}_n + \Delta t(1-\gamma)\ddot{x}_n \tag{4.12}$$

where;

$\tilde{x}_{n+1}$ is the predictor displacement at the $i+1$th time step

$\tilde{\dot{x}}_{n+1}$ is the predictor velocity at the ith time step

The *corrector* step

$$x_{n+1} = \tilde{x}_{n+1} + \Delta t^2 \beta \ddot{x}_{n+1} \tag{4.13}$$

$$\dot{x}_{n+1} = \tilde{\dot{x}}_{n+1} + \Delta t \gamma \ddot{x}_{n+1} \tag{4.14}$$

The α-shifted equation of motion is defined as:

$$M\ddot{x}_{n+1} + (1+\alpha)C\dot{x}_{n+1} - \alpha C\dot{x}_n + (1+\alpha)R_{n+1} - \alpha R_n = (1+\alpha)F_{n+1} - \alpha F_n \tag{4.15}$$

This procedure is known as the α-method. The parameters α and β are chosen from Hilber et al., (1977). The Hilber-Hughes-Taylor (Hilber et al., (1977)) (HHT) numerical integration scheme was developed in order to improve the numerical dissipation to damp out spurious participation of higher modes. The direct integration of the equations of motion is presented using a group of unconditionally stable one-step methods. The HHT scheme showed improved numerical dissipation of higher modes and is unconditionally stable when compared with the Newmark method. Refer to Hilber et al., (1977), Thewalt and Mahin, (1987) or Broderick, (1994) for further details. The parameters α and β are chosen as;

$$\beta = (1-\alpha)^2 / 4 \tag{4.16}$$

$$\gamma = (1-2\alpha)/2 \tag{4.17}$$

for $-1/3 \le \alpha \le 0$, numerical damping of the method is possible. From Equation 4.15 it can be seen that if the relationship between R and x becomes non-linear, then an iterative solution procedure is required. The predictor step is implicit and the corrector step is explicit. The OS method is based on the following approximation of the restoring force;

$$R_{n+1}(x_{n+1}) \approx K^I x_{n+1} + \left(\widetilde{R}_{n+1}(\widetilde{x}_{n+1}) - K^I \widetilde{x}_{n+1}\right) \tag{4.18}$$

where; K^I is a stiffness matrix with stiffness higher than or equal to the tangent stiffness (the elastic stiffness is used if the tangent stiffness is unavailable)

$\widetilde{R}_{n+1}$ is the predictor restoring force at (n+1) time step is measured when the predictor displacement is applied

$\widetilde{x}_{n+1}$ is the predictor displacement at (n+1) time step

Other authors such as Zhang et al., (2005) & Wu et al., (2006) have made developments in OS methods. Zhang et al., (2005) developed an explicit predictor-corrector time integration scheme using polynomial extrapolation to predict the system's response. Wu et al., (2006) noted that the OS method only provides an explicit target displacement but not an explicit target velocity. For a RTHT, when velocity dependent restoring force is required, the method is effectively implicit. Therefore, Wu et al., (2006) proposed a predictor-corrector method based on the OS method that is explicit when applied in a RTHT.

The Explicit Newmark method was utilised in the hybrid testing because it was available in the OpenFresco software and was found to be stable and efficient.

4.3.3.3 Integral Form

The majority of research into numerical integration schemes for the PsD and RTHT is concerned with the fundamental second order differential equation of motion. An approach where the integrated first order form of the equation of motion is used as opposed to the

original second order form has also been implemented (Chang, (1998) & Algaard et al., (2001)). Chang, (1998) first proposed the scheme, in which an incremental form of the explicit Newmark method is integrated as follows;

$$M\dot{x}_{i+1} + Cx_{i+1} + \int R_{i+1}dt = \int F_{i+1}dt \tag{4.19}$$

$$x_{n+1} = \frac{1}{2}\Delta t(\dot{x}_n + \dot{x}_{n+1}) \tag{4.20}$$

$$\int x_{n+1}dt = \Delta t x_n + \frac{1}{2}\Delta t^2 \dot{x}_n \tag{4.21}$$

From Equations 4.19, 4.20 & 4.21, it can be seen that the equation of motion is now solved in terms of change in velocity rather than acceleration (Algaard et al., (2001)).

When using direct integration for PsD testing, cumulative errors may become large if the rapid variation of resistance of the test system is not captured accurately due to non-linear behaviour (Chang et al., (1998)). However, using the first order solution method, errors due to the assumption that the structural properties remain constant throughout a time step (linearisation error) are eliminated by the integration of the restoring force, while the sharp characteristics of the seismic loading are smoothed out by the integration of the applied force (Chang et al., (1998)). The result is an algorithm which is capable of picking up the effects of rapidly varying excitation forces and stiffness changes, while at the same time displaying improved error propagation characteristics over the standard Newmark explicit representation. These characteristics of the integral form make the method appropriate for PsD testing.

4.4 Errors in Hybrid Testing

There are three main sources of error in hybrid testing namely; the structural idealisations the approximations made in the numerical integration of the equation of motion and the experimental set-up.

Structural Idealisation

In general, the physical constraints of available testing facilities restrict the structure that can be tested. Typically these restrictions result in a SDOF or low MDOF system being the limit of the capabilities of the laboratory. In addition to this, the structural idealisation of lumped masses is essential for the implementation of PsD and RTHT methods. Displacement commands are applied at the location of the lumped masses by hydraulic actuators in order to represent the seismic response of the structure. Structures are not discrete entities, so the question arises; how well does the discrete model of the system represent the continuous system? Special consideration is therefore needed when performing a hybrid test to ensure the test specimen and test set-up can accurately replicate the proposed structure under consideration.

Numerical Integration

From Section 4.2, describing the variety of numerical integration schemes available for either PsD testing or RTHT, it is clear that careful selection of the numerical integration scheme is required to minimise possible errors. Numerical integration, by its nature can only provide an approximate solution. While the possible error in each time step may be small, however when these errors are accumulated the overall error may be significant. Structural damping plays an important role in the response of a structure and the exact characteristics of damping may be difficult to model because in reality different types of damping may exist e.g. viscous, Coloumb, etc (Shing and Mahin, (1984)). In a non-linear analysis, energy can be introduced into the model by assuming the force-displacement relationship at each step is constant (linearisation) (Shing and Mahin (1984)).

Experimental Errors

Errors in experimental set-up can be broadly classified as measurement or control errors. In particular, hybrid tests are very sensitive to actuator control errors. Experimental errors are probably of most concern because the nature of the error can result in failure of the test procedure. The experimental errors can then be further sub-divided into either systematic or random errors (Shing and Mahin, (1983)). Examples of experimental errors are; movement in the support connection, flexibility in the reaction frame, feedback noise to the actuator (particularly at small command signals), inaccurate measurement and inaccurate control of the actuator(s). The random and systematic errors will be briefly discussed in the following sections.

4.4.1 Random Errors

The random errors are typically as a result of noise in the measurement system. Noise can be problematic as it can result in a change to the electrical signal being sent during a test. Round-off errors associated with the A/D conversion of the signal can result in random errors (Shing and Mahin, (1983)). The round-off errors are due to floating-point computation. Shing and Mahin, (1987) note that the round-off errors are small in comparison to the systematic errors. Random errors are irregular in nature and have been shown to produce negligible effects (Mosqueda et al., (2005)) when compared to systematic errors.

4.4.2 Systematic Errors

Shing and Mahin, (1987) investigated the experimental feedback errors accumulated in the step-by-step integration procedure in the PsD test. The main experimental errors are restoring force feedback measurement errors and subsequent errors associated with the step-by-step integration procedure.

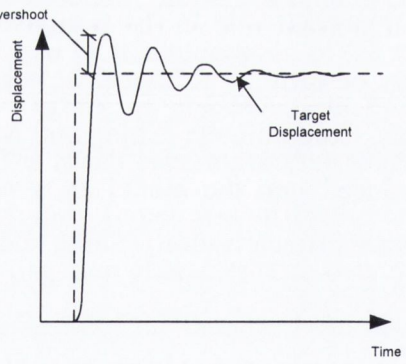

Figure 4.5: Undesired oscillation in displacement controller

Systematic errors introduced by the actuator are of most concern in hybrid testing because they provide undesireable energy effects on the dynamic response of the system (Shing and Manivannan, (1990)). The errors tend to have a dominant frequency that is identical to the numerical response frequency of the structure (Shing and Manivannan, (1990)). Due to the cumulative nature of numerical integration, incrementally small errors introduced to the system will result in resonance-like effects in the error growth. For higher modes, this resonance-like growth of cumulative error occurs faster than for lower modes. In MODF

systems, systematic errors will cause spurious higher mode response due to relatively small convergence errors. In order to prevent this, it is possible to find the dominant frequency by trial tests and then adjusting the servo-control system to improve the actuator performance. Numerical integration with numerical damping can also help to reduce spurious higher mode effects.

Figure 4.5 indicates undesired oscillation resulting in overshoot of the target actuator response. The most common method for control of servo-hydraulic actuators is PID (Proportional Integral Derivative) control. A PID controller is a feedback controller that uses a feedback loop to measure the error in a process and minimise it by adjusting the process control inputs. Proper control tuning of the actuator can help to mitigate this error, however other methods to compensate this have also been implemented. As stated by Bonelli and Bursi, (2004), the undershooting errors introduced by the control system cannot be damped out by the numerical damping provided by the α parameter. The I-Modification error compensation technique proposed by Nakashima and Kato (1987) to compensate for overshoot, was used by Bursi and Shing, (1996) in the α-OS method to correct the displacement and control errors. The restoring force is corrected by the I-Modification algorithm to the known displacement error and predictor stiffness (Bonnet, (2006)). Mosqueda et al., (2005) suggests the use of adaptive Minimal Control Synthesis (MCS) algorithms as opposed to using PID control as this allows an adaptive gain to be changed as the test specimen degrades during an experiment.

4.5 Actuator Delay and Compensation Techniques

Actuator delay represents a major source of inaccuracy in the fast PsD test and RTHT methods (Nakashima et al., (1992)). Figure 4.6 indicates the delay between the input and output signal for a hydraulic actuator. The use of measured forces in the numerical integration scheme assumes that the displacements corresponding to those forces are accurate. The response delay of the actuator causes an increase in the total energy to the system, similar to that caused by equivalent negative damping. If the negative damping is greater than the structural damping, then the response will not converge. Therefore, minimising actuator delay is vitally important in obtaining an accurate solution. Horiuchi et al., (1999) present an actuator delay compensation method for the RTHT method. The

delay is reduced by predicting the displacements one time step ahead, whose length is equal to the time delay of the actuators.

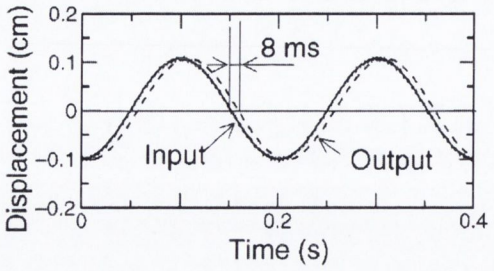

Figure 4.6: Input and output signal for hydraulic actuator (Horiuchi et al., (1999))

As shown in Figure 4.7, the compensation method predicts the actuator displacement after the response delay, δt. The calculated displacement value, x is the value calculated by the numerical integration scheme. The predicted displacement value, x' is that predicted by the compensation method. Inputting the predicted displacement value, x' as the control signal to the actuator (i.e. in place of the calculated value), causes the resulting displacement, x'' to be the same as the calculated displacement, eliminating the actuator delay. Horiuchi et al., (1999) developed a second-order polynomial fit that could forward predict the command displacement by one whole time-step. The compensation method has been successfully implemented in a number of PsD and RT substructured tests; Darby et al., (1999), Blakeborough et al., (2001) & Darby et al., (2002).

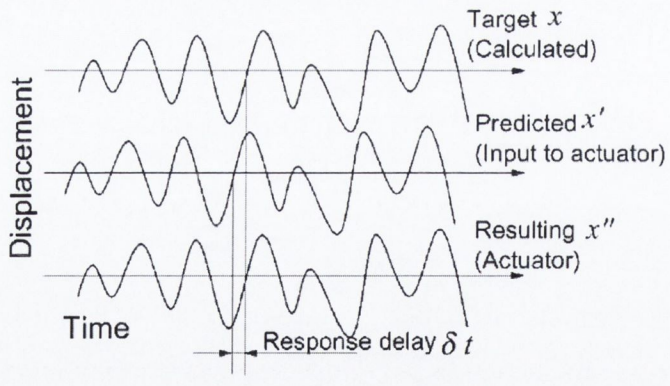

Figure 4.7: Schematic of the prediction method for actuator delay compensation (Horiuchi et al., (1999))

Nakashima and Masaoka, (1999) incorporated the compensation technique developed by Horiuchi et al., (1999) in their extrapolation/interpolation algorithm (also referred to as multi-tasking). In order to conduct a continuous hybrid test, the command signal needs to

be sent to the actuator without any delay. The extrapolation/interpolation method to compensate for any lag consists of generating a command signal at a time step (e.g. 1ms) shorter than the overall integration time step (e.g. 10ms). The command displacement is extrapolated using a polynomial to a target displacement, even if this target displacement is not known. Simultaneously, a separate task is performed to predict the next target displacement. When this task is complete, the interpolation phase corrects the extrapolated command displacement at the sub time steps increments (1ms) to achieve the predicted next target displacement. The procedure therefore allows continuous hybrid testing.

A version of the polynomial approximation by Nakashima and Masaoka, (1999) has been implemented in an event-driven strategy by Stojadinovic et al., (2006). The event-driven strategy was developed by Mosqueda, (2003a) and used by Stojadinovic et al., (2006) to perform geographically distributed hybrid tests, and is the method implemented in this project. The event-driven strategy is used in this project to perform continuous hybrid tests. The details of the event-driven strategy are discussed in Section 4.5.3. Other methods of delay compensation exist, such as the adaptive polynomial based forward prediction algorithm proposed by Wallace et al., (2005). The compensation method uses an error driven adaptive feedback controller as an outer-loop control strategy. It is shown that the method allows the forward prediction algorithm to accurately cope with frequency dependent system behaviour and operate with no prior knowledge of the system characteristics (Wallace et al., (2005)).

4.6 Current Implementation of Hybrid Test Method

A considerable volume of research to date has been undertaken on improving both the hardware and software involved in hybrid testing. However, most of this research has been individually developed by the particular host research body to suit their specific test and laboratory facilities. In the United States, there has been a drive towards a generic hybrid simulation framework. This framework is called OpenFresco (Open Framework for Experimental Setup and Control) (Schellenberg et al., (2009a)). As stated by Schellenberg et al., (2009c) the fundamental idea of OpenFresco is to allow testing to be undertaken at different laboratories, with different test equipment and without specialised knowledge required for the underlying software. To this end, OpenFresco has been used in conjunction with OpenSees to perform hybrid tests in this project. The remainder of this

section will briefly describe the hybrid test equipment used in this thesis, the processes involved a hybrid test and the event driven strategy used to undertake a continuous hybrid test.

4.6.1 Hybrid Test Facility at Trinity College Dublin

The hybrid testing facility in the structures laboratory at Trinity College Dublin comprises of an MTS real-time hybrid test system (MTS Systems Corporation). The hardware consists of a Series 111 MTS Accumulator and a high speed linear hydraulic actuator with a 150kN capacity and 250mm (±125mm) stroke. The computer hardware comprises of a Dell Precision Dual-Core Simulation Host PC (or 'Simulation PC'), a Dell Precision Dual-Core Real-time xPC Target PC (or 'Target PC'), a HP Pentium IV Test PC (or 'Test PC') and a two-channel MTS 493 Real-time Controller (or 'Servo-controller') as shown in Figure 4.8. The digital controller has closed loop PID control. The Structural Test System (STS) software provides the user interface for PID control and calibration of the actuator. The actuator tuning properties employed in the experiments undertaken in this project can be found in Table 4.1. The system is capable of running real-time (RTHT) and soft-real-time hybrid tests (soft-RTHT). The soft-RTHT differs from a RTHT in that it uses OpenSees and OpenFresco to perform the hybrid test. The term 'soft' is used because the test is performed at an extended time scale. The soft-RTHT is discussed in more detail later in this section.

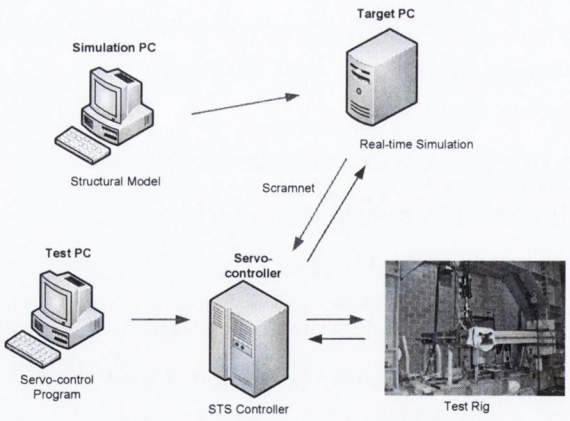

Figure 4.8: Schematic of hardware and data communication for a RTHT (McCrum and Broderick, (2010))

The RTHT communication between the hardware and software is shown in Figure 4.8. In a real-time test, Simulink (Mathworks, (2010)) is used to create the dynamic model of the

structure. The structural model is created on the Simulation PC and then downloaded onto the Target PC through a fibre optic cable. The sole task of the Target PC is to run the model in real-time using Mathworks xPC Target (Mathworks, (2010)). The Target PC has no user interface, and receives commands from the Simulation PC. The Target PC sends commands to the Structural Test System (STS) controller via the shared reflective memory called SCRAMNet GT150 (Shared Common Random Access Memory Network). The Test PC provides the user interface to the Servo-controller, and allows pre-test tuning and control of the actuator through a PID controller. The command displacement is then sent from the Servo-controller to the MTS actuator. The measured force and displacement are sent back to the Servo-controller and then back to the Target PC, where the data is used to calculate the next time step command displacement, making the process close-looped.

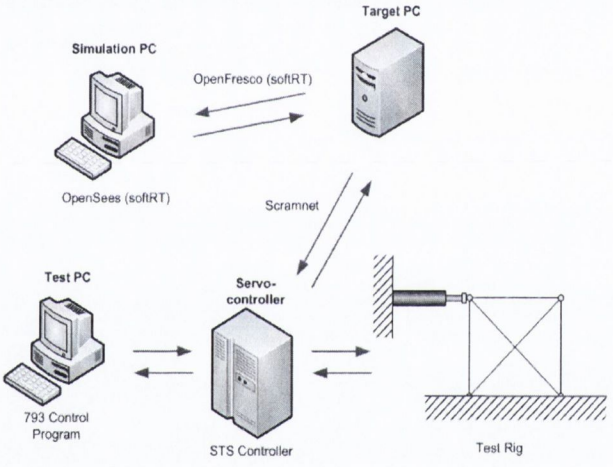

Figure 4.9: Schematic of hardware and data communication for a soft-RTHT (McCrum, (2010))

A soft-RTHT works in a similar way to the RTHT described above, however the simulation (structural model) is created with OpenSees on the Simulation PC instead of using Simulink. As can be seen from Figure 4.9, the communication between the finite element model and the test hardware is dealt with by OpenFresco as opposed to Simulink in the RTHT. The details of OpenFresco will be given in the next section.

Table 4.1: Control parameters for MTS controller

Control Parameters	*Values*
Proportional Gain	45.0 V/V
Integral Gain	5.0 1/sec
Integral Authority	10.0 %FS
Derivate Gain	0.0 sec
Feedforward	0.0 sec
Dynamic Force Frequency	1.0 Hz
Bandwidth	1000.0 Hz

4.6.2 OpenFresco Architecture

In the previous section, the communication process in a hybrid test was explained. The details of the software architecture used in the communication process will next be explained. OpenFresco is an object oriented framework for hybrid simulation. The link between a finite element model (created using any generic finite element software) and the laboratory test equipment/control system is provided by OpenFresco. The development of OpenFresco is closely related to that of OpenSees, making OpenSees the most ideal finite element modelling framework to use in conjunction with OpenFresco. The use of OpenFresco as shown in Figure 4.9 is termed a soft-RTHT. A soft-RTHT runs at an expanded timescale because the finite element framework, namely OpenSees, cannot provide commands at real-time (discussed in greater detail later in this section). The option of using a RTHT is not achievable when OpenSees is being employed to simulate the numerical substructure. Using a soft-RTHT, which is very similar to a continuous PsD test, is suitable for many investigations including the concentrically braced frames structure considered in this project in which the test structure does not have a velocity dependent dynamic response. Although there is a reduced time scale associated with a soft-RTHT, the ease of implementation with OpenSees makes the use of soft-RTHT most appropriate when a detailed representation of the numerical substructure is desired. The complex material property and analysis parameter libraries available in OpenSees can be fully utilised in a soft-RTHT.

The multi-tier software architecture of OpenFresco can be seen in Figure 4.10. The structure consists of three tiers; a client tier, one or two middle server tiers and a backend server tier. In Figure 4.10 the blue box represents the finite element software for the

computational simulation. The green boxes represent OpenFresco processes, and the gray box represents the laboratory control systems. With respect to the local and distributed simulations in Figure 4.10, the red box shows the processes that occur on the client side, the purple box shows the processes that occur on the middle tier server side, and the orange box shows the processes that occur on the server side. On the left hand side of Figure 4.10, the *LocalExpSite* is used for running a local test at one laboratory. On the right hand side of Figure 4.10, *ShadowExpSite* and *ActorExpSite* are required on the client and server side respectively to undertake a geographically distributed test. Following the OpenFresco convention, "trial data" refers to any data being sent from the finite element software towards the laboratory and "daq data" refers to data being sent from the laboratory towards the finite element software.

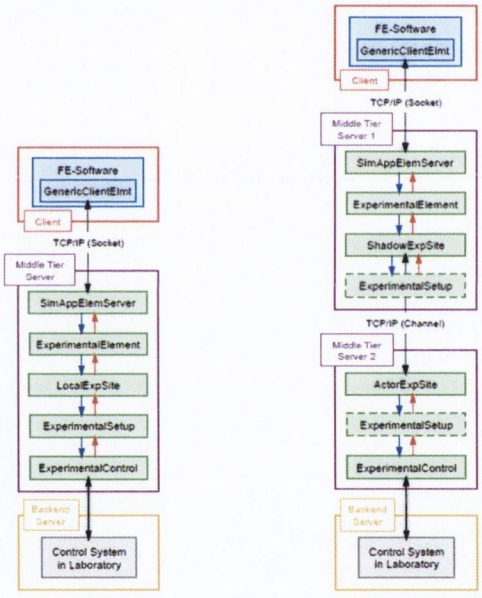

Figure 4.10: Three tier architecture for local (left) and distributed (right) simulation (Schellenberg et al., (2009c))

The Middle Tier in Figure 4.10 provides the link between the computational modelling package and the data control & acquisition in the laboratory. A local hybrid test will be performed during a validation test and the full test schedule, subsequently only the local hybrid test will be discussed herein. Within the Middle Tier, the *ExperimentalElement* represents the real-world experimental element being tested and transforms the global trial displacements to control displacements for the basic coordinate system for the experimental element. The *LocalExpSite* represents the real-world laboratory where the test is being undertaken where the global trial displacements are stored. The

ExperimentalSetup transforms the trial displacements into actuator control displacements. Finally, the *ExperimentalControl* converts the trial displacements for the actuator to into control signals for the respective control system in the laboratory. Following the imposition of physical displacements, the measured force from the load cell is converted into a vector of forces by the *ExperimentalControl*, then transformed from load cell forces to basic element forces by the *ExperimentalSetup*, stored by the *ExperimentalSite* and then transformed from the basic element forces to global forces. The data is used to solve the equation of motion for the next timestep.

OpenFresco supports the implementation of a small number of generic experimental elements. The experimental element can be represented as a beam-column element, a two node link, a generic element or an inverted v-brace element. The generic elements offer the user a relatively easy way of initially using the software framework. The experimental truss element has one axial dof and is defined by two nodes. The experimental beam-column element formulation is based on three (two-dimensional) or six (three-dimensional) dof. The experimental two node link element is defined by two nodes and can have 1 to 6 dof uncoupled from each other for one-, two- or three-dimensional representation. The experimental generic element can be defined by any number of nodes and any number of dof. The experimental inverted v-brace elements are defined by three nodes and can only be represented in two-dimensions.

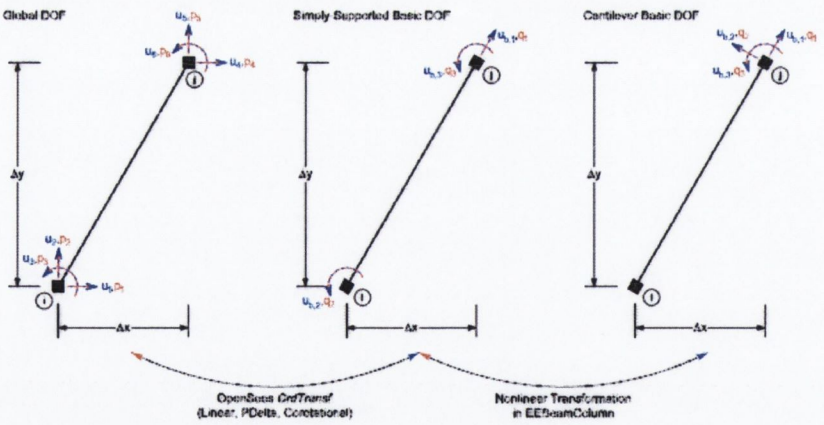

Figure 4.11: Experimental beam-column element (Schellenberg, (2008))

The beam-column element will be used in the validation model and final test model to represent the experimental substructure. The experimental element in OpenFresco utilises the coordinate transformation (*CrdTransf*) class in OpenSees to transfer the element global

dof to the basic element dof (Schellenberg, (2008)). In OpenSees, the *CrdTransf* can be linear, p-delta and corotational geometric transformations. The coordinate transformation enables the linear or nonlinear effects to be accounted for without affecting the implementation of the frame elements themselves. The transformation of the global dof for the beam-column element is shown in Figure 4.11. However, the simply supported basic dof system is not suited to experimental testing because there are rotational dof at each end of the element that are very difficult to achieve in a test setup. The simply supported dof are transformed to a cantilever basic dof system as shown in Figure 4.11. For explicit mathematical formulation of the transformation of the trial displacements from the basic to cantilever system and back again, refer to Schellenberg, (2008).

The procedure of implementing a two-dimensional experimental beam-column element in OpenFresco is detailed in Section 4.7. The procedure in which OpenFresco implements the experimental element into the numerical substructure for a three-dimensional structure is detailed in Chapter Five, Section 5.6. OpenFresco has a number of experimental setups predefined, such as no transformation, one actuator, two actuators, three actuators, inverted v-brace and aggregator. It is also possible to perform hybrid tests using different experimental control hardware such as dSpace, xPC Target and SCRAMNet. For a more detailed description of the capabilities of OpenFresco refer to Schellenberg, (2008), Schellenberg et al., (2009b) or Schellenberg et al., (2009c).

4.6.3 Current Implementation of Event Driven Strategies

The delay compensation technique adopted in the current implementation of hybrid testing is implemented using the event-driven strategy proposed by Mosqueda, (2003a). The following section is a short description of the numerical processes involved in running a continuous soft-RTHT. The hybrid test facility at the structures laboratory in Trinity College Dublin consists of a system that is capable of running geographically distributed hybrid tests as well as local RTHT. The delay compensation method used in the system was developed by Mosqueda, (2003a) to implement a geographically distributed hybrid test and has been further refined by Schellenberg, (2008). If the test parameters and specimen are chosen correctly, then the test will run continuously.

In modern testing equipment, it is not untypical for the computational driver and servo-hydraulic control system to run at two different sampling rates. The computational driver is

run at a rate that depends on the numerical integration of the equation of motion in the finite element software, typically 0.01s. However, the servo-hydraulic control system generally runs at a much higher sampling frequency. SCRAMNet runs at a sampling rate of 1/1024s. Not only are the sampling rates different, but while the servo-hydraulic control system samples at a constant rate, the numerical integration runs at a non-deterministic rate, particularly during a nonlinear response such as yielding or buckling (Schellenberg et al., (2009c)). The solution to this problem proposed by Schellenberg et al., (2009c) is the use of a predictor-corrector technique. The predictor-corrector technique here should not be confused with the integration predictor-corrector procedure used for solving the equation of motion, and is based on the extrapolate/interpolate polynomial approximation developed by Nakashima and Masaoka, (1999).

It can be beneficial in terms of computational efficiency to apply the concept of multi-tasking to undertake tasks on separate processors (Mosqueda et al., (2005)). Figure 4.12 indicates the three-looped control architecture used to undertake hybrid tests. The inner control loop consists of a PID servo-control loop tuned to the optimum parameters. The tasks for the inner-control loop are run on the Servo-controller. The outer control loop is the numerical integration loop integrating the equation of motion. The outer control task is run on a separate local processor than the servo control loop. The intermediate control loop is termed the predictor-corrector control loop in Figure 4.12. As described previously, this control loop allows synchronisation between the outer and inner control loops, which perform their tasks at different time scales.

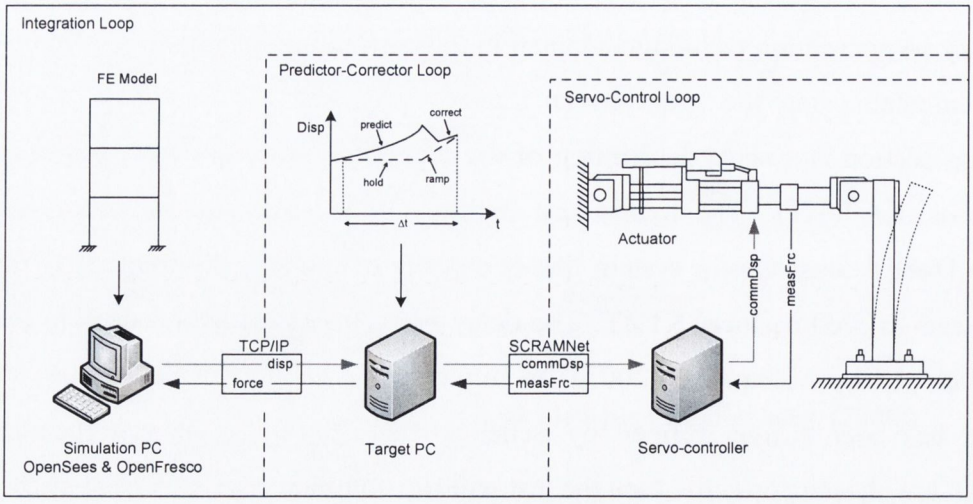

Figure 4.12: Schematic of the control loops in the implementation of a soft-RTHT using SCRAMNet experimental control (Schellenberg et al., (2009b))

The event driven strategy is applicable to geographically distributed hybrid tests, however in a local test, if there is a delay in the sending of the next command target displacement to the servo-control due to excessive iteration in the numerical integration then this communication delay is dealt with in the same manner as a communication delay over the internet in a distributed test. Figure 4.13 indicates the state transition diagram for an event driven hybrid test. Five states exist in the state transition diagram; *extrapolate*, *interpolate*, *slow*, *hold* and *free vibration*. The *extrapolate* and *interpolate* transition states have been described above. The default state is *extrapolate*, where the commands are predicted based on previously computed displacements and the integrator computes the next target displacement (Mosqueda et al., (2005)). The state changes from *extrapolate* to *interpolate* after the next target displacement is received by the controller. The *D-update* event is then generated. Once the target displacement has been applied to the physical substructure and the target displacement is achieved, event *D_target* is then generated. The state then transitions back to extrapolate where the updated measured displacement is sent to the numerical integration algorithm for the next time step.

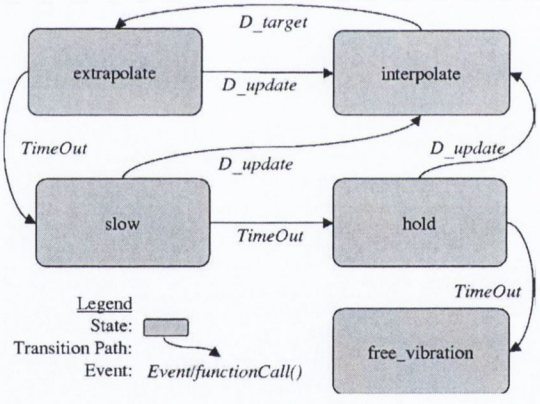

Figure 4.13: State transition diagram used in a hybrid test (Stojadinovic et al., (2006))

As stated by Stojadinovic et al., (2006), the advantage of an event driven strategy is that logic can be used to handle excessive delays. If the system remains in the extrapolate state for too long, the actuator can deviate from the target (Nakashima and Masaoka, (1999)). In order to overcome excessive delays, Mosqueda et al., (2005) proposed to allow a change of state to slow down the actuator. In the *slow* state, the extrapolation occurs at a reduced velocity resulting in more time being available to receive a command update. When the next target displacement is received, the state transitions to *interpolate*. Alternatively, if the target displacement is not received after a specified number of steps, the state transitions to a *hold* state to allow the target displacement to be received. If no target displacement is

received (possibly due to integrator crashing), the *hold* state times out (*TimeOut*) to force the system into *free_vibration*. The *free_vibration* state allows unloading of the structure in a highly damped free vibration.

Schellenberg, (2008) updated the extrapolate/interpolate states to utilise predictor/corrector algorithms to improve synchronisation between the integration and actuator control process in the event-driven strategy. The proposed predictor/corrector algorithm improves performance by generating continuous displacement commands (Schellenberg, (2008)). A further improvement to the event-driven strategy is an adaptive time stepping strategy. The previous strategy (Mosqueda et al., (2005)) spent approximately 80% of the simulation time step in the prediction state, leaving only 20% available for the correction state. If the predicted displacements were not accurate, there was not sufficient time to correct the displacement. The solution was to create a predictor that predicted the displacement a number of time steps ahead rather than just one time step ahead (Schellenberg, (2008)). The event driven strategy described above is implemented in the validation test described in the next section.

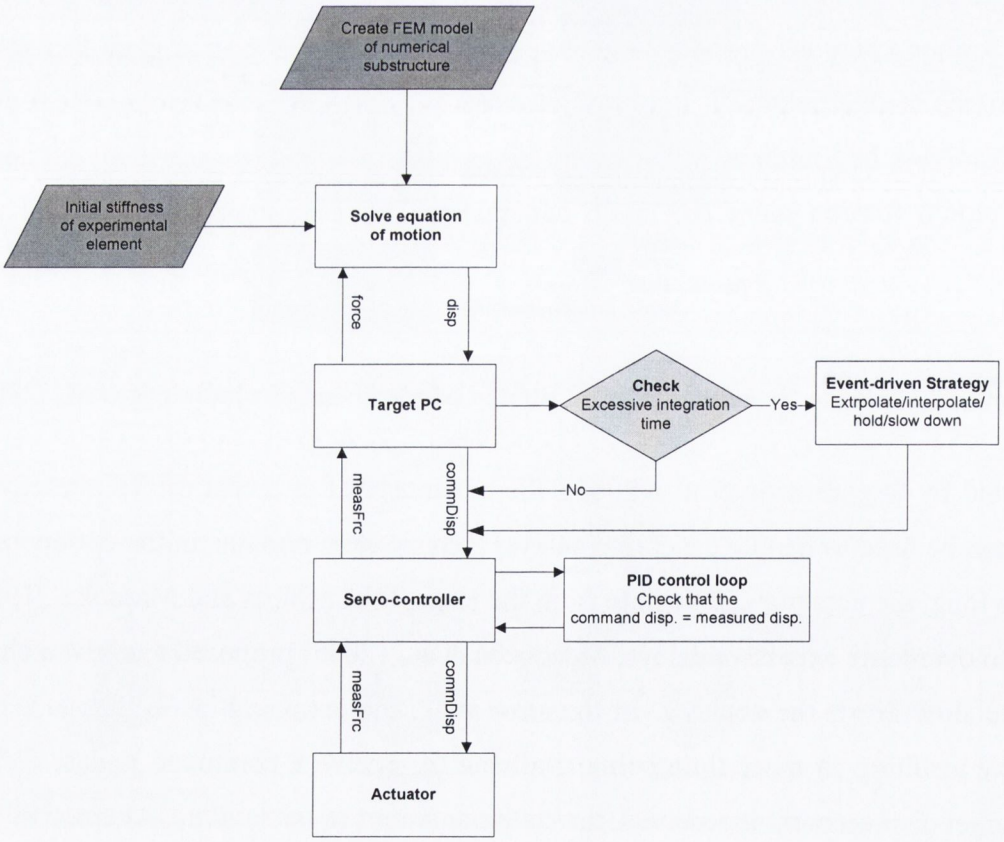

Figure 4.14: Flowchart of hybrid test implemented at Trinity College Dublin testing facility

A summary of the processes involved in performing a hybrid test at structures laboratory at Trinity College Dublin, as described in this section are given below in Figure 4.14.

4.7 Hybrid Test Verification

A verification test was undertaken to validate the implementation of the hybrid test procedure prior to undertaking the full testing schedule (described in Chapter Five). The commonly tested two dimensional substructured steel column portal frame substructure test was employed for this purpose. The laboratory test setup and obtained results are described in this section.

Objective

The main objective of the validation experiment is to evaluate the implementation of the hybrid test procedure. To ensure the hybrid experimental procedure was implemented correctly, the displacement, velocity and acceleration response of the test specimen were to be compared to a comparative purely numerical model. The equilibrium of the test would be checked by comparing the base shear of the test structure (i.e. actuator force) to that of the comparative numerical model. The effectiveness of the event-driven strategy will be investigated by assessing the hold and slow-down phase actuator tracking during these phases of the test.

Scope

The proposed hybrid validation experiment was only to be conducted in two-dimensions. A soft-RTHT is to be implemented in the validation test as this type of experiment will be implemented in the full test schedule. It was not necessary to perform a RTHT within the scope of the validation test. The validation test is performed in the linear elastic range only, so that modelling issues associated with nonlinearity in the comparative numerical model are not of concern. The peak allowable displacement during the test was defined as the upper limit of the linear elastic portal frame displacement. The experimental element had to have significant stiffness to allow actuator displacement of a few millimetres such that reasonable values of actuator displacement could be evaluated.

4.7.1 Substructured Portal Frame Test Setup

The proposed hybrid validation test is a two-dimensional substructured steel portal frame test illustrated in Figure 4.15, in which one steel column is physically tested (physical substructure). As indicated in Figure 4.15(a), the physical substructure consists of a 150x90mm channel section. As shown in Figure 4.15(b), the numerical substructure consists of an elastic beam-column element with a high elastic stiffness representing the beam member, and a simulated experimental beam-column element with the same properties as the physical substructure representing the other column member. The base of the portal frame columns was fixed and the top of the column elements was pinned. The mass was applied to Node 3 and Node 4 (masses not shown in Figure 4.15(b)). The damping was numerically applied to the structure using mass proportional Rayleigh damping. The experimental setup chosen in OpenFresco is the One Actuator setup. The numerically modelled column was simulated using SimDomain. This specific test is a template of a verification test used in a soft-RTHT and has been undertaken by others (Schellenberg, 2008). The Tcl script of the hybrid test model of the portal frame can be seen in Appendix A1. The Tcl script for the purely numerical model of the portal frame can be seen in Appendix A2. It is important to point out that the yield strength and elastic modulus of test specimen had to be estimated because the specimen used was taken from the laboratory but did not have its material properties labelled on it. The extended time scale of the test was approximately 20 times slower than the simulated model.

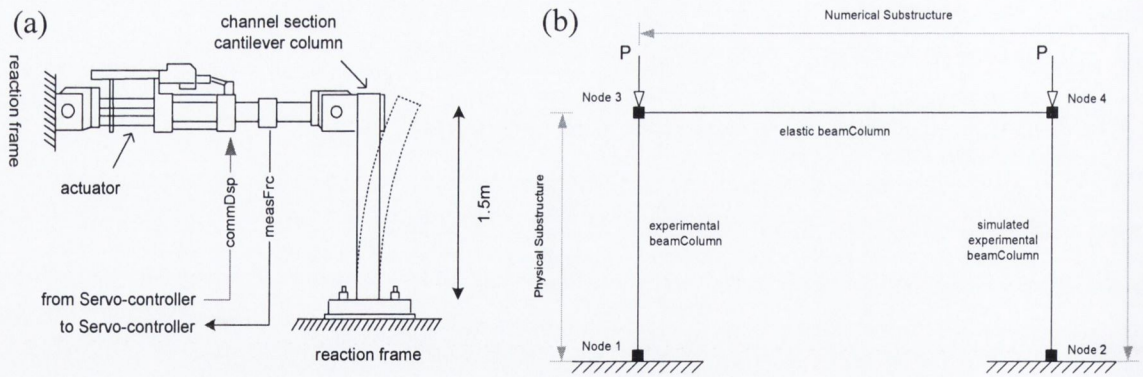

Figure 4.15: Substructured test of two-dimensional portal frame validation test

Initially it was intended to use a steel member I-section as the physical substructure in the hybrid test. However, the stiffness of the steel member I-section specimens readily available in the laboratory was too low which would have resulted in too small actuator displacements. A channel section was available with no lead-in time and was therefore

utilised. The channel section is tested in its stronger axis. It was observed during the test that the channel section was rotating around its longitudinal axis. The connection from the actuator to the test specimen was centred on the centroid of the channel section and the threaded bolts were tightened equally either side (perhaps the shear centre would have been more appropriate). However, due to the additional stiffness of one side of the specimen and possible inconsistencies in the connection detail, a slight twisting deformation occurred. This torsion may have lead to inaccuracies in the test results as these effects are three-dimensional, whereas the model was only defined in two-dimensions.

To initiate the numerical integration for the analysis, the test specimen needs to have its stiffness defined. The formation of the initial stiffness matrix of the test specimen is described as follows;

Figure 4.16: Cantilever frame element degrees of freedom

The full plane frame stiffness matrix for a pinned-fixed beam-column element shown in Figure 4.16 is given below:

$$K_E = \begin{matrix} \\ \\ \\ \\ \\ \\ \\ \end{matrix} \begin{matrix} \mathbf{1} & \mathbf{2} & \mathbf{3} & \mathbf{4} & \mathbf{5} & \mathbf{6} \end{matrix} \begin{bmatrix} \frac{AE}{L} & 0 & 0 & -\frac{AE}{L} & 0 & 0 \\ 0 & \frac{3EI}{L^3} & 0 & 0 & -\frac{3EI}{L^3} & \frac{3EI}{L^2} \\ 0 & 0 & 0 & 0 & 0 & 0 \\ -\frac{AE}{L} & 0 & 0 & \frac{AE}{L} & 0 & 0 \\ 0 & -\frac{3EI}{L^3} & 0 & 0 & \frac{3EI}{L^3} & -\frac{3EI}{L^2} \\ 0 & \frac{3EI}{L^2} & 0 & 0 & -\frac{3EI}{L^2} & \frac{3EI}{L} \end{bmatrix} \begin{matrix} \mathbf{1} \\ \mathbf{2} \\ \mathbf{3} \\ \mathbf{4} \\ \mathbf{5} \\ \mathbf{6} \end{matrix} \quad (4.22)$$

where, E is the Young's Modulus (N/mm^2)

A is the area of the section (mm^2)

I is the second moment of area of the section (mm^4)

L is the effective length of the member (mm)

The 6x6 cantilever frame element stiffness matrix in Equation 4.22 can be reduced. Degrees of freedom 1-3 are all zero due to the cantilever fixity; therefore the stiffness matrix reduces to:

$$K_E = \begin{matrix} \\ 4 \\ 5 \\ 6 \end{matrix} \begin{matrix} \begin{matrix} 4 & 5 & 6 \end{matrix} \\ \begin{bmatrix} \frac{AE}{L} & 0 & 0 \\ 0 & \frac{3EI}{L^3} & -\frac{3EI}{L^2} \\ 0 & -\frac{3EI}{L^2} & \frac{3EI}{L} \end{bmatrix} \end{matrix} \tag{4.23}$$

The element stiffness matrix in Equation 4.23 represents the initial stiffness for the experimental beam-column element in the test model. The experimental setup chosen in OpenFresco is the One Actuator setup. This test only accounts for one degree of freedom as there is only one actuator. In a two-dimensional test, the vertical displacements and rotational degree of freedom are ignored and only the lateral displacements are considered. The initial stiffness provides sufficient information required to initiate the first command displacement using numerical integration.

4.7.2 Results from Verification Test

The test portal frame was subjected to a scaled North-South component of the Taiwan earthquake of 14th of November 1986, selected from the PEER database (PEER, (2000)). The results for the lateral displacement of Node 3 (refer to Figure 4.15) on the simulated model and the hybrid test are compared in Figure 4.17. The largest difference in lateral displacement is 0.28mm, which corresponds to 4% of the maximum displacement demand. The root-mean-square (rms) values of the test displacement and simulated displacement differ by 10.3%. This indicates servo hydraulic control system achieved reasonably accurate actuator displacement tracking; however the twisting of the test specimen during the experiment was thought to add to the displacement error along with the servo hydraulic control. From Figure 4.17, it can be seen that the displacement response was predicted reasonably accurately by the numerical model. The level of damping chosen was 5%, however this value may not have been correct for this specimen as the peak displacements do not match well in Figure 4.17 indicating the higher frequencies were not being damped adequately in the simulated model. It appears from Figure 4.17 that some yielding takes place around 15s as there is an upward shift in the test displacement compared to the simulated displacement.

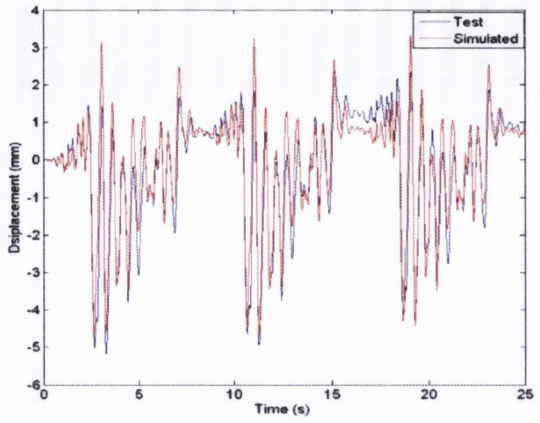

Figure 4.17: Lateral displacement vs. time for the simulated model and test data for Node 3 (refer to Figure 4.15) of portal frame model

Figure 4.18 and Figure 4.19 compare the lateral velocity and lateral acceleration of Node 3 for the simulated model and the hybrid test data, respectively. As can be seen in Figure 4.18, the test data velocity and simulated velocity are observed to match closely. The largest difference in lateral velocity between the test and simulated velocities is 5247.5cm/s, which corresponds to 8.1% of the maximum velocity demand. The rms values of the test velocity and simulated velocity differ by 4.9%. As can be seen in Figure 4.19, the test data velocity and simulated acceleration are observed to match closely. The largest difference in lateral acceleration between the test and simulated velocities is 0.066m/s^2, which corresponds to 4.1% of the maximum acceleration demand. The rms values of the test acceleration and simulated acceleration differ by 3.2%.

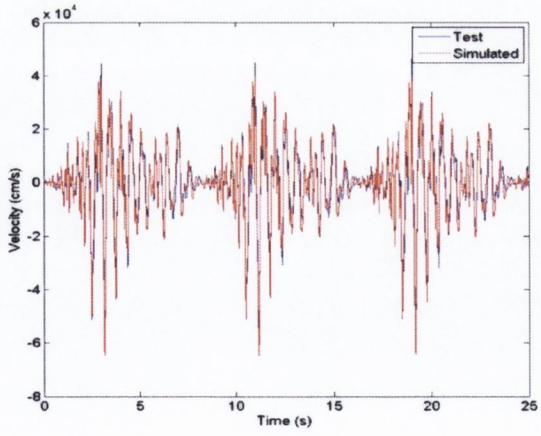

Figure 4.18: Lateral velocity vs. time for the simulated model and test data for Node 3 (refer to Figure 4.15) of portal frame model

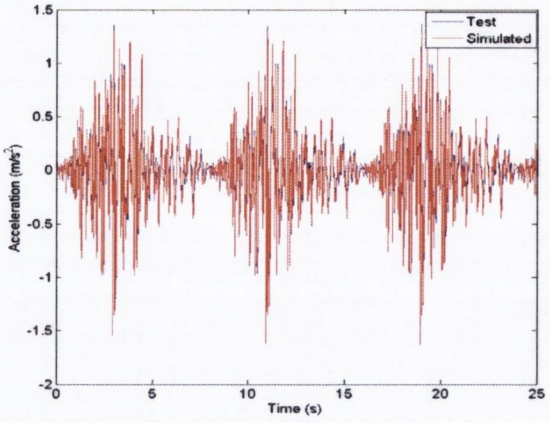

Figure 4.19: Lateral acceleration vs. time for the simulated model and test data for Node 3 (refer to Figure 4.15) of portal frame model

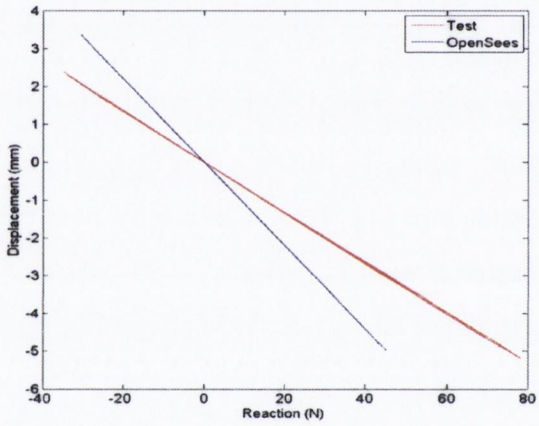

Figure 4.20: Base shear vs. displacement for the simulated model and test data for Node 3 (refer to Figure 4.15) of portal frame model

As discussed above, the verification test results provided validation of the test method and gave confidence to extend the test procedure to more complex models. As can be seen from Figure 4.17, the period of the results from the test and the simulated results show very good agreement. The test results are slightly shifted downwards, which indicates that some damage settlement in the specimen or connection. Figure 4.20 presents the base shear versus roof displacement displayed in the test data and simulated model. The results in Figure 4.20 indicate the force equilibrium in the test and numerical model did not show good agreement. The simulated model overestimated the test specimen's stiffness. The test specimen also shows nonlinearity in the hysteretic response. However, the test specimen only displaced a maximum of approximately 5mm, which is below the yield displacement of the test specimen. Therefore the test specimen hysteresis is unexpected. It is expected

that not having the exact yield strength and elastic modulus properties of test specimen resulted in the overestimation of the stiffness.

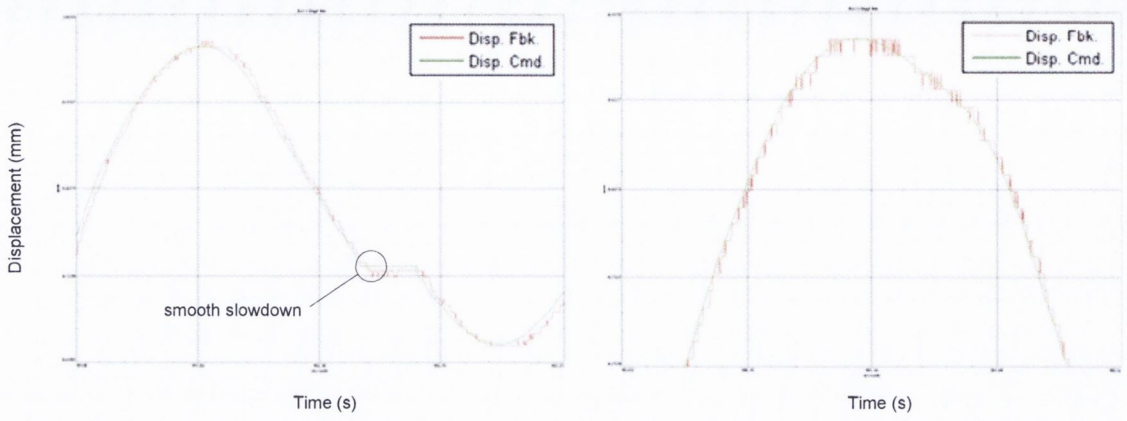

Figure 4.21: (a) Graph of command displacement and feedback displacement vs. time (b) close-up of command displacement and feedback displacement from validation test

Figure 4.21 compares the command and feedback displacement signals. As can be seen in Figure 4.21(a) & (b), the actuator displacement command signal (green line) is smooth, indicating the predictor-corrector model used in the test was performing well. The feedback displacement signal (measured displacement) does not always follow the command signal because there is a small tracking error. When a delay occurred, the command displacement signal made a smooth transition into the hold state, as can be seen in Figure 4.21(a). However, when the new target displacement was received, the command displacement signal was not smooth and there was an abrupt change in the displacement command. The results of the validation test indicate some inaccuracies in the test method and set-up, however overall the system has been shown to be performing well.

4.8 Chapter Overview

This chapter has briefly described the development of the hybrid test method from its origins as the pseudodynamic test (PsD) method to its current form as the RTHT method. Key aspects such as delay compensation and numerical integration techniques used in PsD and RTHT were introduced and the proposed numerical integration and delay compensation scheme adopted in this project have been detailed. A two-dimensional validation test investigating a cantilever column within a steel portal frame was described. The results of the validation test indicated that the hybrid test method had been adequately implemented. The next chapter will detail the proposed test set-up for the application of the

soft-RTHT method to an investigation of the earthquake response of plan irregular concentrically braced frame structures.

Terminology:

A useful synopsis of the terminology in relation to hybrid testing is provided;

- Definition of a pseudodynamic (**PsD**) test is a dynamic test run at elongated time e.g. the test is run 30 or 100 times slower than reality.
- A real-time test (**RT**) is a dynamic test run at actual time i.e. one second in the test is one second in reality.
- A hybrid (**HT**) or substructured test is a test where the critical part of the structure is physically tested and the rest of the structure is numerically modelled. The physical results from the test feed into the numerical model and are used to calculate the next command displacement from numerical integration for the next timestep.
- A 'soft' real-time hybrid test (**soft-RTHT**) is essentially a PsD test. The term soft-RT results from using the current event-driven strategy to perform dynamic testing is referred to as
- A 'hard' real-time hybrid test (**hard-RTHT**) is a one to one correspondence between the simulation time and the actual test time.

CHAPTER FIVE – Experimental Programme Set-up

5.1 Introduction

This chapter presents the practical design of the proposed experimental set-up and the proposed numerical modelling strategy implemented in the hybrid test programme. Details of the variation of the parameters affecting the torsional response of braced plan irregular structures to be studied during the experimental programme will be detailed. The practical issues associated with the test set-up, such as geometric and actuator capacity constraints will be discussed. The details of the final OpenFresco and OpenSees models used in the test will be given.

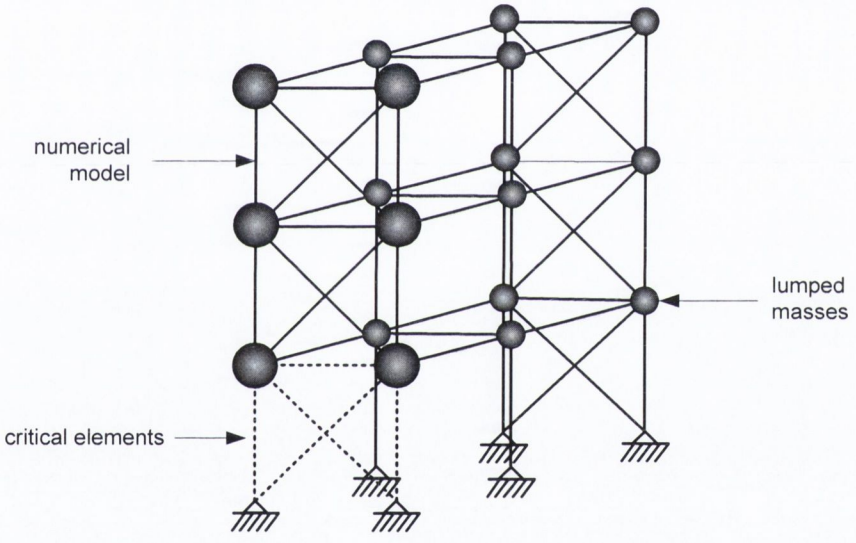

Figure 5.1: Uneven distribution of mass towards one side of structure

Figure 5.1 illustrates the uneven distribution of the mass in the plan irregular concentrically braced structure investigated in this thesis. The additional mass distributed towards one side of the structure creates an additional demand on the bracing; in particular the behaviour of the first-storey braced frame is critical to the overall response of the structure, as shown in Figure 5.1. The objectives of the experimental programme are;

- Assess the effects of important structural parameters affecting the seismic response of braced plan irregular structures. These parameters have been identified as the lateral torsional frequency ratio, Ω_θ and the static eccentricity, e_s. Varying the levels of static

eccentricity and lateral torsional frequency ratio within the experimental programme will allow an assessment of the effect they have on the seismic response.

- Assess the adequacy of the Eurocode 8 (CEN, (2004)) torsional effects factor at improving the seismic response of braced structures with mass eccentricity. Varying the brace section sizes in the first-storey braced frame within the experimental programme will allow an assessment of the effect the torsional effects factor in design has on the seismic response. The next section will detail the parameter selection for the experimental programme.

5.2 Experimental Programme

It is important to choose an appropriate number of parameters to vary during the experimental programme. At a basic level, the tests will be used to validate the numerical modelling approach to be used in future parametric studies. However, more importantly, the testing programme needs to observe the effect of varying important structural parameters on the torsional response of the proposed plan irregular structure being investigated. The fundamental parameters to be varied during the testing programme are shown in Table 5.1. A brief description of the choice of final test parameters is given below;

Table 5.1: Experimental Programme

Test Series Number	*Brace Size (mm)*	*Normalised Slenderness,* $\overline{\lambda}$	*Static Eccentricity,* e_s	*Lateral Torsional Freq. Ratio,* Ω_θ	*Plan Aspect Ratio*
1	30x30x3 SHS	1.68	0.15	0.75	2.0
2	50x30x3 RHS	1.57	0.15	0.75	2.0
3	30x30x3 SHS	1.68	0.15	1.25	2.0
4	50x30x3 RHS	1.57	0.15	1.25	2.0

Static Eccentricity

The static eccentricity, e_s was chosen to reflect realistic possible values. As stated in Chapter Three, Section 3.6.1, the static eccentricity is to be varied from $0.0L$ to $0.15L$ (where L is the total length of the building in the direction under consideration). The

response of the structure at the maximum static eccentricity of $0.15L$ was chosen for each of the tests as can be seen in Table 5.1. The static eccentricity will be varied in one direction only.

Lateral Torsional Frequency Ratio

As described in Chapter Three, Section 3.5.2, the lateral torsional frequency ratio, Ω_θ is the parameter that best characterises the level of torsional resistance of the structure (i.e. if $\Omega_\theta < 1$, then the structure is torsionally flexible and if $\Omega_\theta > 1$, then the structure is torsionally stiff). The upper and lower bounds reflect realistic levels of torsional stiffness and torsional flexibility were chosen as $\Omega_\theta = 1.25$ and $\Omega_\theta = 0.75$ respectively. Both of the upper and lower bounds of Ω_θ will be investigated in two sets of comparative tests, as can be seen in Table 5.1.

Plan Aspect Ratio

Contradictory evidence by researchers has stated that the plan aspect ratio has either no effect or a considerable effect on the response of plan irregular structures. Upper and lower bounds of 1.0 and 3.0 respectively were to be investigated. In the experimental programme, the value of plan aspect ratio of 2.0 was chosen. Due to the limited number of proposed tests, the plan aspect ratio was not varied in the four tests and the effect of this parameter was to be purely computationally assessed.

Slenderness

The upper and lower bounds of non-dimensional slenderness are 2.0 and 1.3, respectively, as defined by Eurocode 8 (CEN, (2004)). The structure designed for plan irregularity using the torsional effects factor resulted in bracing of size 50x30x3mm RHS on the SS first-storey braced frame, with a non-dimensional slenderness of $\overline{\lambda} = 1.57$. The structure not designed for plan irregularity resulted in bracing of size 30x30x3mm SHS SS first-storey braced frame, with a non-dimensional slenderness of $\overline{\lambda} = 1.68$. The effect of the torsionally designed and torsionally undesigned structure will be compared in the testing regime as shown in Table 5.1.

Time History Selection

As described in Chapter 3, Section 3.6.5, the A/V ratio is a useful method of classifying an earthquake record's intensity and energy characteristics. A preliminary computational test model was subjected to each of the 7 No. time histories selected in that section (see Table

3.2). In preliminary numerical analyses of the proposed test structure it was found that the Taiwan record and El Centro record resulted in the greatest ductility demand and damage of the test structure, namely the SS first-storey brace members. Of these, the Taiwan time history was selected for application in the test programme as it produced a smoother and more regular response over the duration of the time history. The El Centro excitation has greatest amplitude in the first 5 to 10 seconds with most of the energy dissipated over the first 5 to 10 seconds. The Taiwan time history provides a more gradual build-up in intensity over the duration of the response making it more appropriate to use during a hybrid test.

The two main parameters that are varied in the tests are the slenderness, $\overline{\lambda}$ and the lateral torsional frequency ratio, Ω_θ. The more slender ($\overline{\lambda} = 1.68$) section is the brace member that has been not been designed to resist the torsional response and the less slender ($\overline{\lambda} = 1.57$) section is the section that has been designed to take account of the torsional response. The lateral torsional frequency ratio, Ω_θ is varied to represent a torsionally stiff and torsionally flexible structure by varying the nodal masses. Varying the above mentioned parameters as shown in Table 5.1 will provide sufficient validation data for the comparative numerical model.

5.3 Experimental Set-up

In this section, the structural design procedure for the first-storey (ground floor) concentrically braced test frame will be given. The practical issues encountered in designing the test set-up such as the physical limitations of the size of the reaction frame and the capacity of the actuator will be detailed.

5.3.1 Design of Test Frame

The proposed test frame was designed according to Eurocode 3 (CEN, (2005)) and Eurocode 8 (CEN, (2004)). The hysteretic behaviour of braces and the design procedure for a concentrically braced framed steel structure was outlined in Chapter Three. A brief description of the design of the proposed test structure and the plan irregularity design considerations will be discussed. Appendix B contains the entire set of fabrication

drawings of the experimental frame and can be referred by the reader to clarify any of the experimental frame details.

Design Method

The proposed structure was designed according to Eurocode 8 (CEN, (2004)) using the lateral force method of analysis, where the earthquake action is represented by equivalent static forces that are applied to the structure. A brief description of the design process is outlined.

Design Actions

The permanent action from an assumed reinforced concrete floor is 7.2kN/m^2, and the variable action is 3.5kN/m^2 (2.5kN/m^2 for office loading and 1.0kN/m^2 for partitions). The soil is assumed Type B, the peak ground acceleration, a_g is assumed as 3.5m/s^2. The behaviour factor, q for a concentrically braced steel structure designed for medium ductility class (DCM) is 4. From these values an elastic target response spectrum for design is calculated. The target response spectrum gives the peak response of a SDOF system as a function of damping and natural period (Elghazouli, (2009)). Only the horizontal component of the earthquake time history is considered. Using the lateral force method of analysis in Eurocode 8 (CEN, (2004)), the distribution of the seismic pushover forces are calculated.

Design of Concentric Bracing

The test structure is assumed to resist the lateral actions by concentric bracing only and no frame resistance. The tension brace is assumed to resist all the lateral action while the pre-buckling resistance of the compression brace is not considered. In this case and with most concentrically braced frames, the limiting factor in the design is the non-dimensional slenderness.

Design of Beams and Columns

The beams and columns were designed to ensure adequate overstrength to the combined seismic, permenant and variable action effects. As a precaution, web stiffeners are provided to the columns and beam at the locations where the gusset plate connects to the respective columns and beam. The stiffeners are required to prevent any possibility of local buckling on the columns and beam. The columns and beam were to be used in every test, therefore no damage was acceptable.

Design of Gusset Plate Connections

The gusset plate connections are designed using the design action obtained from the lateral force method and applying an appropriate overstrength factor. The overstrength factor depends on the type of structure and is calculated by the ratio of α_u/α_1, where α_u is the value by which the horizontal seismic design action is multiplied in order to achieve first plastic action of any member and α_1 is the value by which the horizontal seismic design action is multiplied in order to achieve a number of plastic hinges and structural instability. The overstrength factor aims to ensure that the connection remains non-ductile throughout the response, so the element is then termed non-dissipative. The ductility and energy dissipation in an inelastic response of the structure is provided by the bracing members and not the connections. The gusset plate design in this thesis provided certain difficulties. For one, a typical gusset plate connection is connected to the beam and column intersection at the corner of a frame. In the proposed experimental set-up as shown in Figure 5.2, the gusset plates cannot be connected to both the beam flange and column flange. For the top gusset plate connection, the gusset plate is only connected to the beam flange to allow for the rotation of the stub section connecting the beam to the column. A stiffener plate is provided where the gusset plate connection would normally be connected to the column. Similarly, for the bottom gusset plate connection, the gusset plate is only connected to the column flange to allow for the rotation of the stub section connecting the column to the support. A stiffener plate is provided where the gusset plate connection would normally be connected to the beam below.

The tension capacity of the gusset plate connection was calculated using Whitmore's width (Whitmore, (1952)). The alignment of the brace member connection in the gusset plate will provide a trilinear yield line due to out-of-plane buckling of the brace member. The spacing around the brace member connection in the gusset plate facilitates the out-of-plane buckling and is similar to trilinear yield line proposed by Wijesundara, (2009). In order to form a linear yield line in the gusset plate due to out-of-plane buckling, AISC, (2005) specifies a free space of two times the gusste plate thickness between the brace end and a line that connects the re-entrant corners of the gusset plate. However, it was not possible to implement these guidelines due to the constraint of the gusset plate only being connected to the test frame on one side.

In case any yielding occurred in the gusset plates, the gusset plate connections were replaced after each test. The connection bolts were either M16 Gr. 8.8 ordinary bolts or

M20 Gr. 8.8 ordinary bolts and were tightened according to BS EN 1090-2 (British Standards Institution, (2008)).

Torsional Effects Design

The only exception to the above mentioned design is the design to resist torsion. As noted in Chapter Two, Section 2.5.1, the torsional effects are considered in the seismic design using the torsional effects factor, δ. In preliminary analyses, it was observed that the SS of the structure that has the mass distributed towards it has a greater ductility demand. The torsional effects factor, δ results in an increased design seismic pushover action, resulting in a larger brace section being required to resist the design pushover action. Therefore, the bracing members on the SS of the torsionally unbalanced structure resist a greater design action. The effect of the torsional response of the structure and the adequacy of the proposed Eurocode 8 (CEN, (2004)) design method using the torsional effects factor, δ are the main areas of consideration of the proposed experimental study.

5.3.2 Practical Considerations for Experimental Set-up

The dimensions of the test structure had to allow the test frame to fit into the available reaction frame in the test laboratory. As shown in Figure 5.2, the reaction frame actually consists of two identical reaction frames mounted side-by-side and connected via cross members. The test frame was mounted between the two reaction frames as shown in Figure 5.2. Testing the structure between the two reaction frames allowed a larger and more realistic sized frame to be tested. Two horizontal members spanning between the reaction frames supported the test frame as can be seen in Figure 5.2. Testing between the two reaction frames also allowed the frame to move freely in the direction of actuation without any restrictions. A roller guide was mounted on the reaction frame, as shown in Figure 5.2, in order to prevent the test frame displacing laterally out-of-plane and impacting the reaction frames.

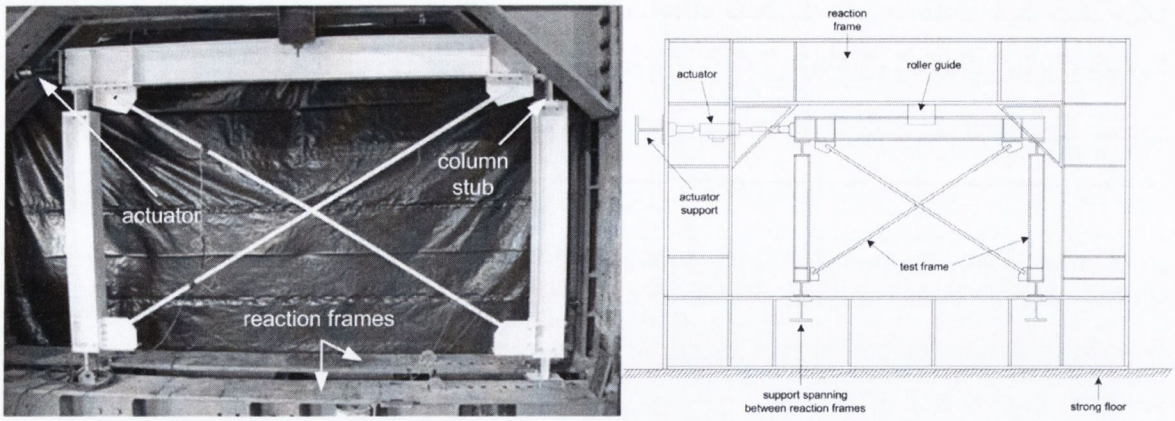

Figure 5.2: Elevation view of test frame and reaction frame with 30x30x3 SHS braces (left) schematic and (right) photograph

It was originally proposed to use a fully pinned connection in the braced frame consisting of a rotating pin joint, both at the column bases and column to beam connections. However, as explained in Chapter Four, Section 4.3, the hybrid test method can fail due to small displacement error being imposed on the test structure or being sent back from the actuator to the numerical model. A small discrepancy in the rotating joint could allow some 'wobble' in the test frame resulting in spurious displacements being imposed on the structure or being sent back to the numerical model. The fabrication tolerances required to construct the pinned joints would have been very small. In order to overcome possible fabrication issues, the pinned supports provided in the experimental set-up are column stub sections to allow almost free rotation in the plane of the test frame whilst preventing any spurious displacements in the test frame.

The force capacity of the actuator limited the size of the brace sections that could be tested. As stated in Chapter Four, the capacity of the actuator is 150kN and the limit of the stroke is ±125mm. It is important to keep the load in the actuator below approximately 80% of the force capacity so that linearity in the actuator is maintained and the actuator can perform accurately. Based on the dimensions of the test set-up allowed by the reaction frame, the bracing members are inclined at 37.1°. A maximum force of 150kN from the actuator will provide a force of 188.18kN in the tension brace, if the tension brace alone resisted the action. However, a contribution to the lateral resistance of the frame is also provided by the compression brace. It was important not to approach the force capacity of the actuator in order to protect the actuator from damage. The tests are conducted at a slow speed meaning the dynamic rating of the actuator would not be a limiting constraint. The stroke of the actuator would not be a constraint because the concentrically braced frame is

very stiff resulting in a yield displacement and any subsequent hysteretic displacement response being far below the stroke capacity of ±125mm. The seismic design of the frame using the Eurocode 8 (CEN, (2004)) torsional effects factor indicated that a 50x30x3mm RHS should be employed. The 50x30x3mm RHS section has a yield force of 101.99kN corresponding to an actuator force of 81.3kN, which is well within the actuator capacity. The compression brace has a buckling capacity of 41.6kN corresponding to an actuator force of 33.2kN. The combined lateral force in the actuator is approximately 114.5kN for the test specimen with 50x30x3mm RHS sections, well below the actuator capacity of 150kN. The frame designed without the torsional effects factor required 30x30x3mm SHS sections in the first-storey on the SS of the structure; implying a tension brace yield force of 73.8kN (actuator force 58.8kN) and a brace buckling load of 26.1kN (actuator force 20.8kN). The combined lateral force required from the actuator is approximately 84.9kN, well below the actuator capacity of 150kN.

5.4 Instrumentation of Experimental Setup

The internal load cell and LVDT in the actuator record the force and displacement, respectively at Node 12 as shown in Figure 5.3. Data recorded on the Test PC consists of displacement and force feedback from the internal LVDT and load cell in the actuator. The data is fed back from the actuator to the Test PC at the Scramnet frequency of 1/1024s. Data recorded on the Host PC consists of displacement and force feedback from the STS PC at larger time steps equal to the integration step for the particular earthquake record e.g. typically 0.01s. Refer to Chapter Four, Section 4.5.1 for a more detailed description of the test procedure and data communication.

External LVDT's are located at Node 12 and Node 13 as indicated in Figure 5.3. The LVDT at Node 12 provides an external verification measure for the internal LVDT in the actuator. The LVDT at Node 13 measures the out-of-plane displacement of the concentric bracing. The LVDT's used in the experimental programme are RDP ACT 2000C displacement transducers with a range of ±50mm and a ±0.5mm linearity error.

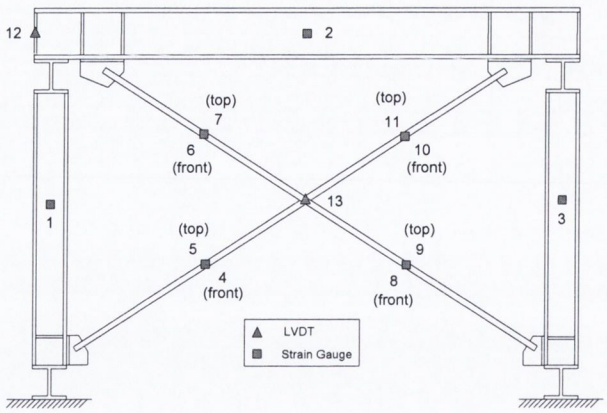

Figure 5.3: Locations of strain gauges and LVDT's on experimental set-up

Strain gauges were used to record the strain at different locations on the test frame. The strain gauges used were Radionics Ltd. mild steel foil gauges, 5mm in length with a resistance of 120Ω and a measurable strain of 3-4%. Each test specimen had 11 No. strain gauges attached at various locations as indicated in Figure 5.3. As can be seen in Figure 5.3, strain gauges Nos. 1 & 3 were used to record the strain (and corresponding axial load by calculation) in the two columns. Similarly, strain gauge No. 2 was used to record the strain (and corresponding axial load by calculation) in the beam. Strain gauges Nos. 3-11 were used to record the strain in the brace members at the locations of expected yield. For example as shown in Figure 5.3, strain gauge No. 6 is located on the front face of the braced section and records the out-of-plane buckling strain at mid-span of the brace. Strain gauge No. 7 is located on the top face of the braced section and records the in-plane buckling strain at mid-span of the brace.

5.5 Numerical Modelling of Experimental Set-up

This section will detail the numerical modelling of the test set-up using OpenSees. As discussed previously, various considerations in the design of the frame were tailored to the actuator capacity, reaction frame size and realism of the test structure. Details of the numerical modelling assumptions and aspects of the model, including sensitivity analyses on the test model, will be discussed.

The numerical model used in the sensitivity analysis is based on 3D dynamic models from Chapter Three. Nonlinear beam-column elements with fiber cross sections defining the sectional properties of the member under consideration are used as frame elements. Elastic

elements are used to define elements with elastic sectional properties of the member. A recap of the modelling parameters as follows:

- Nonlinear beam column element used to represent the brace members
- 2 No. elements to represent brace member
- 0.1% out-of-plane lack of straightness at the mid-length node to induce buckling in brace members
- 7 No. integration points along each element
- Dynamic analysis carried out using HHT and Krylov Newton algorithm
- Constraints applied using penalty method
- Giuffré-Menegotto-Pinto uniaxial steel material model (Menegotto and Pinto, (1973)))

Within the sensitivity analysis, the number of cross section subdivisions of each patch element making up the cross-sectional representation of the member at each integration point will be varied.

5.5.1 Sensitivity Analysis

To ensure that the computation of the command displacement does not result in an excessively long hold phase in the event driven strategy, the numerical model needs to be computationally efficient. Reducing the computational effort and time required in the numerical integration step is achieved by trying to ensure the number of iterations remains small and the hold phase in the event driven strategy is not required. An example of such a strategy to reduce the computational effort is given by Stauffer et al., (2007), where the FEM complexity and size of the proposed structural model was reduced in order to run a fast hybrid test as efficiently as possible at the CU NEES FHT laboratory (University of Colorado). Reducing the number of integration points and using linear elements where applicable are examples of ways of reducing the computational effort whilst maintaining the numerical accuracy of the model. A sensitivity analysis was therefore carried out to optimise the OpenSees model for the twin goals of accuracy and efficiency. The sensitivity analysis composed of comparing key results and computation times for five different modelling strategies, each involving varying levels of model complexity. The numerical model used in the sensitivity analysis has idealised pinned connections representing the support conditions.

The parameters of the full three-dimensional model of the plan irregular structure used to assess the different strategies are:

- Brace members of slenderness 1.68
- Plan aspect ratio of 2.0
- No mass eccentricity
- Lateral torsional frequency ratio of 1.0 i.e. neither torsionally stiff nor torsionally flexible
- Taiwan earthquake excitation (N-S component recorded at Smart1 11/14/86) scaled 200%

The following five modelling strategies were investigated to the full three-dimensional numerical model of the plan irregular structure in order to reduce the computational effort and time;

Strategy 1: Full Model – Nonlinear Beam, Column and Brace Elements

Strategy 2: As per Strategy 1 with Beams as Elastic Elements

Strategy 3: As per Strategy 2 with Reduced Column & Brace Element Subdivisions

Strategy 4: As per Strategy 3 with Reduced Column & Brace Member Subdivisions

Strategy 5: As per Strategy 4 with Elastic Column Elements

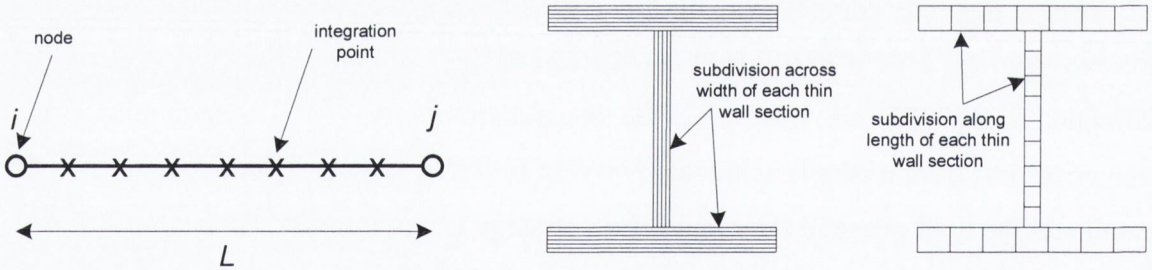

Figure 5.4: Categories of numerical subdivisions implmented in modelling strategies (left) integration points along an element, (centre) subdivisions across width of thin wall sections and (right) subdivisions along length of thin wall sections

The subdivisions for the finite elements composing the members are categorised as follows:

A: Number of integration points along the length of each element

B: Number of cross section subdivisions across the width of each thin wall of the section

C: Number of cross section subdivisions along the length of each thin wall of the section

Table 5.2: Model strategies and subdivisions

Strategy No.	*Beam*			*Column*			*Brace*		
	A	*B*	*C*	*A*	*B*	*C*	*A*	*B*	*C*
No. 1	7	7	15	7	7	15	7	7	15
No. 2	Elastic	Elastic	Elastic	7	7	15	7	7	15
No. 3	Elastic	Elastic	Elastic	7	5	10	7	5	10
No. 4	Elastic	Elastic	Elastic	7	3	5	7	3	5
No. 5	Elastic	Elastic	Elastic	Elastic	Elastic	Elastic	7	3	5

The categories of the subdivisions used in the proposed modelling strategies are illustrated in Figure 5.4. In each three-dimensional model, the beams, columns and braces have model refinements as set out in Table 5.2. For example, Strategy No. 2 has elastic beam-column elements modelling the beam members (A, B, C = Elastic). The column members are modelled as nonlinear beam-column elements with 7 No. integration points along the length of each element, 7 No. cross section subdivisions across the width of each thin wall of the section and 15 No. cross section subdivisions along the length of each thin wall of the section (A = 7, B = 7, C = 15). The brace members are modelled as nonlinear beam-column elements with 7 No. integration points along the length of each element, 7 No. cross section subdivisions across the width of each thin wall of the section and 15 No. cross section subdivisions along the length of each thin wall of the section (A = 7, B = 7, C = 15).

Table 5.3: Reduced computational effort strategies

Strategy No.	*Fundamental Period (s)*	*Time to execution (s)*	*Percentage Quicker (%)*	*Peak Displacement (mm)*	*Percentage Difference (%)*
Strategy 1	0.267	1332.9	0.0	2.42	0.0
Strategy 2	0.291	1110.2	16.7	2.49	2.7
Strategy 3	0.291	771.9	42.1	2.50	2.9
Strategy 4	0.352	544.8	29.1	1.26	48.2
Strategy 5	0.449	502.7	62.3	1.01	58.3

The simulations were performed on a Dell Optiplex 760 with an Intel Core Duo E4800 3.0 GHz Processor with 3.25GB of RAM using Windows XP. The results of the reduced

computational effort sensitivity analysis of the above mentioned strategies for the SS of the structure are given in Table 5.3. The results indicate an expected reduction in computational time and an increase in relative error with a reduction of computational complexity. The peak roof displacement is used as the reference for accuracy to compare each of the Strategies. The fundamental period of the structure is also used as a guide to model strategy accuracy. From the results in Table 5.3, Strategy 3 was selected for use in future models, as it predicts a similar fundamental period as Strategy 1 (the most complex model), with a relative peak displacement error of only 2.9%. Strategy 3 is 42.1% quicker than Strategy 1, giving Strategy 3 an improved chance of not requiring a hold-phase during the hybrid test. The displacement errors in Strategy Nos. 4 & 5 (48.2% & 58.3% respectively) combined with incorrect fundamental periods means these strategies have too large errors to be used as the modelling strategy. It can be seen that in Strategy 5, having elastic column members resulted in a significant impact on the predictions of fundamental period and peak displacement. Comparing Strategy 1 and Strategy 5, the axial and lateral load in a column member is underestimated by 13% and 42%, respectively (results not shown here). The elastic rather than nonlinear beam-column representation of the column members significantly underestimates the lateral force. The reason for this is that nonlinear element used here is force based and considers the spread of plasticity along the element, whereas the elastic element provides an estimation of force based on sectional properties alone.

5.5.2 Final Numerical Model of Test Frame

The numerical modelling approach using OpenSees for concentrically braced structures subjected to earthquake excitation was described in Chapter Three, Section 3.5. As per the dynamic validation tests in Section 3.5, the importance of the stub section being explicitly modelled was shown. Preliminary hybrid test data was used to validate the computational model. The important aspects of the numerical model representation of the test structure are as follows (as per Strategy 3):

- Columns are modelled with nonlinear beam-column elements with 7 No. integration points along their length and subdivided across their section into 10 No. elements along each thin-walled section and 5 No. elements across thin-walled section.

- Beams are modelled with elastic beam column elements with relevant section properties defined.
- Brace members are modelled with nonlinear beam-column elements with 7 No. integration points along their length and subdivided across their section into 10 No. elements along each thin-walled section and 5 No. elements across thin-walled section. The initial out-of-plane camber is 0.1% of the brace member's length.
- The gusset plates were modelled as elastic beam-column elements with a relatively high stiffness to replicate the structural stiffness of the gusset plates in the test set-up.
- The stub sections were modelled explicitly as nonlinear beam-column elements. One beam-column element represented one of the section flanges with length equal to the flange thickness and fiber cross section defined as the in-plan dimensions of the flange. The other flange of the stub section was similarly defined. The web was represented by a nonlinear beam-column element with length equal to the height of the web and fiber cross section defined as the in-plan dimensions of the web.
- Gravity loads were not applied to the structure because the stub sections would fail due to buckling of the web section under gravity load.

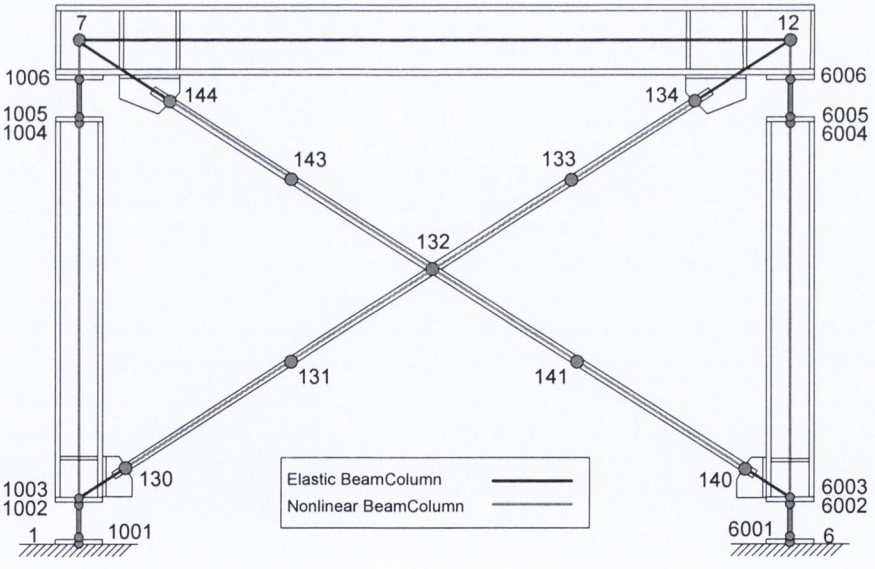

Figure 5.5: Elevation view of numerical representation of test structure (actuator and reaction frame not shown)

The final numerical model representation of the test frame can be seen in Figure 5.5. Note the nonlinear beam-column elements representing the column and bracing members. The

beam and gusset plates are modelled using elastic beam-column elements. The end restraint of the over-designed gusset plates was expected to result in a fixed connection in-plan and a semi-rigid connection out-of-plane. The over-design of the gusset plates in conjunction with the expected response resulted in the gusset plates being modelled as elastic beam-column elements with a high elastic stiffness.

The remainder of the proposed three-storey concentrically braced structure is numerically modelled as part of the numerical substructure. The FS first-storey braced frame is modelled as per the test structure. However, the upper storeys are modelled with idealised pinned connections rather than modelling the pinned joints as per the test column stub connections. The main reason for this is to reduce the uneccesary complexity of the numerical model.

5.6 Hybrid Test Representation

The final combined computational and hybrid simulation model in OpenFresco will be presented in this section. Details of the hybrid test implementation and numerical representation of the physical substructure will be given.

5.6.1 Hybrid Test Substructure

In order to undertake a substructured hybrid test using OpenFresco, the structural properties of the physical substructure need to be made available for OpenFresco. The experimental substructure needs to be explicitly defined in OpenFresco. An initial stiffness matrix for a beam column element is used as a structural simplification for the SS first storey concentrically braced frame. Figure 5.6 indicates the soft-RTHT substructure simplification required to perform the test. The initial stiffness of the physical substructure is required by OpenFresco to calculate the first command displacement for the actuator. When OpenSees is used as the finite element software the experimental element is directly embedded in OpenFresco. The experimental element therefore acts like a regular element in OpenSees. There is a high degree of compatability between OpenFresco and OpenSees as compared to other computational drivers because OpenFresco was initially developed

with OpenSees in mind as the companion finite element software. At runtime, OpenSees has direct access to the all the OpenFresco commands (Schellenberg, (2008)).

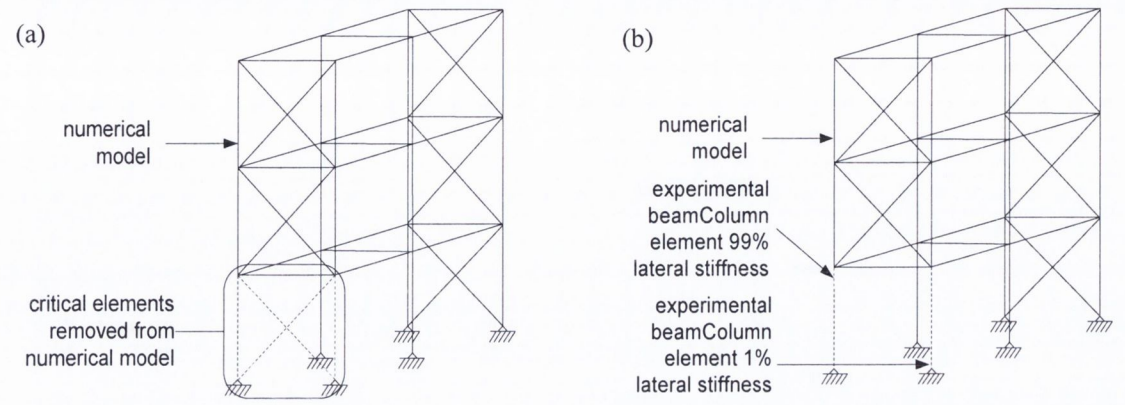

Figure 5.6: Concentrically braced three-storey steel structure (lumped masses not shown) (a) purely numerical model indicating critical elements and (b) numerical model including experimental elements

Three different approaches were attempted to replicate the physical substructure shown in Figure 5.6(a) in OpenFresco, and are summarised as follows;

1. One cantilever column with lateral stiffness of the physical substructure. The initial stiffness was obtained by performing preliminary tests on the physical substructure. cantilever was required to ensure stability of the structure. The cantilever column was located at the centre of the bay with a fixed-fixed end connectivity. The beam supported by the cantilever had a high stiffness to prevent deflection. This approach proved unsuccessful as the OpenFresco model was unstable.
2. An approach to represent the lateral stiffness of the physical substructure using two column members similar to that shown in Figure 5.6(b). In order to provide stability to the structure, two cantilever columns with fixed-pinned connectivity were used. The lateral stiffness of the concentrically braced frame was applied to both members with each column having 50% of the lateral stiffness. Somewhat surprisingly, this approach proved unsuccessful as the OpenFresco model was unstable.
3. The approach shown in Figure 5.6(b) was then implemented. In this approach, 99% of the lateral stiffness provided by the frame was applied to one of the column members (LHS column) and 1% of the lateral stiffness was applied to the other column member (RHS column) as shown in Figure 5.6(b). Both cantilever elements had an axial stiffness equal to that of the actual test columns. With only one actuator available for testing, the experimental element with 1% lateral stiffness was simulated using SimDomain in OpenFresco. The force and displacement feedback from the experiment were taken from

the experimental beam-column element that had 99% of the braced frame lateral stiffness. This approach proved successful.

The approach taken in OpenFresco to replicate the lateral stiffness of the physical substructure using the experimental beam-column element defined in OpneFresco with 99% of the lateral stiffness in one element is valid because with only one actuator, only one degree of freedom at one node location can be tested. However, it would be expected that the 50% lateral stiffness approach should have also been successful. OpenFresco is requires continuous input from users in order to develop, so it is not unexpected for certain aspects to require further investigation.

Appendix C1 contains the hybrid test two-dimensional model script and Appendix C2 contains the OpenSees two-dimensional model script of the experimental structure used in the experiments. Appendix C3 contains the hybrid test three-dimensional model script and Appendix C4 contains the final OpenSees model three-dimensional script of the overall structure.

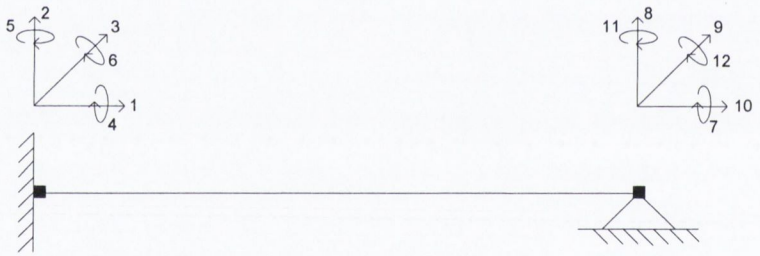

Figure 5.7: Fixed-pinned space frame element degrees-of-freedom

As mentioned above, the initial stiffness matrix of the experimental elements needed to be defined for the hybrid test. In the implementation described above, the braced frame is represented by two column elements with fixed-pinned end fixities. The initial stiffness matrix for the beam-column element was derived from a space frame element for the three-dimensional model as shown in Figure 5.7. The stiffness matrix for a fixed-pinned beam-column element in three-dimensions shown in Figure 5.7 is given below;

$$K_E = \begin{bmatrix} \frac{AE}{L} & 0 & 0 & 0 & 0 & 0 & \frac{-AE}{L} & 0 & 0 & 0 & 0 & 0 \\ 0 & \frac{3EI_z}{L^3} & 0 & 0 & 0 & \frac{3EI_z}{L^2} & 0 & \frac{-3EI_z}{L^3} & 0 & 0 & 0 & 0 \\ 0 & 0 & \frac{3EI_y}{L^3} & 0 & \frac{3EI_y}{L^2} & 0 & 0 & 0 & \frac{-3EI_y}{L^3} & 0 & 0 & 0 \\ 0 & 0 & 0 & \frac{GJ}{L} & 0 & 0 & 0 & 0 & 0 & \frac{-GJ}{L} & 0 & 0 \\ 0 & 0 & \frac{3EI_y}{L^2} & 0 & \frac{3EI_y}{L} & 0 & 0 & 0 & \frac{-3EI_y}{L^2} & 0 & 0 & 0 \\ 0 & \frac{3EI_z}{L^2} & 0 & 0 & 0 & \frac{3EI_z}{L} & 0 & \frac{-3EI_z}{L^2} & 0 & 0 & 0 & 0 \\ \frac{AE}{L} & 0 & 0 & 0 & 0 & 0 & \frac{AE}{L} & 0 & 0 & 0 & 0 & 0 \\ 0 & \frac{-3EI_z}{L^3} & 0 & 0 & 0 & \frac{-3EI_z}{L^2} & 0 & \frac{3EI_z}{L^3} & 0 & 0 & 0 & 0 \\ 0 & 0 & \frac{3EI_y}{L^3} & 0 & \frac{-3EI_y}{L} & 0 & 0 & 0 & \frac{3EI_y}{L^3} & 0 & 0 & 0 \\ 0 & 0 & 0 & \frac{-GJ}{L} & 0 & 0 & 0 & 0 & 0 & \frac{GJ}{L} & 0 & 0 \\ 0 & 0 & 0 & 0 & 0 & 0 & 0 & 0 & 0 & 0 & 0 & 0 \\ 0 & 0 & 0 & 0 & 0 & 0 & 0 & 0 & 0 & 0 & 0 & 0 \end{bmatrix} \quad (5.1)$$

where; E is the Young's Modulus (N/mm^2)

A is the area of the section (mm^2)

I_z is the second moment of area about the major-axis (mm^4)

I_y is the second moment of area about the major-axis (mm^4)

G is the shear modulus (N/mm^2)

J is the torsional constant of the section (mm^4)

L is the effective length of the member (mm)

The 12x12 cantilever space frame stiffness matrix in Equation 5.1 can be reduced. Degrees of freedom 1-6 are all zero due to the cantilever fixity; therefore the stiffness matrix reduces to:

$$K_E = \begin{bmatrix} \frac{AE}{L} & 0 & 0 & 0 & 0 & 0 \\ 0 & \frac{3EI_z}{L^3} & 0 & 0 & 0 & 0 \\ 0 & 0 & \frac{3EI_y}{L^3} & 0 & 0 & 0 \\ 0 & 0 & 0 & \frac{GJ}{L} & 0 & 0 \\ 0 & 0 & 0 & 0 & 0 & 0 \\ 0 & 0 & 0 & 0 & 0 & 0 \end{bmatrix} \quad (5.2)$$

The major axis second moment of area (I_z) of the bracing members provide the lateral stiffness in the major axis (i.e. in the plane of the test frame) and the minor axis second

moment of area (I_y) of the column sections provide the stiffness in the minor axis (i.e. out of the plane of the test frame).

The stiffness matrix given in Equation 5.2 was used as the initial stiffness of the physical substructure in OpenFresco. One experimental element (LHS column in Figure 5.4(b)) had 99% of the in-plane lateral stiffness and the same axial and torsional stiffness of the initial stiffness matrix in Equation 5.2. The other experimental element (RHS column in Figure 5.4(b)) had 1% of the in-plane lateral stiffness and the same axial and torsional stiffness of the initial stiffness matrix in Equation 5.2. Refer to Appendix C3 for details of the OpenFresco model of the test structure incorporating the experimental element stiffness matrix.

5.6.2 Hybrid Test Numerical Integration

As mentioned in Chapter Four, the explicit Newmark integrator has been widely used in hybrid testing due to its computational efficiency. The explicit Newmark with fixed number of iterations was utilised during this research. A fixed number of iterations (maximum of 5 No. iterations chosen) were used throughout the testing to prevent excessive iteration during an integration time step. An excessive number of iterations in the integration time steps would result in delay in the command displacement for the next time step being sent to the actuator. This could result in a hold and pause phase in the soft-RTHT procedure causing unwanted force relaxation in the experimental specimen. Simulations of each experiment were undertaken prior to the test being performed to ensure no excessive hold phases and possible timing out of the numerical integration would occur.

Other available methods of numerical integration in OpenFresco include the collocation method, HHT method and the α-OS method. The explicit Newmark with fixed number of iterations was found to be the simplest and most reliable numerical integrator during preliminary testing. The explicit Newmark method with fixed number of iterations consistently resulted in the no timing-out during simulations and was chosen mainly for this reliability.

5.7 Chapter Overview

This chapter has described the key parameters affecting the seismic response of braced plan irregular structures and the investigation of these parameters in the experimental programme. The design of the experimental set-up was detailed, including practical and numerical modelling considerations. A sensitivity analysis was undertaken to ensure an adequate numerical model representation was chosen. The final soft-RTHT numerical and physical substructures were described in detail in this chapter. The next chapter will detail the test results obtained from the experimental programme.

CHAPTER SIX – Experimental Results

6.1 Introduction

This chapter presents the experimental results from four series of tests (24 No. tests in total). The schedule of tests is shown in Table 6.1. The tests are divided into four categories representing different levels of slenderness and lateral torsional frequency ratio, as discussed in Chapter Five, Section 5.3.

Each series of tests is referred to as Test 1, Test 2, Test 3 and Test 4, and each sub-test is referred to as Test 1A, Test 1B, Test 1C, etc as per Table 6.1. The tests conducted without braces were used to gauge the contribution of the pinned frame to the overall lateral stiffness (Test 1A, Test 2A, Test 3A & Test 4A). In effect, these tests evaluated how well the column stub connections replicated idealised pinned connections. An elastic cyclic sawtooth test was then performed on the test structure with the concentric bracing present to determine the initial stiffness of the test frame (Test 1B, Test 2B, Test 3B & Test 4B). Next, a two-dimensional elastic test was performed to validate the two-dimensional numerical model (Test 1C, Test 2C, Test 3C & Test 4C). A three-dimensional elastic test was performed to validate in the elastic region the three-dimensional numerical model against the test results (Test 1D, Test 2D, Test 3D & Test 4D) and a three-dimensional inelastic test was then performed to validate the inelastic region of the three-dimensional numerical model against the test results (Test 1E, Test 2E, Test 3E & Test 4E). Finally, a three-dimensional inelastic test with increased level of ground acceleration input excitation was performed to damage the test specimens to a greater extent than the previous inelastic test (Test 1F, Test 2F, Test 3F & Test 4F).

Two- and three-dimensional numerical models will be validated against test results by comparing roof displacement and acceleration on the SS of the structures. The base shear versus displacement hysteresis plots will provide a force equilibrium check between the test and numerical model. The test and numerically modelled strain in the braces will also be compared.

Table 6.1: Summary of test schedule

Test ID	*Input Excitation*	*Test Type*	*Scaling Factor*	*Brace Size*	$\overline{\lambda}$	e_s	Ω_θ
1A	Cyclic	Elastic	-	No Braces	1.68	0.15	0.75
1B	Cyclic	Elastic	-	30x30x3SHS	1.68	0.15	0.75
1C	Scaled Taiwan 2D	Elastic	0.03	30x30x3SHS	1.68	0.15	0.75
1D	Scaled Taiwan 3D	Elastic	0.4	30x30x3SHS	1.68	0.15	0.75
1E	Taiwan 3D	Inelastic	1.0	30x30x3SHS	1.68	0.15	0.75
1F	Scaled Taiwan 3D	Inelastic	2.0	30x30x3SHS	1.68	0.15	0.75
2A	Cyclic	Elastic	-	No Braces	1.57	0.15	0.75
2B	Cyclic	Elastic	-	50x30x3RHS	1.57	0.15	0.75
2C	Scaled Taiwan 2D	Elastic	0.03	50x30x3RHS	1.57	0.15	0.75
2D	Scaled Taiwan 3D	Elastic	0.4	50x30x3RHS	1.57	0.15	0.75
2E	Taiwan 3D	Inelastic	1.0	50x30x3RHS	1.57	0.15	0.75
2F	Scaled Taiwan	Inelastic	2.0	50x30x3RHS	1.57	0.15	0.75
3A	Cyclic	Elastic	-	No Braces	1.68	0.15	1.25
3B	Cyclic	Elastic	-	30x30x3SHS	1.68	0.15	1.25
3C	Scaled Taiwan 2D	Elastic	0.03	30x30x3SHS	1.68	0.15	1.25
3D	Scaled Taiwan 3D	Elastic	0.4	30x30x3SHS	1.68	0.15	1.25
3E	Taiwan 3D	Inelastic	1.0	30x30x3SHS	1.68	0.15	1.25
3F	Scaled Taiwan	Inelastic	2.0	30x30x3SHS	1.68	0.15	1.25
4A	Cyclic	Elastic	-	No Braces	1.57	0.15	1.25
4B	Cyclic	Elastic	-	50x30x3RHS	1.57	0.15	1.25
4C	Scaled Taiwan 2D	Elastic	0.03	50x30x3RHS	1.57	0.15	1.25
4D	Scaled Taiwan 3D	Elastic	0.4	50x30x3RHS	1.57	0.15	1.25
4E	Taiwan 3D	Inelastic	1.0	50x30x3RHS	1.57	0.15	1.25
4F	Scaled Taiwan 3D	Inelastic	2.0	50x30x3RHS	1.57	0.15	1.25

6.2 TEST 1 Experimental Results

The following section will detail the experimental results obtained for both elastic and inelastic tests of the group TEST 1 experiments. These tests employed 30x30x3mm SHS concentric brace specimens with normalised slenderness of 1.68. The main test results for each sub-test will be given, including a brief description of the results.

6.2.1 TEST 1A – Cyclic Sawtooth: No Braces

TEST 1A was used to calculate the stiffness of the test frame without any braces providing lateral stiffness. The displacement and force feedback from the experiment were used to calculate the lateral stiffness of the unbraced test frame as 30N/mm.

6.2.2 TEST 1B – Cyclic Sawtooth: With Braces

TEST 1B was used to calculate the initial lateral stiffness of the concentrically braced test frame. The displacement and force feedback from the experiment were used to calculate the lateral stiffness of the test frame with braces, which was calculated as 9995N/mm. This value represents the lateral stiffness of the experimental element in the hybrid test model (refer to Chapter Five, Section 5.6 for details) which is input into the OpenFresco model in subsequent tests (TESTS 1C-F). The test data from TEST 1B are presented in Appendix D1.

6.2.3 TEST 1C – 2D Elastic

In TEST 1C the response of the test structure to earthquake ground motion was examined in a hybrid test. The scaled Taiwan ground acceleration time history used in the experiment is presented in Figure 6.1. The peak ground acceleration is 0.005*g*.

The main results from the test can be seen in Figure 6.2 to Figure 6.4. The maximum lateral displacement of the roof during the test was 3.34mm, as shown in Figure 6.2. As can be seen in Figure 6.2, the variation in lateral roof displacement throughout the test matches the numerical model predictions well, with a 4.9% difference in peak lateral displacement. The periods of the test structure and numerical model show good agreement. Similarly, as can be seen in Figure 6.3, the variation in lateral roof acceleration throughout the test matches the numerical predictions well, with a 4.2% difference in peak lateral acceleration. A maximum lateral roof acceleration of -0.08m/s^2 was observed during the test.

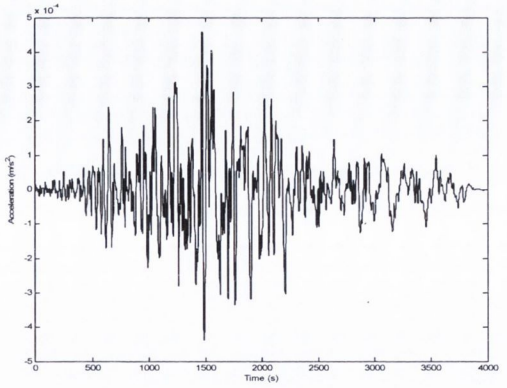

Figure 6.1: Scaled Taiwan input time history for elastic 2D test

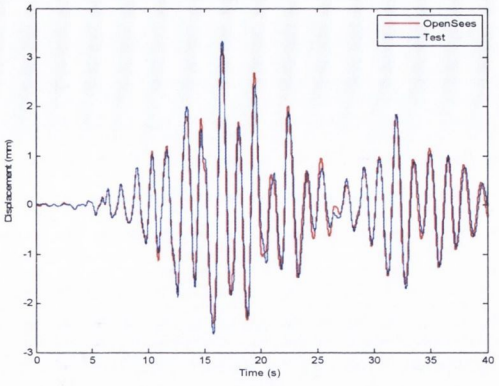

Figure 6.2: Graph of roof displacement vs. time for OpenSees model and test results

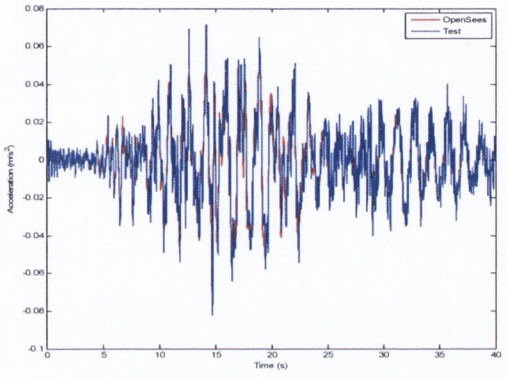

Figure 6.3: Graph of roof acceleration vs. time for OpenSees model and test results

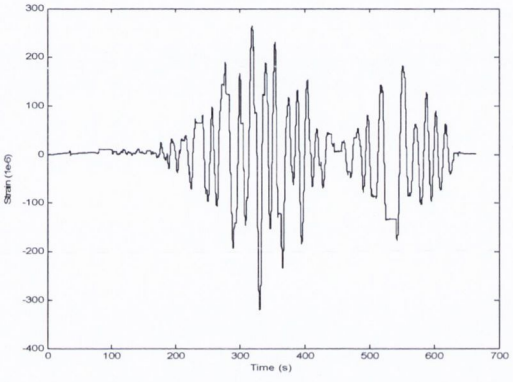

Figure 6.4: Graph of strain vs. time at strain gauge No. 4

The test data for strain gauge No. 4 is shown in Figure 6.4. It can be seen from Figure 6.4 the strain does not reach yield during the experiment. The other strain gauge test data from TEST 1C are presented in Appendix D2. (Refer to Chapter Five, Section 5.3 for details of the location of the strain gauges on the test structure).

6.2.4 TEST 1D – Elastic 3D: Taiwan Scaled

The three-dimensional test model in TEST 1D had a lateral torsional frequency ratio of 0.75 (i.e. torsionally flexible) and a plan aspect ratio of 2.0. Its response to the Taiwan earthquake scaled to a peak ground acceleration of 0.06*g* was examined in a hybrid test.

The main results for the test can be seen in Figure 6.6 to Figure 6.9. The maximum lateral displacement of the roof during the test was 4.52mm, as shown in Figure 6.6. As can be seen in Figure 6.6, the variation in lateral roof displacement throughout the test matches the numerical model predictions well, with a 4.6% difference in peak lateral displacement.

The periods of the test structure and numerical model show good agreement. Similarly, as can be seen in Figure 6.7, the variation in lateral roof acceleration throughout the test matches the numerical predictions well, with a 14.9% difference in peak lateral acceleration. The maximum lateral roof acceleration observed during the test was 1.34m/s^2.

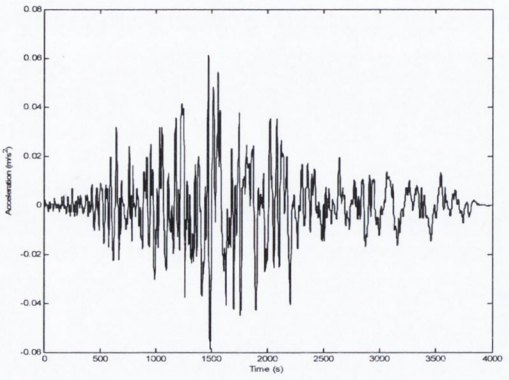

Figure 6.5: Scaled Taiwan input time history for elastic 3D test

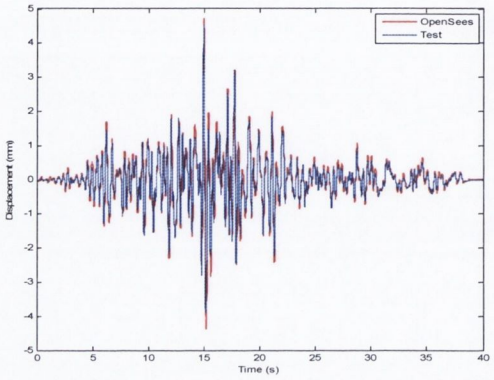

Figure 6.6: Graph of roof displacement vs. time for OpenSees model and test results

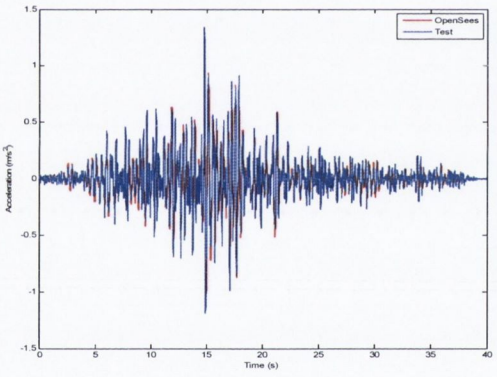

Figure 6.7: Graph of roof acceleration vs. time for OpenSees model and test data

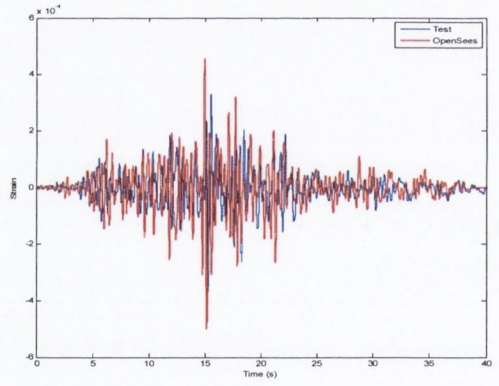

Figure 6.8: Graph of strain vs. time at strain gauge No. 4 for OpenSees model and test data

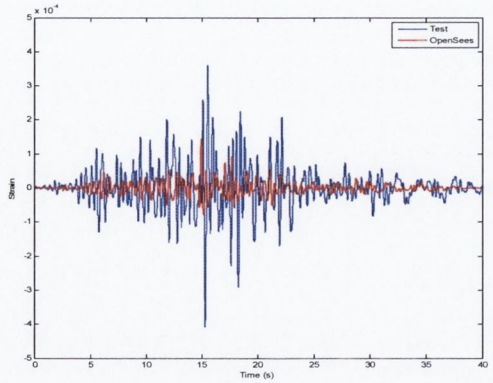

Figure 6.9: Graph of strain vs. time at strain gauge No. 5 for OpenSees model and test data

Figure 6.8 and Figure 6.9 compare the experimentally measured and numerically modelled brace strains at strain gauges No. 4 and No. 5, respectively. As can be seen from Figure 6.8, at location No. 4 the numerically modelled brace strains and the recorded strains from the experiment were in the same order of magnitude and show reasonable agreement. The peak strain recorded during the test was $-3.68e^{-4}$ whereas the peak numerically modelled strain was $-5.01e^{-4}$ representing a difference of 26.5%, with the numerically modelled strains being larger. As can be seen from Figure 6.9, the numerically modelled brace strains at stain gauge location No. 5 underestimated the recorded strains from the experiment. The peak recorded strain during the test was $-4.09e^{-4}$ whereas the peak numerically modelled strain was $-1.44e^{-4}$ representing a difference of 80.9%, with the numerically modelled strains being smaller. Although there is a considerable difference between the test strains and numerically modelled strains for strain gauge No. 5, they are of the same order of magnitude.

The results for the remainder of the strain gauges for TEST 1D are presented in Appendix D3.

6.2.5 TEST 1E – Inelastic 3D: Taiwan

The test model in TEST 1E possessed the same lateral torsional frequency ratio and plan aspect ratio as TEST 1D. In this test, an external LVDT was placed on the actuator head plate to validate the feedback displacement from the actuator internal LVDT. During the experiment, the number of iterations required by the numerical model caused the numerical integration to 'time-out' such that the numerical commands were no longer sent to the actuator and the test terminated. (There is a more detailed description of the timing-out during a test in Chapter Four, Section 4.5). The test ran for approximately 23 seconds of the simulation before this occurred. The excitation had reached maximum amplitude and was diminishing towards the end of the excitation, so the most important results were not affected by the premature end of the test.

The main results for the test can be seen in Figure 6.11 to Figure 6.19. The maximum lateral displacement of the roof during the test was 11.51mm, as shown in Figure 6.11. As can be seen in Figure 6.11, the variation in lateral roof displacement throughout the test matches the numerical model predictions well, with a 3.2% difference in peak lateral displacement. The periods of the test structure and numerical model show good agreement.

Similarly, as can be seen in Figure 6.13, the variation in lateral roof acceleration throughout the test matches the numerical predictions well, with a 13.9% difference in peak lateral acceleration. The maximum lateral roof acceleration observed during the test was 3.29m/s^2.

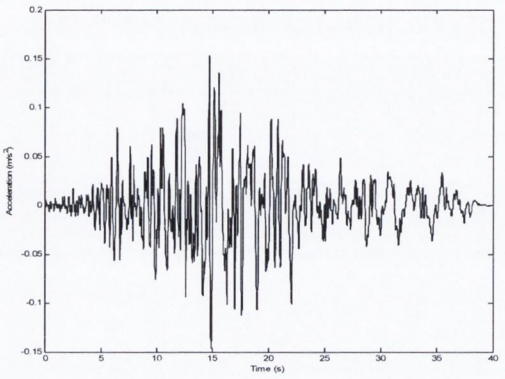

Figure 6.10: Scaled Taiwan input time history for inelastic 3D test

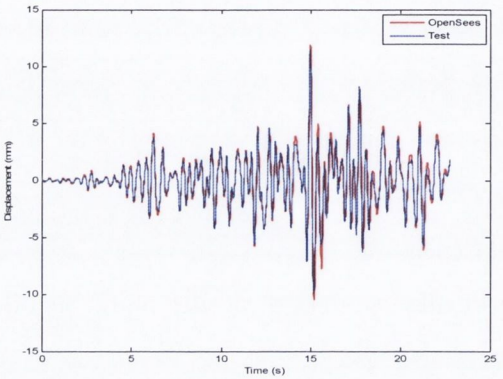

Figure 6.11: Graph of roof displacement vs. time for OpenSees model and test results

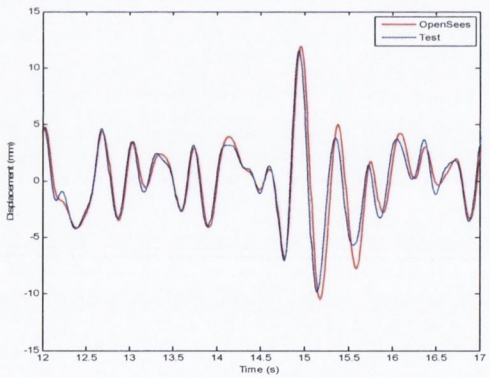

Figure 6.12: Close-up of roof displacement vs. time for OpenSees model and test data

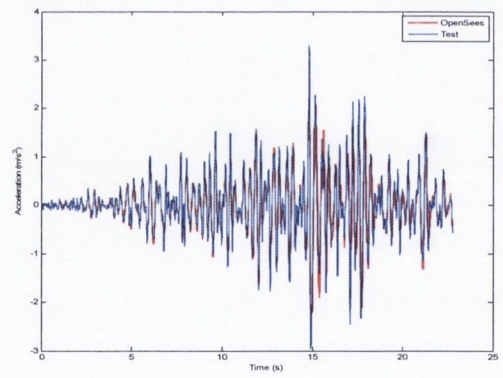

Figure 6.13: Graph of acceleration vs. time for OpenSees model and test data

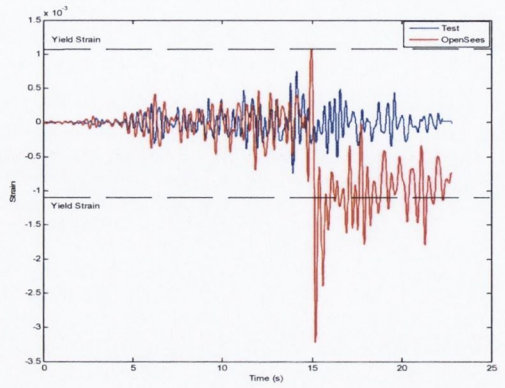

Figure 6.14: Graph of strain vs. time at gauge No. 4 for OpenSees and test data

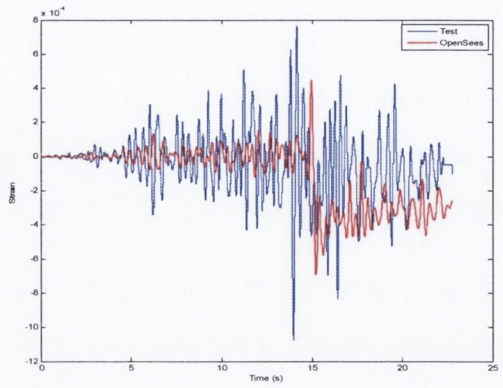

Figure 6.15: Graph of strain vs. time at strain gauge No. 5 for OpenSees model and test data

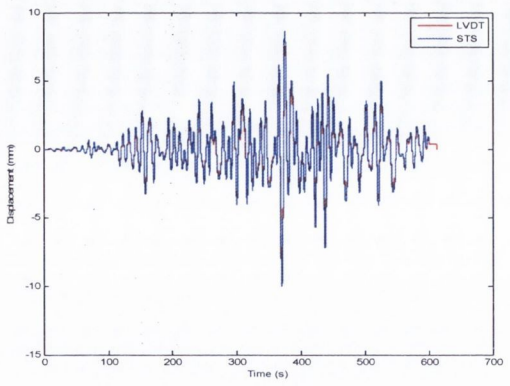

Figure 6.16: Graph of displacement vs. time for actuator with STS and LVDT

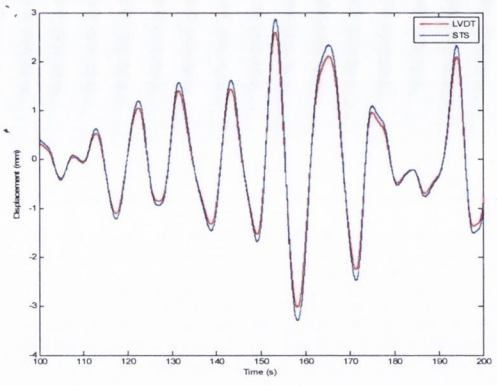

Figure 6.17: Close-up of displacement vs. time for actuator with STS and LVDT

Figure 6.14 and Figure 6.15 show the test strains and numerically modelled strains at strain gauge No. 4 and strain gauge No. 5, respectively. As can be seen from Figure 6.14 the numerically modelled strains in the bracing at stain gauge location No. 4 and the recorded strains from the experiment differ considerably, indicating poor numerical modelling of the strains at this location. The peak recorded strain during the test was $-7.38e^{-4}$. The peak numerically modelled strain was $-3.22e^{-3}$. The peak numerically modelled and peak test strains at strain gauge location No. 4 differed by 335%, with the numerically modelled strains being larger. The numerical model predicted yielding and potentially buckling of the brace member at strain gauge No. 4 at approximately 15s. The specific value of the peak strain is not as important as the information it provides in terms of possible prediction of yielding and buckling. As can be seen from Figure 6.15, the numerically modelled strains in the bracing at stain gauge location No. 5 and the recorded strains from the experiment were closer in order of magnitude: the peak recorded strain during the test being $1.08e^{-3}$, whereas the peak numerically modelled strain was $4.47e^{-4}$ representing a difference of 58.5%.

As can be seen in Figure 6.14 and Figure 6.15, the brace member did not yield during the experiment. Comparing Figure 6.14 and Figure 6.15, it is evident that the strains at strain gauge No. 4 were modelled less accurately as compared to the strains at strain gauge No. 5. A possible reason for this is that the numerical model allows for out-of-plane buckling through an initial camber in both axes of the brace members. However, in reality the brace member will predominantly buckle in one plane only, resulting in different levels of strain on each perpendicular face of the brace section. The numerical model does not account for this possible behaviour as initially it allows for the possibility of buckling in- and out-of-

plane. This behaviour was observed throughout the experimental programme where on one face of the brace section the strains are modelled more accurately compared to the face perpendicular to it.

In Figure 6.16, it can be seen that the external LVDT applied to the actuator head plate and the STS recorded actuator displacement from the internal actuator LVDT match reasonably well. Figure 6.17 is a close-up of the external LVDT and STS actuator displacements. The peak displacement error between the STS recorded data and the external LVDT was 7.9%. In the next experiment, TEST 2, it was observed that the external LVDT was calibrated incorrectly and found to have an error of 3.5%. The corrected LVDT data is shown in Figure 6.17. The error is therefore within acceptable limits. The results for strain gauge No. 4 and No. 5 are shown above, however all of the raw strain gauge data and LVDT data for TEST 1E can be found in Appendix D4.

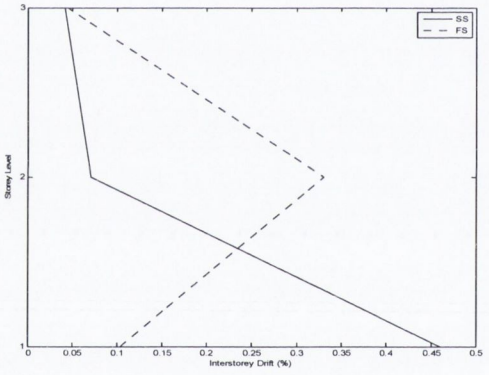

Figure 6.18: Graph of SS and FS test peak interstorey drifts

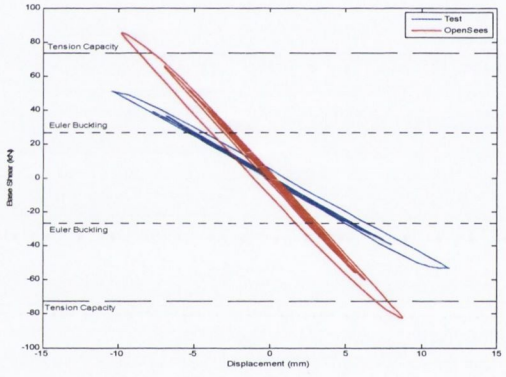

Figure 6.19: Base shear vs. displacement for OpenSees and test data

The interstorey drifts of the SS and FS of the experimental structure are shown in Figure 6.18. It can be seen from Figure 6.18 the interstorey drifts are the largest on the SS first-storey. None of the interstorey drifts exceed the assumed Eurocode 8 (CEN, (2004)) limit of 0.5%. The variation in interstorey drift between the SS and FS can be seen in Figure 6.18 and indicates the influence of a torsional rather than a purely translational response in the test structure. It should be noted that numerical substructure was modelled with idealised pinned co0nnections during each hybrid test.

The hysteresis plot of base shear against displacement for the test specimen and numerical model can be seen in Figure 6.19. As shown in Figure 6.19 the force in the brace specimens exceeds their buckling load but not their yield load. The numerical model overestimates the initial stiffness of the test specimen. The hysteresis plot for the test

shows some nonlinear behaviour with slightly reduced stiffness in one large displacement cycle. The peak ductility demand recorded during TEST 1E was 0.88, indicating the structure did not exceed yield displacement.

It should be noted that the stub connections have a significant effect on the response of the structure. The lateral force from the test is transferred to the reaction frame through shear in the stub connections. For example, in this test, 69% of the peak displacement of 9.83mm was due to the shear force in the stub section. The P-Δ effect in the column stub due to the axial load was taken into consideration in the numerical model.

6.2.6 TEST 1F – Inelastic 3D: Taiwan Scaled 2.0

The test model in TEST 1F possessed the same lateral torsional frequency ratio and plan aspect ratio as TEST 1D. The input excitation was scaled by a factor of 2.0. In this test, external LVDTs were placed on the actuator head plate and at the cross-point of the braces in order to measure out-of-plane displacement of the braces.

The main results for the test can be seen in Figure 6.21 to Figure 6.26. The maximum positive and negative lateral displacements of the roof of the structure observed during the test were 22.73mm & -18.64mm, as can be seen in Figure 6.21. The maximum numerically modelled lateral displacements were 26.09mm & -27.06mm representing a 12.9% overestimation of the observed peak lateral roof displacement on the positive side and 31.1% on the negative side. As shown in Figure 6.22 the periods of the test structure and numerical model do not show good agreement, particularly after yielding in the braces occurs at 15s. As can be seen in Figure 6.23, the test lateral acceleration at the roof matches reasonably well the numerical model. The maximum lateral roof acceleration of the structure during the test was 6.38m/s^2 as can be seen in Figure 6.23. The maximum numerically modelled lateral roof acceleration of the structure was 4.56m/s^2 as can be seen in Figure 6.23. There is a 28.6% difference in peak lateral acceleration between the numerical model and test data.

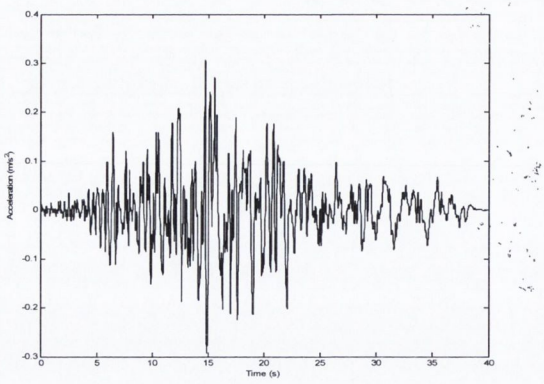

Figure 6.20: Scaled Taiwan input time history for inelastic 3D test

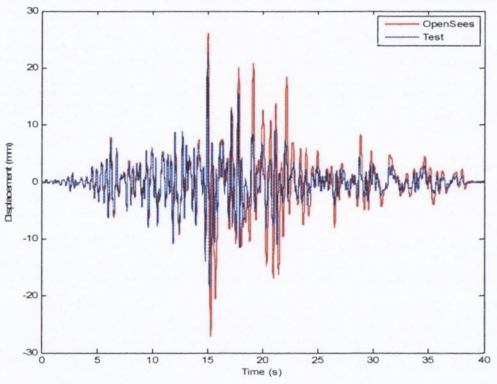

Figure 6.21: Graph of roof displacement vs. time for OpenSees model and test results

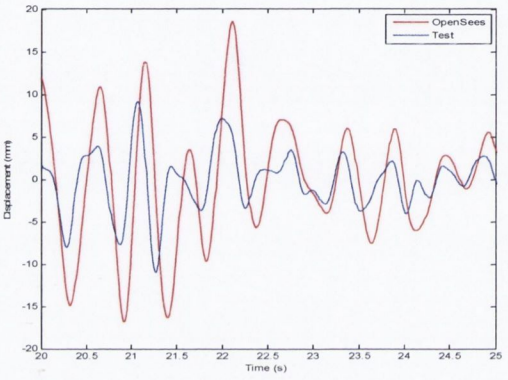

Figure 6.22: Close-up of roof displacement vs. time for OpenSees model and test data

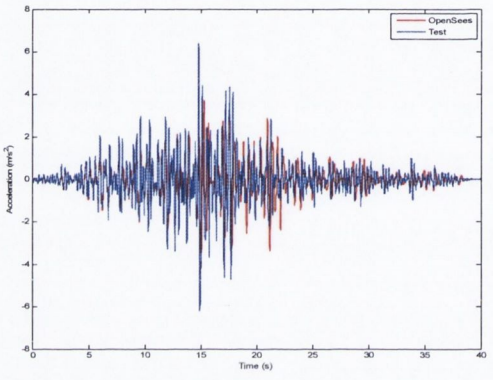

Figure 6.23: Graph of acceleration vs. time for OpenSees model and test results

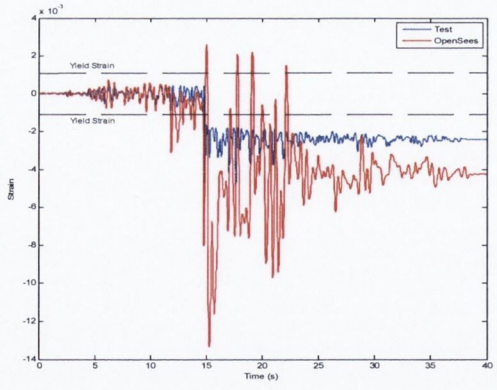

Figure 6.24: Graph of strain vs. time at gauge No. 4 for OpenSees and test data

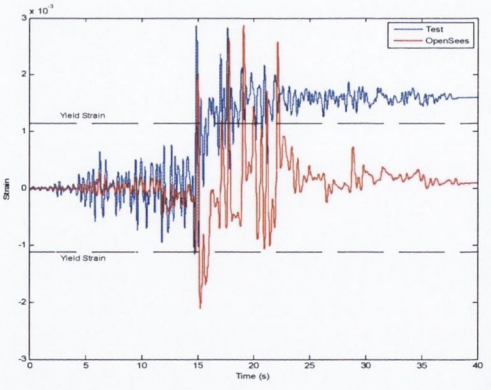

Figure 6.25: Graph of strain vs. time at strain gauge No. 5 for OpenSees model and test data

Figure 6.24 and Figure 6.23 show the test strains and numerically modelled strains at strain gauge No. 4 and strain gauge No. 5, respectively. As can be seen from Figure 6.24, the numerically modelled strains in the bracing at stain gauge location No. 4 and the recorded strains from the experiment were not in the same order of magnitude and showed poor agreement. The peak recorded strain during the test was $-4.81e^{-3}$. The peak numerically

modelled strain was $-1.34e^{-2}$. The peak numerically modelled and peak test strains at strain gauge location No. 4 differed by 64.1%, with the numerically modelled strains being larger. It can be seen from Figure 6.24 that the numerical model correctly predicts the initiation of yielding, but overestimates the strains. As can be seen from Figure 6.25, the numerically modelled strains in the bracing at stain gauge location No. 5 and the recorded strains from the experiment were in the same order of magnitude. The peak recorded strain during the test was $2.87e^{-3}$. The peak numerically modelled strain was $2.88e^{-3}$. The peak numerically modelled and peak test strains at strain gauge location No. 5 differed by 0.3%, with the numerically modelled strains being smaller. However, the negative peak numerically modelled strain overestimated the negative peak strain by 47.2% as can be seen in Figure 6.25. The numerically modelled strains at strain gauge location No. 5 underestimated the response, particularly after yielding. Although there is a considerable difference in the peak test strains and peak numerically modelled strains, particularly for strain gauge No. 4, the numerical model successfully predicts the initiation of yielding at approximately 15s.

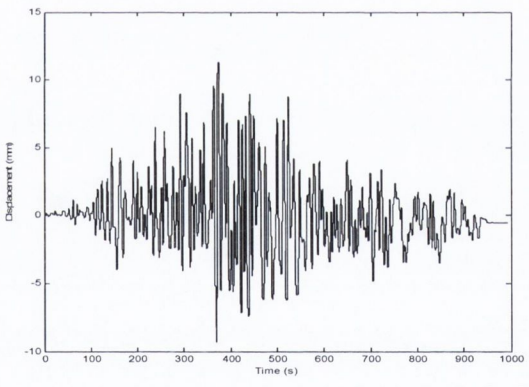

Figure 6.26: Graph of displacement vs. time for LVDT and OpenSees at Node 13

Figure 6.27: Photo of test frame after TEST 1F

Figure 6.26 shows the observed variation in the out-of-plane displacement at the cross-point node (refer to Node 13 in Figure 5.3 in Chapter Five) of the concentric bracing. The peak out-of-plane displacement was 11.3mm. The peak lateral displacement of the test was 22.73mm. The lateral displacement was approximately twice the brace out-of-plane displacement at the cross point of the braces. The displaced shape of the concentric bracing can be seen at the end of TEST 1F in Figure 6.27 showing the buckled shape of the bracing members. No local buckling was observed in either bracing member.

The results for strain gauge No. 4 and No. 5 are shown above, however all of the raw strain gauge data and LVDT data can be found in Appendix D5 for TEST 1F.

The interstorey drifts of the SS and FS of the experimental structure are shown in Figure 6.28. It can be seen from Figure 6.28 the interstorey drifts are the largest on the SS first-storey. The first-storey SS interstorey drift of 0.91% exceeded the assumed Eurocode 8 (CEN, (2004) limit of 0.5%. The variation in interstorey drift between the SS and FS can be seen in Figure 6.28 and indicates a torsional rather than a purely translational response in the test structure.

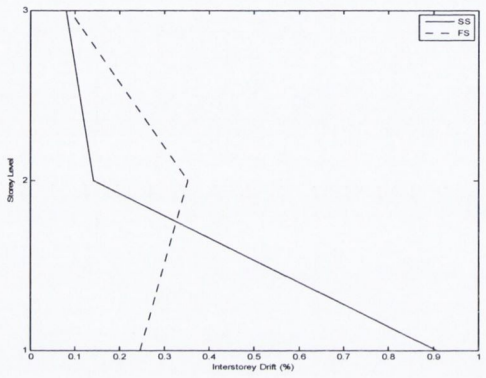

Figure 6.28: Graph of SS and FS test peak interstorey drifts

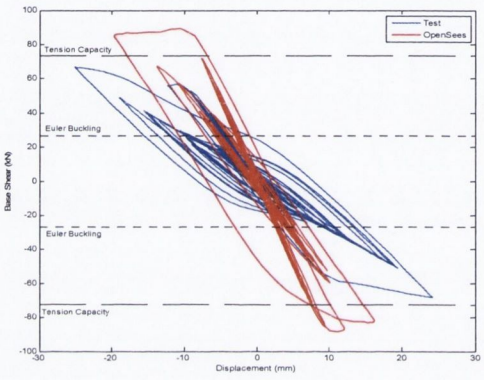

Figure 6.29: Base shear vs. displacement for OpenSees and test data

The hysteresis plot of base shear against displacement for the test specimen and numerical model can be seen in Figure 6.29. As shown in Figure 6.29 the force in the brace specimens exceeds their buckling load, but not their yield load. The numerical model overestimates the initial stiffness of the test specimen. The hysteresis plot for the test shows considerable nonlinear behaviour with severely reduced stiffness. It is thought the nonlinear behaviour in TEST 2E affected TEST 2F, as the peak ductility demand recorded during TEST1F was 1.74, indicating the structure did exceed yield displacement.

6.3 TEST 2 Experimental Results

The following section will detail the test results for both elastic and inelastic tests for all sub-tests of TEST 2. These tests employed 50x30x3mm RHS concentric brace specimens with normalised slenderness of 1.57. The main test results for each sub-test will be given, including a brief description of the results. After TEST 1F the braces were removed and

the stub connections at the base had permanent lateral deformation pushing the test columns inwards making the removal of the braces difficult. The stubs had yielded at the web to flange connection.

6.3.1 TEST 2A – Cyclic Sawtooth: No Braces

TEST 2A was used to calculate the stiffness of the test frame without any braces providing lateral stiffness. The displacement and force feedback from the experiment were used to calculate the lateral stiffness of the unbraced test frame as 38.6N/mm.

6.3.2 TEST 2B – Cyclic Sawtooth: With Braces

TEST 1B was used to calculate the initial lateral stiffness of the concentrically braced test frame. The displacement and force feedback from the experiment were used to calculate the lateral stiffness of the test frame with braces, which was calculated as 11383N/mm. This value represents the lateral stiffness of the experimental element in the hybrid test model (refer to Chapter Five, Section 5.6 for details) which is input into the OpenFresco model in subsequent tests (TESTS 2C-F). The test data from TEST 2B are presented in Appendix D6.

6.3.3 TEST 2C – 2D Elastic

In TEST 2C the response of the test structure to earthquake ground motion was examined in a hybrid test. The scaled Taiwan ground acceleration time history used in the experiment is presented in Figure 6.30. The peak ground acceleration is 0.005*g*.

The main results from the test can be seen in Figure 6.31 to Figure 6.33. The maximum lateral displacement of the roof during the test was 3.14mm, as shown in Figure 6.31. As can be seen in Figure 6.31, the variation in lateral roof displacement throughout the test matches the numerical model predictions well, with a 2.1% difference in peak lateral displacement. The periods of the test structure and numerical model show good agreement. However, as can be seen in Figure 6.32, the variation in lateral roof acceleration throughout the test matches the numerical predictions poorly, with a 30.0% difference in peak lateral acceleration. The maximum lateral roof acceleration observed during the test

was 0.08m/s^2. The low amplitude and noisy nature of the test acceleration response may be a reason for the poor predictive accuracy of the numerical model.

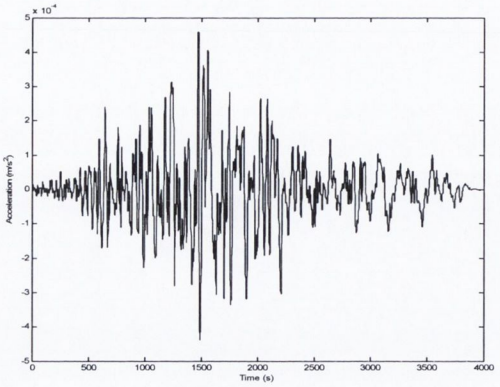

Figure 6.30: Scaled Taiwan input time history for elastic 2D test

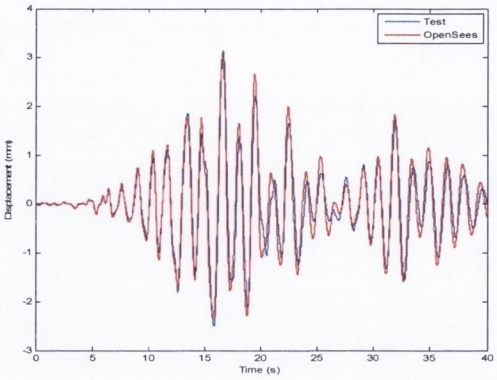

Figure 6.31: Graph of roof displacement vs. time for OpenSees model and test results

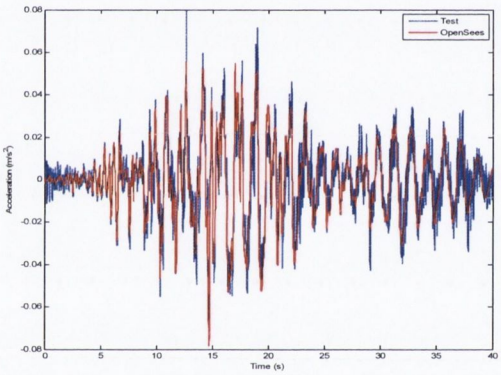

Figure 6.32: Graph of roof acceleration vs. time for OpenSees model and test results

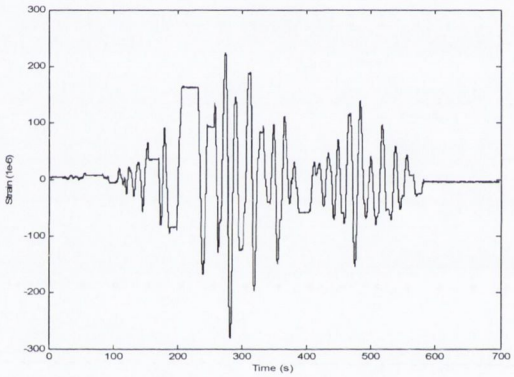

Figure 6.33: Graph of strain vs. time at strain gauge No. 4

The test data for strain gauge No. 4 is shown in Figure 6.33. It can be seen from Figure 6.33 the strain does not reach yield during the experiment. The other strain gauge test data from TEST 2C are presented in Appendix D7.

6.3.4 TEST 2D – Elastic 3D: Taiwan Scaled

The three-dimensional test model in TEST 2D had a lateral torsional frequency ratio of 0.75 (i.e. torsionally flexible) and a plan aspect ratio of 2.0. Its response to the Taiwan earthquake scaled to a peak ground acceleration of 0.06*g* was examined in a hybrid test.

The main results for the test can be seen in Figure 6.35 to Figure 6.38. The maximum lateral displacement of the roof during the test was 4.53mm, as shown in Figure 6.35. As

can be seen in Figure 6.35, the variation in lateral roof displacement throughout the test matches the numerical model predictions well, with a 4.9% difference in peak lateral displacement. The periods of the test structure and numerical model show good agreement. Similarly, as can be seen in Figure 6.36, the variation in lateral roof acceleration throughout the test matches the numerical predictions well, with an 8.9% difference in peak lateral acceleration. The maximum lateral roof acceleration observed during the test was 1.25m/s^2.

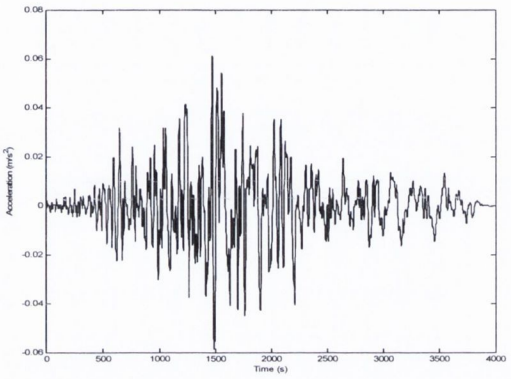

Figure 6.34: Scaled Taiwan input time history for elastic 3D test

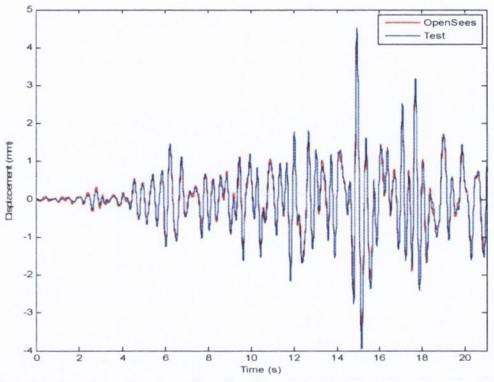

Figure 6.35: Graph of roof displacement vs. time for OpenSees model and test results

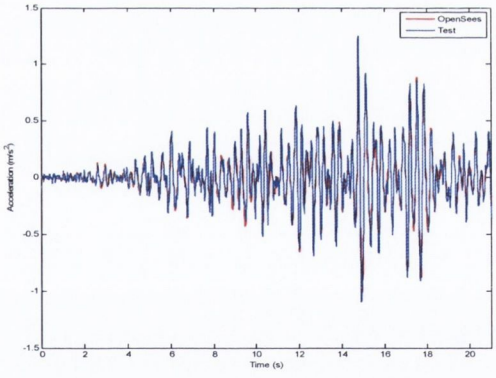

Figure 6.36: Graph of roof acceleration vs. time for OpenSees model and test data

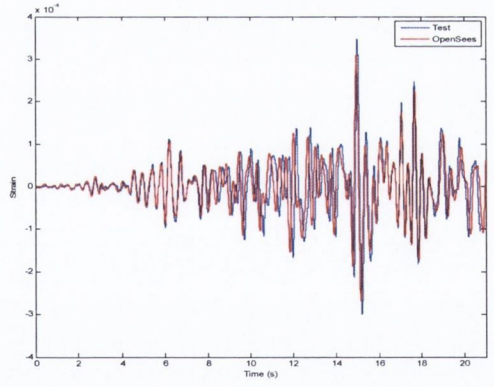

Figure 6.37: Graph of strain vs. time at strain gauge No. 4 for OpenSees model and test data

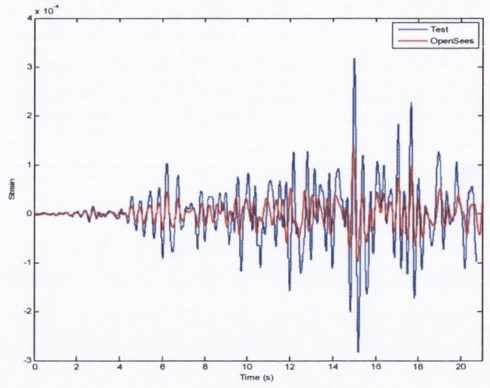

Figure 6.38: Graph of strain vs. time at strain gauge No. 5 for OpenSees model and test data

Figure 6.37 and Figure 6.38 compare the experimentally measured and numerically modelled brace strains at strain gauges No. 4 and No. 5, respectively. As can be seen from Figure 6.37, at location No. 4 the numerically modelled brace strains and the recorded strains from the experiment were in the same order of magnitude and show reasonable agreement. The peak strain recorded during the test was $-3.46e^{-4}$ whereas the peak numerically modelled strain was $-3.09e^{-4}$ representing a difference of 10.8%, with the numerically modelled strains being larger. As can be seen from Figure 6.38, the numerically modelled brace strains at stain gauge location No. 5 underestimated the recorded strains from the experiment. The peak recorded strain during the test was $3.17e^{-4}$ whereas the peak numerically modelled strain was $1.37e^{-4}$ representing a difference of 56.8%, with the numerically modelled strains being smaller. Although there is a considerable difference between the test strains and numerically modelled strains for strain gauge No. 5, they are of the same order of magnitude.

TEST 2D stopped prematurely at approximately 21 seconds during the experiment due to the numerical integration timing-out. The excitation had reached maximum amplitude and was diminishing towards the end of the excitation, so the most important results were not affected by this. The results for the remainder of the strain gauges for TEST 2D can be found in Appendix D8.

6.3.5 TEST 2E – Inelastic 3D: Taiwan

The test model in TEST 2E possessed the same lateral torsional frequency ratio and plan aspect ratio as TEST 2D. TEST 2E stopped prematurely at approximately 25.5 seconds

during the experiment due to the numerical integration timing-out. The excitation had reached maximum amplitude and was diminishing towards the end of the excitation, so the most important results were not affected by this.

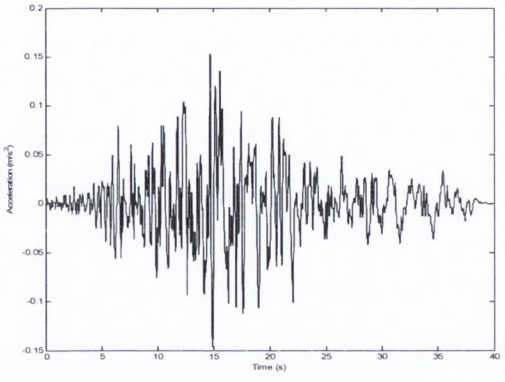

Figure 6.39: Scaled Taiwan input time history for inelastic 3D test

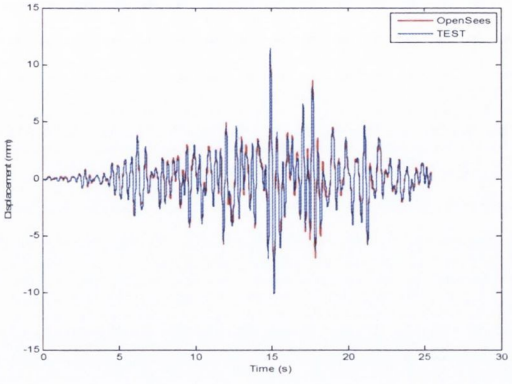

Figure 6.40: Graph of roof displacement vs. time for OpenSees model and test results

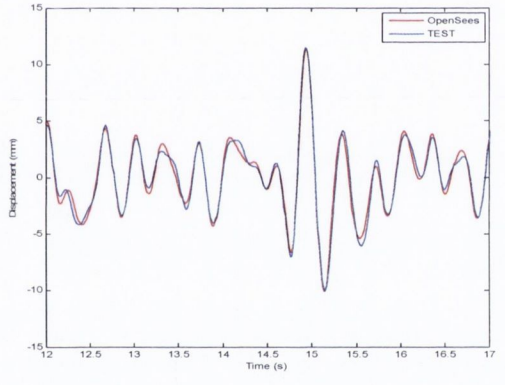

Figure 6.41: Close-up of roof displacement vs. time for OpenSees model and test

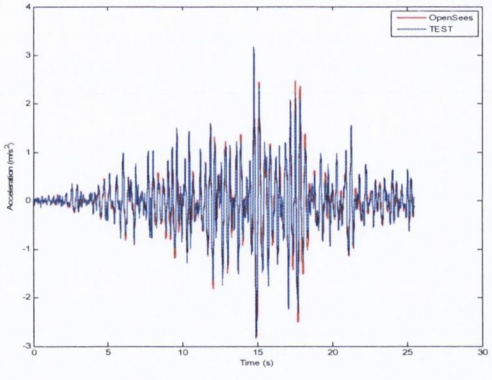

Figure 6.42: Graph of acceleration vs. time data for OpenSees model and test results

The main results for the test can be seen in Figure 6.40 to Figure 6.46. The maximum lateral displacement of the roof during the test was 11.41mm, as shown in Figure 6.40. As can be seen in Figure 6.40, the variation in lateral roof displacement throughout the test matches the numerical model predictions well, with a 0.5% difference in peak lateral displacement. As shown in Figure 6.41 the periods of the test structure and numerical model show good agreement. Similarly, as can be seen in Figure 6.42, the variation in lateral roof acceleration throughout the test matches the numerical predictions well, with a 6.4% difference in peak lateral acceleration. The maximum lateral roof acceleration observed during the test was 3.17m/s^2.

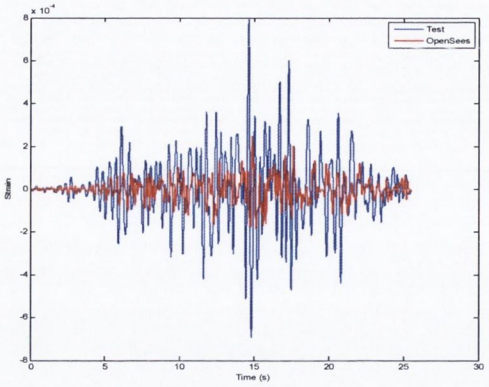

Figure 6.43: Graph of strain vs. time at gauge No. 4 for OpenSees and test data

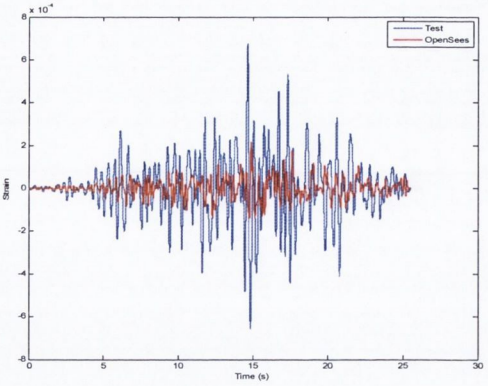

Figure 6.44: Graph of strain vs. time at strain gauge No. 5 for OpenSees model and test data

Figure 6.43 and Figure 6.44 show the test strains and numerically modelled strains at strain gauge No. 4 and strain gauge No. 5, respectively. As can be seen from Figure 6.43 the numerically modelled strains in the bracing at stain gauge location No. 4 and the recorded strains from the experiment differ considerably, indicating poor numerical modelling of the strains at this location. The peak recorded strain during the test was $7.93e^{-4}$. The peak numerically modelled strain was $2.47e^{-4}$. The peak numerically modelled and peak test strains at strain gauge location No. 4 differed by 68.8%, with the numerically modelled strains being larger. Yielding did not occur in either the test or numerical model. As can be seen from Figure 6.44, the numerically modelled strains in the bracing at stain gauge location No. 5 and the recorded strains from the experiment were in the same order of magnitude with the peak recorded strain during the test being $6.77e^{-4}$, whereas the peak numerically modelled strain was $2.15e^{-4}$ representing a difference of 68.1%.

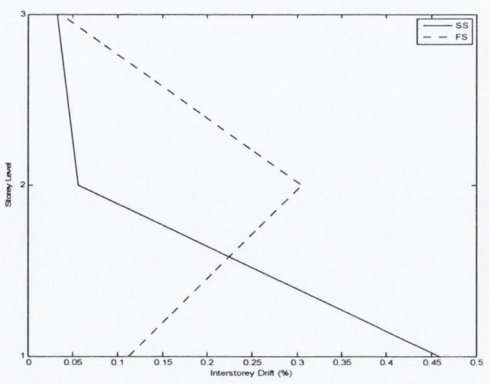

Figure 6.45: Graph of SS and FS test peak interstorey drifts

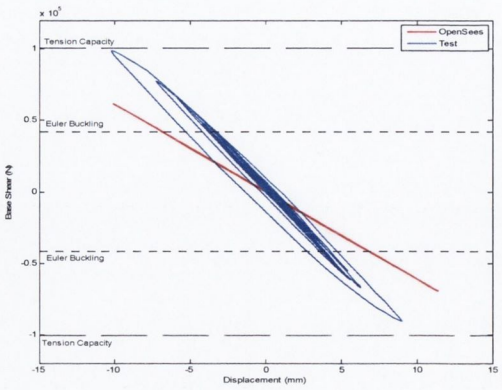

Figure 6.46: Base shear vs. displacement for OpenSees and test data

The interstorey drifts of the SS and FS of the experimental structure are shown in Figure 6.45. It can be seen from Figure 6.45 the interstorey drifts are the largest on the SS ground-storey. None of the interstorey drifts exceed the assumed Eurocode 8 (CEN, (2004) limit of 0.5%. The variation in interstorey drift between the SS and FS can be seen in Figure 6.45 and indicates a torsional rather than a purely translational response in the test structure.

The hysteresis plot of base shear against displacement for the test specimen and numerical model can be seen in Figure 6.46. As shown in Figure 6.46 the force in the brace specimens exceeds their buckling load, but not their yield load. The numerical model underestimates the initial stiffness of the test specimen. Unlike TEST 1E & 1F, the stiffness is underestimated by the numerical model. As mentioned previously, at the end of TEST 1F the braces were removed and the stub connections at the base had permanent lateral displacement pushing the test columns inwards making the removal of the braces difficult. This permanent deformation in the stubs may have lead to a change in stiffness of the overall test frame accounting for the numerical model underestimation of stiffness. It can be seen from the remainder of the test results that the numerical model underestimates the test stiffness. The hysteresis plot for the test shows some nonlinear behaviour with slightly reduced stiffness in a few of the larger displacement responses. The test specimen reached buckling load but not yield as can be seen in Figure 6.46. The peak ductility demand recorded during TEST2E was 0.88, indicating the structure did not exceed yield displacement.

6.3.6 TEST 2F – Inelastic 3D: Taiwan Scaled 2.0

The test model in TEST 2F possessed the same lateral torsional frequency ratio and plan aspect ratio as TEST 2D. The input excitation was scaled by a factor of 2.0. TEST 2E stopped prematurely at approximately 30 seconds during the experiment due to the numerical integration timing-out. The excitation had reached maximum amplitude and was diminishing towards the end of the excitation, so the most important results were not affected by this.

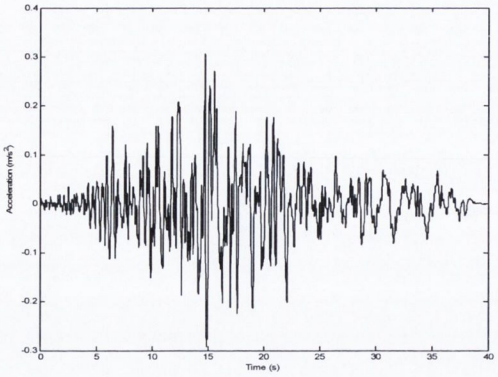

Figure 6.47: Scaled Taiwan input time history for inelastic 3D test

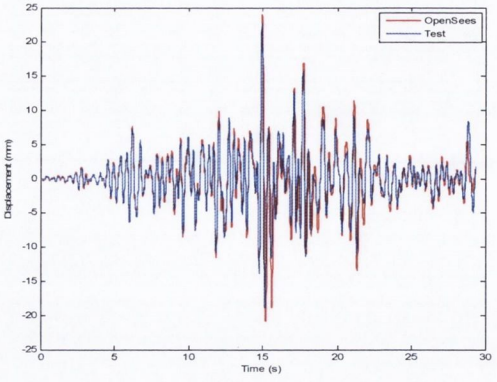

Figure 6.48: Graph of roof displacement vs. time for OpenSees model and test results

The main results for the test can be seen in Figure 6.48 to Figure 6.56. The maximum positive and negative lateral displacements of the roof of the structure observed during the test were 22.66mm & -18.91mm, as can be seen in Figure 6.48. The maximum numerically modelled lateral displacements were 24.03mm & -20.84mm representing a 5.7% overestimation of the observed peak lateral roof displacement on the positive side and 9.25% on the negative side. As shown in Figure 6.49 the periods of the test structure and numerical model show reasonable agreement. As can be seen in Figure 6.50, the test lateral acceleration at the roof matches reasonably well the numerical model. The maximum lateral roof acceleration of the structure during the test was 6.12m/s^2 as can be seen in Figure 6.50. The maximum numerically modelled lateral roof acceleration of the structure was 5.92m/s^2 as can be seen in Figure 6.50. There is a 3.3% difference in peak lateral acceleration between the numerical model and test data.

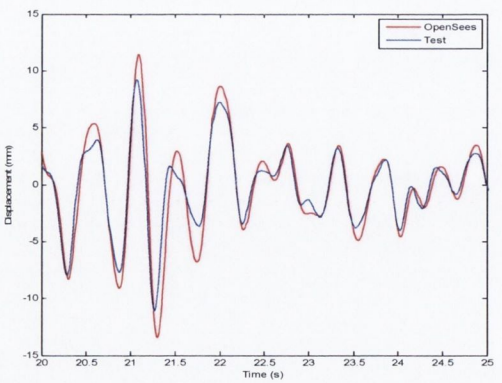

Figure 6.49: Close-up of roof displacement vs. time for OpenSees model and test data

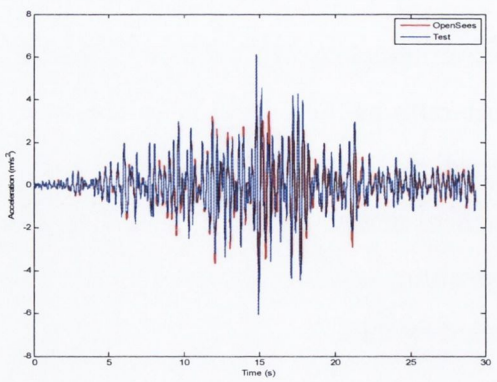

Figure 6.50: Graph of acceleration vs. time for OpenSees and test results

Figure 6.51 and Figure 6.52 show the test strain and numerically modelled strain at strain gauge No. 4 and strain gauge No. 5, respectively. As can be seen from Figure 6.51, the numerically modelled strains in the bracing at stain gauge location No. 4 and the recorded strains from the experiment showed poor agreement. The peak recorded strain during the test was $1.418e^{-3}$. It can be seen in Figure 6.51 that yielding occurs during the test, but is not predicted by the numerical model. The peak numerically modelled strain was $4.88e^{-4}$. The peak numerically modelled and peak test strains at strain gauge location No. 4 differed by 65.6%, with the numerically modelled strains being smaller. As can be seen from Figure 6.52, the numerically modelled strains in the bracing at stain gauge location No. 5 and the recorded strains from the experiment were in the same order of magnitude. The peak recorded strain during the test was $8.85e^{-4}$. The peak numerically modelled strain was $4.34e^{-4}$. The peak numerically modelled and peak test strains at strain gauge location No. 5 differed by 50.9%, with the numerically modelled strains being smaller. The numerical model underestimates the strains in brace members and does not predict yielding.

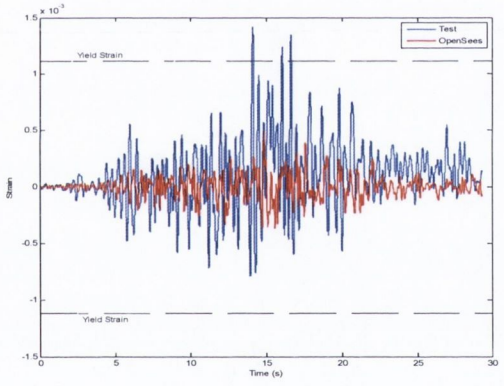

Figure 6.51: Graph of strain vs. time at gauge No. 4 for OpenSees and test data

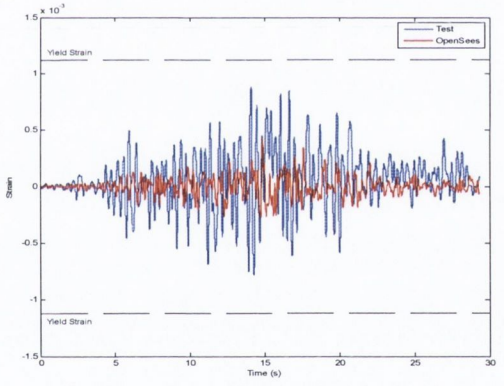

Figure 6.52: Graph of strain vs. time at strain gauge No. 5 for OpenSees model and test data

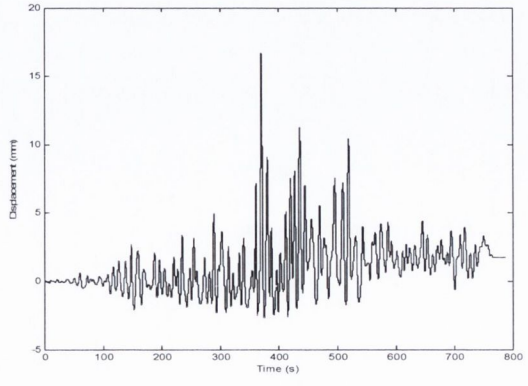

Figure 6.53: Graph of displacement vs. time for LVDT and OpenSees at Node 13

Figure 6.54: Photo of test frame after TEST 2F

Figure 6.53 shows the observed variation in out-of-plane displacement at the cross-point node (refer to Node 13 in Figure 5.3 in Chapter Five) of the concentric bracing. The peak out-of-plane displacement was 16.68mm. The peak lateral displacement of the test was 22.66mm. The lateral displacement was approximately 1.36 times the brace out-of-plane displacement. The displaced shape of the concentric bracing can be seen at the end of TEST 2F in Figure 6.54. The buckled shape is not as pronounced as TEST 1F. No local buckling was observed in either bracing member.

The results for strain gauge No. 4 and No. 5 are shown above, however all of the raw strain gauge data and LVDT data can be found in Appendix D10 for TEST 2F.

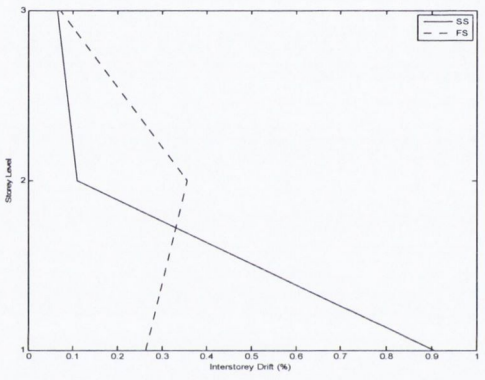

Figure 6.55: Graph of SS and FS test peak interstorey drifts

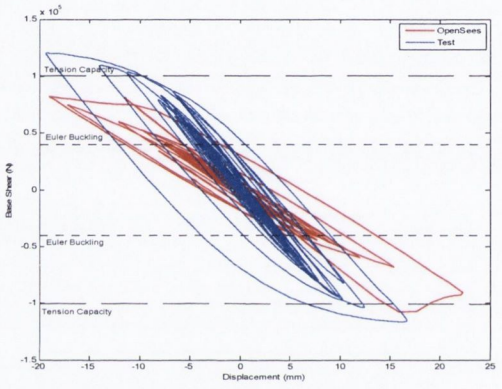

Figure 6.56: Base shear vs. displacement for OpenSees and test data

The interstorey drifts of the SS and FS of the experimental structure are shown in Figure 6.55. It can be seen from Figure 6.55 the interstorey drifts are the largest on the SS first-storey. The first-storey interstorey drift of 0.9% exceeded the assumed Eurocode 8 (CEN, (2004) limit of 0.5%. The variation in interstorey drift between the SS and FS can be seen in Figure 6.55 with the SS interstorey drifts differing from the FS interstorey drifts indicating a torsional rather than purely translational response in the structure.

The hysteresis plot of base shear against displacement for the test specimen and numerical model can be seen in Figure 6.56. As shown in Figure 6.56 the force in the brace specimens exceeds their buckling and yield loads. The numerical model underestimates the initial stiffness of the test specimen. The hysteresis plot for the test shows considerable nonlinear behaviour with some reduced stiffness in the larger displacement response cycles. The peak ductility demand recorded during TEST 2F was 1.73, indicating the structure did exceed yield displacement.

6.4 TEST 3 Experimental Results

The following section will detail the experimental results obtained for both elastic and inelastic tests for the group TEST 3 experiments. These tests employed 30x30x3mm SHS concentric brace specimens with normalised slenderness of 1.68. The main test results for each sub-test will be given, including a brief description of the results.

6.4.1 TEST 3A – Cyclic Sawtooth: No Braces

TEST 3A was used to calculate the stiffness of the test frame without any braces providing lateral stiffness. The displacement and force feedback from the experiment were used to calculate the lateral stiffness of the unbraced test frame as 31.8N/mm.

6.4.2 TEST 3B – Cyclic Sawtooth: With Braces

TEST 3B was used to calculate the initial lateral stiffness of the concentrically braced test frame. The displacement and force feedback from the experiment were used to calculate the lateral stiffness of the test frame with braces, which was calculated as 10094N/mm. This value represents the lateral stiffness of the experimental element in the hybrid test model (refer to Chapter Five, Section 5.6 for details) which is input into the OpenFresco model in subsequent tests (TESTS 3C-F). The test data from TEST 3B are presented in Appendix D1.

6.4.3 TEST 3C – 2D Elastic

In TEST 3C the response of the test structure to earthquake ground motion was examined in a hybrid test. The scaled Taiwan ground acceleration time history used in the experiment is presented in Figure 6.57. The peak ground acceleration is 0.005*g*.

The main results from the test can be seen in Figure 6.58 to Figure 6.60. The maximum lateral displacement of the roof during the test was -1.26mm, as shown in Figure 6.58. As can be seen in Figure 6.58, the variation in lateral roof displacement throughout the test matches the numerical model predictions reasonably well, with an 11.9% difference in peak lateral displacement. The periods of the test structure and numerical model show good agreement. However, as can be seen in Figure 6.59, the variation in lateral roof

acceleration throughout the test matches the numerical predictions poorly, with a 38.4% difference in peak lateral acceleration. The maximum lateral roof acceleration observed during the test was -0.19m/s^2. The low amplitude and noisy nature of the test acceleration response may be a reason for the poor predictive accuracy of the numerical model.

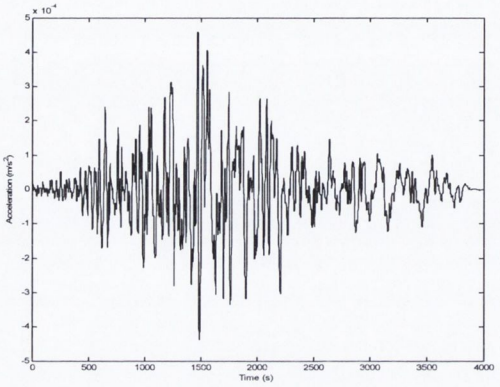

Figure 6.57: Scaled Taiwan input time history for elastic 2D test

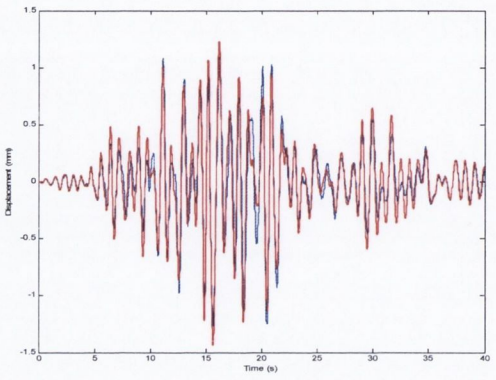

Figure 6.58: Graph of roof displacement vs. time for OpenSees model and test results

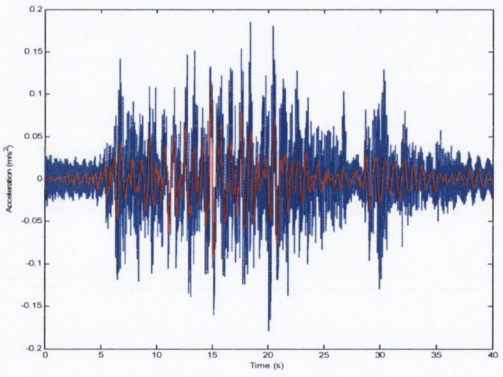

Figure 6.59: Graph of roof acceleration vs. time for OpenSees model and test results

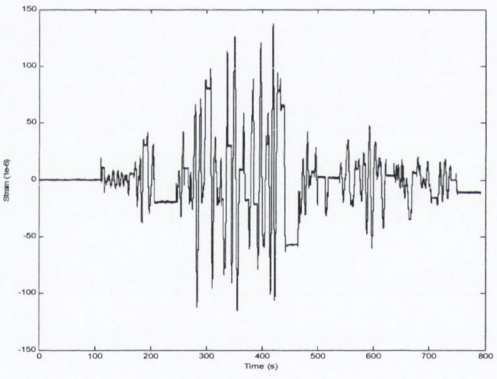

Figure 6.60: Graph of strain vs. time at strain gauge No. 4

The test data for strain gauge No. 4 is shown in Figure 6.60. It can be seen from Figure 6.60 the strain does not reach yield during the experiment. The other strain gauge test data from TEST 3C are presented in Appendix D12.

6.4.4 TEST 3D – Elastic 3D: Taiwan Scaled

The three-dimensional test model in TEST 3D had a lateral torsional frequency ratio of 1.25 (i.e. torsionally stiff) and a plan aspect ratio of 2.0. Its response to the Taiwan earthquake scaled to a peak ground acceleration of 0.06*g* was examined in a hybrid test. It is important to note that when initially running this experiment, an error occurred in running the wrong file and a much higher displacement was applied to the structure

resulting in slight yielding of the specimen before the test was manually terminated. As can be seen in Figure 6.65, there is a slight upward shift of the test strain data compared to the numerical model indicating slight yielding prior to the test being run again correctly.

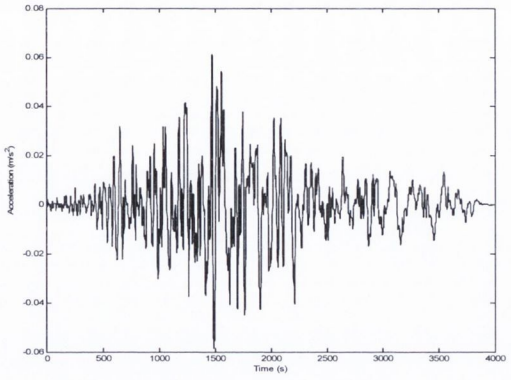

Figure 6.61 Scaled Taiwan input time history for elastic 3D test

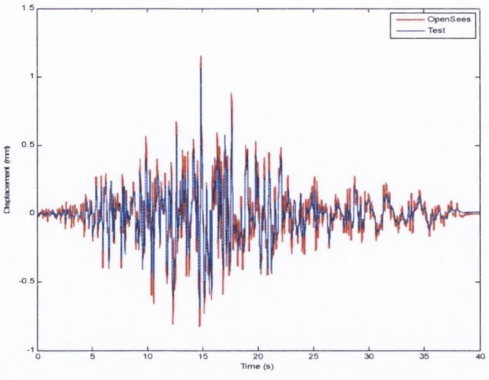

Figure 6.62 Graph of roof displacement vs. time for OpenSees model and test

The main results for the test can be seen in Figure 6.62 to Figure 6.65. The maximum lateral displacement of the roof during the test was 1.06mm, as shown in Figure 6.62. As can be seen in Figure 6.62, the variation in lateral roof displacement throughout the test matches the numerical model predictions well, with an 8.6% difference in peak lateral displacement. The periods of the test structure and numerical model show good agreement. However, as can be seen in Figure 6.63, the variation in lateral roof acceleration throughout the test matches the numerical predictions reasonably poorly, with a 19.7% difference in peak lateral acceleration. The maximum lateral roof acceleration observed during the test was -0.68m/s^2.

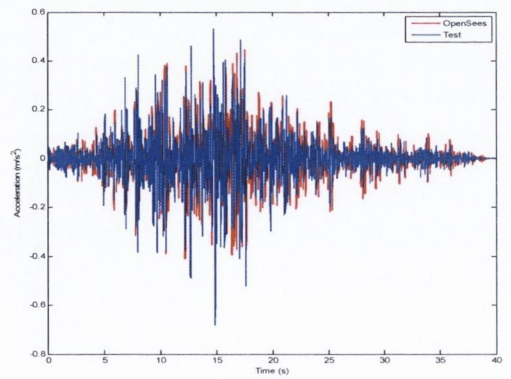

Figure 6.63 Graph of roof acceleration vs. time for OpenSees model and test data

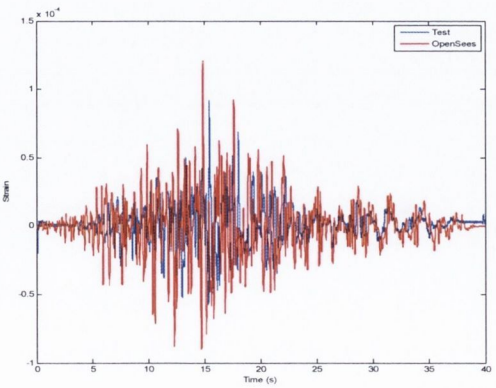

Figure 6.64 Graph of strain vs. time at strain gauge No. 4 for OpenSees model and test data

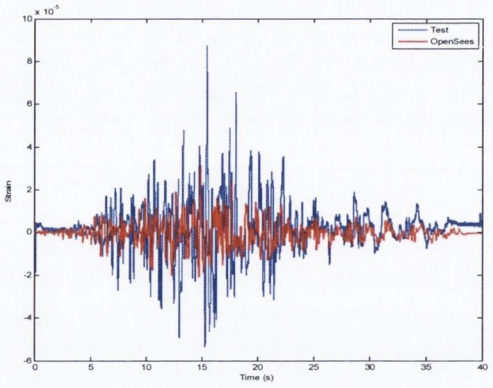

Figure 6.65 Graph of strain vs. time at strain gauge No. 5 for OpenSees model and test data

Figure 6.64 and Figure 6.65 compare the experimentally measured and numerically modelled brace strains at strain gauges No. 4 and No. 5, respectively. As can be seen from Figure 6.64, at location No. 4 the numerically modelled brace strains and the recorded strains from the experiment show reasonable agreement. The peak strain recorded during the test was $9.19e^{-5}$ whereas the peak numerically modelled strain was $1.21e^{-4}$ representing a difference of 23.9%, with the numerically modelled strains being larger. As can be seen from Figure 6.65, the numerically modelled brace strains at stain gauge location No. 5 underestimated the recorded strains from the experiment. The peak recorded strain during the test was $8.73e^{-5}$ whereas the peak numerically modelled strain was $3.15e^{-5}$ representing a difference of 63.9%, with the numerically modelled strains being smaller. Although there is a considerable difference between the test strains and numerically modelled strains for strain gauge No. 5, they are of the same order of magnitude.

The results for the remainder of the strain gauges for TEST 3D can be found in Appendix D13.

6.4.5 TEST 3E – Inelastic 3D: Taiwan

The test model in TEST 3E possessed the same lateral torsional frequency ratio and plan aspect ratio as TEST 3D. The test ran for approximately 27 seconds of the simulation before the test timed out. The excitation had reached maximum amplitude and was diminishing towards the end of the excitation, so the most important results were not affected by the premature end of the test.

The main results for the test can be seen in Figure 6.67 to Figure 6.73. The maximum lateral displacement of the roof during the test was 2.69mm, as shown in Figure 6.67. As

can be seen in Figure 6.67, the variation in lateral roof displacement throughout the test matches the numerical model predictions reasonably well, with an 8.5% difference in peak lateral displacement. The periods of the test structure and numerical model show good agreement. However, as can be seen in Figure 6.69, the variation in lateral roof acceleration throughout the test matches the numerical predictions reasonably poorly, with a 25.2% difference in peak lateral acceleration. The maximum lateral roof acceleration observed during the test was -1.88m/s^2. The numerical model results for TEST 3E do not show as good agreement with the test data as compared to TEST 1E or TEST 2E. The expected reason for this is the premature yielding of the brace specimens during TEST 3D as explained previously in Section 6.4.4.

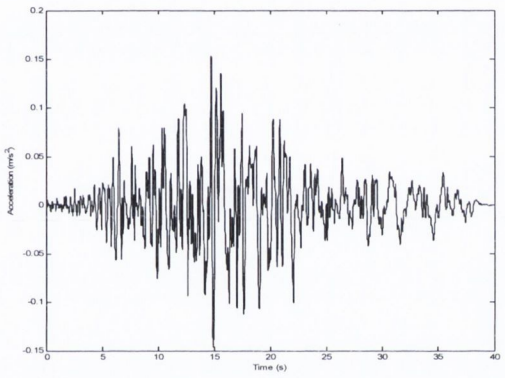

Figure 6.66: Scaled Taiwan input time history for inelastic 3D test

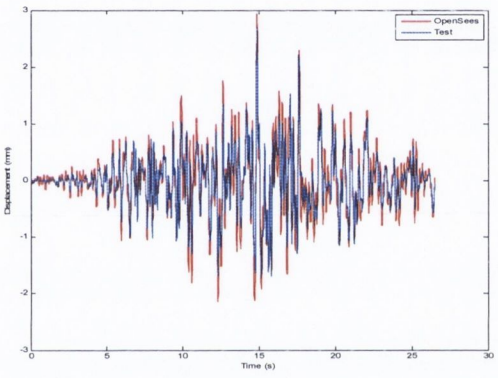

Figure 6.67: Graph of roof displacement time for OpenSees model and test results

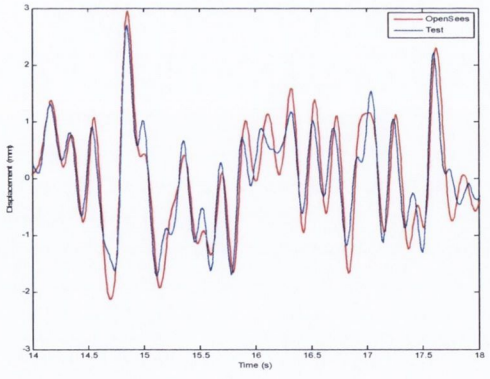

Figure 6.68: Close-up of roof displacement vs. time for OpenSees model and test data

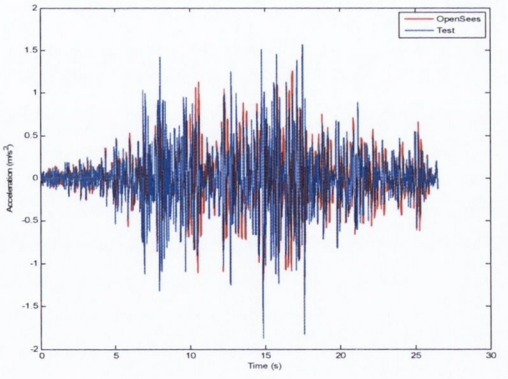

Figure 6.69: Graph of acceleration vs. time for OpenSees model and test results

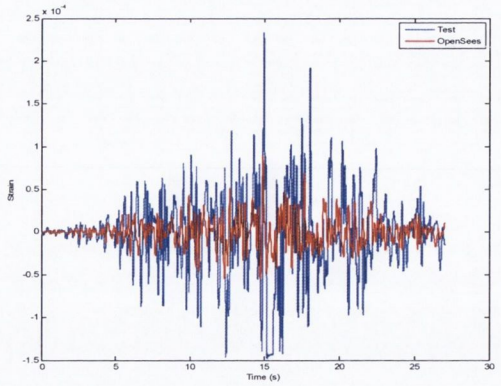

Figure 6.70: Graph of strain vs. time at gauge No. 4 for OpenSees and test data

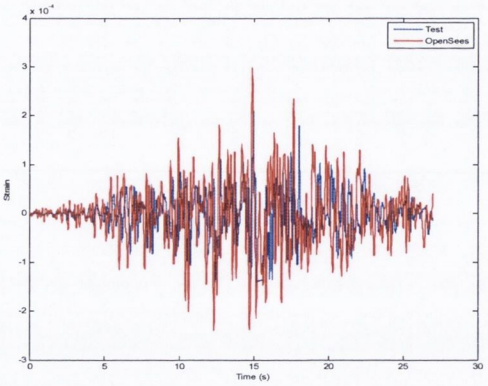

Figure 6.71: Graph of strain vs. time at strain gauge No. 5 for OpenSees model and test data

Figure 6.70 and Figure 6.71 show the test strains and numerically modelled strains at strain gauge No. 4 and strain gauge No. 5, respectively. The strain in the bracing members did not reach the yield strain of $1.12e^{-3}$. As can be seen from Figure 6.70 the numerically modelled strains in the bracing at stain gauge location No. 4 and the recorded strains from the experiment differ considerably, indicating poor numerical modelling of the strains at this location. The peak recorded strain during the test was $2.33e^{-4}$. The peak numerically modelled strain was $8.95e^{-5}$. The peak numerically modelled and peak test strains at strain gauge location No. 4 differed by 61.6%, with the numerically modelled strains being larger. As can be seen from Figure 6.71, the numerically modelled strains in the bracing at stain gauge location No. 5 and the recorded strains from the experiment were in the same order of magnitude with the peak recorded strain during the test being $2.17e^{-4}$, whereas the peak numerically modelled strain was $2.98e^{-4}$ representing a difference of 27.3%.

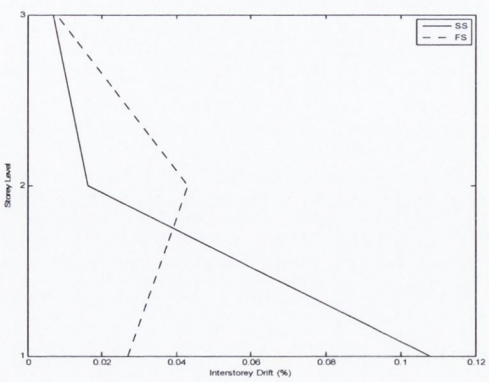

Figure 6.72: Graph of SS and FS test peak interstorey drifts

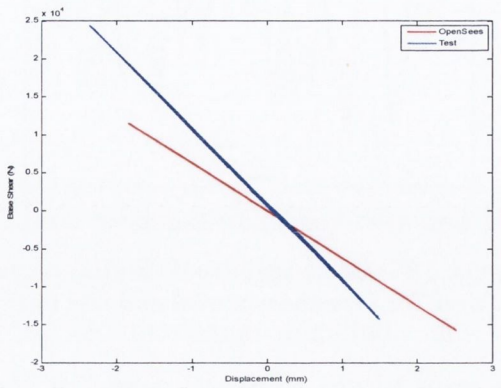

Figure 6.73: Base shear vs. displacement for OpenSees and test data

The interstorey drifts of the SS and FS of the experimental structure are shown in Figure 6.72. It can be seen from Figure 6.72 the interstorey drifts are the largest on the SS first-storey. None of the interstorey drifts exceed the assumed Eurocode 8 (CEN, (2004) limit of 0.5%. The variation in interstorey drift between the SS and FS can be seen in Figure 6.72 indicating a torsional rather than purely translational response in the structure.

The hysteresis plot of base shear against displacement for the test specimen and numerical model can be seen in Figure 6.73. As shown in Figure 6.73 the force in the brace specimens do not exceed their buckling or yield loads. The numerical model underestimates the initial stiffness of the test specimen. The hysteresis plot for the test shows slight nonlinear behaviour with no stiffness deterioration. The peak ductility demand recorded during TEST 3E was 0.206, indicating the structure did not exceed yield displacement.

6.4.6 TEST 3F – Inelastic 3D: Taiwan Scaled 2.0

The test model in TEST 3F possessed the same lateral torsional frequency ratio and plan aspect ratio as TEST 3D. The input excitation was scaled by a factor of 2.0.

The main results for the test can be seen in Figure 6.75 to Figure 6.81. The maximum positive and negative lateral displacements of the roof of the structure observed during the test were 5.38mm & -3.44mm, as can be seen in Figure 6.75. The maximum numerically modelled lateral displacements were 5.51mm & -3.44mm representing a 2.4% overestimation of the observed peak lateral roof displacement on the positive side and 14.1% on the negative side. As shown in Figure 6.76 the periods of the test structure and numerical model show good agreement. As can be seen in Figure 6.77, the test lateral acceleration at the roof matches reasonably poorly with the numerical model. The maximum lateral roof acceleration of the structure during the test was -3.67m/s^2 as can be seen in Figure 6.77. The maximum numerically modelled lateral roof acceleration of the structure was -2.49m/s^2 as can be seen in Figure 6.77. There is a 32.1% difference in peak lateral acceleration between the numerical model and test data.

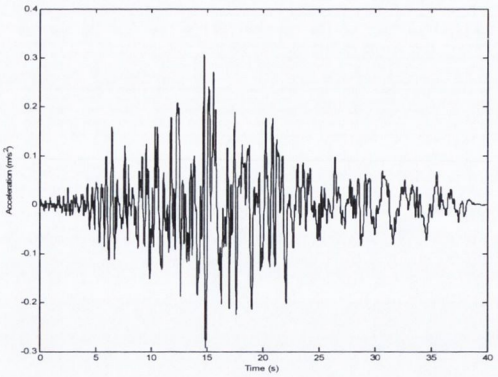

Figure 6.74: Scaled Taiwan input time history for inelastic 3D test

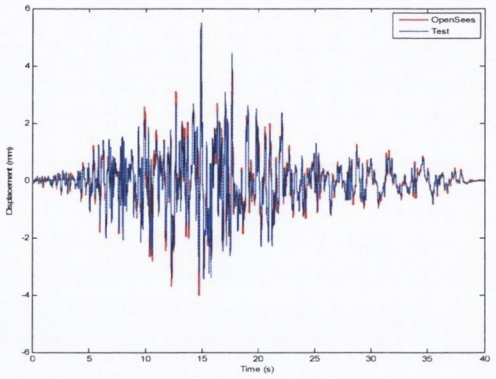

Figure 6.75: Graph of roof displacement vs. time for OpenSees model and test results

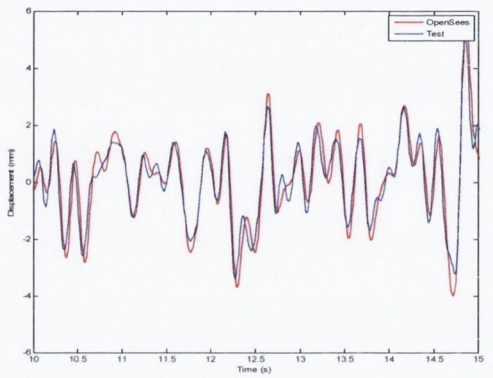

Figure 6.76: Close-up of roof displacement vs. time for OpenSees model and test data

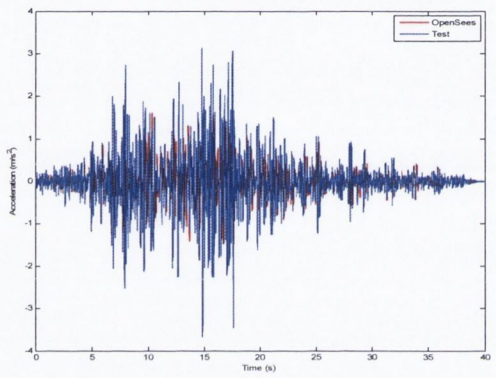

Figure 6.77: Graph of acceleration vs. time for OpenSees model and test results

Figure 6.78 and Figure 6.79 show the test strains and numerically modelled strains at strain gauge No. 4 and strain gauge No. 5, respectively. As can be seen from Figure 6.78, the numerically modelled strains in the bracing at stain gauge location No. 4 and the recorded strains from the experiment were in the same order of magnitude and showed good agreement. The peak recorded strain during the test was $4.52e^{-4}$. The peak numerically modelled strain was $5.36e^{-4}$. The peak numerically modelled and peak test strains at strain gauge location No. 4 differed by 15.8%, with the numerically modelled strains being larger. It can be seen from Figure 6.79 that the numerical model overestimates the strains. As can be seen from Figure 6.79, the numerically modelled strains in the bracing at stain gauge location No. 5 and the recorded strains from the experiment were in the same order of magnitude. The peak recorded strain during the test was $4.16e^{-4}$. The peak numerically modelled strain was $1.79e^{-4}$. The peak numerically modelled and peak test strains at strain gauge location No. 5 differed by 56.8%, with the numerically modelled strains being

smaller. The numerically modelled strains at strain gauge location No. 5 underestimated the response.

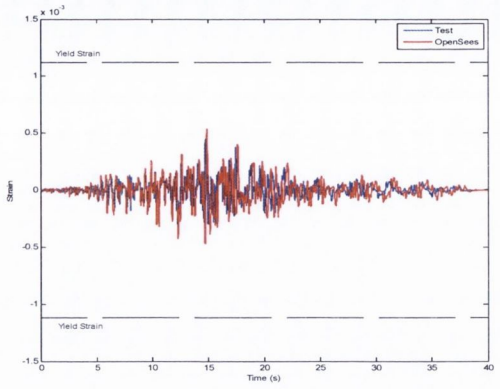

Figure 6.78: Graph of strain vs. time at gauge No. 4 for OpenSees and test data

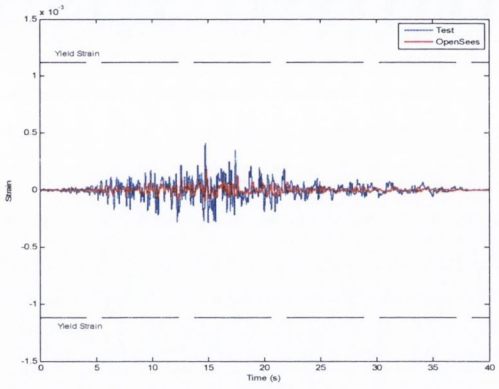

Figure 6.79: Graph of strain vs. time at strain gauge No. 5 for OpenSees model and test data

The observed variation in the out-of-plane displacement at the cross-point node (refer to Node 13 in Figure 5.3 in Chapter Five) of the concentric bracing can be found in Appendix D15. The peak out-of-plane displacement was 3.74mm. The peak lateral displacement of the test frame was 5.38mm. The lateral displacement was approximately 1.44 times the brace out-of-plane displacement. The displaced shape of the concentric bracing after TEST 3F can be seen in Figure 6.82. No local buckling was observed in either bracing member.

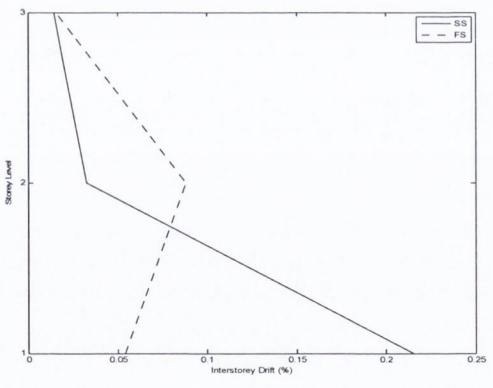

Figure 6.80: Graph of SS and FS test peak interstorey drifts

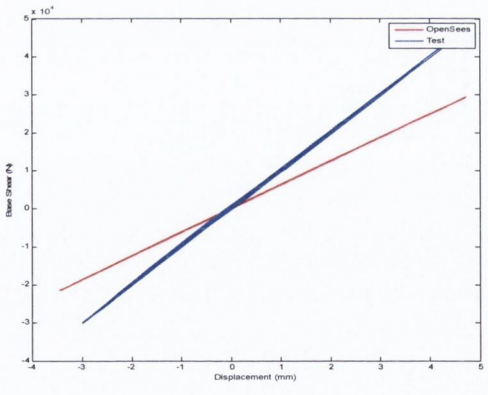

Figure 6.81: Base shear vs. displacement for OpenSees and test data

The interstorey drifts of the SS and FS of the experimental structure are shown in Figure 6.80. It can be seen from Figure 6.80 the interstorey drifts are the largest at the SS first-storey. None of the interstorey drifts exceed the assumed Eurocode 8 (CEN, (2004) limit of 0.5%. The variation in interstorey drift between the SS and FS can be seen in Figure 6.80

with the SS interstorey drifts being greater than FS interstorey drifts indicating a torsional rather than purely translational response in the structure.

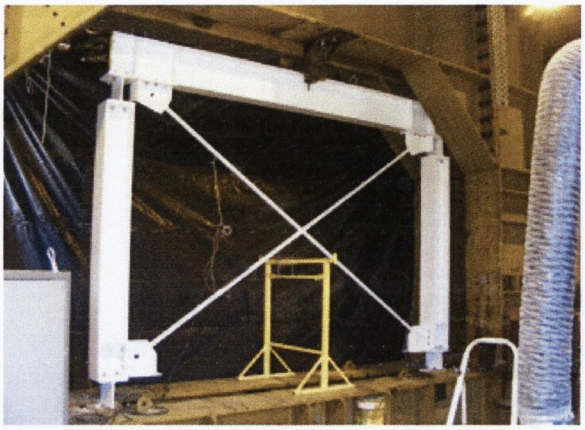

Figure 6.82: Photo of test frame after TEST 3F

The hysteresis plot of base shear against displacement for the test specimen and numerical model can be seen in Figure 6.81. As shown in Figure 6.81 the force in the brace specimens did not exceed their buckling or yield loads. The numerical model underestimates the stiffness of the test specimen. The hysteresis plot for the test shows slight nonlinear behaviour with no stiffness deterioration. The photo of the test frame after TEST 3F in Figure 6.82 also indicates no buckling in the bracing members. The peak ductility demand recorded during TEST 3F was 0.413, indicating the structure did not exceed yield displacement.

6.5 TEST 4 Experimental Results

The following section will detail the experimental results obtained for both elastic and inelastic TEST 4 group of experiments. These tests employed 50x30x3mm RHS concentric brace specimens with normalised slenderness of 1.57. The main test results for each sub-test will be given, including a brief description of the results.

6.5.1 TEST 4A – Cyclic Sawtooth: No Braces

TEST 4A was used to calculate the stiffness of the test frame without any braces providing lateral stiffness. The displacement and force feedback from the experiment were used to calculate the lateral stiffness of the unbraced test frame as 34N/mm.

6.5.2 TEST 4B — Cyclic Sawtooth: With Braces

TEST 4B was used to calculate the initial lateral stiffness of the concentrically braced test frame. The displacement and force feedback from the experiment were used to calculate the lateral stiffness of the test frame with braces, which was calculated as 12136N/mm. This value represents the lateral stiffness of the experimental element in the hybrid test model (refer to Chapter Five, Section 5.6 for details) which is input into the OpenFresco model in subsequent tests (TESTS 4C-F). The test data from TEST 4B are presented in Appendix D16.

6.5.3 TEST 4C – 2D Elastic

In TEST 4C the response of the test structure to earthquake ground motion was examined in a hybrid test. The scaled Taiwan ground acceleration time history used in the experiment is presented in Figure 6.83. The peak ground acceleration is 0.005*g*.

The main results from the test can be seen in Figure 6.84 to Figure 6.86. The maximum lateral displacement of the roof during the test was -1.23mm, as shown in Figure 6.84. As can be seen in Figure 6.84, the variation in lateral roof displacement throughout the test matches the numerical model predictions reasonably poorly, with a 20.6% difference in peak lateral displacement. The periods of the test structure and numerical model show good agreement. Similarly, as can be seen in Figure 6.85, the variation in lateral roof acceleration throughout the test matches the numerical predictions poorly, with a 31.8% difference in peak lateral acceleration. The maximum lateral roof acceleration observed during the test was 0.18m/s^2. The low amplitude and noisy nature of the test acceleration response may be the reason for the poor predictive accuracy of the numerical model.

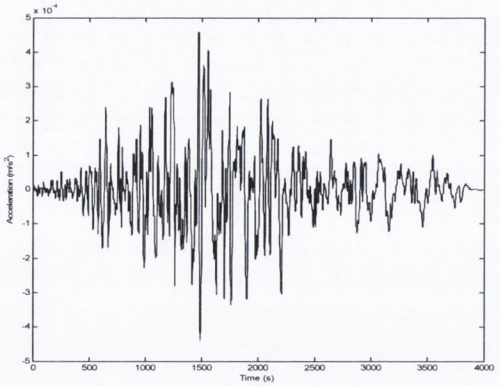

Figure 6.83: Scaled Taiwan input time history for elastic 2D test

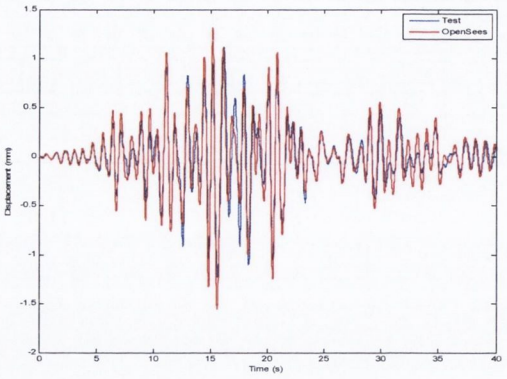

Figure 6.84: Graph of roof displacement vs. time for OpenSees model and test results

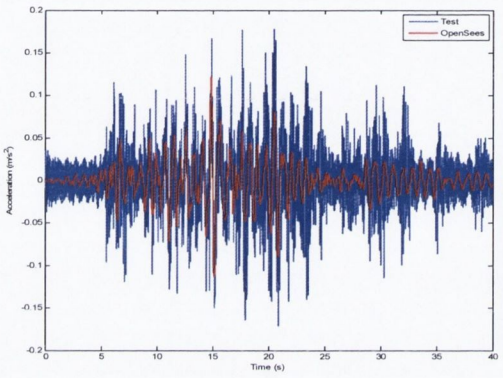

Figure 6.85: Graph of roof acceleration vs. time for OpenSees model and test results

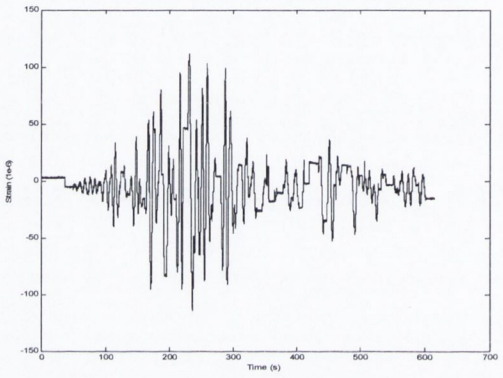

Figure 6.86: Graph of strain vs. time at strain gauge No. 4

The test data for strain gauge No. 4 is shown in Figure 6.86. It can be seen from Figure 6.86 the strain does not reach yield during the experiment. The other strain gauge test data from TEST 4C are presented in Appendix D17.

6.5.4 TEST 4D – Elastic 3D: Taiwan Scaled

The three-dimensional test model in TEST 4D had a lateral torsional frequency ratio of 1.25 (i.e. torsionally stiff) and a plan aspect ratio of 2.0. Its response to the Taiwan earthquake scaled to a peak ground acceleration of 0.06*g* was examined in a hybrid test.

The main results for the test can be seen in Figure 6.88 to Figure 6.91. The maximum lateral displacement of the roof during the test was 0.99mm, as shown in Figure 6.88. As can be seen in Figure 6.88, the variation in lateral roof displacement throughout the test matches the numerical model predictions well, with a 3.6% difference in peak lateral displacement. The periods of the test structure and numerical model show good agreement.

Similarly, as can be seen in Figure 6.89, the variation in lateral roof acceleration throughout the test matches the numerical predictions reasonably well, with a 15.2% difference in peak lateral acceleration. The maximum lateral roof acceleration observed during the test was -0.6m/s^2.

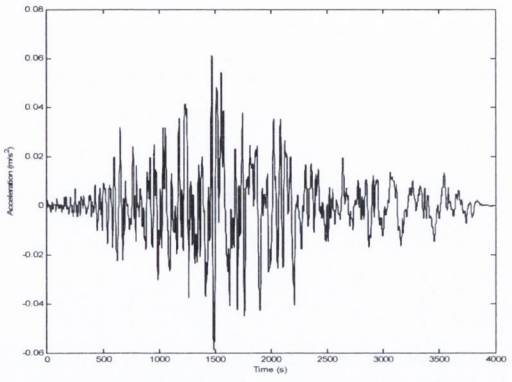

Figure 6.87: Scaled Taiwan input time history for elastic 3D test

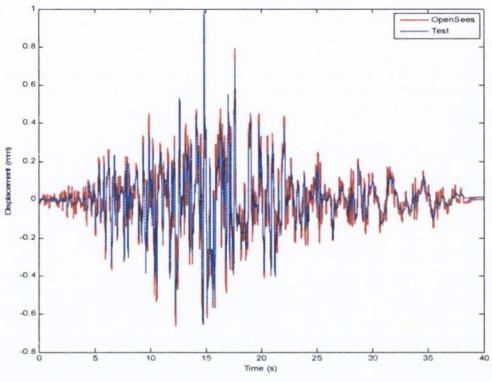

Figure 6.88: Graph of roof displacement vs. time for OpenSees model and test results

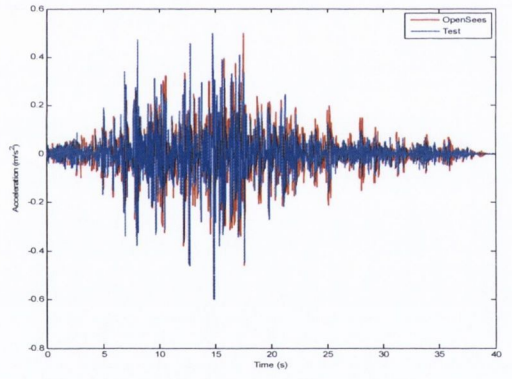

Figure 6.89: Graph of roof acceleration vs. time for OpenSees model and test data

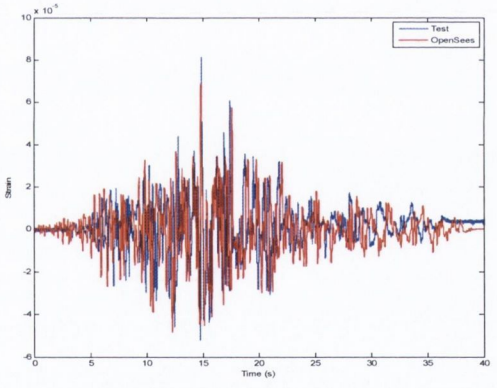

Figure 6.90: Graph of strain vs. time at strain gauge No. 4 for OpenSees model and test data

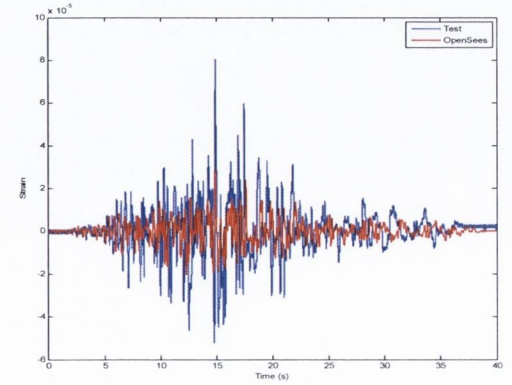

Figure 6.91: Graph of strain vs. time at strain gauge No. 5 for OpenSees model and test data

Figure 6.90 and Figure 6.91 compare the experimentally measured and numerically modelled brace strains at strain gauges No. 4 and No. 5, respectively. As can be seen from Figure 6.90, at location No. 4 the numerically modelled brace strains and the recorded strains from the experiment were in the same order of magnitude and show reasonable agreement. The peak strain recorded during the test was $8.14e^{-5}$ whereas the peak numerically modelled strain was $6.91e^{-5}$ representing a difference of 15.1%, with the numerically modelled strains being larger. As can be seen from Figure 6.91, the numerically modelled brace strains at stain gauge location No. 5 underestimated the recorded strains from the experiment. The peak recorded strain during the test was $8.06e^{-5}$ whereas the peak numerically modelled strain was $2.89e^{-5}$ representing a difference of 64.1%, with the numerically modelled strains being smaller. Although there is a considerable difference between the test strains and numerically modelled strains for strain gauge No. 5, they are of the same order of magnitude.

6.5.5 TEST 4E – Inelastic 3D: Taiwan

The test model in TEST 4E possessed the same lateral torsional frequency ratio and plan aspect ratio as TEST 4D.

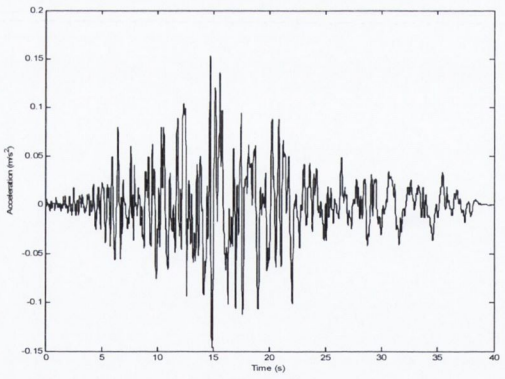

Figure 6.92: Scaled Taiwan input time history for inelastic 3D test

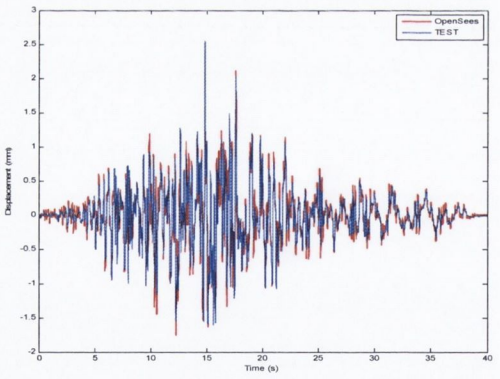

Figure 6.93: Graph of roof displacement vs. time for OpenSees model and test results

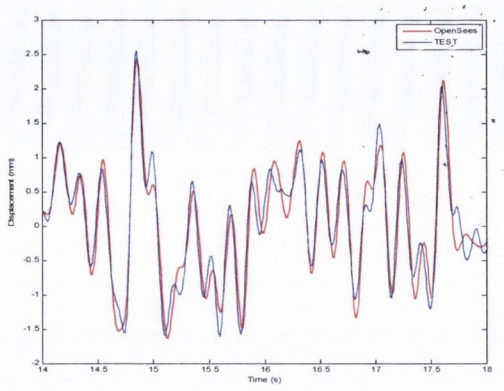

Figure 6.94: Close-up of roof displacement vs. time for OpenSees model and test data

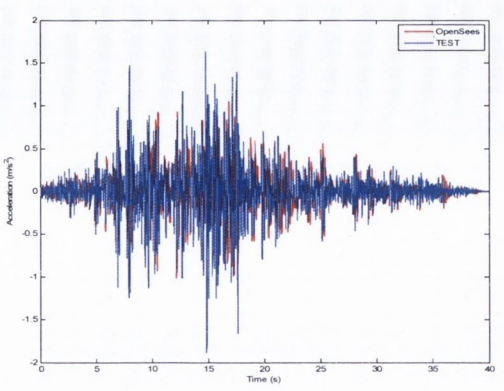

Figure 6.95: Graph of acceleration vs. time for OpenSees model and test results

The main results for the test can be seen in Figure 6.93 to Figure 6.99. The maximum lateral displacement of the roof during the test was 2.42mm, as shown in Figure 6.93. As can be seen in Figure 6.93, the variation in lateral roof displacement throughout the test matches the numerical model predictions well, with a 5.1% difference in peak lateral displacement. As shown in Figure 6.94 the periods of the test structure and numerical model show reasonably good agreement. However, as can be seen in Figure 6.95, the variation in lateral roof acceleration throughout the test matches the numerical predictions poorly, with a 31.6% difference in peak lateral acceleration. The maximum lateral roof acceleration observed during the test was 1.29m/s^2.

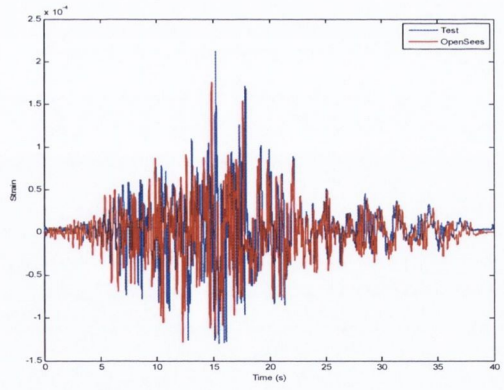

Figure 6.96: Graph of strain vs. time at gauge No. 4 for OpenSees and test data

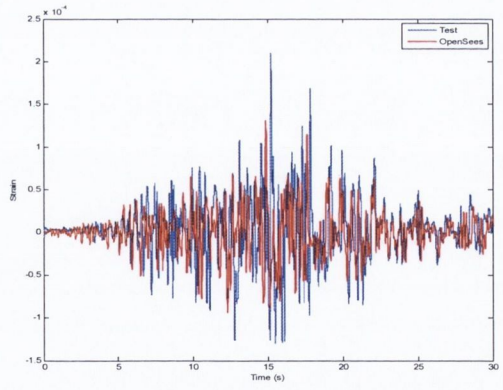

Figure 6.97: Graph of strain vs. time at strain gauge No. 5 for OpenSees model and test data

Figure 6.96 and Figure 6.97 show the test strains and numerical model strains at strain gauge No. 4 and strain gauge No. 5, respectively. The strain in the bracing members did not reach the yield strain of 1.12e^{-3}. As can be seen from Figure 6.96, the numerically modelled strains in the bracing at stain gauge location No. 4 and the recorded strains from

the experiment were in the same order of magnitude and showed good agreement. The peak recorded strain during the test was $2.13e^{-4}$. The peak numerically modelled strain was $1.76e^{-4}$. The peak numerically modelled and peak test strains at strain gauge location No. 4 differed by 17.5%, with the numerically modelled strains being smaller. As can be seen from Figure 6.97, the numerically modelled strains in the bracing at stain gauge location No. 5 and the recorded strains from the experiment were in the same order of magnitude and showed reasonably good agreement. The peak recorded strain during the test was $2.09e^{-4}$. The peak numerically modelled strain was $1.31e^{-4}$. The peak numerically modelled and peak test strains at strain gauge location No. 5 differed by 37.5%, with the numerically modelled strains being smaller. Overall, the peak test strains and peak numerically modelled strains are in the same order of magnitude and indicate good agreement.

The results for strain gauge No. 4 and No. 5 are shown above, however all of the raw strain gauge data and LVDT data can be found in Appendix D19 for TEST 4E.

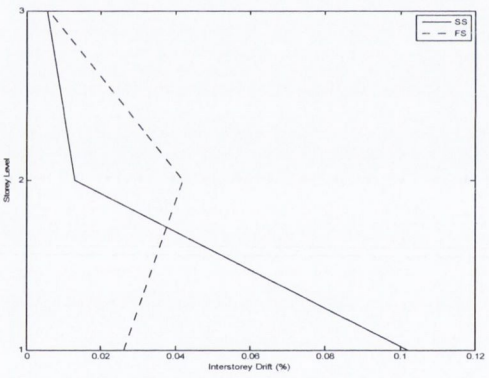

Figure 6.98: Graph of SS and FS test peak interstorey drifts

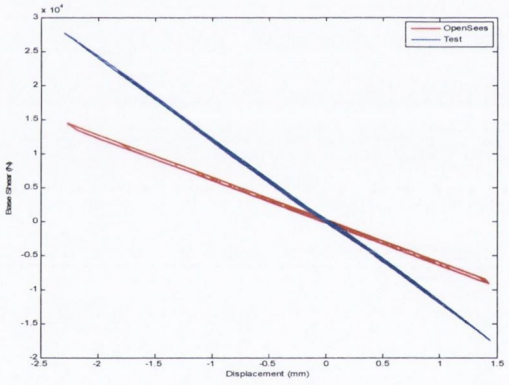

Figure 6.99: Base shear vs. displacement for OpenSees and test data

The interstorey drifts of the SS and FS of the experimental structure are shown in Figure 6.98. It can be seen from Figure 6.98 the interstorey drifts are the largest on the SS first-storey. None of the interstorey drifts exceed the assumed Eurocode 8 (CEN, (2004) limit of 0.5%. The variation in interstorey drift between the SS and FS can be seen in Figure 6.98 indicating a torsional rather than purely translational response in the structure.

The hysteresis plot of base shear against displacement for the test specimen and numerical model can be seen in Figure 6.99. As shown in Figure 6.99 the force in the brace specimens does not exceed their buckling or yield loads. The numerical model underestimates the initial stiffness of the test specimen. The hysteresis plot for the test shows slight nonlinear behaviour with no stiffness deterioration. The peak ductility

demand recorded during TEST 4E was 0.195, indicating the structure did not exceed yield displacement.

6.5.6 TEST 4F – Inelastic 3D: Taiwan Scaled 2.0

The test model in TEST 4F possessed the same lateral torsional frequency ratio and plan aspect ratio as TEST 4D. The input excitation was scaled by a factor of 2.0.

The main results for the test can be seen in Figure 6.101 to Figure 6.107. The maximum positive and negative lateral displacements of the roof of the structure observed during the test were 5.09mm & -3.25mm, as can be seen in Figure 6.101. The maximum numerically modelled lateral displacements were 4.85mm & -3.51mm representing a 4.7% overestimation of the observed peak lateral roof displacement on the positive side and 7.4% on the negative side. As shown in Figure 6.102 the periods of the test structure and numerical model show good agreement. As can be seen in Figure 6.103, the test lateral acceleration at the roof matches reasonably poorly the numerical model. The maximum lateral roof acceleration of the structure during the test was 3.76m/s^2 as can be seen in Figure 6.103. The maximum numerically modelled lateral roof acceleration of the structure was 2.59m/s^2 as can be seen in Figure 6.103. There is a 31.1% difference in peak lateral acceleration between the numerical model and test data.

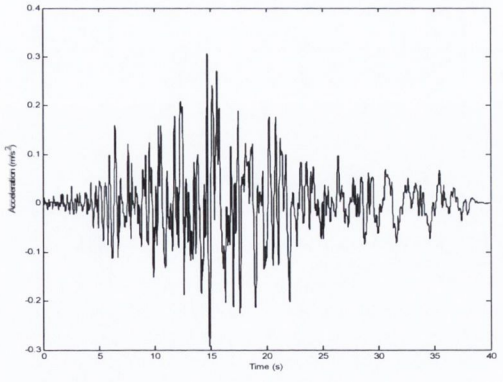

Figure 6.100: Scaled Taiwan input time history for inelastic 3D test

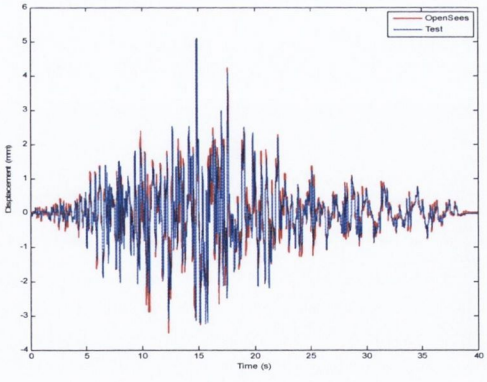

Figure 6.101: Graph of roof displacement vs. time for OpenSees model and test results

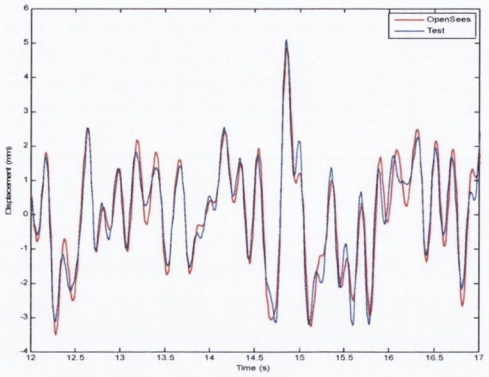

Figure 6.102: Close-up of roof displacement vs. time for OpenSees model and test data

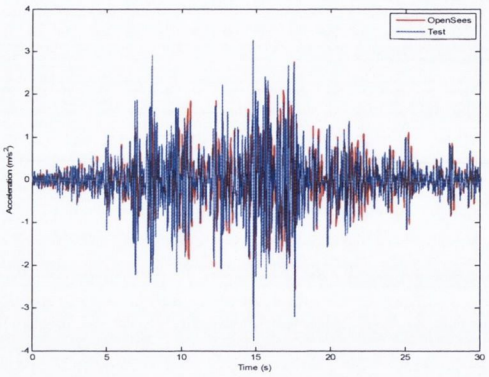

Figure 6.103: Graph of acceleration vs. time for OpenSees model and test results

Figure 6.104 and Figure 6.105 show the test strain and numerical model strain at strain gauge No. 4 and strain gauge No. 5, respectively. As can be seen from Figure 6.104, the numerically modelled strains in the bracing at stain gauge location No. 4 and the recorded strains from the experiment were in the same order of magnitude and show good agreement. The peak recorded strain during the test was $4.18e^{-4}$. The peak numerically modelled strain was $3.50e^{-4}$. The peak numerically modelled and peak test strains at strain gauge location No. 4 differed by 16.2%, with the numerically modelled strains being smaller. As can be seen from Figure 6.105, the numerically modelled strains in the bracing at stain gauge location No. 5 and the recorded strains from the experiment were in the same order of magnitude and show reasonably poor agreement. The peak recorded strain during the test was $4.09e^{-4}$. The peak numerically modelled strain was $1.60e^{-4}$. The peak numerically modelled and peak test strains at strain gauge location No. 5 differed by 60.8%, with the numerically modelled strains being smaller. Although there is a considerable difference between the peak test strains and peak numerically modelled strains for strain gauge No. 5, in general they are in the same order of magnitude.No yielding of the brace specimens was observed during the experiment.

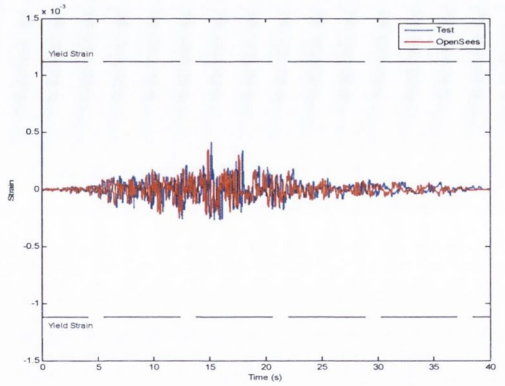

Figure 6.104: Graph of strain vs. time at gauge No. 4 for OpenSees and test data

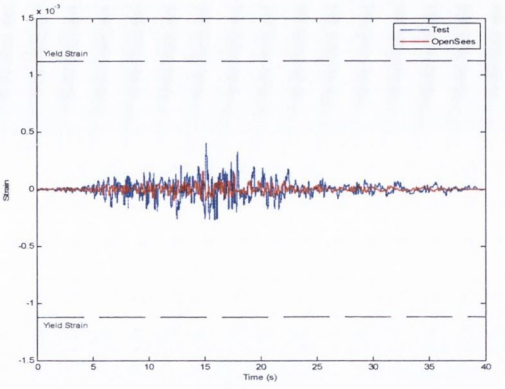

Figure 6.105: Graph of strain vs. time at strain gauge No. 5 for OpenSees model and test data

The out-of-plane displacement for the cross-point node (refer to Node 13 in Figure 5.3 in Chapter Five) of the concentric bracing is presented in Appendix D20. The peak out-of-plane displacement recorded was 2.53mm. The peak lateral displacement of the test frame was 5.09mm. The lateral displacement was approximately twice the brace out-of-plane displacement. The results for strain gauge No. 4 and No. 5 are shown above, however all of the raw strain gauge data and LVDT data can be found in Appendix D20 for TEST 4F.

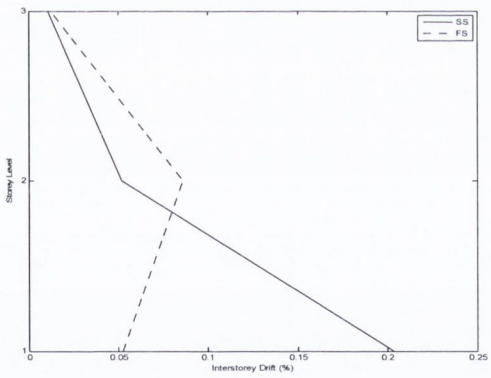

Figure 6.106: Graph of SS and FS test peak interstorey drifts

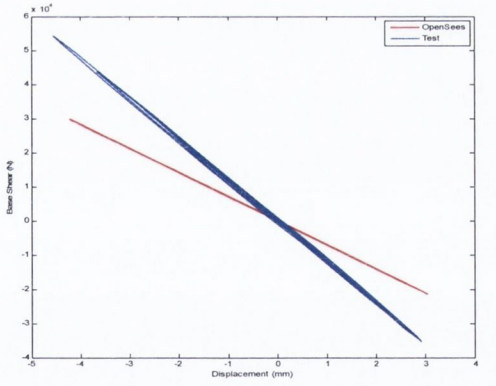

Figure 6.107: Base shear vs. displacement for OpenSees and test data

The interstorey drifts of the SS and FS of the experimental structure are shown in Figure 6.106. It can be seen from Figure 6.106 the interstorey drifts are the largest on the SS first-storey. None of the interstorey drifts exceed the assumed Eurocode 8 (CEN, (2004) limit of 0.5%. The variation in interstorey drift between the SS and FS can be seen in Figure 6.106 indicating a torsional rather than purely translational response in the structure.

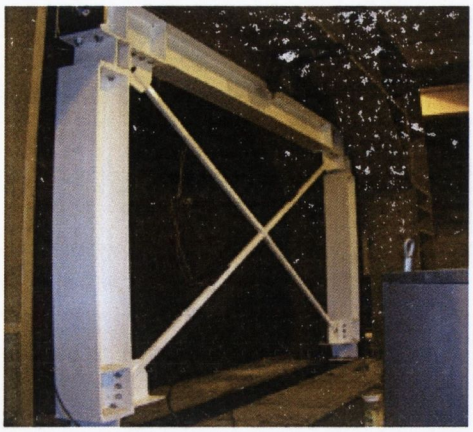

Figure 6.108: Photo of test frame after TEST 4F

The hysteresis plot of base shear against displacement for the test specimen and numerical model can be seen in Figure 6.107. As shown in Figure 6.107 the force in the brace specimens does not exceed their buckling or yield loads. The numerical model underestimates the stiffness of the test specimen. The hysteresis plot for the test shows slight nonlinear behaviour with no stiffness deterioration. The photo of the test frame after TEST 4F in Figure 6.108 also indicates no buckling in the bracing members. The peak ductility demand recorded during TEST 4F was 0.39, indicating the structure did not exceed yield displacement.

6.6 Coupon Tests

Coupon test samples in accordance with BS EN ISO 6892-1:2009, (British Standards Institution, (2009)) were taken from untested brace members in order determine the yield strength (f_y) of each specimen. The yield strength, f_y is needed in to compare the numerical model to the test data. For the 50x30x3 RHS specimens, the mean value for the yield strength is 233.26N/mm^2 and the 30x30x3 SHS specimens, the mean value for the yield strength is 244.13N/mm^2. The steel was specified from the supplier at a grade of 235N/mm^2.

6.7 Results Discussion

The following section will summarise the results from the experimental programme and discuss the conclusions arising from the test results. Firstly, the accuracy of the experimental method will be discussed. Secondly, the accuracy of the numerical model in

comparison to the test data will be discussed. Finally, the effect of parameter variation and corresponding conclusions will be detailed.

6.7.1 Performance of Experimental Procedure

The accuracy of the hybrid test method procedure has been assessed in detail in Chapter Four, Section 4.7, in the validation test. The validation test showed that the hybrid test method could perform well for a simple structural arrangement. The general effectiveness of the hybrid test procedure to perform dynamic experiments on a concentrically braced frame can be assessed from the results in this chapter.

The majority of the experiments in which only small displacement responses were observed required hold phases to facilitate calculation of the next time step command displacement. As noted previously, some tests timed-out due to excessive delays in computing the next target displacement by numerical integration. The timing-out of this process was typically observed when the command displacements became quite small. Small changes in displacement proved difficult for the algorithm to proceed to the next time step within the time limitation. In contrast, the system performed well during periods of large displacement command fluctuation when no hold phases were required. Out of the 24 No. tests in total, the following tests timed-out prematurely; TEST 1E (23s), TEST 2D (21s), TEST 2E (26s), TEST 2F (30s) and TEST 3D (27s). The peak displacement and acceleration for the test structure occurs around 15-17s. The Taiwan ground acceleration time history gradually increases in amplitude to a peak around 15-17s and then gradually reduces in amplitude to the end of the record at 40s. As can be seen from the times at which each experiment timed-out, the peak displacement and peak acceleration were already achieved during each of the experiments. The peak displacement and acceleration results were not affected by the premature end of these tests.

Prior to performing each experiment, a test simulation was undertaken. The simulation of a hybrid test is performed by replacing the experimental element with a numerical element. The model is a purely numerical model, but differs from the OpenSees model. The simulated numerical element that replaces the experimental element uses the initial stiffness matrix of the proposed experimental element. In OpenFresco the numerical element is simulated using SimDomain. SimDomain is used to test that the numerical model, experimental setup and network communication are functioning correctly prior to

conducting an experiment. Each of the simulated experiments ran successfully without any timing-out issues. Hence, the subsequent timing-out of the actual experiments as a result of excessive numerical integration time was not expected.

As can be seen from the experimental results for each series of the four tests, the displacement and acceleration responses were mostly smooth and continuous. Some of the two-dimensional tests with small scale input ground accelerations had a noisy acceleration response due to the low amplitude input excitation.

6.7.2 Accuracy of Numerical Model

A summary of the test data and numerical modelling results for peak lateral displacement, peak lateral acceleration and peak strains at strain gauge No. 4 are given in Table 6.2. The results from strain gauge No. 4 are used as an indicator for the accuracy of the numerically modelled strains. The summary of the test and numerical modelling results for the root-mean-square (rms) values of lateral displacement, lateral acceleration and strain at strain gauge No. 4 are given in Table 6.3. The rms value provides information on the overall signal amplitude rather than just the peak values, allowing a better overall comparison.

The difference between the peak displacement of the test data and numerical model showed an average error of 5.3%, as shown in Table 6.2. It can be seen from Table 6.2 in TEST 1; TESTs 1C, 1D & 1E have similar levels of difference in peak displacement of 4.92%, 4.63% and 3.2%, respectively. However, TEST 1F has a difference in peak numerically modelled and test displacement of 31.1%. In general, the level of accuracy for peak displacements is good, however due to the limited number of tests in each block, if one test does not perform well this can skew the results. Between three of the experiments, good agreement is shown. The difference between the peak acceleration of the test data and numerical model showed an average error of 9.3%, as shown in Table 6.2. Similar to the peak displacements, an error in one experiment slightly skewed the mean peak acceleration error (TEST 1F).

The average difference between the rms values for displacement of all the test data and numerical models is 7.69%, as shown in Table 6.3. The average difference between the rms values for acceleration of all the test data and numerical models is 8.05%, as shown in Table 6.3. It can be seen from Table 6.3 in TEST 4; TESTs 4D, 4E & 4F have similar

levels of difference in rms acceleration of 15.12%, 4.69% and 6.08%, respectively. However, TEST 4C has a difference in rms numerically modelled and test acceleration of 72.24%. In general, the level of accuracy for rms acceleration is reasonable, however due to the limited number of tests in each block, if one test does not perform well this can skew the results. The combined results of peak and rms values indicate the numerical model predicts the acceleration response of the test structure with an acceptable level of accuracy.

The average difference between the peak test strains and peak numerically modelled strains is 20.1%, as shown in Table 6.2. The average difference between the rms values for strains of the test data and numerical model are 121.06%, as shown in Table 6.3. The combined results of peak and rms values indicate the numerical model predicts the strains in the test structure with an unacceptably poor level of accuracy.

In summary, the numerical model shows good agreement with the test data with respect to displacement and accelerations, but the strains show unacceptably poor agreement.

Table 6.2: Summary of peak test and numerical model results

Test ID	*Input Excitation*	*Test Type*	*Scaling Factor*	*Max. Roof Displacement (mm)*	*Disp. Error Model and Test (%)*	*Max. Acceration (m/s^2)*	*Acc. Error Model and Test (%)*	*Max Strain SG4*	*Strain Error (%)*
1A	Cyclic	Elastic	-	-	-	-	-	-	-
1B	Cyclic	Elastic	-	-	-	-	-	-	-
1C	Sc. Taiwan 2D	Elastic	0.03	3.339	4.92	-0.082	4.16	-	-
1D	Sc. Taiwan 3D	Elastic	0.4	4.52	4.63	1.34	14.9	-3.678e-4	26.5
1E	Taiwan 3D	Inelastic	1.0	11.509	3.2	3.298	13.9	-7.381e-4	335
1F	Sc. Taiwan 3D	Inelastic	2.0	-27.055	31.1	4.558	28.6	-4.801e-4	64.04
Mean					7.3		10.2		70.9
COV					1.36		0.76		188.9
2A	Cyclic	Elastic	-	-	-	-	-	-	-
2B	Cyclic	Elastic	-	-	-	-	-	-	-
2C	Sc. Taiwan 2D	Elastic	0.03	3.143	2.13	0.0797	30	-	-
2D	Sc. Taiwan 3D	Elastic	0.4	4.526	4.95	1.252	8.97	3.463e-4	10.8
2E	Taiwan 3D	Inelastic	1.0	11.41	0.53	3.17	6.37	7.932e-4	68.8
2F	Sc. Taiwan 3D	Inelastic	2.0	22.66	9.25	6.12	3.27	1.418e-3	65.57
Mean					2.8		8.1		24.2
COV					0.11		1.10		7.08
3A	Cyclic	Elastic	-	-	-	-	-	-	-
3B	Cyclic	Elastic	-	-	-	-	-	-	-
3C	Sc. Taiwan 2D	Elastic	0.03	-1.264	11.9	0.186	38.4	-	-
3D	Sc. Taiwan 3D	Elastic	0.4	1.06	8.55	0.681	19.7	9.19e-5	23.9
3E	Taiwan 3D	Inelastic	1.0	2.69	8.45	-1.875	25.2	2.333e-4	61.6
3F	Sc. Taiwan 3D	Inelastic	2.0	5.51	14.1	-3.67	32.1	4.517e-4	15.77
Mean					7.2		19.2		16.9
COV					0.06		0.49		3.99
4A	Cyclic	Elastic	-	-	-	-	-	-	-
4B	Cyclic	Elastic	-	-	-	-	-	-	-
4C	Sc. Taiwan 2D	Elastic	0.03	-1.23	20.6	0.178	31.8	-	-
4D	Sc. Taiwan 3D	Elastic	0.4	0.989	3.6	-0.599	15.2	8.14e-5	15.1
4E	Taiwan 3D	Inelastic	1.0	2.42	5.1	1.29	31.6	2.129e-4	17.5
4F	Sc. Taiwan 3D	Inelastic	2.0	5.09	7.4	-3.76	31.1	4.177e-4	16.2
Mean					6.1		18.3		8.1
COV					0.45		0.49		0.01
Mean					**5.3**		**9.3**		**20.1**
COV					**0.03**		**0.24**		**5.89**

Table 6.3: Summary of rms test and numerical model results

Test ID	*Input Excitation*	*Test Type*	*Scaling Factor*	*RMS Roof Displacement (mm)*	*Disp. Error Model and Test (%)*	*RMS Acceration (m/s^2)*	*Acc. Error Model and Test (%)*	*RMS Test Strain* **SG4**	*Strain Error (%)*
1A	Cyclic	Elastic	-	-	-	-	-	-	-
1B	Cyclic	Elastic	-	-	-	-	-	-	-
1C	Sc. Taiwan 2D	Elastic	0.03	0.8916	0.07	0.0195	5.44	-	-
1D	Sc. Taiwan 3D	Elastic	0.4	0.6857	8.92	0.1992	3.67	3.593e-5	118.83
1E	Taiwan 3D	Inelastic	1.0	2.2602	6.11	0.6565	7.48	1.649e-4	310.98
1F	Sc. Taiwan 3D	Inelastic	2.0	3.427	47.07	0.9799	13.52	1.957e-4	96.77
Mean					15.54		7.53		175.53
COV					341.63		13.77		9254.9
2A	Cyclic	Elastic	-	-	-	-	-	-	-
2B	Cyclic	Elastic	-	-	-	-	-	-	-
2C	Sc. Taiwan 2D	Elastic	0.03	0.8128	7.52	0.0179	2.07	-	-
2D	Sc. Taiwan 3D	Elastic	0.4	0.5942	4.67	0.2552	6.01	1.592e-4	7.72
2E	Taiwan 3D	Inelastic	1.0	2.166	0.05	0.6185	1.63	3.035e-4	66.64
2F	Sc. Taiwan 3D	Inelastic	2.0	4.007	11.6	1.119	3.63	1.4013e-4	66.95
Mean					3.63		1.48		47.1
COV					40.14		11.84		775.5
3A	Cyclic	Elastic	-	-	-	-	-	-	-
3B	Cyclic	Elastic	-	-	-	-	-	-	-
3C	Sc. Taiwan 2D	Elastic	0.03	0.3604	3.73	0.03167	26.22	-	-
3D	Sc. Taiwan 3D	Elastic	0.4	0.1609	21.06	0.09365	16.24	9.40e-6	121.5
3E	Taiwan 3D	Inelastic	1.0	0.5143	17.52	0.3685	1.65	4.642e-5	64.23
3F	Sc. Taiwan 3D	Inelastic	2.0	0.8732	5.23	0.6108	24.67	4.135e-5	138.49
Mean					10.02		4.03		65.25
COV					97.5		374.54		8431.14
4A	Cyclic	Elastic	-	-	-	-	-	-	-
4B	Cyclic	Elastic	-	-	-	-	-	-	-
4C	Sc. Taiwan 2D	Elastic	0.03	0.355	10.15	0.0229	72.24	-	-
4D	Sc. Taiwan 3D	Elastic	0.4	0.1505	8.41	0.08677	15.12	5.81e-6	104.86
4E	Taiwan 3D	Inelastic	1.0	0.4034	4.88	0.29053	4.69	8.30e-6	270.92
4F	Sc. Taiwan 3D	Inelastic	2.0	0.8202	3.17	0.5895	6.08	1.966e-5	213.3
Mean					1.57		19.15		196.35
COV					49.42		1010.13		4739.4
Mean					**7.69**		**8.05**		**121.06**
COV					**30.23**		**45.66**		**4305.2**

Table 6.4: Difference in initial stiffness and energy dissipation between test data and numerical model

Test ID	*Test Type*	*Energy Dissipation Test (J)*	*Energy Dissipation Num. Model (J)*	*Difference in Energy Dissipated (%)*	*Test Initial Stiffness (N/mm)*	*Numerically Modelled Init.Stiffness (N/mm)*	*Initial Stiffness Error (%)*	*Init. Stiffness Error 3D Models Only (%)*
1A	Cyclic	-	-	-	-	-	-	-
1B	Cyclic	-	-	-	-	-	-	-
1C	Sc. Taiwan 2D	5774.8	2490.1	56.8	9437.03	4820.44	48.92	-
1D	Sc. Taiwan 3D	2606.3	2490.1	4.46	9505.88	4822.12	49.29	49.29
1E	Taiwan 3D	4437.6	1579.2	64.4	9846.09	5355.09	45.61	45.61
1F	Sc. Taiwan 3D	49204	38564	21.6	9397.57	4397.11	47.64	47.64
Mean				36.8			47.87	47.51
COV				610.5			2.07	2.26
2A	Cyclic	-	-	-	-	-	-	-
2B	Cyclic	-	-	-	-	-	-	-
2C	Sc. Taiwan 2D	7698.9	1971.2	74.4	11505.88	2879.97	74.97	-
2D	Sc. Taiwan 3D	1639.1	395.4	75.9	11408.14	7035.64	38.33	38.33
2E	Taiwan 3D	13580.9	8877.4	34.6	11157.14	6119.4	45.15	45.15
2F	Sc. Taiwan 3D	44249.0	30990	29.9	10733.58	5980.53	44.18	44.18
Mean				53.7			50.68	42.59
COV				461.7			203.54	9.19
3A	Cyclic	-	-	-	-	-	-	-
3B	Cyclic	-	-	-	-	-	-	-
3C	Sc. Taiwan 2D	986.2	265.62	73.1	9835.45	2716.57	72.38	-
3D	Sc. Taiwan 3D	173.8	124.89	28.2	9846.06	6249.79	36.53	36.53
3E	Taiwan 3D	758.9	611.5	19.4	9770.26	6248.55	36.05	36.05
3F	Sc. Taiwan 3D	3839.9	2797.9	27.1	9749.39	6247.13	35.92	35.92
Mean				36.9			45.22	36.16
COV				446.3			245.97	0.067
4A	Cyclic	-	-	-	-	-	-	-
4B	Cyclic	-	-	-	-	-	-	-
4C	Sc. Taiwan 2D	814.7	238.5	70.7	11492.95	3091.13	73.11	-
4D	Sc. Taiwan 3D	137.1	103.2	24.7	11657.17	7069.44	39.35	39.35
4E	Taiwan 3D	970.1	559.9	42.3	11763.63	6607.21	43.83	43.83
4F	Sc. Taiwan 3D	4900.3	2773.6	43.4	12052.01	7070.27	41.34	41.34
Mean				45.3			49.41	41.51
COV				270.6			189.71	3.36
Mean				**43.2**			**48.3**	**41.9**
COV				**48.82**			**4.14**	**16.26**

Energy Dissipation

The force equilibrium of the system was examined to assess the accuracy of the numerical model in representing the test data. In the finite element method, solving for the displacements that minimise the total potential energy of the system ensures an equilibrium solution. Plots of base shear and lateral roof displacement are used to assess the equilibrium of the numerical model. Figure 6.109 below presents a typical hysteretic

response of the TEST 2F structure subjected to a seismic excitation. The area within the hysteresis of such a plot provides an evaluation of the energy dissipated in the structure during the seismic event.

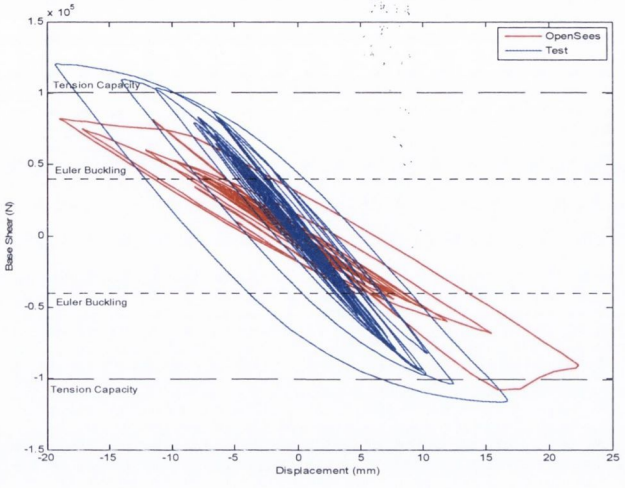

Figure 6.109: Graph of base shear vs. lateral displacement of test structure for TEST 2F

Table 6.4 compares the numerically modelled and experimentally measured energy dissipation during each experiment. In TEST 1, the average difference in energy dissipation between the numerical model and test data was 36.8%. In TEST 2, the average difference in energy dissipation between the numerical model and test data was 53.7%. In TEST 3, the average difference in energy dissipation between the numerical model and test data was 36.9%. In TEST 4, the average difference in energy dissipation between the numerical model and test data was 45.3%. It is evident from these results that the numerical model underestimated the level of energy dissipation that occurred in the structure during each test. It is not unexpected in finite element analysis to observe accurate displacements, but inaccurate forces, especially in nonlinear systems. In terms of displacements, velocities, accelerations and forces in the finite element method, the displacements provide the most reliable and accurate solution. For example, the shape functions and displacements are used to calculate the elemental forces. The shape functions are large and displacements are small. Subsequently, a small error in the displacement translates to a larger error in the computed forces.

Stiffness

Figure 6.109 presents a typical comparison of base shear and lateral displacement between the test data and the numerically modelled results. It can be seen from Figure 6.109 that the numerical model underestimates the stiffness of the frame. Table 6.4 presents the

differences in stiffness between the test data and numerical modelled results. The initial stiffness was calculated from the slope of the base shear versus lateral roof displacement hysteresis plot. The accuracy of the numerical model in predicting the stiffness of the test structure was reasonably poor. The stiffness of the three-dimensional models rather than two-dimensional models was of greater interest as these models capture the torsional response of the entire structure. The hysteresis plots for test and numerical model results for the three-dimensional models show an average 41.9% difference in initial stiffness. Similar to the forces, the calculation of the stiffness of an element in the FEM is based on the displacements. As can be seen from Table 6.4, the average difference in energy dissipation and stiffness throughout all of the tests is 43.2% and 41.9% respectively, both with a similar percentage of error.

Possible Errors

As mentioned in TEST 2, Section 6.3, the test frame base stub sections yielded in the web during TEST 1 and were permanently deformed inwards after the test. The numerical model in TEST 1 overestimated the stiffness of the test structure and then underestimated the stiffness in the remainder of the experiments (TEST 2, 3 & 4). It is thought the reason for some of the inaccuracy in the stiffness estimation of the test structure is due to this. To investigate this, a brief comparison of TEST 1 and TEST 2 is presented.

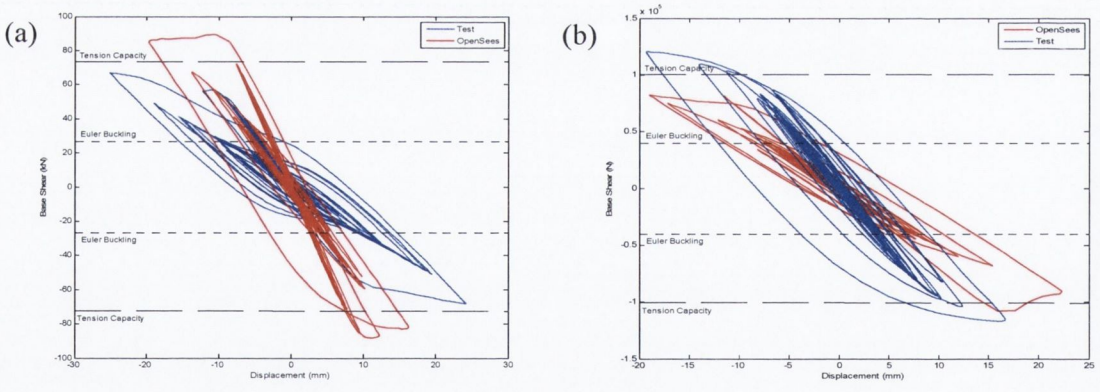

Figure 6.110 Graph of base shear vs. lateral displacement of test structure (a) TEST 1F and (b) TEST 2F

Figure 6.110(a) & (b) presents the numerically modelled and actual test hysteresis of TEST 1F and TEST 2F, respectively. The test structures differed in that TEST 1F had $\overline{\lambda}$ = 1.68 and TEST 2F had $\overline{\lambda}$ = 1.57. Comparing Figure 6.110(a) & (b) it can be seen that the numerical model overestimates the stiffness of the test frame in TEST 1F, while underestimating the stiffness of the test frame in TEST 2F. As mentioned previously, the

stub connections yielded during TEST 1 and were permanently deformed pushing the columns inwards as shown in Figure 6.111. It can be seen in Figure 6.111 the web section has yielded and is acting as a column with fixed-fixed restraints at the web-to-flange connection.

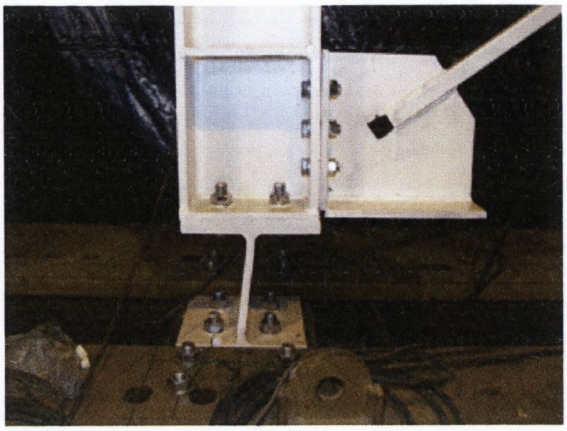

Figure 6.111 Permanent deformation of base stub connection after TEST 1F

For the remainder of the experiment, TEST 3 and TEST 4, the numerical model underestimated the initial stiffness of the test frame similar to TEST 2. It is evident from these observations that the use of the stub pin connection to represent a pinned connection creates errors, and may account for some of the difference in the numerically modelled and actual stiffness.

6.7.3 Effect of Parameter Variation

The main aim of the test series is to evaluate the effect on observed response of the changes in some important structural parameters. The effect of these parameter changes on the torsional response of the plan irregular test structure is of particular importance.

The variation in observed response with the change in torsional stiffness of the structure is evident by comparison of the peak lateral displacements of the torsionally stiff ($\Omega_\theta = 1.25$) and torsionally flexible ($\Omega_\theta = 0.75$) structures. For example, TEST 1F with $\Omega_\theta = 0.75$ had a maximum lateral roof displacement of 27.1mm, and TEST 3F with $\Omega_\theta = 1.25$ had a maximum lateral roof displacement of 5.51mm. Both test specimens in TEST 1F and TEST 3F were identical, having the same level of mass eccentricity, brace section size and being subjected to the same level of ground excitation. The only difference between the structures was the value of Ω_θ due to the different masses. Similarly, TEST 2F with $\Omega_\theta =$

0.75 had a maximum lateral roof displacement of 22.66mm and TEST 4F with Ω_θ = 1.25 had a maximum lateral roof displacement of 5.09mm. It can be seen from this simple comparison between these structures that Ω_θ has a significant effect on the structural response. The torsionally flexible structure has a greater displacement response (over 4 times greater) than the torsionally stiff structure.

The effect of designing the structure against accidental torsion can be seen in the comparison between TEST 1 & TEST 2 and between TEST 3 & TEST 4. For example, the test structures in TEST 3 and TEST 4 possess the same parameters but one was designed against accidental torsion. TEST 3 has 30x30x3mm SHS bracing and TEST 4 has 50x30x3mm RHS bracing. TEST 4F has been designed to resist accidental torsional effects. The maximum roof displacement of the structure for TEST 3F was 5.38mm compared to a maximum roof displacement of the structure for TEST 4F of 5.09mm. This simple comparison indicates that the structural response was not significantly improved by using the Eurocode 8 (CEN, (2004)) design method for accidental torsion. The test structure has only been designed to resist 5% mass eccentricity, as per Eurocode 8 (CEN, (2004)), whereas the structure has been tested with a mass eccentricity of 15%. The rms displacements of the numerical model and test structure differed by 15.54% in TEST 1, but only 3.63% in TEST 2. A similar trend was observed in the rms displacement errors for TEST 3 of 10.02% and for TEST 4 of 1.57%. The results indicate that the structures designed to resist torsion (i.e. TEST 2 & TEST 4) displayed a more reliable response as the numerical model was more capable of accurately predicting the overall displacement response observed in the test data.

The lateral torsional frequency ratio was varied between test structures by altering the mass and hence the natural period of the structure. The reduction/increase of the natural period results in a different level of response amplification for the same earthquake event. This can be seen in Figure 6.112 where the periods of the TEST 1 and TEST 3 structures are shown on the relative displacement response spectrum of the Taiwan earthquake record. The change in the period of the structure accounts for some of the change in the torsional flexibility of the structure. It could be expected that the change in the observed displacement response for each structure would correspond to the change in displacement demand indicated by the spectral values at the different natural periods.

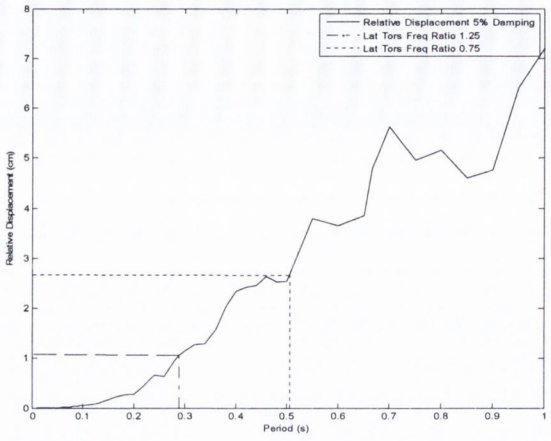

Figure 6.112: Graph of relative displacement vs. period for 5% damping for Taiwan excitation

Shown in Figure 6.112 is the relative displacement response spectrum of the Taiwan excitation (1986) with 5% damping. The relative displacement spectrum is related to the relative velocity spectrum and absolute acceleration response spectrum by the following equations:

$$x_{max} = \frac{T}{2\pi} . S_v \tag{6.1}$$

$$\dot{x}_{max} = S_v \tag{6.2}$$

$$\ddot{x}_{max} = \frac{2\pi}{T} . S_v \tag{6.3}$$

where x_{max} is the maximum value of the relative displacement between the mass and ground in a SDOF system

$\dot{x}_{max}$ is the maximum value of the relative velocity between the mass and ground in a SDOF system

$\ddot{x}_{max}$ is the maximum value of the relative acceleration between the mass and ground in a SDOF system

T is the period of the SDOF system

S_v is the relative velocity between the mass and ground in a SDOF system

(For a detailed description of the derivation of the response spectrum, see Hudson, (1956) or Clough and Penzien, (1993))

The hybrid test undertaken is displacement controlled, making the relative displacement response spectrum an appropriate method of assessing the difference in the responses of the the torsionally stiff and torsionally flexible structures.

The relative displacements expected in test structures corresponding to different periods can be seen in Figure 6.112. The stiffer structure (TEST 3) has a period of 0.289s and a relative displacement demand of 1.107cm compared to the flexible structure (TEST 1) with a period of 0.507s and a relative displacement demand of 2.714cm. The ratio of relative displacement response spectrum demand is 2.714/1.107 = 2.45. The maximum observed roof displacement in TEST 1F is 22.73mm and in TEST 3F is 5.38mm, resulting in a peak displacement ratio of 27.06/5.51 = 4.91. By comparing the relative displacement ratio and peak displacement ratio, it can be estimated that approximately 50% of the change in displacement response is attributed to the change in natural period. Similarly, the ratio of relative displacement response spectrum demand for TEST 2F and TEST 4F is 2.695/1.04 = 2.59. The maximum roof displacement for TEST 2F is 22.66mm and for TEST 4F is 5.09mm, resulting in a peak displacement ratio of 22.66/5.09 = 4.39. By comparing the relative displacement ratio and peak displacement ratio, it can be estimated that 41% of the increase in displacement response is due to the change in period. The remainder of the change in displacement response could be assumed to be due to the change in Ω_θ.

6.8 Chapter Overview

This chapter presented the main test results from a series of hybrid braced frame experiments. Two- and three-dimensional numerical models are compared to the test results to provide validation for the models. The results indicate that the proposed numerical model, as outlined in the Chapter Five, was able to accurately model the displacement response of the test structure. The peak and rms numerically modelled displacements showed good agreement with the test data. The peak and rms numerically modelled accelerations showed acceptable agreement with the test data. The peak and rms numerically modelled strain showed unacceptably poor agreement with the test data. In general, the numerical model underestimated the stiffness of the test structure. Some of the error associated to the underestimation of the initial stiffness was believed to be caused by the numerical modelling of the stub connections. The next chapter will detail the parametric study of a concentrically braced plan irregular structure with the full range of important structural parameters affecting the torsional response being investigated.

CHAPTER SEVEN – Parametric Study

7.1 Introduction

This chapter presents a parametric investigation of the seismic response of concentrically braced plan irregular structures. In the previous chapter, the response of an OpenSees numerical model of the concentrically braced plan irregular structure was compared against hybrid test data, and indicated good predictive capabilities. The three-dimensional numerical model developed in previous chapters will be used to investigate the changes in the response of concentrically braced plan irregular structures caused by variations in important structural parameters. Key parameters such as static eccentricity and lateral torsional frequency ratio are investigated using inelastic time history analysis. The effectiveness of the Eurocode 8 (CEN, (2004)) torsional effects design provision is assessed.

7.2 Parametric Study

This section will provide a brief overview of the important parameters that affect the torsional response of a concentrically braced plan irregular structure. The key parameters affecting the seismic behaviour of the plan irregular structure have been discussed in detail in Chapter Three. Only a limited number of parameters were varied during the test schedule in Chapter Six, a numerical parameter study allows a more complete investigation of the seismic behaviour of concentrically braced plan irregular structures. The key parameters investigated are; static eccentricity, lateral torsional frequency ratio, torsional effects design (brace slenderness) and plan aspect ratio.

Table 7.1: Key parameters and range considered

Parameter	*Range Considered*
$\overline{\lambda}$	1.3, 1.57, 1.68, 2.0
e_s	0.0L, 0.025L, 0.05L, 0.075L, 0.1L, 0.125L, 0.15L
Ω_θ	0.75, 0.875, 1.0, 1.125, 1.25
PA ratio	1.0, 1.5, 2.0, 2.5, 3.0
A/V ratio	0.53, 0.69, 0.74, 0.89, 1.0, 1.33, 1.77

The stochastic nature of earthquake events is considered by subjecting the structure to five earthquake time histories with low, medium and high A/V ratios (see Chapter Three, Section 3.6.5 for details). The important structural properties affecting the structural response of the plan irregular structure and the range of values investigated are listed in Table 7.1.

7.3 Numerical Model

The final three-dimensional numerical model used in the parametric study was the same model used in Chapter Five (Section 5.5.2) with the exception that the stubs used in the experimental setup to mimic a pinned connection are not included in the parametric numerical model. Idealised pinned connections at the column ends replace these stub connections. The final model is summarised as follows;

- Beams are modelled with elastic beam column elements with relevant section properties defined.
- Brace members are modelled with nonlinear beam-column elements with 7 No. integration points along their length and subdivided across their section into 10 No. elements along each thin-walled section and 5 No. elements across thin-walled section. The initial out-of-plane camber is 0.1% of the brace member's length.
- The gusset plates were modelled as elastic beam-column elements with a relatively high stiffness to replicate the structural stiffness of the gusset plates in the test set-up.
- All connections are modelled as idealised pinned connections.

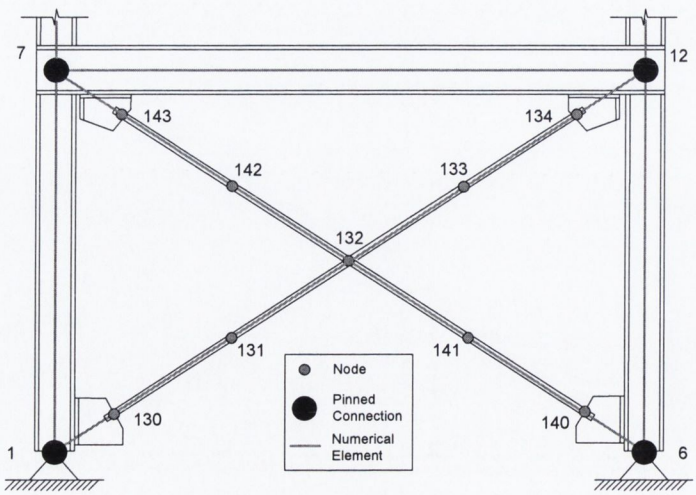

Figure 7.1: Final numerical model of concentrically braced frame for parametric study

The final braced frame numerical model is shown in Figure 7.1. Replacing the stub connections with idealised pinned connections had the effect of stiffening the structure and importantly allowed the structure to be modelled with gravity loads. For example, for the structure with $\Omega_\theta = 0.75$, $e_s = 0.0L$ and $\bar{\lambda} = 1.68$, the period of the parametric numerical model is 0.39s (without stubs) and test numerical model was 0.5s (with stubs). Consequently, the magnitude of the displacements observed during the experimental programme is higher than those displayed by equivalent numerical model without the stub connections. See Appendix E for the OpenSees model of the final braced frame structure.

7.4 Parametric Study Results

The following section provides a summary of the numerical analyses performed on the base model (described below) plan irregular three-storey concentrically braced steel structure. The seismic response is evaluated with respect to displacement ductility demand and interstorey drifts. The displacement ductility demand of the structure, μ_δ is defined as follows;

$$\mu_\delta = \frac{\delta_u}{\delta_y} \tag{7.1}$$

where; δ_u is the maximum displacement of the structure

δ_y is the first yield displacement of the structure

The yield displacement is obtained from a pushover analysis of the concentrically braced frame structure. The yield displacement is the lateral displacement of the structure at which the first yield of the bracing members occurs. The interstorey drift, d_r is defined in Eurocode 8 (CEN, (2004)) as the difference in the average lateral displacements at the top and bottom of the storey under consideration.

7.4.1 Base Model

The base (or reference) model structure was designed using the lateral force method of analysis in Eurocode 8 (CEN, (2004)). The base model structure had a plan aspect (PA) ratio of 2.0, $e_s = 0.0L$, $\Omega_\theta = 1.0$ (neither torsionally stiff nor torsionally flexible) and the lateral stability of the structure was provided by 30x30x3mm SHS concentric bracing ($\bar{\lambda}$ =

1.68) in each storey. The base model has been designed to resist a PGA of 0.35*g*. The base model structure has not been designed to resist any torsional effects. The base model structure was initially subjected to 7 No. earthquakes with varying levels of A/V ratio as described in Chapter Three, Section 3.6.5. The roof displacement response of the base model for all 7 No. unscaled earthquakes can be seen in Figure 7.2. The time histories with low A/V ratios are Taiwan (PGA 0.153*g*), Calitri (PGA 0.177*g*) and El Centro (PGA 0.215*g*), as shown on the left of Figure 7.2. The time histories with medium A/V ratios are Kobe (PGA 0.343*g*) and Friuli (PGA 0.315*g*), as shown in the centre of Figure 7.2. The time histories with high A/V ratios are Spitak (PGA 0.119*g*) and NWCalifornia (PGA 0.11*g*), as shown on the right of Figure 7.2.

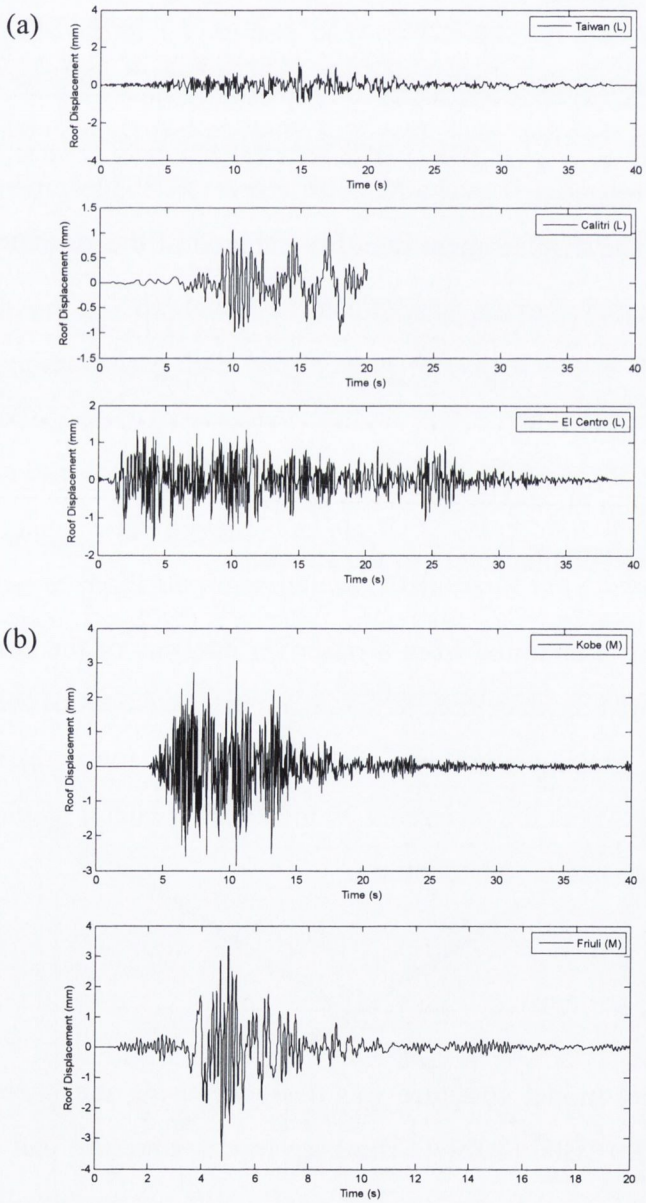

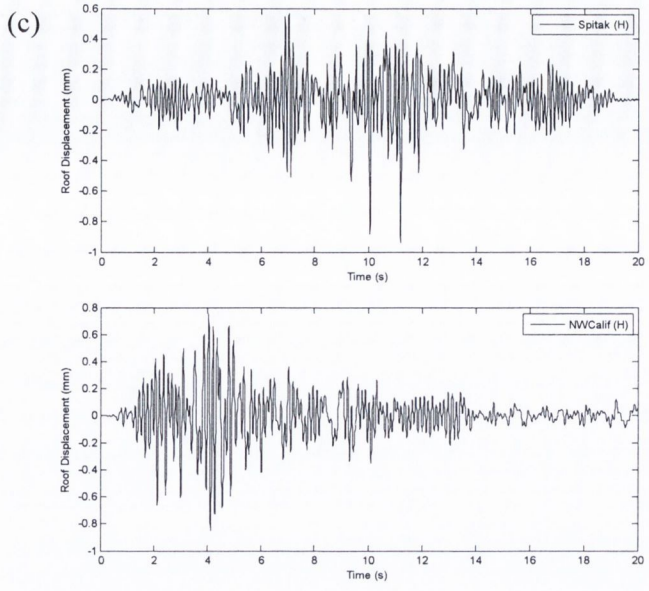

Figure 7.2: Graph of roof displacement vs. time for base model structure for (a) low, (b) medium, and (c) and high A/V ratio time histories

As can be seen from Figure 7.2, the Taiwan, Calitri and El Centro excitations have the medium level of lateral roof displacements and a sustained level of displacement throughout their duration. The Kobe and Friuli excitations result in the greatest lateral roof displacement for the base model structure analysed. The Spitak and NW Calif excitations had the smallest lateral roof displacements compared to the other excitations studied. To investigate the structural response more extensively only five earthquakes were selected; two excitations from low A/V ratio level, one from medium A/V ratio level and two from high A/V ratio level. The time histories selected were; Taiwan (L), El Centro (L), Friuli (M), Spitak (H) & NWCalif (H). The Taiwan excitation was chosen because the excitation provides an even distribution of acceleration gradually increasing to peak acceleration around 15s and then gradually reducing to the end of the excitation. The El Centro excitation was chosen because it has quite a different response compared to the Taiwan excitation, with large accelerations at the very start of the response rather than spread more evenly over the whole response as in the Taiwan excitation. The Kobe excitation has a longer duration than the Friuli excitation, but the Kobe excitation is rather uneventful in the second half of the excitation. Consequently, the Friuli excitation was chosen for the medium A/V ratio time history. For the high A/V ratio, both the Spitak and NWCalif excitations were chosen. The Friuli excitation had the largest PGA (0.315*g*) of the selected time histories. Each acceleration time history was scaled to have the same PGA as the Friuli time history so that the results from the analyses could be compared directly.

It should be noted that each of the above mentioned excitations is scaled to a PGA of $0.315g$ which is less than the assumed design PGA ($a_g = 0.35g$) for the structure. Some yielding of the base model structure is expected during the analyses. Figure 7.3 shows each of the five ground acceleration time histories with equal PGA. The Spitak and NW Calif records have durations of 20s, whereas the Taiwan, Friuli and El Centro records have durations of 40s.

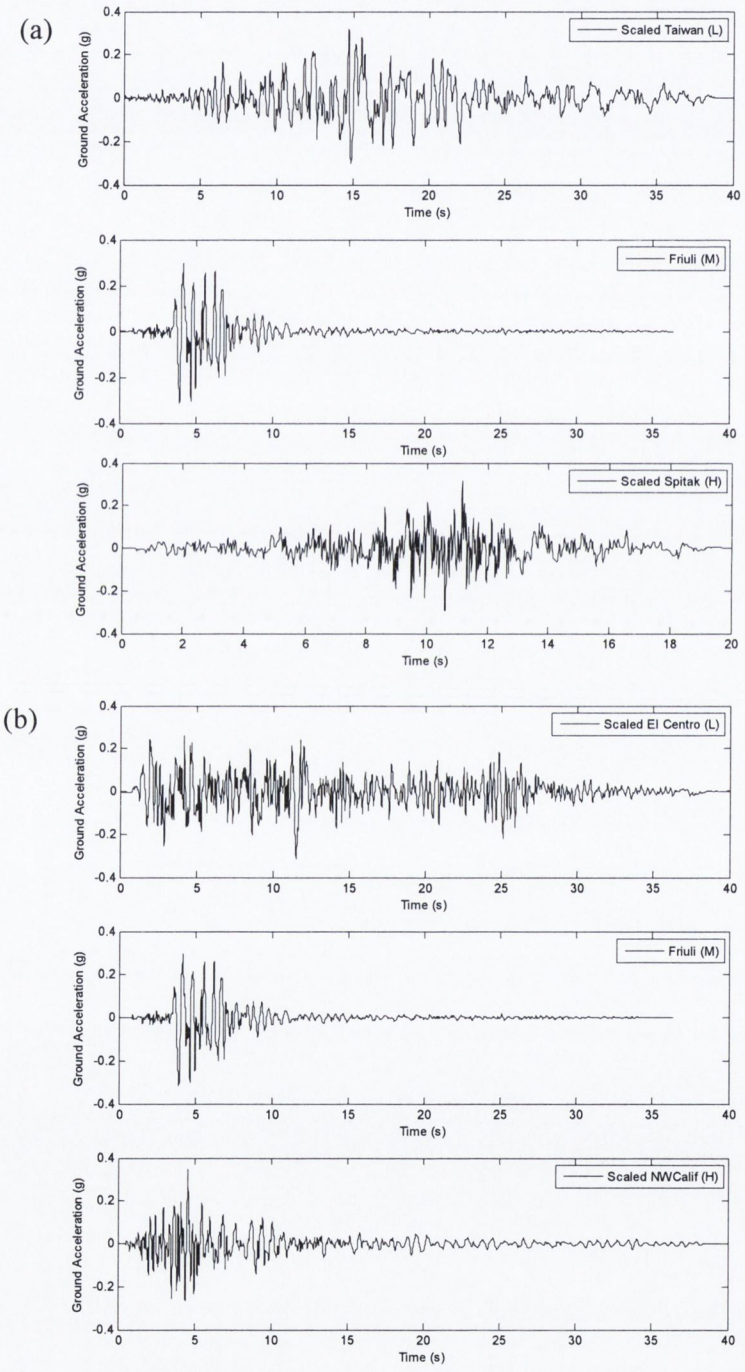

Figure 7.3: Graph of ground acceleration vs. time for (a) Taiwan (L), Friuli (M), Spitak (H), and (b) El Centro (L), Friuli (M), & NW Calif (H) excitations with equal PGA

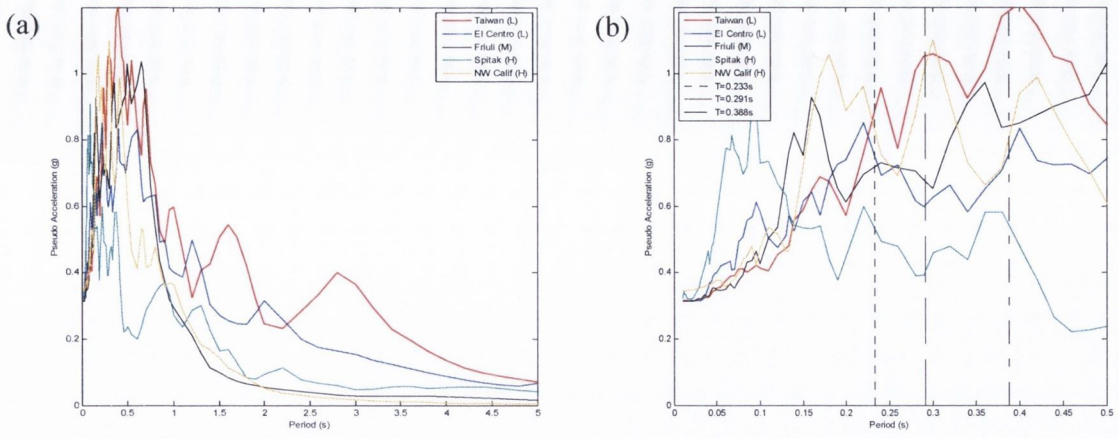

Figure 7.4: (a) Graph of scaled pseudo acceleration vs. period for Taiwan (L), El Centro (L), Friuli (M), Spitak (H) & NW Calif (H) excitations with equal PGA, and (b) close-up indicating three structural periods of structures analysed in relation to response spectrum

The scaled pseudo acceleration response spectrums of the 5 No. earthquake excitations used in the study are shown in Figure 7.4. The overall pseudo acceleration response spectrum can be seen in Figure 7.4(a). A close-up of the pseudo acceleration response spectrum with the periods of three of the structures analysed is shown in Figure 7.4(b). The three structural periods indicated represent the natural periods of the structures with a PA ratio of 2.0, $e_s = 0.0L$, $\bar{\lambda}$ =1.68 and lateral torsional frequency ratios of; $\Omega_\theta = 0.75$ (T = 0.388s), $\Omega_\theta = 1.0$ (T = 0.291s) and $\Omega_\theta = 1.25$ (T = 0.233s). These three structural periods give an indication of the upper and lower bounds of the natural period of the structures under investigation. As can be seen from Figure 7.4(b), the pseudo acceleration responses are similar at all three periods for the El Centro and Spitak excitations. The NW Calif excitation has a similar response at the lower and upper periods, but a higher response for the base model structure (T = 0.291s). The Friuli excitation has a similar level of acceleration for the structures with the two lower structural periods (T = 0.233s & T = 0.291s), but an increased response for the torsionally flexible structure with the larger period (T = 0.388s).

7.4.2 Analyses of Base Model Results

The following results outline the response of the base model structure to the 5 No. earthquakes described in the previous section. The base model structure used in these analyses has a PA ratio of 2.0, $\Omega_\theta = 1.0$, $\bar{\lambda} = 1.68$ and varying levels of e_s. The base model structure has not been designed to resist any torsional effects.

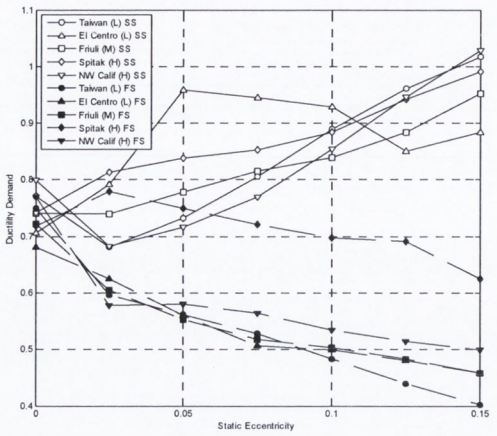

Figure 7.5: Graph of ductility demand vs. static eccentricity for SS & FS for each excitation (Ω_θ = 1.0, PA = 2.0, $\bar{\lambda}$ = 1.68)

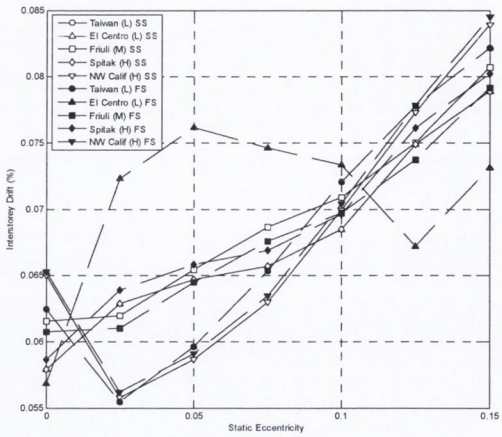

Figure 7.6: Graph of first-storey drift vs. static eccentricity for SS & FS for each excitation (Ω_θ = 1.0, PA = 2.0, $\bar{\lambda}$ = 1.68)

Figure 7.5 compares the variation in displacement ductility demand with static eccentricity for the SS and FS of the base model structure for each of the time histories. With the exception of the El Centro excitation, ductility demand in the SS of the structure increases consistently with static eccentricity. In contrast, with the exception of the Spitak excitation, the ductility demand in the FS of the structure decreases consistently with static eccentricity. Figure 7.6 compares the variation in first-storey drift with static eccentricity for the SS and FS of the base model structure for each of the time histories. The first-storey drifts due to the Spitak and Friuli excitations increase consistently with static eccentricity on both the SS and FS of the structure. The Taiwan and NW California excitations initially display a reduction in drift as the static eccentricity increases from $0.0L$ to $0.025L$, but then experienced increasing drifts with increase in static eccentricity on both the SS and FS of the structure. Figure 7.6 indicates that the first-storey drift is approximately the same for both the SS and FS of the structure, with the exception of the El Centro excitation.

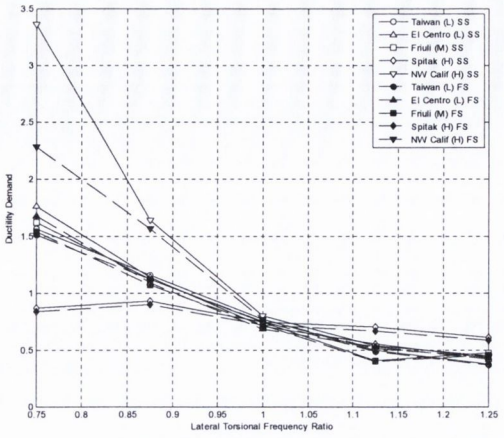

Figure 7.7: Graph of ductility demand vs. Ω_θ for SS & FS for each excitation (e_s = 0.0L, PA = 2.0, $\bar{\lambda}$ = 1.68)

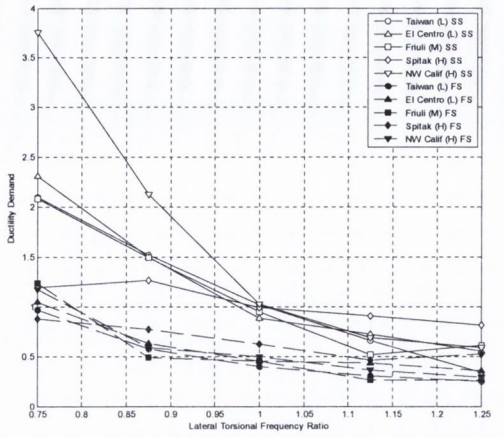

Figure 7.8: Graph of ductility demand vs. Ω_θ for SS & FS for each excitation (e_s = 0.15L, PA = 2.0, $\bar{\lambda}$ = 1.68)

Figure 7.7 compares the change in ductility demand against change in lateral torsional frequency ratio for the SS and FS of the base model structure with no static eccentricity (e_s = 0.0L). Figure 7.8 compares the change in ductility demand against change in lateral torsional frequency ratio for the SS and FS of the base model structure with maximum static eccentricity (e_s = 0.15L). In Figure 7.7 the ductility demands are very similar on the SS and FS of the structure for no static eccentricity (e_s = 0.0L) as can be seen from the overlapping lines in the graphs. With the exception of the NW Calif excitation on the SS of the structure for Ω_θ = 0.75, the ductility demands are approximately the same for both the SS and FS of the structure for all excitations. Figure 7.7 indicates the torsionally flexible (Ω_θ = 0.75) structures are subjected to a larger ductility demand compared to the torsionally stiff (Ω_θ = 1.25) structures. It can be seen from Figure 7.8 the ductility demands are noticeably different on the SS and FS of the structure for maximum static eccentricity (e_s = 0.15L). In particular, the NW Calif excitation has a much larger ductility demand as compared to the other excitations for Ω_θ = 0.75. For the torsionally stiff structures (Ω_θ = 1.125 & 1.25), the response of the structure is more stable. There is a greater variation in the ductility demand for the torsionally flexible structures (Ω_θ = 0.75 & 0.875) as compared to the torsionally stiff structures (Ω_θ = 1.125 & 1.25) as can be seen in both Figure 7.7 and Figure 7.8. For all levels of Ω_θ, the SS ductility demands for e_s = 0.15L are on average 22.1% greater than that of the SS ductility demands for e_s = 0.0L. For all levels of Ω_θ, the FS ductility demands for e_s = 0.15L are on average 51.9% lower than these of the FS ductility demands for e_s = 0.0L.

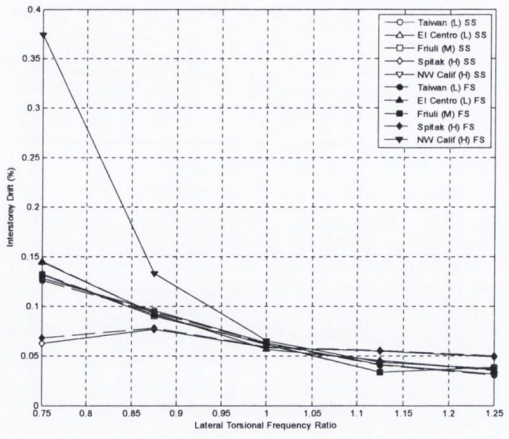

Figure 7.9: Graph of first-storey drift vs. Ω_θ for SS & FS for each excitation (e_s = 0.0L, PA = 2.0, $\bar{\lambda}$ = 1.68)

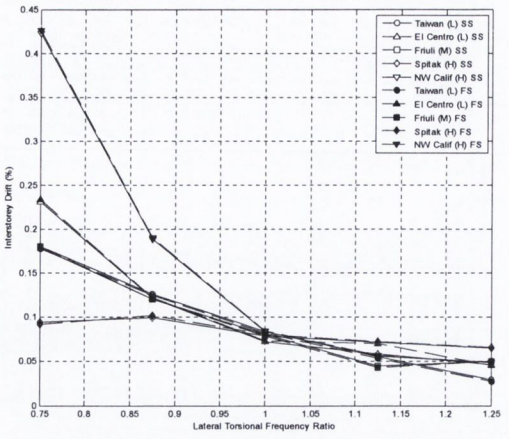

Figure 7.10: Graph of first-storey drift vs. Ω_θ for SS & FS for each excitation (e_s = 0.15L, PA = 2.0, $\bar{\lambda}$ = 1.68)

Figure 7.9 compares the change in first-storey drift against change in lateral torsional frequency ratio for the SS and FS of the base model structure with no static eccentricity (e_s = 0.0L). Figure 7.10 compares the change in first-storey drift against change in lateral torsional frequency ratio for the SS and FS of the base model structure with maximum static eccentricity (e_s = 0.15L). It can be seen from Figure 7.9 the first-storey interstorey drifts are approximately the same on the SS and FS of the structure for no static eccentricity (e_s = 0.0L). Likewise, it can be seen from Figure 7.10 the first-storey interstorey drifts are approximately the same on the SS and FS of the structure for maximum static eccentricity (e_s = 0.15L). Comparing Figure 7.9 and Figure 7.10, the first-storey interstorey drifts for e_s = 0.15L are on average 23.4% greater than that of the first-storey interstorey drifts for e_s = 0.0L on the SS of the structure. Similarly, the first-storey interstorey drifts for e_s = 0.15L are on average 22.7% greater than that of the first-storey interstorey drifts for e_s = 0.0L on the FS of the structure.

The seismic response of the torsionally stiff structures (Ω_θ = 1.125 & 1.25) is more stable. As shown in Figure 7.9 and Figure 7.10, the first-storey interstorey drift is lower for the torsionally stiff structures (Ω_θ = 1.125 & 1.25) as compared to the torsionally flexible structures (Ω_θ = 0.75 & 0.875). The torsionally flexible (Ω_θ = 0.75 & 0.875) structures show a more unstable structural response, particularly the NW Calif excitation for the structure with e_s = 0.15L and Ω_θ = 0.75, in which the first-storey drift is 8.5 times greater than in the structure with e_s = 0.15L and Ω_θ = 1.25. As shown in Figure 7.10 the SS and FS of the Ω_θ = 0.75 structure, the first-storey interstorey drift of 0.43% for the NW Calif

excitation approaches the assumed limit from Eurocode 8 (CEN, 2004) for interstorey drift of 0.5%.

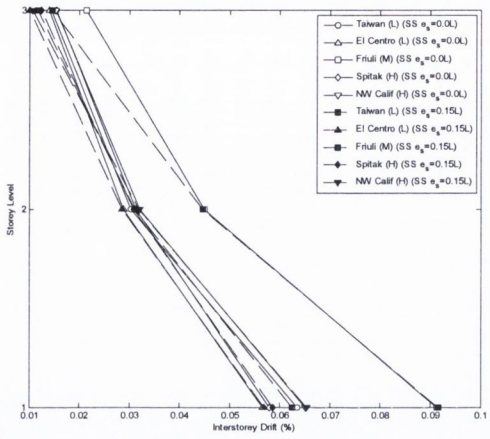

Figure 7.11: Graph of storey level vs. inter-storey drift for SS for each excitation for e_s = 0.0L & e_s = 0.15L (Ω_θ = 1.0)

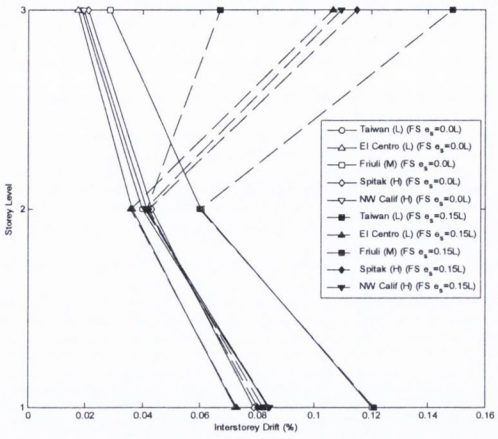

Figure 7.12: Graph of storey level vs. interstorey drift for FS for each excitation for e_s = 0.0L & e_s = 0.15L (Ω_θ = 1.0)

The variation in SS and FS interstorey drift throughout the height of the building is shown for various values of static eccentricity in Figure 7.11 and Figure 7.12, respectively. Figure 7.11 shows the base model performs well in terms of interstorey drift on the SS of the structure for $e_s = 0.0L$ and $e_s = 0.15L$. The Eurocode 8 (CEN, (2004)) interstorey drift limit of 0.5% is assumed as the design criteria limit. It can be seen from Figure 7.11 and Figure 7.12 the interstorey drifts are all below the 0.5% limit for the base model structure.

The interstorey drifts of the SS for $e_s = 0.0L$ and $e_s = 0.15L$ are very similar within each storey. The interstorey drifts of the FS for $e_s = 0.0L$ and $e_s = 0.15L$ are very similar within each storey, with the exception of the third-storey. Unexpectedly, the FS interstorey drifts for the third-storey with $e_s = 0.15L$ had slightly larger interstorey drifts as compared to the SS third-storey interstorey drifts with $e_s = 0.15L$ for all excitations, as shown in Figure 7.12. The FS interstorey drifts are approximately 69.2% greater than the SS interstorey drifts for the third-storey for maximum static eccentricity. It is possible the influence of higher modes affected the third-storey response of this structure to a greater extent than previously observed responses.

The results indicate the base model Eurocode 8 (CEN, (2004)) designed structure with PA ratio of 2.0, $\Omega_\theta = 1.0$, $e_s = 0.0L$ & $0.15L$ and $\bar{\lambda} = 1.68$, performed well with respect to interstorey drifts. The ductility demand on the SS of the structure increases with increasing static eccentricity but reduces with increasing static eccentricity on the FS of the structure.

The torsionally flexible structures have an increased ductility demand as compared to the torsionally stiff structure. This section has provided an overview of the structural behaviour of braced frame plan irregular structures. The next section will describe the structural behaviour of the concentrically braced plan irregular structures more extensively.

7.5 Complete Parametric Investigation

For the purposes of clarity, the average results of the five chosen earthquakes will be used to demonstrate the seismic response of the concentrically braced plan irregular structures, as opposed to presenting the results from each individual earthquake as per the previous section. To simplify the visualisation of the effect of the structural properties and different earthquake results, the mean results will be used with 95% confidence intervals (CI's) where applicable.

7.5.1 Static Eccentricity

The static eccentricity, e_s was varied from $0.0L$ to $0.15L$. Analyses were undertaken on the base model structure with PA ratio of 2.0, $\bar{\lambda}$ = 1.68 and varying levels of Ω_θ and e_s. The behaviour of the structure for a range of static eccentricities at different levels of lateral torsional frequency ratio is shown in Figure 7.13 to Figure 7.22. The mean of the results rather than all individual results from the five time histories are plotted to improve the clarity of the displayed data. A one sample t-test is performed within each group to verify normality and check the significance of the mean value. All of the Anderson-Darling test statistics gave p-values strongly supporting the null-hypothesis that the data comes from a normal distribution. The shaded areas in the figures indicate the limit of the 95% CI's. Tables 7.2 & 7.3 summarise the mean ductility demand and first-storey drift including CI's for the SS and FS, respectively.

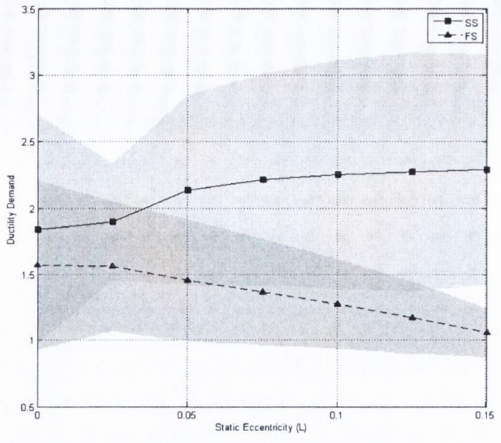

Figure 7.13: Graph of ductility demand vs. static eccentricity for SS & FS for $\Omega_\theta = 0.75$

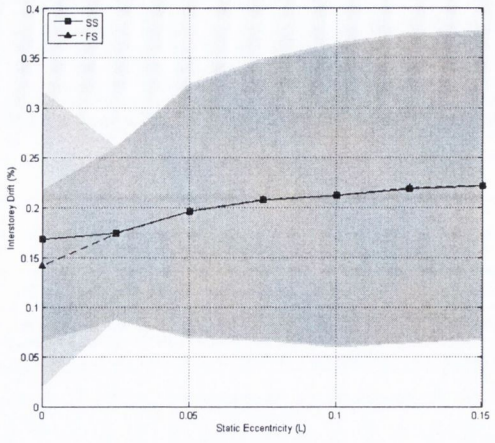

Figure 7.14: Graph of first-storey drift vs. static eccentricity for SS & FS for $\Omega_\theta = 0.75$

Figure 7.13 illustrates the variation in ductility demand with static eccentricity for the Ω_θ = 0.75 structure (torsionally flexible). Ductility demand increases on the SS of the structure from 1.84 for e_s = 0.0L to 2.3 for e_s = 0.15L, while the ductility demand decreases from 1.57 for e_s = 0.0L to 1.06 for e_s = 0.15L on the FS of the structure. The 95% CI's for the SS of the structure are large, as can be seen in Figure 7.13 and Table 7.2, indicating the variability in the SS structural ductility demand for the various earthquakes is reasonably large for the most torsionally flexible structure (Ω_θ = 0.75). For the SS of the Ω_θ = 0.75 structure, the CI's are smaller for e_s = 0.0L compared to e_s = 0.15L. The CI's are larger for e_s = 0.0L compared to e_s = 0.15L on the FS of the Ω_θ = 0.75 structure. As can be seen in Figure 7.13 and Tables 7.2 & 7.3, the 95% CI's for the FS of the structure are smaller than the SS, indicating the FS ductility demand is less variable for the most torsionally flexible structure (Ω_θ = 0.75). Above e_s = 0.075L the ductility demand on the SS can be greater than 3.

Figure 7.14 illustrates the variation in first-storey interstorey drift with static eccentricity for the Ω_θ = 0.75 structure (torsionally flexible). The first-storey drift increases on the SS of the structure from 0.17% for e_s = 0.0L to 0.22% for e_s = 0.15L, while the first-storey drift increases from 0.14% for e_s = 0.0L to 0.22% for e_s = 0.15L on the FS of the structure.

The 95% CI's for the SS of the structure are quite large, indicating the variability in the SS structural first-storey drift for the various earthquakes is reasonably large for the most torsionally flexible structure (Ω_θ = 0.75). The CI's are larger for e_s = 0.15L compared to e_s = 0.0L. In Figure 7.14 and Tables 7.2 & 7.3 it can be seen the first-storey drift response of the SS and FS of the structure is approximately the same, with the exception of e_s = 0.0L. It

appears to be an anomaly that the SS first-storey drift at $e_s = 0.0L$ is greater than the FS first-storey drift at $e_s = 0.0L$ as this was not observed in the other analyses.

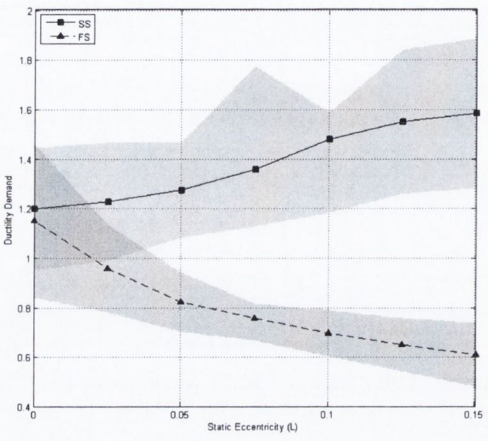

Figure 7.15: Graph of ductility demand vs. static eccentricity for SS & FS for $\Omega_\theta = 0.875$

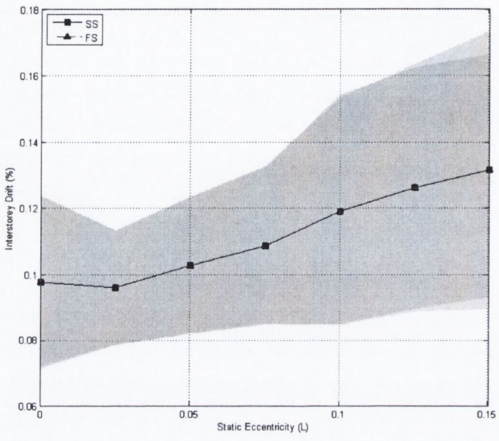

Figure 7.16: Graph of first-storey drift vs. static eccentricity for SS & FS for $\Omega_\theta = 0.875$

Figure 7.15 illustrates the variation in ductility demand with static eccentricity for the $\Omega_\theta = 0.875$ structure (torsionally flexible). The ductility demand shows the same trend as the $\Omega_\theta = 0.75$ structure with ductility demand increasing on the SS and decreasing on the FS of the structure with increasing e_s, however the ductility demands are lower for the $\Omega_\theta = 0.875$ structure compared to the $\Omega_\theta = 0.75$ structure. It can be seen from Figure 7.15 that the SS ductility demand remains below 2 even at $e_s = 0.15L$. The CI's are more consistent at each value of e_s, and are smaller in magnitude for the $\Omega_\theta = 0.875$ structure compared to the $\Omega_\theta = 0.75$ structure. Similar to the $\Omega_\theta = 0.75$ structure, the FS ductility demand is less variable compared to the SS ductility demand (larger CI's).

Figure 7.16 illustrates the variation in first-storey interstorey drift with static eccentricity for the $\Omega_\theta = 0.875$ structure (torsionally flexible). The first-storey drift shows a similar trend as the $\Omega_\theta = 0.75$ structure with the SS and FS first-storey drifts are approximately the same at every value of e_s. As can be seen in Figure 7.16 and Tables 7.2 & 7.3, the peak first-storey drift increases on both SS and FS of the structure from approximately 0.1% for $e_s = 0.0L$ to 0.13% for $e_s = 0.15L$. The peak first-storey drift is less than the first-storey drift of the $\Omega_\theta = 0.75$ structure (0.22% at $e_s = 0.15L$).

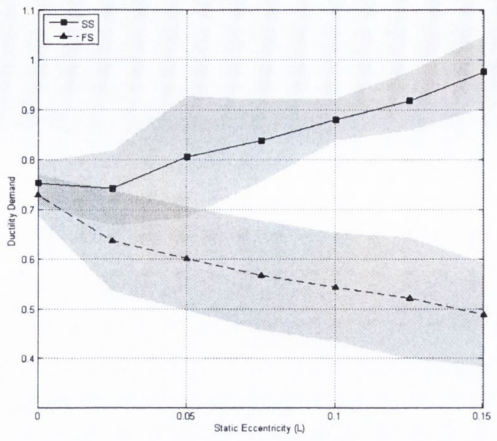

Figure 7.17: Graph of ductility demand vs. static eccentricity for SS & FS for $\Omega_\theta = 1.0$

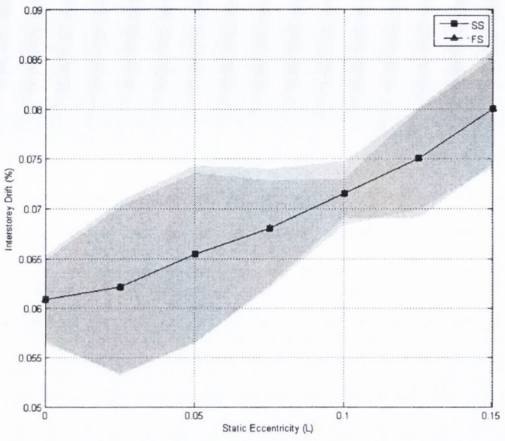

Figure 7.18: Graph of first-storey drift vs. static eccentricity for SS & FS for $\Omega_\theta = 1.0$

Figure 7.17 illustrates the variation in ductility demand with static eccentricity for the Ω_θ = 1.0 structure (neither torsionally stiff nor torsionally flexible). Ductility demand increases on the SS of the structure from 0.75 for $e_s = 0.0L$ to 0.98 for $e_s = 0.15L$, while the ductility demand decreases from 0.73 for $e_s = 0.0L$ to 0.49 for $e_s = 0.15L$ on the FS of the structure. Unlike the torsionally flexible structures (Ω_θ = 0.75 & 0.875), the Ω_θ = 1.0 structure has levels of ductility demand below 1 for all values of e_s, indicating no yield in the structure. The 95% CI's for the SS of the structure are relatively small. As can be seen in Figure 7.17 and Tables 7.2 & 7.3, the 95% CI's for the FS of the structure are larger than the SS, indicating the variability in the FS structural ductility demand for the various earthquakes is more variable than the SS of the structure for the neither torsionally stiff nor torsionally flexible structure (Ω_θ = 1.0). This is in contrast to the torsionally flexible structures.

Figure 7.18 illustrates the variation in first-storey interstorey drift with static eccentricity for the Ω_θ = 1.0 structure (neither torsionally stiff nor torsionally flexible). As can be seen in Figure 7.18 and Table 7.3, the first-storey drift on the SS and FS of the structure increases from 0.06% for $e_s = 0.0L$ to 0.08% for $e_s = 0.15L$. The first-storey drift is approximately the same on the SS and FS of the structure, representing a similar trend to the torsionally flexible structures. The 95% CI's are smaller in comparison to the torsionally flexible structures indicating the variability in the SS structural ductility demand for the various earthquakes is reasonably low for the neither torsionally stiff nor torsionally flexible structure (Ω_θ = 1.0).

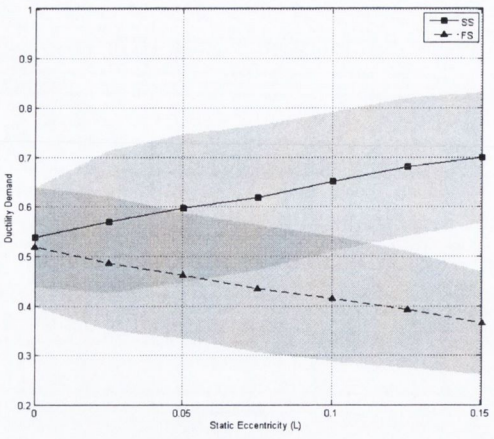

Figure 7.19: Graph of ductility demand vs. static eccentricity for SS & FS for $\Omega_\theta = 1.125$

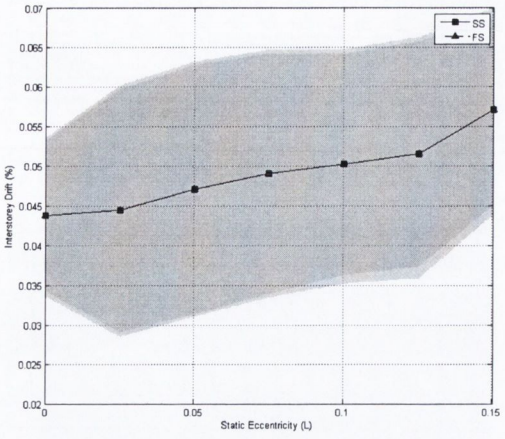

Figure 7.20: Graph of first-storey drift vs. static eccentricity for SS & FS for $\Omega_\theta = 1.125$

Figure 7.19 illustrates variation in ductility demand with static eccentricity for the Ω_θ = 1.125 structure (torsionally stiff). Ductility demand increases on the SS of the structure from 0.537 for $e_s = 0.0L$ to 0.698 for $e_s = 0.15L$, while the ductility demand decreases from 0.518 for $e_s = 0.0L$ to 0.365 for $e_s = 0.15L$ on the FS of the structure. In comparison with the more flexible structures (Ω_θ = 0.75, 0.875 & 1.0), the ductility demand is reduced but shows a similar trend increasing on the SS and decreasing on the FS. The increase and decrease is almost linear unlike the more flexible structures (Ω_θ = 0.75, 0.875 & 1.0). The 95% CI's for the SS of the structure are quite large, as can be seen in Figure 7.19 and Table 7.2, indicating the variability in the SS structural ductility demand for the various earthquakes is reasonably large for the intermediate torsionally stiff structure (Ω_θ = 1.125). The CI's on the SS and FS of the structure are similar for all levels of static eccentricity.

Figure 7.20 illustrates the variation in first-storey interstorey drift with static eccentricity for the structure with Ω_θ = 1.125 (torsionally stiff). As can be seen in Figure 7.20 and Table 7.3, the first-storey drift on the SS and FS increases from 0.04% for $e_s = 0.0L$ to 0.06% for $e_s = 0.15L$. The first-storey drift is approximately the same on the SS and FS of the structure, representing a similar trend to the torsionally flexible structures. The 95% CI's are quite large, indicating the variability in the first-storey drift for the various earthquakes is reasonably large for the intermediate torsionally stiff structure (Ω_θ = 1.125). The first-storey drifts are less than the first-storey drifts of the more flexible structures (Ω_θ = 0.75, 0.875 & 1.0).

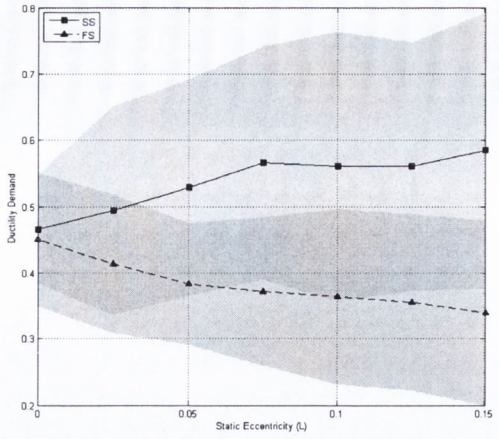

Figure 7.21: Graph of ductility demand vs. static eccentricity for SS & FS for $\Omega_\theta = 1.25$

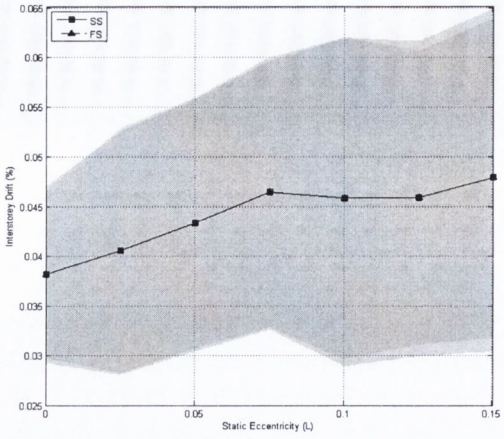

Figure 7.22: Graph of first-storey drift vs. static eccentricity for SS & FS for $\Omega_\theta = 1.25$

Figure 7.21 indicates the variation in ductility demand with static eccentricity for the Ω_θ = 1.25 structure (torsionally stiff). Ductility demand increases on the SS of the structure from 0.47 for $e_s = 0.0L$ to 0.58 for $e_s = 0.15L$, while the ductility demand decreases on the FS of the structure from 0.45 for $e_s = 0.0L$ to 0.34 for $e_s = 0.15L$. In comparison with the more flexible structures (Ω_θ = 0.75, 0.875, 1.0 & 1.125), the ductility demand is reduced but shows a similar trend increasing on the SS and decreasing on the FS. The 95% CI's for the SS and FS of the structure are large, as can be seen in Figure 7.21 and Table 7.2, indicating the variability in the SS structural ductility demand for the various earthquakes is reasonably large for the most torsionally stiff structure (Ω_θ = 1.25). The proportional size of the CI's is larger than any of the previous structures indicating greater variability in the response, but on average the level of ductility demand is reduced as compared to the more torsionally flexible structures (Ω_θ = 0.75, 0.875, 1.0 & 1.125).

Figure 7.22 illustrates the variation in first-storey interstorey drift with static eccentricity for the Ω_θ = 1.25 structure (torsionally stiff). As can be seen in Figure 7.22 and Table 7.3, the first-storey drift on the SS and FS increases from 0.04% for $e_s = 0.0L$ to 0.05% for $e_s = 0.15L$. The first-storey drifts are slightly less compared to the Ω_θ = 1.125 structure. The 95% CI's are large, indicating the variability in the first-storey drift for the various earthquakes is reasonably large for the most torsionally stiff structure (Ω_θ = 1.25). The CI's are larger for $e_s = 0.15L$ compared to $e_s = 0.0L$. The first-storey drifts are less than the first-storey drifts of the more flexible structures (Ω_θ = 0.75, 0.875, 1.0 & 1.1.25).

Summary

The static eccentricity was varied during the parametric study ranging from no static eccentricity ($e_s = 0.0L$) to maximum static eccentricity ($e_s = 0.15L$). The maximum value represents a severe but realistic level of static eccentricity. Results indicate that the ductility demand increases with increasing levels of static eccentricity on the SS of the structure and reduces with increasing levels of static eccentricity on the FS of the structure. The torsionally stiff structures perform better than the torsionally flexible structures having reduced ductility demands and reduced first-storey drifts. Considering all lateral torsional frequency ratios, the SS ductility demand increased on average by nearly 30% from the no static eccentricity case to the maximum static eccentricity case. In contrast, the FS ductility demand decreased on average by just over 30%. The first-storey interstorey drift increases for increasing levels of static eccentricity for all values of lateral torsional frequency ratio. Unlike the ductility demands, the first-storey interstorey drifts increase by a similar amount on both the SS (29.6%) and FS (35.2%) of the structure. The CI's are generally larger at extreme levels of lateral torsional frequency ratio e.g. $\Omega_\theta = 0.75$ & 1.25. No general trend was observed indicating reduced CI's for the torsionally stiff structures compared to the torsionally flexible structures. The level of interstorey drift presented in this section has focussed on the first-storey drift, as this always gave the greatest level of drift for each of the storeys. The level of drift in the other storeys varied such that the ductility demand was always greater on the SS compared to the FS even though the SS and FS first-storey drifts were generally similar. The level of static eccentricity has been observed to be a key parameter affecting the seismic torsional response of plan irregular braced frame type structures.

Table 7.2: Summary of SS mean ductility demand and interstorey drift results

Ω_0	*Static Ecc. (L)*	*Mean Ductility Demand*	*+ 95% CI Ductility Demand*	*- 95% CI Ductility Demand*	Ω_0	*Static Ecc. (L)*	*Mean First-storey Drift*	*+ 95% CI Ductility Demand*	*- 95% CI Ductility Demand*
0.75	0.0	1.835	2.701	0.971	0.75	0.0	0.168	0.316	0.019
	0.025	1.893	2.332	1.454		0.025	0.174	0.261	0.087
	0.05	2.132	2.847	1.417		0.05	0.196	0.321	0.071
	0.075	2.110	3.005	1.417		0.075	0.207	0.346	0.068
	0.1	2.249	3.110	1.389		0.1	0.212	0.362	0.062
	0.125	2.269	3.165	1.373		0.125	0.218	0.372	0.065
	0.15	2.288	3.156	1.420		0.15	0.221	0.374	0.069
Mean		**2.111**			**Mean**		**0.199**		
COV		**0.028**			**COV**		**0.0004**		
0.875	0.0	1.197	1.444	0.950	0.875	0.0	0.098	0.124	0.072
	0.025	1.226	1.464	0.989		0.025	0.096	0.113	0.079
	0.05	1.273	1.465	1.081		0.05	0.102	0.124	0.082
	0.075	1.355	1.585	1.127		0.075	0.109	0.133	0.085
	0.1	1.476	1.771	1.181		0.1	0.119	0.154	0.085
	0.125	1.547	1.837	1.258		0.125	0.126	0.162	0.089
	0.15	1.581	1.882	1.280		0.15	0.131	0.166	0.093
Mean		**1.379**			**Mean**		**0.112**		
COV		**0.021**			**COV**		**0.0002**		
1.0	0.0	0.751	0.795	0.708	1.0	0.0	0.061	0.065	0.056
	0.025	0.741	0.817	0.667		0.025	0.062	0.071	0.053
	0.05	0.705	0.927	0.683		0.05	0.065	0.074	0.057
	0.075	0.837	0.920	0.754		0.075	0.068	0.074	0.062
	0.1	0.879	0.922	0.837		0.1	0.071	0.075	0.068
	0.125	0.917	0.976	0.858		0.125	0.075	0.080	0.069
	0.15	0.975	1.047	0.902		0.15	0.080	0.086	0.074
Mean		**0.829**			**Mean**		**0.069**		
COV		**0.009**			**COV**		**4.15e-5**		
1.125	0.0	0.537	0.637	0.437	1.125	0.0	0.043	0.053	0.034
	0.025	0.569	0.712	0.425		0.025	0.044	0.059	0.029
	0.05	0.596	0.745	0.447		0.05	0.047	0.063	0.031
	0.075	0.617	0.763	0.472		0.075	0.049	0.064	0.034
	0.1	0.649	0.789	0.509		0.1	0.050	0.064	0.036
	0.125	0.679	0.819	0.540		0.125	0.052	0.066	0.037
	0.15	0.698	0.830	0.566		0.15	0.057	0.069	0.045
Mean		**0.621**			**Mean**		**0.049**		
COV		**0.003**			**COV**		**1.78e-5**		
1.25	0.0	0.465	0.547	0.384	1.25	0.0	0.038	0.047	0.029
	0.025	0.494	0.651	0.337		0.025	0.041	0.053	0.028
	0.05	0.528	0.691	0.365		0.05	0.043	0.056	0.031
	0.075	0.566	0.741	0.389		0.075	0.046	0.059	0.033
	0.1	0.560	0.764	0.357		0.1	0.046	0.061	0.029
	0.125	0.560	0.747	0.373		0.125	0.046	0.061	0.031
	0.15	0.584	0.793	0.375		0.15	0.048	0.064	0.032
Mean		**0.537**			**Mean**		**0.044**		
COV		**0.002**			**COV**		**1.05e-5**		

Table 7.3: Summary of FS mean ductility demand and interstorey drift results

Ω_θ	*Static Ecc. (L)*	*Mean Ductility Demand*	*+ 95% CI Ductility Demand*	*- 95% CI Ductility Demand*	Ω_θ	*Static Ecc. (L)*	*Mean First-storey Drift*	*+ 95% CI Ductility Demand*	*- 95% CI Ductility Demand*
0.75	0.0	1.569	2.207	0.931	0.75	0.0	0.142	0.218	0.066
	0.025	1.559	2.048	1.070		0.025	0.174	0.260	0.087
	0.05	1.455	1.914	0.995		0.05	0.196	0.324	0.069
	0.075	1.366	1.767	0.967		0.075	0.208	0.349	0.066
	0.1	1.276	1.612	0.941		0.1	0.212	0.365	0.059
	0.125	1.174	1.447	0.900		0.125	0.219	0.375	0.064
	0.15	1.062	1.244	0.879		0.15	0.222	0.377	0.067
Mean		**1.352**			**Mean**		**0.196**		
COV		**0.032**			**COV**		**0.0007**		
0.875	0.0	1.149	1.458	0.841	0.875	0.0	0.098	0.124	0.072
	0.025	0.958	1.135	0.783		0.025	0.096	0.113	0.079
	0.05	0.823	0.943	0.704		0.05	0.103	0.123	0.082
	0.075	0.758	0.849	0.669		0.075	0.109	0.133	0.085
	0.1	0.697	0.791	0.604		0.1	0.119	0.154	0.085
	0.125	0.651	0.759	0.544		0.125	0.126	0.162	0.089
	0.15	0.611	0.739	0.481		0.15	0.129	0.166	0.093
Mean		**0.807**			**Mean**		**0.114**		
COV		**0.031**			**COV**		**0.0002**		
1.0	0.0	0.728	0.686	0.686	1.0	0.0	0.061	0.065	0.057
	0.025	0.636	0.535	0.535		0.025	0.062	0.070	0.054
	0.05	0.601	0.497	0.497		0.05	0.065	0.074	0.056
	0.075	0.567	0.457	0.457		0.075	0.068	0.073	0.062
	0.1	0.543	0.434	0.434		0.1	0.071	0.073	0.069
	0.125	0.521	0.399	0.399		0.125	0.075	0.080	0.069
	0.15	0.4883	0.384	0.384		0.15	0.079	0.085	0.075
Mean		**0.584**			**Mean**		**0.068**		
COV		**0.006**			**COV**		**4.11e-5**		
1.125	0.0	0.518	0.638	0.398	1.125	0.0	0.044	0.054	0.034
	0.025	0.485	0.520	0.351		0.025	0.044	0.060	0.029
	0.05	0.461	0.587	0.335		0.05	0.047	0.053	0.031
	0.075	0.435	0.563	0.306		0.075	0.049	0.065	0.033
	0.1	0.414	0.541	0.288		0.1	0.050	0.065	0.035
	0.125	0.393	0.510	0.275		0.125	0.051	0.066	0.036
	0.15	0.365	0.468	0.262		0.15	0.057	0.070	0.044
Mean		**0.439**			**Mean**		**0.049**		
COV		**0.002**			**COV**		**1.741e-5**		
1.25	0.0	0.450	0.551	0.349	1.25	0.0	0.0381	0.047	0.029
	0.025	0.413	0.517	0.309		0.025	0.0403	0.052	0.028
	0.05	0.383	0.475	0.292		0.05	0.0431	0.056	0.030
	0.075	0.372	0.484	0.260		0.075	0.0461	0.059	0.033
	0.1	0.364	0.496	0.232		0.1	0.0453	0.062	0.029
	0.125	0.356	0.488	0.223		0.125	0.0457	0.062	0.029
	0.15	0.339	0.479	0.201		0.15	0.0476	0.065	0.030
Mean		**0.383**			**Mean**		**0.043754**		
COV		**0.001**			**COV**		**1.019e-5**		

7.5.2 Lateral Torsional Frequency Ratio

The effect of altering the lateral torsional frequency ratio on the seismic behaviour of the concentrically braced plan irregular structure is presented in this section. Analysis was undertaken on a concentrically braced plan irregular structure with a PA ratio of 2.0 and $\bar{\lambda}$ = 1.68 with a range of static eccentricities and lateral torsional frequency ratios. Results are normalised against the base model structure with a PA ratio of 2.0, Ω_θ = 1.0, e_s = 0.0L and $\bar{\lambda}$ = 1.68. The results displayed in Figure 7.23 to Figure 7.26 display mean values for the five earthquakes. The 95% CI's are not displayed in the figures for the purposes of visual clarity. The results displayed herein are the same results as displayed in the previous

section describing the effect of static eccentricity, however the results have been re-arranged to display the variation of the lateral torsional frequency ratio.

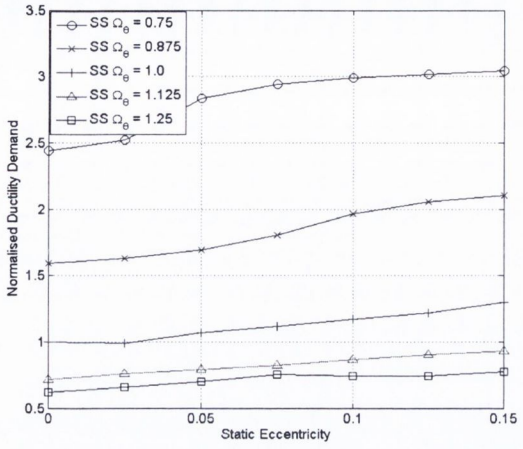

Figure 7.23: Graph of normalised ductility demand vs. static eccentricity for SS

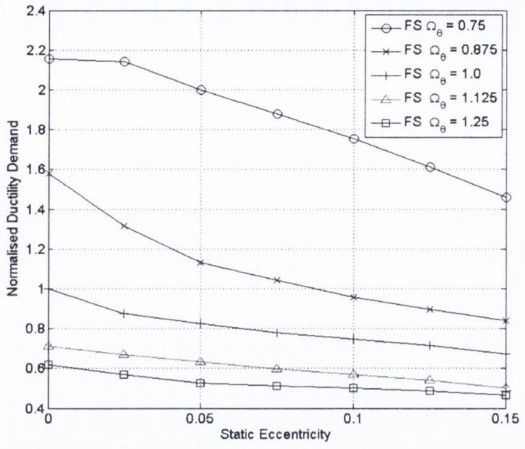

Figure 7.24: Graph of normalised ductility demand vs. static eccentricity for FS

Figure 7.23 illustrates the change in SS normalised ductility demand against static eccentricity for a range of lateral torsional frequency ratios. The torsionally stiff structures (Ω_θ = 1.125 & Ω_θ = 1.25) perform better than the base model structure as can be seen by the normalised ductility demand less than 1.0 for all levels of static eccentricity. The torsionally flexible structures (Ω_θ = 0.75 & Ω_θ = 0.875) perform worse than the base model structure as can be seen by the normalised ductility demand greater than 1.0 for all levels of static eccentricity. The SS normalised ductility demand of the most torsionally flexible structure, Ω_θ = 0.75 is on average 2.83 times that of the base model structure.

Figure 7.24 illustrates the change in FS normalised ductility demand against static eccentricity for a range of lateral torsional frequency ratios. The torsionally stiff structures (Ω_θ = 1.125 & Ω_θ = 1.25) perform better than the base model structure as can be seen by the normalised ductility demand less than 1.0 for all levels of static eccentricity. The torsionally flexible structures (Ω_θ = 0.75 & Ω_θ = 0.875) perform worse than the base model structure as can be seen by the normalised ductility demand greater than 1.0 for all levels of static eccentricity. The FS average normalised ductility demand of the most torsionally flexible structure, Ω_θ = 0.75 is 1.86 times that of the base model structure.

Comparing Figure 7.23 with Figure 7.24, it can be seen that the SS normalised ductility demand increases whilst the FS normalised ductility demand decreases with increase in value of static eccentricity.

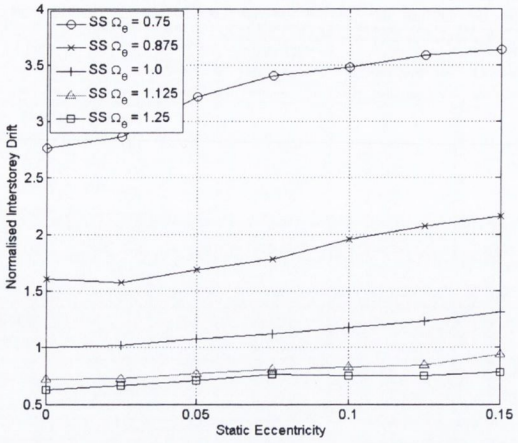

Figure 7.25: Graph of normalised first-storey drift vs. static eccentricity for SS

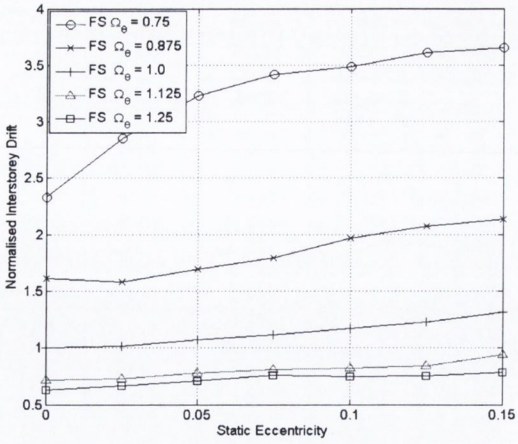

Figure 7.26: Graph of normalised first-storey drift vs. static eccentricity for FS

Figure 7.25 illustrates the change in SS normalised first-storey drift against static eccentricity for a range of lateral torsional frequency ratios. The torsionally stiff structures (Ω_θ = 1.125 & Ω_θ = 1.25) perform better than the base model structure as can be seen by the normalised first-storey drift less than 1.0 for all levels of static eccentricity. The torsionally flexible structures (Ω_θ = 0.75 & Ω_θ = 0.875) perform worse than the base model structure as can be seen by the normalised first-storey drift greater than 1.0 for all levels of static eccentricity. The SS normalised first-storey drift of the most torsionally flexible structure, Ω_θ = 0.75 is on average 3.28 times that of the base model structure.

Figure 7.26 illustrates the change in FS normalised first-storey drift against static eccentricity for a range of lateral torsional frequency ratios. The torsionally stiff structures (Ω_θ = 1.125 & Ω_θ = 1.25) perform better than the base model structure as can be seen by the normalised first-storey drift less than 1.0 for all levels of static eccentricity. The torsionally flexible structures (Ω_θ = 0.75 & Ω_θ = 0.875) perform worse than the base model structure as can be seen by the normalised first-storey drift less than 1.0 for all levels of static eccentricity. The FS average normalised first-storey drift of the most torsionally flexible structure, Ω_θ = 0.75 is 3.22 times that of the base model structure. The SS and FS normalised first-storey drifts are very similar.

Comparing Figure 7.25 with Figure 7.26, it can be seen that the normalised first-storey drifts increase on the SS and FS of the structure with increase in value of static eccentricity. The SS normalised first-storey drifts are approximately the same as the FS normalised first-storey drifts, with the exception of the Ω_θ = 0.75 and e_s = 0.0L structure.

Summary

The lateral torsional frequency ratio ranged from Ω_θ = 0.75 (torsionally flexible) to Ω_θ = 1.25 (torsionally stiff) within the parametric study. The torsionally stiff structures perform better than the torsionally flexible structures. The SS of the structure has a larger ductility demand compared to the FS of the structure for all levels of lateral torsional frequency ratio. The ductility demand on the SS of the Ω_θ = 0.75 structure is nearly 4 times greater than that of the Ω_θ = 1.25 structure. Similarly, the ductility demand on the FS of the Ω_θ = 0.75 structure is 3.5 times greater than that of the Ω_θ = 1.25 structure. On average, the torsionally flexible structures have a ductility demand 3.75 times that of the torsionally stiff structures. The SS ductility demand increases for increasing levels of static eccentricity for all values of lateral torsional frequency ratio. The FS ductility demand decreases for increasing levels of static eccentricity for all values of lateral torsional frequency ratio. Unlike the ductility demands, the first-storey drifts are approximately the same on the SS and FS of the structure. The first-storey drifts increase for increasing levels of static eccentricity for all values of lateral torsional frequency ratio. The level of lateral torsional frequency ratio has been observed to be a key parameter affecting the seismic torsional response of plan irregular braced frame type structures.

7.5.3 Plan Aspect Ratio

The effect of changing the plan aspect (PA) ratio on the seismic behaviour of the concentrically braced plan irregular structures is investigated by varying the PA ratio with the following values; 1.0, 1.5, 2.0, 2.5 to 3.0. The concentrically braced frames have $\bar{\lambda}$ = 1.68, e_s = 0.0L & 0.15L and the PA ratio is varied by increasing/decreasing the dimension of the structure perpendicular to the braced frames. The width of the braced frames remains unchanged. The structures under investigation have Ω_θ ranging from 0.75, 0.875, 1.0, 1.125 to 1.25. Results are normalised against the base model structure with a PA ratio of 2.0, Ω_θ = 1.0, e_s = 0.0L and $\bar{\lambda}$ = 1.68. The results displayed in Figure 7.27 to Figure 7.30 display mean values for the five earthquakes considered. The 95% CI's are not displayed for the purposes of visual clarity.

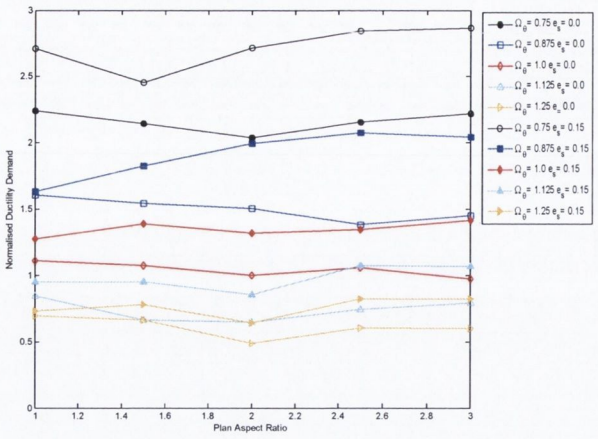

Figure 7.27: Graph of normalised ductility demand vs. PA ratio for SS

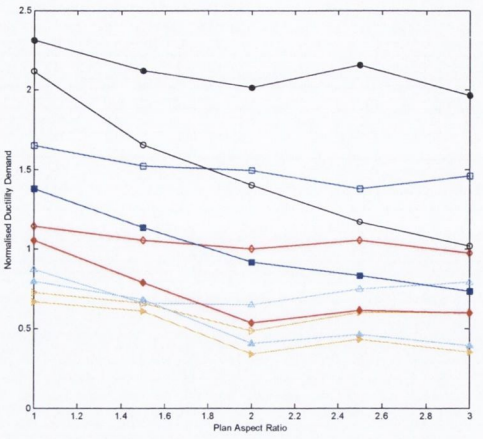

Figure 7.28: Graph of normalised ductility demand vs. PA ratio for FS

Figure 7.27 compares the change in SS normalised ductility demand against PA ratio for varying levels of lateral torsional frequency ratio and static eccentricity. As can be seen from the results in Figure 7.27 combined with the low levels of COV, the ductility demand remains approximately constant for all levels of plan aspect ratio. On average, the SS ductility demand increased by 4.9% from PA ratio of 1.0 to 3.0. The results indicate variation of the PA ratio does not have a large effect on the SS normalised ductility demand. Compared to the base model structure with PA ratio of 2.0, the lower and higher PA ratio structures perform similarly.

Figure 7.28 compares the change in FS normalised ductility demand against plan aspect ratio for varying levels of lateral torsional frequency ratio and static eccentricity. A decrease in the FS normalised ductility demand with increasing PA ratio can be seen in Figure 7.28, particularly the $\Omega_\theta = 0.75$ and $e_s = 0.15L$ structure and the $\Omega_\theta = 0.875$ and $e_s = 0.15L$ structure. On average, the FS ductility demand decreased by 18.1% from PA ratio of 1.0 to 3.0. Compared to the base model structure with PA ratio of 2.0, the lower PA ratio structures have a slightly higher FS normalised ductility demand and the higher PA ratio structures have a slightly lower FS normalised ductility demand.

Figure 7.29 compares the change in SS normalised first-storey drift against plan aspect ratio for varying levels of lateral torsional frequency ratio and static eccentricity. As can be seen in Figure 7.29 the normalised first-storey drift remains approximately constant for all levels of PA ratio. On average, the SS first-storey drift decreased by 2.3% from PA ratio of 1.0 to 3.0. The results indicate variation of the PA ratio does not have a large effect on the SS normalised first-storey drift of the structure.

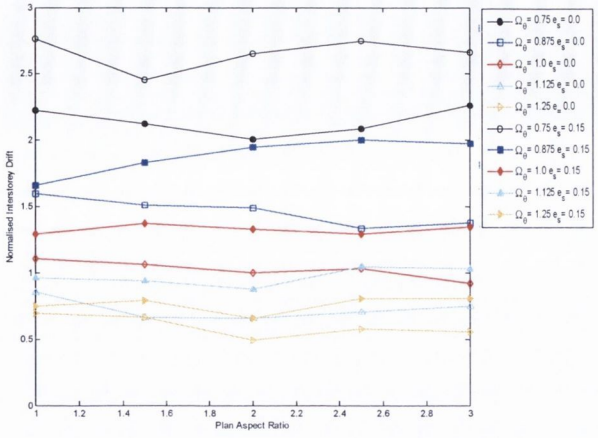

Figure 7.29: Graph of normalised first-storey drift vs. PA ratio for SS

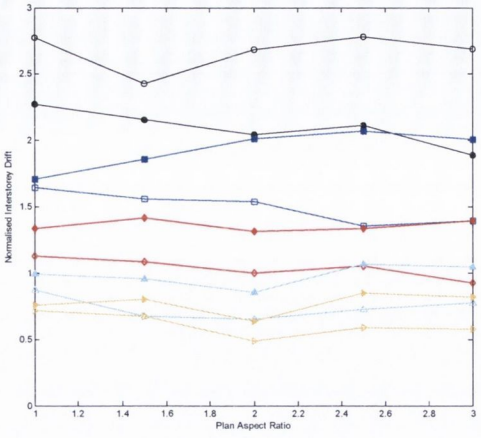

Figure 7.30: Graph of normalised first-storey drift vs. PA ratio for FS

Figure 7.30 compares the change in FS normalised first-storey drift against plan aspect ratio for varying levels of lateral torsional frequency ratio and static eccentricity. As can be seen from the results in Figure 7.30, the normalised first-storey drift remains approximately constant for all levels of PA ratio as per the SS first-storey drift discussed above. On average, the FS first-storey drift decreased by 2.2% from PA ratio of 1.0 to 3.0. The results indicate variation of the PA ratio does not have a significant effect on the FS normalised first-storey drift of the structure.

Summary

The effect of changing the PA ratio on the seismic behaviour of braced plan irregular structures was considered by altering the PA ratio within realistic ranges from 1.0 to 3.0. The SS ductility demand at values of no static eccentricity (e_s = 0.0L) and maximum static eccentricity (e_s = 0.15L) increased by 4.9% from a PA ratio of 1.0 to 3.0, while the SS first-storey drift increased by 2.3% over the same range. No substantial variation was observed in the SS ductility demand or SS first-storey drift. The SS ductility demand and SS first-storey drift are approximately constant for all levels of PA ratio. The FS ductility demand at values of no static eccentricity (e_s = 0.0L) and maximum static eccentricity (e_s = 0.15L) decreased by 18.1% from a PA ratio of 1.0 to 3.0. The FS ductility demand for the torsionally stiff structures (Ω_θ = 1.125 & Ω_θ = 1.25) decreased by 4.6% on average from a PA ratio of 1.0 to 3.0. The FS ductility demand for the torsionally flexible structures (Ω_θ = 0.875 & Ω_θ = 0.75) decreased by 26.9% on average from a PA ratio of 1.0 to 3.0. The FS first-storey drift for no static eccentricity (e_s = 0.0L) and maximum static eccentricity (e_s = 0.15L) decreases by 2.2% across the range of PA ratios and can be considered to be

approximately constant for all levels of PA ratio. The effect of varying the PA ratio is not significant except for the FS ductility demand that reduces for increasing levels of PA ratio.

7.5.4 Design for Torsional Effects

Eurocode 8 (CEN, (2004)) provides an intuitive method of designing structures to resist torsional effects using the lateral pushover method of analysis. The torsional effects provision makes allowance for 5% static eccentricity in the plan of the structure. The structure not designed to take account of torsional effects is referred to as an Excluding Torsional Provision (ETP) structure. The structure designed to take account of torsional effects is referred to as an Including Torsional Provision (ITP) structure. The difference between the ETP and ITP structures is the brace section size on the SS of the structure. The side of the structure closer to the eccentric mass requires additional lateral stiffness to resist the additional demands placed on it by the mass distribution. The ETP structure has a SS brace section size of 30x30x3mm SHS, with $\bar{\lambda}$ = 1.68, whereas the ITP structure has a SS brace section size of 50x30x3mm RHS, with $\bar{\lambda}$ = 1.57. In both structures the FS brace section size is 30x30x3mm SHS ($\bar{\lambda}$ = 1.68). The results are normalised to the base model structure with a PA ratio of 2.0, Ω_θ = 1.0, $e_s = 0.0L$ and $\bar{\lambda}$ = 1.68.

The ETP structural responses have been presented previously and are repeated here to allow easier comparison between the ETP and ITP structural responses. For example, Figure 7.31 is the same graph as Figure 7.23.

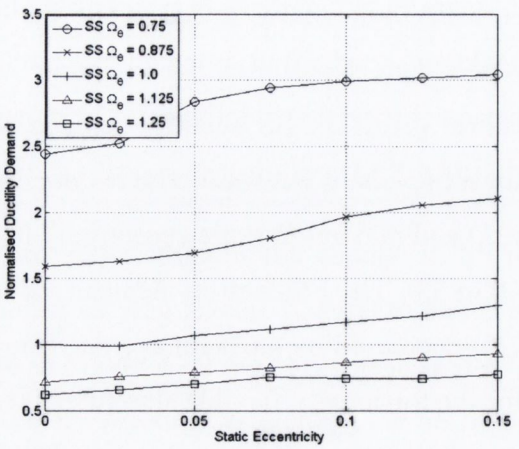

Figure 7.31: Graph of normalised ductility demand vs. static eccentricity for SS of the ETP structure

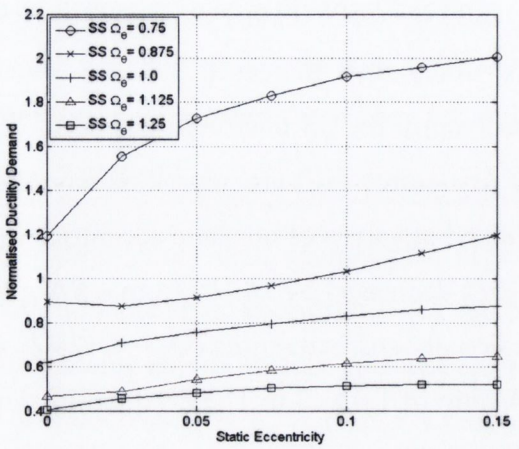

Figure 7.32: Graph of normalised ductility demand vs. static eccentricity for SS of the ITP structure

Figure 7.31 and Figure 7.32 illustrate the variation in SS normalised ductility demand with static eccentricity for varying levels of lateral torsional frequency ratio for the ETP and ITP structures, respectively. Comparing the SS response of the ETP structures in Figure 7.31 and the ITP structures in Figure 7.32, it is evident the ITP structures experience a lower normalised ductility demand than the ETP structures. For Ω_θ = 0.75, the SS normalised ductility demand varies from 2.44 for e_s = 0.0L to 3.04 for e_s = 0.15L in the ETP structure (Figure 7.31) compared to 1.19 for e_s = 0.0L to 2.01 for e_s = 0.15L in the ITP structure (Figure 7.32). The SS normalised ductility demand of the torsionally flexible structures (Ω_θ = 0.75 & Ω_θ = 0.875) are on average 42% smaller in the ITP structure as compared to the ETP structure. For Ω_θ = 1.25, the SS normalised ductility demand varies from 0.62 for e_s = 0.0L to 0.78 for e_s = 0.15L for the ETP structure (Figure 7.31) compared to 0.41 for e_s = 0.0L to 0.52 for e_s = 0.15L for the ITP structure (Figure 7.32). The SS normalised ductility demand of the torsionally stiff structures (Ω_θ = 1.125 & Ω_θ = 1.25) are on average 31.5% smaller in the ITP structure as compared to the ETP structure. The SS normalised ductility demand of the ITP structure is reduced by 35.5% on average for all levels of lateral torsional frequency ratio. The ITP structure reduces the ductility demand of the ETP structure on average by 35.4% for 5% static eccentricity (e_s = 0.05L).

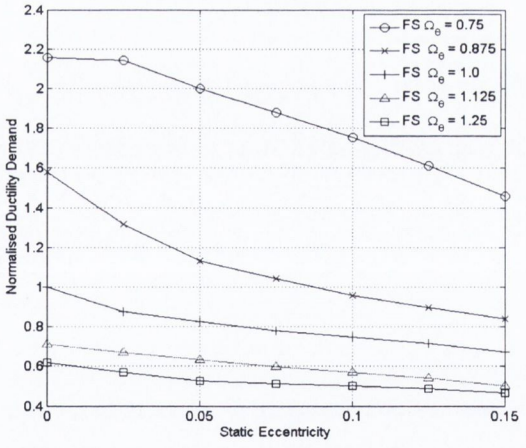

Figure 7.33: Graph of normalised ductility demand vs. static eccentricity for FS of the ETP structure

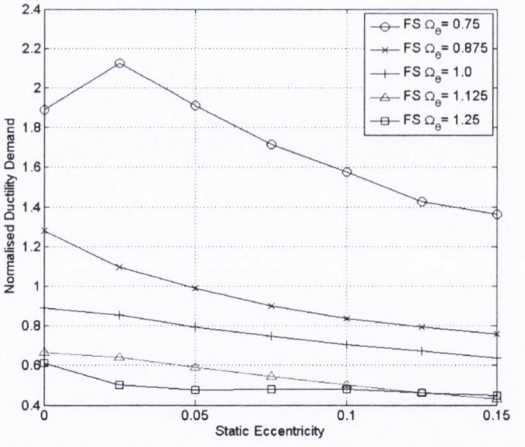

Figure 7.34: Graph of normalised ductility demand vs. static eccentricity for FS of the ITP structure

Figure 7.33 and Figure 7.34 illustrate the variation in FS normalised ductility demand with static eccentricity for varying levels of lateral torsional frequency ratio for the ETP and ITP structures, respectively. Comparing the FS response of the ETP structure in Figure 7.33 and the ITP structure in Figure 7.34, it is evident the ITP structure has slightly reduced normalised ductility demand as compared to the ETP structure. The FS normalised ductility demand of the torsionally stiff structures (Ω_θ = 0.75 & Ω_θ = 0.875) are on average

10.9% smaller in the ITP designed structure as compared to the ETP designed structure. The FS normalised ductility demand of the torsionally flexible structures (Ω_θ = 1.125 & Ω_θ = 1.25) are on average 7.5% smaller in the ITP designed structure as compared to the ETP designed structure. The FS normalised ductility demand of the ITP structure is reduced by 8.5% on average for all levels of lateral torsional frequency ratio. The ITP structure reduces the ductility demand of the ETP structure on average by 7.8% for 5% static eccentricity ($e_s = 0.05L$).

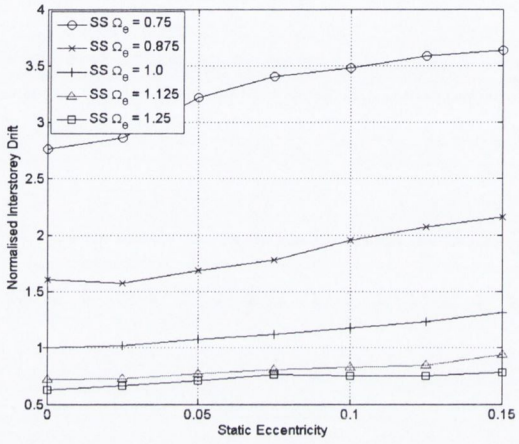

Figure 7.35: Graph of normalised first-storey drift vs. static eccentricity for SS of the ETP structure

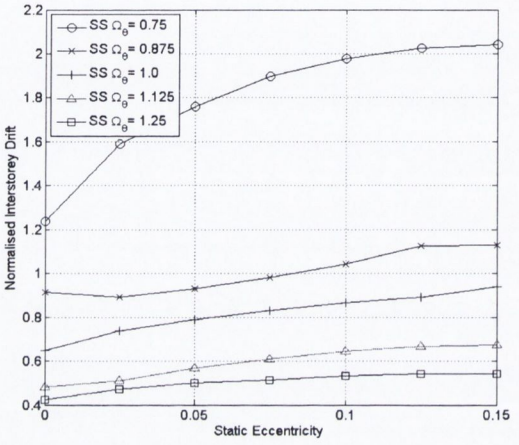

Figure 7.36: Graph of normalised first-storey drift vs. static eccentricity for SS of the ITP structure

Figure 7.35 and Figure 7.36 illustrate the variation in SS normalised first-storey drift with static eccentricity for varying levels of lateral torsional frequency ratio for the ETP and ITP structures, respectively. Comparing the SS response of the ETP structure in Figure 7.35 and the ITP structure in Figure 7.36, it is evident the ITP structure has a reduced normalised first-storey drift compared to the ETP structure. The SS normalised first-storey drifts of the torsionally stiff structures (Ω_θ = 0.75 & Ω_θ = 0.875) are on average 45.4% smaller in the ITP designed structure as compared to the ETP designed structure. The SS normalised first-storey drifts of the torsionally stiff structures (Ω_θ = 1.125 & Ω_θ = 1.25) are on average 28.2% smaller in the ITP structure as compared to the ETP structure. The SS normalised first-storey drift of the ITP structure is reduced by 35.1% on average for all levels of lateral torsional frequency ratio. The ITP structure reduces the first-storey drift of the ETP structure on average by 34.6% for 5% static eccentricity ($e_s = 0.05L$).

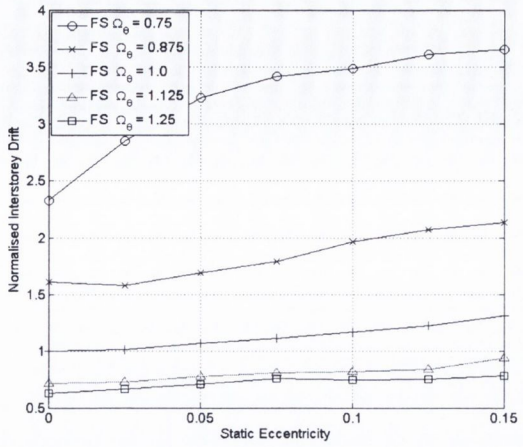

Figure 7.37: Graph of normalised first-storey drift vs. static eccentricity for FS of the ETP structure

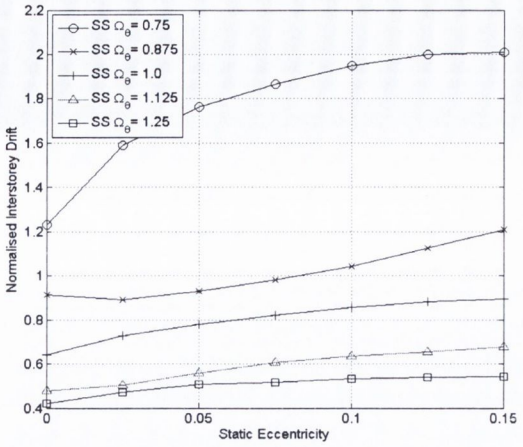

Figure 7.38: Graph of normalised first-storey drift vs. static eccentricity for FS of the ITP structure

Figure 7.37 and Figure 7.38 illustrate the variation in FS normalised first-storey drift against static eccentricity for varying levels of lateral torsional frequency ratio for the ETP and ITP structures, respectively. Comparing the FS response of the ETP structure in Figure 7.37 and the ITP structure in Figure 7.38, it is evident the ITP structure has a reduced normalised first-storey drift compared to the ETP structure. The FS normalised first-storey drifts of the torsionally stiff structures (Ω_θ = 0.75 & Ω_θ = 0.875) are on average 44.8% smaller in the ITP structure as compared to the ETP structure. The FS normalised first-storey drifts of the torsionally stiff structures (Ω_θ = 1.125 & Ω_θ = 1.25) are on average 28.3% smaller in the ITP structure as compared to the ETP structure. The FS normalised first-storey drift of the ITP structure is reduced by 35.1% on average for all levels of lateral torsional frequency ratio. The ITP structure reduces the first-storey drift of the ETP structure on average by 34.7% for 5% static eccentricity ($e_s = 0.05L$).

Summary

The effectiveness of the Eurocode 8 (CEN, (2004)) provision for torsional effects was evaluated by application of the design procedure to the base model concentrically braced plan irregular structure. The base model structure was designed without the torsional effects provision (ETP - Excluding Torsional Provision) was compared to the base model structure designed with the torsional effects provision (ITP - Including Torsional Provision). The normalised ductility demand for all levels of static eccentricity of the ITP structure is reduced by 35.5% on the SS of the structure and 8.5% on the FS of the structure. The normalised first-storey drift for all levels of static eccentricity of the ITP

structure is reduced by 35.1% on the SS of the structure and 35.1% on the FS of the structure. The normalised ductility demand of the most torsionally flexible ITP structure ($\Omega_\theta = 0.75$) is 2.01 times that of the base model structure. Similarly, the normalised first-storey drift of the most torsionally flexible ITP structure ($\Omega_\theta = 0.75$) is 2.04 times that of the base model structure. The results from the ETP and ITP analysis indicate the Eurocode 8 (CEN, (2004)) torsional provision is adequate for torsionally stiff structures, and even reduces the ductility demand on the SS of the structure for the most torsionally flexible structure at high levels of static eccentricity when subjected to earthquake excitation with PGA below the design PGA (e.g. for $\Omega_\theta = 0.75$ and $e_s = 0.15L$ ETP ductility demand of 3.04 compared to ITP ductility demand of 2.01). Likewise, the provision even reduces the FS interstory drift at high levels of static eccentricity. The results are somewhat unexpected as the provision allows for $e_s = 0.05L$ whereas the maximum static eccentricity considered here is three times this value. For the level of static eccentricity accounted for in the provision (up to 5%), the structure performs well.

7.5.5 Over- and Under-designed for Torsional Effects

The previous section detailed the effect on the seismic response of braced frame plan irregular structures when designed to resist torsional effects. Designing the structure to take account of a mass eccentricity of 5% resulted in the bracing increasing in size on the SS of the structure from 30x30x3mm SHS ($\bar{\lambda} = 1.68$) to 50x30x3mm RHS ($\bar{\lambda} = 1.57$). To further investigate the effects of over- and under-designing the structure to resist the torsional effects, time history analysis of frames with varying brace sizes were performed. To comply with Eurocode 8 (CEN, (2004)) provisions, the normalised slenderness in each case adheres to the following limits; $1.3 < \bar{\lambda} \leq 2.0$. A brace dimension of 40x40x5mm SHS results in $\bar{\lambda} = 1.3$ and a brace dimension of 25x25x2.5mm SHS results in $\bar{\lambda} = 2.0$, both at the lower and upper limit bounds, respectively. Brace sections with $\bar{\lambda} = 1.3$ result in an over-design compared to the Eurocode 8 (CEN, (2004)) torsional effects provisions. Brace sections with $\bar{\lambda} = 2.0$ result in an under-design compared to the Eurocode 8 (CEN, (2004)) torsional effects provision. On the FS of the over- and under-designed structures the brace sections remained 30x30x3mm SHS ($\bar{\lambda} = 1.68$), as per the base model structure that has not been designed taking into consideration the torsional effects.

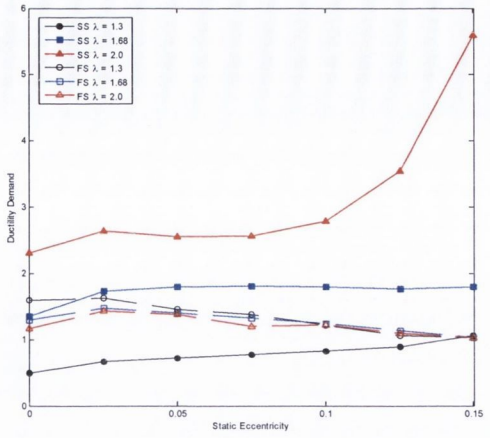

Figure 7.39: Graph of ductility demand vs. static eccentricity for $\Omega_\theta = 0.75$

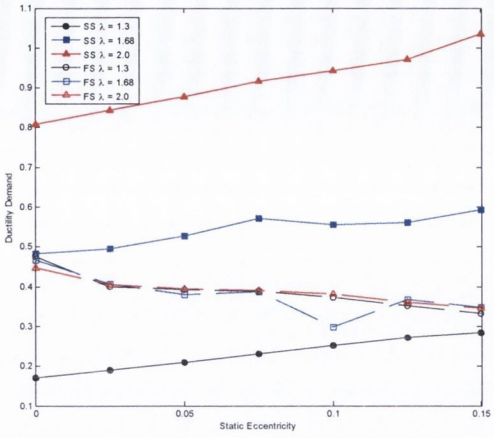

Figure 7.40: Graph of ductility demand vs. static eccentricity for $\Omega_\theta = 1.25$

Figure 7.39 presents the variation in SS and FS ductility demand with static eccentricity for the most torsionally flexible structure (Ω_θ = 0.75) for a range of brace normalised slenderness values. As shown in Figure 7.39, the $\bar{\lambda}$ = 1.3 structure SS ductility demand remains less than 1.0 for all levels of eccentricity (except for $e_s = 0.15L$) showing that the structure did not reach its yield displacement. The $\bar{\lambda}$ = 1.3 structure experiences a FS ductility demand between 1.63 for $e_s = 0.025L$ and 1.03 for $e_s = 0.15L$. The ductility demand is greater on the FS compared to the SS due to the brace section sizes being smaller on the FS ($\bar{\lambda}$ = 1.68). As can be seen in Figure 7.39, the $\bar{\lambda}$ = 1.68 structure experiences a SS ductility demand between 1.35 for $e_s = 0.0L$ and 1.79 for $e_s = 0.15L$, and a FS ductility demand between 1.48 for $e_s = 0.0L$ and 1.03 for $e_s = 0.15L$. The ductility demand is greater on the SS compared to the FS even though the same $\bar{\lambda}$ = 1.68 bracing is used on both SS and FS. As shown in Figure 7.39, the $\bar{\lambda}$ = 2.0 structure experiences a SS ductility demand between 2.31 for $e_s = 0.0L$ and 5.59 for $e_s = 0.15L$, and a FS ductility demand between 1.43 for $e_s = 0.0L$ and 1.03 for $e_s = 0.15L$. The $\bar{\lambda}$ = 2.0 structure performs poorly on the SS of the structure for high levels of static eccentricity. The ductility demand is higher in the $\bar{\lambda}$ = 2.0 structure and lower in the $\bar{\lambda}$ = 1.3 compared to the $\bar{\lambda}$ = 1.68 structure. The $\bar{\lambda}$ = 2.0 structure experiences large ductility demands (> 3) above $e_s = 0.1L$.

Figure 7.40 presents the variation in SS and FS ductility demand with static eccentricity for the most torsionally stiff structure (Ω_θ = 1.25) for a range of brace normalised slenderness values. As can be seen in Figure 7.40, the ductility demand for all of the most torsionally stiff structures (Ω_θ = 1.25) is less than 1.0 for all levels of $\bar{\lambda}$ indicating the structures did not reach yield displacement (except the SS of the $\bar{\lambda}$ = 2.0 structure with ductility demand

of 1.04 for $e_s = 0.15L$). The results in Figure 7.40 for $\Omega_\theta = 1.25$ contrast with those in Figure 7.39 for $\Omega_\theta = 0.75$ in which all of the structures reached yield displacement, except for the SS of the $\bar{\lambda} = 1.3$ structure. Comparing Figure 7.39 and Figure 7.40, the $\Omega_\theta = 1.25$ structures increase in ductility demand is more stable and consistent as compared to the $\Omega_\theta = 0.75$ structures. No large increase in ductility demand was experienced in the $\Omega_\theta = 1.25$ structure with $\bar{\lambda} = 2.0$ above $e_s = 0.1L$ as was observed in the $\Omega_\theta = 0.75$ structure with $\bar{\lambda} = 2.0$ above $e_s = 0.1L$.

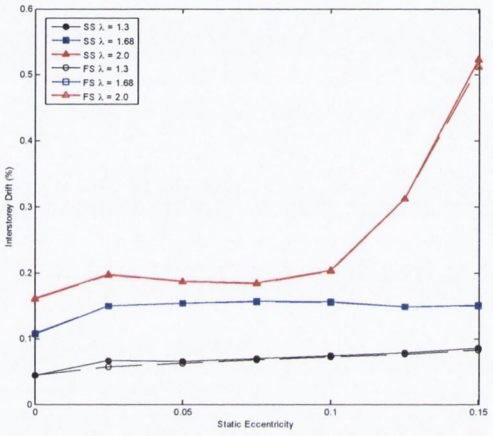

Figure 7.41: Graph of first-storey inter-storey drift vs. static eccentricity for $\Omega_\theta = 0.75$

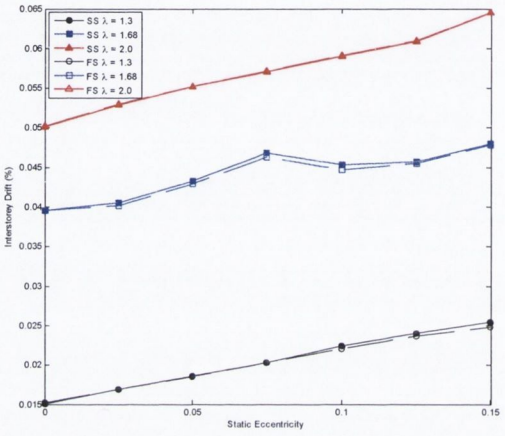

Figure 7.42: Graph of first-storey inter-storey drift vs. static eccentricity for $\Omega_\theta = 1.25$

Figure 7.41 presents the variation in SS and FS first-storey interstorey drift with static eccentricity for the most torsionally flexible structure ($\Omega_\theta = 0.75$) for a range of brace normalised slenderness values. As shown in Figure 7.41, the $\bar{\lambda} = 1.3$ structure experiences a SS first-storey drift between 0.04% for $e_s = 0.0L$ and 0.09% for $e_s = 0.15L$. The $\bar{\lambda} = 1.3$ structure has a FS first-storey drift between 0.04% for $e_s = 0.0L$ and 0.08% for $e_s = 0.15L$. The first-storey drift is approximately the same on the SS and FS even though the stiffness differs on either side. A similar trend is observed in the $\bar{\lambda} = 1.3$ and $\bar{\lambda} = 2.0$ structures. The $\bar{\lambda} = 2.0$ structure performs poorly on the SS and FS of the structure as the first-storey drift exceed the Eurocode 8 (CEN, (2004)) interstorey drift limit of 0.5% for $e_s = 0.15L$. The $\bar{\lambda} = 1.3$ and $\bar{\lambda} = 1.68$ structures perform well in terms of interstorey drift on the SS and FS of the structure. The level of first-storey drift observed is highest in the $\bar{\lambda} = 2.0$ structure and lowest in the $\bar{\lambda} = 1.3$ structure.

Figure 7.42 presents the variation in SS and FS first-storey interstorey drift with static eccentricity for the most torsionally stiff structure ($\Omega_\theta = 1.25$) for a range of brace

normalised slenderness values. The first-storey drift is approximately the same on the SS and FS of the structure. The level of first-storey drift observed is highest in the $\bar{\lambda}$ = 2.0 structure and lowest in the $\bar{\lambda}$ = 1.3 structure.

The $\bar{\lambda}$ = 2.0 structure with Ω_θ = 1.25 performs considerably better than the Ω_θ = 0.75 structure as shown in Figure 7.41. For both the Ω_θ = 0.75 and Ω_θ = 1.25 structures the first-storey drift is higher in the $\bar{\lambda}$ = 2.0 structure and lower in the $\bar{\lambda}$ = 1.3 compared to the $\bar{\lambda}$ = 1.68 structure. Similar to the ductility demands, the Ω_θ = 0.75 structure with $\bar{\lambda}$ = 2.0 experiences large first-storey drifts for values of static eccentricity above 0.1L, whereas the Ω_θ = 1.25 structure with $\bar{\lambda}$ = 2.0 experiences a smaller and more stable drift response.

Summary

Changing the normalised slenderness of the brace members is equivalent to under- or over-designing the structure to resist torsional effects. The under-designed structure ($\bar{\lambda}$ = 2.0) experienced a large SS and FS ductility demand and large first-storey interstorey drifts, with the maximum eccentricity resulting in the first-storey interstorey drift exceeding the Eurocode 8 (CEN, (2004)) interstorey drift limit. Over-designing the brace sections on the SS of the structure ($\bar{\lambda}$ = 1.3) resulted in a greater ductility demand on the FS of the structure compared to the SS of the structure. The under-designed structure ($\bar{\lambda}$ = 2.0) structure experienced a SS ductility demand on average 42.5% greater than the base model structure. The over-designed structure ($\bar{\lambda}$ = 1.3) structure had a SS ductility demand on average 26.7% less than the base model structure. Considering that the static eccentricity is distributed towards the SS of the structure, it is unexpected for the FS ductility demand to exceed the SS ductility demand. The under-designed ($\bar{\lambda}$ = 2.0) and over-designed ($\bar{\lambda}$ = 1.3) structures experience the same first-storey drift on the SS and FS of the structure. It is unexpected the first-storey interstorey drift for both the under- and over-designed structures are effectively the same for both the SS and FS of the structure as the stiffness of the braced frames is different on the SS and FS. The FS of the over-designed structure had increased ductility demand compared to the base model structure caused by the FS bracing having reduced stiffness as compared to the SS bracing. Over-designing the braced irregular structure to resist torsional effects has the unwanted effect of increasing the ductility demand on the FS of the structure.

7.5.6 Influence of Bi-directional Excitation

The influence of bi-directional excitation was investigated by analysing the plan irregular structure with braced frames in the two main horizontal directions and subjecting the structure to bi-directional excitation. The earthquake record used for the bi-directional analysis is the orthogonal record for the particular earthquake. To evaluate the affect of bi-directional excitation on the seismic behaviour, a structure with a PA ratio of 1.0, brace sections sizes of 30x30x3mm SHS ($\bar{\lambda}$ = 1.68) and a range of Ω_θ and e_s values was analysed. It was only possible to investigate a structure with a PA ratio of 1.0 to ensure that the seismic design of the structure in both horizontal directions would remain the same. As a result, the same bracing section sizes could be used in the braced frames in both horizontal directions and allow direct comparison between uni-directional and bi-directional excitation. The results are normalised against the uni-directional excited structure with; PA ratio of 1.0, $\bar{\lambda}$ = 1.68, Ω_θ = 1.0, e_s = 0.0L and bracing in the uni-directional plane of excitation only. It should be noted that the structure analysed in uni-directional and bi-directional excitation is only subjected to uni-axial static eccentricity. The static eccentricity is only applied in one direction.

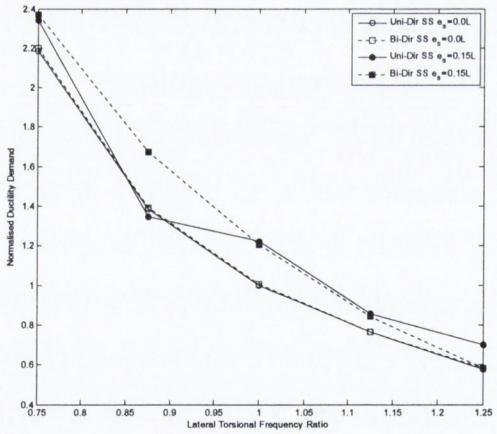

Figure 7.43: Graph of normalised ductility demand vs. Ω_θ for SS of uni- and bi-axial excited structures

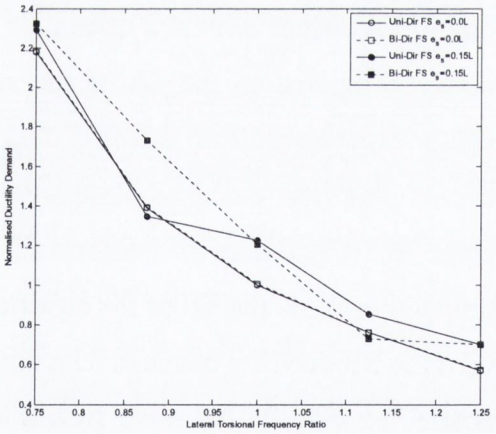

Figure 7.44: Graph of normalised ductility demand vs. Ω_θ for FS of uni- and bi-axial excited structures

Figure 7.43 compares normalised ductility demand against lateral torsional frequency ratio for the SS of the structure subjected to uni-directional and bi-directional excitation for e_s = 0.0L and e_s = 0.15L. It can be seen from Figure 7.43 the normalised ductility demand for the SS of the structure remains similar if the structure is subjected to uni-directional or bi-directional excitation (with the exception of Ω_θ = 0.875 for e_s = 0.15L). For all levels of Ω_θ, the normalised ductility demand for e_s = 0.15L is on average 8.2% greater than the ductility

demand for e_s = 0.0L. The normalised ductility demand reduces with increasing lateral torsional frequency ratio.

Figure 7.44 compares normalised ductility demand against lateral torsional frequency ratio for the FS of the structure subjected to uni-directional and bi-directional excitation for e_s = 0.0L and e_s = 0.15L. It can be seen from Figure 7.44 the normalised ductility demand for the FS of the structure remains similar if the structure is subjected to uni-directional or bi-directional excitation for e_s = 0.0L. The normalised ductility demand for the FS of the structure with e_s = 0.15L differ slightly with the bi-directional excitation producing larger ductility demand. For all levels of Ω_θ, the normalised ductility demand for e_s = 0.15L is on average 8.1% greater than the ductility demand for e_s = 0.0L.

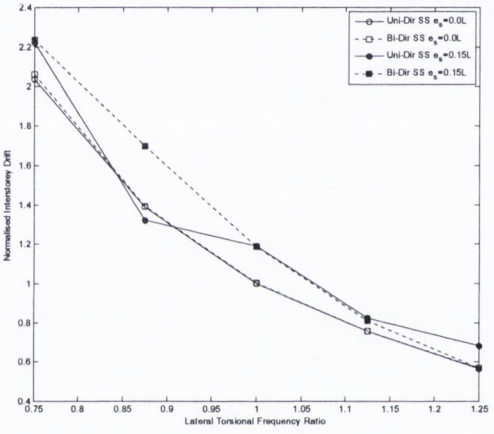

Figure 7.45: Graph of normalised first-storey drift vs. Ω_θ for SS of uni- and bi-axial excited structures

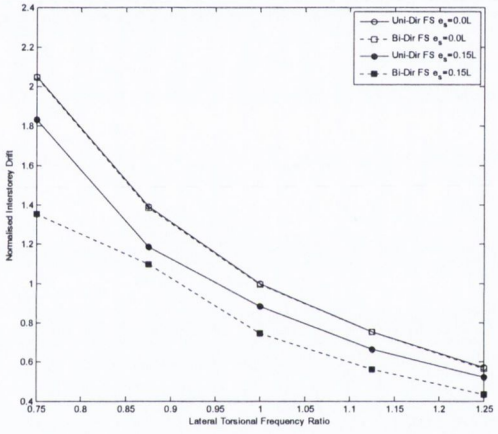

Figure 7.46: Graph of normalised first-storey drift vs. Ω_θ for FS of uni- and bi- axial excited structures

Figure 7.45 compares change in normalised first-storey drift against lateral torsional frequency ratio for the SS of the structure subjected to uni-directional and bi-directional excitation for e_s = 0.0L and e_s = 0.15L. It can be seen in Figure 7.45 the normalised first-storey drift for the SS of the structure remains similar if the structure is subjected to uni-directional or bi-directional excitation (with the exception of Ω_θ = 0.875 for e_s = 0.15L). The normalised first-storey drift for e_s = 0.15L is on average 8.4% greater than the ductility demand for e_s = 0.0L.

Figure 7.46 compares change in normalised first-storey drift against lateral torsional frequency ratio for the FS of the structure subjected to uni-directional and bi-directional excitation for e_s = 0.0L and e_s = 0.15L. It can be seen from Figure 7.46 the normalised first-storey drift for the FS of the structure is approximately the same if the structure is

subjected to uni-directional or bi-directional excitation for $e_s = 0.0L$. As shown in Figure 7.46, the normalised first-storey drift for the uni-directional excited structure with $e_s = 0.15L$ is on average 20.3% greater than the normalised first-storey drift for the bi-directional excited structure with $e_s = 0.15L$. Overall, the normalised first-storey drift for $e_s = 0.15L$ is on average 19.7% greater than the first-storey drift for $e_s = 0.0L$.

Summary

The SS ductility demand for the uni-directionally and bi-directionally excited structures is similar for all levels of lateral torsional frequency ratio and static eccentricity. The FS ductility demand for the uni-directionally and bi-directionally excited structures is similar for all levels of lateral torsional frequency ratio and static eccentricity. The SS first-storey interstorey drift is similar for uni- and bi-directionally excited structures. The FS first-storey interstorey drift is similar for uni- and bi-directionally excited structures with the exception being the uni-directional excited structure with $e_s = 0.15L$ is on average 20.3% greater than the normalised first-storey drift for the bi-directional excited structure. In general, the analysis indicates the bi-directional and uni-directional excited structures have a similar seismic response. The uni-directional excited structure slightly overestimates the ductility demand and interstorey drift for high levels of static eccentricity. However, a few limitations exist preventing definitive conclusions, such as the structure only has static eccentricity applied in one direction and the PA ratio was not varied.

7.5.7 Influence of Level of Ground Acceleration

Structures investigated in the previous sections have all been designed to resist a peak ground acceleration, $a_g = 0.35g$ using the lateral force pushover method, whereas the peak ground acceleration applied to the models was $a_g = 0.315g$. The sensitivity of the seismic response of braced plan irregular structures to the level of excitation exceeding the design value (which is not implausible in reality) was investigated by increasing the level of peak ground acceleration. The increased levels of input peak ground acceleration were applied to the base model structure with a PA ratio of 2.0, $\bar{\lambda} = 1.68$ and a range of Ω_θ and e_s values. The peak ground acceleration was increased from 0.315g to 0.4g, 0.5g and 0.6g. Peak ground accelerations above 0.6g caused numerical model to fail due to a lack of convergence in the solution during numerical integration. On inspection, the out-of-plane

displacements in the bracing members on the SS of the structure at higher levels of static eccentricity are the cause of the failed numerical integration. The results of the analysis are displayed below.

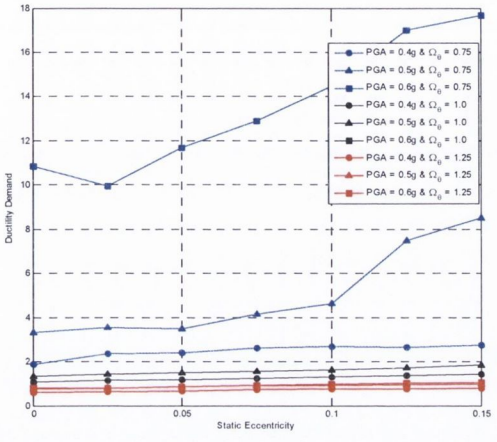

Figure 7.47: Graph of SS ductility demand vs. static eccentricity for a range of Ω_θ and PGA

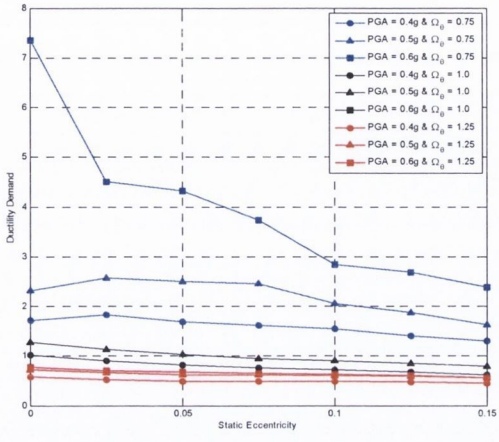

Figure 7.48: Graph of FS ductility demand vs. static eccentricity for a range of Ω_θ and PGA

Figure 7.47 illustrates the variation in SS ductility demand with static eccentricity for a range of lateral torsional frequency ratios and peak ground accelerations. The SS response of the structures subjected to PGA = 0.4*g*, 0.5*g* and 0.6*g* exhibit a predictable behaviour for the Ω_θ = 1.0 or Ω_θ = 1.25 structures with ductility demands below 2.0. As can be seen in Figure 7.47, for PGA = 0.6*g* and Ω_θ = 0.75 on the SS of the structure the ductility demand increases from 10.8 for e_s = 0.0*L* to 17.7 for e_s = 0.15*L*. For PGA = 0.5*g* and Ω_θ = 1.25 on the SS of the structure the ductility demand increases from 0.75 for e_s = 0.0*L* to 0.99 for e_s = 0.15*L*. The torsionally flexible structure (Ω_θ = 0.75) SS response subjected to PGA = 0.5*g* and 0.6*g* exhibits unacceptably high levels of ductility demand. The torsionally stiff structure (Ω_θ = 1.25) SS response subjected to PGA = 0.4*g*, 0.5*g* and 0.6*g* exhibits a predictable and stable behaviour with levels of ductility demand below 2.0 for all levels of static eccentricity.

Figure 7.48 illustrates the variation in FS ductility demand with static eccentricity for a range of lateral torsional frequency ratios and peak ground accelerations. The FS response of the structures subjected to PGA = 0.4*g*, 0.5*g* and 0.6*g* exhibits a predictable behaviour for the Ω_θ = 1.0 or Ω_θ = 1.25 structures with ductility demands below 1.5. As can be seen in Figure 7.48, for PGA = 0.6*g* and Ω_θ = 0.75 on the FS of the structure the ductility demand decreases from 7.4 for e_s = 0.0*L* to 2.4 for e_s = 0.15*L*. For PGA = 0.5*g* and Ω_θ = 1.25 on the FS of the structure the ductility demand decreases from 0.72 for e_s = 0.0*L* to

0.56 for $e_s = 0.15L$. The torsionally flexible structure ($\Omega_\theta = 0.75$) FS response subjected to PGA = $0.6g$ exhibits unacceptably high levels of ductility demand for low levels of static eccentricity. The torsionally stiff structure ($\Omega_\theta = 1.25$) FS response subjected to PGA = $0.4g$, $0.5g$ and $0.6g$ exhibits a predictable and stable behaviour with levels of ductility demand below 1.0 for all levels of static eccentricity.

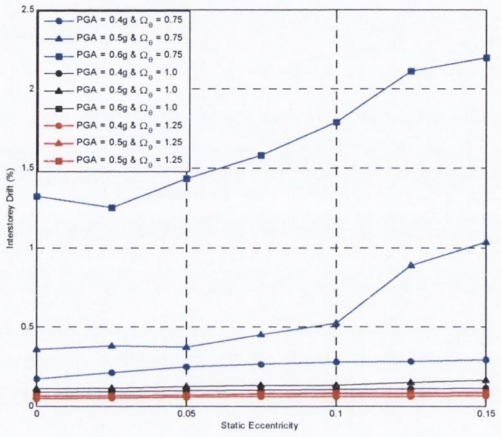

Figure 7.49: Graph of SS first-storey drift vs. static eccentricity for a range of Ω_θ and PGA

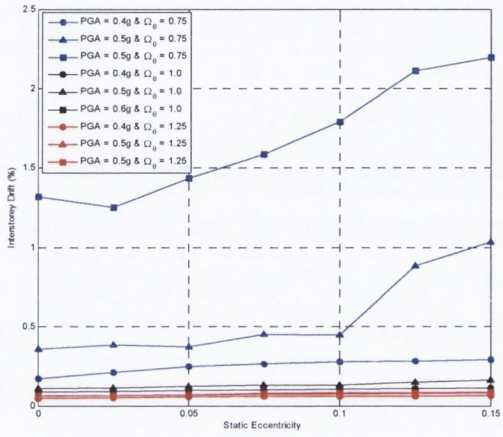

Figure 7.50: Graph of FS first-storey drift vs. static eccentricity for a range of Ω_θ and PGA

Figure 7.49 illustrates the variation in SS first-storey drift with static eccentricity for a range of lateral torsional frequency ratios and peak ground accelerations. It can be seen in Figure 7.49 the PGA = $0.4g$ structure has a first-storey drift below 0.3% for all levels of lateral torsional frequency ratio and static eccentricity. The structures subjected to PGA = $0.5g$ have a first-storey drift below 0.5% for $\Omega_\theta = 1.0$ and $\Omega_\theta = 1.25$ for every level of static eccentricity, but the $\Omega_\theta = 0.75$ structure has a first-storey drift above 0.5% for $e_s \geq 0.1L$. For PGA = $0.6g$ and $\Omega_\theta = 0.75$ on the SS of the structure the first-storey drift increases from 1.3% for $e_s = 0.0L$ to 2.2% for $e_s = 0.15L$. For PGA = $0.4g$ and $\Omega_\theta = 1.25$ on the SS of the structure the first-storey drift increases from 0.07% for $e_s = 0.0L$ to 0.1% for $e_s = 0.15L$. The torsionally flexible structure ($\Omega_\theta = 0.75$) SS response subjected to PGA = $0.5g$ and $0.6g$ exhibits unacceptably high levels of first-storey drift. The torsionally stiff structure ($\Omega_\theta = 1.25$) SS response subjected to PGA = $0.4g$, $0.5g$ and $0.6g$ exhibits a predictable and stable behaviour with levels of first-storey drift below 0.5% for all levels of static eccentricity.

Figure 7.50 illustrates the variation in FS first-storey drift with static eccentricity for a range of lateral torsional frequency ratios and peak ground accelerations. Similar to the torsionally stiff structure ($\Omega_\theta = 1.25$) SS response, the FS response subjected to PGA =

0.4g, 0.5g and 0.6g exhibits a predictable and stable behaviour with levels of first-storey drift below 0.5% for all levels of static eccentricity. However, the torsionally flexible structure ($\Omega_\theta = 0.75$) FS response subjected to PGA = 0.5g and 0.6g exhibits unacceptably high levels of first-storey drift.

Summary

The effect on the seismic response of the braced plan irregular structure caused by levels of peak ground acceleration exceeding the design ground was examined. The base model structure was designed for PGA = 0.35g and was subjected to excitations with PGA = 0.4g, 0.5g and 0.6g. The seismic behaviour of the torsionally flexible structures subjected to excitations with PGA greater (0.5 & 0.6g) than the design PGA display high levels of ductility demand and interstorey drifts exceeding Eurocode 8 (CEN, (2004)) design limits (0.5%). These structures suffer unacceptably large displacements caused by increased levels of inelasticity. Torsionally stiff structures perform well in terms of ductility demand and interstorey drift, while torsionally flexible structures perform poorly at increased levels of peak ground acceleration (0.5g & 0.6g) and static eccentricity.

It is not recommended levels of torsional flexiblity ($\Omega_\theta = 0.875$ & $\Omega_\theta = 0.75$) be allowed in concentrically braced frame plan irregular structures due to their poor performance in situations where the peak ground accelerations exceed the design peak ground acceleration. The ductility demands and interstorey drifts were unacceptably high at increased levels of peak ground acceleration (0.5g & 0.6g) and static eccentricity. A simple design check preventing torsionally flexible structures could be implemented such that $\Omega_\theta \geq 1.0$ for concentrically braced frame plan irregular structures or it could possibly be the case that another form of lateral resisting system should be employed.

7.5.8 Response Attributed to Plan Irregularity and Change in Period of Structure

In Chapter Six, Section 6.7.3, the change in response of the experimental structure was attributed to both the change in period of the structure and the change in plan irregularity. The change in period is quantified by the change in response spectrum displacement and the change in plan irregularity is quantified by the change in peak roof displacement. The results shown in Table 7.4 and Table 7.5 are for structures analysed with $\bar{\lambda} = 1.68$ and a PA

ratio of 2.0. The structures are subjected to five earthquake excitations and the mean results of SS and FS peak roof displacement and response spectrum displacement are shown in Table 7.4 and Table 7.5, respectively. The torsionally stiff (Ω_θ = 1.125 & Ω_θ = 1.25) and torsionally flexible (Ω_θ = 0.875 & Ω_θ = 0.75) structures are compared to Ω_θ = 1.0 structure with equivalent levels of static eccentricity.

The change in response of the structure for a range of lateral torsional frequency ratios and static eccentricities is quantified in two ways; firstly the change in mean peak lateral roof displacement of the structure and secondly the change in mean relative response spectrum displacement due to the change in period of the structure. The torsional stiffness of the structure was altered by increasing/decreasing the mass of the structure. Changing the mass of the structure changed the lateral torsional frequency ratio, but also altered the period of the structure. Increasing or decreasing the period of the structure alters the relative displacement spectral response the structure is subjected to. For example, as shown in Table 7.4 the Ω_θ = 0.75 with e_s = 0.0L structure has a period of 0.3886s giving a relative displacement spectral response of 1.811cm compared to the Ω_θ = 1.25 with e_s = 0.0L structure has a period of 0.2332s giving a mean relative displacement spectral response of 0.572cm. The percentage difference in relative displacement spectral response and mean roof displacement is used to quantify the contribution to the response from the change in period compared to the change in displacement response in the numerical analysis.

Table 7.4: Summary of SS difference in mean peak roof displacement and mean relative response spectrum displacement

Ω_θ	*Static Ecc. (L)*	*Period (s)*	*Mean Roof Disp. (mm)*	*Mean % Difference in Roof Disp. Compared to Ω_θ = 1.0 Structure*	*Mean Relative Resp. Spect. Disp. (cm)*	*Mean % Difference in Resp. Spect. Disp. Compared to Ω_θ = 1.0 Structure*	*Mean % Difference in Roof Disp. Response and Relative Spectral Disp. Response*
0.75	0.0	0.38862	5.593	141.79	1.811	107.52	24.17
	0.025	0.38864	5.719	158.64	1.807	107.75	32.08
	0.05	0.38854	6.472	171.56	1.803	107.89	37.11
	0.075	0.38843	6.700	167.57	1.802	108.39	35.32
	0.1	0.38830	6.797	155.96	1.801	108.72	30.29
	0.125	0.38810	6.843	146.54	1.799	109.05	25.58
	0.15	0.38789	6.902	133.3	1.798	109.43	19.91
Mean							**28.92**
COV							**39.27**
0.875	0.0	0.33314	3.601	58.64	1.204	34.73	40.77
	0.025	0.33310	3.718	67.39	1.202	34.96	48.12
	0.05	0.33303	3.848	60.43	1.201	35.23	14.70
	0.075	0.33293	4.094	63.56	1.201	35.59	44.01
	0.1	0.33281	4.464	68.47	1.200	35.83	47.67
	0.125	0.33264	4.638	67.71	1.199	36.11	46.67
	0.15	0.33246	4.757	61.99	1.199	36.35	41.36
Mean							**44.33**
COV							**8.49**
1.125	0.0	0.25911	1.623	-28.32	0.668	-21.99	-22.35
	0.025	0.25906	1.723	-23.69	0.667	-21.91	-7.51
	0.05	0.25901	1.803	-25.62	0.666	-21.84	-14.75
	0.075	0.25895	1.863	-26.15	0.665	-21.73	-16.90
	0.1	0.25884	1.962	-26.2	0.664	-21.66	-17.32
	0.125	0.25872	2.053	-26.02	0.664	-21.57	-17.10
	0.15	0.25857	2.107	-28.19	0.663	-21.53	-23.63
Mean							**-17.08**
COV							**23.95**
1.25	0.0	0.23319	1.426	-37.91	0.572	-32.15	-15.19
	0.025	0.23316	1.523	-33.74	0.571	-32.04	-5.04
	0.05	0.23311	1.630	-34.13	0.570	-31.91	-6.51
	0.075	0.23304	1.746	-32.35	0.569	-31.71	-1.98
	0.1	0.23296	1.794	-33.62	0.569	-31.57	-6.09
	0.125	0.23284	1.797	-35.92	0.568	-31.43	-12.50
	0.15	0.23271	1.881	-36.88	0.569	-31.29	-15.16
Mean							**-8.92**
COV							**24.02**

Table 7.4 presents the summary of the SS difference in response of the mean spectral displacement due to change in period and SS difference in response of the mean peak roof displacement of the structure. For example, the difference in SS mean spectral displacement response and mean roof displacement for the Ω_θ = 0.75 structure is 28.92% for all levels of static eccentricity. In other words, 28.92% of the SS displacement response of the Ω_θ = 0.75 structure is caused by the plan irregularity of the structure as opposed to purely the change in period of the structure. In Table 7.4 it can be seen that the torsionally flexible structures have a displacement response greater than the Ω_θ = 1.0 structure while the torsionally stiff structures have a displacement response less than the Ω_θ = 1.0 structure. The change in response caused by the change in period being less in the torsionally stiff as compared to the torsionally flexible structures.

Table 7.5: Summary of FS difference in mean peak roof displacement and mean relative response spectrum displacement

Ω_θ	*Static Ecc. (L)*	*Period (s)*	*Mean Roof Disp. (mm)*	*Mean % Difference in Roof Disp. Compared to Ω_θ = 1.0 Structure*	*Mean Relative Resp. Spect. Disp. (cm)*	*Mean % Difference in Resp. Spect. Disp. Compared to Ω_θ = 1.0 Structure*	*Mean % Difference in Roof Disp. Response and Relative Spectral Disp. Response*
0.75	0.0	0.38862	4.721	114.91	1.811	107.52	6.43
	0.025	0.38864	4.704	152.27	1.807	107.75	29.24
	0.05	0.38854	4.389	148.97	1.803	107.89	27.58
	0.075	0.38843	4.135	148.43	1.802	108.39	26.98
	0.1	0.38830	3.865	142.02	1.801	108.72	23.45
	0.125	0.38810	3.561	133.13	1.799	109.05	18.08
	0.15	0.38789	3.215	123.39	1.798	109.43	11.31
Mean							**20.44**
COV							**66.45**
0.875	0.0	0.33314	3.454	57.42	1.204	34.73	39.52
	0.025	0.33310	2.879	53.34	1.202	34.96	34.45
	0.05	0.33303	2.448	38.54	1.201	35.23	8.59
	0.075	0.33293	2.259	35.53	1.201	35.59	0.17
	0.1	0.33281	2.089	30.17	1.200	35.83	18.76
	0.125	0.33264	1.962	26.62	1.199	36.11	35.65
	0.15	0.33246	1.842	25.69	1.199	36.35	41.49
Mean							**25.52**
COV							**229.80**
1.125	0.0	0.25911	1.564	-28.57	0.668	-21.99	-23.03
	0.025	0.25906	1.472	-23.96	0.667	-21.91	-8.56
	0.05	0.25901	1.404	-23.55	0.666	-21.84	-7.26
	0.075	0.25895	1.327	-23.78	0.665	-21.73	-8.62
	0.1	0.25884	1.269	-24.16	0.664	-21.66	-10.34
	0.125	0.25872	1.203	-24.77	0.664	-21.57	-12.92
	0.15	0.25857	1.115	-25.12	0.663	-21.53	-14.29
Mean							**-12.15**
COV							**25.16**
1.25	0.0	0.23319	1.378	-37.97	0.572	-32.15	-15.33
	0.025	0.23316	1.268	-35.33	0.571	-32.04	-9.31
	0.05	0.23311	1.179	-35.94	0.570	-31.91	-11.21
	0.075	0.23304	1.139	-34.66	0.569	-31.71	-8.51
	0.1	0.23296	1.119	-33.64	0.569	-31.57	-6.15
	0.125	0.23284	1.096	-32.51	0.568	-31.43	-3.32
	0.15	0.23271	1.050	-31.27	0.569	-31.29	-0.07
Mean							**-7.70**
COV							**21.95**

Table 7.5 presents the summary of the FS difference in response of the mean spectral displacement due to change in period and FS difference in response of the mean peak roof displacement of the structure. For example, the difference in FS mean spectral displacement response and mean roof displacement for the Ω_θ = 0.75 structure is 20.44% for all levels of static eccentricity. In other words, 20.44% of the SS displacement response of the Ω_θ = 0.75 structure is caused by the irregularity of the structure as opposed to purely the change in period of the structure. In Table 7.5 it can be seen that the torsionally flexible structures have a displacement response greater than the Ω_θ = 1.0 structure while the torsionally stiff structures have a displacement response less than the Ω_θ = 1.0 structure. The change in response caused by the change in period being less in the torsionally stiff as compared to the torsionally flexible structures.

Summary

The change in response caused by the change in period of the structure was less pronounced in the torsionally flexible structures ($\Omega_\theta = 0.875$ & $\Omega_\theta = 0.75$) as compared to the torsionally stiff structures ($\Omega_\theta = 1.125$ & $\Omega_\theta = 1.25$). A larger proportion of the overall displacement response on the SS and FS of the structure is governed by the change in period for the torsionally stiff structures as compared to the torsionally flexible structures. For the torsionally flexible structures, the displacement response of the SS of the structure has an average increase in response due to plan irregularity of 36.6% as compared to the FS of the structure having an average increase in response due to plan irregularity of 22.9%. Similarly for the torsionally stiff structures, the displacement response of the SS of the structure has an average increase in response due to plan irregularity of 13.0% as compared to the FS of the structure having an average increase in response due to plan irregularity of 9.9%.

7.6 Results Discussion

Firstly, the seismic response of a base model structure that is neither torsionally stiff nor torsionally flexible, with varying levels of static eccentricity and lateral torsional frequency ratio and designed using the lateral force method of analysis in Eurocode 8 (CEN, (2004)) was assessed. The base model structure responded well to the five earthquakes applied to it in terms of ductility demand and iterstorey drift. The interstorey drifts are below the Eurocode 8 (CEN, (2004)) limits and the ductility demands in the range of 2-3 are acceptable in seismic design. A summary of the results obtained from the parametric numerical study undertaken in this chapter are discussed in detail hereafter.

Static Eccentricity

The static eccentricity was varied during the parametric study ranging from no static eccentricity ($e_s = 0.0L$) to maximum static eccentricity ($e_s = 0.15L$). The maximum value represents a severe but realistic level of static eccentricity. The ductility demand increases with increasing levels of static eccentricity on the SS of the structure and reduces with increasing levels of static eccentricity on the FS of the structure. The torsionally stiff structures perform better than the torsionally flexible structures having reduced ductility demands and reduced first-storey drifts. Considering all lateral torsional frequency ratios, the SS ductility demand increased on average by nearly 30% from the no static eccentricity

case to the maximum static eccentricity case. In contrast, the FS ductility demand decreased on average by just over 30%. The first-storey interstorey drift increases for increasing levels of static eccentricity for all levels of lateral torsional frequency ratio. Unlike the ductility demands, the first-storey interstorey drifts increase by a similar amount on both the SS (29.6%) and FS (35.2%) of the structure. The CI's are generally larger at extreme levels of lateral torsional frequency ratio e.g. Ω_θ = 0.75 & 1.25. No general trend was observed indicating reduced CI's for the torsionally stiff structures compared to the torsionally flexible structures. The level of interstorey drift presented in this section has focussed on the first-storey drift, as this always gave the greatest level of drift for each of the storeys. The level of drift in the other storeys varied such that the ductility demand was always greater on the SS compared to the FS even though the SS and FS first-storey drifts were generally similar. The level of static eccentricity has been observed to be a key parameter affecting the seismic torsional response of plan irregular braced frame type structures. The results presented here display a trend of increased ductility demand on the SS of the structure observed by other researchers (for example see Goel, (1997), Stathopoulos and Anagnostopoulos, (2003) or Fernández-Dávila and Cruz, (2006)).

Lateral Torsional Frequency Ratio

The lateral torsional frequency ratio ranged from Ω_θ = 0.75 (torsionally flexible) to Ω_θ = 1.25 (torsionally stiff) within the parametric study. The torsionally stiff structures perform better than the torsionally flexible structures. The SS of the structure has a larger ductility demand compared to the FS of the structure for all levels of lateral torsional frequency ratio. The ductility demand on the SS of the Ω_θ = 0.75 structure is nearly 4 times greater than that of the Ω_θ = 1.25 structure. Similarly, the ductility demand on the FS of the Ω_θ = 0.75 structure is 3.5 times greater than that of the Ω_θ = 1.25 structure. On average, the torsionally flexible structures have a ductility demand 3.75 times that of the torsionally stiff structures. The SS ductility demand increases for increasing levels of static eccentricity for all values of lateral torsional frequency ratio. The FS ductility demand decreases for increasing levels of static eccentricity for all values of lateral torsional frequency ratio. Unlike the ductility demands, the first-storey drifts are approximately the same on the SS and FS of the structure. The first-storey drifts increase for increasing levels of static eccentricity for all values of lateral torsional frequency ratio. The level of lateral torsional frequency ratio has been observed to be a key parameter affecting the seismic torsional response of plan irregular braced frame type structures. The results presented here display a well known observation in plan irregular structures that ductility demand and

interstorey drift are larger for torsionally stiff compared to torsionally flexible structures (see Moghadam and Tso, (2000a) or Marusic and Fajfar, (2005)).

Torsionally Designed Structure

The effectiveness of the Eurocode 8 (CEN, (2004)) provision for torsional effects was evaluated by application of the design procedure to the base model concentrically braced plan irregular structure. The base model structure was designed without the torsional effects provision (ETP - Excluding Torsional Provision) and compared to the base model structure designed with the torsional effects provision (ITP - Including Torsional Provision). The normalised ductility demand for all levels of static eccentricity of the ITP structure is reduced by 35.5% on the SS of the structure and 8.5% on the FS of the structure. The normalised first-storey drift for all levels of static eccentricity of the ITP structure is reduced by 35.1% on the SS of the structure and 35.1% on the FS of the structure. The normalised ductility demand of the most torsionally flexible ITP structure ($\Omega_\theta = 0.75$) is 2.01 times that of the base model structure. Similarly, the normalised first-storey drift of the most torsionally flexible ITP structure ($\Omega_\theta = 0.75$) is 2.04 times that of the base model structure. The results from the ETP and ITP analysis indicate the Eurocode 8 (CEN, (2004)) torsional provision is adequate for torsionally stiff structures, and even reduces the ductility demand on the SS of the structure for the most torsionally flexible structure at high levels of static eccentricity. Likewise, the provision even reduces the FS interstory drift at high levels of static eccentricity. The results are somewhat unexpected as the provision allows for $e_s = 0.05L$ whereas the maximum static eccentricity considered here is three times this value. For the level of static eccentricity accounted for in the provision (up to 5%), the structure performs well.

Under- and Over-designed Structure

Changing the normalised slenderness of the brace members is equivalent to under- or over-designing the structure to resist torsional effects. The under-designed structure ($\bar{\lambda} = 2.0$) experienced a large SS and FS ductility demand and large first-storey interstorey drifts, with the maximum eccentricity resulting in the first-storey interstorey drift exceeding the Eurocode 8 (CEN, (2004)) interstorey drift limit. Over-designing the brace sections on the SS of the structure ($\bar{\lambda} = 1.3$) resulted in a greater ductility demand on the FS of the structure compared to the SS of the structure. The under-designed structure ($\bar{\lambda} = 2.0$) structure experienced a SS ductility demand on average 42.5% greater than the base model

structure. The over-designed structure ($\bar{\lambda}$ = 1.3) structure had a SS ductility demand on average 26.7% less than the base model structure. Considering that the static eccentricity is distributed towards the SS of the structure, it is unexpected for the FS ductility demand to exceed the SS ductility demand. The under-designed ($\bar{\lambda}$ = 2.0) and over-designed ($\bar{\lambda}$ = 1.3) structures experience the same first-storey drift on their SS and FS of the structure. It is unexpected the first-storey interstorey drift for both the under- and over-designed structures are effectively the same for both the SS and FS of the structure as the stiffness of the braced frames is different on the SS and FS. The FS of the over-designed structure had increased ductility demand compared to the base model structure caused by the FS bracing having reduced stiffness as compared to the SS bracing. Over-designing the braced irregular structure to resist torsional effects has the unwanted effect of increasing the ductility demand on the FS of the structure.

Bi-directional Excitation

The SS & FS ductility demand for the uni-directionally and bi-directionally excited structures is similar for all levels of lateral torsional frequency ratio and static eccentricity. The SS first-storey interstorey drift is similar for uni- and bi-directionally excited structures. The FS first-storey interstorey drift is similar for uni- and bi-directionally excited structures with the single exception being the uni-directional excited structure with $e_s = 0.15L$ is on average 20.3% greater than the normalised first-storey drift for the bi-directional excited structure. In general, the analysis indicates the bi-directional and uni-directional excited structures have a similar seismic response. The uni-directional excited structure slightly overestimates the ductility demand and interstorey drift for high levels of static eccentricity. However, a few limitations exist preventing definitive conclusions, such as the structure only has static eccentricity applied in one direction and the PA ratio was not varied. Other authors, such as Ghersi and Rossi, (2001) or Stathopoulos and Anagnostopoulos, (2003) also observed the influence of the bi-directional excitation on the seismic response of plan irregular structures being minimal as compared to uni-directional excitation.

Plan Aspect Ratio

The effect of changing the PA ratio on the seismic behaviour of braced plan irregular structures was considered by altering the PA ratio within realistic ranges from 1.0 to 3.0. The SS ductility demand at values of no static eccentricity ($e_s = 0.0L$) and maximum static eccentricity ($e_s = 0.15L$) increased by 4.9% from a PA ratio of 1.0 to 3.0, while the SS

first-storey drift increased by 2.3% over the same range. No substantial variation was observed in the SS ductility demand or SS first-storey drift. The SS ductility demand and SS first-storey drift are approximately constant for all levels of PA ratio. The FS ductility demand at values of no static eccentricity ($e_s = 0.0L$) and maximum static eccentricity ($e_s = 0.15L$) decreased by 18.1% from a PA ratio of 1.0 to 3.0. The FS first-storey drift for values of no static eccentricity ($e_s = 0.0L$) and maximum static eccentricity ($e_s = 0.15L$) decreases by 2.2% across the range of PA ratios and can be considered to be approximately constant for all levels of PA ratio. The effect of varying the PA ratio is not large except for the FS ductility demand that reduces for increasing levels of PA ratio.

Level of Ground Acceleration

The effect on the seismic response of the braced plan irregular structure caused by levels of ground acceleration exceeding the design ground was examined. The base model structure was designed for PGA = 0.35g and was subjected to excitations with PGA = 0.4g, 0.5g and 0.6g. The seismic behaviour of the torsionally flexible structures subjected to excitations with PGA greater (0.5g & 0.6g) than the design PGA produce high levels of ductility demand and interstorey drifts exceeding Eurocode 8 (CEN, (2004)) design limits (0.5%). Subjecting the structure to excitations with PGA exceeding the design PGA, the structures suffers unacceptably large displacements caused by increased levels of inelasticity in the structure. Torsionally stiff structures perform well in terms of ductility demand and interstorey drift. Torsionally flexible structures perform poorly at increased levels of peak ground acceleration (0.5g & 0.6g) and static eccentricity. It is not recommended levels of torsional flexiblity ($\Omega_\theta = 0.875$ & $\Omega_\theta = 0.75$) be allowed in concentrically braced plan irregular structures due to their poor performance in situations where the peak ground accelerations exceed the design peak ground acceleration. A simple design check preventing torsionally flexible structures could be implemented such that $\Omega_\theta \geq 1.0$ for plan irregular structures. Moghadam and Tso, (2000a) also recommended that a minimum torsional stiffness condition should be stipulated in Annex A to Eurocode 8 (CEN, (1994)). Moghadam and Tso, (2000a) note that the torsionally flexible structures have a torsion dominant first mode such that the codified torsional provision are not applicable as they assume a translational dominant first mode.

Change in Response due to Plan Irregularity or Change in Period

The change in response caused by the change in period of the structure was less pronounced in the torsionally flexible structures ($\Omega_\theta = 0.875$ & $\Omega_\theta = 0.75$) as compared to

the torsionally stiff structures (Ω_θ = 1.125 & Ω_θ = 1.25). A larger proportion of the overall displacement response on the SS and FS of the structures is governed by the change in period for the torsionally stiff structures as compared to the torsionally flexible structures. For the torsionally flexible structures, the displacement response of the SS of the structure experienced an average increase in response due to plan irregularity of 36.6% as compared to the FS of the structure having an average increase in response due to plan irregularity of 22.9%. Similarly for the torsionally stiff structures, the displacement response of the SS of the structure experienced an average increase in response due to plan irregularity of 13.0% as compared to the FS of the structure having an average increase in response due to plan irregularity of 9.9%.

7.7 Chapter Overview

A detailed parametric investigation into the main parameters affecting the seismic response of concentrically braced plan irregular structures was presented in this chapter. The investigation into the effect of static eccentricity indicated a greater ductility demand exists on the SS compared to the FS of the structure as a result of increasing the level of the static eccentricity. Torsionally stiff structures performed better than torsionally flexible structures having reduced ductility demands and interstorey drifts. Designing braced plan irregular structures to resist the torsional effects using Eurocode 8 (CEN, (2004)) provisions improved the performance of the structure for levels of static eccentricity accounted for in the design provision. Over-designing the braced plan irregular structure to resist torsional effects has the unwanted effect of increasing the ductility demand on the FS of the structure and under-designing the structure resulted in poor seismic response for the torsioanlly flexible structures. Investigating the seismic response of the plan irregular structure subjected to peak ground accelerations exceeding the design peak ground acceleration indicated the torsionally flexible structures performed poorly with very high levels of ductility demand and interstorey drifts exceeding design limits. It is recommended restricting design to torsionally stiff structures with $\Omega_\theta \geq 1.0$ for braced plan irregular structures. Bi-directional excitation was investigated, but shown to have a minimal effect on the torsional response. Likewise, altering the plan aspect ratio of the structure did not significantly alter the response of the structure. The next chapter will summarise the main conclusions from the thesis.

CHAPTER EIGHT - Conclusions

8.1 Summary

In this thesis, the seismic behaviour of concentrically braced plan irregular structures has been investigated experimentally and numerically. An experimental programme consisting of 24 No. substructured soft-RTHTs of a single-storey concentrically braced frame was undertaken to better understand the seismic behaviour of concentrically braced plan irregular structures. The concentrically braced frame formed the physical substructure of a three-storey concentrically braced plan irregular structure with the remainder of the structure simultaneously modelled during the experiments using OpenSees. A series of elastic and inelastic seismic tests were performed on the physical substructure to investigate the seismic response of plan irregular structures by varying key structural parameters during the experimental programme. The results from the experimental programme were used to validate a purely numerical model for predicting the seismic response of braced plan irregular structures. An in-depth numerical parametric investigation of the key parameters affecting the seismic behaviour of braced plan irregular structures was undertaken. In particular, the appropriateness of the current Eurocode 8 (CEN, (2004)) torsional effects factor design provision when applied to braced plan irregular structures was evaluated.

8.2 Conclusions

The conclusions from this thesis can be divided into two main categories; (1) hybrid testing and (2) seismic response of plan irregular braced frame structures. Firstly, the hybrid testing conclusions are as follows;

- The hybrid test method was implemented successfully in this thesis in the form of a soft-RTHT. The hybrid test method is a relatively recently developed dynamic testing procedure and few experiments of the type implemented in this thesis have been carried out. Testing consisted of substructured soft-RTHT validation experiments on a simple portal frame structure, followed by a comprehensive experimental programme on substructured concentrically braced frames. Both the validation test and full experimental programme tests were implemented successfully.

- The hybrid test method makes use of the concept of substructuring, where the critical part of the structure is physically tested whilst the remainder of the structure is numerically modelled. The critical part of the structure typically has a highly nonlinear or rate dependent behaviour making it difficult to model numerically with a high degree of accuracy. The rest of the structure, whose response is numerically modelled, typically has a more predictable elastic or slightly nonlinear response. Employing substructuring allows the physical test to be performed at full scale, avoiding the scaling issues associated with shake table testing.

- The soft-RTHT method implemented in this thesis has been specifically developed to perform geographically distributed hybrid tests. The concept of multi-tasking is used in the hybrid test system to improve computational efficiency by performing separate tasks on separate PCs, namely; PID control on the Servo-controller PC, a predictor-corrector algorithm on the Target PC and the finite element simulations on the Simulation PC. An event-driven strategy designed to handle excessive communication delays has been employed in the implementation of the hybrid test in this thesis. Within the event-driven strategy, a predictor-corrector algorithm allows the command state to transition from *extrapolate* to *interpolate* to *slow* to *hold* to time-out. If there is a delay in receiving the target command, the system extrapolates the target command. If the delay persists, the system slows down and holds the actuator at the current target command. If the hold phase continues for too long, the system times out and the experiment is terminated. On some occasions during the experimental programme, the system timed out unexpectedly. Simulations were run prior to every test to help ensure that timing out would not take place during physical testing. Timing out typically occurred during small displacement commands and not during peak displacement responses.

- Validation Test: The results of a two-dimensional validation experiment on a simple elastic structural model indicated reasonably accurate performance in comparison to equivalent numerically simulated results, even though some unwanted torsion was observed in the experimental substructure. The peak and rms values for lateral displacement, acceleration and velocity of the test specimen differed by between 4-10% compared to the simulation, showing good agreement. The force equilibrium in the test and numerical model did not show good agreement, with the simulated model overestimating the test specimen's stiffness. The test specimen also displayed

unexpected nonlinearity in its hysteretic response. The actuator displacement command signal was observed to be smooth, indicating that the predictor-corrector model used in the test performed well. The feedback displacement signal (measured displacement) did not always follow the command signal due to a small tracking error.

- Full Experimental Programme Tests: The results of a three-dimensional substructured concentrically braced frame soft-RTHTs indicated good agreement with an equivalent Opensees numerical model in both the linear and nonlinear range. The difference between the peak and rms displacement and acceleration response of the test data and numerical model was on average between 4-10%, indicating good agreement. The difference between the test strain response and numerically modelled strain was on average 20% (peak) and 121% (rms), showing very poor agreement. Comparison of the base shears and lateral roof displacements from three-dimensional experimental and numerical models indicates that the OpenSees model achieves a poor representation of the stiffness of the test structure, underestimating the experimental stiffness by approximately 40%.

A parametric study was performed using time history analyses averaged from five earthquake records with brace ductility demand and interstorey drift presented in the results as the key response indicators. From the parametric study, the plan irregular response conclusions are as follows:

- The static eccentricity was varied during the parametric study ranging from no static eccentricity ($e_s = 0.0L$) to maximum static eccentricity ($e_s = 0.15L$), representing severe but realistic levels of static eccentricity. Ductility demand was found to increase with increasing levels of static eccentricity on the stiff side (SS) of the structure and reduce with increasing levels of static eccentricity on the flexible side (FS) of the structure. (The SS refers to the side of the structure closer to the centre of mass). Torsionally stiff structures performed better than torsionally flexible structures having lower ductility demands and first-storey drifts. Across all levels of lateral torsional frequency ratio, the effect of increasing the level of static eccentricity lead to the average SS ductility demand increasing by up to 30% and the average FS ductility demand decreasing by eccentricity similar amount. The first-storey interstorey drift increases for increasing levels of static eccentricity for all levels of lateral torsional frequency ratio. Unlike the ductility demands, the first-storey interstorey drifts increase by a similar amounts (up to

30% approximately) on both the SS and FS of the structure. The level of static eccentricity has been shown to be a key parameter affecting the seismic torsional response of braced plan irregular structures.

- The lateral torsional frequency ratio (Ω_θ) provides a parameter describing the torsional flexibility/stiffness of a structure. A value of lateral torsional frequency ratio of $\Omega_\theta < 1.0$ means the structure is torsionally flexible and a value of $\Omega_\theta > 1.0$ means the structure is torsionally stiff. The values investigated within the parametric study ranged from Ω_θ = 0.75, 0.875, 1.0, 1.125, representing realistic but severe levels of torsional flexibility/stiffness. Torsionally stiff structures were observed to perform better than torsionally flexible structures. The SS of the structure experienced a larger ductility demand than the FS of the structure for all levels of lateral torsional frequency ratio. The ductility demand on the SS of the $\Omega_\theta = 0.75$ structure was observed to be four times greater than that of the $\Omega_\theta = 1.25$ structure. Similarly, the ductility demand on the FS of the $\Omega_\theta = 0.75$ structure was observed to be 3.5 times greater than that of the $\Omega_\theta = 1.25$ structure. On average, the torsionally flexible structures experienced a ductility demand 3.75 times that of the torsionally stiff structures. The level of lateral torsional frequency ratio has been shown to be a key parameter affecting the seismic torsional response of plan irregular braced frame type structures.

- The Eurocode 8 (CEN, (2004)) accidental eccentricity design provision provides an intuitive method of accounting for low levels of static eccentricity. A torsional effects factor is used in design to increase the lateral pushover action applied to the side of the structure closer to the centre of mass. For the braced plan irregular structure, the design provision results in increased brace section sizes on the SS of the structure. The effectiveness of the Eurocode 8 (CEN, (2004)) provision for torsional effects was evaluated by application of the design procedure to the base model concentrically braced plan irregular structure. The response of the base model structure designed without the torsional effects provision (ETP - Excluding Torsional Provision) was compared to the base model structure designed with the torsional effects provision (ITP - Including Torsional Provision). The ductility demand of the ITP structure is reduced by 35.5% on the SS of the structure and 8.53% on the FS of the structure compared to the ETP structure. The first-storey drift of the ITP structure is reduced by 35.0% on the SS of the structure and 35.0% on the FS of the structure as compared to the ETP

structure. The results from the ETP and ITP analysis indicate that the Eurocode 8 (CEN, (2004)) torsional provision is adequate for torsionally stiff structures, and even reduces the ductility demand on the SS of the structure for the most torsionally flexible structure at high levels of static eccentricity when subjected to earthquake excitation with PGA below the design PGA. Likewise, the provision even reduces the FS interstory drift at high levels of static eccentricity. The results are somewhat unexpected as the provision allows for $e_s = 0.05L$ whereas the maximum static eccentricity considered here is three times this value. For the level of static eccentricity accounted for in the provision (up to 5%), the structure performs well.

- Changing the normalised slenderness of the brace members on the SS of the structure is equivalent to under- or over-designing the structure to resist torsional effects. The Eurocode 8 (CEN, (2004)) accidental eccentricity design provision required SS bracing with $\bar{\lambda} = 1.57$, whereas the structure not designed to take account of accidental eccentricity required SS bracing with $\bar{\lambda} = 1.68$ (base model). The under-designed structure ($\bar{\lambda} = 2.0$) experienced large SS and FS ductility demands and large first-storey interstorey drifts, with the maximum eccentricity resulting in the first-storey interstorey drift exceeding the Eurocode 8 (CEN, (2004)) interstorey drift limit. Over-designing the brace sections on the SS of the structure ($\bar{\lambda} = 1.3$) resulted in the ductility demand on the FS of the structure exceeding that on the SS of the structure. The under-designed structure ($\bar{\lambda} = 2.0$) experienced an average SS ductility demand over 40% greater than the base model structure. In contrast, the over-designed structure (with SS bracing of $\bar{\lambda} = 1.3$) experienced a SS ductility demand on average almost 30% less than the base model structure. The effect of over- and under-designing a structure to resist torsional effects has a large influence on the seismic response of the structure. The FS of the over-designed structure also had increased ductility demand compared to the base model structure caused by the FS bracing having reduced stiffness as compared to the SS bracing. Over-designing the braced irregular structure to resist torsional effects has the unwanted effect of increasing the ductility demand on the FS of the structure. Applying excessive stiffness and strength to the SS of the structure is not a solution to reduce global demands.

- The effect of applying the ground excitation in two orthogonal directions as opposed to one direction only during analysis was investigated by applying bi-directional excitation to the structure with a PA ratio of 1.0. The structure with a PA ratio of 1.0 had equal frame widths in both horizontal directions allowing the same brace sections to be used, facilitating direct comparison of the bi-directional to the uni-directional excited structures. The analysis indicates the bi-directional and uni-directional excited structures have a similar seismic response. However, a few limitations exist that prevent definitive conclusions, such as the structure only has static eccentricity applied in one direction and the PA ratio was not varied.

- The effect of changing the PA ratio on the seismic behaviour of braced plan irregular structures was considered by altering the PA ratio within realistic ranges from 1.0 to 3.0. The effect of varying the PA ratio is not significant with the exception of the FS ductility demand that decreases notably for higher levels of PA ratio.

- The effect on the seismic response of braced plan irregular structures caused by levels of ground acceleration exceeding the design ground was examined. The base model structure was designed for PGA = 0.35g and was subjected to excitations with PGA = 0.4g, 0.5g and 0.6g. Torsionally flexible structures subjected to excitations with PGA greater than the design PGA displayed high levels of ductility demand and interstorey drifts exceeding Eurocode 8 (CEN, (2004)) design limits (0.5%). Excitations with PGA exceeding the design PGA lead to the structure suffering unacceptably large lateral displacements caused by increased levels of inelasticity in the structure. Torsionally stiff structures perform well in terms of ductility demand and interstorey drift. Torsionally flexible structures perform poorly at increased levels of peak ground acceleration (0.5g & 0.6g), especially with high levels of static eccentricity. It is recommended that levels of torsional flexibility (Ω_θ = 0.875 & Ω_θ = 0.75) should not be allowed in plan irregular braced frame structures due to their poor performance in situations where the peak ground accelerations exceed the design peak ground acceleration. A simple design check preventing torsionally flexible structures could be implemented such that a design provision of $\Omega_\theta \geq 1.0$ is required for plan irregular braced frame structures.

- In the parametric study, varying the lateral torsional frequency ratio of the braced plan irregular structures required the mass of the structure to be altered. The results of this is a change in the fundamental period of vibration of the structure. Changing the fundamental period will influence the displacement demand on the structure, as quantified by the displacement response spectrum. It is important to quantify the separate contributions to the total observed variation in response attributable to the change in fundamental period on one hand, and to plan irregularity effects (level of e_s and Ω_θ) on the other. The proportion of the change in response attributable to the fundamental period of the structure was lower in the torsionally flexible structures (Ω_θ = 0.875 & Ω_θ = 0.75) than in the torsionally stiff structures (Ω_θ = 1.125 & Ω_θ = 1.25).

8.3 Recommendations for Further Work

There are two main aspects to possible further research namely; (1) hybrid testing and (2) plan irregularity. Firstly the recommendations for further research related to hybrid testing are described as follows;

- The soft-RTHT procedure was an introductory step towards hybrid testing at Trinity College Dublin; however limitations in the method exist. It is essentially a PsD test with an extended time scale and the method's applicability can be limited by the experimental procedure, such as being inapplicable to velocity dependent systems. The real-time hybrid test method which allows testing of rate dependent systems should be implemented as the next phase of the development of the dynamic testing facilities in the TCD Structures Laboratory.

- Implementation of the RTHT procedure at the dynamic laboratory at Trinity College Dublin would allow greater system control over the test procedure. The current soft-RTHT system employs an event-driven strategy more suited to online distributed tests. Implementation of the RTHT method would allow a user to define tailored numerical integrators and delay compensation techniques using Simulink rather than relying on the defined integrators in OpenFresco.

- The ability to perform multiple degrees of freedom experiments with multiple actuators would extend the possibilities of potential test set-ups enormously. The current one

actuator set-up only allows for a one degree of freedom test. OpenFresco offers multiple actuator test set-ups and would provide a first step towards multi-degree of freedom hybrid testing. However, multiple actuation would require acquisition of one or more high speed actuators to allow multiple degree of freedom testing at real-time. Multi-degree of freedom hybrid tests have been carried out before, however their implementation could improve the understanding of the seismic response of plan irregular structures by locating actuators on the SS and FS of the structure, thus physically applying torsion to a structure.

- The hybrid tests described in this thesis were the first of their kind to be carried out at the Structural Engineering Laboratory at Trinity College Dublin. The hybrid validation experiments and the braced frame plan irregular experiments utilised a substructured soft-RTHT procedure. An important extension to the development of the hybrid test method would be to perform a hybrid test with physically applied gravity loads on the test specimen. The additional stiffness and p-delta effects resulting from the application of the gravity loads could have a significant effect on the response. In order to investigate collapse in a physical rather than numerical manner, the stub connections could be replaced with more realistic pinned connections or a frame type connection that exist in reality. The numerical model used in the parametric study essentially reflects this scenario. The gravity loads could then be applied to the structure using hydraulic jacks and more realistic test results could be achieved. To the best of the author's knowledge, a substructured soft-RTHT with physically applied gravity load has not been implemented to date.

- A medium term goal could be the development of geographically distributed testing. Distributed testing already exists and is ready for implementation in the soft-RTHT set-up through the application of the event driven strategy. The soft-RTHT procedure implemented in this thesis was developed specifically for this purpose. An achievable goal could be to perform 'locally' distributed tests, for example from a location within the university campus. The 'locally' geographically distributed tests would need to have user defined random delays to replicate realistic internet communication delays. Once the procedure has been successfully implemented, the limitations of distributed tests are the communication infrastructure around the host laboratory and between potential remote sites.

- The fundamental validation of the hybrid test procedure would be the comparison of test results with fully dynamic shake table test results, as has been the case for numerous hybrid experimental tests previously. Existing shake table test results such as Goggins, (2004) or other proposed shake table tests in the future could be used for validation. The most realistic dynamic test to compare the accuracy of a hybrid test procedure is through shake table test results. Comparing fully dynamic test results with substructured hybrid tests using the facility in the dynamics laboratory at Trinity College Dublin would provide increased confidence in the accuracy of the experimental procedure.

Secondly, the recommendations for further research related to plan irregularity are detailed hereafter;

- The OpenSees numerical model has been shown to adequately predict the nonlinear response of concentrically braced frame plan irregular structures. Extending this model to a larger and more realistic structure would lead to a greater understanding of the seismic behaviour of multi-storey braced plan irregular structures. A structure with different plan configurations and more bays/storeys could allow for better understanding of the interaction between the response of the SS and FS of the structure and effects of static eccentricity and torsional stiffness in a more realistic structure. A purely numerical parametric study utilising the parallel computing abilities of OpenSees or the use of high performance computers would allow for an extensive investigation.

- Stiffness irregularity has been investigated by proxy by implementation in design of the Eurocode 8 (CEN, (2004)) accidental eccentricity provision using the torsional effects factor. The stiffness eccentricity was not explicitly investigated in this thesis. A parametric study similar to that on static eccentricity investigated in this thesis, but applied to variations in stiffness eccentricity would provide complementary information on the seismic response of braced plan irregular structures.

- The affect of strength eccentricity on the seismic response of plan irregular structures needs further investigation. Strength and stiffness are related, such that increasing the strength increases the stiffness of a lateral force resisting element. A desirable distribution of strength and stiffness that can reduce the torsional response of plan irregular structures requires investigation. Methods of design such as the direct

displacement-based seismic approach would achieve a given performance limit rather than be bounded by a given performance limit and may prove more suitable than the current force-based seismic design approach in Eurocode 8 (CEN, (2004)).

- The highly nonlinear seismic response of torsionally flexible braced plan irregular structures was shown to be unsatisfactory with unacceptably high levels of ductility demand and interstorey drift. An approach to mitigate the seismic response of torsionally flexible structures by application of passive or active control is worth investigation. Passive control has interested researchers already, so the possibility of implementing active control strategies for plan irregularity presents an interesting opportunity. In terms of seismic design, active control is preferable because it can have an effect over a larger frequency range and is adaptive, whereas passive control typically is designed for a narrow frequency band only. A holistic multi-strategy adaptive control approach providing the best possible control for combined seismic, wind and irregularity loading scenarios would be worth investigation. Real-time hybrid testing could be implemented to validate the adaptive control strategy in a rate-dependent experimental set-up.

References

ACTIVESTATE (2010) ActiveTcl 8.5.8.1.291945 Regents of the University of California, Sun Microsystems, Inc., Scriptics Corporation, ActiveState Corporation.

AISC (2005) Seismic provisions for structural steel buildings. Chicago, American Institute of Steel Construction.

ALGAARD, W. (2001) Integrated implementation system for pseudodynamic testing. *PhD thesis, Civil Engineering.* University of Glasgow, UK.

ALGAARD, W., AGAR, A. & BICANIC, N. (2001) Enhanced integral form of the Newmark time stepping scheme for pseudodynamic testing. *Engineering Computations,* 18, 676 - 689.

AMERICAN SOCIETY OF CIVIL ENGINEERS (2005) Minimum design loads for buildings and other structures. *7-05.* Reston, VA.

ASCE (2000) Steel moment frames after Northridge. *Journal of Sturctural Engineering,* 126.

AZIMINEJAD, A. & MOGHADAM, A. S. (2009) Performance of asymmetric multistory shear buildings with different strength distributions. *Journal of Applied Sciences,* 9, 1082-1089.

BAUSCHINGER, J. (1886) Mittheilungen XV: Ueber die veraenderung der elasticitaetsgrenze und der festigheit des eisens und stahls durch strecken und quetschen durch einwaermen und abkuhlen und durch wiederholte beanspruchung. Mechanisch-technischen Laboratorium., Koeniglichen Hochschule in Muenchen, Munich

BLACK, R. G., WENGER, W. A. B. & POPOV, E. P. (1980) Inelastic buckling of steel struts under cyclic load reversals. Berkeley, CA: Earthquake Engineering Research Center, University of California, Berkeley.

BLAKEBOROUGH, A., MERRIMAN, P. A. & WILLIAMS, M. S. (1997) The Northridge, California earthquake of 17 January 1994: a field report by EEFIT. *Earthquake Engineering Field Investigation Team.* London.

BLAKEBOROUGH, A., WILLIAMS, M. S. & DARBY, A. P. (2001) The development of real-time substructure testing. *Philosophical Transactions of The Royal Society* 359, 1869-1891.

BONELLI, A. & BURSI, O. S. (2004) Generalized-α methods for seismic structural testing. *Earthquake Engineering & Structural Dynamics,* 33, 1067-1102.

BONNET, P. A. (2006) The development of multi-axis real-time substructure testing. *PhD thesis, Department of Engineering Science.* University of Oxford.

BOUSIAS, S. N., FARDIS, M. N., SPATHIS, A. L. & KOSMOPOULOS, A. J. (2007) Pseudodynamic response of torsionally unbalanced two-storey test structure. *Earthquake Engineering & Structural Dynamics,* 36, 1065-1087.

BOUTROS, M. K. (1999) Cyclic behaviour of partly plastic pinned circular tubes: II. Testing and verification of the model. *Thin-Walled Structures,* 33, 69-82.

BOZORGNIA, Y. & TSO, W. K. (1986) Inelastic earthquake response of asymmetric structures. *Journal of Structural Engineering, ASCE,* 112, 383-400.

BRITISH STANDARDS INSTITUTION (2008) BS EN 1090-2:2008 *Execution of steel structures and aluminium structures Part 2: Technical requirements for the execution of steel structures.* BSi, United Kingdom.

BRITISH STANDARDS INSTITUTION (2009) BS EN ISO 6892-1:2009. *Metallic materials - Tensile testing - Part 1: Method of test at room temperature.* BSi, United Kingdom.

BRODERICK, B. M. (1994) Seismic testing, analysis and design of composite frames. *PhD thesis, Department of Civil Engineering, Imperial College of Science, Technology and Medicine.* University of London.

BUCHET, P. & PEGON, P. (1994) PSD testing with substructuring: implementation and use. *JRC Special Publication No. I.94.25, Ispra, Italy*, 21 pages.

BURSI, O. S. & SHING, P.-S. B. (1996) Evaluation of some implicit time-stepping algorithms for pseudodynamic tests. *Earthquake Engineering & Structural Dynamics,* 25, 333-355.

CARRION, J. E. & SPENCER, F. B., JR. (2007) Model-based strategies for real-time hybrid testing. *NSEL Report Series.* Report No. NSEL-006 ed., University of Illinois at Urbana-Champaign.

CEN (1994) Eurocode 8: Design provisions for earthquake resistance of structures. *ENV 1998-1-1/2/3.* European Committee for Standardization.

CEN (2002) Eurocode 8: Draft No. 5 Design of structures for earthquake resistance – Part 1: General rules, seismic actions and rules for buildings. *PrEH 1998-1.* BSi, United Kingdom.

CEN (2004) Eurocode 8: Design of structures for earthquake resistance – Part 1: General rules, seismic actions and rules for buildings. *BS EN 1998-1:2004.* BSi, United Kingdom.

CEN (2005) Eurocode 3: Design of steel structures – Part 1-1: General rules and rules for buildings. *BS EN 1993-1-1:2005.* BSi, United Kingdom.

CHANDLER, A. M. & DUAN, X. N. (1997) Performance of asymmetric code-designed buildings for serviceability and ultimate limit states. *Earthquake Engineering & Structural Dynamics,* 26, 717-735.

CHANDLER, A. M., DUAN, X. N. & RUTENBERG, A. (1996) Seismic torsional response: assumptions, controversies and research progress. *European Earthquake Engineering*, 37-50.

CHANDLER, A. M. & POMONIS, A. (1997) The Northridge, California earthquake of 17 January 1994: a field report by EEFIT. *Earthquake Engineering Field Investigation Team.* London.

CHANG, S.-Y., TSAI, K.-C. & CHEN, K.-C. (1998) Improved time integration for pseudodynamic tests. *Earthquake Engineering & Structural Dynamics,* 27, 711-730.

CHANG, S. Y. (1998) A time integration pseudodynamic algorithm. *Proceedings of the 11th European Conference on Earthquake Engineering.* Roterdam, Holland.

CHAPRA, S. C. & CANALE, R. P. (2006) *Numerical Methods for Engineers*, McGraw Hill.

CHOPRA, A. K. & GOEL, R. K. (2003) A modal pushover analysis procedure to estimate seismic demands for unsymmetric-plan buildings: Theory and preliminary evaluation. Earthquake Engineering Research Center, University of California, Berkeley.

CLOUGH, R. W. & PENZIEN, J. (1993) *Dynamics of structures,* New York, McGraw-Hill.

COELHO, E., CAPOS COSTA, A., CANDEIAS, M. J., FALCAO, S. & MENDES, L. (2005) Shake table tests of a 3-storey irregular RC structure designed for gravity loads. *SPEAR Workshop.* Ispra, Italy.

COMBESCURE, D. & PEGON, P. (1997) α-Operator splitting time integration technique for pseudodynamic testing error propagation analysis. *Soil Dynamics and Earthquake Engineering,* 16, 427-443.

COMMISSION OF THE EUOPEAN COMMUNITIES (1989) 'Eurocode EC8: structures in seismic regions; Part 1 general design and building' (draft). *Report EUR 12266 EN.* Brussels.

COMMUNITIES, C. O. T. E. (1993) Eurocode 8: Design for structures in seismic regions, Part 1, General and Building Report EUR12266EN, Brussels.

CORRENZA, J. C., HUTCHINSON, G. L. & CHANDLER, A. M. (1994) Effect of transverse load-resisting elements on inelastic earthquake response of eccentric-plan buildings. *Earthquake Engineering & Structural Dynamics,* 23, 75-89.

CORRENZA, J. C., HUTCHINSON, G. L. & CHANDLER, A. M. (1995) Seismic response of flexible-edge elements in code-designed torsionally unbalanced structures. *Engineering Structures,* 17, 158-166.

DARBY, A. P., BLAKEBOROUGH, A. & WILLIAMS, M. S. (1999) Real-time substructure tests using hydraulic actuator. *Journal of Engineering Mechanics,* 125, 1133-1139.

DARBY, A. P., WILLIAMS, M. S. & BLAKEBOROUGH, A. (2002) Stability and delay compensation for real-time substructure testing. *Journal of Engineering Mechanics,* 128, 1276-1284.

DE LA LLERA, J. C. & CHOPRA, A. K. (1994) Accidental torsion in buildings due to stiffness uncertainty. *Earthquake Engineering & Structural Dynamics,* 23, 117-136.

DE LA LLERA, J. C. & CHOPRA, A. K. (1995) Understanding the inelastic seismic behaviour of asymmetric-plan buildings. *Earthquake Engineering & Structural Dynamics,* 24, 549-572.

DE LA LLERA, J. C. & CHOPRA, A. K. (1996) Inelastic behavior of asymmetric multistory buildings. *Journal of Structural Engineering, ASCE,* 122, 597-606.

DE STEFANO, M., MARINO, E. & ROSSI, P. (2006) Effect of overstrength on the seismic behaviour of multi-storey regularly asymmetric buildings. *Bulletin of Earthquake Engineering,* 4, 23-42.

DE STEFANO, M. & PINTUCCHI, B. (2002) A model for analyzing inelastic seismic response of plan-irregular building structures. *15th ASCE Engineering Mechanic Conference.* Columbia University, New York, USA.

DE STEFANO, M. & PINTUCCHI, B. (2003) Mass-eccentric building structures: effects of asymmetric distribution of axial forces in vertical resisting elements. *Pacific Conference on Earthquake Engineering.* Christchurch, New Zealand.

DE STEFANO, M. & PINTUCCHI, B. (2008) A review of research on seismic behaviour of irregular building structures since 2002. *Bulletin of Earthquake Engineering,* 6, 285-308.

DE STEFANO, M. & RUTENBERG, A. (1998) Predicting the dynamic response of asymmetric multistory wall-frame structures by pushover analysis: two case studies. *Proceedings of the 11th European Conference on Eartrhquake Engineering.* Balkema, Rotterdam.

DERMITZAKIS, S. N. & MAHIN, S. A. (1985) Development of substructuring techniques for on-line computer controlled seismic performance testing. *Report UCB/EERC - 85/04.* Earthquake Engineering Research Center, University of California, Berkeley.

DICLELI, M. & CALIK, E. E. (2008) Physical theory hysteretic model for steel braces. *Journal of Structural Engineering, ASCE,* 134, 1215-1228.

DIMIG, J., SHIELD, C., FRENCH, C., BAILEY, F. & CLARK, A. (1999) Effective force testing: A method of seismic simulation for structural testing. *Journal of Structural Engineering, ASCE,* 125, 1028-1037.

DIMOVA, S. & ALASHKI, I. (2003) Seismic design of symmetric structures for accidental torsion. *Bulletin of Earthquake Engineering,* 1, 303-320.

DING, X. (2006) Redundancy in steel braced frames under seismic excitations. Ph.D. thesis, University of Illinois at Urbana-Champaign.

DUAN, X. N. & CHANDLER, A. M. (1993) Inelastic seismic response of code-designed multistorey frame buildings with regular asymmetry. *Earthquake Engineering & Structural Dynamics,* 22, 431-445.

DUTTA, S. C. & DAS, P. K. (2002) Inelastic seismic response of code-designed reinforced concrete asymmetric buildings with strength degradation. *Engineering Structures,* 24, 1295-1314.

ELGHAZOULI, A. (2009) *Seismic design of buildings to Eurocode 8*, Spon Press.

ELGHAZOULI, A. (2010) Assessment of European seismic design procedures for steel framed structures. *Bulletin of Earthquake Engineering,* 8, 65-89.

ELGHAZOULI, A. Y. (2003) Seismic design procedures for concentrically braced frames. *Proceedings of the Institution of Civil Engineers, Structures and Buildings,* 156, 381-394.

ELKHORAIBI, T. & MOSALAM, K. M. (2007) Generalized hybrid simulation framework for structural systems subjected to seismic loading. Pacific Earthquake Engineering Research Center.

ERDURAN, E. & RYAN, K. L. (2011) Effects of torsion on the behavior of peripheral steel-braced frame systems. *Earthquake Engineering & Structural Dynamics,* 40, 491-507.

FAJFAR, P. & GASPERSIC, P. (1996) The N2 method for the seismic damage analysis of RC buildings. *Earthquake Engineering & Structural Dynamics,* 25, 31-46.

FAJFAR, P., MAGLIULO, G., MARUŠIC, D. & PERUŠ, I. (2002) Simplified non-linear analysis of asymmetric buildings. *Proceedings of the third European workshop on the seismic behaviour of irregular and complex structures.* Florence, Italy.

FAJFAR, P., MARUSIC, D. & PERUS, I. (2005) Torsional effects in the pushover-based seismic analysis of buildings. *Journal of Earthquake Engineering,* 9, 831-854.

FARDIS, M. N. & NEGRO, P. (2005) SPEAR International Workshop. *European Commission Joint Research Centre.* Ispra, Italy.

FELL, B. V., MYERS, A. T., DEIERLEIN, G. G. & KANVINDE, A. M. (2006) Testing and simulation of ultra-low cycle fatigue and fracture in steel braces. *Proceedings of the 8th U.S. National Conference on Earthquake Engineering.* San Fransisco, USA.

FEMA (2000) Prestandard and commentary for the seismic rehabilitation of buildings - FEMA 356. Federal Emergency Management Agency, Washington DC, USA.

FERNÁNDEZ-DÁVILA, V. I. & CRUZ, E. F. (2006) Parametric study of the non-linear seismic response of three-dimensional building models. *Engineering Structures,* 28, 756-770.

FERRAIOLI, M., AVOSSA, A. M. & FERRI, A. (2010) Pushover procedure for inelastic torsion analysis of buildings. *14th European Conference on Earthquake Engineering.* Ohrid, Macedonia.

GHERSI, A., MARINO, E. & ROSSI, P. (2007) Static versus modal analysis: influence on inelastic response of multi-storey asymmetric buildings. *Bulletin of Earthquake Engineering,* 5, 511-532.

GHERSI, A. & ROSSI, P. P. (2001) Influence of bi-directional ground motions on the inelastic response of one-storey in-plan irregular systems. *Engineering Structures,* 23, 579-591.

GIORDANO, A., GUADAGNUOLO, M. & FAELLA, G. (2008) Pushover analysis of plan irregular masonry buildings. *The 14th World Conference on Earthquake Engineering.* Beijing, China.

GOEL, R. K. (1997) Seismic response of asymmetric systems: Energy-based approach. *Journal of Structural Engineering, ASCE,* 123, 1444-1453.

GOEL, R. K. (1998) Effects of supplemental viscous damping on seismic response of asymmetric-plan systems. *Earthquake Engineering & Structural Dynamics,* 27, 125-141.

GOEL, R. K. & CHOPRA, A. K. (1990) Inelastic seismic response of one-storey, asymmetric-plan systems: Effects of stiffness and strength distribution. *Earthquake Engineering & Structural Dynamics,* 19, 949-970.

GOGGINS, J. (2004) Earthquake resistant hollow and filled steel braces. *PhD thesis, Civil, Structural & Environmental Engineering.* University of Dublin, Trinity College, Ireland.

GOGGINS, J. M., BRODERICK, B. M., ELGHAZOULI, A. Y. & LUCAS, A. S. (2005) Experimental cyclic response of cold-formed hollow steel bracing members. *Engineering Structures,* 27, 977-989.

GOGGINS, J. M., BRODERICK, B. M., ELGHAZOULI, A. Y. & LUCAS, A. S. (2006) Behaviour of tubular steel members under cyclic axial loading. *Journal of Constructional Steel Research,* 62, 121-131.

HAKUNO, M., SHIDAWARA, M. & HARA, T. (1969) Dynamic destructive test of a cantilever beam controlled by an analog-computer. *Trans. Jpn. Soc. Civ. Engrs.*, 1-9.

HEJAL, R. & CHOPRA, A. K. (1987) Earthquake response of torsionally-coupled buildings. *Report No. UCB/EERC 87-20.* Earthquake Engineering Research Center, University of California, Berkeley.

HEREDIA-ZAVONI, E. & MACHICAO-BARRIONUEVO, R. (2004) Response to orthogonal components of ground motion and assessment of percentage combination rules. *Earthquake Engineering & Structural Dynamics,* 33, 271-284.

HILBER, H. M., HUGHES, T. J. R. & TAYLOR, R. L. (1977) Improved numerical dissipation for time integration algorithms in structural dynamics. *Earthquake Engineering & Structural Dynamics,* 5, 283-292.

HILL, R. (1998) *The mathematical theory of plasticity,* Oxford, Clarendon Press.

HORIUCHI, T., INOUE, M. & KONNO, T. (2000) Development of a real-time hybrid experimental system using a shaking table. *12th World Conference on Earthquake Engineering.* Auckland, New Zealand.

HORIUCHI, T., INOUE, M., KONNO, T. & NAMITA, Y. (1999) Real-time hybrid experimental system with actuator delay compensation and its application to a piping system with energy absorber. *Earthquake Engineering & Structural Dynamics,* 28, 1121-1141.

HUANG, Y. & MAHIN, S. A. (2008) A cyclic damaged plasticity model: Implementation and applications. *10th International LS-DYNA User Conference.* Michigan, USA.

HUANG, Y. & MAHIN, S. A. (2010) Simulating the inelastic seismic behavior of steel braced frames including the effects of low-cycle fatigue. *PEER Report 2010/104.* University of California, Berkeley.

HUDSON, D. E. (1956) Response spectrum techniques in engineering seismology. *Proceedings of the 1st World Conference on Earthquake Engineering* Earthquake Engineering Research Institute, Berkeley, California.

HUGHES, T. J. R., PISTER, K. S. & TAYLOR, R. L. (1979) Implicit-explicit finite elements in nonlinear transient analysis. *Computer Methods in Applied Mechanics and Engineering,* 17-18, 159-182.

ICBO (1997) 1997 Uniform building code, volume 2 structural engineering design provisions. International Conference of Building Officials. California, Whittier.

IGARASHAI, A., IEMURA, H., TANAKA, H. & TSURUTA, D. (2004) Experimental simulation of coupled response of structural systems using the substructured hybrid shake table test method. *13th World Conference on Earthquake Engineering.* Vancouver, Canada.

IKEDA, K. & MAHIN, M. A. (1984) A refined physical theory model for predicting the seismic behaviour of braced steel frames. *UCB/EERC-84/12.* Earthquake Engineering Research Center, University of California, Berkeley.

IKEDA, K., MAHIN, M. A. & DERMITZAKIS, S. N. (1984) Phenomenological modelling of steel braces under cyclic loading. *UCB/EERC-84/09.* Earthquake Engineering Research Center, University of California, Berkeley.

JAIN, A. K., HANSON, R. D. & GOEL, S. C. (1978) Inelastic response of restrained steel tubes. *Journal of the Structural Division, ASCE,* 104, 897-910.

JEONG, S.-H. & ELNASHAI , A. S. (2005) Analytical assessment of an irregular RC frame for full-Scale 3D pseudo-dynamic testing part II: condition assessment and test deployment. *Journal of Earthquake Engineering,* 9, 265-284.

JEONG, S.-H. & ELNASHAI, A. S. (2005) Anaytical assessment of an irregular RC frame for full-scale 3D pseudo-dynamic testing part I: analytical model verification. *Journal of Earthquake Engineering,* 9, pages 95-128

JIN, J. & EL-TAWIL, S. (2003) Inelastic cyclic model for steel braces. *Journal of Engineering Mechanics,* 129, 548-557.

KANVINDE, A. M. & DEIERLEIN, G. G. (2007) Cyclic void growth model to assess ductile fracture initiation in structural steels due to ultra low cycle fatigue. *Journal of Engineering Mechanics,* 133, 701-712.

KARAVASILIS, T. L., BAZEOS, N. & BESKOS, D. E. (2008) Seismic response of plane steel MRF with setbacks: Estimation of inelastic deformation demands. *Journal of Constructional Steel Research,* 64, 644-654.

KHATIB, F., MAHIN, S. A. & PISTER, K. S. (1988) Seismic behavior of concentrically braced steel frames. *UCB/EERC-88/01.* Earthquake Engineering Research Center, University of California, Berkeley.

KILAR, V. & FAJFAR, P. (1997) Simple push-over analysis of asymmteric buildings. *Earthquake Engineering & Structural Dynamics,* 26, 233-249.

KOREN, D. & KILAR, V. (2011) The applicability of the N2 method to the estimation of torsional effects in asymmetric base-isolated buildings. *Earthquake Engineering & Structural Dynamics,* 40, 867-886.

KRESLIN, M. & FAJFAR, P. (2010) Seismic evaluation of an existing complex RC building. *Bulletin of Earthquake Engineering,* 8, 363-385.

LEE, D. M. (1980) Base isolation for torsion reduction in asymmetric structures under earthquake loading. *Earthquake Engineering & Structural Dynamics,* 8, 349-359.

LEE, J. J. & AB-MALEK, K. (2010) Base isolation using seismic rubber bearings for asymmetric buildings. *14th European Conference on Earthquake Engineering.* Ohrid, Macedonia.

LI, H.-N. & LI, X.-L. (2009) Experiment and analysis of torsional seismic responses for asymmetric structures with semi-active control by MR dampers *Smart Materials and Structures,* 18, 1-10.

LIGNOS, D. & GANTES, C. J. (2005) Seismic demands for steel braced frames with stiffness irregularities based on modal pushover analysis. *Proceedings of the 4th European Workshop on the Seismic Behaviour of Irregular and Complex Structures.* Thessaloniki, Greece.

LIN, W.-H. & CHOPRA, A. K. (2003) Asymmetric one-storey elastic systems with non-linear viscous and viscoelastic dampers: Simplified analysis and supplemental

damping system design. *Earthquake Engineering & Structural Dynamics,* 32, 579-596.

LONGO, A., MONTUORI, R. & PILUSO, V. (2008) Failure mode control of x-braced frames under seismic actions. *Journal of Earthquake Engineering,* 12, 728 - 759.

MAGONETTE, G. (2001) Development and application of large-scale continuous pseudo-dynamic testing techniques. *Phil. Trans. R. Soc. Lond,* 359, 1771-1799.

MAHIN, S. A., SHING, P.-S. B., THEWALT, C. R. & HANSON, R. D. (1989) Pseudodynamic test method: current status and future directions. *Journal of Structural Engineering, ASCE,* 115, 2113-2128.

MAISON, B. F. & POPOV, E. P. (1980) Cyclic response prediction for braced steel frames. *Journal of Structural Division, ASCE,* 106, 1401-1416.

MARUSIC, D. & FAJFAR, P. (2005) On the inelastic seismic response of asymmetric buildings under bi-axial excitation. *Earthquake Engineering & Structural Dynamics,* 34, 943-963.

MASI, A., DOLCE, M. & CATERINA, F. (1997) Seismic response of irregular multi-storey buildings with flexible inelastic diaphragms. *The Structural Design of Tall Buildings,* 6, 99-124.

MATHWORKS (2010) Matlab & Simulink 2010a. Natick, MA, USA.

MAZZONI, S., MCKENNA, F., SCOTT, M. H. & FENVES, G. L. (2006) OpenSees command language manual. University of Claifornia, Berkeley.

MCCLINTOCK, F. A. & ARGON, A. S. (1966) *Mechanical behavior of materials*, Addison-Wesley Publishing Co., Reading, MA.

MCCRUM, D. P. (2010) Seismic analysis and hybrid testing of a concentrically braced asymmetric irregular structure (presentation). *SECED Young Engineers Conference.* University College London.

MCCRUM, D. P. & BRODERICK, B. M. (2010) Seismic analysis using the real-time hybrid test method *Joint Symposium on Bridge & Infrastructure Research in Ireland and Concrete Research in Ireland.* University College Cork & Cork Institute of Technology, Ireland.

MCKENNA, F., FENVES, G. L. & SCOTT, M. H. (2000) Open system for earthquake engineering simulation. University of California, Berkeley.

MENEGOTTO, M. & PINTO, P. E. (1973) Method of analysis for cyclically loaded reinforced concrete plane frames including changes in geometry and nonelastic behavior of elements under combined normal force and bending. *Proceedings of IABSE Symposium on Resistance and Ultimate Deformability of Structures Acted on by Well Defined Repeated Loads.* Lisbon, Portugal.

MIRI, M. & MARAMAEE, S. (2009) The effects of asymmetric bracing on steel structures under seismic loads. *World Academy of Science, Engineering and Technology.*

MOGHADAM, A. S. & TSO, W. K. (1996) Seismic response of regular asymmetrical RC ductile frame buildings. IN RAMASCO, R. & RUTENBERG, A. (Eds.) *Proc. European Workshop on the Seismic Behaviour of Asymmetric and Set-Back Structures.* Capri-Naples, Italy.

MOGHADAM, A. S. & TSO, W. K. (2000a) Extension of eurocode 8 torsional provisions to multi-storey buildings. *Journal of Earthquake Engineering,* 4, 25-41.

MOGHADAM, A. S. & TSO, W. K. (2000b) Pushover analysis for asymmetric and set-back multi-story buildings. *12th World Conference on Earthquake Engineering.* Auckland, New Zealand.

MOLA, E. & NEGRO, P. (2005) Full scale psd testing of the torsionally unbalanced SPEAR structure in the 'as-built' and retrofitted configurations. *SPEAR Workshop.* Ispra, Italy.

MOLINA, F. J., VERZELETTI, G., MAGONETTE, G., BUCHET, P., RENDA, V., GERADIN, M., PARDUCCI, A., MEZZI, M., PACCHIAROTTI, A., FEDERICI, L. & MASCELLONI, S. (2002) Pseudodynamic tests on rubber base isolators with numerical substructuring of the superstructure and strain-rate effect compensation. *Earthquake Engineering & Structural Dynamics,* 31, 1563-1582.

MOSQUEDA, G. (2003a) Continuous hybrid simulation with geographically distributed substructures. *Department of Civil and Environmental Engineering.* University of California, Berkeley.

MOSQUEDA, G. (2003b) Continuous hybrid simulation with geographically distributed substructures. . *University of California, Berkeley.* University of California, Berkeley.

MOSQUEDA, G., STOJADINOVIC, B. & MAHIN, S. A. (2005) Implementation and accuracy of continuous hybrid simulation with geographically distributed substructures. *UCB/EERC 2005-02.* Earthquake Engineering Research Center. University of California, Berkeley.

MYSLIMAJ, B. & TSO, W. K. (2005) A design-oriented approach to strength distribution in single-story asymmetric systems with elements having strength-dependent stiffness. *Earthquake Spectra,* 21, 197-212.

NAKASHIMA, M., KAMINOSO, T., ISHIDA, M. & ANDO, K. (1990) Integration techniques for substructuring pseudodynamic test. *Proceedings 4th US National Conference On Earthquake Engineering.* Palm Springs, CA, USA.

NAKASHIMA, M. & KATO, H. (1987) Experimental error growth behavior and error growth control in on-line computer test control method. *Building Research Institute.* Ministry of Construction, Tsukuba, Japan.

NAKASHIMA, M., KATO, H. & TAKAOKA, E. (1992) Development of real-time pseudo dynamic testing. *Earthquake Engineering & Structural Dynamics,* 21, 79-92.

NAKASHIMA, M. & MASAOKA, N. (1999) Real-time on-line test for MDOF systems. *Earthquake Engineering & Structural Dynamics,* 28, 393-420.

NEILD, S. A., STOTEN, D. P., DRURY, D. & WAGG, D. J. (2005) Control issues relating to real-time substructuring experiments using a shaking table. *Earthquake Engineering & Structural Dynamics,* 34, 1171-1192.

NEWMARK, N. M. (1959) A method of computation for structural dynamics. *Journal of Engineering Mechanics Division, ASCE,* 85, 67-94.

PAN, P., TOMOFUJI, H., WANG, T., NAKASHIMA, M., OHSAKI, M. & MOSALAM, K. M. (2006) Development of peer-to-peer (P2P) internet online hybrid test system. *Earthquake Engineering & Structural Dynamics,* 35, 867–890.

PAULAY, T. (1998) Torsional mechanisms in ductile building systems. *Earthquake Engineering & Structural Dynamics,* 27, 1101-1121.

PEER (2000) Pacific Earthquake Engineering Research Center. Regents of the University of California.

PEGON, P. & PINTO, A. V. (2000) Pseudo-dynamic testing with substructuring at the ELSA Laboratory. *Earthquake Engineering & Structural Dynamics,* 29, 905-925.

PENELIS, G. G. & KAPPOS, A. J. (2005) Inelastic torsional effects in 3D pushover analysis of buildings. *4th European Workshop on the Seismic Behaviour of Irregular and Complex Structures.* Thessaloniki, Greece.

PERUŠ, I. & FAJFAR, P. (2005) On the inelastic torsional response of single-storey structures under bi-axial excitation. *Earthquake Engineering & Structural Dynamics,* 34, 931-941.

PETTI, L. & DE IULIIS, M. (2008) Torsional seismic response control of asymmetric-plan systems by using viscous dampers. *Engineering Structures,* 30, 3377-3388.

PINTO, A., PEGON, P., MAGONETTE, G., MOLINA, J., BUCHET, P. & G., T. (2002) Pseudodynamic tests on a large-scale model of an existing RC bridge using non-linear substructuring and asynchronous motion. European Laboratory for Structural Assessment, Ispra, Italy.

PINTO, A., TAUCER, F. & DIMOVA, S. (2007) Pre-normative research needs to achieve improved design guidelines for seismic protection in the EU. *EUR 22858 EN.* JRC Scientific and Technical Reports.

POPOV, E. P. & BLACK, R. G. (1981) Steel struts under severe cyclic loadings. *Journal of the Structural Division, ASCE,* 107, 1857-1881.

REINHORN, A., SIVASELVAN, V., LIANG, Z. & SHAO, X. (2004) Real-time dynamic hybrid testing of structural systems. *Proceedings of the 13th World Conference on Earthquake Engineering.* Vancouver, Canada.

ROSENBLEUTH, E. (1957) Considerations on torsion, overturning and drift limitations. *Proceedings SEAOC Conference.* Coronado, California, USA.

ROSENBLEUTH, E. & MELI, R. (1986) The 1985 earthquake: causes and effects in Mexico City. *Concrete International,* 23-34.

RUTENBERG, A., EISENBERGER, M. & SHOHET, G. (1992) Inelastic seismic response of code designed single storey asymmetric structures. *Engineering Structures,* 14, 91-102.

RUTENBERG, A. & TSO, W. K. (2004) Horizontally irregular structures: some recent develeopments. IN FAJFAR, P. & KRAWINKLER, H. (Eds.) *Performance-Based Seismic Design Concepts and Implementation. Proceedings of an International Workshop.* Bled, Slovenia.

SADEK, A. W. & TSO, W. K. (1989) Strength eccentricity concept for inelastic analysis of asymmetrical structures. *Engineering Structures,* 11, 189-194.

SALEEM, K., PARRA-FUENTE, J., OJAGHI, M., WILLIAMS, M. & BLAKEBOROUGH, A. (2008) UK-NEES: grid services architecture for earthquake. *Proceedings of the WSEAS International Conference on Applied Computing Conference.* Istanbul, Turkey, World Scientific and Engineering Academy and Society (WSEAS).

SCHELLENBERG, A. (2008) Advanced implementation of hybrid simulation. *PhD thesis, Civil Engineering.* University of California, Berkeley.

SCHELLENBERG, A., KIM, H. K., TAKAHASHI, Y., FENVES, G. L. & MAHIN, S. A. (2009a) OpenFresco. University of California, Berkeley.

SCHELLENBERG, A., KIM, H. K., YOSHIKAZU, T. & MAHIN, S. A. (2009b) OpenFresco command language manual. University of California, Berkeley.

SCHELLENBERG, A., MAHIN, S. A. & FENVES, G. L. (2009c) Advanced implementation of hybrid simulation. *Pacific Earthquake Engineering Research Center.*

SCHELLENBERG, A. & YANG, T. (2006) OpenSees Navigator. University of California, Berkeley.

SHAO, X., REINHORN, A. M. & SIVASELVAN, M. V. (2011) Real-time hybrid simulation using shake tables and dynamic actuators. *Journal of Structural Engineering, ASCE,* 137, 748-760.

SHIELD, C., FRENCH, C. W. & TIMM, J. (2001) Development and implementation of the effective force testing method for seismic simulation of large–scale structures. *Philosophical Transaction of the Royal Society: Theme Issue on Dynamic Testing of Structures,* A359, 1911-1929.

SHING, P. B. & MAHIN, S. A. (1983) Experimental error propagation in pseudodynamic testing. *Report UCB/EERC-83/12.* Earthquake Engineering Research Center, University of California, Berkeley.

SHING, P. B. & MAHIN, S. A. (1984) Pseudodynamic test method for seismic performance evaluation: theory and implementation. *Report UCB/EERC-84/01.* Earthquake Engineering Research Center, University of California, Berkeley.

SHING, P. B. & MAHIN, S. A. (1985) Computational aspects of a seismic performance test method using on-line computer control. *Earthquake Engineering & Structural Dynamics,* 13, 507-526.

SHING, P. B. & MAHIN, S. A. (1987) Cumulative experimental errors in pseudodynamic tests. *Earthquake Engineering & Structural Dynamics,* 15, 409-424.

SHING, P. B. & MANIVANNAN, T. (1990) On the accuracy of implicit algorithm for pseudodynamic tests. *Earthquake Engineering & Structural Dynamics,* 19, 631-651.

SHING, P. B., NAKASHIMA, M. & BURSI, O. S. (1996) Application of pseudodynamic test method to structural research. *Earthquake Spectra,* 12, 29-56.

SHING, P. B., VANNAN, M. T. & CATER, E. (1991) Implicit time integration for pseudodynamic tests. *Earthquake Engineering & Structural Dynamics,* 20, 551-576.

SHING, P. B., WEI, Z., JUNG, R. & STAUFFER, E. (2004) NEES fast hybrid test system at the University of Colorado. *Proceedings of the 13th World Conference in Earthquake Engineering.* Vancouver, Canada.

SIMSIR, C., DALGIÇ, M., LÜBBEN, T., IRRETIER, A., WOLFF, M. & ZOCH, H. W. (2010) The Bauschinger effect in the supercooled austenite of SAE 52100 steel. *Acta Materialia,* 58, 4478-4491.

SINGH, M. P., SINGH, S. & MORESCHI, L. M. (2002) Tuned mass dampers for response control of torsional buildings. *Earthquake Engineering & Structural Dynamics,* 31, 749-769.

STATHOPOULOS, K. G. & ANAGNOSTOPOULOS, S. A. (2003) Inelastic earthquake response of single-story asymmetric buildings: an assessment of simplified shear-beam models. *Earthquake Engineering & Structural Dynamics,* 32, 1813-1831.

STATHOPOULOS, K. G. & ANAGNOSTOPOULOS, S. A. (2005) Inelastic torsion of multistorey buildings under earthquake excitations. *Earthquake Engineering & Structural Dynamics,* 34, 1449-1465.

STAUFFER, E., HAUSSMANN, G., SMITH, K. & WALLEN, R. (2007) Fast hybrid testing at CU NEES: benchmark tests. *NEES at CU Boulder.* University of Colorado, Boulder, Colorado, USA.

STOJADINOVIC, B., MOSQUEDA, G. & MAHIN, S. A. (2006) Event-driven control system for geographically distributed hybrid simulation. *Journal of Structural Engineering, ASCE,* 132, 68-77.

TAKAHASHI, Y. & FENVES, G. L. (2006) Software framework for distributed experimental–computational simulation of structural systems. *Earthquake Engineering & Structural Dynamics,* 35, 267-291.

TAKAHASHI, Y. & OHI, K. (1984) A correlation study in pseudodynamic on-line tests vs. shake table tests. *Structural Stability Research Council, Annual Technical Session and Meeting.* San Fransisco, California, USA.

TAKANASHI, K. & NAKASHIMA, M. (1987) Japanese activities on on-line testing. *Journal of Engineering Mechanics,* 113, 1014-1032.

TAKANASHI, K., UDAGAWA, K., SEKI, M., OKADA, T. & TANAKA, H. (1975) Non-linear earthquake response analysis of structures by a computer-actuator on-line system (part 1 detail of the system). *Transcript of the Architectural Institute of Japan.*

TENA-COLUNGA, A. & GÓMEZ-SOBERÓN, L. (2002) Torsional response of base-isolated structures due to asymmetries in the superstructure. *Engineering Structures,* 24, 1587-1599.

THEWALT, C. R. & MAHIN, S. A. (1987) Hybrid solution techniques for generalized pseudodynamic testing. *UCB/EERC-87/09.* Earthquake Engineering Research Center, University of California, Berekeley.

TRAHAIR, N. S., BRADFORD, M. A., NETHERCOT, D. A. & GARDNER, L. (2008) *The behaviour and design of steel structures to EC3*, Taylor & Francis.

TREMBLAY, R., ARCHAMBAULT, M. H. & FILIATRAULT, A. (2003) Seismic Response of Concentrically Braced Steel Frames Made with Rectangular Hollow Bracing Members. *Journal of Structural Engineering,* 129, 1626-1636.

TROMBETTI, T., BARRASSO, P., CREWE, A., DE STEFANO, M., GASPARINI, G., NUDO, R., RUTENBERG, A., SILVESTRI, S. & TAYLOR, C. A. (2004) Shake table testing of symmetric and asymmetric three-storey steel frame structures. *13th World Conference on Earthquake Engineering.* Vancouver, Canada.

TSO, W. K. & BOZORGNIA, Y. (1986) Effective eccentricity for inelastic seismic response of buildings. *Earthquake Engineering & Structural Dynamics,* 14, 413-427.

TSO, W. K. & MYSLIMAJ, B. (2003) A yield displacement distribution-based approach for strength assignment to lateral force-resisting elements having strength dependent stiffness. *Earthquake Engineering & Structural Dynamics,* 32, 2319-2351.

TSO, W. K., ZHU, T. J. & HEIDEBRECHT, A. C. (1992) Engineering implication of ground motion A/V ratio. *Soil Dynamics and Earthquake Engineering,* 11, 133-144.

UBC (1997) Uniform building code. International Conference of Building Officials, Whittier, California, USA.

URIZ, P., FILIPPOU, F. C. & MAHIN, S., A. (2008) Model for cyclic inelastic buckling of steel braces. *Journal of Structural Engineering, ASCE,* 134, 619-628.

VANNAN, M. T. (1991) The pseudodynamic test method with substructuring application. *PhD thesis, College of Engineering and Applied Sciences.* Boulder, Colorado, University of Calorado.

WALLACE, M. I., WAGG, D. J. & NEILD, S. A. (2005) An adaptive polynomial based forward prediction algorithm for multi-actuator real-time dynamic substructuring. *Proceedings of the Royal Society A: Mathematical, Physical and Engineering Science,* 461, 3807–3826.

WANG, J.-F. & LIN, C.-C. (2005) Seismic performance of multiple tuned mass dampers for soil-irregular building interaction systems. *International Journal of Solids and Structures,* 42, 5536-5554.

WHITMORE, R. E. (1952) Experimental investigation of stresses in gusset plates. Knoxville, Tennesse, University of Tennesse.

WIJESUNDARA, K. K. (2009) Design of concentrically braced steel frames with rhs shape braces. Università degli Studi di Pavia & Istituto Universitario di Studi Superiori.

WILLIAMS, M. S. & BLAKEBOROUGH, A. (2001) Laboratory testing of structures under dynamic loads: an introductory review. *Philosophical Transactions of the Royal Society of London,* Series A, 1651-1670.

WU, B., BAO, H., OU, J. & TIAN, S. (2005) Stability and accuracy analysis of the central difference method for real-time substructure testing. *Earthquake Engineering & Structural Dynamics,* 34, 705-718.

WU, B., WANG, Q., BENSON SHING, P. & OU, J. (2007) Equivalent force control method for generalized real-time substructure testing with implicit integration. *Earthquake Engineering & Structural Dynamics,* 36, 1127-1149.

WU, B., XU, G., WANG, Q. & WILLIAMS, M. S. (2006) Operator-splitting method for real-time substructure testing. *Earthquake Engineering & Structural Dynamics,* 35, 293-314.

YOSHIDA, O., DYKE, S. J., GIACOSA, L. M. & TRUMAN, K. Z. (2003) Experimental verification of torsional response control of asymmetric buildings using MR dampers. *Earthquake Engineering & Structural Dynamics,* 32, 2085-2105.

ZAYAS, V. A., POPOV, E. P. & MAHIN, S. A. (1980) Cyclic inelasticbuckling of tubular steel braces. *UCB/EERC-80/16.* Earthquake Engineering Research Center, Berkeley, California, USA.

ZHANG, Y., SAUSE, R., RICLES, J. M. & NAITO, C. J. (2005) Modified predictor–corrector numerical scheme for real-time pseudo dynamic tests using state-space formulation. *Earthquake Engineering & Structural Dynamics,* 34, 271-288.

ZHAO, J., FRENCH, C., SHIELD, C. & POSBERGH, T. (2003) Considerations for the development of real-time dynamic testing using servo-hydraulic actuation. *Earthquake Engineering & Structural Dynamics,* 32, 1773-1794.

ZHAO, J., FRENCH, C. W., SHIELD, C. & POSBERGH, T. (2006) Comparison of tests of a nonlinear structure using a shake table and the EFT method. *Journal of Structural Engineering, ASCE,* 132, 1473-1481.

ZIENKIEWICZ, O. C. & TAYLOR, R. L. (2005) *The finite element method for solid and structural mechanics*, Butterworth Heinemann.

Appendix A1 - Two Dimensional Portal Frame OpenFresco Hybrid Simulation

```
# FileName: 2DPortalFrame_Local.tcl
# Author: Daniel McCrum
# Email: mccrumdp@tcd.ie
# Last Altered: January, 2011.

# Description:
# This file contains the tcl input to perform a local
# hybrid simulation of a one bay frame comprising of
# 150 x 90 Channel Section column substructure.
# The specimens are simulated using the xPC Target

#       ---> _____________________________
#            |                            |          ^
#            |                            |          |
#            |                            |          | 1500mm
#            |                            |          |
#            |                            |          v
#          XXX                          XXX
#
#            <------------------------------------->
#                          2500mm

# Units: N m sec
wipe all;
file mkdir Data;                    # Create directory for data

# ------------------------------
# Start of model generation
# ------------------------------
# create ModelBuilder (with two-dimensions and 3 DOF/node)
model BasicBuilder -ndm 2 -ndf 3

# ------------------------------
# Load OpenFresco package
# ------------------------------
# (make sure all dlls are in the same folder as openSees.exe)
loadPackage OpenFresco

# ------------------------------
# Define geometry for model
# ------------------------------
set withGravity 1;
set Pc 47320;
set P [expr 0.5*$Pc];
set mass3 [expr $P/9810];
set mass4 [expr $P/9810];
# node $tag $xCrd $yCrd $mass
node 1    0.0   0.0
node 2    2500   0.0
node 3    0.0   1500  -mass $mass3 $mass3 0.0
node 4    2500   1500  -mass $mass4 $mass4 0.0

# set the boundary conditions
# fix $tag $DX $DY $RZ
fix 1  1  1  1
fix 2  1  1  1

# ------------------------------
# Define materials
# ------------------------------
# uniaxialMaterial Steel02 $matTag $Fy $E $b $R0 $cR1 $cR2 $a1 $a2 $a3 $a4
#uniaxialMaterial Steel02 1 235 210000 0.03 18.5 0.925 0.15 0.0 1.0 0.0 1.0
uniaxialMaterial Steel02 1 235 1886.453 0.03 18.5 0.925 0.15 0.0 1.0 0.0 1.0

# ------------------------------
# Define experimental control
# ------------------------------
```

```
# expControl SimUniaxialMaterials $tag $matTags
#expControl SimUniaxialMaterials 1 1
expControl xPCtarget     1    1 "148.150.204.191"  22222  DMC_RTTest_soft  "C:/STS/Model"
expControl SimUniaxialMaterials 2 1

# ------------------------------
# Define experimental setup
# ------------------------------
# expSetup OneActuator $tag <-control $ctrlTag> $dir -sizeTrialOut $t $o <-trialDispFact $f> ...
expSetup OneActuator 1 -control 1 2 -sizeTrialOut 3 3
expSetup OneActuator 2 -control 2 2 -sizeTrialOut 3 3

# ------------------------------
# Define experimental site
# ------------------------------
# expSite LocalSite $tag $setupTag
expSite LocalSite 1 1
expSite LocalSite 2 2

# ------------------------------
# Define geometric transformation
# ------------------------------
geomTransf PDelta 1
geomTransf Linear 2
#geomTransf Corotational 3

# ------------------------------
# Define experimental elements
# ------------------------------
# left and right columns
# expElement beamColumn $eleTag $iNode $jNode $transTag -site $siteTag -initStif $Kij <-iMod> <-rho $rho>
expElement beamColumn 1 3 1 1 -site 1 -initStif 405440 0 0 0 1885.893 -2828.840 0 -2828.840 4243.260
expElement beamColumn 2 4 2 1 -site 2 -initStif 405440 0 0 0 1885.893 -2828.840 0 -2828.840 4243.260

# ------------------------------
# Define numerical elements
# ------------------------------
# 203UC60 Beam
# element elasticBeamColumn $eleTag $iNode $jNode $A $E $Iz $transfTag
element elasticBeamColumn 3 3 4 7640 210e3 6125e4 2

if {$withGravity} {
   # Define gravity loads
   # --------------------
   # Create a Plain load pattern with a Linear TimeSeries
   pattern Plain 1 "Linear" {
      # Create nodal loads at nodes 2
      #    nd    FX          FY  MZ
      load  3   0.0  [expr -$P] 0.0
      load  4   0.0  [expr -$P] 0.0
   }
   # ------------------------------
   # End of model generation
   # ------------------------------


   # ------------------------------
   # Start of analysis generation
   # ------------------------------
   # Create the system of equation
   system BandGeneral
   # Create the DOF numberer
   numberer Plain
   # Create the constraint handler
   constraints Plain
   # Create the convergence test
   test EnergyIncr 1.0e-6 10

   # Create the integration scheme
   integrator LoadControl 0.1
   # Create the solution algorithm
   algorithm Newton
   # Create the analysis object
   analysis Static
   # ------------------------------
   # End of analysis generation
   # ------------------------------
```

```
    # ------------------------------
    # Start of recorder generation
    # ------------------------------
    # create a Recorder object for the nodal displacements at node 2
    recorder Node -file Data/Gravity_Dsp.out -time -node 3 4 -dof 1 2 3 disp
    recorder Element -file Data/Gravity_Frc.out -time -ele 1 2 3 force

    # ---------------------------------
    # End of recorder generation
    # ---------------------------------

    # ------------------------------
    # Perform the gravity analysis
    # ------------------------------
    # perform the gravity load analysis, requires 10 steps to reach the load level
    if {[analyze 10] == 0} {
        puts "\nGravity load analysis completed"
    } else {
        puts "\nGravity load analysis failed"
        exit -1
    }

    # ------------------------------
    # Start of model generation
    # ------------------------------
    # Set the gravity loads to be constant & reset the time in the domain
    loadConst -time 0.0
    remove recorders
}

# ------------------------------
# Define dynamic loads
# ------------------------------
# set time series to be passed to uniform excitation
set dt 0.01
set scale 0.5
set accelSeries "Path -filePath Taiwan.txt -dt $dt -factor [expr 9810*$scale]"

# create UniformExcitation load pattern
# pattern UniformExcitation $tag $dir
pattern UniformExcitation  2 1 -accel $accelSeries

# calculate the rayleigh damping factors for nodes & elements
set alphaM    1.2797;   # D = alphaM*M
set betaK     0.0;      # D = betaK*Kcurrent
set betaKinit  0.0;     # D = beatKinit*Kinit
set betaKcomm  0.0;     # D = betaKcomm*KlastCommit

# set the rayleigh damping
rayleigh $alphaM $betaK $betaKinit $betaKcomm;

# ------------------------------
# End of model generation
# ------------------------------

# ------------------------------
# Start of analysis generation
# ------------------------------
# create the system of equations
system BandGeneral

# create the DOF numberer
numberer Plain

# create the constraint handler
constraints Plain

# create the convergence test
test FixedNumIter 5
#test NormDispIncr 1E-8 25

# create the integration scheme
integrator NewmarkHSFixedNumIter 0.5 0.25
#integrator NewmarkHSIncrReduct 0.5 0.25 0.8
#integrator HHTHSFixedNumIter 0.5
#integrator HHTHSIncrReduct 0.5 0.8
#integrator CollocationHSFixedNumIter 1.5
```

```
#integrator CollocationHSIncrReduct 1.5 0.8
#integrator AlphaOS 0.9

# create the solution algorithm
algorithm Newton
#algorithm Linear

# create the analysis object
analysis Transient
# ------------------------------
# End of analysis generation
# ------------------------------

# ------------------------------
# Start of recorder generation
# ------------------------------
# create the recorder objects
recorder Node -file Data/Node_Dsp.out -time -node    3 4 -dof 1 2 3 disp
recorder Node -file Data/Node_Vel.out -time -node    3 4 -dof 1 2 3 vel
recorder Node -file Data/Node_Acc.out -time -node    3 4 -dof 1 2 3 accel
recorder Node -file Data/Node_Rxn.out -time -node 1 2 3 4 -dof 1 2 3 reactionIncludingInertia

recorder Element -file Data/Elmt_glbFrc.out  -time -ele 1 2 3 forces
expRecorder Control -file Data/Control_ctrlDsp.out -time -control 1 2 ctrlDisp
expRecorder Control -file Data/Control_daqDsp.out  -time -control 1 2 daqDisp
expRecorder Control -file Data/Control_daqFrc.out  -time -control 1 2 daqForce

expRecorder Control -file Data/Control_ctrlDsp.out -time -control 1 ctrlDisp
expRecorder Control -file Data/Control_ctrlVel.out -time -control 1 ctrlVel
expRecorder Control -file Data/Control_daqDsp.out  -time -control 1 daqDisp
expRecorder Control -file Data/Control_daqFrc.out  -time -control 1 daqForce

expRecorder Setup -file Data/Setup_trialDsp.out -time -setup 1 trialDisp
expRecorder Setup -file Data/Setup_trialVel.out -time -setup 1 trialVel
expRecorder Setup -file Data/Setup_trialAcc.out -time -setup 1 trialAccel
expRecorder Setup -file Data/Setup_outDsp.out -time -setup 1 outDisp
expRecorder Setup -file Data/Setup_outFrc.out -time -setup 1 outForce
expRecorder Setup -file Data/Setup_ctrlDsp.out -time -setup 1 ctrlDisp
expRecorder Setup -file Data/Setup_ctrlVel.out -time -setup 1 ctrlVel
expRecorder Setup -file Data/Setup_ctrlAcc.out -time -setup 1 ctrlAccel
expRecorder Setup -file Data/Setup_daqDsp.out -time -setup 1 daqDisp
expRecorder Setup -file Data/Setup_daqFrc.out -time -setup 1 daqForce

# ---------------------------------
# End of recorder generation
# ---------------------------------

# ------------------------------
# Finally perform the analysis
# ------------------------------
# perform an eigenvalue analysis
set pi 3.14159265358979
set lambda [eigen -fullGenLapack 4]
puts "\nEigenvalues at start of transient:"
puts "lambda        omega         period"
foreach lambda $lambda {
   if {$lambda > 0.0} {
      set omega [expr pow($lambda,0.5)]
      set period [expr 2*$pi/pow($lambda,0.5)]
      puts "$lambda  $omega  $period"
   }
}

# open output file for writing
set outFileID [open elapsedTime.txt w]
# perform the transient analysis
set tTot [time {
   for {set i 1} {$i < 2500} {incr i} {
      set t [time {analyze  1  [expr $dt/1.0]}]
      puts $outFileID $t
                  #puts "step $i"
   }
}]
puts "\nElapsed Time = $tTot \n"
# close the output file
close $outFileID
wipe
```

Appendix A2 - Two Dimensional Portal Frame OpenSees Numerical Model

```
# FileName: 2DPortalFrame.tcl
# Author: Daniel McCrum
# Email: mccrumdp@tcd.ie
# Last Altered: January 2010.

# Description:
# This file contains the tcl input to perform an OpenSees
# numerical model simulation of a 2D portal frame comprising of
# 150 x 90 channel section columns.


#       --->_____________________________
#           |                            |          ^
#           |                            |          |
#           |                            |          | 1.5m
#           |                            |          |
#           |                            |          v
#         XXX                          XXX
#
#           <------------------------------------->
#                          2.5m

# Units: N m kg
wipe all;
file mkdir Data;                    # Create directory for data
source ChanSection.tcl;

# ------------------------------
# Start of model generation
# ------------------------------
# create ModelBuilder (with two-dimensions and 2 DOF/node)
model BasicBuilder -ndm 2 -ndf 3

# ------------------------------
# Define geometry for model
# ------------------------------
set g 9.81;
set mass3 [expr (47320/$g)*0.5];
set mass4 [expr (47320/$g)*0.5];

set LCol 1.500;
set LBeam 2.500;

# node $tag $xCrd $yCrd $mass
node 1    0.0     0.00
node 2    $LBeam   0.00
node 3    0.0     $LCol
node 4    $LBeam   $LCol

mass 3 $mass3 0. 0.
mass 4 $mass4 0. 0.

# set the boundary conditions
# fix $tag $DX $DY
fix 1   1  1  1
fix 2   1  1  1

# ------------------------------
# Define materials
# ------------------------------
# uniaxialMaterial Steel02 $matTag $Fy $E $b $R0 $cR1 $cR2 $a1 $a2 $a3 $a4
set matID 1;
uniaxialMaterial Steel02 $matID 235e6 1886.453e6 0.03 18.5 0.925 0.15 0.0 1.0 0.0 1.0

# ------------------------------
# Define sections
# ------------------------------
# Column Parameters:
```

```
# 150 x 90 Channel Section
set colSecID 2;
set d 0.15;                    # Overall section depth 150
set b 0.088;                   # Overall section width 90
set t 0.008;                   # Web thickness 8
set T1 0.0014;                 # Flange thickness 14
set T2 0.006;                  # Flange thickness 6
set bb 0.01;
set subFLen 10;                # sub-division across flange length
set subFThk 5;                 # sub-division across flange thickness
set subWLen 10;                # sub-division across web length
set subWThk 5;                 # sub-division across web thickness
ChanSection $colSecID $matID $d $b $t $T1 $T2 $subWLen $subWThk $subFLen $subFThk
puts "ChanSection defined";

# ------------------------------
# Define elements
# ------------------------------
# left and right columns
# Coordinate transformation
set ColTransfTag 10;
set ColTransfType PDelta;
geomTransf $ColTransfType $ColTransfTag;              # columns have PDelta effects
set numintgrPtsCol 7;

element nonlinearBeamColumn 1 1 3 $numintgrPtsCol $colSecID $ColTransfTag
element nonlinearBeamColumn 2 2 4 $numintgrPtsCol $colSecID $ColTransfTag

# Beam
set BeamTransfTag 11;
set BeamTransfType Linear;
geomTransf $BeamTransfType $BeamTransfTag;
element elasticBeamColumn 3 3 4 7640e-6 210e9 61.25e-6 $BeamTransfTag

# calculate the rayleigh damping factors for nodes & elements
set alphaM    1.2797;             # D = alphaM*M
set betaK     0.0;                # D = betaK*Kcurrent
set betaKinit  0.0;               # D = beatKinit*Kinit
set betaKcomm  0.0;               # D = betaKcomm*KlastCommit

# set the rayleigh damping
rayleigh $alphaM $betaK $betaKinit $betaKcomm;

# ------------------------------
# End of model generation
# ------------------------------
# ------------------------------
# Start of analysis generation
# ------------------------------
system BandGeneral ;
numberer Plain ;
constraints Plain ;
test EnergyIncr 1.0e-5 10 ;

# create the integrator
#integrator NewmarkExplicit 0.5 ;
set gamma 0.8;
integrator HHT $gamma ;

# create the solution algorithm
algorithm Linear ;

# create the analysis object
analysis Transient ;
# ------------------------------
# End of analysis generation
# ------------------------------

# ------------------------------
# Start of recorder generation
# ------------------------------
# create the recorder objects
recorder Node -file Data/Node_Dsp.out -time -node 3 4 -dof 1 disp
recorder Node -file Data/Node_Vel.out -time -node 3 4 -dof 1 vel
recorder Node -file Data/Node_Acc.out -time -node 3 4 -dof 1 accel
recorder Node -file Data/Node_Rxn.out -time -node 1 2 -dof 1 2 reaction

recorder Element -file Data/Elmt_Frc.out     -time -ele 1 2 3 forces
```

```
recorder Element -file Data/Elmt_ctrlDsp.out -time -ele 1 2  ctrlDisp
recorder Element -file Data/Elmt_daqDsp.out  -time -ele 1 2  daqDisp


# ------------------------------------
# Define Display
# ------------------------------------

source DisplayPlane.tcl;
source DisplayModel3D.tcl;

set xPixels 500;        # height of graphical window in pixels
set yPixels 500;        # height of graphical window in pixels
set xLoc 5;             # horizontal location of graphical window (0=upper left-most corner)
set yLoc 5;             # vertical location of graphical window (0=upper left-most corner)
set dAmp 10;            # Relative amplification factor for deformations
set ShapeType1 DeformedShape;
set windowTitle "2D Frame Deformed Shape";
set viewPlane ZY;
set nEigen 0;
recorder display $windowTitle $xLoc $yLoc $xPixels $yPixels  -wipe ; # display recorder

DisplayPlane $ShapeType1 $dAmp $viewPlane $nEigen 0;
recorder plot Data/Node_Acc.out Accel-Z 5 510 500 500 -columns 1 2; # Plot Load vs Disp
recorder plot Data/Node_Dsp.out FloorDrift-Z 515 510 500 500 -columns 1 2; # Plot Load vs Disp

set xLoc1 510;
set yLoc1 5;
set ShapeType DeformedShape;
DisplayModel3D $ShapeType $dAmp $xLoc1 $yLoc1 $xPixels $yPixels $nEigen
# ---------------------------------
# End of recorder generation
# ---------------------------------

# DYNAMIC LOADS
set iGMfile "Taiwan.txt Taiwan.txt" ;        # ground-motion filenames
set iGMdirection "1 2";                      # ground-motion directions
set iGMfact "9.81 0.0";                      # ground-motion scaling factor

# set up ground-motion-analysis parameters
set DtAnalysis 0.01;              # select suitable time-step Dt for analysis
set TmaxAnalysis 25;              # maximum duration of ground-motion analysis

# ------------------------------------
# Perform Dynamic  Analysis
# ------------------------------------
# The following commands are unique to the Uniform Earthquake excitation
set IDloadTag 400;    # for uniformSupport excitation
# Uniform EXCITATION: acceleration input
foreach GMdirection $iGMdirection GMfile $iGMfile GMfact $iGMfact {
        incr IDloadTag;
#       set inFile $iGMfile;
#       set outFile $GMfile.g3;                 # set variable holding new filename (PEER files have .at2/dt2 extension)
#       ReadSMDFile $inFile $outFile dt;        # call procedure to convert the ground-motion file
#       set GMfatt [expr $g*$GMfact];           # data in input file is in g Unifts -- ACCELERATION TH
        set AccelSeries "Series -dt $DtAnalysis -filePath $iGMfile -factor  $iGMfact";          # time series information
        pattern UniformExcitation  $IDloadTag  $GMdirection -accel  $AccelSeries  ; # create Unifform excitation
}

set Nsteps [expr int($TmaxAnalysis/$DtAnalysis)];
set ok [analyze $Nsteps $DtAnalysis];        # actually perform analysis; returns ok=0 if analysis was successful

if {$ok != 0} {     ;    # if analysis was not successful.
        # change some analysis parameters to achieve convergence
        # performance is slower inside this loop
        # Time-controlled analysis
        set ok 0;
        set controlTime [getTime];
        while {$controlTime < $TmaxAnalysis && $ok == 0} {
                set ok [analyze 1 $DtAnalysis]
                set controlTime [getTime]
                set ok [analyze 1 $DtAnalysis]
                if {$ok != 0} {
                        puts "Trying Newton with Initial Tangent .."
                        test NormDispIncr   $Tol 1000  0
                        algorithm Newton -initial
                        set ok [analyze 1 $DtAnalysis]
                        test $TestType $Tol $maxNumIter  0
```

```
                        algorithm $algorithmType
                }
                if {$ok != 0} {
                        puts "Trying Broyden .."
                        algorithm Broyden 8
                        set ok [analyze 1 $DtAnalysis]
                        algorithm $algorithmType
                }
                if {$ok != 0} {
                        puts "Trying NewtonWithLineSearch .."
                        algorithm NewtonLineSearch .8
                        set ok [analyze 1 $DtAnalysis]
                        algorithm $algorithmType
                }
        }
};      # end if ok !0


puts "Ground Motion Done. End Time: [getTime]"
set fmt1 "%s Analysis Result: CtrlNode %.2i, dof %.1i, Disp=%.4f %s";

# ------------------------------
# If Convergence Fails
# ------------------------------

set LunitTXT "m";
set IDctrlNode 3;
set IDctrlDOF 1;

if {$ok != 0 } {
        puts [format $fmt1 "PROBLEM WITH DYNAMIC ANALYSIS" $IDctrlNode $IDctrlDOF [nodeDisp $IDctrlNode
$IDctrlDOF] $LunitTXT]
} else {
        puts [format $fmt1 "DYNAMIC ANALYSIS COMPLETE:"  $IDctrlNode $IDctrlDOF [nodeDisp $IDctrlNode $IDctrlDOF]
$LunitTXT]
}
wipe
# --------------------------------
# End of analysis
# --------------------------------
```

Appendix B – Test Frame Fabrication Drawings

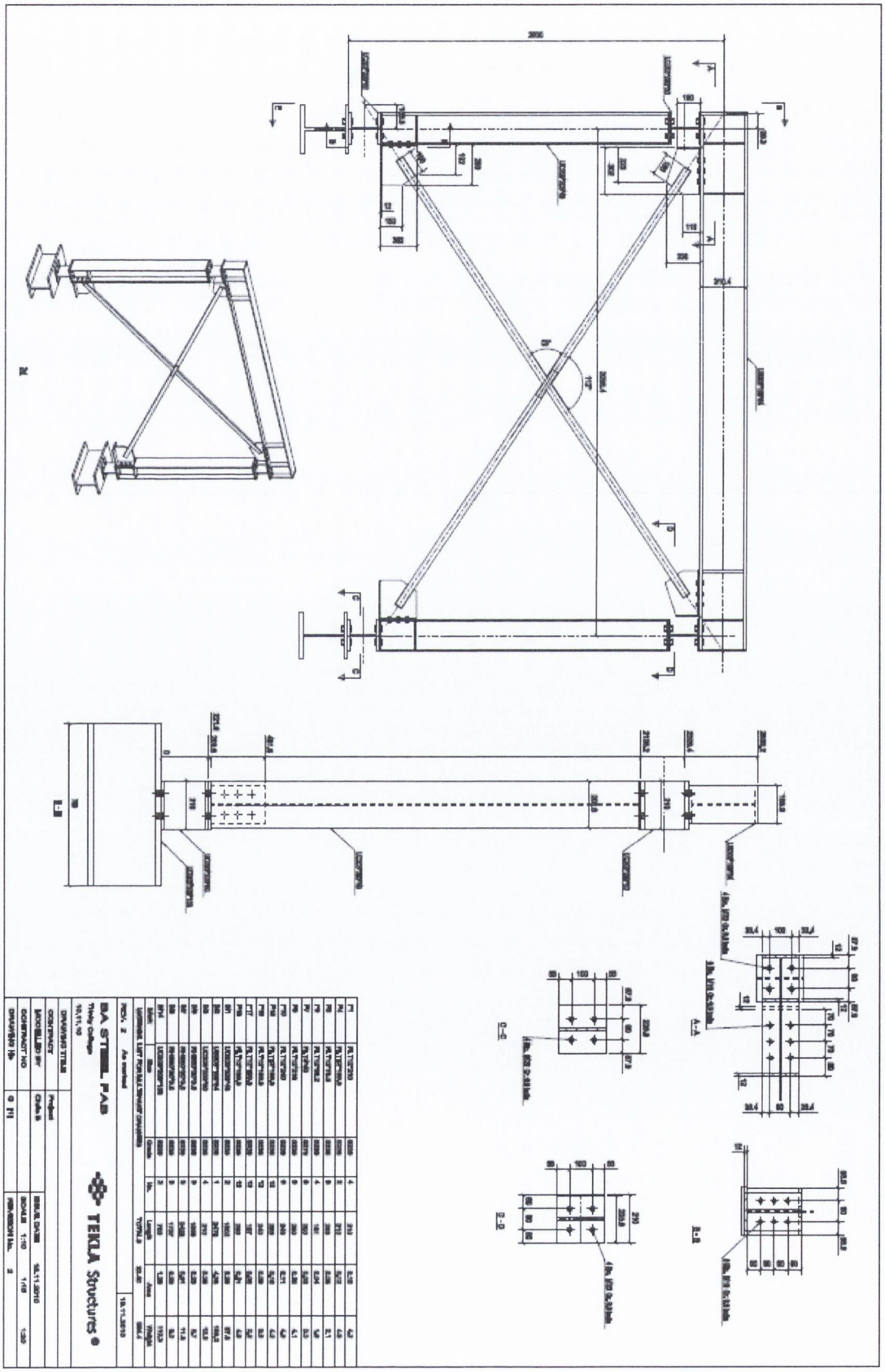

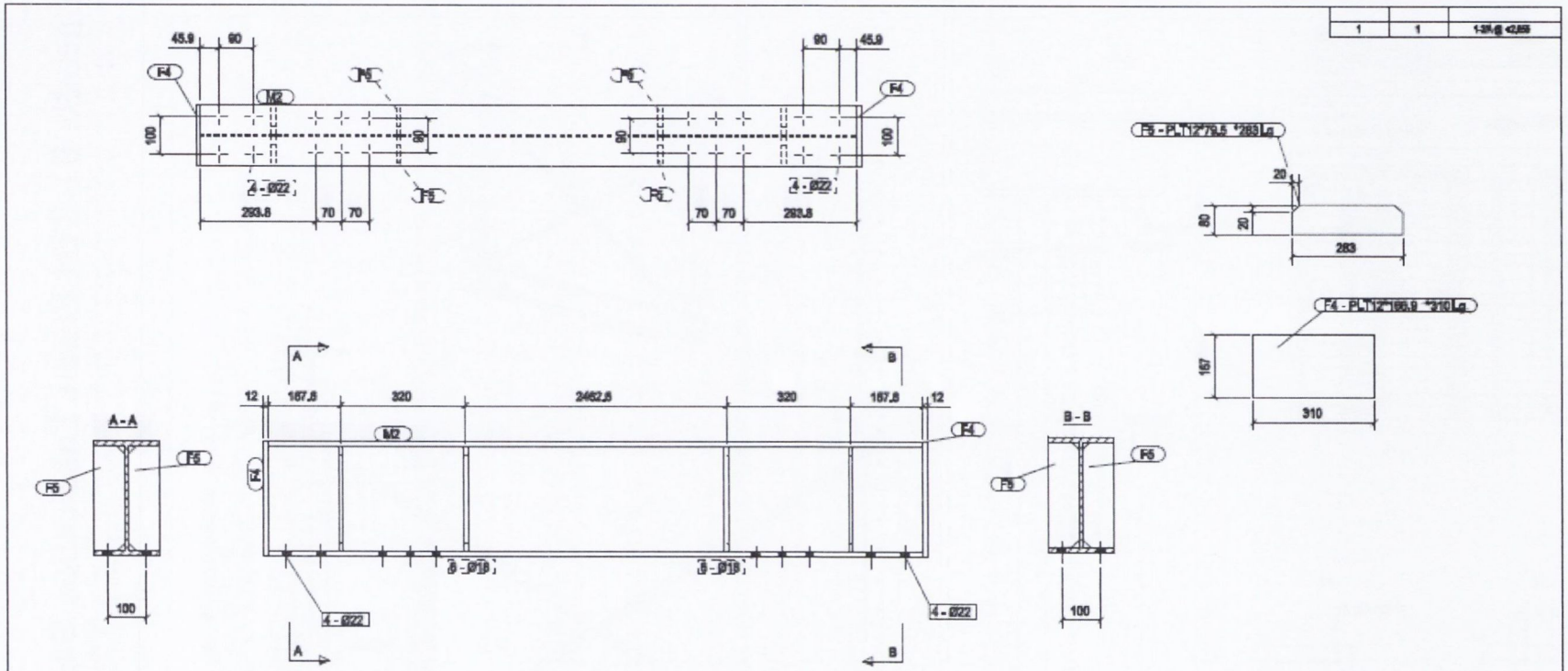

ONE BEAM REQ'D AS DRAWN MK'D B5

PRELIM	MARK	QTY	PROFILE	GRADE	LTH (mm)	AREA (m²)	WEIGHT (kg)	REV	DATE	DESCRIPTION
	F4	2	PLT12*166.9	S235	310	0.230	9.8			
	F5	8	PLT12*79.5	S235	283	0.421	16.7			
	M2	1	UB305*165*54	S235	3478	4.363	186.2			

TEKLA Structures ®

DRAWING TITLE: BEAM
CONTRACT NAME: Project
ISSUE DATE:
DRAWN BY:
CHECKED BY:

CONTRACT NO: 0
MARK: B5
Rev:

PAINT SPEC:
U.N.O: WELD: 6.0mm HOLES: Ø22 mm

TOTAL: AREA EACH: 5.03 m² AREA ALL: 5.03 m² WEIGHT EACH: 0.21 T WEIGHT ALL: 0.21 T

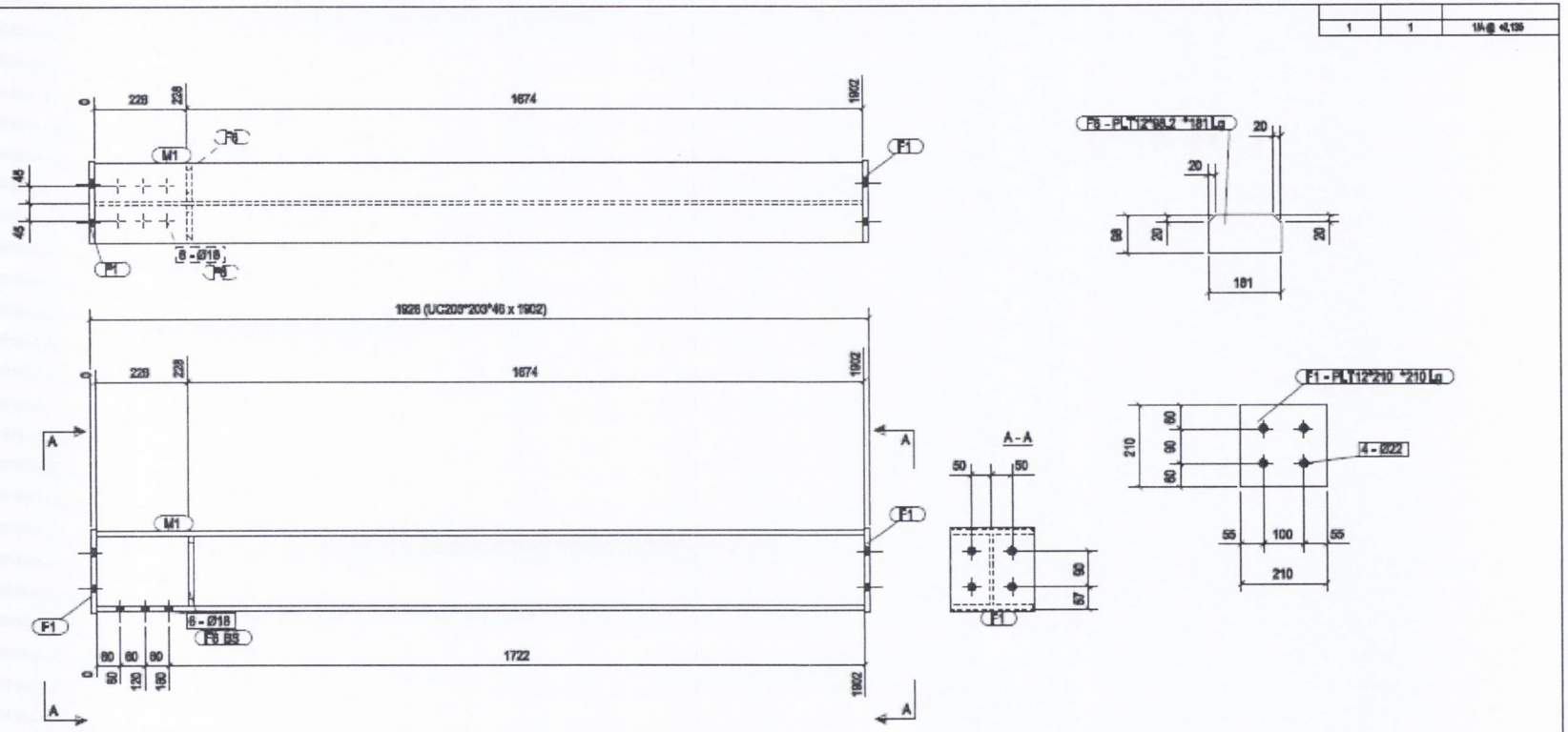

2 COLUMN's REQ'D AS DRAWN MK'D C2

PRELIM	MARK	QTY	PROFILE	GRADE	LTH (mm)	AREA (m²)	WEIGHT (kg)	REV	DATE	DESCRIPTION
	F1	2	PLT12*210	S235	210	0.197	8.3			
	F6	2	PLT12*98.2	S235	181	0.082	3.3			
	M1	1	UC203*203*46	S235	1902	2.283	87.8			

PAINT SPEC:

TEKLA AREA EACH: 2.54 m² AREA ALL: 2.54 m² WEIGHT EACH: 0.10 T WEIGHT ALL: 0.10 T U.N.O: WELD: 8.0mm HOLES: Ø22 mm

TEKLA Structures ®

DRAWING TITLE: COLUMN
CONTRACT NAME: Project
ISSUE DATE:
DRAWN BY:
CHECKED BY:

CONTRACT NO:	MARK:	Rev:
0	C2	

1	6	SA @ 1,482
		SB @ 1,482
		SC @ 1,482
		SA @ 1,482
		SB @ 1,482
		SC @ 1,482

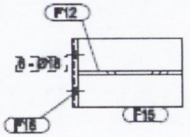

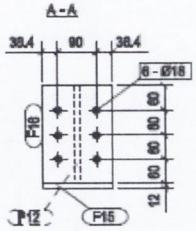

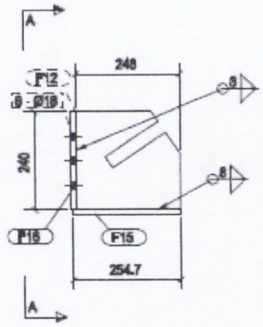

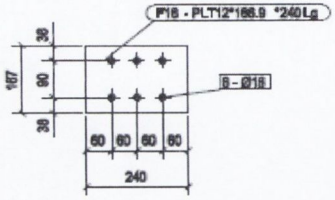

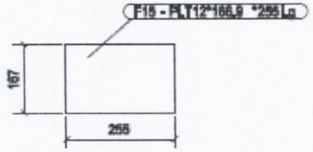

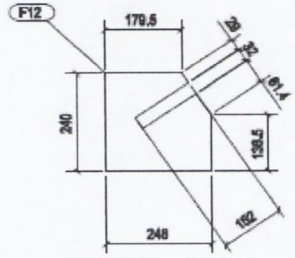

6 STUBS REQ'D AS DRAWN MK'D BS2

PRELIM	MARK	QTY	PROFILE	GRADE	LTH (mm)	AREA (m²)	WEIGHT (kg)	REV	DATE	DESCRIPTION
	F12	1	PLT12*240	S235	248	0.117	4.8			
	F15	1	PLT12*166.9	S235	255	0.095	4.0			
	F16	1	PLT12*166.9	S235	240	0.090	3.8			

TEKLA AREA EACH: 0.30 m² AREA ALL: 1.81 m² WEIGHT EACH: 0.01 T WEIGHT ALL: 0.08 T

PAINT SPEC:

U.N.O: WELD: 6.0mm HOLES: Ø22 mm

TEKLA Structures ®

DRAWING TITLE: STUB

CONTRACT NAME: Project

ISSUE DATE:

DRAWN BY:

CHECKED BY:

CONTRACT NO:	MARK:	Rev:
0	BS2	

1	0	BA @ ±2,345
		BB @ ±2,345
		BC @ ±2,345
		BA @ ±2,345
		BB @ ±2,345
		BC @ ±2,345

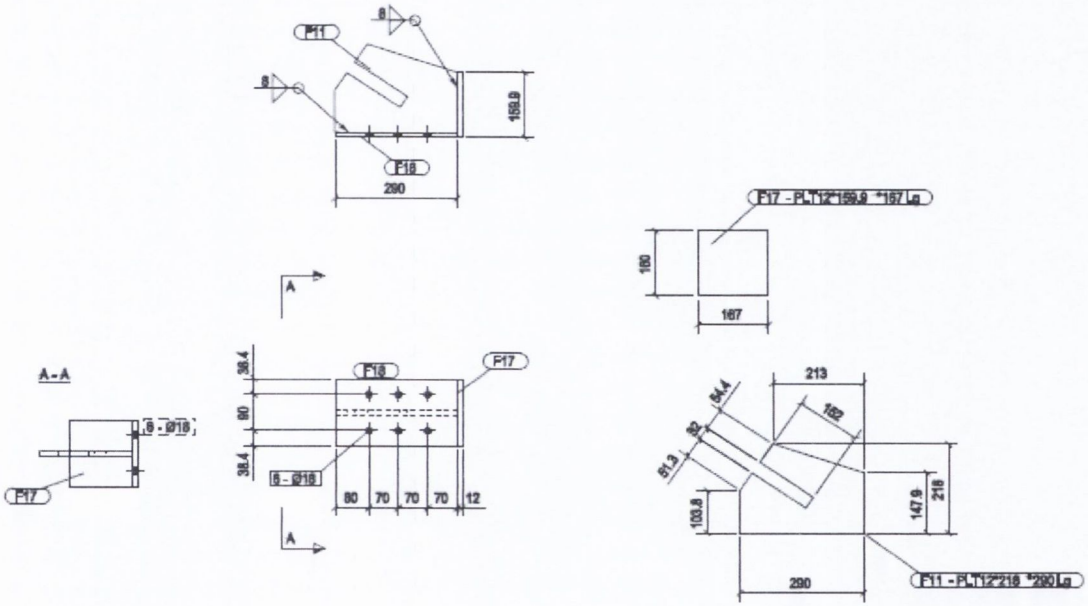

6 STUBS REQ'D AS DRAWN MK'D TS2

PRELIM	MARK	QTY	PROFILE	GRADE	LTH (mm)	AREA (m²)	WEIGHT (kg)	REV	DATE	DESCRIPTION
	F11	1	PLT12*216	S235	290	0.107	4.4			
	F17	1	PLT12*159.9	S235	167	0.081	2.5			
	F18	1	PLT12*166.9	S235	290	0.108	4.8			

TEKLA Structures ®

DRAWING TABLE:	STUB
CONTRACT NAME:	Project
ISSUE DATE:	
DRAWN BY:	
CHECKED BY:	

CONTRACT NO:	MARK:	Rev:
0	TS2	

PAINT SPEC:

TOTAL AREA EACH: 0.28 m² AREA ALL: 1.66 m² WEIGHT EACH: 0.01 T WEIGHT ALL: 0.07 T U.N.O. WELD: 8.0mm HOLES: Ø22 mm

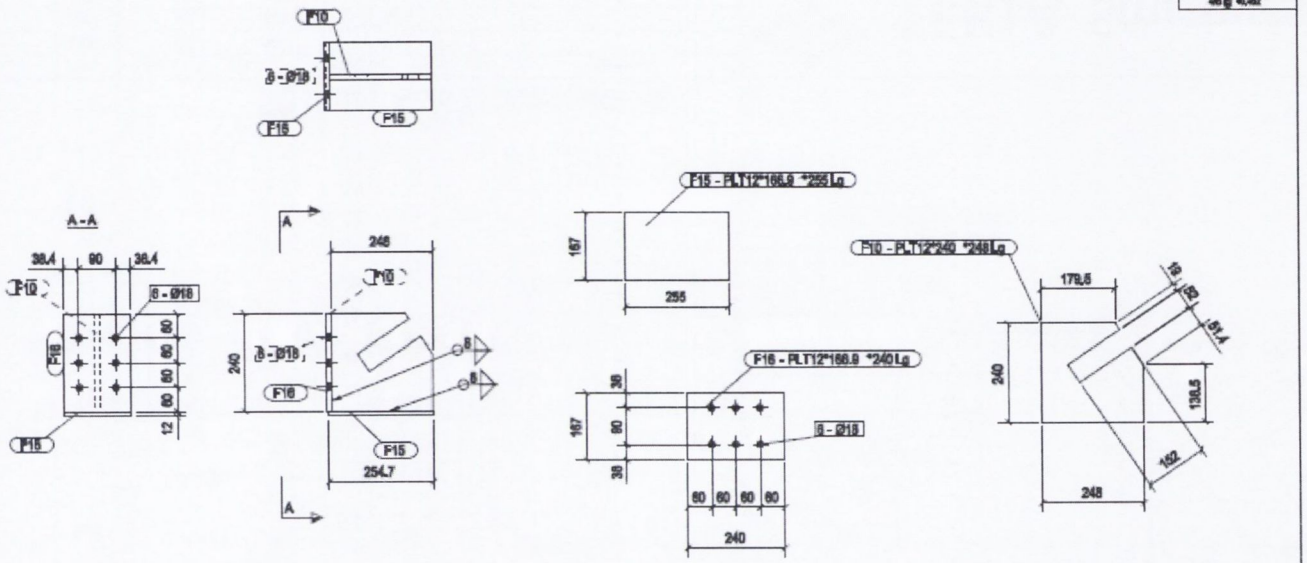

6 STUBS REQ'D AS DRAWN MK'D BS1

PRELIM	MARK	QTY	PROFILE	GRADE	LTH (mm)	AREA (m^2)	WEIGHT (kg)	REV	DATE	DESCRIPTION
	F10	1	PLT12*240	S235	248	0.111	4.5			
	F15	1	PLT12*166.9	S235	255	0.095	4.0			
	F16	1	PLT12*166.9	S235	240	0.090	3.8			

TEKLA Structures ®

DRAWING TITLE: STUB
CONTRACT NAME: Project
ISSUE DATE:
DRAWN BY:
CHECKED BY:

CONTRACT NO: 0
MARK: BS1
Rev:

PAINT SPEC:
U.N.O: WELD: 6.0mm HOLES: Ø22 mm

TEKLA AREA EACH: 0.30 m^2 AREA ALL: 1.78 m^2 WEIGHT EACH: 0.01 T WEIGHT ALL: 0.07 T

1	6	1A @ 42.5/6
		2A @ 42.5/6
		3A @ 42.5/6
		3B @ 42.5/6
		4A @ 42.5/6
		4B @ 42.5/6

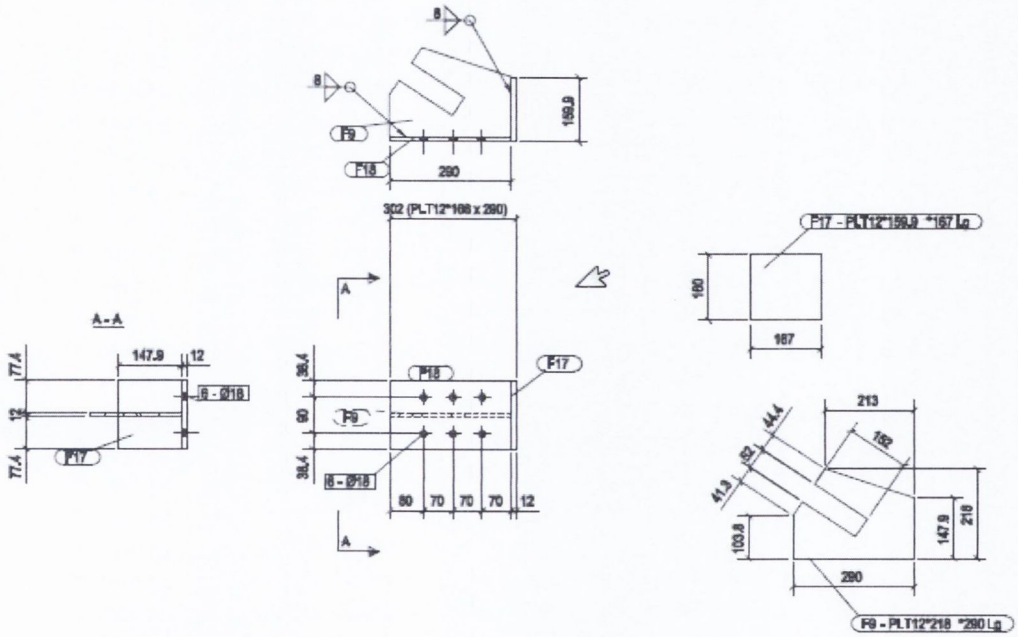

6 STUBS REQ'D AS DRAWN MK'D TS1

PRELIM	MARK	QTY	PROFILE	GRADE	LTH (mm)	AREA (m²)	WEIGHT (kg)	REV	DATE	DESCRIPTION
	F9	1	PLT12*218	S235	290	0.101	4.1			
	F17	1	PLT12*159.9	S235	167	0.081	2.5			
	F18	1	PLT12*168.9	S235	290	0.108	4.8			

TEKLA Structures ®

DRAWING TITLE: STUB
CONTRACT NAME: Project
ISSUE DATE:
DRAWN BY:
CHECKED BY:

CONTRACT NO:	MARK:	Rev:
0	TS1	

PAINT SPEC:

TEKLA AREA EACH: 0.27 m² AREA ALL: 1.62 m² WEIGHT EACH: 0.01 T WEIGHT ALL: 0.07 T

WELD: 8.0mm HOLES: Ø22 mm

4	B2

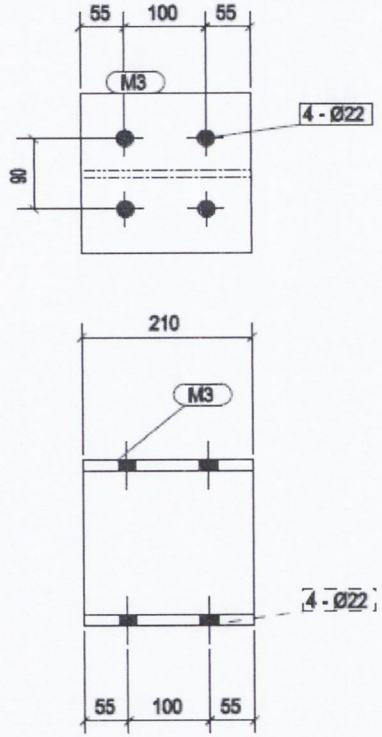

4 BEAMS REQ'D AS DRAWN MK'D M3

TEKLA Structures ®				QTY: 4	PROFILE: UC203*203*60	SURFACE AREA: 0.3 m²/ea.	1.0 m²/tot.	
				GRADE: S235	LENGTH: 210	WEIGHT: 12.4 kg/ea.	0.05 T tot.	
				CONTRACT NAME: Project		CONTRACT NO: 0	MARK: M3	
				DRAWN BY:	CHECKED BY:			
REV	DATE	DESCRIPTION		U.S.C:	ISSUE DATE:			

2	B8

2 BEAMS REQ'D AS DRAWN MK'D M14

TEKLA Structures ®

			QTY: 2	PROFILE: UC305*305*158	SURFACE AREA: 1.3 m^2/ea.	2.6 m^2 tot.	
			GRADE: S235	LENGTH: 700	WEIGHT: 109.6 kg/ea.	0.22 T tot.	
			CONTRACT NAME: Project		CONTRACT NO: 0	MARK: M14	
			DRAWN BY:	CHECKED BY:			
REV	DATE	DESCRIPTION	U.M.O:	ISSUE DATE:			

Appendix C1 - Two Dimensional Concentrically Braced Frame Hybrid Test Model

```
# FileName: TestFrame2D_1.tcl
# Author: Daniel McCrum
# Email: mccrumdp@tcd.ie
# Last Altered: March, 2011.

# Description:
# This file contains the tcl input to perform a local
# hybrid simulation of a ground storey one bay braced frame
# comprising of 203 UC 46 columns and 30x30x3SHS braced sections
# as part of a three storey 2D braced frame mmodel.
#          ____________________________
#          |                          |        ^
#          |                          |        |
#          |                          |        | 2200mm
#          |                          |        |
#          |__________________________|        v
#          |                          |        ^
#          |                          |        |
#          |                          |        | 2200mm
#          |                          |        |
#          |                          |        v
#     --->  ____________________________
#          |                          |        ^
#          |                          |        |
#          |                          |        | 2500mm
#          |                          |        |
#          |                          |        v
#       XXX                        XXX
#
#          <--------------------------------->
#                      3300mm

# Units: N mm Mg sec

wipe all;
file mkdir Data;                # Create directory for data
file mkdir Data1;               # Create directory for data
file mkdir Data2;               # Create directory for data
file mkdir DataExp;             # Create directory for data

# ------------------------------
# Start of model generation
# ------------------------------
# create ModelBuilder (with two-dimensions and 3 DOF/node)
model BasicBuilder -ndm 2 -ndf 3

source HSsection.tcl;

# --------------------------------
# Load OpenFresco package
# --------------------------------
# (make sure all dlls are in the same folder as openSees.exe)
loadPackage OpenFresco

# --------------------------------
# Define mass for model
# --------------------------------
# The nodal masses represent a lateral torsional frequency
# ratio of 0.85 for the stiff side of the structure.
set Pc1 86.385;        # Mass in Mg
set Pc2 43.192;        # Mass in Mg
set Pc3 21.596;        # Mass in Mg

set P1 [expr 0.5*0.53333*1.981*$Pc1];
```

```
set P2 [expr 0.5*0.53333*1.981*$Pc2];
set P3 [expr 0.5*0.53333*1.981*$Pc3];

set mass3 [expr $P1];
set mass4 [expr $P1];

set mass5 [expr $P2];
set mass6 [expr $P2];

set mass7 [expr $P3];
set mass8 [expr $P3];

# ---------------------------------
# Define geometry for model
# ---------------------------------
set Lbeam1 3296;
set Lcol1 2500;
set Lcol2 2200;

# node $tag $xCrd $yCrd $mass
node  1    0.0          0.0
node  2    $Lbeam1      0.0
node  3    0.0          $Lcol1                          -mass $mass3 $mass3 0.0
node  4    $Lbeam1      $Lcol1                          -mass $mass4 $mass4 0.0
node  5    0.0          [expr $Lcol1+$Lcol2]            -mass $mass5 $mass6 0.0
node  6    $Lbeam1      [expr $Lcol1+$Lcol2]            -mass $mass6 $mass6 0.0
node  7    0.0          [expr $Lcol1+(2*$Lcol2)]         -mass $mass7 $mass7 0.0
node  8    $Lbeam1      [expr $Lcol1+(2*$Lcol2)]        -mass $mass8 $mass8 0.0

# Duplicate nodes
node  23   0.0                $Lcol1
node  24   $Lbeam1            $Lcol1

node  25   0.0                [expr $Lcol1+$Lcol2]
node  26   $Lbeam1            [expr $Lcol1+$Lcol2]

node  35   0.0                [expr $Lcol1+$Lcol2]
node  36   $Lbeam1            [expr $Lcol1+$Lcol2]

node  47   0.0                [expr $Lcol1+(2*$Lcol2)]
node  48   $Lbeam1            [expr $Lcol1+(2*$Lcol2)]

# SECOND STOREY
node 230   [expr ($Lbeam1/4)-4]          [expr $Lcol1+($Lcol2/4)+4]
node 231   [expr (2*$Lbeam1/4)-6]        [expr $Lcol1+(2*$Lcol2/4)+6]
node 232   [expr (3*$Lbeam1/4)-4]        [expr $Lcol1+(3*$Lcol2/4)+4]

node 235   [expr (3*$Lbeam1/4)-4]        [expr $Lcol1+($Lcol2/4)+4]
node 237   [expr (1*$Lbeam1/4)-4]        [expr $Lcol1+(3*$Lcol2/4)+4]

# THIRD STOREY
node 330   [expr ($Lbeam1/4)-4]          [expr ($Lcol1+$Lcol2)+($Lcol2/4)+4]
node 331   [expr (2*$Lbeam1/4)-6]        [expr ($Lcol1+$Lcol2)+(2*$Lcol2/4)+6]
node 332   [expr (3*$Lbeam1/4)-4]        [expr ($Lcol1+$Lcol2)+(3*$Lcol2/4)+4]

node 335   [expr (3*$Lbeam1/4)-4]        [expr ($Lcol1+$Lcol2)+($Lcol2/4)+4]
node 337   [expr (1*$Lbeam1/4)-4]        [expr ($Lcol1+$Lcol2)+(3*$Lcol2/4)+4]

# set the boundary conditions
# fix $tag $DX $DY $RZ
fix 1   1  1  1
fix 2   1  1  1

# ---------------------------------
# Define materials
# ---------------------------------
set steelTag 1;

# uniaxialMaterial Steel02 $matTag $Fy $E $b $R0 $cR1 $cR2 $a1 $a2 $a3 $a4
uniaxialMaterial Steel02 1 244.13 159290 0.03 18.5 0.925 0.15 0.0 1.0 0.0 1.0

uniaxialMaterial Elastic 7 5000000

# Brace Parameters:
# 30 x 30 x 3 RHS
set braceFiberSecTag 10;
set d 30;                    # Overall section depth 30
set b 30;                    # Overall section width 30
```

```
set t 3;                        # Thickness 2.5
set subFLen 10;                 # sub-division across flange length
set subFThk 5;                  # sub-division across flange thickness
set subWLen 10;                 # sub-division across web length
set subWThk 5;                  # sub-division across web thickness
HSsection $braceFiberSecTag $steelTag $d $b $t $subWLen $subWThk $subFLen $subFThk
puts "HSSection defined";

# ---------------------------------
# Define experimental control
# ---------------------------------
# expControl SimUniaxialMaterials $tag $matTags
#expControl SimUniaxialMaterials 1 1
expControl xPCtarget     1    1 "148.150.204.191"  22222  DMC_RTTest_soft  "C:/STS/Model"
expControl SimUniaxialMaterials 2 1

# ---------------------------------
# Define experimental setup
# ---------------------------------
# expSetup OneActuator $tag <-control $ctrlTag> $dir -sizeTrialOut $t $o <-trialDispFact $f> ...
expSetup OneActuator 1 -control 1 2 -sizeTrialOut 3 3
expSetup OneActuator 2 -control 2 2 -sizeTrialOut 3 3


# ---------------------------------
# Define experimental site
# ---------------------------------
# expSite LocalSite $tag $setupTag
expSite LocalSite 1 1
expSite LocalSite 2 2

# ---------------------------------
# Define geometric transformation
# ---------------------------------
geomTransf PDelta 1
geomTransf Linear 2
#geomTransf Corotational 3

# ---------------------------------
# Define experimental elements
# ---------------------------------
expElement beamColumn 1 3 1 1 -site 1 -initStif [expr 3.0696e10] [expr -18418176*0.99] 0 [expr -18418176*0.99] [expr
28388.69*0.01] 0 0 0 0
expElement beamColumn 2 4 2 1 -site 2 -initStif [expr 3.0696e10] [expr -18418176*0.01] 0 [expr -18418176*0.01] [expr
28388.69*0.01] 0 0 0 0

# ---------------------------------
# Define numerical elements
# ---------------------------------
# 305x156x40UB Beam
# element elasticBeamColumn $eleTag $iNode $jNode $A $E $Iz $transfTag
element elasticBeamColumn 3 3 4 5130 210e3 8503e4 2
element elasticBeamColumn 4 5 6 5130 210e3 8503e4 2
element elasticBeamColumn 5 7 8 5130 210e3 8503e4 2

# 203UC46 Column
# element elasticBeamColumn $eleTag $iNode $jNode $A $E $Iz $transfTag
element elasticBeamColumn 10 3 5 5870 210e3 4568e4 1
element elasticBeamColumn 11 4 6 5870 210e3 4568e4 1

element elasticBeamColumn 12 5 7 5870 210e3 4568e4 1
element elasticBeamColumn 13 6 8 5870 210e3 4568e4 1

# Zero Length Elements

#element zeroLength $eleTag $iNode $jNode -mat $matTag1 $matTag2... -dir $dir1 $dir2 ... <-orient $x1 $x2 $x3 $yp1 $yp2 $yp3>
element zeroLength 200 3 23 -mat 7 7 -dir 1 2
element zeroLength 201 4 24 -mat 7 7 -dir 1 2

element zeroLength 202 5 25 -mat 7 7 -dir 1 2
element zeroLength 203 6 26 -mat 7 7 -dir 1 2

element zeroLength 204 5 35 -mat 7 7 -dir 1 2
element zeroLength 205 6 36 -mat 7 7 -dir 1 2

element zeroLength 206 7 47 -mat 7 7 -dir 1 2
element zeroLength 207 8 48 -mat 7 7 -dir 1 2
```

```
set numintgrPts 7;

# Brace Members
# Second storey
element dispBeamColumn 100 23 230 $numintgrPts $braceFiberSecTag 2
element dispBeamColumn 101 230 231 $numintgrPts $braceFiberSecTag 2
element dispBeamColumn 102 231 232 $numintgrPts $braceFiberSecTag 2
element dispBeamColumn 103 232 26 $numintgrPts $braceFiberSecTag 2

element dispBeamColumn 104 24 235 $numintgrPts $braceFiberSecTag 2
element dispBeamColumn 105 235 231 $numintgrPts $braceFiberSecTag 2
element dispBeamColumn 106 231 237 $numintgrPts $braceFiberSecTag 2
element dispBeamColumn 107 237 25 $numintgrPts $braceFiberSecTag 2

# Third storey
element dispBeamColumn 110 35 330 $numintgrPts $braceFiberSecTag 2
element dispBeamColumn 111 330 331 $numintgrPts $braceFiberSecTag 2
element dispBeamColumn 112 331 332 $numintgrPts $braceFiberSecTag 2
element dispBeamColumn 113 332 48 $numintgrPts $braceFiberSecTag 2

element dispBeamColumn 114 36 335 $numintgrPts $braceFiberSecTag 2
element dispBeamColumn 115 335 331 $numintgrPts $braceFiberSecTag 2
element dispBeamColumn 116 331 337 $numintgrPts $braceFiberSecTag 2
element dispBeamColumn 117 337 47 $numintgrPts $braceFiberSecTag 2

# ---------------------------------
# Define dynamic loads
# ---------------------------------
# set time series to be passed to uniform excitation
set dt 0.01
set scale 0.03
set accelSeries "Path -filePath Taiwan40.txt -dt $dt -factor [expr 9810*$scale]"

# create UniformExcitation load pattern
# pattern UniformExcitation $tag $dir
pattern UniformExcitation  2 1 -accel $accelSeries

# calculate the rayleigh damping factors for nodes & elements
set alphaM    0.849;   # D = alphaM*M (or 0.368 for T = 3.416)
set betaK     0.0;     # D = betaK*Kcurrent
set betaKinit  0.0;    # D = beatKinit*Kinit
set betaKcomm  0.0;    # D = betaKcomm*KlastCommit

# set the rayleigh damping
rayleigh $alphaM $betaK $betaKinit $betaKcomm;

# ---------------------------------
# End of model generation
# ---------------------------------

# ---------------------------------
# Start of analysis generation
# ---------------------------------
# create the system of equations
system BandGeneral

# create the DOF numberer
numberer Plain

# create the constraint handler
constraints Plain

# create the convergence test
test FixedNumIter 5
#test NormDispIncr 1E-8 25

# create the integration scheme
#integrator NewmarkHSFixedNumIter 0.5 0.25
#integrator NewmarkHSIncrReduct 0.5 0.25 0.8
#integrator HHTHSFixedNumIter 0.5
#integrator HHTHSIncrReduct 0.5 0.8
integrator CollocationHSFixedNumIter 1.5
#integrator CollocationHSIncrReduct 1.5 0.8
#integrator AlphaOS 0.9
# create the solution algorithm
algorithm Newton
#algorithm Linear
```

```
# create the analysis object
analysis Transient
# ------------------------------
# End of analysis generation
# ------------------------------

# ------------------------------
# Start of recorder generation
# ------------------------------
# create the recorder objects
recorder Node -file Data/Node_Dsp.out -time -node    3 4 -dof 1 2 3 disp
recorder Node -file Data/Node_Vel.out -time -node    3 4 -dof 1 2 3 vel
recorder Node -file Data/Node_Acc.out -time -node    3 4 -dof 1 2 3 accel
recorder Node -file Data/Node_Rxn.out -time -node 1 2 -dof 1 2 reactionIncludingInertia

recorder Node -file Data/Node_DspRoof.out -time -node    7 8 -dof 1 2 3 disp
recorder Node -file Data/Node_VelRoof.out -time -node    7 8 -dof 1 2 3 vel
recorder Node -file Data/Node_AccRoof.out -time -node    7 8 -dof 1 2 3 accel

# SECOND STOREY
# Brace axial load
recorder Element -file Data1/Brace1Ele1local.out -time -ele 101 localForce
recorder Element -file Data1/Brace2Ele1local.out -time -ele 105 localForce

recorder Node -file Data1/Node3_Dsp.out -time -node 3 -dof 1 disp
recorder Node -file Data1/Node4_Dsp.out -time -node 4 -dof 1 disp

# Stress/Strain in Braces
recorder Element -file Data1/Br1sec7Top.out -time -ele 101 section $numintgrPts fiber 25 0 $steelTag stressStrain; # Mid Brace Stress
recorder Element -file Data1/Br1sec1Top.out -time -ele 101 section 1 fiber 25 0 $steelTag stressStrain; # Brace End Stress

recorder Element -file Data1/Br2sec7Side.out -time -ele 105 section $numintgrPts fiber 0 25 $steelTag stressStrain; # Mid Brace Stress
recorder Element -file Data1/Br2sec1Side.out -time -ele 105 section 1 fiber 0 25 $steelTag stressStrain; # Brace End Stress

# THIRD STOREY
# Brace axial load
recorder Element -file Data2/Brace1Ele1local.out -time -ele 111 localForce
recorder Element -file Data2/Brace2Ele1local.out -time -ele 115 localForce

recorder Node -file Data2/Node5_Dsp.out -time -node 5 -dof 1 disp
recorder Node -file Data2/Node6_Dsp.out -time -node 6 -dof 1 disp

# Stress/Strain in Braces
recorder Element -file Data2/Br1sec7Top.out -time -ele 111 section $numintgrPts fiber 25 0 $steelTag stressStrain; # Mid Brace Stress
recorder Element -file Data2/Br1sec1Top.out -time -ele 111 section 1 fiber 25 0 $steelTag stressStrain; # Brace End Stress

recorder Element -file Data2/Br2sec7Side.out -time -ele 115 section $numintgrPts fiber 0 25 $steelTag stressStrain; # Mid Brace Stress
recorder Element -file Data2/Br2sec1Side.out -time -ele 115 section 1 fiber 0 25 $steelTag stressStrain; # Brace End Stress


recorder Element -file DataExp/Elmt_glbFrc.out  -time -ele 1 2 forces
expRecorder Control -file DataExp/Control_ctrlDsp.out -time -control 1 2 ctrlDisp
expRecorder Control -file DataExp/Control_daqDsp.out  -time -control 1 2 daqDisp
expRecorder Control -file DataExp/Control_daqFrc.out  -time -control 1 2 daqForce

expRecorder Control -file DataExp/Control_ctrlDsp.out -time -control 1 ctrlDisp
expRecorder Control -file DataExp/Control_ctrlVel.out -time -control 1 ctrlVel
expRecorder Control -file DataExp/Control_daqDsp.out  -time -control 1 daqDisp
expRecorder Control -file DataExp/Control_daqFrc.out  -time -control 1 daqForce

expRecorder Setup -file DataExp/Setup_trialDsp.out -time -setup 1 trialDisp
expRecorder Setup -file DataExp/Setup_trialVel.out -time -setup 1 trialVel
expRecorder Setup -file DataExp/Setup_trialAcc.out -time -setup 1 trialAccel
expRecorder Setup -file DataExp/Setup_outDsp.out -time -setup 1 outDisp
expRecorder Setup -file DataExp/Setup_outFrc.out -time -setup 1 outForce
expRecorder Setup -file DataExp/Setup_ctrlDsp.out -time -setup 1 ctrlDisp
expRecorder Setup -file DataExp/Setup_ctrlVel.out -time -setup 1 ctrlVel
expRecorder Setup -file DataExp/Setup_ctrlAcc.out -time -setup 1 ctrlAccel
expRecorder Setup -file DataExp/Setup_daqDsp.out -time -setup 1 daqDisp
expRecorder Setup -file DataExp/Setup_daqFrc.out -time -setup 1 daqForce

# ---------------------------------
# End of recorder generation
# ---------------------------------

# ------------------------------
# Finally perform the analysis
# ------------------------------
```

```
# perform an eigenvalue analysis
set pi 3.14159265358979
set lambda [eigen -fullGenLapack 4]
puts "\nEigenvalues at start of transient:"
puts "lambda        omega         period"
foreach lambda $lambda {
   if {$lambda > 0.0} {
      set omega [expr pow($lambda,0.5)]
      set period [expr 2*$pi/pow($lambda,0.5)]
      puts "$lambda  $omega  $period"
   }
}

# open output file for writing
set outFileID [open Data/elapsedTime.txt w]
# perform the transient analysis
set tTot [time {
   for {set i 1} {$i < 4000} {incr i} {
      set t [time {analyze  1  [expr $dt/1.0]}]
      puts $outFileID $t
                  #puts "step $i"
   }
}]
puts "\nElapsed Time = $tTot \n"
# close the output file
close $outFileID

wipe
# ---------------------------------
# End of analysis
# ---------------------------------
```

Appendix C2 - Two Dimensional Concentrically Braced Frame OpenSees Model

```
# FileName: Frame2D.tcl
# Author: Daniel McCrum
# Email: mccrumdp@tcd.ie
# Last Altered: January, 2011.

# Description:
# This file contains the tcl script for an OpenSees model
# of three-storey two bay concentrically braced plan irregular
# structure

#          _____________________
#         |                     |        ^
#         |                     |        |
#         |                     |        | 2200mm
#         |                     |        |
#         |_____________________|        v
#         |                     |        ^
#         |                     |        |
#         |                     |        | 2200mm
#         |                     |        |
#         |                     |        v
#          _____________________
#         |                     |        ^
#         |                     |        |
#         |                     |        | 2500mm
#         |                     |        |
#         |                     |        v
#       XXX                   XXX
#
#          <--------------------------------->
#                        3300mm

# Units: N m sec
wipe all;
file mkdir Data;                # Create directory for data
file mkdir Data1;               # Create directory for data
file mkdir Data2;               # Create directory for data
file mkdir DataExp;             # Create directory for data

# ------------------------------
# Start of model generation
# ------------------------------
# create ModelBuilder (with two-dimensions and 3 DOF/node)
model BasicBuilder -ndm 2 -ndf 3

source HEsection1.tcl;
source HSsection.tcl;
source FlanSection.tcl;
source WebSection.tcl;

# ---------------------------------
# Define geometry for model
# ---------------------------------
set withGravity 1;

set Lbeam1 3300;                # beam 1 length
set Lcol1  2500;                # column length
set Lcol2  2200;

# node $tag $xCrd $yCrd $mass
node  1    0.0                  0.0
node  2    $Lbeam1              0.0
node  3    0.0                  $Lcol1
node  4    $Lbeam1              $Lcol1
```

```
node 5   0.0                [expr $Lcol1+$Lcol2]
node 6   $Lbeam1            [expr $Lcol1+$Lcol2]
node 7   0.0                [expr $Lcol1+2*$Lcol2]
node 8   $Lbeam1            [expr $Lcol1+2*$Lcol2]

set hfl 14.2;
set hweb 181;

node 111  0.0               $hfl
node 112  0.0               [expr $hfl + $hweb]
node 113  0.0               [expr (2*$hfl) + $hweb]
node 114  0.0               [expr $Lcol1 - (2*$hfl + $hweb)]
node 115  0.0               [expr $Lcol1 - ($hfl + $hweb)]
node 116  0.0               [expr $Lcol1 - $hfl]

node 211  $Lbeam1           $hfl
node 212  $Lbeam1           [expr $hfl + $hweb]
node 213  $Lbeam1           [expr 2*$hfl + $hweb]
node 214  $Lbeam1           [expr $Lcol1 - (2*$hfl + $hweb)]
node 215  $Lbeam1           [expr $Lcol1 - ($hfl + $hweb)]
node 216  $Lbeam1           [expr $Lcol1 - $hfl]

# FIRST STOREY
# Brace Members
node 130  [expr 970.4-4]                [expr 858.6+4]
node 131  [expr 1650]                   [expr 1302.3]
node 132  [expr 2267.7-4]               [expr 1734.8+4]

node 135  [expr 2329.6-4]               [expr 858.6+4]
node 137  [expr 1032.3-4]               [expr 1734.8+4]

# Gusset nodes
node 121  323.5                         [expr (2*$hfl+$hweb)+227.35]
node 221  [expr $Lbeam1-323.5]          [expr (2*$hfl+$hweb)+227.35]

node 311  386.5                         [expr $Lcol1-267.84]
node 411  [expr $Lbeam1-386.5]          [expr $Lcol1-267.84]

# SECOND STOREY
# Brace Members
node 230  [expr ($Lbeam1/4)-4]                  [expr $Lcol1+($Lcol2/4)+4]
node 231  [expr (2*$Lbeam1/4)-6]                [expr $Lcol1+(2*$Lcol2/4)+6]
node 232  [expr (3*$Lbeam1/4)-4]                [expr $Lcol1+(3*$Lcol2/4)+4]

node 235  [expr (3*$Lbeam1/4)-4]                [expr $Lcol1+($Lcol2/4)+4]
node 237  [expr (1*$Lbeam1/4)-4]                [expr $Lcol1+(3*$Lcol2/4)+4]

# THIRD STOREY
# Brace members
node 330  [expr ($Lbeam1/4)-4]                  [expr ($Lcol1+$Lcol2)+($Lcol2/4)+4]
node 331  [expr (2*$Lbeam1/4)-6]                [expr ($Lcol1+$Lcol2)+(2*$Lcol2/4)+6]
node 332  [expr (3*$Lbeam1/4)-4]                [expr ($Lcol1+$Lcol2)+(3*$Lcol2/4)+4]

node 335  [expr (3*$Lbeam1/4)-4]                [expr ($Lcol1+$Lcol2)+($Lcol2/4)+4]
node 337  [expr (1*$Lbeam1/4)-4]                [expr ($Lcol1+$Lcol2)+(3*$Lcol2/4)+4]

# Duplicate nodes for brace end connections
node 101  323.5                         [expr (2*$hfl+$hweb)+227.35]
node 102  [expr $Lbeam1-323.5]          [expr (2*$hfl+$hweb)+227.35]

node 103  386.5                         [expr $Lcol1-267.84]
node 104  [expr $Lbeam1-386.5]          [expr $Lcol1-267.84]

node 13   0.0               $Lcol1
node 14   $Lbeam1           $Lcol1

node 23   0.0               $Lcol1
node 24   $Lbeam1           $Lcol1

node 25   0.0               [expr $Lcol1+$Lcol2]
node 26   $Lbeam1           [expr $Lcol1+$Lcol2]

node 35   0.0               [expr $Lcol1+$Lcol2]
node 36   $Lbeam1           [expr $Lcol1+$Lcol2]

node 47   0.0               [expr $Lcol1+2*$Lcol2]
node 48   $Lbeam1           [expr $Lcol1+2*$Lcol2]
```

```
# ---------------------------------
# Define mass for model
# ---------------------------------
# The nodal masses represent a lateral torsional frequency
# ratio of 0.85 for the stiff side of the structure.
set Pc1 86.385;         # Mass in Mg
set Pc2 43.192;         # Mass in Mg
set Pc3 21.596;         # Mass in Mg

set P1 [expr 0.5*0.53333*1.981*$Pc1];
set P2 [expr 0.5*0.53333*1.981*$Pc2];
set P3 [expr 0.5*0.53333*1.981*$Pc3];

set mass3 [expr $P1];
set mass4 [expr $P1];

set mass5 [expr $P2];
set mass6 [expr $P2];

set mass7 [expr $P3];
set mass8 [expr $P3];

mass  3 $mass3 $mass3 0.0
mass  4 $mass4 $mass4 0.0
mass  5 $mass5 $mass5 0.0
mass  6 $mass6 $mass6 0.0
mass  7 $mass7 $mass7 0.0
mass  8 $mass8 $mass8 0.0

# set the boundary conditions
# fix $tag $DX $DY $RZ
fix 1   1  1  1
fix 2   1  1  1

fix 121 0 0 0
fix 221 0 0 0

fix 311 0 0 0
fix 411 0 0 0

equalDOF 101 121      1 2 3
equalDOF 102 221      1 2 3

equalDOF 103 311 1 2 3
equalDOF 104 411 1 2 3

equalDOF 3 13 1 2 3
equalDOF 4 14 1 2 3

equalDOF 3 23 1 2 3
equalDOF 4 24 1 2 3

equalDOF 5 25 1 2 3
equalDOF 6 26 1 2 3

equalDOF 5 35 1 2 3
equalDOF 6 36 1 2 3

equalDOF 7 47 1 2 3
equalDOF 8 48 1 2 3

# ---------------------------------
# Define materials
# ---------------------------------
set steelTag 1;
set matID 2;
set matStiff 3;
# uniaxialMaterial Steel02 $matTag $Fy $E $b $R0 $cR1 $cR2 $a1 $a2 $a3 $a4
uniaxialMaterial Steel02 $steelTag 244.13 159290 0.03 18.5 0.925 0.15 -0.045 1.0 0.045 1.0

uniaxialMaterial Steel02 $matID 235 210000 0.03 18.5 0.925 0.15 -0.045 1.0 0.045 1.0

uniaxialMaterial Steel02 $matStiff 235 70000 0.03 18.5 0.925 0.15 -0.045 1.0 0.045 1.0

set E 210000;
set poisson 0.3;
set G [expr $E/([expr 2*(1+$poisson)])];      # Torsional Stiffness
```

```
# ----------------------------------
# Define Sections
# ----------------------------------

# Column Parameters:
# 203 UC 46
set col2secID 2;
set col2FiberSecTag 3;
set d 203;                  # Overall section depth
set b 203;                  # Overall section width
set t 7.2;                  # Web thickness
set T 11;                   # Flange thickness
set dw [expr $d - 2*$T];    # Depth of web
set y [expr $d/2];
set subFLen 10;             # sub-division across flange length
set subFThk 5;              # sub-division across flange thickness
set subWLen 10;             # sub-division across web length
set subWThk 5;              # sub-division across web thickness
HEsection1 $col2FiberSecTag $matID $d $b $dw $t $subWLen $subWThk $subFLen $subFThk
puts "HESection1 defined";


# Brace Parameters:
# 30 x 30 x 3 RHS
set braceFiberSecTag 8;
set d 30;                   # Overall section depth 30
set b 30;                   # Overall section width 30
set t 3;                    # Thickness 2.5
set subFLen 10;             # sub-division across flange length
set subFThk 5;              # sub-division across flange thickness
set subWLen 10;             # sub-division across web length
set subWThk 5;              # sub-division across web thickness
HSsection $braceFiberSecTag $steelTag $d $b $t $subWLen $subWThk $subFLen $subFThk
puts "HSSection defined";

# Flange
set flangeFiberSecTag 10;
set d 209;                  # Overall section depth
set b 210;                  # Overall section width
set subLen 10;              # sub-division across length
set subThk 5;               # sub-division across thickness
FlanSection $flangeFiberSecTag $matStiff $d $b $subLen $subThk
puts "FlanSection defined";

# Web
set webFiberSecTag 12;
set d 181;                  # Overall section depth
set b 9.4;                  # Overall section width
set subLen 15;              # sub-division across length
set subThk 7;               # sub-division across thickness
WebSection $webFiberSecTag $matStiff $d $b $subLen $subThk
puts "WebSection defined";

# ----------------------------------
# Define geometric transformation
# ----------------------------------
geomTransf PDelta 1
geomTransf Linear 2
#geomTransf Corotational 3
set numintgrPts 7;


# ----------------------------------
# Define numerical elements
# ----------------------------------
# Columns
# FIRST STOREY
element nonlinearBeamColumn 1 1 111 $numintgrPts $flangeFiberSecTag 1
element nonlinearBeamColumn 2 111 112 $numintgrPts $webFiberSecTag 1
element nonlinearBeamColumn 3 112 113 $numintgrPts $flangeFiberSecTag 1
element nonlinearBeamColumn 4 113 114 $numintgrPts $col2FiberSecTag 1
element nonlinearBeamColumn 5 114 115 $numintgrPts $flangeFiberSecTag 1
element nonlinearBeamColumn 6 115 116 $numintgrPts $webFiberSecTag 1
element nonlinearBeamColumn 7 116 3 $numintgrPts $flangeFiberSecTag 1

element nonlinearBeamColumn 10 2 211 $numintgrPts $flangeFiberSecTag 1
element nonlinearBeamColumn 11 211 212 $numintgrPts $webFiberSecTag 1
element nonlinearBeamColumn 12 212 213 $numintgrPts $flangeFiberSecTag 1
```

```
element nonlinearBeamColumn 13 213 214 $numintgrPts $col2FiberSecTag 1
element nonlinearBeamColumn 14 214 215 $numintgrPts $flangeFiberSecTag 1
element nonlinearBeamColumn 15 215 216 $numintgrPts $webFiberSecTag 1
element nonlinearBeamColumn 16 216 4 $numintgrPts $flangeFiberSecTag 1

# SECOND STOREY
element nonlinearBeamColumn 20 3 5 $numintgrPts $col2FiberSecTag 1
element nonlinearBeamColumn 21 4 6 $numintgrPts $col2FiberSecTag 1

# THIRD STOREY
element nonlinearBeamColumn 22 5 7 $numintgrPts $col2FiberSecTag 1
element nonlinearBeamColumn 23 6 8 $numintgrPts $col2FiberSecTag 1

# 305x165x54 UB Beam
# element elasticBeamColumn $eleTag $iNode $jNode $A $E $Iz $transfTag
set Ebeam 210000;
set Abeam 68.8e2;
set Izbeam 11700e4;
element elasticBeamColumn 30 3 4 $Abeam $Ebeam $Izbeam 2
element elasticBeamColumn 31 5 6 $Abeam $Ebeam $Izbeam 2
element elasticBeamColumn 32 7 8 $Abeam $Ebeam $Izbeam 2


# Brace Members
# First storey
element nonlinearBeamColumn 50 121 130 $numintgrPts $braceFiberSecTag 2
element nonlinearBeamColumn 51 130 131 $numintgrPts $braceFiberSecTag 2
element nonlinearBeamColumn 52 131 132 $numintgrPts $braceFiberSecTag 2
element nonlinearBeamColumn 53 132 411 $numintgrPts $braceFiberSecTag 2

element nonlinearBeamColumn 54 221 135 $numintgrPts $braceFiberSecTag 2
element nonlinearBeamColumn 55 135 131 $numintgrPts $braceFiberSecTag 2
element nonlinearBeamColumn 56 131 137 $numintgrPts $braceFiberSecTag 2
element nonlinearBeamColumn 57 137 311 $numintgrPts $braceFiberSecTag 2

set Egus 500000;                    # Large stiffness
set Agus 1800;                      # 150mm x 12mm thk
set Izgus 337.5e4;      # 12 x 150^3/12
element elasticBeamColumn 60 113 121 $Agus $Egus $Izgus 1
element elasticBeamColumn 61 213 221 $Agus $Egus $Izgus 1

element elasticBeamColumn 62 3 311 $Agus $Egus $Izgus 1
element elasticBeamColumn 63 4 411 $Agus $Egus $Izgus 1

# Second storey
element nonlinearBeamColumn 100 23 230 $numintgrPts $braceFiberSecTag 2
element nonlinearBeamColumn 101 230 231 $numintgrPts $braceFiberSecTag 2
element nonlinearBeamColumn 102 231 232 $numintgrPts $braceFiberSecTag 2
element nonlinearBeamColumn 103 232 26 $numintgrPts $braceFiberSecTag 2

element nonlinearBeamColumn 104 24 235 $numintgrPts $braceFiberSecTag 2
element nonlinearBeamColumn 105 235 231 $numintgrPts $braceFiberSecTag 2
element nonlinearBeamColumn 106 231 237 $numintgrPts $braceFiberSecTag 2
element nonlinearBeamColumn 107 237 25 $numintgrPts $braceFiberSecTag 2

# Third storey
element nonlinearBeamColumn 110 35 330 $numintgrPts $braceFiberSecTag 2
element nonlinearBeamColumn 111 330 331 $numintgrPts $braceFiberSecTag 2
element nonlinearBeamColumn 112 331 332 $numintgrPts $braceFiberSecTag 2
element nonlinearBeamColumn 113 332 48 $numintgrPts $braceFiberSecTag 2

element nonlinearBeamColumn 114 36 335 $numintgrPts $braceFiberSecTag 2
element nonlinearBeamColumn 115 335 331 $numintgrPts $braceFiberSecTag 2
element nonlinearBeamColumn 116 331 337 $numintgrPts $braceFiberSecTag 2
element nonlinearBeamColumn 117 337 47 $numintgrPts $braceFiberSecTag 2


# --------------------------------
# Define dynamic loads
# --------------------------------
# set time series to be passed to uniform excitation
set dt 0.01
set scale 0.03
set accelSeries "Path -filePath Taiwan40.txt -dt $dt -factor [expr 9810*$scale]"

# create UniformExcitation load pattern
# pattern UniformExcitation $tag $dir
pattern UniformExcitation  2 1 -accel $accelSeries
```

```
# ---------------------------------
# End of model generation
# ---------------------------------

# ---------------------------------
# Start of analysis generation
# ---------------------------------

#constraints Transformation ;
set alphaSP 1e12;
set alphaMP 1e12;
constraints Penalty $alphaSP $alphaMP ;
numberer RCM ;
system UmfPack ;
set Tol 1.e-5;
set maxNumIter 1000;
test NormDispIncr $Tol $maxNumIter ;
#algorithm ModifiedNewton ;
algorithm KrylovNewton ;
set gamma 0.8;
integrator HHT $gamma ;
analysis Transient ;

# ---------------------------------
# Define Dampnig
# ---------------------------------
set xDamp 0.1;                  # 5.0% damping ratio assumed
set MpropSwitch 1.0;
set KcurrSwitch 0.0;
set KcommSwitch 1.0;
set KinitSwitch 0.0;
set nEigenI 1;                  # mode 1
set nEigenJ 3;                  # mode 3
set type frequency;
set lambdaN [eigen $type [expr $nEigenJ]];          # eigenvalue analysis for nEigenJ modes
set lambdaI [lindex $lambdaN [expr $nEigenI-1]];    # eigenvalue mode i
set lambdaJ [lindex $lambdaN [expr $nEigenJ-1]];    # eigenvalue mode j
set omegaI [expr pow($lambdaI,0.5)];
set omegaJ [expr pow($lambdaJ,0.5)];
set alphaM [expr $MpropSwitch*$xDamp*(2*$omegaI*$omegaJ)/($omegaI+$omegaJ)];    # M-prop. damping; D = alphaM*M
set betaKcurr [expr $KcurrSwitch*2.*$xDamp/($omegaI+$omegaJ)];          # current-K;     +beatKcurr*KCurrent
set betaKcomm [expr $KcommSwitch*2.*$xDamp/($omegaI+$omegaJ)];          # last-committed K;   +betaKcomm*KlastCommitt
set betaKinit [expr $KinitSwitch*2.*$xDamp/($omegaI+$omegaJ)];          # initial-K;     +beatKinit*Kini
rayleigh $alphaM $betaKcurr $betaKinit $betaKcomm;                      # RAYLEIGH damping

#set T1 [expr 2*3.141592654/$omegaI];
#set Omega1 [expr $omegaI];
#puts "The first period is: $T1";
#puts "Omega 1 is: $Omega1";
#puts "The first frequency is: [expr 1/$T1]";
#
#set T3 [expr 2*3.141592654/$omegaJ];
#set Omega3 [expr $omegaJ];
#puts "The third period is: $T3";
#puts "Omega 3 is: $Omega3";
#puts "The third frequency is: [expr 1/$T3]";

## calculate the rayleigh damping factors for nodes & elements
#set alphaM    0.425;            # D = alphaM*M
#set betaK     0.0;              # D = betaK*Kcurrent
#set betaKinit  0.0;             # D = beatKinit*Kinit
#set betaKcomm  0.0;             # D = betaKcomm*KlastCommit
#
## set the rayleigh damping
#rayleigh $alphaM $betaK $betaKinit $betaKcomm;

# ---------------------------------
# End of analysis generation
# ---------------------------------


# ---------------------------------
# Start of recorder generation
# ---------------------------------
# create the recorder objects
recorder Node -file Data/Node_Dsp.out -time -node    3 4 -dof 1 2 3 disp
recorder Node -file Data/Node_Vel.out -time -node    3 4 -dof 1 2 3 vel
recorder Node -file Data/Node_Acc.out -time -node    3 4 -dof 1 2 3 accel
```

```
recorder Node -file Data/Node_Rxn.out -time -node 1 2 -dof 1 2 reactionIncludingInertia

recorder Node -file Data/Node_DspRoof.out -time -node    7 8 -dof 1 2 3 disp
recorder Node -file Data/Node_VelRoof.out -time -node    7 8 -dof 1 2 3 vel
recorder Node -file Data/Node_AccRoof.out -time -node    7 8 -dof 1 2 3 accel

# Brace axial load
recorder Element -file Data/Brace1Ele1local.out -time -ele 51 localForce
recorder Element -file Data/Brace2Ele1local.out -time -ele 55 localForce

# Stress/Strain in Braces
recorder Element -file Data/Br2sec7Top.out -time -ele 51 section $numintgrPts fiber 25 0 $steelTag stressStrain; # Mid Brace Stress
recorder Element -file Data/Br2sec7Side.out -time -ele 51 section $numintgrPts fiber 0 25 $steelTag stressStrain; # Brace End Stress

recorder Element -file Data/Br1sec7Top.out -time -ele 55 section $numintgrPts fiber 25 0 $steelTag stressStrain; # Mid Brace Stress
recorder Element -file Data/Br1sec7Side.out -time -ele 55 section $numintgrPts fiber 0 25 $steelTag stressStrain; # Brace End Stress


# SECOND STOREY
# Brace axial load
recorder Element -file Data1/Brace1Ele1local.out -time -ele 101 localForce
recorder Element -file Data1/Brace2Ele1local.out -time -ele 105 localForce

recorder Node -file Data1/Node3_Dsp.out -time -node 3 -dof 1 disp
recorder Node -file Data1/Node4_Dsp.out -time -node 4 -dof 1 disp

# Stress/Strain in Braces
recorder Element -file Data1/Br1sec7Top.out -time -ele 101 section $numintgrPts fiber 25 0 $steelTag stressStrain; # Mid Brace Stress
recorder Element -file Data1/Br1sec1Top.out -time -ele 101 section 1 fiber 25 0 $steelTag stressStrain; # Brace End Stress

recorder Element -file Data1/Br2sec7Side.out -time -ele 105 section $numintgrPts fiber 0 25 $steelTag stressStrain; # Mid Brace Stress
recorder Element -file Data1/Br2sec1Side.out -time -ele 105 section 1 fiber 0 25 $steelTag stressStrain; # Brace End Stress


# THIRD STOREY
# Brace axial load
recorder Element -file Data2/Brace1Ele1local.out -time -ele 111 localForce
recorder Element -file Data2/Brace2Ele1local.out -time -ele 115 localForce

recorder Node -file Data2/Node5_Dsp.out -time -node 5 -dof 1 disp
recorder Node -file Data2/Node6_Dsp.out -time -node 6 -dof 1 disp

# Stress/Strain in Braces
recorder Element -file Data2/Br1sec7Top.out -time -ele 111 section $numintgrPts fiber 25 0 $steelTag stressStrain; # Mid Brace Stress
recorder Element -file Data2/Br1sec1Top.out -time -ele 111 section 1 fiber 25 0 $steelTag stressStrain; # Brace End Stress

recorder Element -file Data2/Br2sec7Side.out -time -ele 115 section $numintgrPts fiber 0 25 $steelTag stressStrain; # Mid Brace Stress
recorder Element -file Data2/Br2sec1Side.out -time -ele 115 section 1 fiber 0 25 $steelTag stressStrain; # Brace End Stress



# ---------------------------------
# End of recorder generation
# ---------------------------------

# -------------------------------------
# Define Display
# -------------------------------------
source DisplayPlane.tcl;
source DisplayModel3D.tcl;

set xPixels 500;                # height of graphical window in pixels
set yPixels 500;                # height of graphical window in pixels
set xLoc 5;                     # horizontal location of graphical window (0=upper left-most corner)
set yLoc 5;                     # vertical location of graphical window (0=upper left-most corner)
set dAmp 10;                    # Relative amplification factor for deformations
set ShapeType1 DeformedShape;
set windowTitle "2D Frame Deformed Shape";
set viewPlane ZY;
set nEigen 0;
recorder display $windowTitle $xLoc $yLoc $xPixels $yPixels  -wipe ; # display recorder

DisplayPlane $ShapeType1 $dAmp $viewPlane $nEigen 0;
recorder plot Data/Node_AccRoof.out Accel-Z 5 510 500 500 -columns 1 2; # Plot Load vs Disp
recorder plot Data/Node_DspRoof.out FloorDrift-Z 515 510 500 500 -columns 1 2; # Plot Load vs Disp

set xLoc1 510;
set yLoc1 5;
```

```
set ShapeType DeformedShape;
DisplayModel3D $ShapeType $dAmp $xLoc1 $yLoc1 $xPixels $yPixels $nEigen

# ------------------------------
# Finally perform the analysis
# ------------------------------
# perform an eigenvalue analysis
set pi 3.14159265358979
set lambda [eigen -fullGenLapack 4]
puts "\nEigenvalues at start of transient:"
puts "lambda        omega         period"
foreach lambda $lambda {
   if {$lambda > 0.0} {
      set omega [expr pow($lambda,0.5)]
      set period [expr 2*$pi/pow($lambda,0.5)]
      puts "$lambda  $omega  $period"
   }
}

# open output file for writing
set outFileID [open Data/elapsedTime.txt w]
# perform the transient analysis
set tTot [time {
   for {set i 1} {$i < 4000} {incr i} {
      set t [time {analyze  1  [expr $dt/1.0]}]
      puts $outFileID $t
                  #puts "step $i"
   }
}]
puts "\nElapsed Time = $tTot \n"
# close the output file
close $outFileID

wipe
# --------------------------------
# End of analysis
# --------------------------------
```

Appendix C3 - Three Dimensional Concentrically Braced Frame Hybrid Test Model

```
# FileName: PortalFrame_Local_Test.tcl
# Author: Daniel McCrum
# Email: mccrumdp@tcd.ie
# Last Altered: March, 2011.

# Description:
# This file contains the tcl input to perform a 3D local
# hybrid simulation of a concentrically braced plan
# irregular structure
#
#          _____________________
#         |                     |        ^
#         |                     |        |
#         |                     |        | 2200mm
#         |                     |        |
#         |_____________________|        v
#         |                     |        ^
#         |                     |        |
#         |                     |        | 2200mm
#         |                     |        |
#         |                     |        v
#      --->_____________________
#         |                     |        ^
#         |                     |        |
#         |                     |        | 2500mm
#         |                     |        |
#         |                     |        v
#        XXX                   XXX
#
#           <--------------------------------->
#                        3300mm
```

```
# Units: N mm Mg sec

wipe all;
file mkdir Data;                # Create directory for general data
file mkdir Data1;               # Create directory for first storey data
file mkdir Data2;               # Create directory for second storey data
file mkdir DataExp;             # Create directory for experimental data

source HEsection1.tcl;
source HSsection1.tcl;
source HSsection.tcl;

# ------------------------------------
# Start of model generation
# ------------------------------------
# create ModelBuilder (with two-dimensions and 3 DOF/node)
model BasicBuilder -ndm 3 -ndf 6
# ------------------------------------
# Load OpenFresco package
# ------------------------------------
# (make sure all dlls are in the same folder as openSees.exe)
loadPackage OpenFresco
# ------------------------------------
# Define geometry for model
# ------------------------------------
set Lcol1 2500;
set Lcol2 2200;
set Lbeam1 3300;
set Lbeam2 3300;

# Plan Aspect Ratio equal to 2.0
#set Lbeam1 3296;               # beam 1 length
#set Lbeam2 3300;               # beam 2 length
```

```
#set Lcol1  2427;              # column length
#set Lcol2  2200;

# nodal coords.
#          X                    Y                    Z
node 1  0                      0                    0
node 2  0                      0                    $Lbeam2
node 3  0                      0                    [expr $Lbeam2*2]
node 4  [expr $Lbeam1]         0                    [expr $Lbeam2*2]
node 5  [expr $Lbeam1]         0                    $Lbeam2
node 6  [expr $Lbeam1]         0                    0

# FIRST FLOOR
node 7  0                      $Lcol1               0
node 8  0                      $Lcol1               $Lbeam2
node 9  0                      $Lcol1               [expr $Lbeam2*2]
node 10 [expr $Lbeam1]         $Lcol1               [expr $Lbeam2*2]
node 11 [expr $Lbeam1]         $Lcol1               $Lbeam2
node 12 [expr $Lbeam1]         $Lcol1               0


# SECOND FLOOR
node 27  0                     [expr $Lcol1+$Lcol2]     0
node 28  0                     [expr $Lcol1+$Lcol2]     $Lbeam2
node 29  0                     [expr $Lcol1+$Lcol2]     [expr $Lbeam2*2]
node 30  [expr $Lbeam1]        [expr $Lcol1+$Lcol2]     [expr $Lbeam2*2]
node 31  [expr $Lbeam1]        [expr $Lcol1+$Lcol2]     $Lbeam2
node 32  [expr $Lbeam1]        [expr $Lcol1+$Lcol2]     0

# THIRD FLOOR
node 47  0                     [expr $Lcol1+($Lcol2*2)]  0
node 48  0                     [expr $Lcol1+($Lcol2*2)]  $Lbeam2
node 49  0                     [expr $Lcol1+($Lcol2*2)]  [expr $Lbeam2*2]
node 50  [expr $Lbeam1]        [expr $Lcol1+($Lcol2*2)]  [expr $Lbeam2*2]
node 51  [expr $Lbeam1]        [expr $Lcol1+($Lcol2*2)]  $Lbeam2
node 52  [expr $Lbeam1]        [expr $Lcol1+($Lcol2*2)]  0

# Duplicate nodes for brace end zerolength sections
# FIRST STOREY
#node 111  0                   0                    0
node 113  0                    0                    [expr $Lbeam2*2]
node 114  [expr $Lbeam1]       0                    [expr $Lbeam2*2]
#node 116  [expr $Lbeam1]      0                    0
#node 117  0                   $Lcol1               0
node 119  0                    $Lcol1               [expr $Lbeam2*2]
node 210  [expr $Lbeam1]       $Lcol1               [expr $Lbeam2*2]
#node 212  [expr $Lbeam1]      $Lcol1               0

# SECOND STOREY
node 311  0                    $Lcol1               0
node 313  0                    $Lcol1               [expr $Lbeam2*2]
node 314  [expr $Lbeam1]       $Lcol1               [expr $Lbeam2*2]
node 316  [expr $Lbeam1]       $Lcol1               0

node 317  0                    [expr $Lcol1+$Lcol2]     0
node 319  0                    [expr $Lcol1+$Lcol2]     [expr $Lbeam2*2]
node 410  [expr $Lbeam1]       [expr $Lcol1+$Lcol2]     [expr $Lbeam2*2]
node 412  [expr $Lbeam1]       [expr $Lcol1+$Lcol2]     0

# THIRD STOREY
node 511  0                    [expr $Lcol1+$Lcol2]     0
node 513  0                    [expr $Lcol1+$Lcol2]     [expr $Lbeam2*2]
node 514  [expr $Lbeam1]       [expr $Lcol1+$Lcol2]     [expr $Lbeam2*2]
node 516  [expr $Lbeam1]       [expr $Lcol1+$Lcol2]     0

node 517  0                    [expr $Lcol1+($Lcol2*2)]  0
node 519  0                    [expr $Lcol1+($Lcol2*2)]  [expr $Lbeam2*2]
node 610  [expr $Lbeam1]       [expr $Lcol1+($Lcol2*2)]  [expr $Lbeam2*2]
node 612  [expr $Lbeam1]       [expr $Lcol1+($Lcol2*2)]  0

# Brace imperfection nodes 0.1% out-of-straight at mid-length
set delta1 4;
set delta2 6;
# FIRST STOREY
# RHS Brace Members
node 150   [expr ($Lbeam1/4)-$delta1]   [expr ($Lcol1/4)+$delta1]   [expr $delta2+$Lbeam2*2]
node 151   [expr (2*$Lbeam1/4)-$delta2]  [expr (2*$Lcol1/4)+$delta2]  [expr $Lbeam2*2]
node 152   [expr (3*$Lbeam1/4)-$delta1]  [expr (3*$Lcol1/4)+$delta1]  [expr $delta2+$Lbeam2*2]
```

```
node 160  [expr (3*$Lbeam1/4)-$delta1]   [expr ($Lcol1/4)+$delta1]        [expr $delta2+$Lbeam2*2]
node 161  [expr ($Lbeam1/4)-$delta1]     [expr (3*$Lcol1/4)+$delta1]     [expr $delta2+$Lbeam2*2]


# SECOND STOREY
# LHS Brace Members
node 230  [expr ($Lbeam1/4)-$delta1]     [expr $Lcol1+($Lcol2/4)+$delta1]          -$delta1
node 231  [expr (2*$Lbeam1/4)-$delta2]   [expr $Lcol1+(2*$Lcol2/4)+$delta2]       -$delta2
node 232  [expr (3*$Lbeam1/4)-$delta1]   [expr $Lcol1+(3*$Lcol2/4)+$delta1]       -$delta1

node 235  [expr (3*$Lbeam1/4)-$delta1]   [expr $Lcol1+($Lcol2/4)+$delta1]          $delta1
#node 236  [expr (2*$Lbeam1/4)-$delta2]  [expr $Lcol1+(2*$Lcol2/4)+$delta2]       $delta2
node 237  [expr (1*$Lbeam1/4)-$delta1]   [expr $Lcol1+(3*$Lcol2/4)+$delta1]       $delta1

# RHS Brace Members
node 250 [expr ($Lbeam1/4)-$delta1]      [expr $Lcol1+($Lcol2/4)+$delta1]          [expr -$delta1+$Lbeam2*2]
node 251 [expr (2*$Lbeam1/4)-$delta2]    [expr $Lcol1+(2*$Lcol2/4)+$delta2]       [expr -$delta2+$Lbeam2*2]
node 252 [expr (3*$Lbeam1/4)-$delta1]    [expr $Lcol1+(3*$Lcol2/4)+$delta1]       [expr -$delta1+$Lbeam2*2]


node 255 [expr (3*$Lbeam1/4)-$delta1]    [expr $Lcol1+($Lcol2/4)+$delta1]          [expr $delta1+$Lbeam2*2]
#node 256 [expr (2*$Lbeam1/4)-$delta2]   [expr $Lcol1+(2*$Lcol2/4)+$delta2]       [expr $delta2+$Lbeam2*2]
node 257 [expr (1*$Lbeam1/4)-$delta1]    [expr $Lcol1+(3*$Lcol2/4)+$delta1]       [expr $delta1+$Lbeam2*2]


# THIRD STOREY
# LHS Brace Members
node 330  [expr ($Lbeam1/4)-$delta1]     [expr ($Lcol1+$Lcol2)+($Lcol2/4)+$delta1]          -$delta1
node 331  [expr (2*$Lbeam1/4)-$delta2]   [expr ($Lcol1+$Lcol2)+(2*$Lcol2/4)+$delta2]       -$delta2
node 332  [expr (3*$Lbeam1/4)-$delta1]   [expr ($Lcol1+$Lcol2)+(3*$Lcol2/4)+$delta1]       -$delta1

node 335  [expr (3*$Lbeam1/4)-$delta1]   [expr ($Lcol1+$Lcol2)+($Lcol2/4)+$delta1]          $delta1
#node 336  [expr (2*$Lbeam1/4)-$delta2]  [expr ($Lcol1+$Lcol2)+(2*$Lcol2/4)+$delta2]       $delta2
node 337  [expr (1*$Lbeam1/4)-$delta1]   [expr ($Lcol1+$Lcol2)+(3*$Lcol2/4)+$delta1]       $delta1

# RHS Brace Members
node 350 [expr ($Lbeam1/4)-$delta1]      [expr ($Lcol1+$Lcol2)+($Lcol2/4)+$delta1]          [expr -$delta1+$Lbeam2*2]
node 351 [expr (2*$Lbeam1/4)-$delta2]    [expr ($Lcol1+$Lcol2)+(2*$Lcol2/4)+$delta2]       [expr -$delta2+$Lbeam2*2]
node 352 [expr (3*$Lbeam1/4)-$delta1]    [expr ($Lcol1+$Lcol2)+(3*$Lcol2/4)+$delta1]       [expr -$delta1+$Lbeam2*2]


node 355 [expr (3*$Lbeam1/4)-$delta1]    [expr ($Lcol1+$Lcol2)+($Lcol2/4)+$delta1]          [expr $delta1+$Lbeam2*2]
#node 356 [expr (2*$Lbeam1/4)-$delta2]   [expr ($Lcol1+$Lcol2)+(2*$Lcol2/4)+$delta2]       [expr $delta2+$Lbeam2*2]
node 357 [expr (1*$Lbeam1/4)-$delta1]    [expr ($Lcol1+$Lcol2)+(3*$Lcol2/4)+$delta1]       [expr $delta1+$Lbeam2*2]

# ------------------------------------
# Define masses
# ------------------------------------
set massTotal1 86385;          # Mass in Mg
set massTotal2 43192;
set massTotal3 21596;

# Level of mass eccentricity
set eccmult1 0.53333333;       # Mass eccentricity factor for LHS Frame
set eccmult2 0.23333333;       # Mass eccentricity factor for Centre Frame
set eccmult3 0.23333333;       # Mass eccentricity factor for RHS Frame

# lateral torsional frequency ratio multiplier
#set factor1 2.74; # for lateral tors freq of 1.15
#set factor1 2.02; # for lateral tors freq of 1.00
set factor1 1.981; # for lateral tors freq of 0.85

# Nodal masses
# FIRST FLOOR
mass 7 [expr $massTotal1*0.5*$eccmult1*$factor1/9810] 0. [expr $massTotal1*0.5*$eccmult1*$factor1/9810] 1.0e-9 1.0e-9 1.0e-9;
mass 8 [expr $massTotal1*0.5*$eccmult2*$factor1/9810] 0. [expr $massTotal1*0.5*$eccmult2*$factor1/9810] 1.0e-9 1.0e-9 1.0e-9;
mass 9 [expr $massTotal1*0.5*$eccmult3*$factor1/9810] 0. [expr $massTotal1*0.5*$eccmult3*$factor1/9810] 1.0e-9 1.0e-9 1.0e-9;
mass 10 [expr $massTotal1*0.5*$eccmult3*$factor1/9810] 0. [expr $massTotal1*0.5*$eccmult3*$factor1/9810] 1.0e-9 1.0e-9 1.0e-9;
mass 11 [expr $massTotal2*0.5*$eccmult2*$factor1/9810] 0. [expr $massTotal1*0.5*$eccmult2*$factor1/9810] 1.0e-9 1.0e-9 1.0e-9;
mass 12 [expr $massTotal1*0.5*$eccmult1*$factor1/9810] 0. [expr $massTotal1*0.5*$eccmult1*$factor1/9810] 1.0e-9 1.0e-9 1.0e-9;

# SECOND FLOOR
mass 27 [expr $massTotal2*0.5*$eccmult1*$factor1/9810] 0. [expr $massTotal2*0.5*$eccmult1*$factor1/9810] 1.0e-9 1.0e-9 1.0e-9;
mass 28 [expr $massTotal2*0.5*$eccmult2*$factor1/9810] 0. [expr $massTotal2*0.5*$eccmult2*$factor1/9810] 1.0e-9 1.0e-9 1.0e-9;
mass 29 [expr $massTotal2*0.5*$eccmult3*$factor1/9810] 0. [expr $massTotal2*0.5*$eccmult3*$factor1/9810] 1.0e-9 1.0e-9 1.0e-9;
mass 30 [expr $massTotal2*0.5*$eccmult3*$factor1/9810] 0. [expr $massTotal2*0.5*$eccmult3*$factor1/9810] 1.0e-9 1.0e-9 1.0e-9;
mass 31 [expr $massTotal2*0.5*$eccmult2*$factor1/9810] 0. [expr $massTotal2*0.5*$eccmult2*$factor1/9810] 1.0e-9 1.0e-9 1.0e-9;
```

```
mass 32 [expr $massTotal2*0.5*$eccmult1*$factor1/9810] 0. [expr $massTotal2*0.5*$eccmult1*$factor1/9810] 1.0e-9 1.0e-9 1.0e-9;

# THIRD FLOOR
mass 47 [expr $massTotal3*0.5*$eccmult1*$factor1/9810] 0. [expr $massTotal3*0.5*$eccmult1*$factor1/9810] 1.0e-9 1.0e-9 1.0e-9;
mass 48 [expr $massTotal3*0.5*$eccmult2*$factor1/9810] 0. [expr $massTotal3*0.5*$eccmult2*$factor1/9810] 1.0e-9 1.0e-9 1.0e-9;
mass 49 [expr $massTotal3*0.5*$eccmult3*$factor1/9810] 0. [expr $massTotal3*0.5*$eccmult3*$factor1/9810] 1.0e-9 1.0e-9 1.0e-9;
mass 50 [expr $massTotal3*0.5*$eccmult3*$factor1/9810] 0. [expr $massTotal3*0.5*$eccmult3*$factor1/9810] 1.0e-9 1.0e-9 1.0e-9;
mass 51 [expr $massTotal3*0.5*$eccmult2*$factor1/9810] 0. [expr $massTotal3*0.5*$eccmult2*$factor1/9810] 1.0e-9 1.0e-9 1.0e-9;
mass 52 [expr $massTotal3*0.5*$eccmult1*$factor1/9810] 0. [expr $massTotal3*0.5*$eccmult1*$factor1/9810] 1.0e-9 1.0e-9 1.0e-9;

# set the boundary conditions
# fix $tag $DX $DY $DZ $RX $RY $RZ
fix 1   1 1 1 1 1 1
fix 6   1 1 1 1 1 1

#fix 1   1 1 1 0 1 0
#fix 6   1 1 1 0 1 0

fix 2   1 1 1 0 1 0
fix 5   1 1 1 0 1 0

fix 3   1 1 1 0 1 0
fix 4   1 1 1 0 1 0

# ------------------------------------
# Define materials
# ------------------------------------
set matID 1;
# uniaxialMaterial Steel02 $matTag $Fy $E $b $R0 $cR1 $cR2 $a1 $a2 $a3 $a4
uniaxialMaterial Steel02 1 235 210000 0.03 18.5 0.925 0.15 0.0 1.0 0.0 1.0
#uniaxialMaterial Steel02 $matID 235 25330 0.03 18.5 0.925 0.15 0.0 1.0 0.0 1.0
uniaxialMaterial Elastic 7 5000000

set E 210e3;
set poisson 0.3;
set G [expr $E/([expr 2*(1+$poisson)])];      # Torsional Stiffness

# ------------------------------------
# Define experimental control
# ------------------------------------
# expControl SimUniaxialMaterials $tag $matTags
#expControl SimUniaxialMaterials 1 1
expControl xPCtarget      1     1 "148.150.204.191"  22222  DMC_RTTest_soft  "C:/STS/Model"
expControl SimUniaxialMaterials 2 1

# ------------------------------------
# Define experimental setup
# ------------------------------------
# expSetup OneActuator $tag <-control $ctrlTag> $dir -sizeTrialOut $t $o <-trialDispFact $f> ...
expSetup OneActuator 1 -control 1 2 -sizeTrialOut 6 6
expSetup OneActuator 2 -control 2 2 -sizeTrialOut 6 6

# ------------------------------------
# Define experimental site
# ------------------------------------
# expSite LocalSite $tag $setupTag
expSite LocalSite 1 1
expSite LocalSite 2 2

# ------------------------------------
# Define section parameters
# ------------------------------------
# Column Parameters:
# 203 UC 46
set col2secID 20;
set col2FiberSecTag 21;
set d 203;                      # Overall section depth
set b 203;                      # Overall section width
set t 7.2;                      # Web thickness
set T 11;                       # Flange thickness
set dw [expr $d - 2*$T];        # Depth of web
set y [expr $d/2];
set subFLen 10;                 # sub-division across flange length
set subFThk 5;                  # sub-division across flange thickness
set subWLen 10;                 # sub-division across web length
set subWThk 5;                  # sub-division across web thickness
HEsection1 $col2FiberSecTag $matID $d $b $dw $t $subWLen $subWThk $subFLen $subFThk
puts "HESection1 defined";
```

```
# column torsional stiffness
set col2TorsTag 79;
set J9 8070000;
set GJ9 [expr $G*$J9];
uniaxialMaterial Elastic $col2TorsTag $GJ9; # Define column torsional stiffness
section Aggregator $col2secID $col2TorsTag T -section $col2FiberSecTag; # attach torsion and flexure

# Beam Parameters:
# 305x165x40UB Beam
set Ebeam 210000;
set Abeam 5130;
set Izbeam 6740e4;
set Iybeam 8503e4;
set Jbeam 47.2e4;

# Brace Parameters:
# 30 x 30 x 3 RHS
set bracesecID 7;
set braceFiberSecTag 8;
set d 30;                    # Overall section depth 30
set b 30;                    # Overall section width 30
set t 3;                     # Thickness 2.5
set subFLen 10;              # sub-division across flange length
set subFThk 5;               # sub-division across flange thickness
set subWLen 10;              # sub-division across web length
set subWThk 5;               # sub-division across web thickness
HSsection $braceFiberSecTag $matID $d $b $t $subWLen $subWThk $subFLen $subFThk
puts "HSSection defined";

# Brace torsional stiffness
set braceTorsTag 73;
set J4 6.15e8;
set GJ4 [expr $G*$J4];
uniaxialMaterial Elastic $braceTorsTag $GJ4;  # Define column torsional stiffness
section Aggregator $bracesecID $braceTorsTag T -section $braceFiberSecTag; # attach torsion and flexure

# Brace Parameters:
# 30 x 30 x 3 RHS
set bracesecID1 9;
set braceFiberSecTag1 10;
set d 30;                    # Overall section depth 30
set b 30;                    # Overall section width 30
set t 3;                     # Thickness 2.5
set subFLen 10;              # sub-division across flange length
set subFThk 5;               # sub-division across flange thickness
set subWLen 10;              # sub-division across web length
set subWThk 5;               # sub-division across web thickness
HSsection1 $braceFiberSecTag1 $matID $d $b $t $subWLen $subWThk $subFLen $subFThk
puts "HSSection1 defined";

# Brace torsional stiffness
set braceTorsTag1 75;
set J5 6.15e8;
set GJ5 [expr $G*$J5];
uniaxialMaterial Elastic $braceTorsTag1 $GJ5;  # Define column torsional stiffness
section Aggregator $bracesecID1 $braceTorsTag1 T -section $braceFiberSecTag1; # attach torsion and flexure

# ------------------------------------
# Define geometric transformation
# ------------------------------------
# Coordinate transformation
set ColTransfTag 10;
set Beam1TransfTag 20;
set BraceTransfTag 30;
geomTransf PDelta $ColTransfTag 0 0 1
geomTransf Linear $Beam1TransfTag 0 -1 0
geomTransf Corotational $BraceTransfTag 0 -1 0
set numintgrPtsCol 7;
set numintgrPtsBrace 7;

# ------------------------------------
# Define experimental elements
# ------------------------------------
# left and right columns
#expElement beamColumn 1 1 3 10 -site 1 -initStif 1889.0 0.0 0.0 -1416800.0 0.0 7543.57 0.0 0.0 0.0 0.0 6353846.15 0.0 -1416800.0
0.0 0.0 1416.8e6
#expElement beamColumn 1 1 3 10 -site 1 -initStif 405440 0 0 0 0 0 0 473.13 0 0 0 -711200 0 0 1885.9 0 2828840 0 0 0 0 6353846.15 0
0 0 0 2828840 0 1885.9 0 0 -711200 0 0 0 1066.8e6
```

```
#expElement beamColumn 1 1 7 $ColTransfTag -site 1 -initStif 405440 0 0 0 0 0 0 7543.57 0 0 0 -5657680 0 0 1885.9 0 1422400 0 0 0
0 6353846.15 0 0 0 0 1422400 0 1422400000 0 0 -5657680 0 0 0 5657680000
#expElement beamColumn 2 6 12 $ColTransfTag -site 2 -initStif 405440 0 0 0 0 0 0 7543.57 0 0 0 -5657680 0 0 1885.9 0 1422400 0 0
0 0 6353846.15 0 0 0 0 1422400 0 1422400000 0 0 -5657680 0 0 0 5657680000

expElement beamColumn 1 1 7 $ColTransfTag -site 1 -initStif [expr 986160] 0 0 0 0 0 0 [expr 124.19*0.99] 0 0 0 0 0 0 [expr
33.68*0.99] 0 0 0 0 0 0 [expr 26640000*0.99] 0 0 0 0 0 0 0 0 0 0 0 0 0 0
expElement beamColumn 2 6 12 $ColTransfTag -site 2 -initStif [expr 986160] 0 0 0 0 0 0 [expr 124.19*0.01] 0 0 0 0 0 0 [expr
33.68*0.01] 0 0 0 0 0 0 [expr 26640000*0.01] 0 0 0 0 0 0 0 0 0 0 0 0 0 0

# ------------------------------------
# Define numerical elements
# ------------------------------------
# FIRST STOREY
# Middle
element dispBeamColumn 3 5 11 $numintgrPtsCol $col2secID $ColTransfTag
element dispBeamColumn 4 2 8 $numintgrPtsCol $col2secID $ColTransfTag

# RHS
element dispBeamColumn 5 3 9 $numintgrPtsCol $col2secID $ColTransfTag
element dispBeamColumn 6 4 10 $numintgrPtsCol $col2secID $ColTransfTag

# SECOND STOREY
element dispBeamColumn 11 7 27 $numintgrPtsCol $col2secID $ColTransfTag
element dispBeamColumn 12 8 28 $numintgrPtsCol $col2secID $ColTransfTag
element dispBeamColumn 13 9 29 $numintgrPtsCol $col2secID $ColTransfTag

element dispBeamColumn 14 10 30 $numintgrPtsCol $col2secID $ColTransfTag
element dispBeamColumn 15 11 31 $numintgrPtsCol $col2secID $ColTransfTag
element dispBeamColumn 16 12 32 $numintgrPtsCol $col2secID $ColTransfTag

# THIRD STOREY
element dispBeamColumn 21 27 47 $numintgrPtsCol $col2secID $ColTransfTag
element dispBeamColumn 22 28 48 $numintgrPtsCol $col2secID $ColTransfTag
element dispBeamColumn 23 29 49 $numintgrPtsCol $col2secID $ColTransfTag

element dispBeamColumn 24 30 50 $numintgrPtsCol $col2secID $ColTransfTag
element dispBeamColumn 25 31 51 $numintgrPtsCol $col2secID $ColTransfTag
element dispBeamColumn 26 32 52 $numintgrPtsCol $col2secID $ColTransfTag


# Beams
element elasticBeamColumn 30 7 12 $Abeam $Ebeam $G $Jbeam $Iybeam $Izbeam $Beam1TransfTag
element elasticBeamColumn 31 8 11 $Abeam $Ebeam $G $Jbeam $Iybeam $Izbeam $Beam1TransfTag
element elasticBeamColumn 32 9 10 $Abeam $Ebeam $G $Jbeam $Iybeam $Izbeam $Beam1TransfTag

element elasticBeamColumn 33 7 8 $Abeam $Ebeam $G $Jbeam $Iybeam $Izbeam $Beam1TransfTag
element elasticBeamColumn 34 8 9 $Abeam $Ebeam $G $Jbeam $Iybeam $Izbeam $Beam1TransfTag
element elasticBeamColumn 35 10 11 $Abeam $Ebeam $G $Jbeam $Iybeam $Izbeam $Beam1TransfTag
element elasticBeamColumn 36 11 12 $Abeam $Ebeam $G $Jbeam $Iybeam $Izbeam $Beam1TransfTag

# SECOND STOREY
element elasticBeamColumn 40 27 32 $Abeam $Ebeam $G $Jbeam $Iybeam $Izbeam $Beam1TransfTag
element elasticBeamColumn 41 28 31 $Abeam $Ebeam $G $Jbeam $Iybeam $Izbeam $Beam1TransfTag
element elasticBeamColumn 42 29 30 $Abeam $Ebeam $G $Jbeam $Iybeam $Izbeam $Beam1TransfTag

element elasticBeamColumn 43 27 28 $Abeam $Ebeam $G $Jbeam $Iybeam $Izbeam $Beam1TransfTag
element elasticBeamColumn 44 28 29 $Abeam $Ebeam $G $Jbeam $Iybeam $Izbeam $Beam1TransfTag
element elasticBeamColumn 45 30 31 $Abeam $Ebeam $G $Jbeam $Iybeam $Izbeam $Beam1TransfTag
element elasticBeamColumn 46 31 32 $Abeam $Ebeam $G $Jbeam $Iybeam $Izbeam $Beam1TransfTag

# THIRD STOREY
element elasticBeamColumn 50 47 52 $Abeam $Ebeam $G $Jbeam $Iybeam $Izbeam $Beam1TransfTag
element elasticBeamColumn 51 48 51 $Abeam $Ebeam $G $Jbeam $Iybeam $Izbeam $Beam1TransfTag
element elasticBeamColumn 52 49 50 $Abeam $Ebeam $G $Jbeam $Iybeam $Izbeam $Beam1TransfTag

element elasticBeamColumn 53 47 48 $Abeam $Ebeam $G $Jbeam $Iybeam $Izbeam $Beam1TransfTag
element elasticBeamColumn 54 48 49 $Abeam $Ebeam $G $Jbeam $Iybeam $Izbeam $Beam1TransfTag
element elasticBeamColumn 55 50 51 $Abeam $Ebeam $G $Jbeam $Iybeam $Izbeam $Beam1TransfTag
element elasticBeamColumn 56 51 52 $Abeam $Ebeam $G $Jbeam $Iybeam $Izbeam $Beam1TransfTag

# Zero Length Elements
# Ground Floor
element zeroLength 500 3 113 -mat 7 7 7 -dir 1 2 3
element zeroLength 501 4 114 -mat 7 7 7 -dir 1 2 3

# First Floor Bottom
element zeroLength 502 9 119 -mat 7 7 7 -dir 1 2 3
```

```
element zeroLength 503 10 210 -mat 7 7 7 -dir 1 2 3

# First Floor Top
element zeroLength 504 7 311 -mat 7 7 7 -dir 1 2 3
element zeroLength 505 9 313 -mat 7 7 7 -dir 1 2 3
element zeroLength 506 10 314 -mat 7 7 7 -dir 1 2 3
element zeroLength 507 12 316 -mat 7 7 7 -dir 1 2 3

# Second Floor Bottom
element zeroLength 508 27 317 -mat 7 7 7 -dir 1 2 3
element zeroLength 509 29 319 -mat 7 7 7 -dir 1 2 3
element zeroLength 510 30 410 -mat 7 7 7 -dir 1 2 3
element zeroLength 511 32 412 -mat 7 7 7 -dir 1 2 3

# Second Floor Top
element zeroLength 512 27 511 -mat 7 7 7 -dir 1 2 3
element zeroLength 513 29 513 -mat 7 7 7 -dir 1 2 3
element zeroLength 514 30 514 -mat 7 7 7 -dir 1 2 3
element zeroLength 515 32 516 -mat 7 7 7 -dir 1 2 3

# Third Floor
element zeroLength 516 47 517 -mat 7 7 7 -dir 1 2 3
element zeroLength 517 49 519 -mat 7 7 7 -dir 1 2 3
element zeroLength 518 50 610 -mat 7 7 7 -dir 1 2 3
element zeroLength 519 52 612 -mat 7 7 7 -dir 1 2 3

# Brace members
# Two element braces
# FIRST STOREY
# RHS Bay
element dispBeamColumn 172 113 150 $numintgrPtsBrace $bracesecID1 $BraceTransfTag
element dispBeamColumn 173 150 151 $numintgrPtsBrace $bracesecID1 $BraceTransfTag
element dispBeamColumn 174 151 152 $numintgrPtsBrace $bracesecID1 $BraceTransfTag
element dispBeamColumn 175 152 210 $numintgrPtsBrace $bracesecID1 $BraceTransfTag

element dispBeamColumn 182 114 160 $numintgrPtsBrace $bracesecID1 $BraceTransfTag
element dispBeamColumn 183 160 151 $numintgrPtsBrace $bracesecID1 $BraceTransfTag
element dispBeamColumn 184 151 161 $numintgrPtsBrace $bracesecID1 $BraceTransfTag
element dispBeamColumn 185 161 119 $numintgrPtsBrace $bracesecID1 $BraceTransfTag

# SECOND STOREY
# LHS Bay
element dispBeamColumn 230 311 230 $numintgrPtsBrace $bracesecID $BraceTransfTag
element dispBeamColumn 231 230 231 $numintgrPtsBrace $bracesecID $BraceTransfTag
element dispBeamColumn 232 231 232 $numintgrPtsBrace $bracesecID $BraceTransfTag
element dispBeamColumn 233 232 412 $numintgrPtsBrace $bracesecID $BraceTransfTag

element dispBeamColumn 240 316 235 $numintgrPtsBrace $bracesecID $BraceTransfTag
element dispBeamColumn 241 235 231 $numintgrPtsBrace $bracesecID $BraceTransfTag
element dispBeamColumn 242 231 237 $numintgrPtsBrace $bracesecID $BraceTransfTag
element dispBeamColumn 243 237 317 $numintgrPtsBrace $bracesecID $BraceTransfTag

# RHS Bay
element dispBeamColumn 270 313 250 $numintgrPtsBrace $bracesecID $BraceTransfTag
element dispBeamColumn 271 250 251 $numintgrPtsBrace $bracesecID $BraceTransfTag
element dispBeamColumn 272 251 252 $numintgrPtsBrace $bracesecID $BraceTransfTag
element dispBeamColumn 273 252 410 $numintgrPtsBrace $bracesecID $BraceTransfTag

element dispBeamColumn 280 314 255 $numintgrPtsBrace $bracesecID $BraceTransfTag
element dispBeamColumn 281 255 251 $numintgrPtsBrace $bracesecID $BraceTransfTag
element dispBeamColumn 282 251 257 $numintgrPtsBrace $bracesecID $BraceTransfTag
element dispBeamColumn 283 257 319 $numintgrPtsBrace $bracesecID $BraceTransfTag

# THIRD STOREY
# LHS Bay
element dispBeamColumn 330 511 330 $numintgrPtsBrace $bracesecID $BraceTransfTag
element dispBeamColumn 331 330 331 $numintgrPtsBrace $bracesecID $BraceTransfTag
element dispBeamColumn 332 331 332 $numintgrPtsBrace $bracesecID $BraceTransfTag
element dispBeamColumn 333 332 612 $numintgrPtsBrace $bracesecID $BraceTransfTag

element dispBeamColumn 340 516 335 $numintgrPtsBrace $bracesecID $BraceTransfTag
element dispBeamColumn 341 335 331 $numintgrPtsBrace $bracesecID $BraceTransfTag
element dispBeamColumn 342 331 337 $numintgrPtsBrace $bracesecID $BraceTransfTag
element dispBeamColumn 343 337 517 $numintgrPtsBrace $bracesecID $BraceTransfTag

# RHS Bay
element dispBeamColumn 370 513 350 $numintgrPtsBrace $bracesecID $BraceTransfTag
element dispBeamColumn 371 350 351 $numintgrPtsBrace $bracesecID $BraceTransfTag
```

```
element dispBeamColumn 372 351 352 $numintgrPtsBrace $bracesecID $BraceTransfTag
element dispBeamColumn 373 352 610 $numintgrPtsBrace $bracesecID $BraceTransfTag

element dispBeamColumn 380 514 355 $numintgrPtsBrace $bracesecID $BraceTransfTag
element dispBeamColumn 381 355 351 $numintgrPtsBrace $bracesecID $BraceTransfTag
element dispBeamColumn 382 351 357 $numintgrPtsBrace $bracesecID $BraceTransfTag
element dispBeamColumn 383 357 519 $numintgrPtsBrace $bracesecID $BraceTransfTag

# ------------------------------------
# Define dynamic loads
# ------------------------------------
# set time series to be passed to uniform excitation
set dt 0.01
set scale 1.0
set accelSeries "Path -filePath Taiwan40.txt -dt $dt -factor [expr 9810*$scale]"

# create UniformExcitation load pattern
# pattern UniformExcitation $tag $dir
pattern UniformExcitation  2 1 -accel $accelSeries

# calculate the rayleigh damping factors for nodes & elements
set alphaM    1.282;              # D = alphaM*M Gives damping ratio 0.05
set betaK     0.0;                # D = betaK*Kcurrent
set betaKinit  0.0;               # D = beatKinit*Kinit
set betaKcomm  0.0;               # D = betaKcomm*KlastCommit

# set the rayleigh damping
rayleigh $alphaM $betaK $betaKinit $betaKcomm;

# ------------------------------------
# End of model generation
# ------------------------------------

# ------------------------------------
# Start of analysis generation
# ------------------------------------
# create the system of equations
system BandGeneral
# create the DOF numberer
numberer Plain
# create the constraint handler
constraints Plain
# create the convergence test
test FixedNumIter 5
#test NormDispIncr 1E-8 25
# create the integration scheme
integrator NewmarkHSFixedNumIter 0.5 0.25
#integrator NewmarkHSIncrReduct 0.5 0.25 0.8
#integrator HHTHSFixedNumIter 0.5
#integrator HHTHSIncrReduct 0.5 0.8
#integrator CollocationHSFixedNumIter 1.5
#integrator CollocationHSIncrReduct 1.5 0.8
#integrator AlphaOS 0.9
# create the solution algorithm
algorithm Newton
#algorithm Linear

# create the analysis object
analysis Transient
# ------------------------------------
# End of analysis generation
# ------------------------------------

# ------------------------------------
# Recorders
# ------------------------------------

# Record displacements at cantilever tip
recorder Node -file Data/RoofDispSS.out -time -node 47 -dof 1 disp;
recorder Node -file Data/RoofAccelSS.out -time -node 47 -dof 1 accel;

recorder Node -file Data/RoofDispFS.out -time -node 49 -dof 1 disp;
recorder Node -file Data/RoofAccelFS.out -time -node 49 -dof 1 accel;

recorder Node -file Data/RoofDispCentre8.out -time -node 48 -dof 1 2 3 disp;
recorder Node -file Data/RoofAccelCentre8.out -time -node 48 -dof 1 2 3 accel;

recorder Node -file Data/DBase.out -time -node 1 2 3 -dof 1 2 3 disp;
```

```
# Column Base Shear
recorder Node -file Data/RBase1.out -time -node 1 -dof 1 2 3 reaction;
recorder Node -file Data/RBase2.out -time -node 2 -dof 1 2 3 reaction;
recorder Node -file Data/RBase3.out -time -node 3 -dof 1 2 3 reaction;

recorder Node -file Data/RBase4.out -time -node 4 -dof 1 2 3 reaction;
recorder Node -file Data/RBase5.out -time -node 5 -dof 1 2 3 reaction;
recorder Node -file Data/RBase6.out -time -node 6 -dof 1 2 3 reaction;

recorder Node -file Data/ActuatorNodeF.out -time -node 7 -dof 1 2 3 4 5 6 reaction;
recorder Node -file Data/ActuatorNodeD.out -time -node 7 -dof 1 2 3 disp;

# Displacement for drift
recorder Node -file Data/DispSS1.out -time -node 7 -dof 1 2 3 disp;
recorder Node -file Data/DispFS1.out -time -node 12 -dof 1 2 3 disp;

recorder Node -file Data/DispSS2.out -time -node 27 -dof 1 2 3 disp;
recorder Node -file Data/DispFS2.out -time -node 32 -dof 1 2 3 disp;

# ------------------------------------
# Stiff Side Brace Data
# ------------------------------------
# Brace axial load
recorder Element -file Data/SSBrace2Ele1local.out -time -ele 132 localForce
recorder Element -file Data/SSBrace1Ele1local.out -time -ele 142 localForce
recorder Node -file Data/SSBrace1EndForce.out -time -node 116 -dof 1 2 3 reaction;
recorder Node -file Data/SSBrace2EndForce.out -time -node 111 -dof 1 2 3 reaction;
recorder Node -file Data/SSBrace1EndForce1.out -time -node 6 -dof 1 2 3 reaction;
recorder Node -file Data/SSBrace2EndForce1.out -time -node 1 -dof 1 2 3 reaction;

# Brace curvature
recorder Node -file Data/SSBrace1Curv.out -time -node 132 -dof 4 5 6 disp;
recorder Node -file Data/SSBrace2Curv.out -time -node 137 -dof 4 5 6 disp;

# Stress/Strain in braces
recorder Element -file Data/SSBr2sec7Top.out -time -ele 133 section $numintgrPtsBrace fiber 25 0 $matID stressStrain;
recorder Element -file Data/SSBr2sec1Top.out -time -ele 133 section 1 fiber 25 0 $matID  stressStrain;
recorder Element -file Data/SSBr2sec7Side.out -time -ele 133 section $numintgrPtsBrace fiber 0 25 $matID stressStrain;
recorder Element -file Data/SSBr2sec1Side.out -time -ele 133 section 1 fiber 0 25 $matID stressStrain;
recorder Element -file Data/SSBr1sec7Top.out -time -ele 143 section $numintgrPtsBrace fiber 25 0 $matID stressStrain;
recorder Element -file Data/SSBr1sec1Top.out -time -ele 143 section 1 fiber 25 0 $matID stressStrain;
recorder Element -file Data/SSBr1sec7Side.out -time -ele 143 section $numintgrPtsBrace fiber 0 25 $matID stressStrain;
recorder Element -file Data/SSBr1sec1Side.out -time -ele 143 section 1 fiber 0 25 $matID stressStrain;

# Gusset plate/brace end node
recorder Node -file Data/SSGussetNd.out -time -node 130 -dof 1 2 3 4 5 6 reaction;
recorder Node -file Data/SSGussetNd1.out -time -node 131 -dof 1 2 3 4 5 6 reaction;

# ------------------------------------
# Flexible Side Brace Data
# ------------------------------------

# Brace axial load
recorder Element -file Data/FSBrace2Ele1local.out -time -ele 172 localForce
recorder Element -file Data/FSBrace1Ele1local.out -time -ele 182 localForce

recorder Node -file Data/FSBrace1EndForce.out -time -node 113 -dof 1 2 3 reaction;
recorder Node -file Data/FSBrace2EndForce.out -time -node 114 -dof 1 2 3 reaction;


# Brace curvature
recorder Node -file Data/FSBrace1Curv.out -time -node 172 -dof 4 5 6 disp;
recorder Node -file Data/FSBrace2Curv.out -time -node 182 -dof 4 5 6 disp;

# Stress/Strain in Braces
recorder Element -file Data/FSBr2sec7Top.out -time -ele 173 section $numintgrPtsBrace fiber 25 0 $matID stressStrain; # Mid Brace
recorder Element -file Data/FSBr2sec1Top.out -time -ele 173 section 1 fiber 25 0 $matID stressStrain; # Brace End Stress

recorder Element -file Data/FSBr2sec7Side.out -time -ele 173 section $numintgrPtsBrace fiber 0 25 $matID stressStrain; # Mid
recorder Element -file Data/FSBr2sec1Side.out -time -ele 173 section 1 fiber 0 25 $matID stressStrain; # Brace End Stress
recorder Element -file Data/FSBr1sec7Top.out -time -ele 183 section $numintgrPtsBrace fiber 25 0 $matID stressStrain; # Mid Brace
recorder Element -file Data/FSBr1sec1Top.out -time -ele 183 section 1 fiber 25 0 $matID stressStrain; # Brace End Stress
recorder Element -file Data/FSBr1sec7Side.out -time -ele 183 section $numintgrPtsBrace fiber 0 25 $matID stressStrain; # Mid Brace
recorder Element -file Data/FSBr1sec1Side.out -time -ele 183 section 1 fiber 0 25 $matID stressStrain; # Brace End Stress

puts "Regular recorders defined" ;
expRecorder Control -file DataExp/Control_ctrlDsp.out -time -control 1 ctrlDisp
expRecorder Control -file DataExp/Control_ctrlVel.out -time -control 1 ctrlVel
```

```
expRecorder Control -file DataExp/Control_daqDsp.out  -time -control 1 daqDisp
expRecorder Control -file DataExp/Control_daqFrc.out  -time -control 1 daqForce

expRecorder Setup -file DataExp/Setup_trialDsp.out -time -setup 1 trialDisp
expRecorder Setup -file DataExp/Setup_trialVel.out -time -setup 1 trialVel
expRecorder Setup -file DataExp/Setup_trialAcc.out -time -setup 1 trialAccel
expRecorder Setup -file DataExp/Setup_outDsp.out -time -setup 1 outDisp
expRecorder Setup -file DataExp/Setup_outFrc.out -time -setup 1 outForce
expRecorder Setup -file DataExp/Setup_ctrlDsp.out -time -setup 1 ctrlDisp
expRecorder Setup -file DataExp/Setup_ctrlVel.out -time -setup 1 ctrlVel
expRecorder Setup -file DataExp/Setup_ctrlAcc.out -time -setup 1 ctrlAccel
expRecorder Setup -file DataExp/Setup_daqDsp.out -time -setup 1 daqDisp
expRecorder Setup -file DataExp/Setup_daqFrc.out -time -setup 1 daqForce

puts "expRecorders defined" ;

# ------------------------------------
# Stiff Side Brace Data 2nd Storey
# ------------------------------------

# Brace axial load
recorder Element -file Data1/SSBrace2Ele1local.out -time -ele 232 localForce
recorder Element -file Data1/SSBrace1Ele1local.out -time -ele 242 localForce

# Brace curvature
recorder Node -file Data1/SSBrace1Curv.out -time -node 232 -dof 4 5 6 disp;
recorder Node -file Data1/SSBrace2Curv.out -time -node 237 -dof 4 5 6 disp;

# Stress/Strain in braces
recorder Element -file Data1/SSBr2sec7Top.out -time -ele 233 section $numintgrPtsBrace fiber 25 0 $matID stressStrain;
recorder Element -file Data1/SSBr2sec1Top.out -time -ele 233 section 1 fiber 25 0 $matID stressStrain;
recorder Element -file Data1/SSBr2sec7Side.out -time -ele 233 section $numintgrPtsBrace fiber 0 25 $matID stressStrain;
recorder Element -file Data1/SSBr2sec1Side.out -time -ele 233 section 1 fiber 0 25 $matID stressStrain;
recorder Element -file Data1/SSBr1sec7Top.out -time -ele 243 section $numintgrPtsBrace fiber 25 0 $matID stressStrain;
recorder Element -file Data1/SSBr1sec1Top.out -time -ele 243 section 1 fiber 25 0 $matID stressStrain;
recorder Element -file Data1/SSBr1sec7Side.out -time -ele 243 section $numintgrPtsBrace fiber 0 25 $matID stressStrain;
recorder Element -file Data1/SSBr1sec1Side.out -time -ele 243 section 1 fiber 0 25 $matID stressStrain;

# ------------------------------------
# Flexible Side Brace Data 2nd Storey
# ------------------------------------

# Brace axial load
recorder Element -file Data1/FSBrace2Ele1local.out -time -ele 272 localForce
recorder Element -file Data1/FSBrace1Ele1local.out -time -ele 282 localForce

# Brace curvature
recorder Node -file Data1/FSBrace1Curv.out -time -node 272 -dof 4 5 6 disp;
recorder Node -file Data1/FSBrace2Curv.out -time -node 282 -dof 4 5 6 disp;

# Stress/Strain in Braces
recorder Element -file Data1/FSBr2sec7Top.out -time -ele 273 section $numintgrPtsBrace fiber 25 0 $matID stressStrain; # Mid Brace
recorder Element -file Data1/FSBr2sec1Top.out -time -ele 273 section 1 fiber 25 0 $matID stressStrain; # Brace End Stress
recorder Element -file Data1/FSBr2sec7Side.out -time -ele 273 section $numintgrPtsBrace fiber 0 25 $matID stressStrain; # Mid Brace
recorder Element -file Data1/FSBr2sec1Side.out -time -ele 273 section 1 fiber 0 25 $matID stressStrain; # Brace End Stress
recorder Element -file Data1/FSBr1sec7Top.out -time -ele 283 section $numintgrPtsBrace fiber 25 0 $matID stressStrain; # Mid Brace
recorder Element -file Data1/FSBr1sec1Top.out -time -ele 283 section 1 fiber 25 0 $matID stressStrain; # Brace End Stress
recorder Element -file Data1/FSBr1sec7Side.out -time -ele 283 section $numintgrPtsBrace fiber 0 25 $matID stressStrain; # Mid Brace
recorder Element -file Data1/FSBr1sec1Side.out -time -ele 283 section 1 fiber 0 25 $matID stressStrain; # Brace End Stress

# ------------------------------------
# Stiff Side Brace Data 3rd Storey
# ------------------------------------
# Brace axial load
recorder Element -file Data2/SSBrace2Ele1local.out -time -ele 332 localForce
recorder Element -file Data2/SSBrace1Ele1local.out -time -ele 342 localForce

# Brace curvature
recorder Node -file Data2/SSBrace1Curv.out -time -node 332 -dof 4 5 6 disp;
recorder Node -file Data2/SSBrace2Curv.out -time -node 337 -dof 4 5 6 disp;

# Stress/Strain in braces
recorder Element -file Data2/SSBr2sec7Top.out -time -ele 333 section $numintgrPtsBrace fiber 25 0 $matID stressStrain;
recorder Element -file Data2/SSBr2sec1Top.out -time -ele 333 section 1 fiber 25 0 $matID stressStrain;
recorder Element -file Data2/SSBr2sec7Side.out -time -ele 333 section $numintgrPtsBrace fiber 0 25 $matID stressStrain;
recorder Element -file Data2/SSBr2sec1Side.out -time -ele 333 section 1 fiber 0 25 $matID stressStrain;
recorder Element -file Data2/SSBr1sec7Top.out -time -ele 343 section $numintgrPtsBrace fiber 25 0 $matID stressStrain;
recorder Element -file Data2/SSBr1sec1Top.out -time -ele 343 section 1 fiber 25 0 $matID stressStrain;
```

```
recorder Element -file Data2/SSBr1sec7Side.out -time -ele 343 section $numintgrPtsBrace fiber 0 25 $matID stressStrain;
recorder Element -file Data2/SSBr1sec1Side.out -time -ele 343 section 1 fiber 0 25 $matID stressStrain;

# ------------------------------------
# Flexible Side Brace Data 3rd Storey
# ------------------------------------
# Brace axial load
recorder Element -file Data2/FSBrace2Ele1local.out -time -ele 372 localForce
recorder Element -file Data2/FSBrace1Ele1local.out -time -ele 382 localForce

# Brace curvature
recorder Node -file Data2/FSBrace1Curv.out -time -node 372 -dof 4 5 6 disp;
recorder Node -file Data2/FSBrace2Curv.out -time -node 382 -dof 4 5 6 disp;

# Stress/Strain in Braces
recorder Element -file Data2/FSBr2sec7Top.out -time -ele 373 section $numintgrPtsBrace fiber 25 0 $matID stressStrain; # Mid Brace
recorder Element -file Data2/FSBr2sec1Top.out -time -ele 373 section 1 fiber 25 0 $matID stressStrain; # Brace End Stress
recorder Element -file Data2/FSBr2sec7Side.out -time -ele 373 section $numintgrPtsBrace fiber 0 25 $matID stressStrain; # Mid Brace
recorder Element -file Data2/FSBr2sec1Side.out -time -ele 373 section 1 fiber 0 25 $matID stressStrain; # Brace End Stress
recorder Element -file Data2/FSBr1sec7Top.out -time -ele 383 section $numintgrPtsBrace fiber 25 0 $matID stressStrain; # Mid Brace
recorder Element -file Data2/FSBr1sec1Top.out -time -ele 383 section 1 fiber 25 0 $matID stressStrain; # Brace End Stress
recorder Element -file Data2/FSBr1sec7Side.out -time -ele 383 section $numintgrPtsBrace fiber 0 25 $matID stressStrain; # Mid Brace
recorder Element -file Data2/FSBr1sec1Side.out -time -ele 383 section 1 fiber 0 25 $matID stressStrain; # Brace End Stress

# ------------------------------
# Finally perform the analysis
# ------------------------------
# perform an eigenvalue analysis
set pi 3.14159265358979
set lambda [eigen -fullGenLapack 4]
puts "\nEigenvalues at start of transient:"
puts "lambda      omega      period"
foreach lambda $lambda {
   if {$lambda > 0.0} {
      set omega [expr pow($lambda,0.5)]
      set period [expr 2*$pi/pow($lambda,0.5)]
      puts "$lambda  $omega  $period"
   }
}

# open output file for writing
set outFileID [open Data/elapsedTime.txt w]
# perform the transient analysis
set tTot [time {
   for {set i 1} {$i < 4000} {incr i} {
      set t [time {analyze  1  [expr $dt/1.0]}]
      puts $outFileID $t
                  #puts "step $i"
   }
}]
puts "\nElapsed Time = $tTot \n"
# close the output file
close $outFileID

wipe
# --------------------------------
# End of analysis
# --------------------------------
```

Appendix C4 - Three Dimensional Concentrically Braced Frame OpenSees Model

```
# FileName: TestFrame_Local_3D.tcl
# Author: Daniel McCrum
# Email: mccrumdp@tcd.ie
# Last Altered: May, 2011.

# Description:
# This file contains the final numerical model of the three-
# storey concentrically braced torsionally unbalanced structure
# with varying

# Model Information:
# PA RATIO:                 2.0
# SLENDERNESS:              1.68
# LATERAL. TORS. FREQ.:     0.75
# MASS ECCENTRICITY:        0.15L
#
#          _____________________
#         |                     |        ^
#         |                     |        |
#         |                     |        | 2200mm
#         |                     |        |
#         |_____________________|        v
#         |                     |        ^
#         |                     |        |
#         |                     |        | 2200mm
#         |                     |        |
#         |                     |        v
#          _____________________
#         |                     |        ^
#         |                     |        |
#         |                     |        | 2500mm
#         |                     |        |
#         |                     |        v
#       XXX                   XXX
#
#          <--------------------------------->
#                  PA ratio dependent

# Units: N mm sec Mg
wipe all;
file mkdir Data;        # Create directory for general data
file mkdir Data1;       # Create directory for first storey data
file mkdir Data2;       # Create directory for second storey data

source HEsection1.tcl;
source HSsection1.tcl;
source HSsection.tcl;

# ------------------------------------
# Start of model generation
# ------------------------------------
# create ModelBuilder (with two-dimensions and 3 DOF/node)
model BasicBuilder -ndm 3 -ndf 6
# ------------------------------------
# Define geometry for model
# ------------------------------------

set Lcol1 2500;
set Lcol2 2200;
set Lbeam1 3300;                # Change for Plan Aspect Ratio
set Lbeam2 3300;                # Change for Plan Aspect Ratio

# nodal coords.
#           X                   Y                   Z
node 1  0                       0                   0
node 2  0                       0                   $Lbeam2
```

```
node 3  0                          0                          [expr $Lbeam2*2]
node 4  [expr $Lbeam1]             0                          [expr $Lbeam2*2]
node 5  [expr $Lbeam1]             0                          $Lbeam2
node 6  [expr $Lbeam1]             0                          0

# FIRST FLOOR
node 7  0                          $Lcol1                     0
node 8  0                          $Lcol1                     $Lbeam2
node 9  0                          $Lcol1                     [expr $Lbeam2*2]
node 10 [expr $Lbeam1]             $Lcol1                     [expr $Lbeam2*2]
node 11 [expr $Lbeam1]             $Lcol1                     $Lbeam2
node 12 [expr $Lbeam1]             $Lcol1                     0


# SECOND FLOOR
node 27 0                          [expr $Lcol1+$Lcol2]       0
node 28 0                          [expr $Lcol1+$Lcol2]       $Lbeam2
node 29 0                          [expr $Lcol1+$Lcol2]       [expr $Lbeam2*2]
node 30 [expr $Lbeam1]             [expr $Lcol1+$Lcol2]       [expr $Lbeam2*2]
node 31 [expr $Lbeam1]             [expr $Lcol1+$Lcol2]       $Lbeam2
node 32 [expr $Lbeam1]             [expr $Lcol1+$Lcol2]       0

# THIRD FLOOR
node 47 0                          [expr $Lcol1+($Lcol2*2)]   0
node 48 0                          [expr $Lcol1+($Lcol2*2)]   $Lbeam2
node 49 0                          [expr $Lcol1+($Lcol2*2)]   [expr $Lbeam2*2]
node 50 [expr $Lbeam1]             [expr $Lcol1+($Lcol2*2)]   [expr $Lbeam2*2]
node 51 [expr $Lbeam1]             [expr $Lcol1+($Lcol2*2)]   $Lbeam2
node 52 [expr $Lbeam1]             [expr $Lcol1+($Lcol2*2)]   0

# Duplicate nodes for brace end zerolength sections
# FIRST STOREY
node 111 0                         0                          0
node 113 0                         0                          [expr $Lbeam2*2]
node 114 [expr $Lbeam1]            0                          [expr $Lbeam2*2]
node 116 $Lbeam1                   0                          0

node 117 0                         $Lcol1                     0
node 119 0                         $Lcol1                     [expr $Lbeam2*2]
node 210 [expr $Lbeam1]            $Lcol1                     [expr $Lbeam2*2]
node 212 [expr $Lbeam1]            $Lcol1                     0

# SECOND STOREY
node 311 0                         $Lcol1                     0
node 313 0                         $Lcol1                     [expr $Lbeam2*2]
node 314 [expr $Lbeam1]            $Lcol1                     [expr $Lbeam2*2]
node 316 [expr $Lbeam1]            $Lcol1                     0

node 317 0                         [expr $Lcol1+$Lcol2]       0
node 319 0                         [expr $Lcol1+$Lcol2]       [expr $Lbeam2*2]
node 410 [expr $Lbeam1]            [expr $Lcol1+$Lcol2]       [expr $Lbeam2*2]
node 412 [expr $Lbeam1]            [expr $Lcol1+$Lcol2]       0

# THIRD STOREY
node 511 0                         [expr $Lcol1+$Lcol2]       0
node 513 0                         [expr $Lcol1+$Lcol2]       [expr $Lbeam2*2]
node 514 [expr $Lbeam1]            [expr $Lcol1+$Lcol2]       [expr $Lbeam2*2]
node 516 [expr $Lbeam1]            [expr $Lcol1+$Lcol2]       0

node 517 0                         [expr $Lcol1+($Lcol2*2)]   0
node 519 0                         [expr $Lcol1+($Lcol2*2)]   [expr $Lbeam2*2]
node 610 [expr $Lbeam1]            [expr $Lcol1+($Lcol2*2)]   [expr $Lbeam2*2]
node 612 [expr $Lbeam1]            [expr $Lcol1+($Lcol2*2)]   0

# Brace imperfection nodes 0.1% out-of-straight at mid-length
set delta1 4;
set delta2 6;
# FIRST STOREY
# LHS Brace Members
node 130  [expr ($Lbeam1/10)]              [expr($Lcol1/10)]                0.0
node 131  [expr ($Lbeam1/10)+(((($Lbeam1/2)-($Lbeam1/10))/2)-$delta1]   [expr ($Lcol1/10)+(((($Lcol1/2)-($Lcol1/10))/2)+$delta1]
          [expr $delta2]
node 132  [expr (2*$Lbeam1/4)-$delta2]     [expr (2*$Lcol1/4)+$delta2]      0.0
node 133  [expr ($Lbeam1/2)+(((($Lbeam1/2)-($Lbeam1/10))/2)-$delta1]    [expr ($Lcol1/2)+(((($Lcol1/2)-($Lcol1/10))/2)+$delta1]
          [expr $delta2]
node 134  [expr $Lbeam1-($Lbeam1/10)]      [expr $Lcol1-($Lcol1/10)]        0.0

node 140  [expr $Lbeam1-($Lbeam1/10)]                [expr ($Lcol1/10)]                    0.0
```

```
node 141  [expr ($Lbeam1/2)+(($Lbeam1/2)-($Lbeam1/10))/2)-$delta1]    [expr ($Lcol1/10)+(($Lcol1/2)-($Lcol1/10))/2)+$delta1]
          [expr $delta2]
node 142  [expr ($Lbeam1/10)+(($Lbeam1/2)-($Lbeam1/10))/2)-$delta1]   [expr ($Lcol1/2)+(($Lcol1/2)-($Lcol1/10))/2)+$delta1]
          [expr $delta2]
node 143  [expr ($Lbeam1/10)]                    [expr $Lcol1-($Lcol1/10)]                    0.0

# RHS Brace Members
node 150  [expr ($Lbeam1/10)]                    [expr ($Lcol1/10)]                           [expr $Lbeam2*2]
node 151  [expr ($Lbeam1/10)+(($Lbeam1/2)-($Lbeam1/10))/2)-$delta1]   [expr ($Lcol1/10)+(($Lcol1/2)-($Lcol1/10))/2)+$delta1]
          [expr $delta1+$Lbeam2*2]
node 152  [expr (2*$Lbeam1/4)-$delta2]           [expr (2*$Lcol1/4)+$delta2]                  [expr $delta2+$Lbeam2*2]
node 153  [expr ($Lbeam1/2)+(($Lbeam1/2)-($Lbeam1/10))/2)-$delta1]    [expr ($Lcol1/2)+(($Lcol1/2)-($Lcol1/10))/2)+$delta1]
          [expr $delta1+$Lbeam2*2]
node 154  [expr $Lbeam1-($Lbeam1/10)]            [expr $Lcol1-($Lcol1/10)]                    [expr $Lbeam2*2]

node 160  [expr $Lbeam1-($Lbeam1/10)]            [expr ($Lcol1/10)]                           [expr $Lbeam2*2]
node 161  [expr ($Lbeam1/2)+(($Lbeam1/2)-($Lbeam1/10))/2)-$delta1]    [expr ($Lcol1/10)+(($Lcol1/2)-($Lcol1/10))/2)+$delta1]
          [expr $delta2+$Lbeam2*2]
node 162  [expr ($Lbeam1/10)+(($Lbeam1/2)-($Lbeam1/10))/2)-$delta1]   [expr ($Lcol1/2)+(($Lcol1/2)-($Lcol1/10))/2)+$delta1]
          [expr $delta2+$Lbeam2*2]
node 163  [expr ($Lbeam1/10)]                    [expr $Lcol1-($Lcol1/10)]                    [expr $Lbeam2*2]

# SECOND STOREY
# LHS Brace Members
node 230  [expr ($Lbeam1/10)]                    [expr $Lcol1+($Lcol2/10)]                    0.0
node 231  [expr ($Lbeam1/10)+(($Lbeam1/2)-($Lbeam1/10))/2)-$delta1]   [expr $Lcol1+($Lcol2/10)+(($Lcol2/2)-
($Lcol2/10))/2)+$delta1]          [expr $delta2]
node 232  [expr (2*$Lbeam1/4)-$delta2]           [expr $Lcol1+(2*$Lcol2/4)+$delta2]           0.0
node 233  [expr ($Lbeam1/2)+(($Lbeam1/2)-($Lbeam1/10))/2)-$delta1]    [expr $Lcol1+($Lcol2/2)+(($Lcol2/2)-
($Lcol2/10))/2)+$delta1]          [expr $delta2]
node 234  [expr $Lbeam1-($Lbeam1/10)]            [expr $Lcol1+$Lcol2-($Lcol2/10)]             0.0

node 240  [expr $Lbeam1-($Lbeam1/10)]            [expr $Lcol1+($Lcol2/10)]                    0.0
node 241  [expr ($Lbeam1/2)+(($Lbeam1/2)-($Lbeam1/10))/2)-$delta1]    [expr $Lcol1+($Lcol2/10)+(($Lcol2/2)-
($Lcol2/10))/2)+$delta1]          [expr $delta2]
node 242  [expr ($Lbeam1/10)+(($Lbeam1/2)-($Lbeam1/10))/2)-$delta1]   [expr $Lcol1+($Lcol2/2)+(($Lcol2/2)-
($Lcol2/10))/2)+$delta1]          [expr $delta2]
node 243  [expr ($Lbeam1/10)]                    [expr $Lcol1+$Lcol2-($Lcol2/10)]             0.0

# RHS Brace Members
node 250  [expr ($Lbeam1/10)]                    [expr $Lcol1+($Lcol2/10)]                    [expr $Lbeam2*2]
node 251  [expr ($Lbeam1/10)+(($Lbeam1/2)-($Lbeam1/10))/2)-$delta1]   [expr $Lcol1+($Lcol2/10)+(($Lcol2/2)-
($Lcol2/10))/2)+$delta1]          [expr $delta1+$Lbeam2*2]
node 252  [expr (2*$Lbeam1/4)-$delta2]           [expr $Lcol1+(2*$Lcol2/4)+$delta2]           [expr $delta2+$Lbeam2*2]
node 253  [expr ($Lbeam1/2)+(($Lbeam1/2)-($Lbeam1/10))/2)-$delta1]    [expr $Lcol1+($Lcol2/2)+(($Lcol2/2)-
($Lcol2/10))/2)+$delta1]          [expr $delta1+$Lbeam2*2]
node 254  [expr $Lbeam1-($Lbeam1/10)]            [expr $Lcol1+$Lcol2-($Lcol2/10)]             [expr $Lbeam2*2]

node 260  [expr $Lbeam1-($Lbeam1/10)]            [expr $Lcol1+($Lcol2/10)]                    [expr $Lbeam2*2]
node 261  [expr ($Lbeam1/2)+(($Lbeam1/2)-($Lbeam1/10))/2)-$delta1]    [expr $Lcol1+($Lcol2/10)+(($Lcol2/2)-
($Lcol2/10))/2)+$delta1]          [expr $delta2+$Lbeam2*2]
node 262  [expr ($Lbeam1/10)+(($Lbeam1/2)-($Lbeam1/10))/2)-$delta1]   [expr $Lcol1+($Lcol2/2)+(($Lcol2/2)-
($Lcol2/10))/2)+$delta1]          [expr $delta2+$Lbeam2*2]
node 263  [expr ($Lbeam1/10)]                    [expr $Lcol1+$Lcol2-($Lcol2/10)]             [expr $Lbeam2*2]

# THIRD STOREY
# LHS Brace Members
node 330  [expr ($Lbeam1/10)]                    [expr ($Lcol1+$Lcol2)+($Lcol2/10)]           0.0
node 331  [expr ($Lbeam1/10)+(($Lbeam1/2)-($Lbeam1/10))/2)-$delta1]   [expr ($Lcol1+$Lcol2)+($Lcol2/10)+(($Lcol2/2)-
($Lcol2/10))/2)+$delta1]          [expr $delta2]
node 332  [expr (2*$Lbeam1/4)-$delta2]           [expr ($Lcol1+$Lcol2)+(2*$Lcol2/4)+$delta2]  0.0
node 333  [expr ($Lbeam1/2)+(($Lbeam1/2)-($Lbeam1/10))/2)-$delta1]    [expr ($Lcol1+$Lcol2)+($Lcol2/2)+(($Lcol2/2)-
($Lcol2/10))/2)+$delta1]          [expr $delta2]
node 334  [expr $Lbeam1-($Lbeam1/10)]            [expr ($Lcol1+$Lcol2)+$Lcol2-($Lcol2/10)]    0.0

node 340  [expr $Lbeam1-($Lbeam1/10)]            [expr ($Lcol1+$Lcol2)+($Lcol2/10)]           0.0
node 341  [expr ($Lbeam1/2)+(($Lbeam1/2)-($Lbeam1/10))/2)-$delta1]    [expr ($Lcol1+$Lcol2)+($Lcol2/10)+(($Lcol2/2)-
($Lcol2/10))/2)+$delta1]          [expr $delta2]
node 342  [expr ($Lbeam1/10)+(($Lbeam1/2)-($Lbeam1/10))/2)-$delta1]   [expr ($Lcol1+$Lcol2)+($Lcol2/2)+(($Lcol2/2)-
($Lcol2/10))/2)+$delta1]          [expr $delta2]
node 343  [expr ($Lbeam1/10)]              [expr ($Lcol1+$Lcol2)+$Lcol2-($Lcol2/10)]        0.0

# RHS Brace Members
node 350  [expr ($Lbeam1/10)]              [expr ($Lcol1+$Lcol2)+($Lcol2/10)]        [expr $Lbeam2*2]
node 351  [expr ($Lbeam1/10)+(($Lbeam1/2)-($Lbeam1/10))/2)-$delta1]   [expr ($Lcol1+$Lcol2)+($Lcol2/10)+(($Lcol2/2)-
($Lcol2/10))/2)+$delta1]          [expr $delta1+$Lbeam2*2]
node 352  [expr (2*$Lbeam1/4)-$delta2]     [expr ($Lcol1+$Lcol2)+(2*$Lcol2/4)+$delta2]       [expr $delta2+$Lbeam2*2]
```

```
node 353  [expr ($Lbeam1/2)+(((($Lbeam1/2)-($Lbeam1/10))/2)-$delta1]  [expr ($Lcol1+$Lcol2)+($Lcol2/2)+(((($Lcol2/2)-
($Lcol2/10))/2)+$delta1]  [expr $delta1+$Lbeam2*2]
node 354  [expr $Lbeam1-($Lbeam1/10)]  [expr ($Lcol1+$Lcol2)+$Lcol2-($Lcol2/10)]  [expr $Lbeam2*2]

node 360  [expr $Lbeam1-($Lbeam1/10)]  [expr ($Lcol1+$Lcol2)+($Lcol2/10)]  [expr $Lbeam2*2]
node 361  [expr ($Lbeam1/2)+(((($Lbeam1/2)-($Lbeam1/10))/2)-$delta1]  [expr ($Lcol1+$Lcol2)+($Lcol2/10)+(((($Lcol2/2)-
($Lcol2/10))/2)+$delta1]  [expr $delta2+$Lbeam2*2]
node 362  [expr ($Lbeam1/10)+(((($Lbeam1/2)-($Lbeam1/10))/2)-$delta1]  [expr ($Lcol1+$Lcol2)+($Lcol2/2)+(((($Lcol2/2)-
($Lcol2/10))/2)+$delta1]  [expr $delta2+$Lbeam2*2]
node 363  [expr ($Lbeam1/10)]  [expr ($Lcol1+$Lcol2)+$Lcol2-($Lcol2/10)]  [expr $Lbeam2*2]

# ------------------------------------
# Define masses
# ------------------------------------
set massTotal1 86385;        # Mass in Mg
set massTotal2 43192;
set massTotal3 21596;

# Level of mass eccentricity
set eccmult1 0.53333333;     # Mass eccentricity factor for LHS Frame
set eccmult2 0.23333333;     # Mass eccentricity factor for Centre Frame
set eccmult3 0.23333333;     # Mass eccentricity factor for RHS Frame

# lateral torsional frequency ratio multiplier
set factor1 1.981;           # for lateral torsional frequency ratio of 0.75

# Nodal masses
# FIRST FLOOR
mass 7 [expr $massTotal1*0.5*$eccmult1*$factor1/9810] 0. [expr $massTotal1*0.5*$eccmult1*$factor1/9810] 1.0e-9 1.0e-9 1.0e-9;
mass 8 [expr $massTotal1*0.5*$eccmult2*$factor1/9810] 0. [expr $massTotal1*0.5*$eccmult2*$factor1/9810] 1.0e-9 1.0e-9 1.0e-9;
mass 9 [expr $massTotal1*0.5*$eccmult3*$factor1/9810] 0. [expr $massTotal1*0.5*$eccmult3*$factor1/9810] 1.0e-9 1.0e-9 1.0e-9;
mass 10 [expr $massTotal1*0.5*$eccmult3*$factor1/9810] 0. [expr $massTotal1*0.5*$eccmult3*$factor1/9810] 1.0e-9 1.0e-9 1.0e-9;
mass 11 [expr $massTotal1*0.5*$eccmult2*$factor1/9810] 0. [expr $massTotal1*0.5*$eccmult2*$factor1/9810] 1.0e-9 1.0e-9 1.0e-9;
mass 12 [expr $massTotal1*0.5*$eccmult1*$factor1/9810] 0. [expr $massTotal1*0.5*$eccmult1*$factor1/9810] 1.0e-9 1.0e-9 1.0e-9;

# SECOND FLOOR
mass 27 [expr $massTotal2*0.5*$eccmult1*$factor1/9810] 0. [expr $massTotal2*0.5*$eccmult1*$factor1/9810] 1.0e-9 1.0e-9 1.0e-9;
mass 28 [expr $massTotal2*0.5*$eccmult2*$factor1/9810] 0. [expr $massTotal2*0.5*$eccmult2*$factor1/9810] 1.0e-9 1.0e-9 1.0e-9;
mass 29 [expr $massTotal2*0.5*$eccmult3*$factor1/9810] 0. [expr $massTotal2*0.5*$eccmult3*$factor1/9810] 1.0e-9 1.0e-9 1.0e-9;
mass 30 [expr $massTotal2*0.5*$eccmult3*$factor1/9810] 0. [expr $massTotal2*0.5*$eccmult3*$factor1/9810] 1.0e-9 1.0e-9 1.0e-9;
mass 31 [expr $massTotal2*0.5*$eccmult2*$factor1/9810] 0. [expr $massTotal2*0.5*$eccmult2*$factor1/9810] 1.0e-9 1.0e-9 1.0e-9;
mass 32 [expr $massTotal2*0.5*$eccmult1*$factor1/9810] 0. [expr $massTotal2*0.5*$eccmult1*$factor1/9810] 1.0e-9 1.0e-9 1.0e-9;

# THIRD FLOOR
mass 47 [expr $massTotal3*0.5*$eccmult1*$factor1/9810] 0. [expr $massTotal3*0.5*$eccmult1*$factor1/9810] 1.0e-9 1.0e-9 1.0e-9;
mass 48 [expr $massTotal3*0.5*$eccmult2*$factor1/9810] 0. [expr $massTotal3*0.5*$eccmult2*$factor1/9810] 1.0e-9 1.0e-9 1.0e-9;
mass 49 [expr $massTotal3*0.5*$eccmult3*$factor1/9810] 0. [expr $massTotal3*0.5*$eccmult3*$factor1/9810] 1.0e-9 1.0e-9 1.0e-9;
mass 50 [expr $massTotal3*0.5*$eccmult3*$factor1/9810] 0. [expr $massTotal3*0.5*$eccmult3*$factor1/9810] 1.0e-9 1.0e-9 1.0e-9;
mass 51 [expr $massTotal3*0.5*$eccmult2*$factor1/9810] 0. [expr $massTotal3*0.5*$eccmult2*$factor1/9810] 1.0e-9 1.0e-9 1.0e-9;
mass 52 [expr $massTotal3*0.5*$eccmult1*$factor1/9810] 0. [expr $massTotal3*0.5*$eccmult1*$factor1/9810] 1.0e-9 1.0e-9 1.0e-9;

# ------------------------------------
# Define the boundary conditions
# ------------------------------------
# fix $tag $DX $DY $DZ $RX $RY $RZ
fix 1   1 1 1 0 1 0
fix 6   1 1 1 0 1 0

fix 2   1 1 1 0 1 0
fix 5   1 1 1 0 1 0

fix 3   1 1 1 0 1 0
fix 4   1 1 1 0 1 0


# Zero Length Elements
# Ground Floor
equalDOF 1 111 1 2 3 5
equalDOF 6 116 1 2 3 5

equalDOF 3 113 1 2 3 5
equalDOF 4 114 1 2 3 5

# First Floor Bottom
equalDOF 7 117 1 2 3 5
equalDOF 12 212 1 2 3 5

equalDOF 9 119 1 2 3 5
```

```
equalDOF 10 210 1 2 3 5

# First Floor Top
equalDOF 7 311 1 2 3 5
equalDOF 9 313 1 2 3 5
equalDOF 10 314 1 2 3 5
equalDOF 12 316 1 2 3 5
# Second Floor Bottom
equalDOF 27 317 1 2 3 5
equalDOF 29 319 1 2 3 5
equalDOF 30 410 1 2 3 5
equalDOF 32 412 1 2 3 5

# Second Floor Top
equalDOF 27 511 1 2 3 5
equalDOF 29 513 1 2 3 5
equalDOF 30 514 1 2 3 5
equalDOF 32 516 1 2 3 5

# Third Floor
equalDOF 47 517 1 2 3 5
equalDOF 49 519 1 2 3 5
equalDOF 50 610 1 2 3 5
equalDOF 52 612 1 2 3 5

# ------------------------------------
# Define materials
# ------------------------------------
set matID 1;
set steelTag 2;
set matStiff 3;
# uniaxialMaterial Steel02 $matTag $Fy $E $b $R0 $cR1 $cR2 $a1 $a2 $a3 $a4
uniaxialMaterial Steel02 $matID 235 210000 0.03 18.5 0.925 0.15 0.0 1.0 0.0 1.0
uniaxialMaterial Steel02 $steelTag 244.13 159290 0.03 18.5 0.925 0.15 -0.045 1.0 0.045 1.0
uniaxialMaterial Elastic $matStiff 1000000

set E 210e3;
set poisson 0.3;
set G [expr $E/([expr 2*(1+$poisson)])];      # Torsional Stiffness

# ------------------------------------
# Define section parameters
# ------------------------------------
# Column Parameters:
# 203 UC 46
set col2secID 20;
set col2FiberSecTag 21;
set d 203;                    # Overall section depth
set b 203;                    # Overall section width
set t 7.2;                    # Web thickness
set T 11;                     # Flange thickness
set dw [expr $d - 2*$T];      # Depth of web
set y [expr $d/2];
set subFLen 10;               # sub-division across flange length
set subFThk 5;                # sub-division across flange thickness
set subWLen 10;               # sub-division across web length
set subWThk 5;                # sub-division across web thickness
HEsection1 $col2FiberSecTag $matID $d $b $dw $t $subWLen $subWThk $subFLen $subFThk
puts "HESection1 defined";

# column torsional stiffness
set col2TorsTag 79;
set J9 8070000;
set GJ9 [expr $G*$J9];
uniaxialMaterial Elastic $col2TorsTag $GJ9; # Define column torsional stiffness
section Aggregator $col2secID $col2TorsTag T -section $col2FiberSecTag; # attach torsion and flexure
# Beam Parameters:
# 305x165x40UB Beam
set Ebeam 210000;
set Abeam 5130;
set Izbeam 6740e4;
set Iybeam 8503e4;
set Jbeam 47.2e4;

# Brace Parameters:
# 30 x 30 x 3 RHS
set bracesecID 7;
set braceFiberSecTag 8;
```

```
set d 30;                    # Overall section depth 30
set b 30;                    # Overall section width 30
set t 3;                     # Thickness 2.5
set subFLen 10;              # sub-division across flange length
set subFThk 5;               # sub-division across flange thickness
set subWLen 10;              # sub-division across web length
set subWThk 5;               # sub-division across web thickness
HSsection $braceFiberSecTag $steelTag $d $b $t $subWLen $subWThk $subFLen $subFThk
puts "HSSection defined";

# Brace torsional stiffness
set braceTorsTag 73;
set J4 6.15e8;
set GJ4 [expr $G*$J4];
uniaxialMaterial Elastic $braceTorsTag $GJ4;  # Define column torsional stiffness
section Aggregator $bracesecID $braceTorsTag T -section $braceFiberSecTag; # attach torsion and flexure

# Brace Parameters:
# 30 x 30 x 3 RHS
set bracesecID1 9;
set braceFiberSecTag1 10;
set d 30;                    # Overall section depth 30
set b 30;                    # Overall section width 30
set t 3;                     # Thickness 2.5
set subFLen 10;              # sub-division across flange length
set subFThk 5;               # sub-division across flange thickness
set subWLen 10;              # sub-division across web length
set subWThk 5;               # sub-division across web thickness
HSsection1 $braceFiberSecTag1 $steelTag $d $b $t $subWLen $subWThk $subFLen $subFThk
puts "HSSection1 defined";

# Brace torsional stiffness
set braceTorsTag1 75;
set J5 6.15e8;
set GJ5 [expr $G*$J5];
uniaxialMaterial Elastic $braceTorsTag1 $GJ5;  # Define column torsional stiffness
section Aggregator $bracesecID1 $braceTorsTag1 T -section $braceFiberSecTag1; # attach torsion and flexure

# ------------------------------------
# Define geometric transformation
# ------------------------------------
# Coordinate transformation
set ColTransfTag 10;
set Beam1TransfTag 20;
set BraceTransfTag 30;
geomTransf PDelta $ColTransfTag 0 0 1
geomTransf Linear $Beam1TransfTag 0 -1 0
geomTransf Corotational $BraceTransfTag 0 -1 0
set numintgrPtsCol 7;
set numintgrPtsBrace 7;

# ------------------------------------
# Define numerical elements
# ------------------------------------
# COLUMNS
# FIRST STOREY
# LHS
element nonlinearBeamColumn 1 1 7 $numintgrPtsCol $col2secID $ColTransfTag
element nonlinearBeamColumn 2 6 12 $numintgrPtsCol $col2secID $ColTransfTag

# Middle
element nonlinearBeamColumn 8 5 11 $numintgrPtsCol $col2secID $ColTransfTag
element nonlinearBeamColumn 9 2 8 $numintgrPtsCol $col2secID $ColTransfTag

# RHS
element nonlinearBeamColumn 10 3 9 $numintgrPtsCol $col2secID $ColTransfTag
element nonlinearBeamColumn 11 4 10 $numintgrPtsCol $col2secID $ColTransfTag

# SECOND STOREY
element nonlinearBeamColumn 21 7 27 $numintgrPtsCol $col2secID $ColTransfTag
element nonlinearBeamColumn 22 8 28 $numintgrPtsCol $col2secID $ColTransfTag
element nonlinearBeamColumn 23 9 29 $numintgrPtsCol $col2secID $ColTransfTag

element nonlinearBeamColumn 24 10 30 $numintgrPtsCol $col2secID $ColTransfTag
element nonlinearBeamColumn 25 11 31 $numintgrPtsCol $col2secID $ColTransfTag
element nonlinearBeamColumn 26 12 32 $numintgrPtsCol $col2secID $ColTransfTag

# THIRD STOREY
```

```
element nonlinearBeamColumn 31 27 47 $numintgrPtsCol $col2secID $ColTransfTag
element nonlinearBeamColumn 32 28 48 $numintgrPtsCol $col2secID $ColTransfTag
element nonlinearBeamColumn 33 29 49 $numintgrPtsCol $col2secID $ColTransfTag

element nonlinearBeamColumn 34 30 50 $numintgrPtsCol $col2secID $ColTransfTag
element nonlinearBeamColumn 35 31 51 $numintgrPtsCol $col2secID $ColTransfTag
element nonlinearBeamColumn 36 32 52 $numintgrPtsCol $col2secID $ColTransfTag


# BEAMS
# FIRST STOREY
element elasticBeamColumn 50 7 12 $Abeam $Ebeam $G $Jbeam $Iybeam $Izbeam $Beam1TransfTag
element elasticBeamColumn 51 8 11 $Abeam $Ebeam $G $Jbeam $Iybeam $Izbeam $Beam1TransfTag
element elasticBeamColumn 52 9 10 $Abeam $Ebeam $G $Jbeam $Iybeam $Izbeam $Beam1TransfTag

element elasticBeamColumn 53 7 8 $Abeam $Ebeam $G $Jbeam $Iybeam $Izbeam $Beam1TransfTag
element elasticBeamColumn 54 8 9 $Abeam $Ebeam $G $Jbeam $Iybeam $Izbeam $Beam1TransfTag
element elasticBeamColumn 55 10 11 $Abeam $Ebeam $G $Jbeam $Iybeam $Izbeam $Beam1TransfTag
element elasticBeamColumn 56 11 12 $Abeam $Ebeam $G $Jbeam $Iybeam $Izbeam $Beam1TransfTag

# SECOND STOREY
element elasticBeamColumn 60 27 32 $Abeam $Ebeam $G $Jbeam $Iybeam $Izbeam $Beam1TransfTag
element elasticBeamColumn 61 28 31 $Abeam $Ebeam $G $Jbeam $Iybeam $Izbeam $Beam1TransfTag
element elasticBeamColumn 62 29 30 $Abeam $Ebeam $G $Jbeam $Iybeam $Izbeam $Beam1TransfTag

element elasticBeamColumn 63 27 28 $Abeam $Ebeam $G $Jbeam $Iybeam $Izbeam $Beam1TransfTag
element elasticBeamColumn 64 28 29 $Abeam $Ebeam $G $Jbeam $Iybeam $Izbeam $Beam1TransfTag
element elasticBeamColumn 65 30 31 $Abeam $Ebeam $G $Jbeam $Iybeam $Izbeam $Beam1TransfTag
element elasticBeamColumn 66 31 32 $Abeam $Ebeam $G $Jbeam $Iybeam $Izbeam $Beam1TransfTag

# THIRD STOREY
element elasticBeamColumn 70 47 52 $Abeam $Ebeam $G $Jbeam $Iybeam $Izbeam $Beam1TransfTag
element elasticBeamColumn 71 48 51 $Abeam $Ebeam $G $Jbeam $Iybeam $Izbeam $Beam1TransfTag
element elasticBeamColumn 72 49 50 $Abeam $Ebeam $G $Jbeam $Iybeam $Izbeam $Beam1TransfTag

element elasticBeamColumn 73 47 48 $Abeam $Ebeam $G $Jbeam $Iybeam $Izbeam $Beam1TransfTag
element elasticBeamColumn 74 48 49 $Abeam $Ebeam $G $Jbeam $Iybeam $Izbeam $Beam1TransfTag
element elasticBeamColumn 75 50 51 $Abeam $Ebeam $G $Jbeam $Iybeam $Izbeam $Beam1TransfTag
element elasticBeamColumn 76 51 52 $Abeam $Ebeam $G $Jbeam $Iybeam $Izbeam $Beam1TransfTag

# Brace members
# Two element braces
# FIRST STOREY
# LHS Bay
element elasticBeamColumn 151 111 130 $Abeam 700000 $G $Jbeam $Iybeam $Izbeam $Beam1TransfTag
element nonlinearBeamColumn 152 130 131 $numintgrPtsBrace $bracesecID1 $BraceTransfTag
element nonlinearBeamColumn 153 131 132 $numintgrPtsBrace $bracesecID1 $BraceTransfTag
element nonlinearBeamColumn 154 132 133 $numintgrPtsBrace $bracesecID1 $BraceTransfTag
element nonlinearBeamColumn 155 133 134 $numintgrPtsBrace $bracesecID1 $BraceTransfTag
element elasticBeamColumn 156 134 212 $Abeam 700000 $G $Jbeam $Iybeam $Izbeam $Beam1TransfTag

element elasticBeamColumn 161 116 140 $Abeam 700000 $G $Jbeam $Iybeam $Izbeam $Beam1TransfTag
element nonlinearBeamColumn 162 140 141 $numintgrPtsBrace $bracesecID1 $BraceTransfTag
element nonlinearBeamColumn 163 141 132 $numintgrPtsBrace $bracesecID1 $BraceTransfTag
element nonlinearBeamColumn 164 132 142 $numintgrPtsBrace $bracesecID1 $BraceTransfTag
element nonlinearBeamColumn 165 142 143 $numintgrPtsBrace $bracesecID1 $BraceTransfTag
element elasticBeamColumn 166 143 117 $Abeam 700000 $G $Jbeam $Iybeam $Izbeam $Beam1TransfTag

# RHS Bay
element elasticBeamColumn 171 113 150 $Abeam 700000 $G $Jbeam $Iybeam $Izbeam $Beam1TransfTag
element nonlinearBeamColumn 172 150 151 $numintgrPtsBrace $bracesecID $BraceTransfTag
element nonlinearBeamColumn 173 151 152 $numintgrPtsBrace $bracesecID $BraceTransfTag
element nonlinearBeamColumn 174 152 153 $numintgrPtsBrace $bracesecID $BraceTransfTag
element nonlinearBeamColumn 175 153 154 $numintgrPtsBrace $bracesecID $BraceTransfTag
element elasticBeamColumn 176 154 210 $Abeam 700000 $G $Jbeam $Iybeam $Izbeam $Beam1TransfTag

element elasticBeamColumn 181 114 160 $Abeam 700000 $G $Jbeam $Iybeam $Izbeam $Beam1TransfTag
element nonlinearBeamColumn 182 160 161 $numintgrPtsBrace $bracesecID $BraceTransfTag
element nonlinearBeamColumn 183 161 152 $numintgrPtsBrace $bracesecID $BraceTransfTag
element nonlinearBeamColumn 184 152 162 $numintgrPtsBrace $bracesecID $BraceTransfTag
element nonlinearBeamColumn 185 162 163 $numintgrPtsBrace $bracesecID $BraceTransfTag
element elasticBeamColumn 186 163 119 $Abeam 700000 $G $Jbeam $Iybeam $Izbeam $Beam1TransfTag

# SECOND STOREY
# LHS Bay
element elasticBeamColumn 230 311 230 $Abeam 700000 $G $Jbeam $Iybeam $Izbeam $Beam1TransfTag
element nonlinearBeamColumn 231 230 231 $numintgrPtsBrace $bracesecID1 $BraceTransfTag
element nonlinearBeamColumn 232 231 232 $numintgrPtsBrace $bracesecID1 $BraceTransfTag
```

```
element nonlinearBeamColumn 233 232 233 $numintgrPtsBrace $bracesecID1 $BraceTransfTag
element nonlinearBeamColumn 234 233 234 $numintgrPtsBrace $bracesecID1 $BraceTransfTag
element elasticBeamColumn 235 234 412 $Abeam 700000 $G $Jbeam $Iybeam $Izbeam $Beam1TransfTag

element elasticBeamColumn 240 316 240 $Abeam 700000 $G $Jbeam $Iybeam $Izbeam $Beam1TransfTag
element nonlinearBeamColumn 241 240 241 $numintgrPtsBrace $bracesecID1 $BraceTransfTag
element nonlinearBeamColumn 242 241 232 $numintgrPtsBrace $bracesecID1 $BraceTransfTag
element nonlinearBeamColumn 243 232 242 $numintgrPtsBrace $bracesecID1 $BraceTransfTag
element nonlinearBeamColumn 244 242 243 $numintgrPtsBrace $bracesecID1 $BraceTransfTag
element elasticBeamColumn 245 243 317 $Abeam 700000 $G $Jbeam $Iybeam $Izbeam $Beam1TransfTag

# RHS Bay
element elasticBeamColumn 270 313 250 $Abeam 700000 $G $Jbeam $Iybeam $Izbeam $Beam1TransfTag
element nonlinearBeamColumn 271 250 251 $numintgrPtsBrace $bracesecID $BraceTransfTag
element nonlinearBeamColumn 272 251 252 $numintgrPtsBrace $bracesecID $BraceTransfTag
element nonlinearBeamColumn 273 252 253 $numintgrPtsBrace $bracesecID $BraceTransfTag
element nonlinearBeamColumn 274 253 254 $numintgrPtsBrace $bracesecID $BraceTransfTag
element elasticBeamColumn 275 254 410 $Abeam 700000 $G $Jbeam $Iybeam $Izbeam $Beam1TransfTag

element elasticBeamColumn 280 314 260 $Abeam 700000 $G $Jbeam $Iybeam $Izbeam $Beam1TransfTag
element nonlinearBeamColumn 281 260 261 $numintgrPtsBrace $bracesecID $BraceTransfTag
element nonlinearBeamColumn 282 261 252 $numintgrPtsBrace $bracesecID $BraceTransfTag
element nonlinearBeamColumn 283 252 262 $numintgrPtsBrace $bracesecID $BraceTransfTag
element nonlinearBeamColumn 284 262 263 $numintgrPtsBrace $bracesecID $BraceTransfTag
element elasticBeamColumn 285 263 319 $Abeam 700000 $G $Jbeam $Iybeam $Izbeam $Beam1TransfTag


# THIRD STOREY
# LHS Bay
element elasticBeamColumn 330 511 330 $Abeam 700000 $G $Jbeam $Iybeam $Izbeam $Beam1TransfTag
element nonlinearBeamColumn 331 330 331 $numintgrPtsBrace $bracesecID1 $BraceTransfTag
element nonlinearBeamColumn 332 331 332 $numintgrPtsBrace $bracesecID1 $BraceTransfTag
element nonlinearBeamColumn 333 332 333 $numintgrPtsBrace $bracesecID1 $BraceTransfTag
element nonlinearBeamColumn 334 333 334 $numintgrPtsBrace $bracesecID1 $BraceTransfTag
element elasticBeamColumn 335 334 612 $Abeam 700000 $G $Jbeam $Iybeam $Izbeam $Beam1TransfTag

element elasticBeamColumn 340 516 340 $Abeam 700000 $G $Jbeam $Iybeam $Izbeam $Beam1TransfTag
element nonlinearBeamColumn 341 340 341 $numintgrPtsBrace $bracesecID1 $BraceTransfTag
element nonlinearBeamColumn 342 341 332 $numintgrPtsBrace $bracesecID1 $BraceTransfTag
element nonlinearBeamColumn 343 332 342 $numintgrPtsBrace $bracesecID1 $BraceTransfTag
element nonlinearBeamColumn 344 342 343 $numintgrPtsBrace $bracesecID1 $BraceTransfTag
element elasticBeamColumn 345 343 517 $Abeam 700000 $G $Jbeam $Iybeam $Izbeam $Beam1TransfTag

# RHS Bay
element elasticBeamColumn 370 513 350 $Abeam 700000 $G $Jbeam $Iybeam $Izbeam $Beam1TransfTag
element nonlinearBeamColumn 371 350 351 $numintgrPtsBrace $bracesecID $BraceTransfTag
element nonlinearBeamColumn 372 351 352 $numintgrPtsBrace $bracesecID $BraceTransfTag
element nonlinearBeamColumn 373 352 353 $numintgrPtsBrace $bracesecID $BraceTransfTag
element nonlinearBeamColumn 374 353 354 $numintgrPtsBrace $bracesecID $BraceTransfTag
element elasticBeamColumn 375 354 610 $Abeam 700000 $G $Jbeam $Iybeam $Izbeam $Beam1TransfTag

element elasticBeamColumn 380 514 360 $Abeam 700000 $G $Jbeam $Iybeam $Izbeam $Beam1TransfTag
element nonlinearBeamColumn 381 360 361 $numintgrPtsBrace $bracesecID $BraceTransfTag
element nonlinearBeamColumn 382 361 352 $numintgrPtsBrace $bracesecID $BraceTransfTag
element nonlinearBeamColumn 383 352 362 $numintgrPtsBrace $bracesecID $BraceTransfTag
element nonlinearBeamColumn 384 362 363 $numintgrPtsBrace $bracesecID $BraceTransfTag
element elasticBeamColumn 385 363 519 $Abeam 700000 $G $Jbeam $Iybeam $Izbeam $Beam1TransfTag


# ------------------------------------
# Define dynamic loads
# ------------------------------------
# set time series to be passed to uniform excitation
set dt 0.01
set scale 1.0
set accelSeries "Path -filePath Taiwan40.txt -dt $dt -factor [expr 9810*$scale]"
# create UniformExcitation load pattern for uni-directional excitation
# pattern UniformExcitation $tag $dir
pattern UniformExcitation  2 1 -accel $accelSeries

# ------------------------------------
# End of model generation
# ------------------------------------

# ------------------------------------
# Define Display
# ------------------------------------
source DisplayPlane.tcl;
```

```
source DisplayModel3D.tcl;
set xPixels 500;        # height of graphical window in pixels
set yPixels 500;        # height of graphical window in pixels
set xLoc 5;             # horizontal location of graphical window (0=upper left-most corner)
set yLoc 5;             # vertical location of graphical window (0=upper left-most corner)
set dAmp 10;            # Relative amplification factor for deformations
set ShapeType1 DeformedShape;
set windowTitle "2D Frame Deformed Shape";
set viewPlane ZY;
set nEigen 0;
recorder display $windowTitle $xLoc $yLoc $xPixels $yPixels  -wipe ; # display recorder

DisplayPlane $ShapeType1 $dAmp $viewPlane $nEigen 0;
recorder plot Data/RoofAccelSS.out Accel-Z 5 510 500 500 -columns 1 2; # Plot Load vs Disp
recorder plot Data/RoofDispSS.out FloorDrift-Z 515 510 500 500 -columns 1 2; # Plot Load vs Disp

set xLoc1 510;
set yLoc1 5;
set ShapeType DeformedShape;
DisplayModel3D $ShapeType $dAmp $xLoc1 $yLoc1 $xPixels $yPixels $nEigen

# ------------------------------------
# Start of analysis generation
# ------------------------------------
#constraints Transformation ;
set alphaSP 1e12;
set alphaMP 1e12;
constraints Penalty $alphaSP $alphaMP ;
#constraints Lagrange $alphaSP $alphaMP ;
numberer RCM ;
system UmfPack ;
set Tol 1.e-5;
set maxNumIter 1000;
test NormDispIncr $Tol $maxNumIter ;
#algorithm ModifiedNewton ;
algorithm KrylovNewton ;
set gamma 0.8;
integrator HHT $gamma ;
analysis Transient ;

# ------------------------------------
# End of analysis generation
# ------------------------------------

# ------------------------------------
# Define Dampnig
# ------------------------------------
set xDamp 0.1;                  # 10% damping ratio assumed
set MpropSwitch 1.0;
set KcurrSwitch 0.0;
set KcommSwitch 1.0;
set KinitSwitch 0.0;
set nEigenI 1;                  # mode 1
set nEigenJ 3;                  # mode 3
set type frequency;
set lambdaN [eigen $type [expr $nEigenJ]];          # eigenvalue analysis for nEigenJ modes
set lambdaI [lindex $lambdaN [expr $nEigenI-1]];    # eigenvalue mode i
set lambdaJ [lindex $lambdaN [expr $nEigenJ-1]];    # eigenvalue mode j
set omegaI [expr pow($lambdaI,0.5)];
set omegaJ [expr pow($lambdaJ,0.5)];
set alphaM [expr $MpropSwitch*$xDamp*(2*$omegaI*$omegaJ)/($omegaI+$omegaJ)];# M-prop. damping; D = alphaM*M
set betaKcurr [expr $KcurrSwitch*2.*$xDamp/($omegaI+$omegaJ)];          # current-K;     +beatKcurr*KCurrent
set betaKcomm [expr $KcommSwitch*2.*$xDamp/($omegaI+$omegaJ)];          # last-committed K;   +betaKcomm*KlastCommitt
set betaKinit [expr $KinitSwitch*2.*$xDamp/($omegaI+$omegaJ)];          # initial-K;     +beatKinit*Kini
rayleigh $alphaM $betaKcurr $betaKinit $betaKcomm;                      # RAYLEIGH damping

set T1 [expr 2*3.141592654/$omegaI];
set Omega1 [expr $omegaI];
puts "The first period is: $T1";
puts "Omega 1 is: $Omega1";
puts "The first frequency is: [expr 1/$T1]";

set T3 [expr 2*3.141592654/$omegaJ];
set Omega3 [expr $omegaJ];
puts "The third period is: $T3";
puts "Omega 3 is: $Omega3";
puts "The third frequency is: [expr 1/$T3]";
```

```
# ------------------------------------
# Recorders
# ------------------------------------
# Record displacements at cantilever tip
recorder Node -file Data/RoofDispSS.out -time -node 47 -dof 1 disp;
recorder Node -file Data/RoofAccelSS.out -time -node 47 -dof 1 accel;
recorder Node -file Data/RoofDispFS.out -time -node 49 -dof 1 disp;
recorder Node -file Data/RoofAccelFS.out -time -node 49 -dof 1 accel;
recorder Node -file Data/RoofDispCentre8.out -time -node 48 -dof 1 2 3 disp;
recorder Node -file Data/RoofAccelCentre8.out -time -node 48 -dof 1 2 3 accel;
recorder Node -file Data/DBase.out -time -node 1 2 3 -dof 1 2 3 disp;

# Column Base Shear
recorder Node -file Data/RBase1.out -time -node 1 -dof 1 2 3 reaction;
recorder Node -file Data/RBase2.out -time -node 2 -dof 1 2 3 reaction;
recorder Node -file Data/RBase3.out -time -node 3 -dof 1 2 3 reaction;
recorder Node -file Data/RBase4.out -time -node 4 -dof 1 2 3 reaction;
recorder Node -file Data/RBase5.out -time -node 5 -dof 1 2 3 reaction;
recorder Node -file Data/RBase6.out -time -node 6 -dof 1 2 3 reaction;
recorder Node -file Data/ActuatorNodeF.out -time -node 7 -dof 1 2 3 4 5 6 reaction;
recorder Node -file Data/ActuatorNodeD.out -time -node 7 -dof 1 2 3 disp;

# Displacement for drift
recorder Node -file Data/DispSS1.out -time -node 7 -dof 1 2 3 disp;
recorder Node -file Data/DispFS1.out -time -node 12 -dof 1 2 3 disp;
recorder Node -file Data/DispSS2.out -time -node 27 -dof 1 2 3 disp;
recorder Node -file Data/DispFS2.out -time -node 32 -dof 1 2 3 disp;

# ------------------------------------
# Stiff Side Brace Data
# ------------------------------------
# Brace axial load
recorder Element -file Data/SSBrace2Ele1local.out -time -ele 152 localForce
recorder Element -file Data/SSBrace1Ele1local.out -time -ele 162 localForce
recorder Node -file Data/SSBrace1EndForce.out -time -node 162 -dof 1 2 3 reaction;
recorder Node -file Data/SSBrace2EndForce.out -time -node 152 -dof 1 2 3 reaction;
recorder Node -file Data/SSBrace1EndForce1.out -time -node 116 -dof 1 2 3 reaction;
recorder Node -file Data/SSBrace2EndForce1.out -time -node 111 -dof 1 2 3 reaction;

# Brace curvature
recorder Node -file Data/SSBrace1Curv.out -time -node 141 -dof 4 5 6 disp;
recorder Node -file Data/SSBrace2Curv.out -time -node 131 -dof 4 5 6 disp;

# Stress/Strain in braces
recorder Element -file Data/SSBr2sec7Top.out -time -ele 152 section $numintgrPtsBrace fiber 25 0 $matID stressStrain;
recorder Element -file Data/SSBr2sec1Top.out -time -ele 152 section 1 fiber 25 0 $matID  stressStrain;
recorder Element -file Data/SSBr2sec7Side.out -time -ele 152 section $numintgrPtsBrace fiber 0 25 $matID stressStrain;
recorder Element -file Data/SSBr2sec1Side.out -time -ele 152 section 1 fiber 0 25 $matID stressStrain;
recorder Element -file Data/SSBr1sec7Top.out -time -ele 162 section $numintgrPtsBrace fiber 25 0 $matID stressStrain;
recorder Element -file Data/SSBr1sec1Top.out -time -ele 162 section 1 fiber 25 0 $matID stressStrain;
recorder Element -file Data/SSBr1sec7Side.out -time -ele 162 section $numintgrPtsBrace fiber 0 25 $matID stressStrain;
recorder Element -file Data/SSBr1sec1Side.out -time -ele 162 section 1 fiber 0 25 $matID stressStrain;

# Gusset plate/brace end node
recorder Node -file Data/SSGussetNd.out -time -node 130 -dof 1 2 3 4 5 6 reaction;
recorder Node -file Data/SSGussetNd1.out -time -node 140 -dof 1 2 3 4 5 6 reaction;

# ------------------------------------
# Flexible Side Brace Data
# ------------------------------------
# Brace axial load
recorder Element -file Data/FSBrace2Ele1local.out -time -ele 172 localForce
recorder Element -file Data/FSBrace1Ele1local.out -time -ele 182 localForce
recorder Node -file Data/FSBrace1EndForce.out -time -node 113 -dof 1 2 3 reaction;
recorder Node -file Data/FSBrace2EndForce.out -time -node 114 -dof 1 2 3 reaction;

# Brace curvature
recorder Node -file Data/FSBrace1Curv.out -time -node 172 -dof 4 5 6 disp;
recorder Node -file Data/FSBrace2Curv.out -time -node 182 -dof 4 5 6 disp;

# Stress/Strain in Braces
recorder Element -file Data/FSBr2sec7Top.out -time -ele 172 section $numintgrPtsBrace fiber 25 0 $matID stressStrain; # Mid Brace
recorder Element -file Data/FSBr2sec1Top.out -time -ele 172 section 1 fiber 25 0 $matID stressStrain; # Brace End Stress
recorder Element -file Data/FSBr2sec7Side.out -time -ele 172 section $numintgrPtsBrace fiber 0 25 $matID stressStrain; # Mid Brace
recorder Element -file Data/FSBr2sec1Side.out -time -ele 172 section 1 fiber 0 25 $matID stressStrain; # Brace End Stress
recorder Element -file Data/FSBr1sec7Top.out -time -ele 182 section $numintgrPtsBrace fiber 25 0 $matID stressStrain; # Mid Brace
recorder Element -file Data/FSBr1sec1Top.out -time -ele 182 section 1 fiber 25 0 $matID stressStrain; # Brace End Stress
recorder Element -file Data/FSBr1sec7Side.out -time -ele 182 section $numintgrPtsBrace fiber 0 25 $matID stressStrain; # Mid Brace
```

```
recorder Element -file Data/FSBr1sec1Side.out -time -ele 182 section 1 fiber 0 25 $matID stressStrain; # Brace End Stress
puts "Regular recorders defined" ;

# ------------------------------------
# Stiff Side Brace Data 2nd Storey
# ------------------------------------
# Brace axial load
recorder Element -file Data1/SSBrace2Ele1local.out -time -ele 231 localForce
recorder Element -file Data1/SSBrace1Ele1local.out -time -ele 241 localForce

# Brace curvature
recorder Node -file Data1/SSBrace1Curv.out -time -node 241 -dof 4 5 6 disp;
recorder Node -file Data1/SSBrace2Curv.out -time -node 231 -dof 4 5 6 disp;

# Stress/Strain in braces
recorder Element -file Data1/SSBr2sec7Top.out -time -ele 231 section $numintgrPtsBrace fiber 25 0 $matID stressStrain;
recorder Element -file Data1/SSBr2sec1Top.out -time -ele 231 section 1 fiber 25 0 $matID stressStrain;
recorder Element -file Data1/SSBr2sec7Side.out -time -ele 231 section $numintgrPtsBrace fiber 0 25 $matID stressStrain;
recorder Element -file Data1/SSBr2sec1Side.out -time -ele 231 section 1 fiber 0 25 $matID stressStrain;
recorder Element -file Data1/SSBr1sec7Top.out -time -ele 241 section $numintgrPtsBrace fiber 25 0 $matID stressStrain;
recorder Element -file Data1/SSBr1sec1Top.out -time -ele 241 section 1 fiber 25 0 $matID stressStrain;
recorder Element -file Data1/SSBr1sec7Side.out -time -ele 241 section $numintgrPtsBrace fiber 0 25 $matID stressStrain;
recorder Element -file Data1/SSBr1sec1Side.out -time -ele 241 section 1 fiber 0 25 $matID stressStrain;

# ------------------------------------
# Flexible Side Brace Data 2nd Storey
# ------------------------------------
# Brace axial load
recorder Element -file Data1/FSBrace2Ele1local.out -time -ele 271 localForce
recorder Element -file Data1/FSBrace1Ele1local.out -time -ele 281 localForce

# Brace curvature
recorder Node -file Data1/FSBrace1Curv.out -time -node 261 -dof 4 5 6 disp;
recorder Node -file Data1/FSBrace2Curv.out -time -node 251 -dof 4 5 6 disp;

# Stress/Strain in Braces
recorder Element -file Data1/FSBr2sec7Top.out -time -ele 271 section $numintgrPtsBrace fiber 25 0 $matID stressStrain; # Mid Brace
recorder Element -file Data1/FSBr2sec1Top.out -time -ele 271 section 1 fiber 25 0 $matID stressStrain; # Brace End Stress
recorder Element -file Data1/FSBr2sec7Side.out -time -ele 271 section $numintgrPtsBrace fiber 0 25 $matID stressStrain; # Mid Brace
recorder Element -file Data1/FSBr2sec1Side.out -time -ele 271 section 1 fiber 0 25 $matID stressStrain; # Brace End Stress
recorder Element -file Data1/FSBr1sec7Top.out -time -ele 281 section $numintgrPtsBrace fiber 25 0 $matID stressStrain; # Mid Brace
recorder Element -file Data1/FSBr1sec1Top.out -time -ele 281 section 1 fiber 25 0 $matID stressStrain; # Brace End Stress
recorder Element -file Data1/FSBr1sec7Side.out -time -ele 281 section $numintgrPtsBrace fiber 0 25 $matID stressStrain; # Mid Brace
recorder Element -file Data1/FSBr1sec1Side.out -time -ele 281 section 1 fiber 0 25 $matID stressStrain; # Brace End Stress

# ------------------------------------
# Stiff Side Brace Data 3rd Storey
# ------------------------------------

# Brace axial load
recorder Element -file Data2/SSBrace2Ele1local.out -time -ele 331 localForce
recorder Element -file Data2/SSBrace1Ele1local.out -time -ele 341 localForce

# Brace curvature
recorder Node -file Data2/SSBrace1Curv.out -time -node 341 -dof 4 5 6 disp;
recorder Node -file Data2/SSBrace2Curv.out -time -node 331 -dof 4 5 6 disp;
# Stress/Strain in braces
recorder Element -file Data2/SSBr2sec7Top.out -time -ele 331 section $numintgrPtsBrace fiber 25 0 $matID stressStrain;
recorder Element -file Data2/SSBr2sec1Top.out -time -ele 331 section 1 fiber 25 0 $matID stressStrain;
recorder Element -file Data2/SSBr2sec7Side.out -time -ele 331 section $numintgrPtsBrace fiber 0 25 $matID stressStrain;
recorder Element -file Data2/SSBr2sec1Side.out -time -ele 331 section 1 fiber 0 25 $matID stressStrain;
recorder Element -file Data2/SSBr1sec7Top.out -time -ele 341 section $numintgrPtsBrace fiber 25 0 $matID stressStrain;
recorder Element -file Data2/SSBr1sec1Top.out -time -ele 341 section 1 fiber 25 0 $matID stressStrain;
recorder Element -file Data2/SSBr1sec7Side.out -time -ele 341 section $numintgrPtsBrace fiber 0 25 $matID stressStrain;
recorder Element -file Data2/SSBr1sec1Side.out -time -ele 341 section 1 fiber 0 25 $matID stressStrain;

# ------------------------------------
# Flexible Side Brace Data 3rd Storey
# ------------------------------------
# Brace axial load
recorder Element -file Data2/FSBrace2Ele1local.out -time -ele 371 localForce
recorder Element -file Data2/FSBrace1Ele1local.out -time -ele 381 localForce

# Brace curvature
recorder Node -file Data2/FSBrace1Curv.out -time -node 361 -dof 4 5 6 disp;
recorder Node -file Data2/FSBrace2Curv.out -time -node 351 -dof 4 5 6 disp;

# Stress/Strain in Braces
```

```
recorder Element -file Data2/FSBr2sec7Top.out -time -ele 371 section $numintgrPtsBrace fiber 25 0 $matID stressStrain; # Mid Brace
recorder Element -file Data2/FSBr2sec1Top.out -time -ele 371 section 1 fiber 25 0 $matID stressStrain; # Brace End Stress
recorder Element -file Data2/FSBr2sec7Side.out -time -ele 371 section $numintgrPtsBrace fiber 0 25 $matID stressStrain; # Mid Brace
recorder Element -file Data2/FSBr2sec1Side.out -time -ele 371 section 1 fiber 0 25 $matID stressStrain; # Brace End Stress
recorder Element -file Data2/FSBr1sec7Top.out -time -ele 381 section $numintgrPtsBrace fiber 25 0 $matID stressStrain; # Mid Brace
recorder Element -file Data2/FSBr1sec1Top.out -time -ele 381 section 1 fiber 25 0 $matID stressStrain; # Brace End Stress
recorder Element -file Data2/FSBr1sec7Side.out -time -ele 381 section $numintgrPtsBrace fiber 0 25 $matID stressStrain; # Mid Brace
recorder Element -file Data2/FSBr1sec1Side.out -time -ele 381 section 1 fiber 0 25 $matID stressStrain; # Brace End Stress

# ------------------------------
# Finally perform the analysis
# ------------------------------
# perform an eigenvalue analysis
set pi 3.14159265358979
set lambda [eigen -fullGenLapack 4]
puts "\nEigenvalues at start of transient:"
puts "lambda      omega      period"
foreach lambda $lambda {
   if {$lambda > 0.0} {
      set omega [expr pow($lambda,0.5)]
      set period [expr 2*$pi/pow($lambda,0.5)]
      puts "$lambda  $omega  $period"
   }
}
# open output file for writing
set outFileID [open Data/elapsedTime.txt w]
# perform the transient analysis
set tTot [time {
   for {set i 1} {$i < 4000} {incr i} {
      set t [time {analyze  1  [expr $dt/1.0]}]
      puts $outFileID $t
                  #puts "step $i"
   }
}]
puts "\nElapsed Time = $tTot \n"
# close the output file
close $outFileID
set fmt1 "%s Analysis Result: CtrlNode %.2i, dof %.1i, Disp=%.4f %s";

# ------------------------------
# If Convergence Fails
# ------------------------------
set LunitTXT "m";
set IDctrlNode 48;
set IDctrlDOF 3;

if {$ok != 0 } {
            puts [format $fmt1 "PROBLEM WITH DYNAMIC ANALYSIS" $IDctrlNode $IDctrlDOF [nodeDisp $IDctrlNode
$IDctrlDOF] $LunitTXT]
} else {
            puts [format $fmt1 "DYNAMIC ANALYSIS COMPLETE:"  $IDctrlNode $IDctrlDOF [nodeDisp $IDctrlNode $IDctrlDOF]
$LunitTXT]
}
wipe
```

Appendix D1 – Test 1B Results

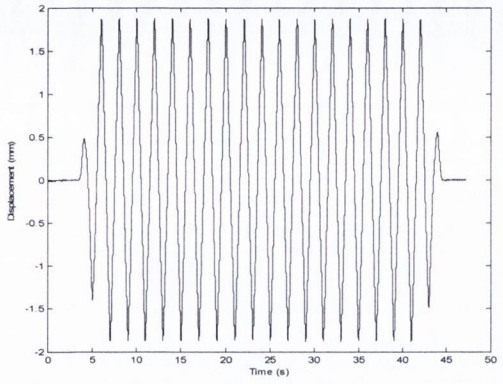

Figure D1.1: Displacement command vs. time

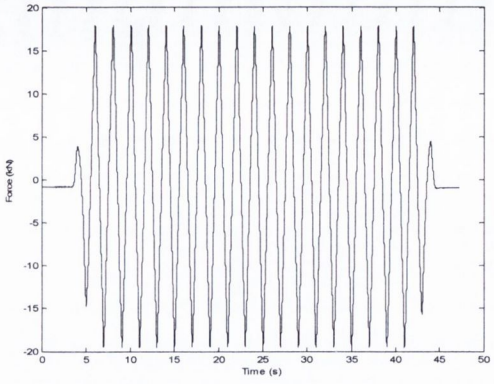

Figure D1.2: Force feedback vs. time

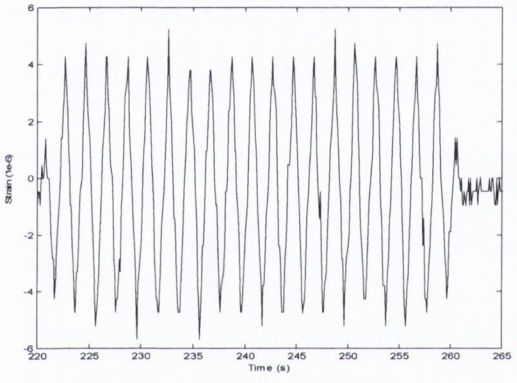

Figure D1.3: Strain Gauge 1

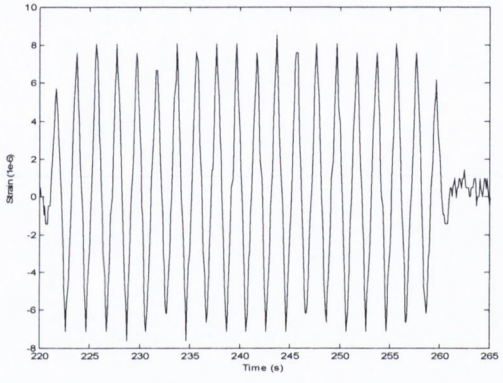

Figure D1.4: Strain Gauge 2

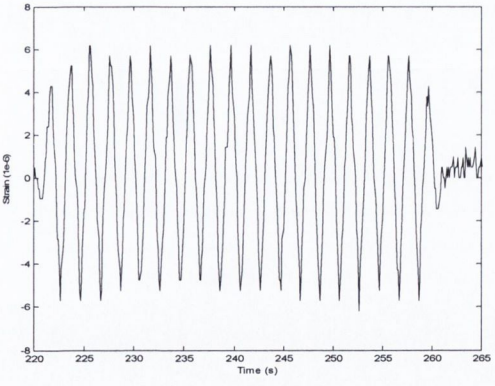

Figure D1.5: Strain Gauge 3

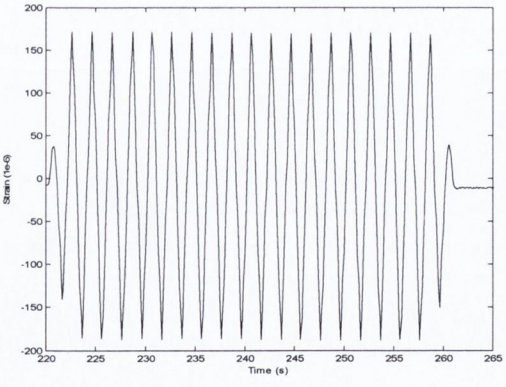

Figure D1.6: Strain Gauge 4

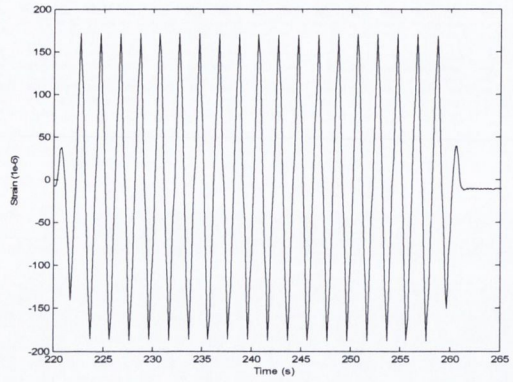

Figure D1.7: Strain Gauge 5

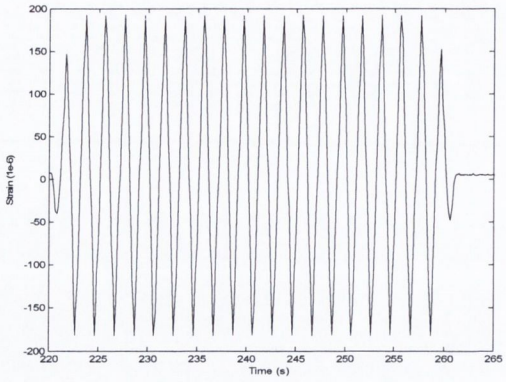

Figure D1.8: Strain Gauge 6

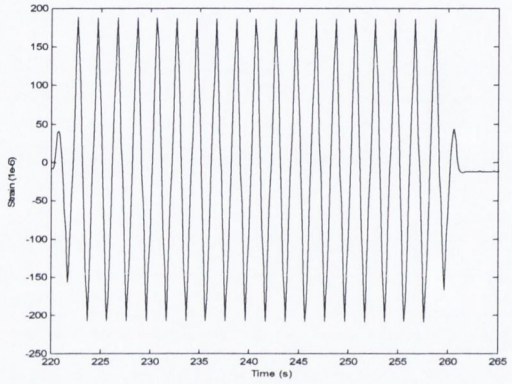

Figure D1.9: Strain Gauge 7

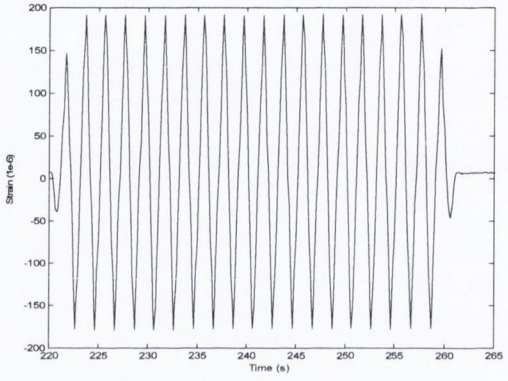

Figure D1.10: Strain Gauge 8

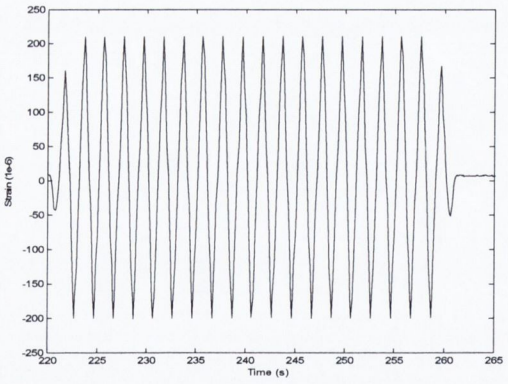

Figure D1.11: Strain Gauge 9

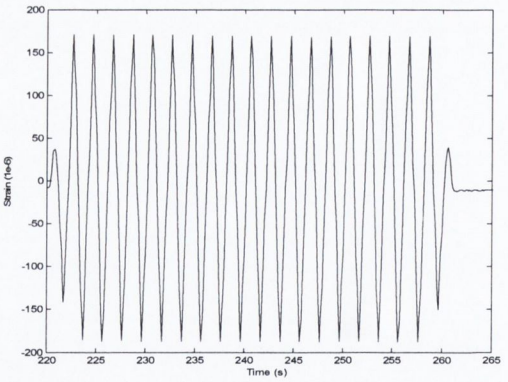

Figure D1.12: Strain Gauge 10

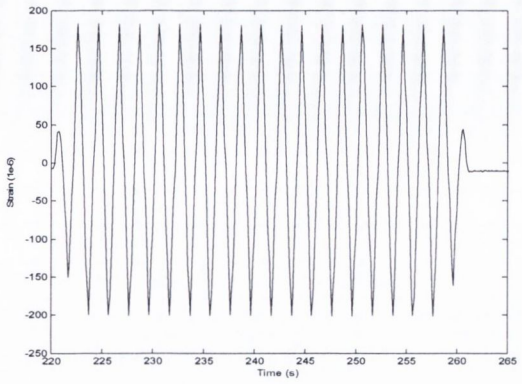

Figure D1.13: Strain Gauge 11

Appendix D2 – Test 1C Results

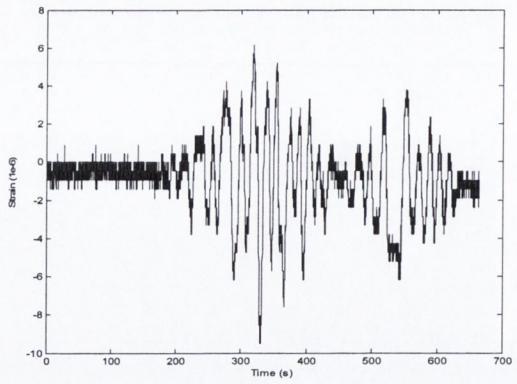

Figure D2.1: Strain Gauge 1

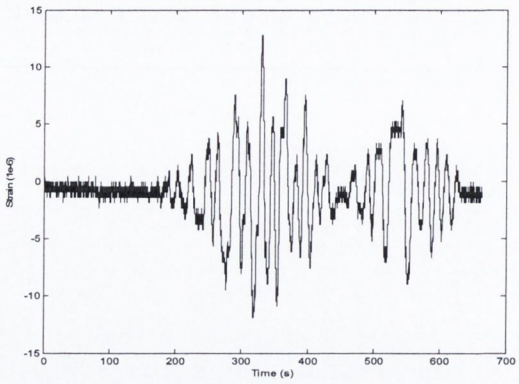

Figure D2.2: Strain Gauge 2

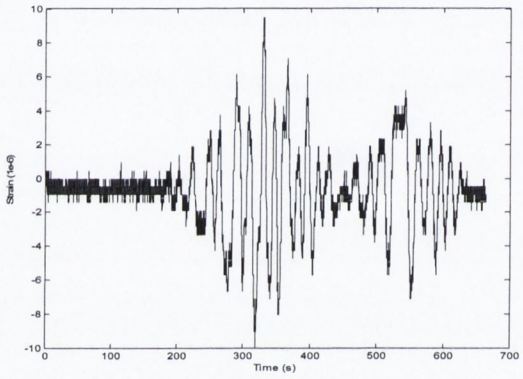

Figure D2.3: Strain Gauge 3

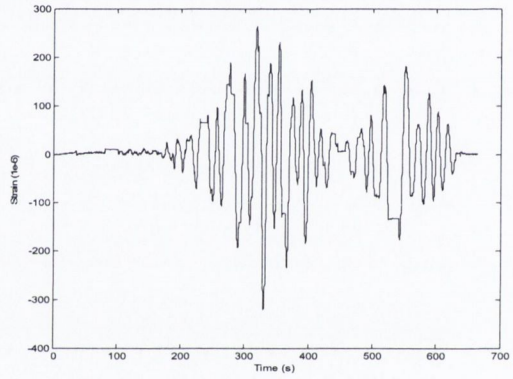

Figure D2.4: Strain Gauge 4

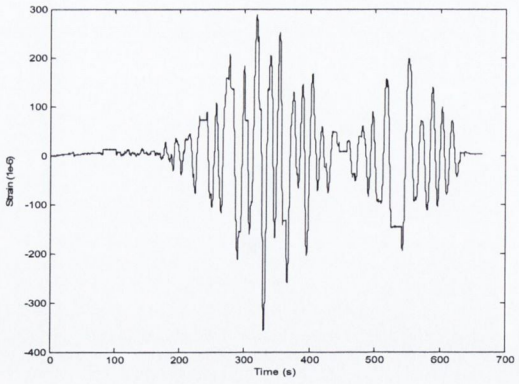

Figure D2.5: Strain Gauge 5

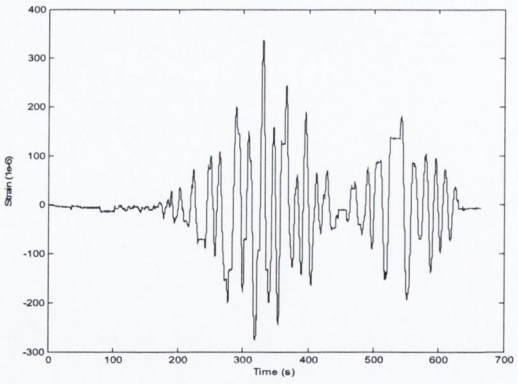

Figure D2.6: Strain Gauge 6

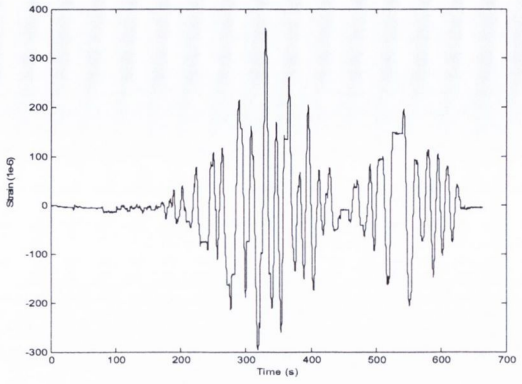

Figure D2.7: Strain Gauge 7

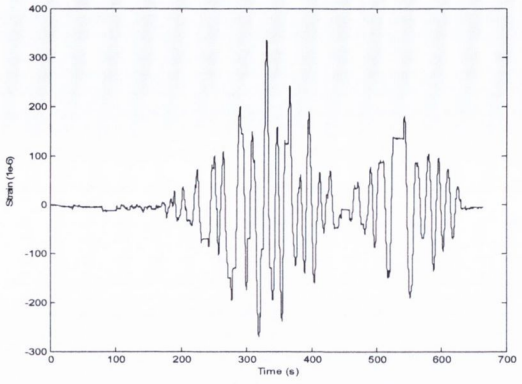

Figure D2.8: Strain Gauge 8

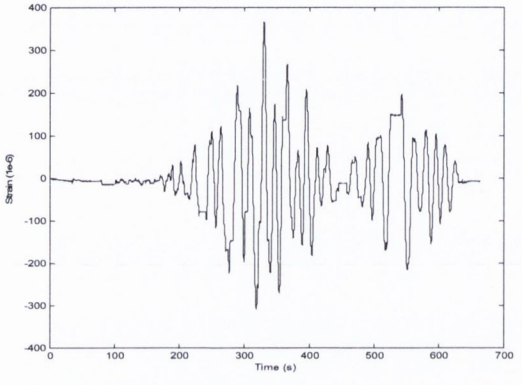

Figure D2.9: Strain Gauge 9

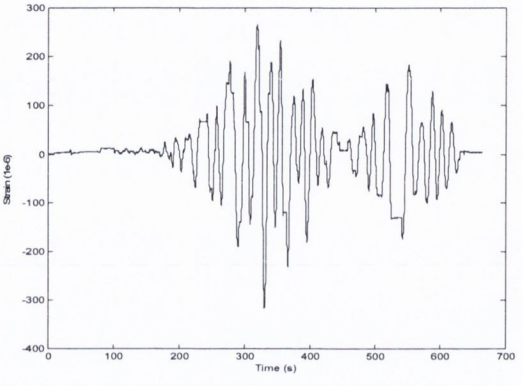

Figure D2.10: Strain Gauge 10

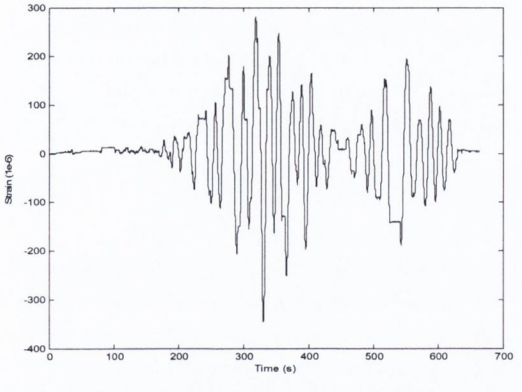

Figure D2.11: Strain Gauge 11

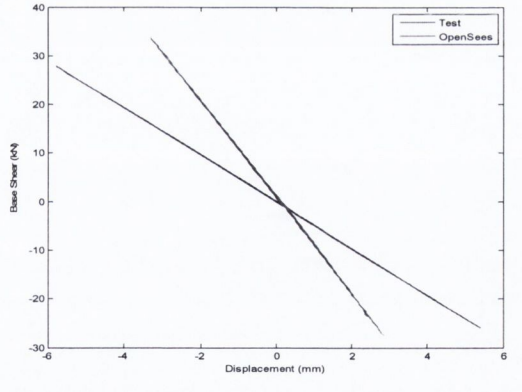

Figure D2.12: Base shear vs. displacement at Node 12

Appendix D3 – Test 1D Results

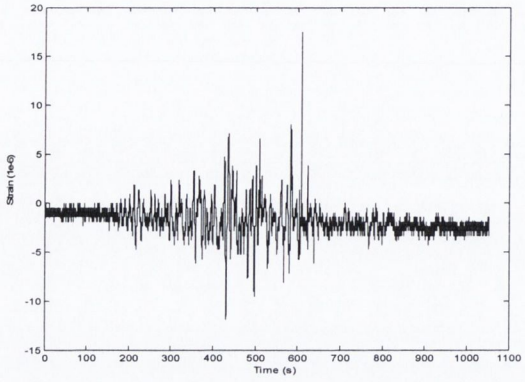

Figure D3.1: Strain Gauge 1

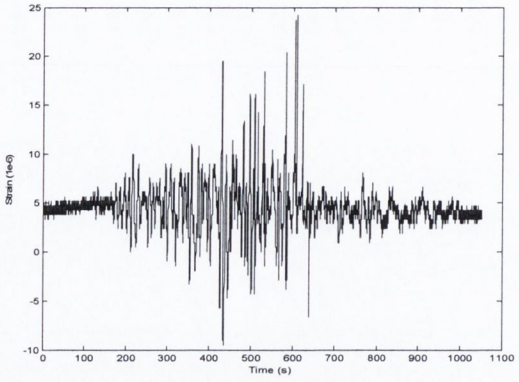

Figure D3.2: Strain Gauge 2

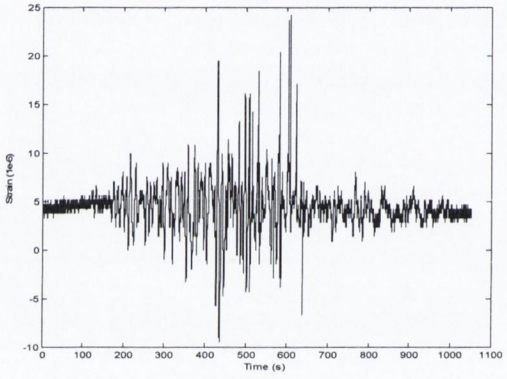

Figure D3.3: Strain Gauge 3

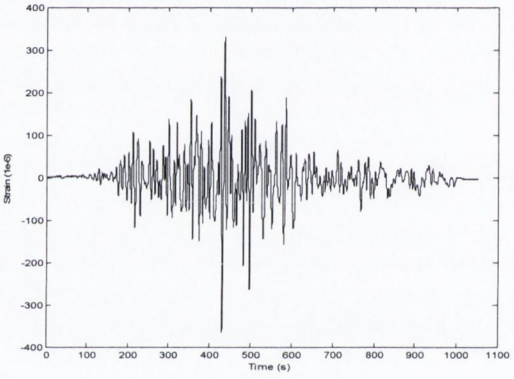

Figure D3.4: Strain Gauge 4

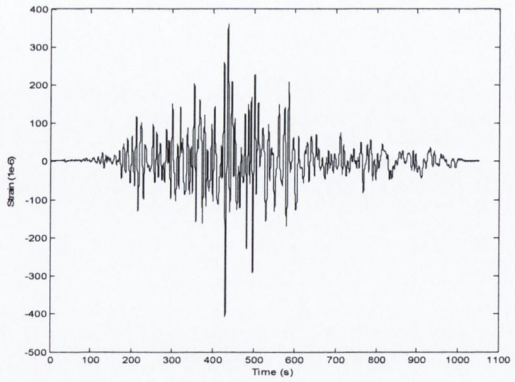

Figure D3.5: Strain Gauge 5

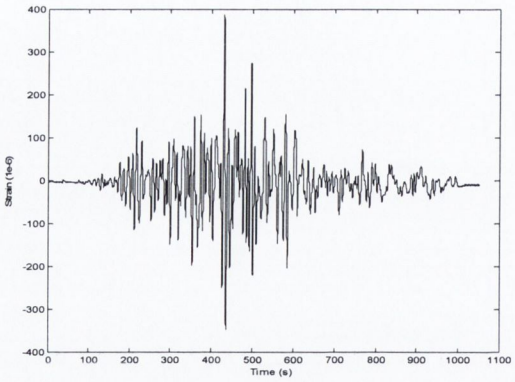

Figure D3.6: Strain Gauge 6

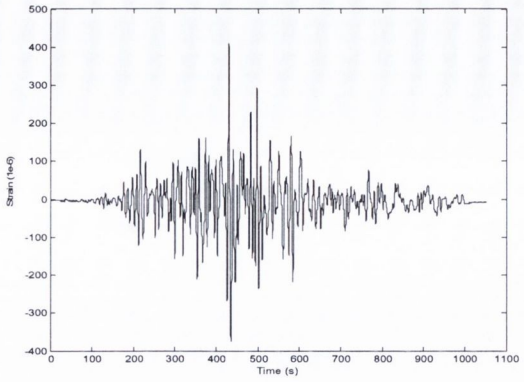

Figure D3.7: Strain Gauge 7

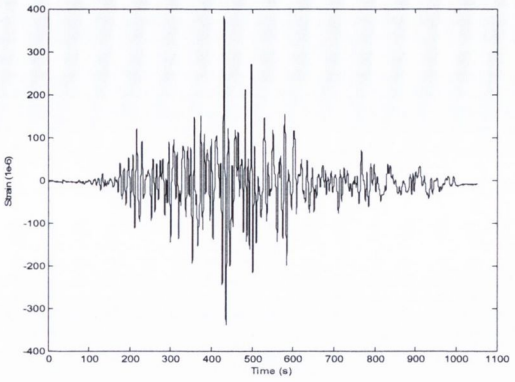

Figure D3.8: Strain Gauge 8

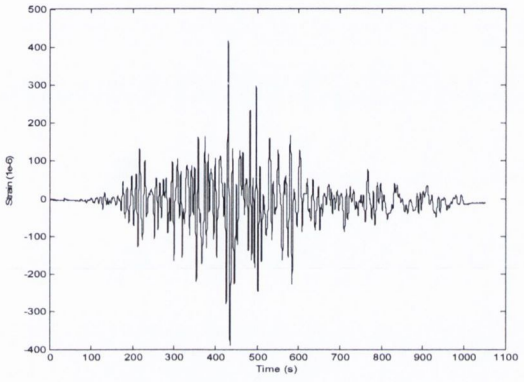

Figure D3.9: Strain Gauge 9

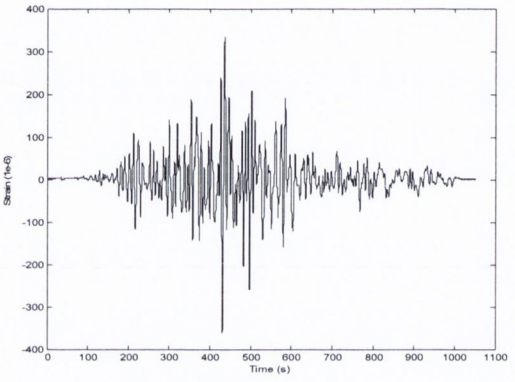

Figure D3.10: Strain Gauge 10

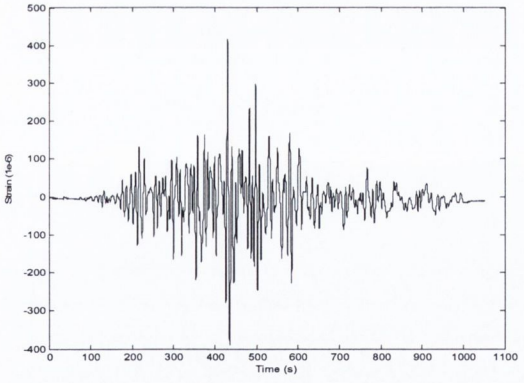

Figure D3.11: Strain Gauge 11

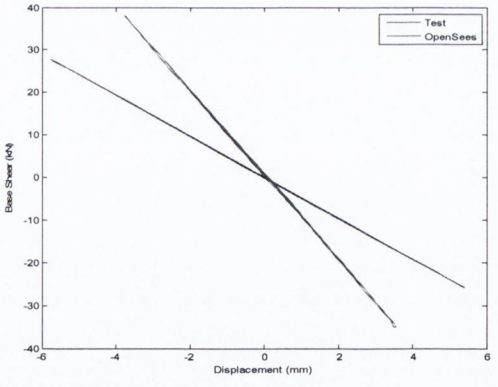

Figure D3.12: Base shear vs. displacement at Node 12

Appendix D4 – Test 1E Results

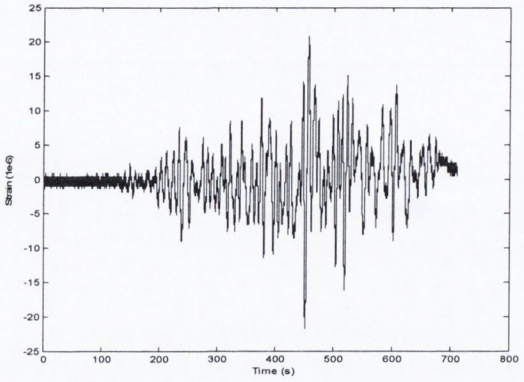

Figure D4.1: Strain Gauge 1

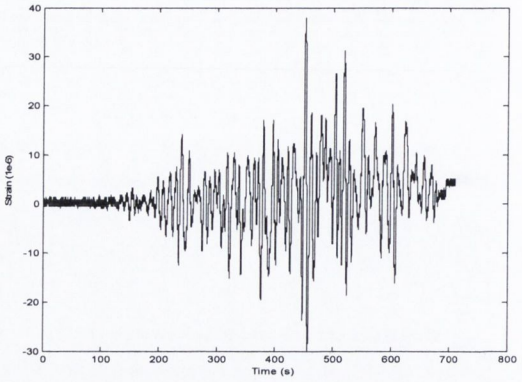

Figure D4.2: Strain Gauge 2

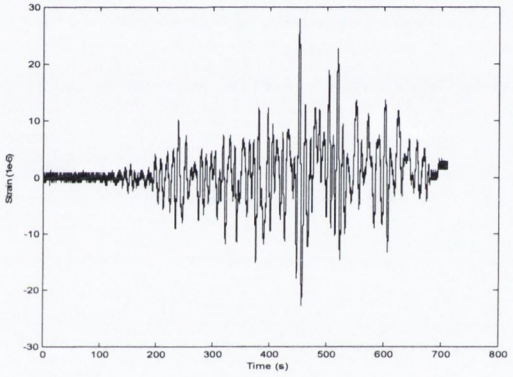

Figure D4.3: Strain Gauge 3

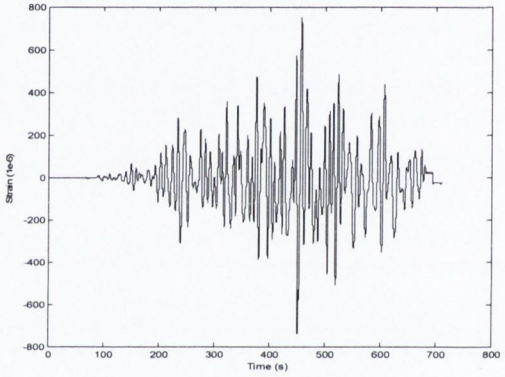

Figure D4.4: Strain Gauge 4

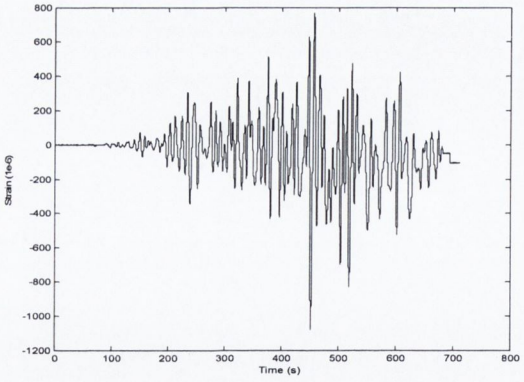

Figure D4.5: Strain Gauge 5

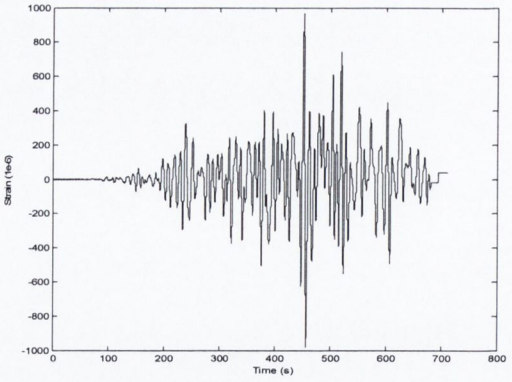

Figure D4.6: Strain Gauge 6

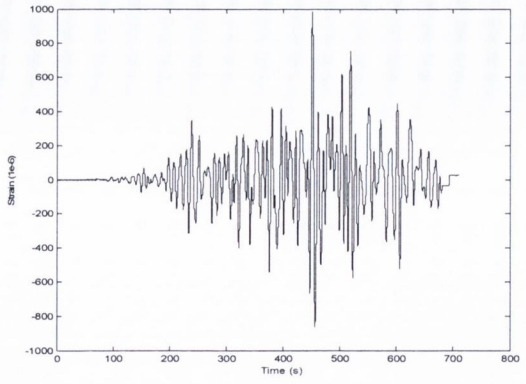

Figure D4.7: Strain Gauge 7

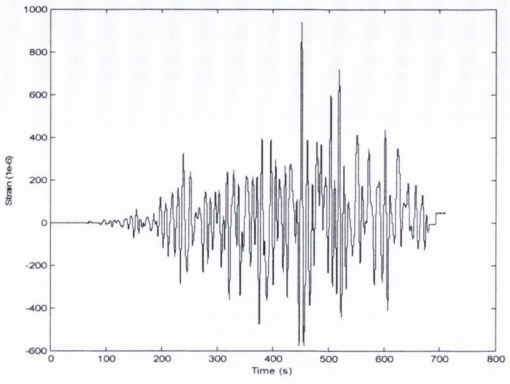

Figure D4.8: Strain Gauge 8

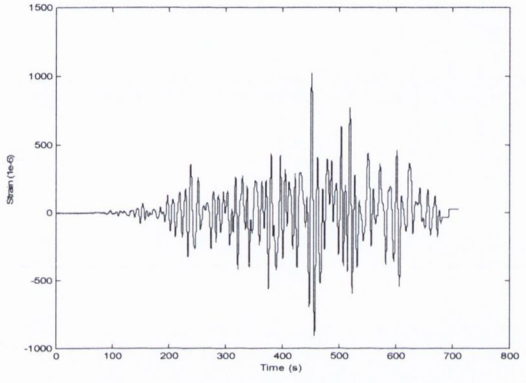

Figure D4.9: Strain Gauge 9

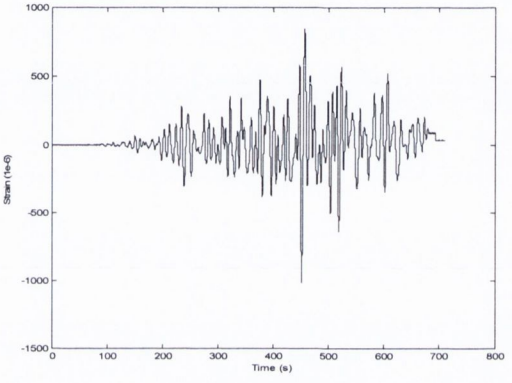

Figure D4.10: Strain Gauge 10

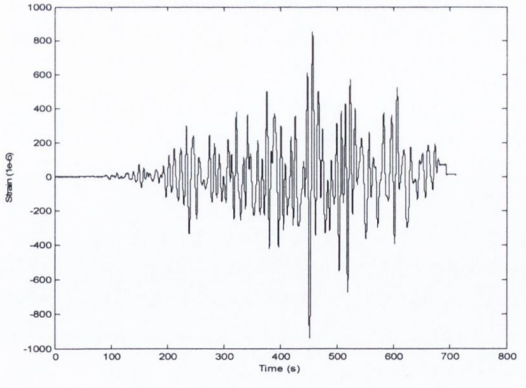

Figure D4.11: Strain Gauge 11

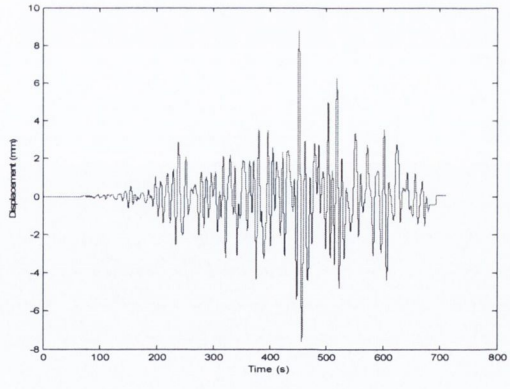

Figure D4.12: LVDT at Node 12

Appendix D5 – Test 1F Results

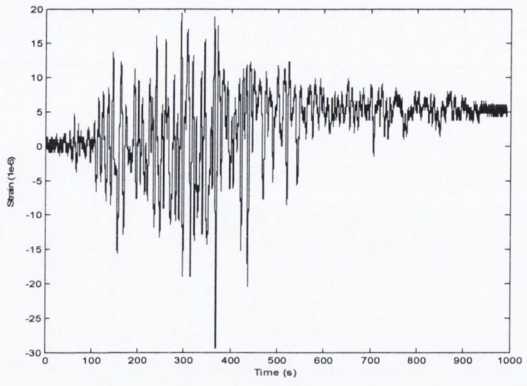

Figure D5.1: Strain Gauge 1

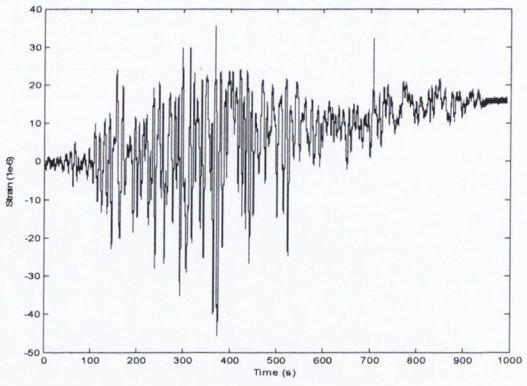

Figure D5.2: Strain Gauge 2

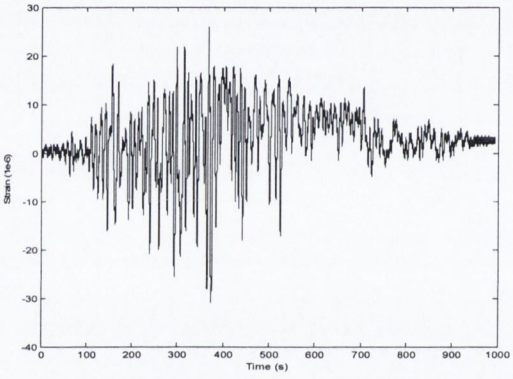

Figure D5.3: Strain Gauge 3

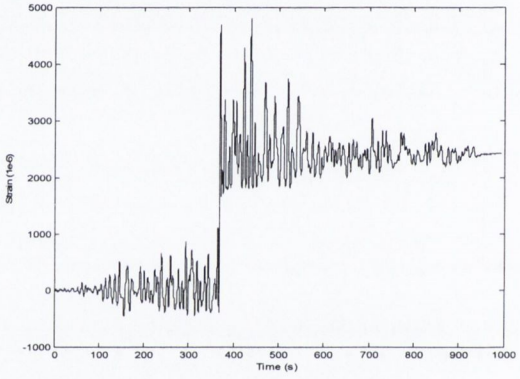

Figure D5.4: Strain Gauge 4

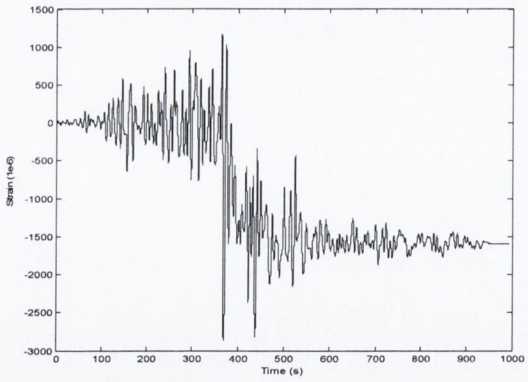

Figure D5.5: Strain Gauge 5

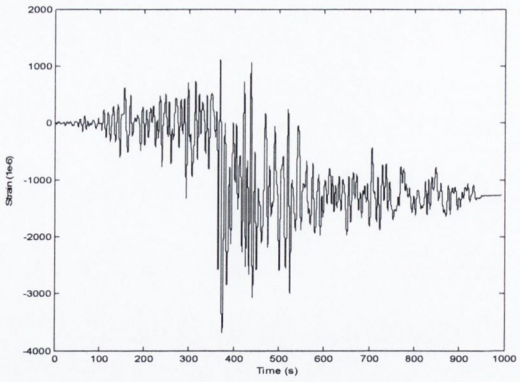

Figure D5.6: Strain Gauge 6

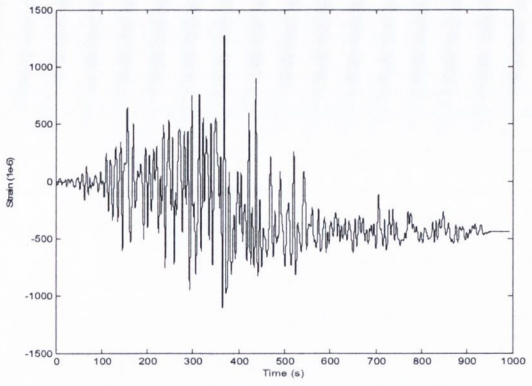

Figure D5.7: Strain Gauge 7

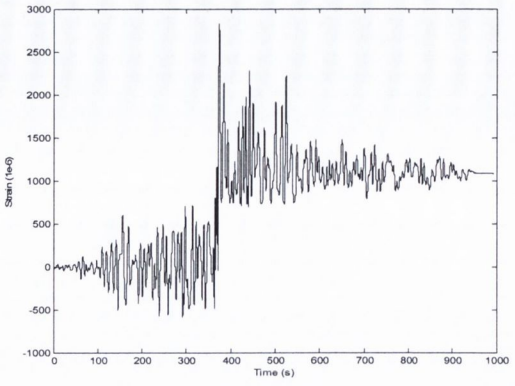

Figure D5.8: Strain Gauge 8

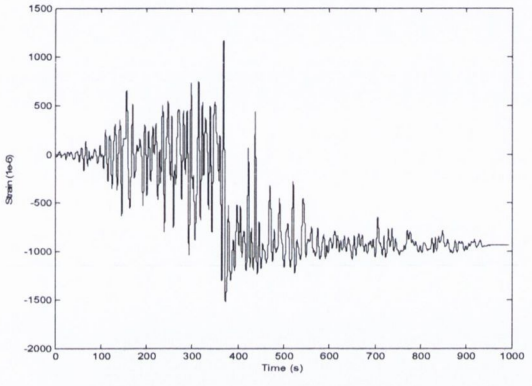

Figure D5.9: Strain Gauge 9

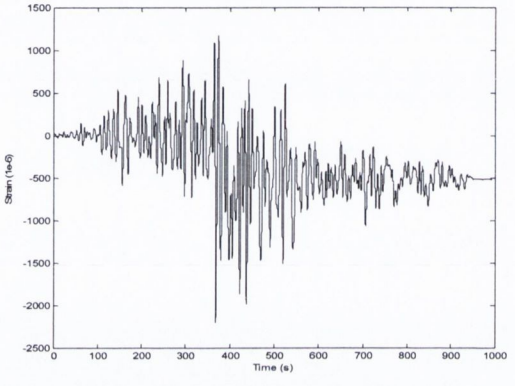

Figure D5.10: Strain Gauge 10

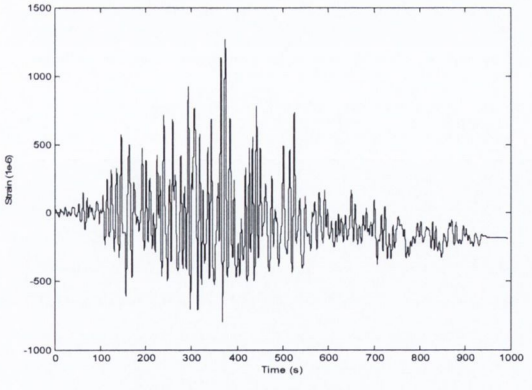

Figure D5.11: Strain Gauge 11

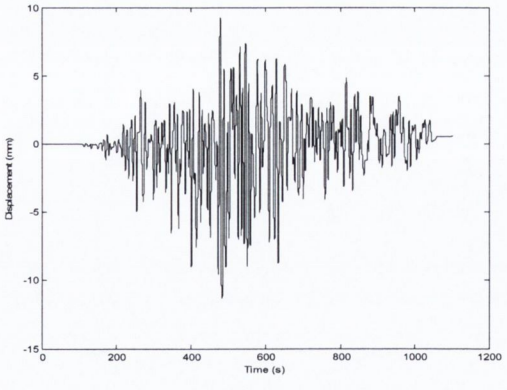

Figure D5.12: LVDT at Node 13

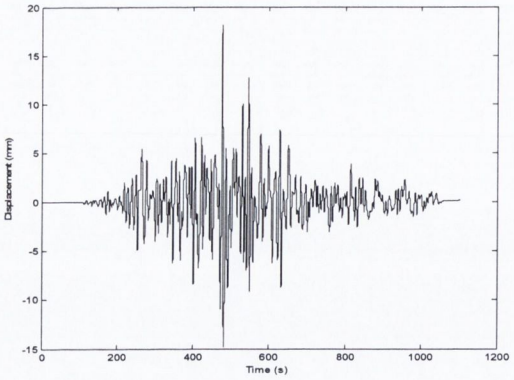

Figure D5.13: Strain Gauge 12

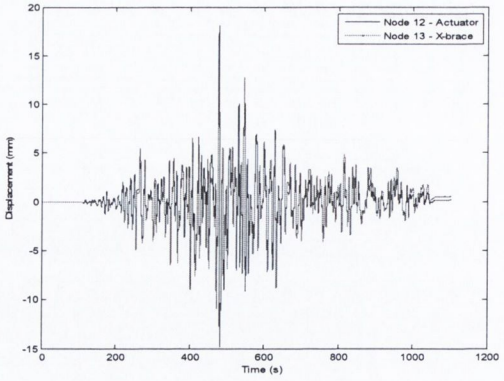

Figure D5.14: LVDT at Node 12 & Node 13

Appendix D6 – Test 2B Results

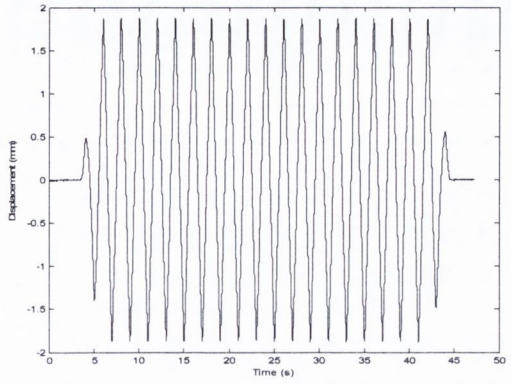

Figure D6.1: Displacement command vs. time

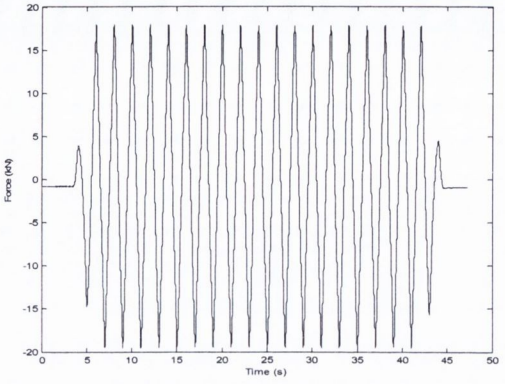

Figure D6.2: Force feedback vs. time

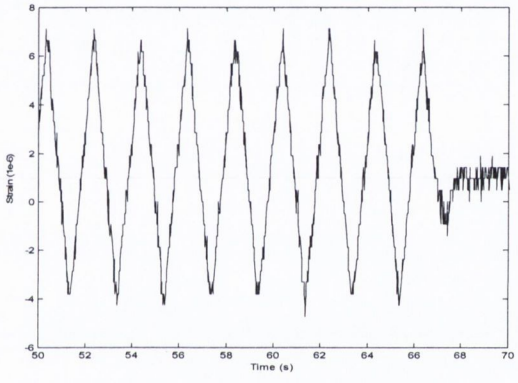

Figure: D6.3 Strain Gauge 1

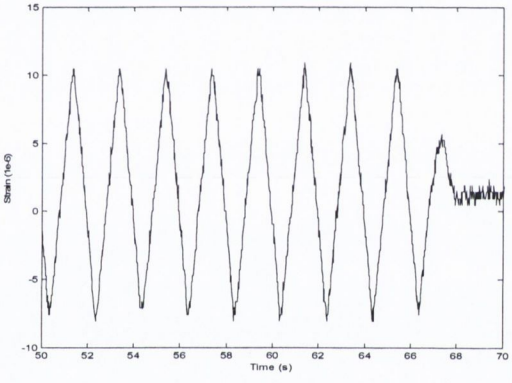

Figure D6.4: Strain Gauge 2

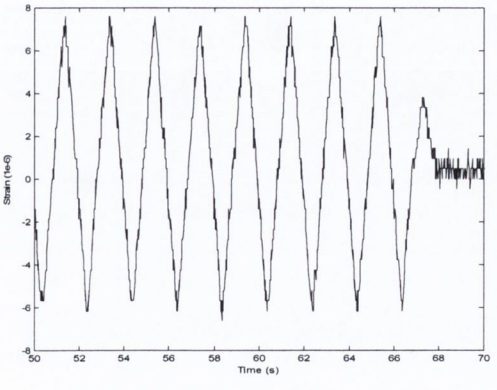

Figure D6.5: Strain Gauge 3

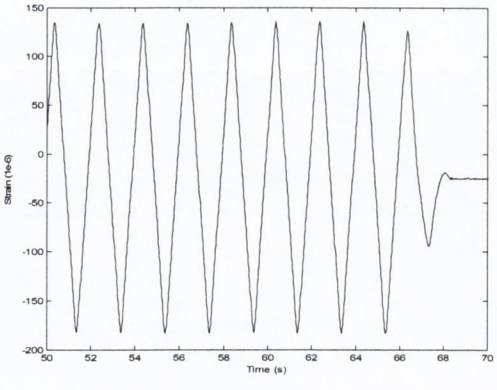

Figure D6.6: Strain Gauge 4

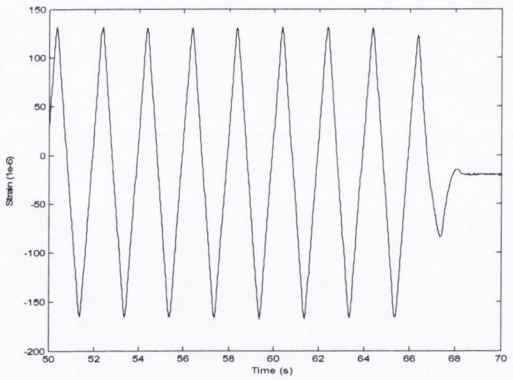

Figure D6.6: Strain Gauge 5

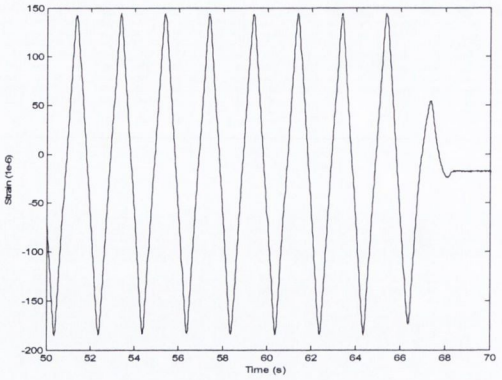

Figure D6.7: Strain Gauge 6

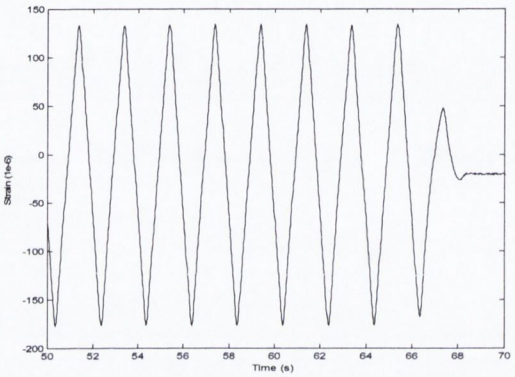

Figure D6.8: Strain Gauge 7

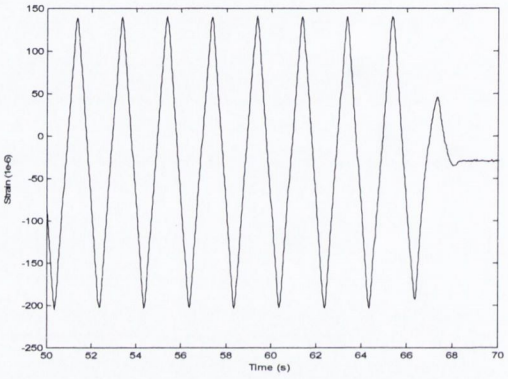

Figure D6.9: Strain Gauge 8

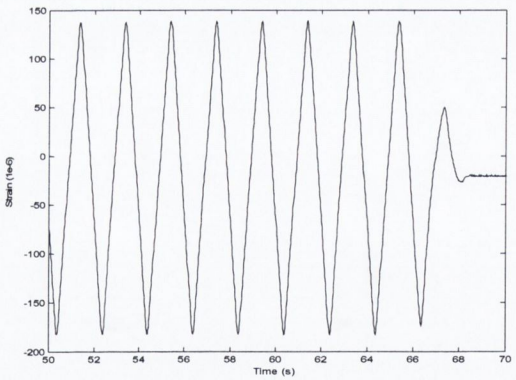

Figure D6.10: Strain Gauge 9

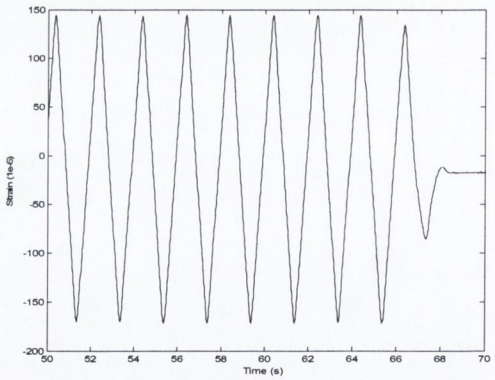

Figure D6.11: Strain Gauge 10

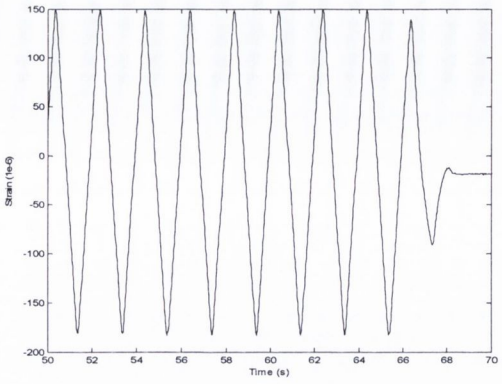

Figure D6.12: Strain Gauge 11

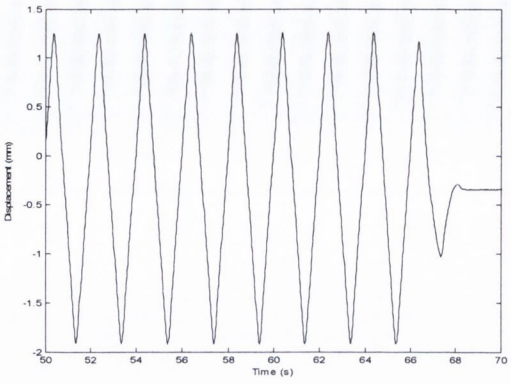

Figure D6.13: LVDT at Node 13

Appendix D7 – Test 2C Results

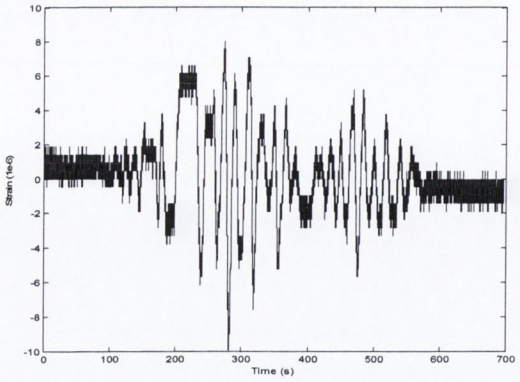

Figure D7.1: Strain Gauge 1

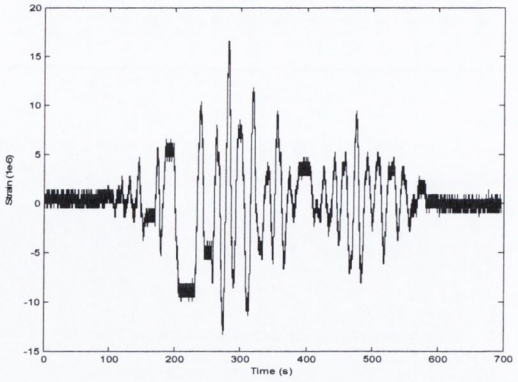

Figure D7.2: Strain Gauge 2

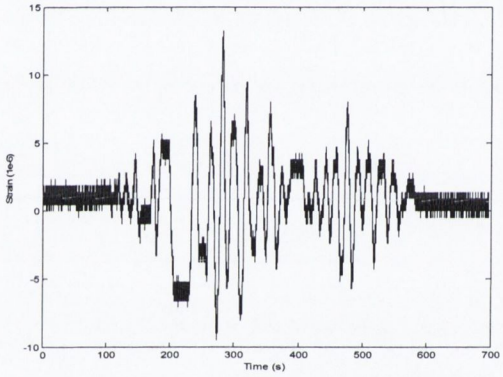

Figure D7.3: Strain Gauge 3

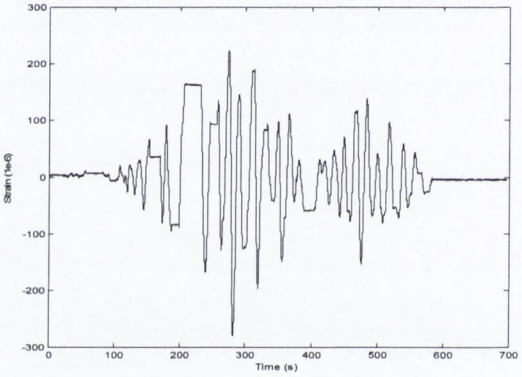

Figure D7.4: Strain Gauge 4

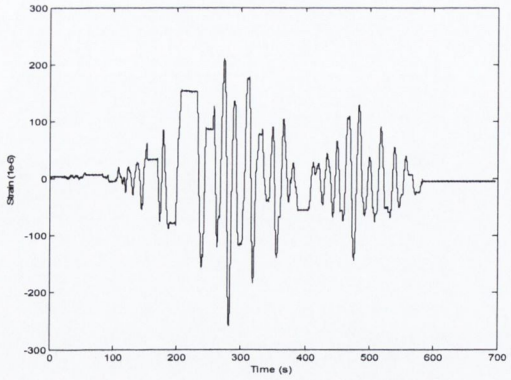

Figure D7.5: Strain Gauge 5

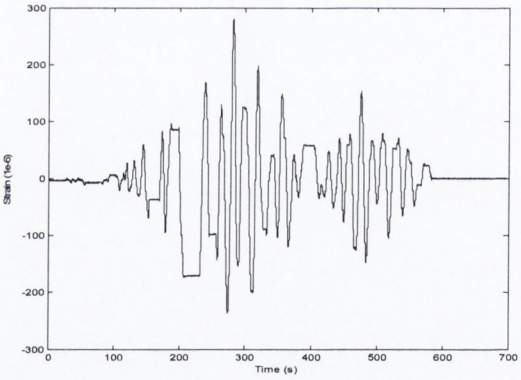

Figure D7.6: Strain Gauge 6

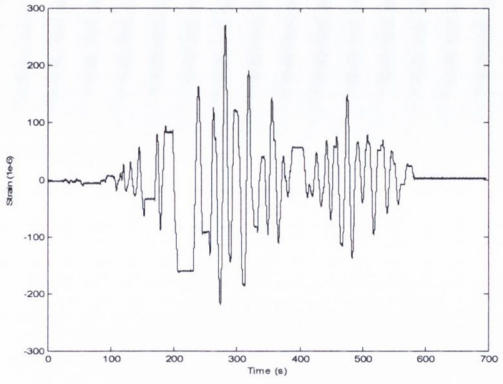

Figure D7.7: Strain Gauge 7

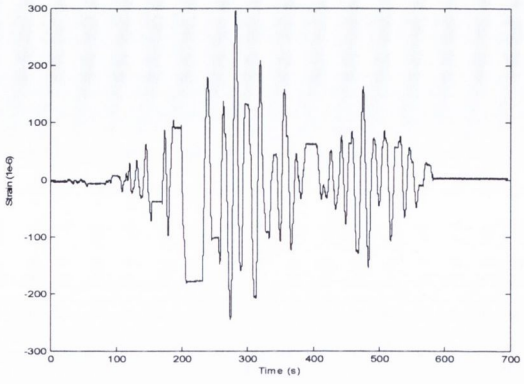

Figure D7.8: Strain Gauge 8

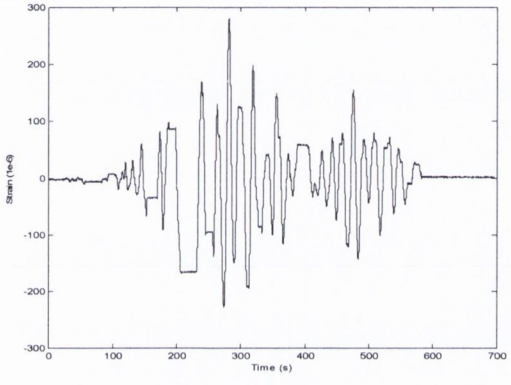

Figure D7.9: Strain Gauge 9

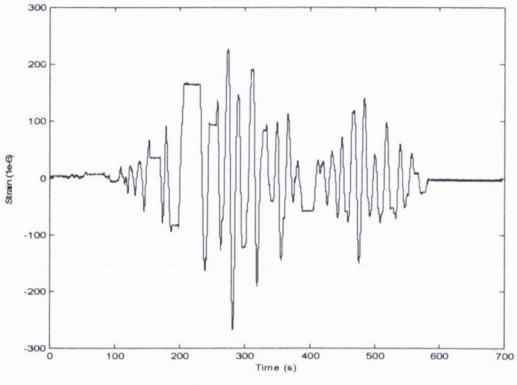

Figure D7.10: Strain Gauge 10

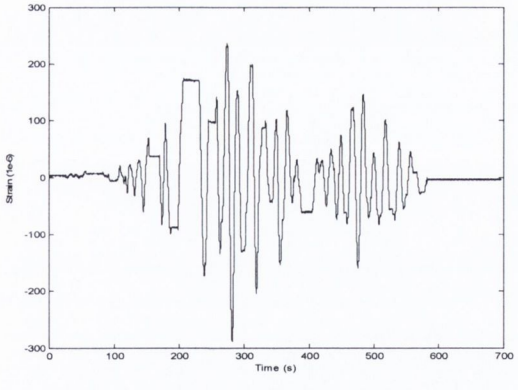

Figure D7.11: Strain Gauge 11

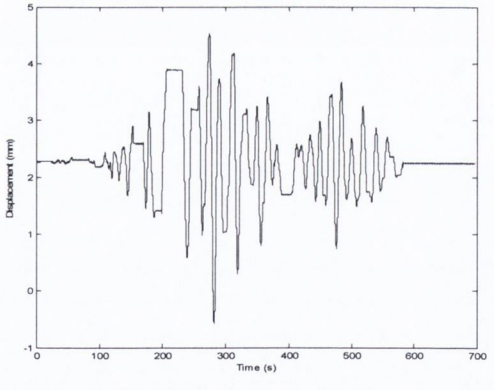

Figure D7.12: LVDT at Node 13

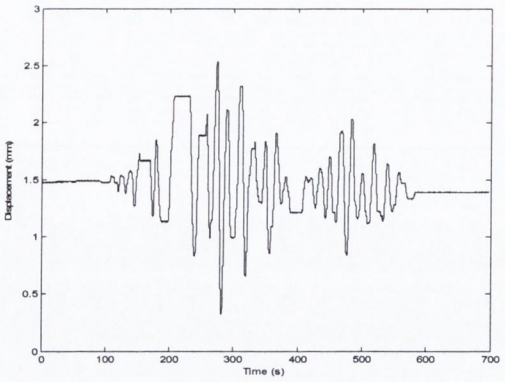

Figure D7.13: LVDT at Node 12

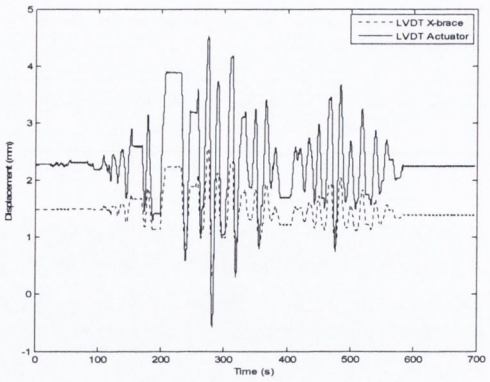

Figure D7.14: LVDT at Node 12 & 13

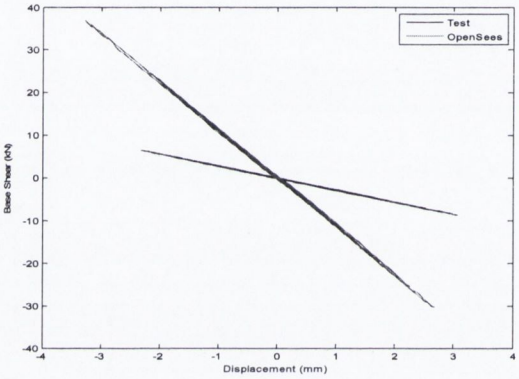

Figure D7.15: Base shear vs. displacement at Node 12

Appendix D8 – TEST 2D Results

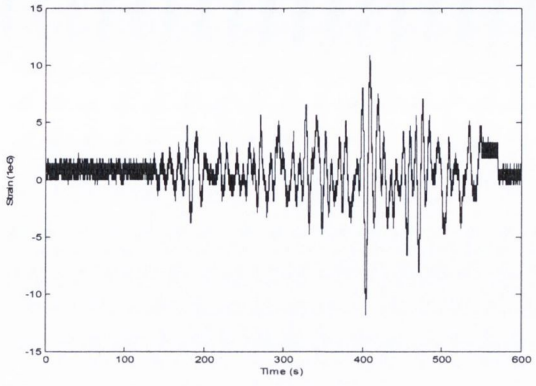

Figure D8.1: Strain Gauge 1

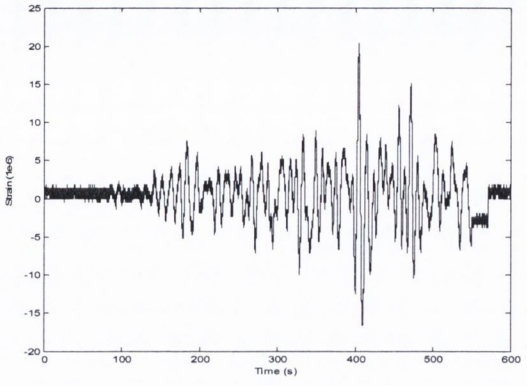

Figure D8.2: Strain Gauge 2

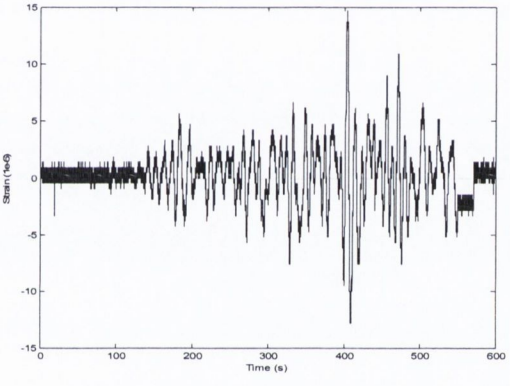

Figure D8.3: Strain Gauge 3

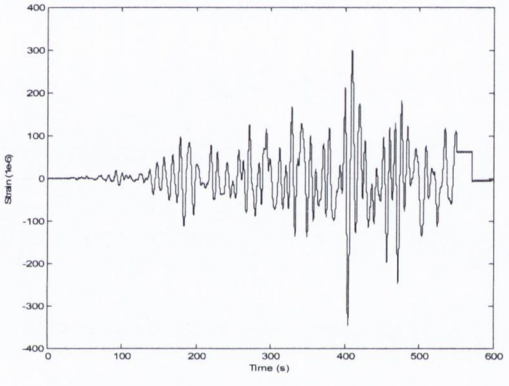

Figure D8.4: Strain Gauge 4

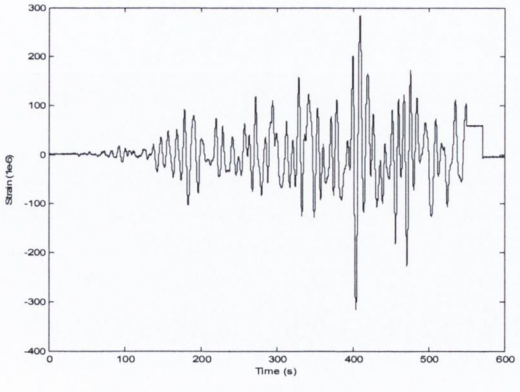

Figure D8.5: Strain Gauge 5

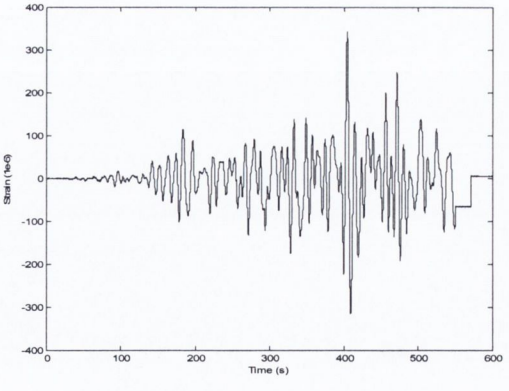

Figure D8.6: Strain Gauge 6

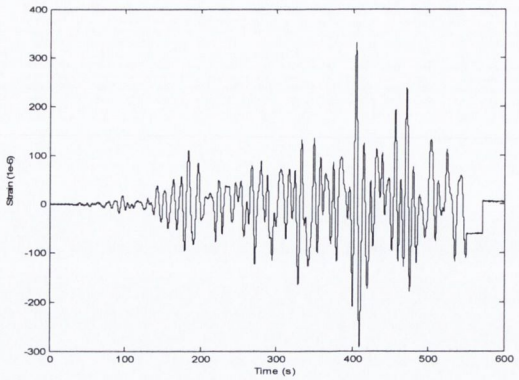

Figure D8.7: Strain Gauge 7

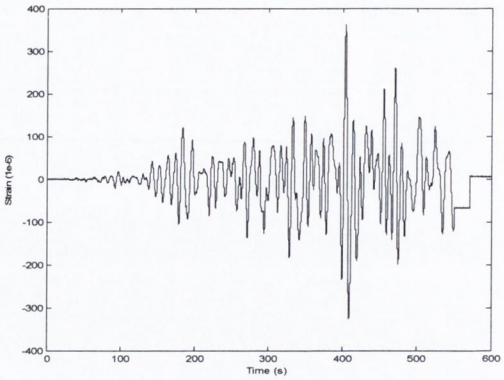

Figure D8.8: Strain Gauge 8

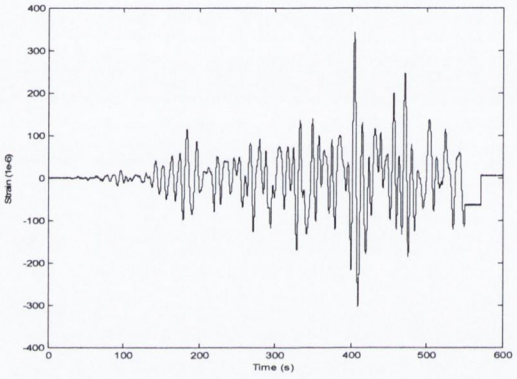

Figure D8.9: Strain Gauge 9

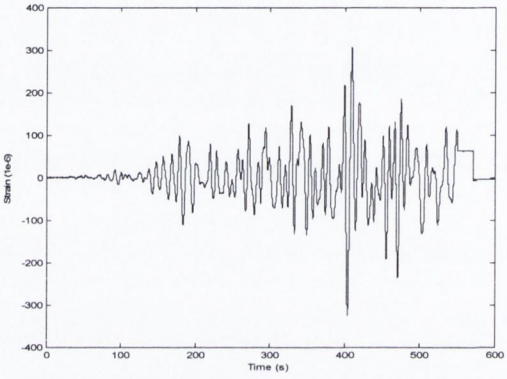

Figure D8.10: Strain Gauge 10

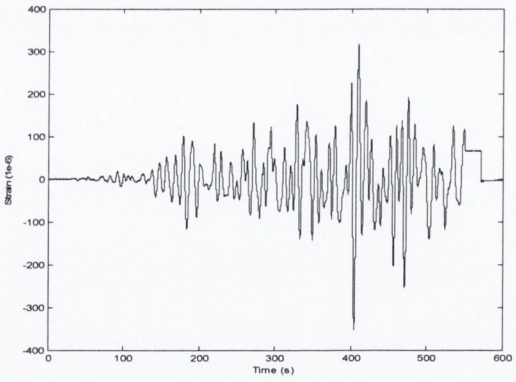

Figure D8.11: Strain Gauge 11

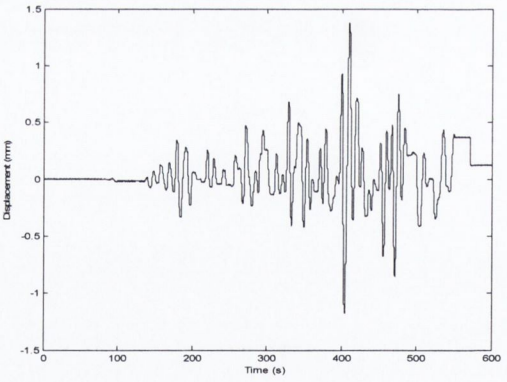

Figure D8.12: LVDT at Node 13

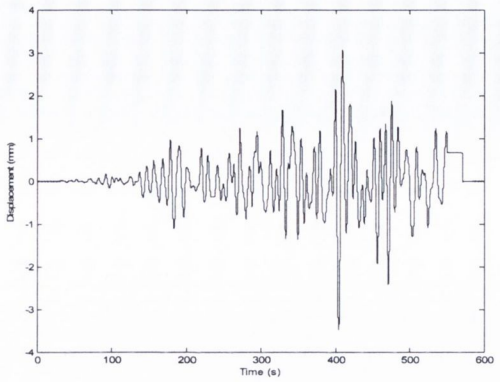

Figure D8.13: Strain Gauge 12

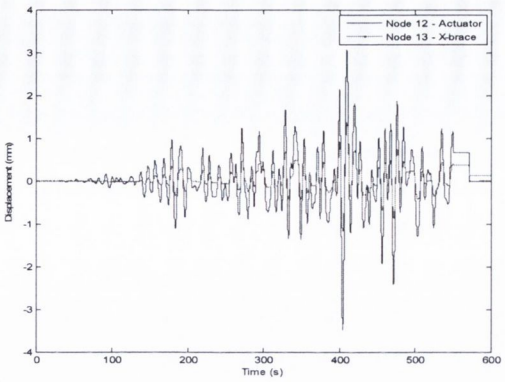

Figure D8.14: LVDT at Node 12 & 13

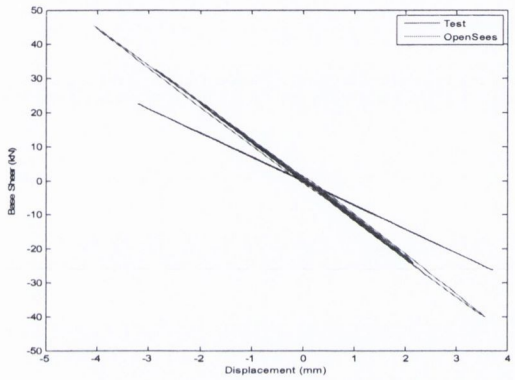

Figure D8.15: Base shear vs. displacement at Node 12

Appendix D9 – TEST 2E Results

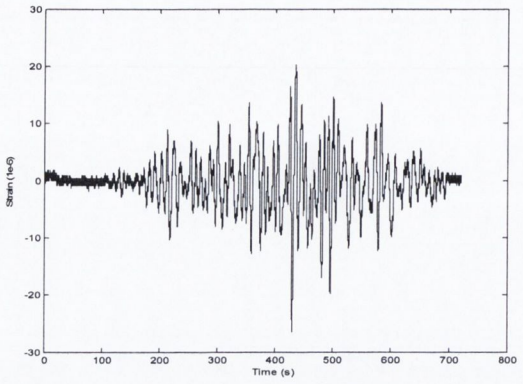

Figure D9.1: Strain Gauge 1

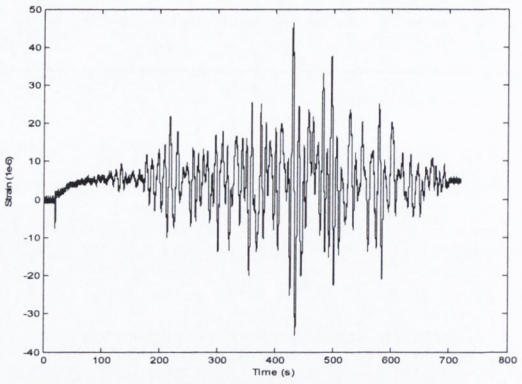

Figure D9.2: Strain Gauge 2

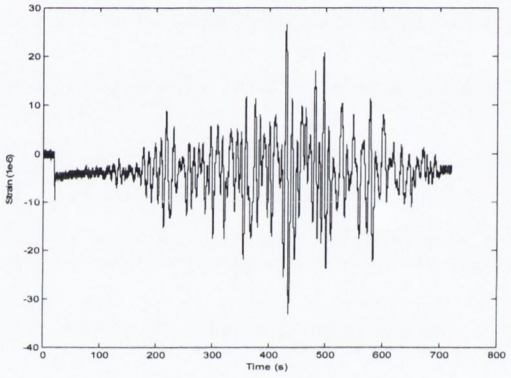

Figure D9.3: Strain Gauge 3

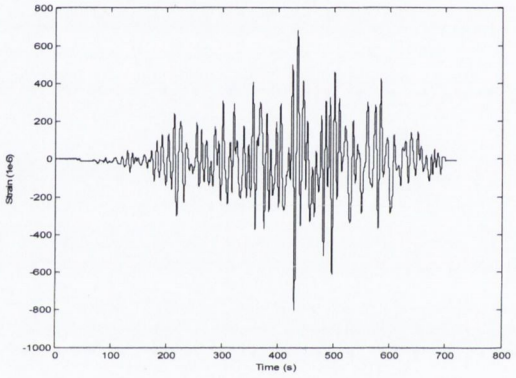

Figure D9.4: Strain Gauge 4

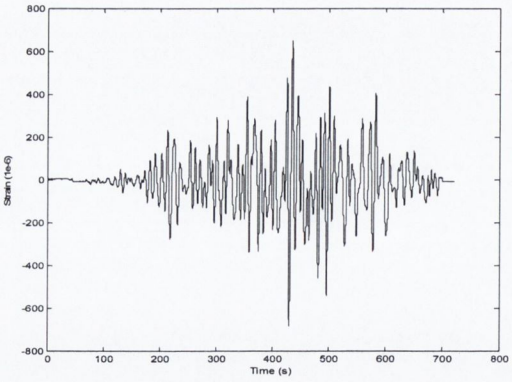

Figure D9.5: Strain Gauge 5

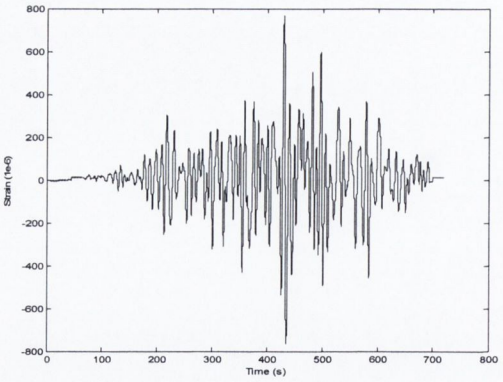

Figure D9.6: Strain Gauge 6

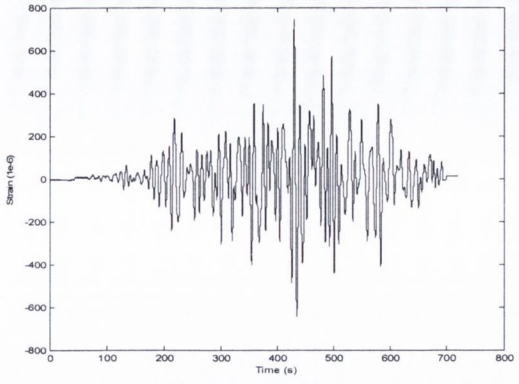

Figure D9.7: Strain Gauge 7

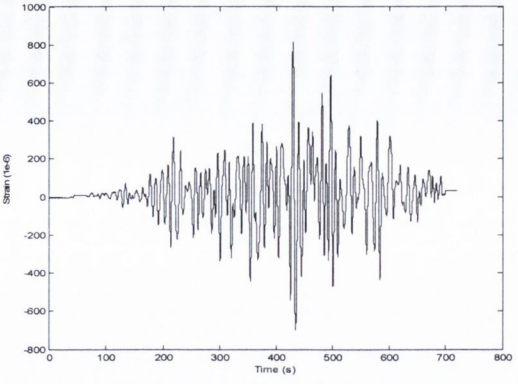

Figure D9.8: Strain Gauge 8

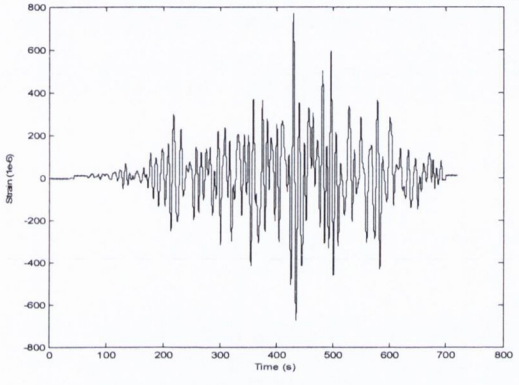

Figure D9.9: Strain Gauge 9

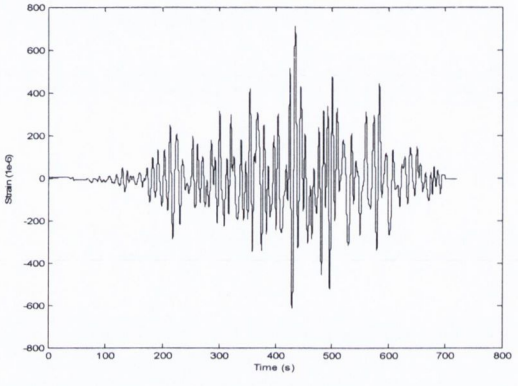

Figure D9.10: Strain Gauge 10

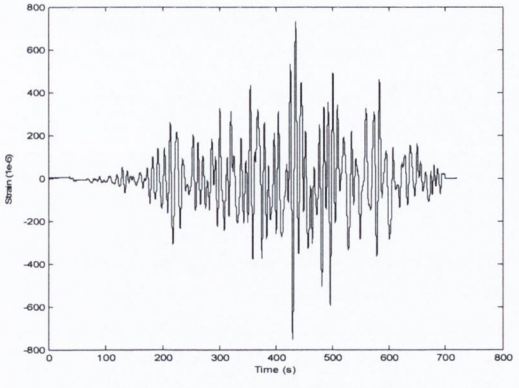

Figure D9.11: Strain Gauge 11

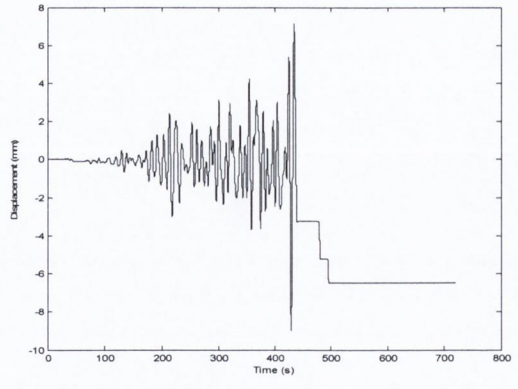

Figure D9.12: LVDT at Node 13

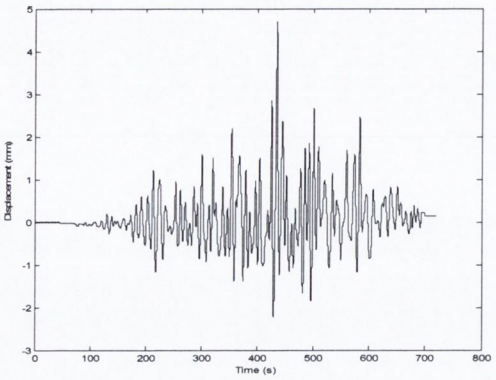

Figure D9.13: Strain Gauge 12

Appendix D10 – TEST 2F Results

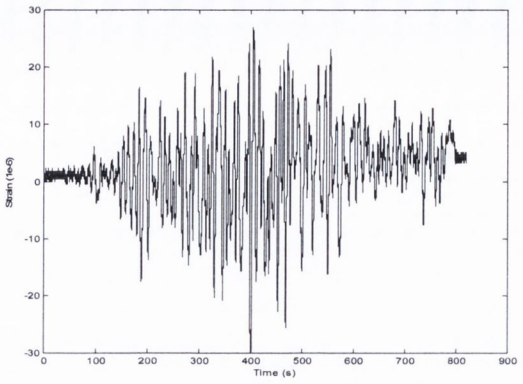

Figure D10.1: Strain Gauge 1

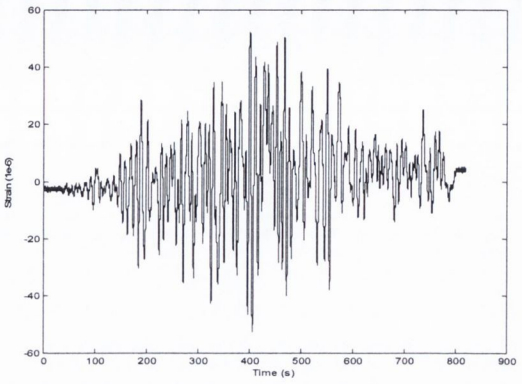

Figure D10.2: Strain Gauge 2

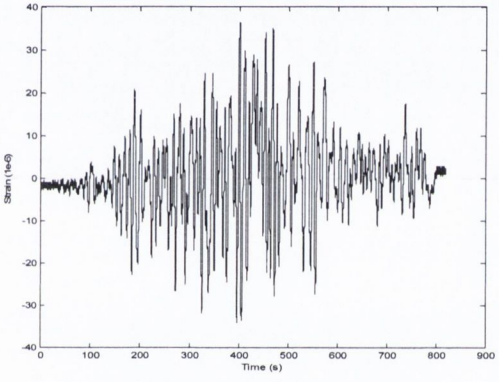

Figure D10.3: Strain Gauge 3

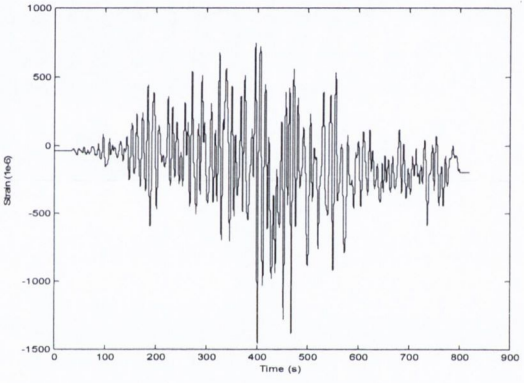

Figure D10.4: Strain Gauge 4

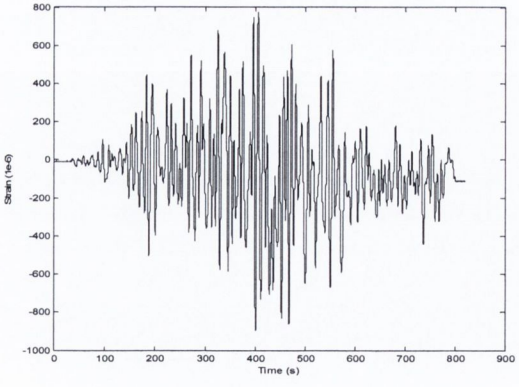

Figure D10.5: Strain Gauge 5

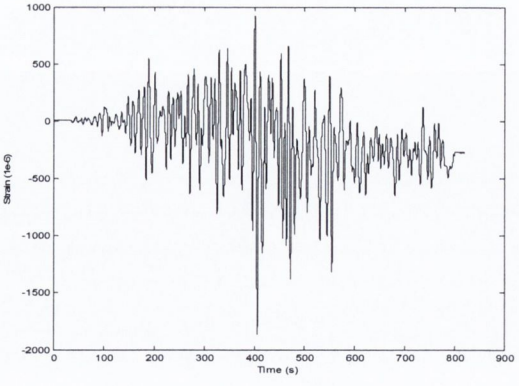

Figure D10.6: Strain Gauge 6

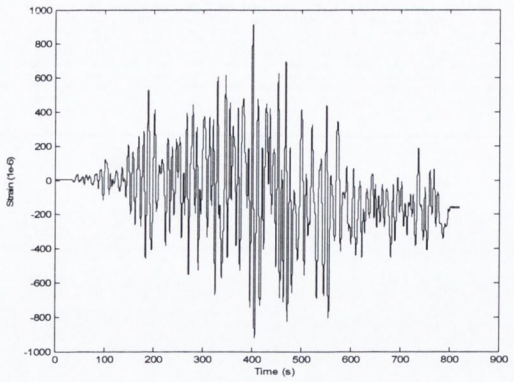

Figure D10.7: Strain Gauge 7

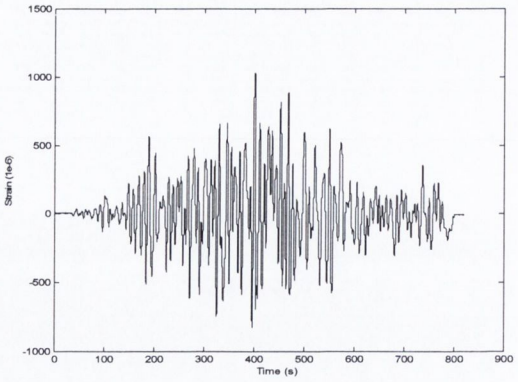

Figure D10.8: Strain Gauge 8

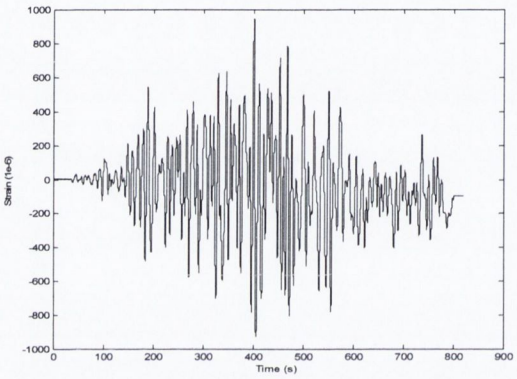

Figure D10.9: Strain Gauge 9

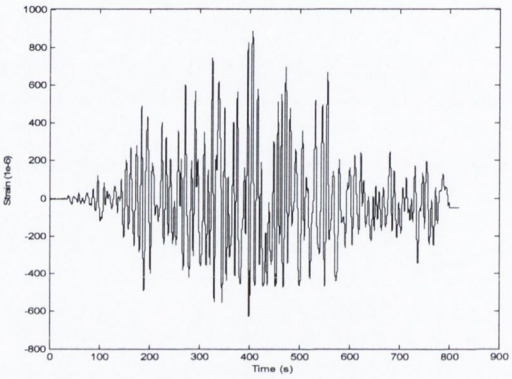

Figure D10.10: Strain Gauge 10

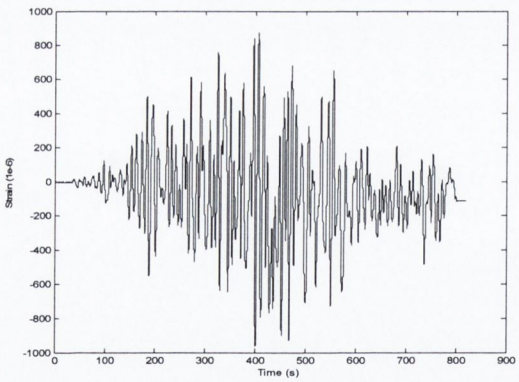

Figure D10.11: Strain Gauge 11

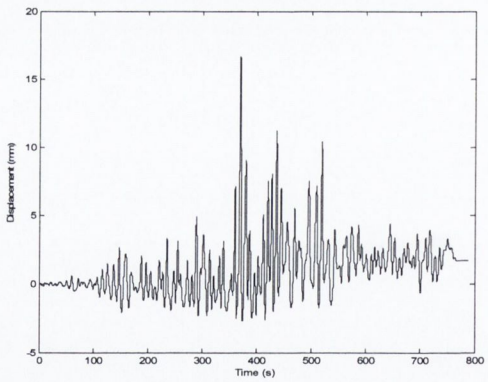

Figure D10.12: LVDT at Node 13

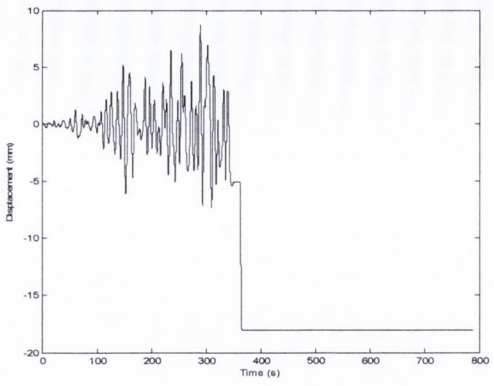

Figure D10.12: LVDT at Node 12

Appendix D11 – Test 3B Results

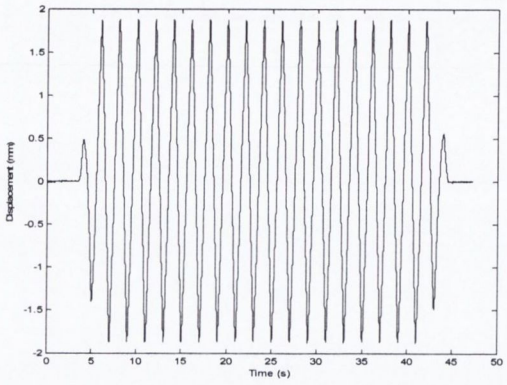

Figure D11.1: Displacement command vs. time

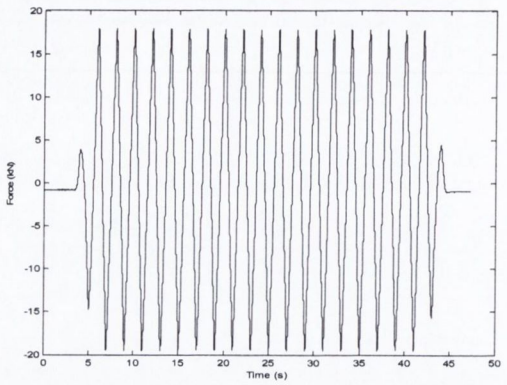

Figure D11.2: Force feedback vs. time

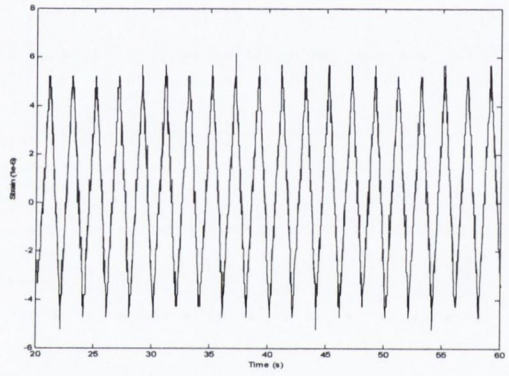

Figure D11.3: Strain Gauge 1

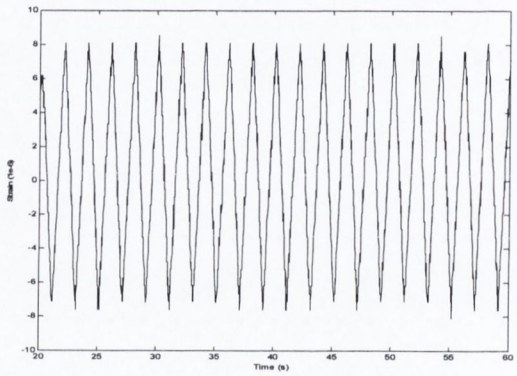

Figure D11.4: Strain Gauge 2

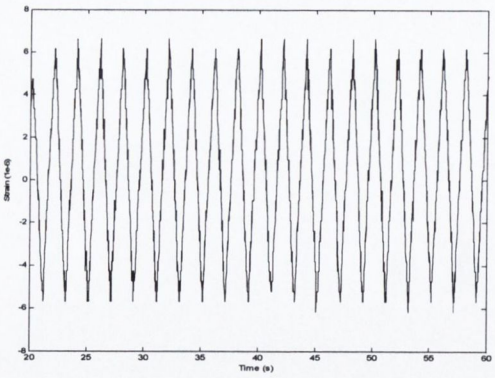

Figure D11.5: Strain Gauge 3

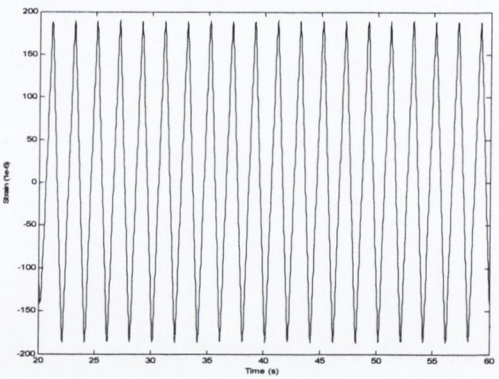

Figure D11.6: Strain Gauge 4

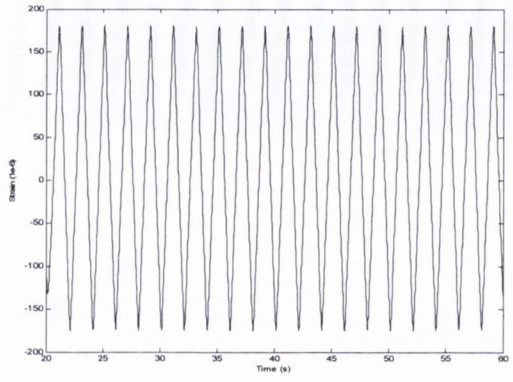

Figure D11.7: Strain Gauge 5

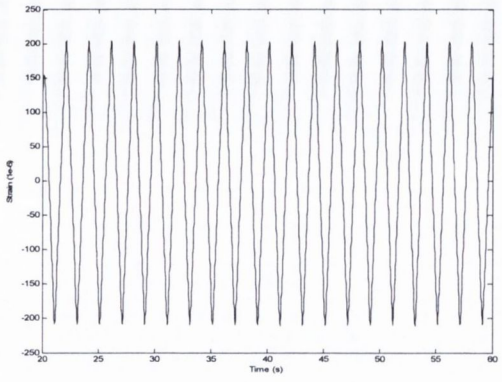

Figure D11.8: Strain Gauge 6

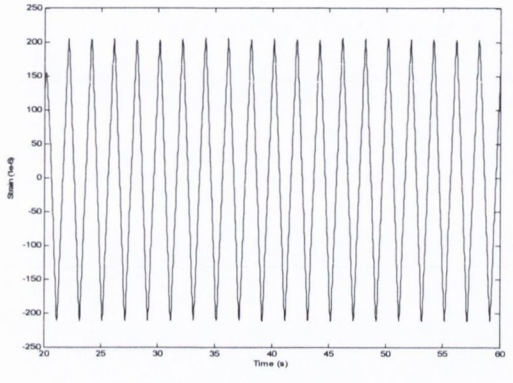

Figure D11.9: Strain Gauge 7

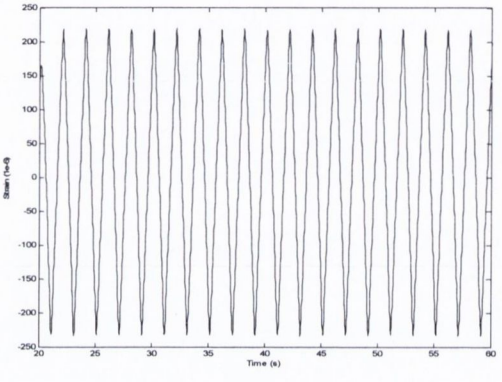

Figure D11.10: Strain Gauge 8

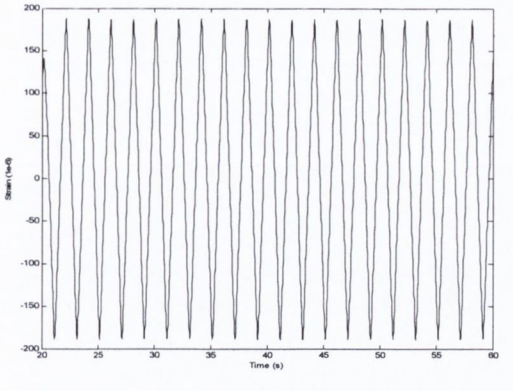

Figure D11.11: Strain Gauge 9

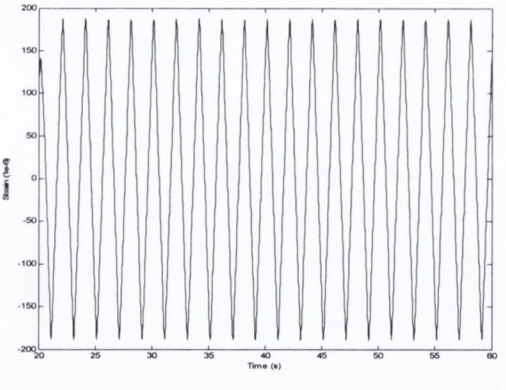

Figure D11.12: Strain Gauge 10

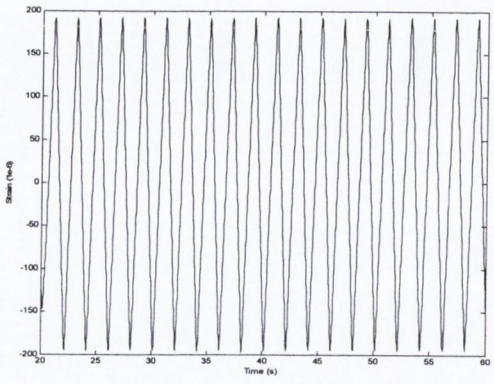

Figure D11.13: Strain Gauge 11

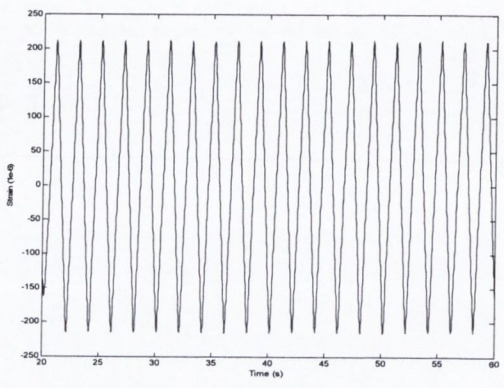

Figure D11.14: LVDT at Node 13

Appendix D12 – Test 3C Results

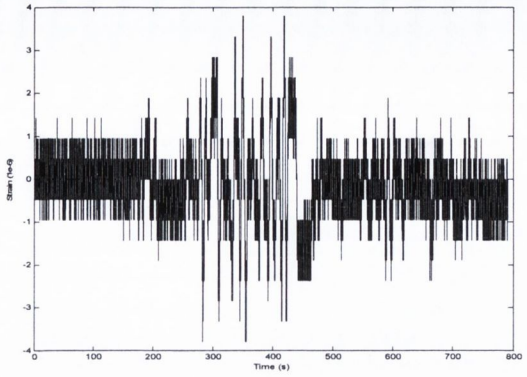

Figure D12.1: Strain Gauge 1

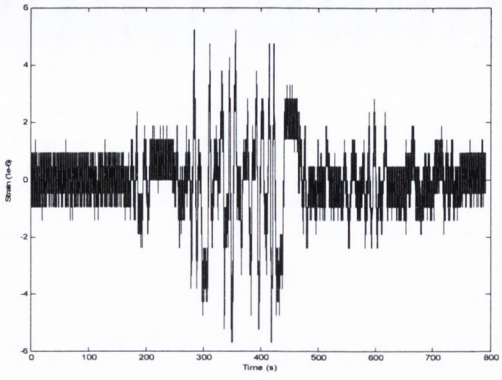

Figure D12.2: Strain Gauge 2

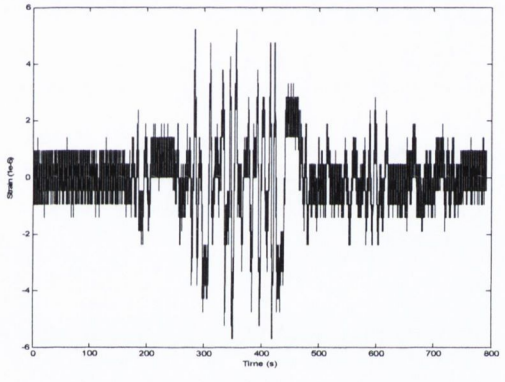

Figure D12.3: Strain Gauge 3

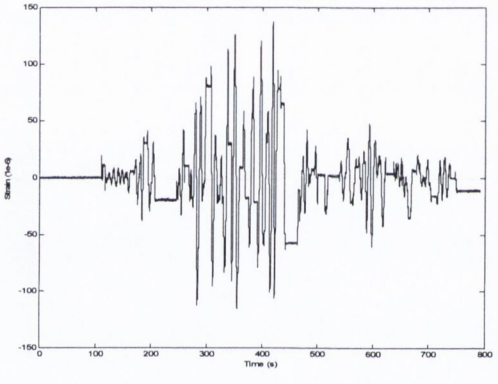

Figure D12.4: Strain Gauge 4

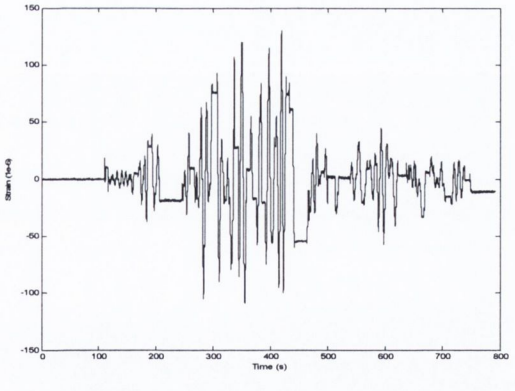

Figure D12.5: Strain Gauge 5

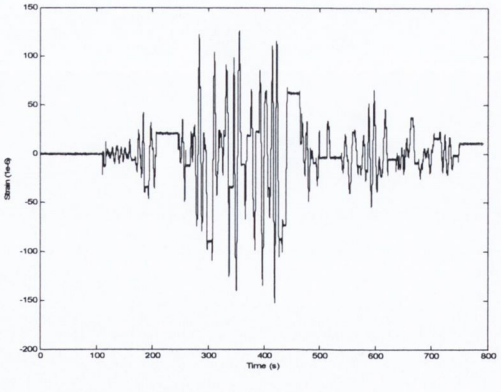

Figure D12.6: Strain Gauge 6

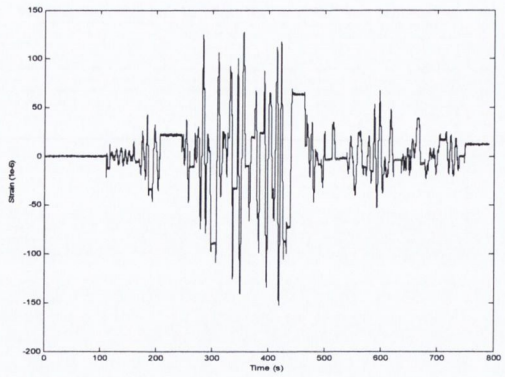

Figure D12.7: Strain Gauge 7

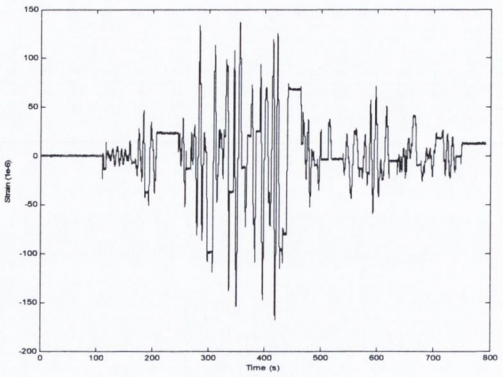

Figure D12.8: Strain Gauge 8

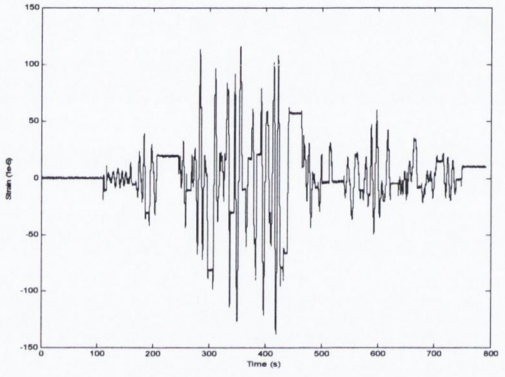

Figure D12.9: Strain Gauge 9

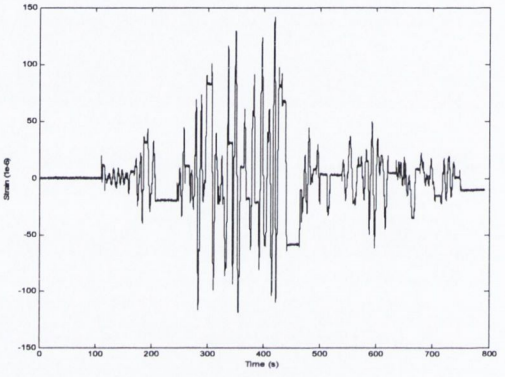

Figure D12.10: Strain Gauge 10

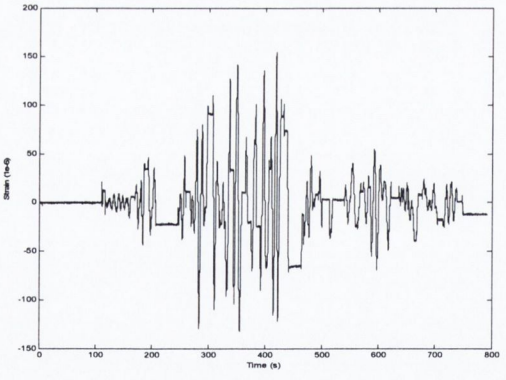

Figure D12.11: Strain Gauge 11

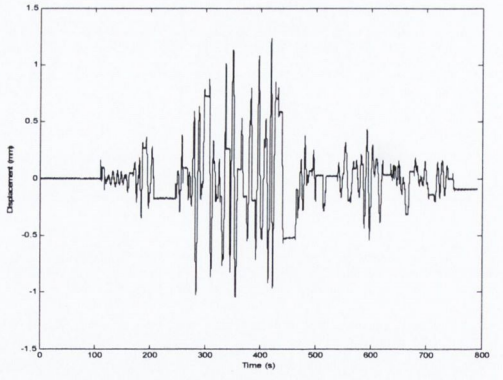

Figure D12.12: LVDT at Node 12

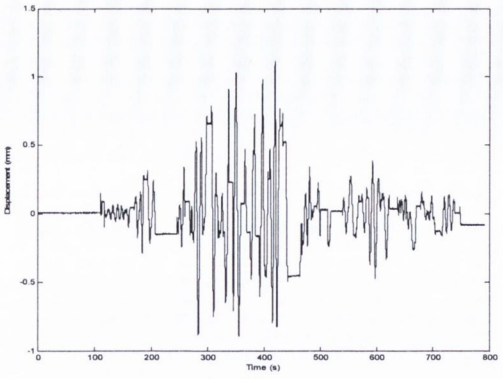

Figure D12.13: LVDT at Node 13

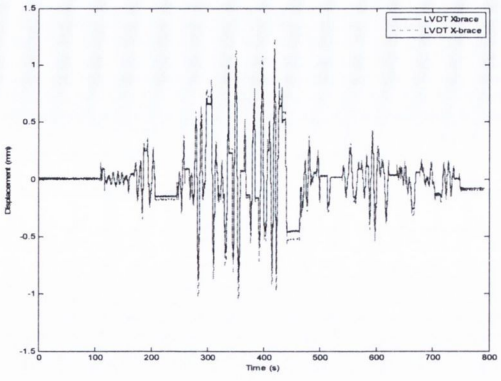

Figure D12.14: LVDT at Nodes 12 & 13

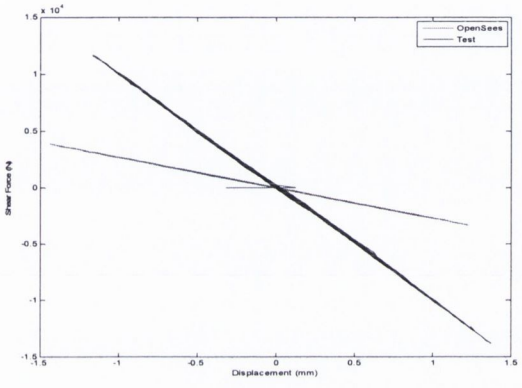

Figure D12.15: Base shear vs. displacement at Node 12

Appendix D13 – TEST 3D Results

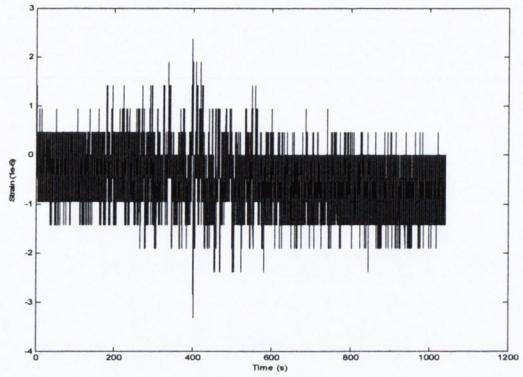

Figure D13.1: Strain Gauge 1

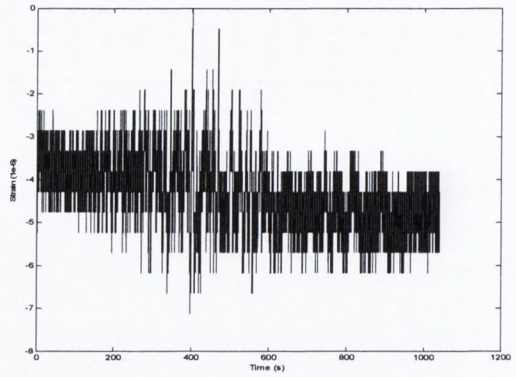

Figure D13.2: Strain Gauge 2

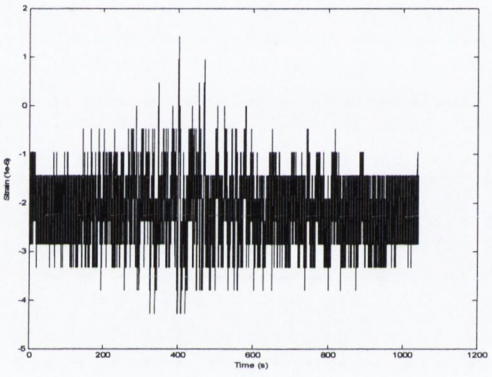

Figure D13.3: Strain Gauge 3

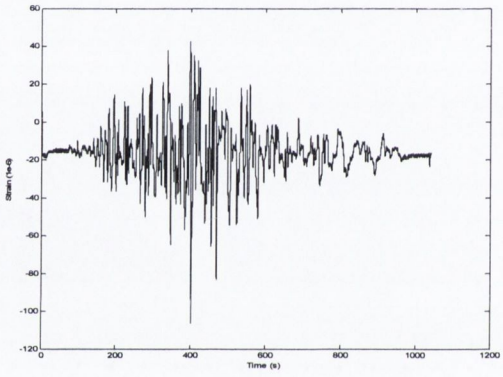

Figure D13.4: Strain Gauge 4

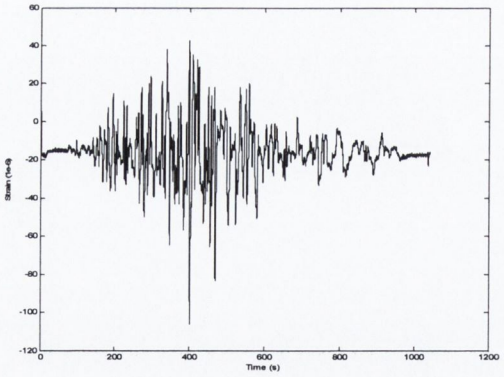

Figure D13.5: Strain Gauge 5

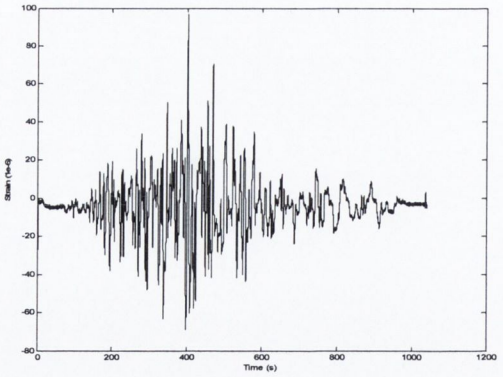

Figure D13.6: Strain Gauge 6

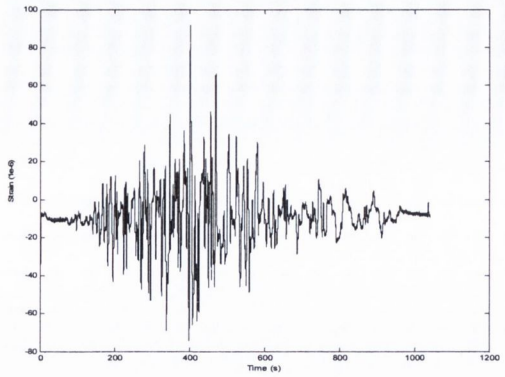

Figure D13.7: Strain Gauge 7

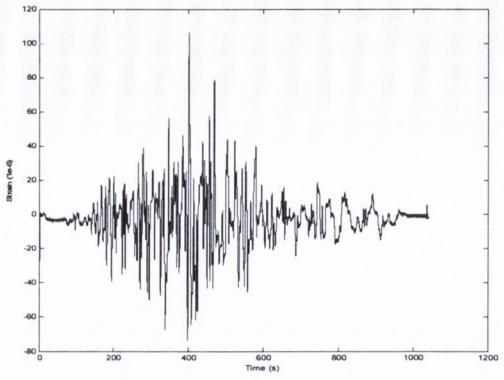

Figure D13.8: Strain Gauge 8

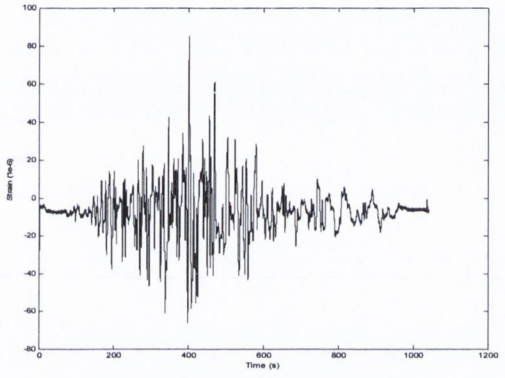

Figure D13.9: Strain Gauge 9

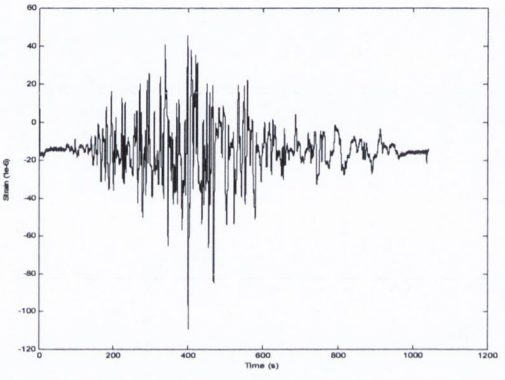

Figure D13.10: Strain Gauge 10

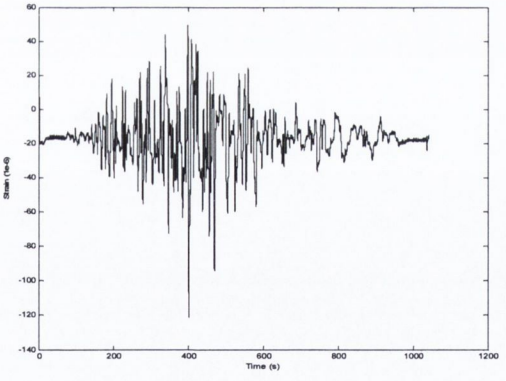

Figure D13.11: Strain Gauge 11

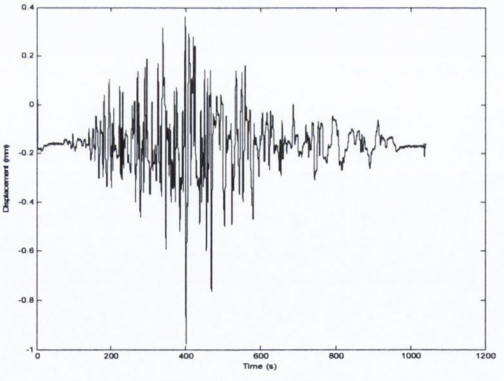

Figure D13.12: LVDT at Node 12

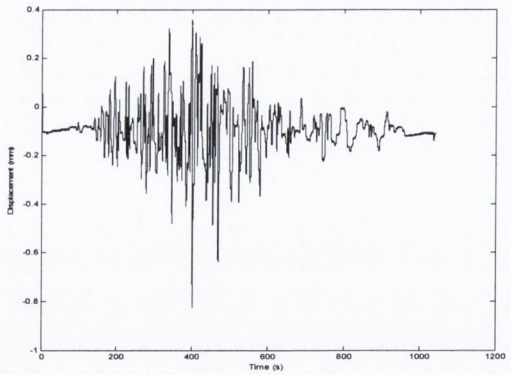

Figure D13.13: LVDT at Node 13

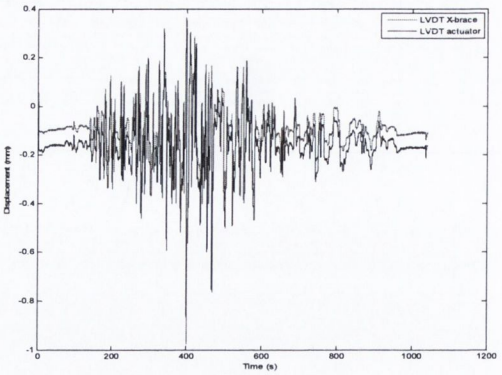

Figure D13.14: LVDT at Node 12 & 13

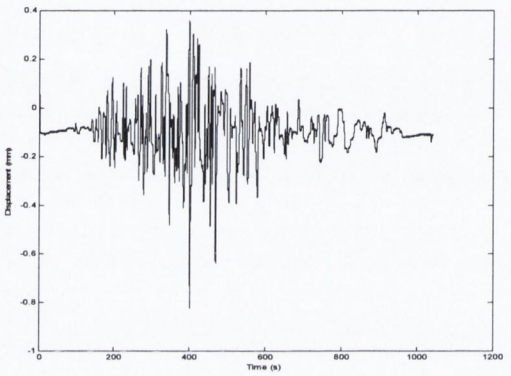

Figure D13.15: Base shear vs. displacement at Node 12

Appendix D14 – TEST 3E Results

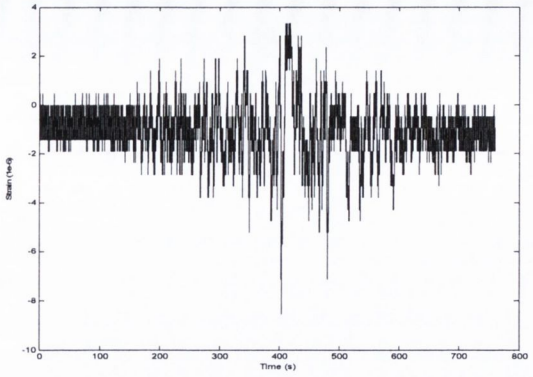

Figure D14.1: Strain Gauge 1

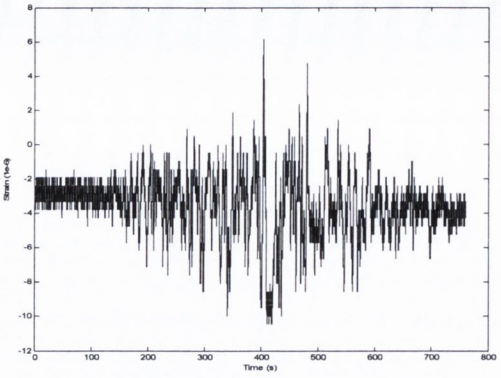

Figure D14.2: Strain Gauge 2

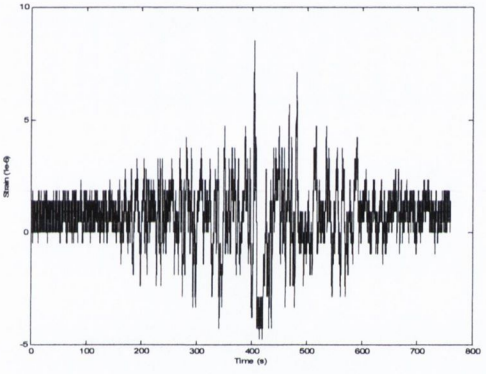

Figure D14.3: Strain Gauge 3

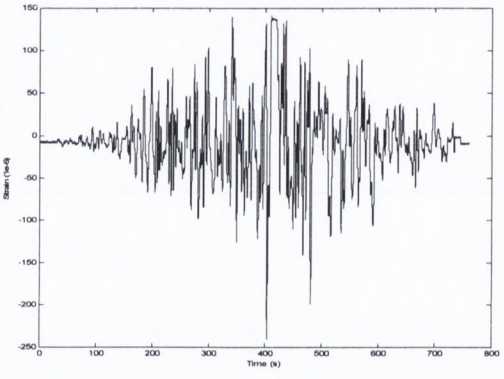

Figure D14.4: Strain Gauge 4

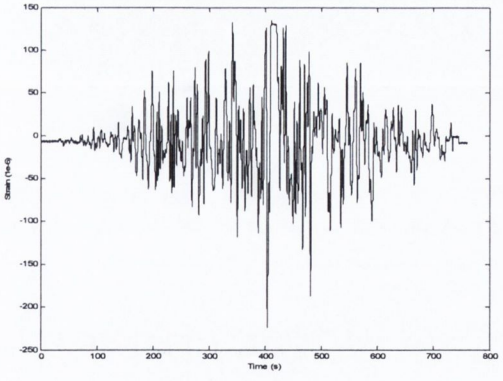

Figure D14.5: Strain Gauge 5

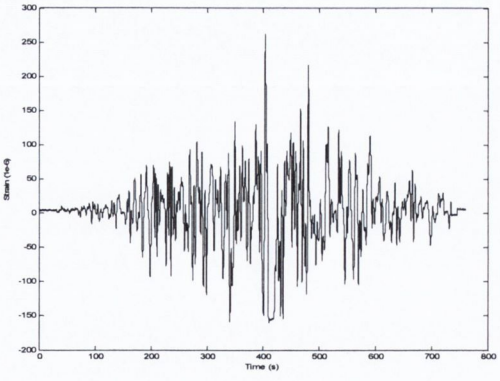

Figure D14.6: Strain Gauge 6

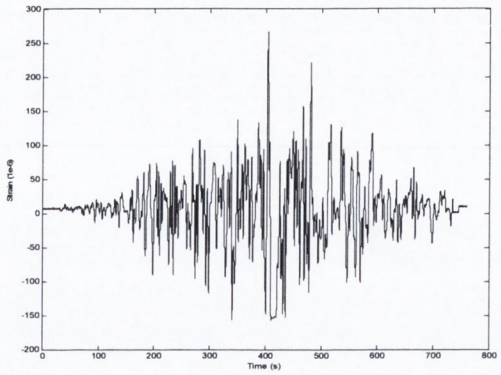

Figure D14.7: Strain Gauge 7

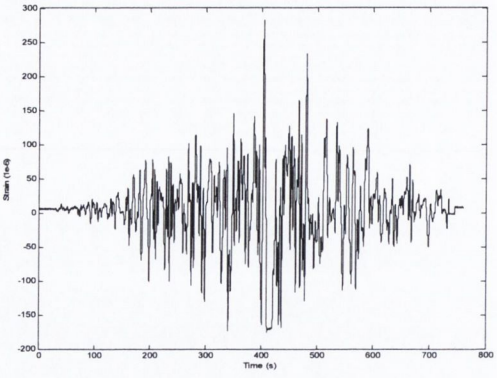

Figure D14.8: Strain Gauge 8

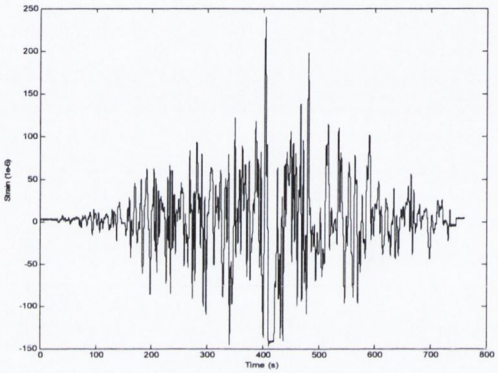

Figure D14.9: Strain Gauge 9

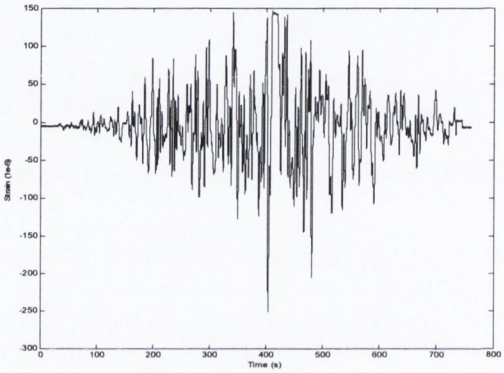

Figure D14.10: Strain Gauge 10

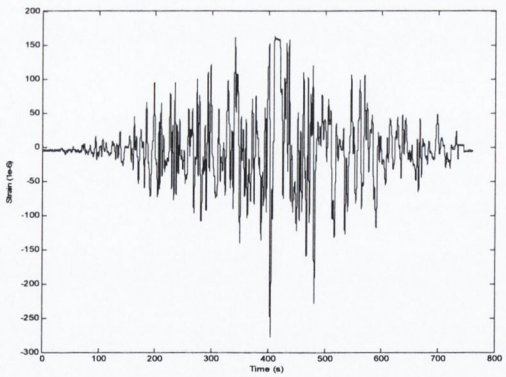

Figure D14.11: Strain Gauge 11

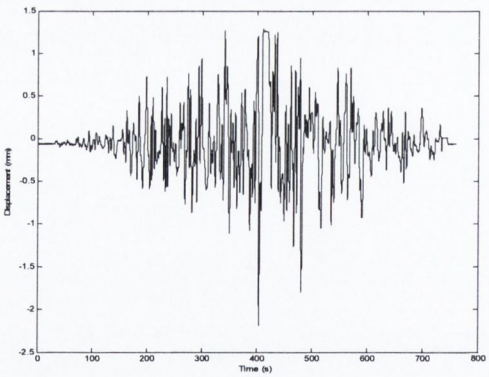

Figure D14.12: LVDT at Node 12

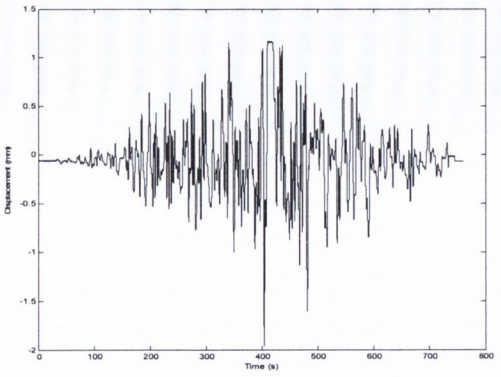

Figure D14.13: LVDT at Node 13

Appendix D15 – TEST 3F Results

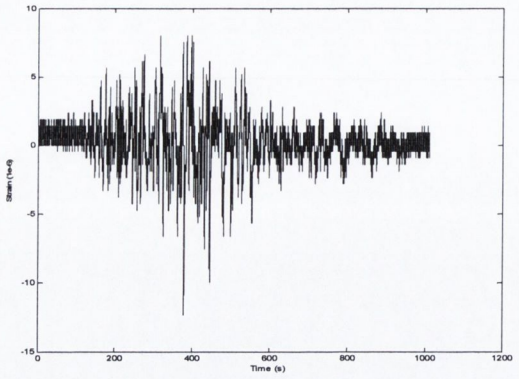

Figure D15.1: Strain Gauge 1

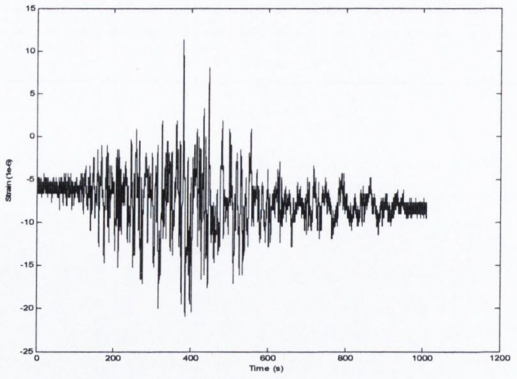

Figure D15.2: Strain Gauge 2

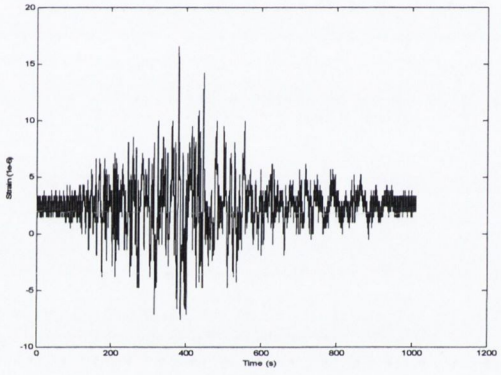

Figure D15.3: Strain Gauge 3

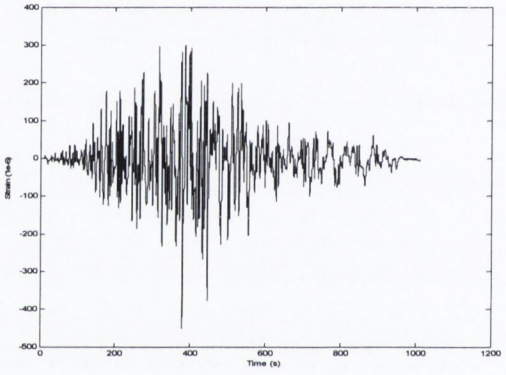

Figure D15.4: Strain Gauge 4

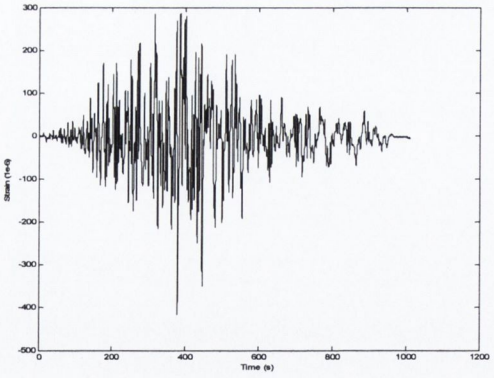

Figure D15.5: Strain Gauge 5

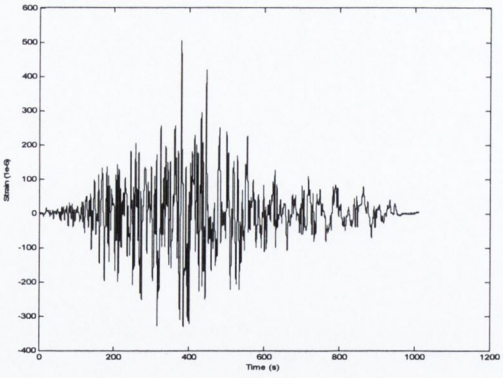

Figure D15.6: Strain Gauge 6

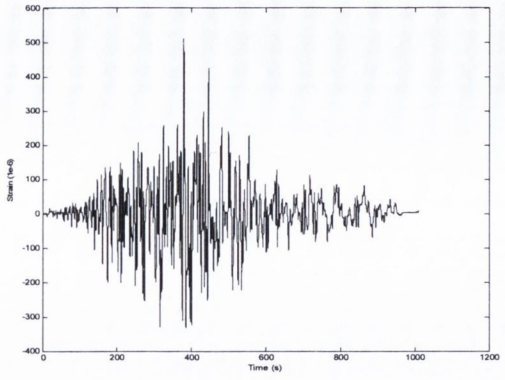

Figure D15.7: Strain Gauge 7

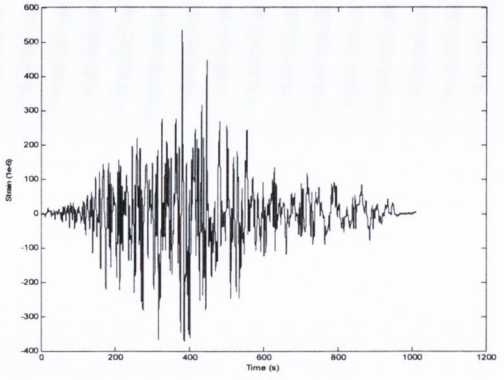

Figure D15.8: Strain Gauge 8

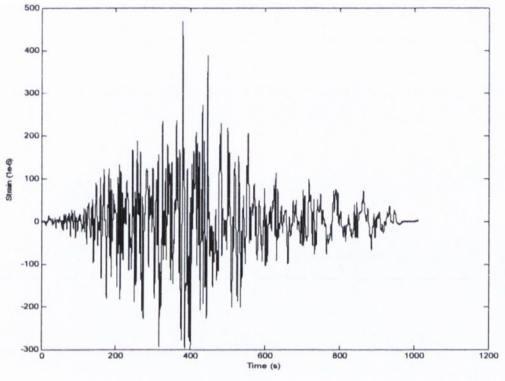

Figure D15.9: Strain Gauge 9

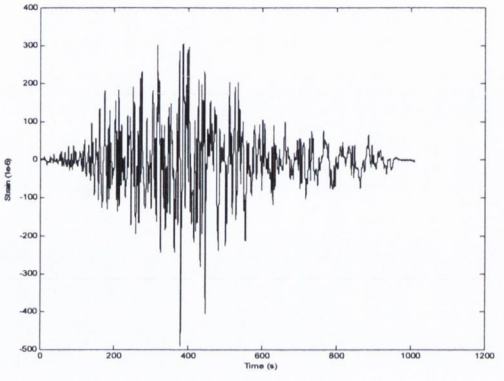

Figure D15.10: Strain Gauge 10

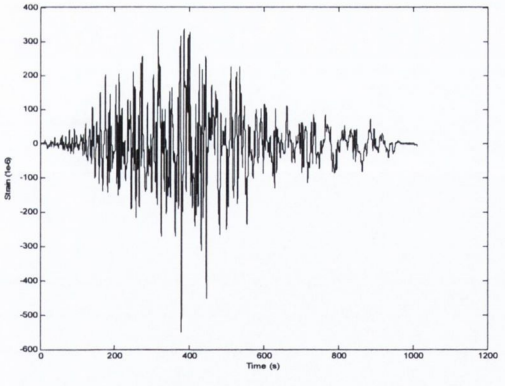

Figure D15.11: Strain Gauge 11

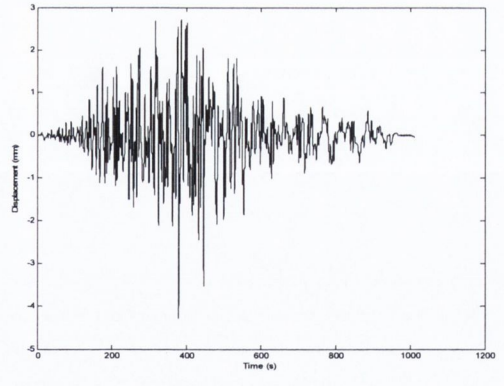

Figure D15.12: LVDT at Node 12

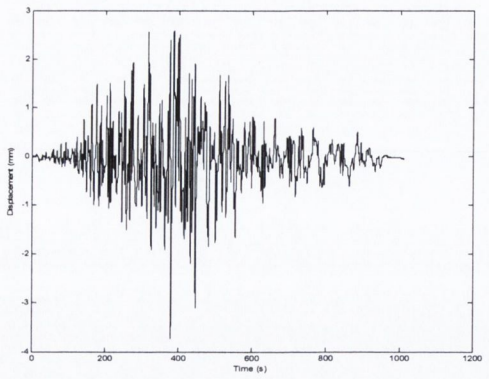

Figure D15.13: LVDT at Node 13

Appendix D16 – Test 4B Results

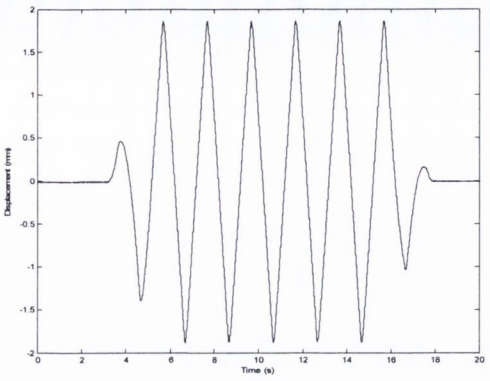

Figure D16.1: Displacement command vs. time

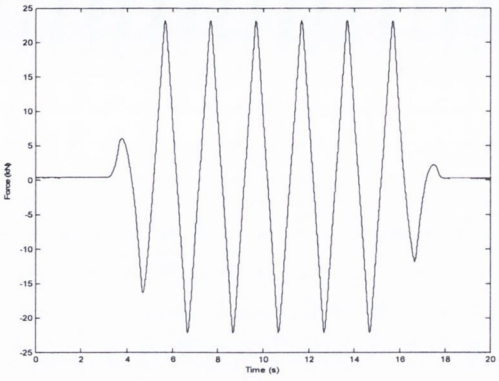

Figure D16.2: Force feedback vs. time

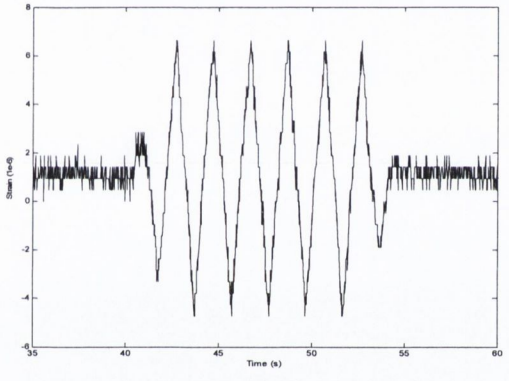

Figure D16.3: Strain Gauge 1

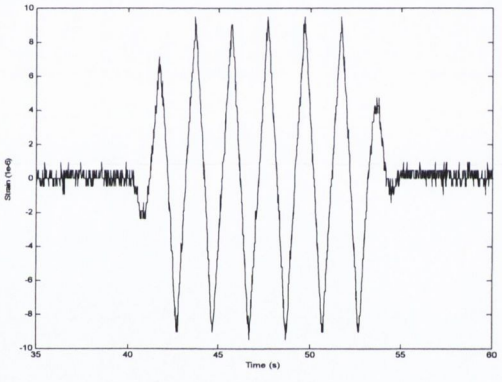

Figure D16.4: Strain Gauge 2

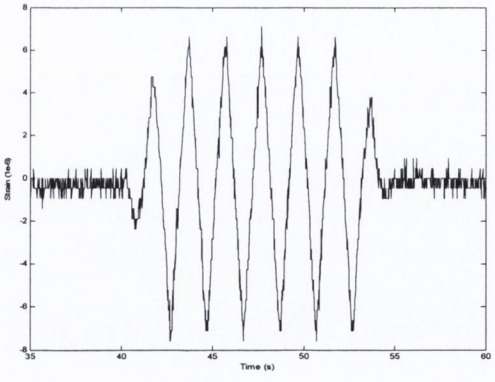

Figure D16.5: Strain Gauge 3

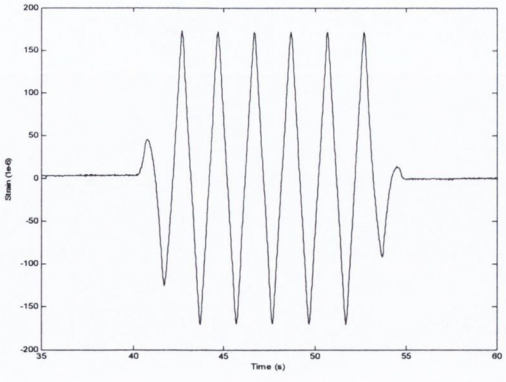

Figure D16.6: Strain Gauge 4

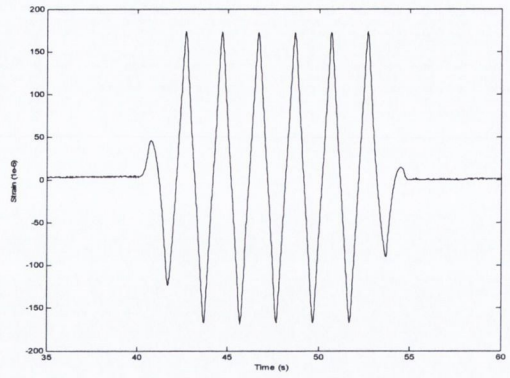

Figure D16.7: Strain Gauge 5

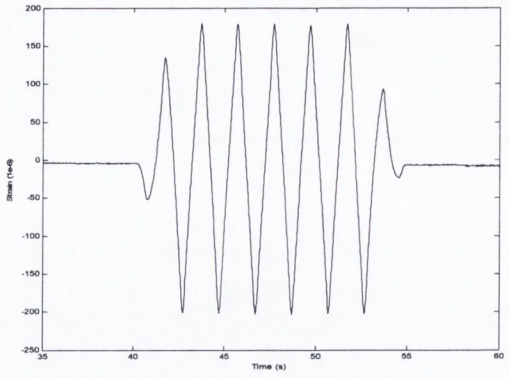

Figure D16.8: Strain Gauge 6

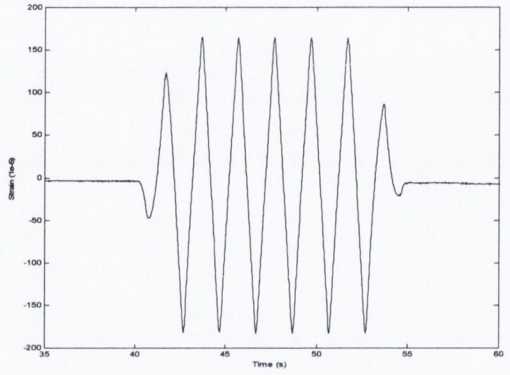

Figure D16.9: Strain Gauge 7

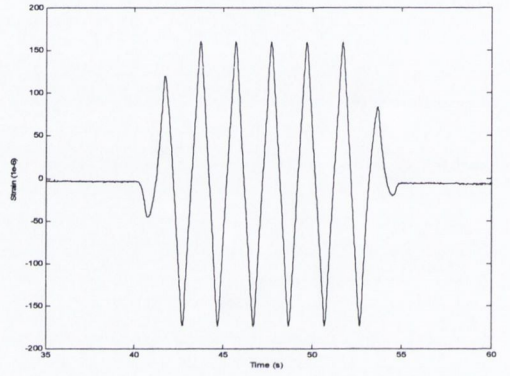

Figure D16.10: Strain Gauge 8

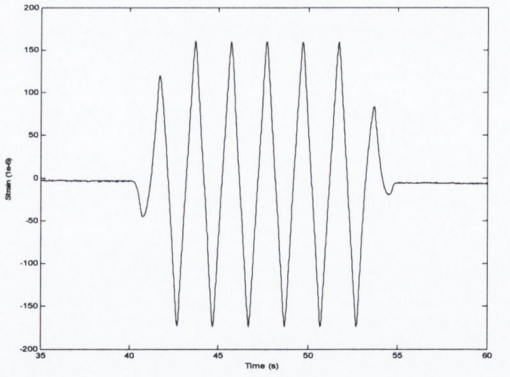

Figure D16.11: Strain Gauge 9

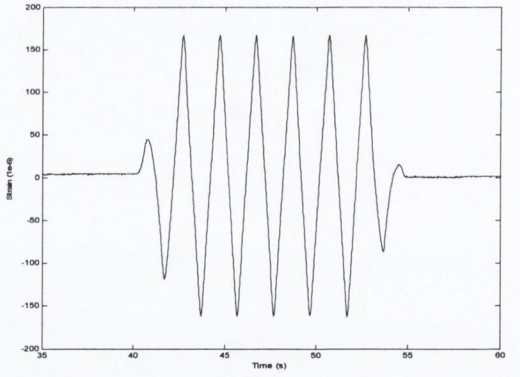

Figure D16.12: Strain Gauge 10

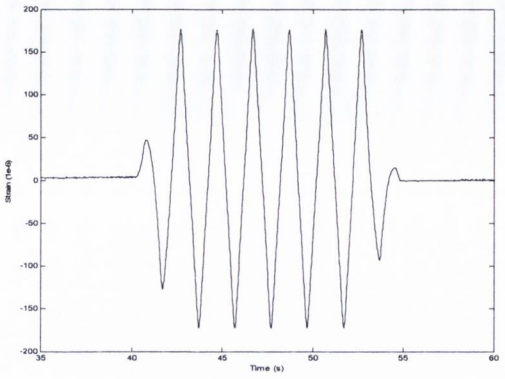

Figure D16.13: Strain Gauge 11

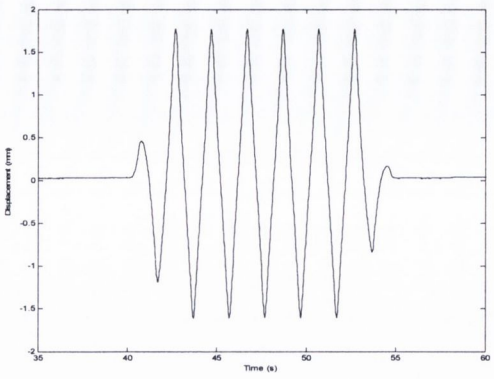

Figure D16.14: LVDT at Node 12

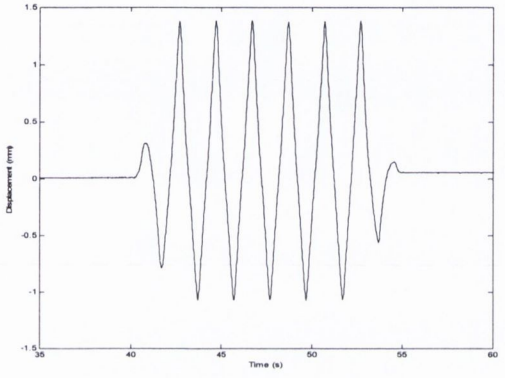

Figure D16.15: LVDT at Node 13

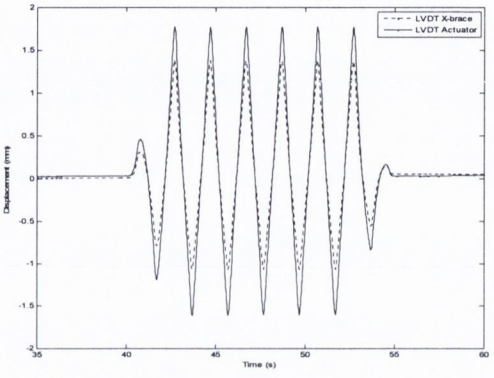

Figure D16.16: LVDT at Node 12 & 13

Appendix D17 – Test 4C Results

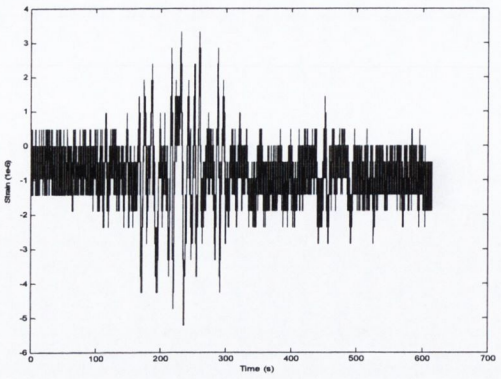

Figure D17.1: Strain Gauge 1

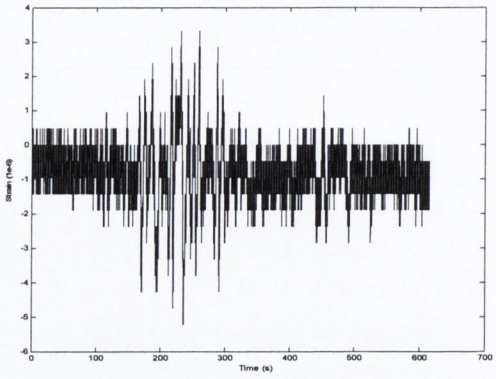

Figure D17.2: Strain Gauge 2

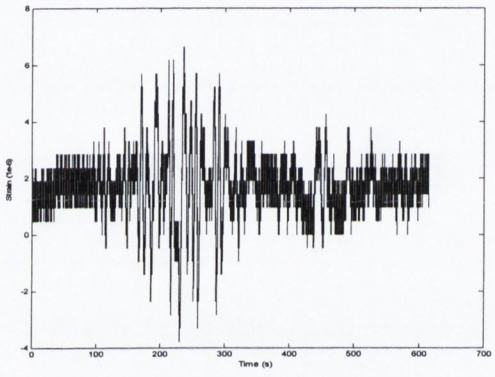

Figure D17.3: Strain Gauge 3

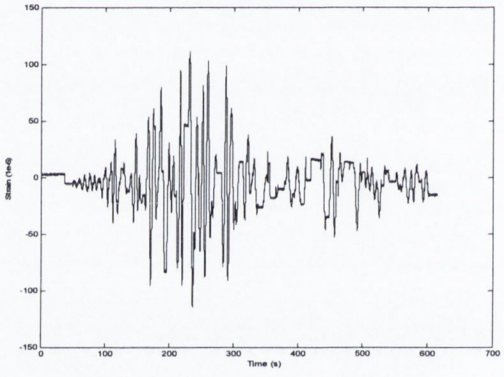

Figure D17.4: Strain Gauge 4

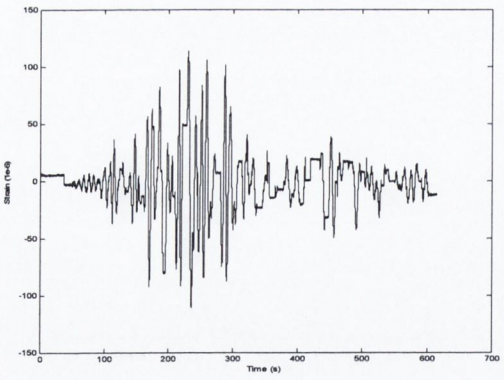

Figure D17.5: Strain Gauge 5

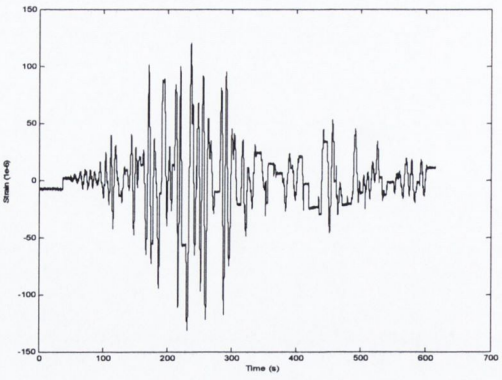

Figure D17.6: Strain Gauge 6

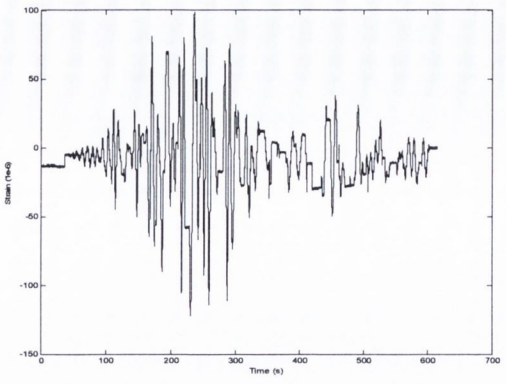

Figure D17.7: Strain Gauge 7

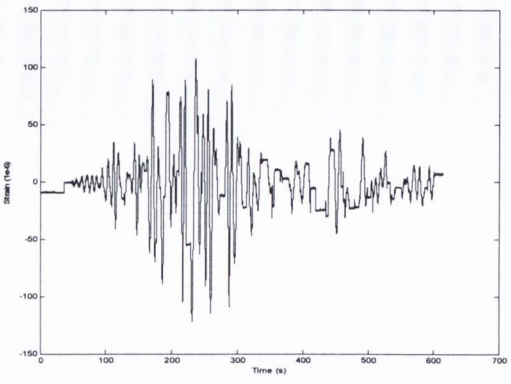

Figure D17.8: Strain Gauge 8

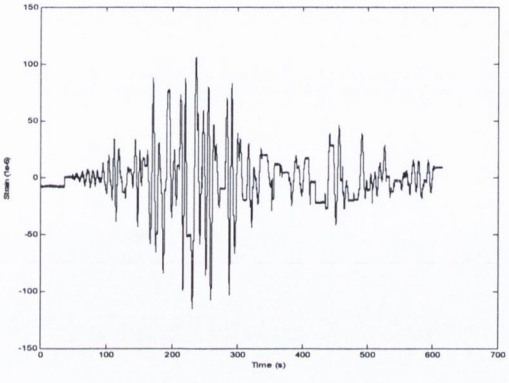

Figure D17.9: Strain Gauge 9

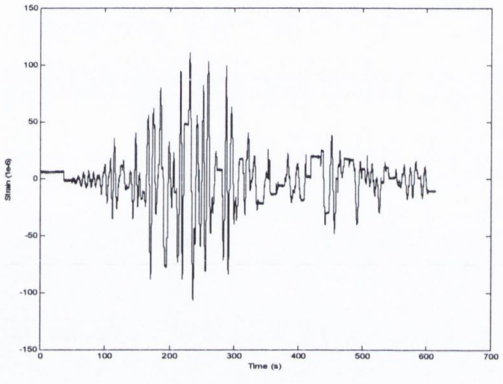

Figure D17.10: Strain Gauge 10

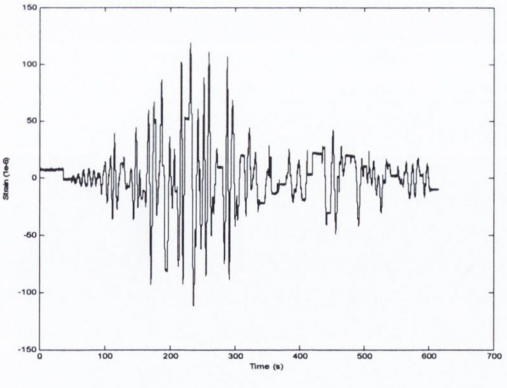

Figure D17.11: Strain Gauge 11

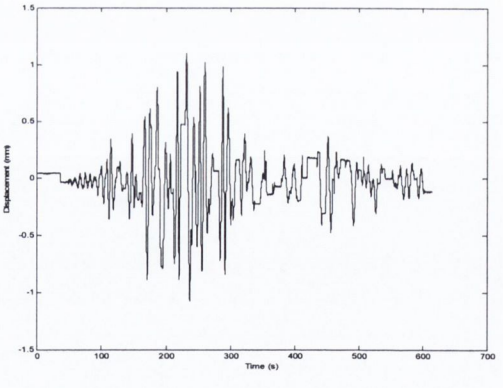

Figure D17.12: LVDT at Node 12

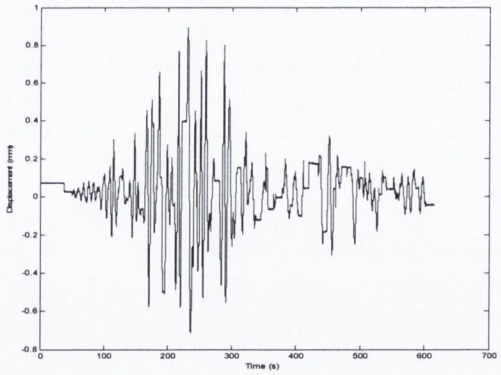

Figure D17.13: LVDT at Node 13

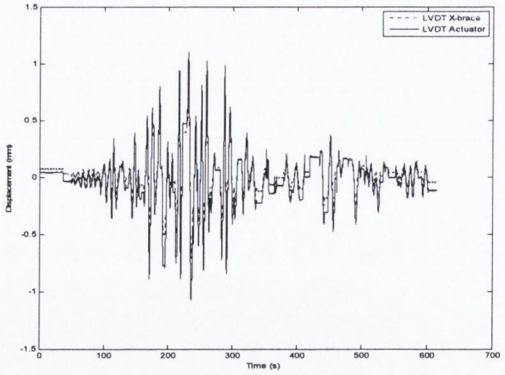

Figure D17.14: LVDT at Node 12 & 13

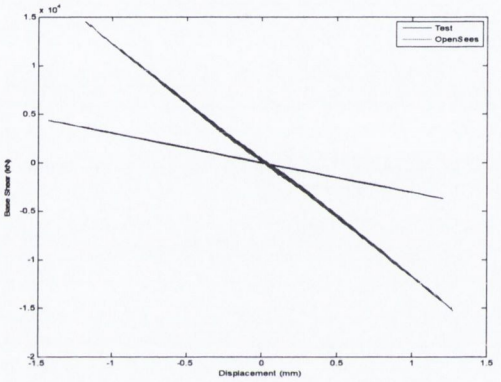

Figure D17.15: Base shear vs. displacement at Node 12

Appendix D18 – TEST 3D Results

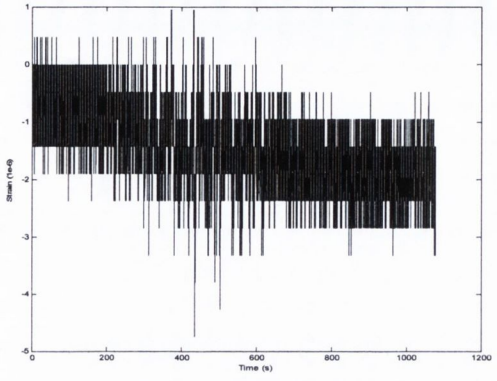

Figure D18.1: Strain Gauge 1

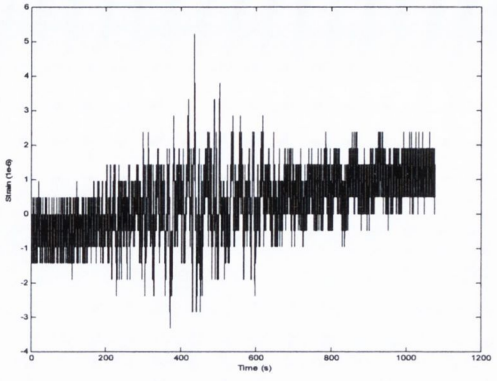

Figure D18.2: Strain Gauge 2

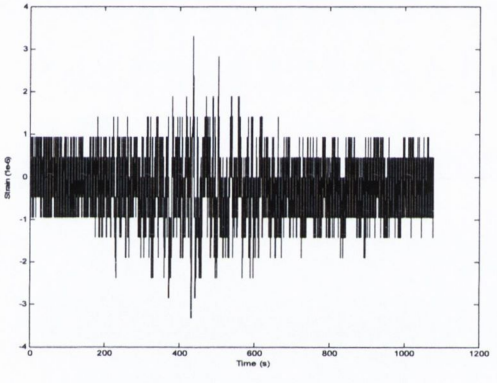

Figure D18.3: Strain Gauge 3

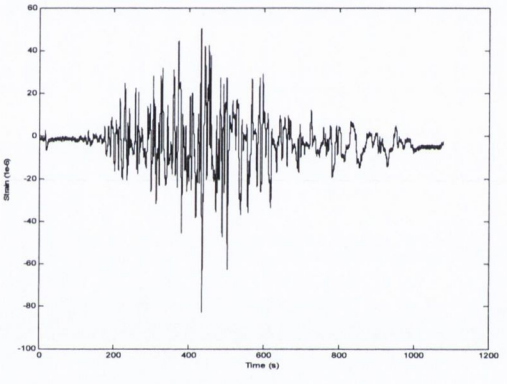

Figure D18.4: Strain Gauge 4

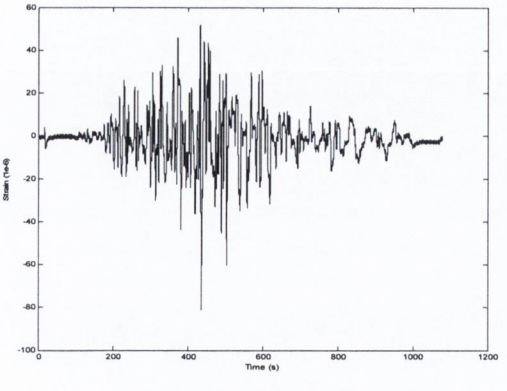

Figure D18.5: Strain Gauge 5

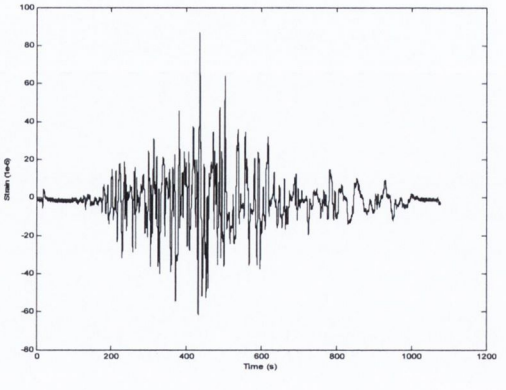

Figure D18.6: Strain Gauge 6

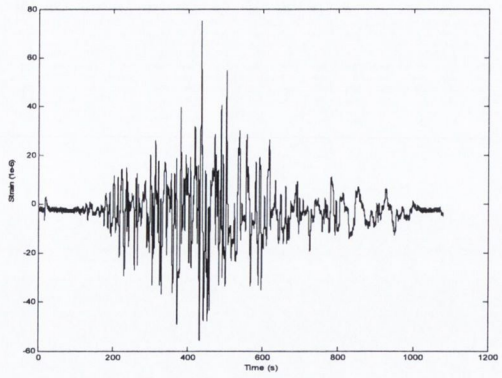

Figure D18.7: Strain Gauge 7

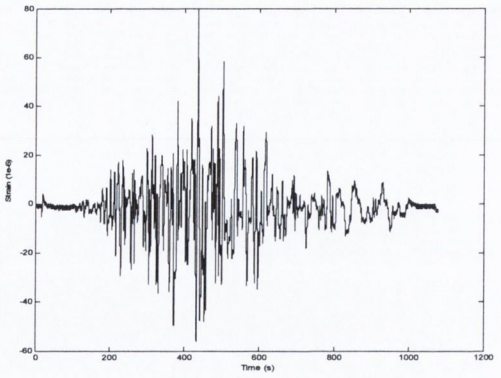

Figure D18.8: Strain Gauge 8

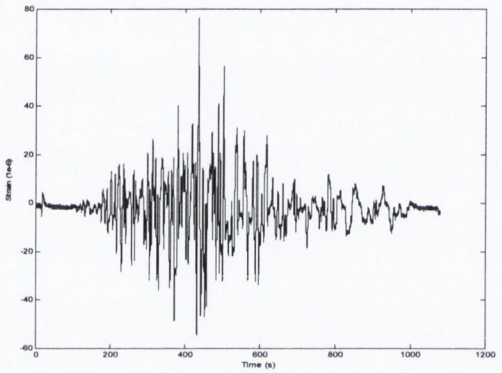

Figure D18.9: Strain Gauge 9

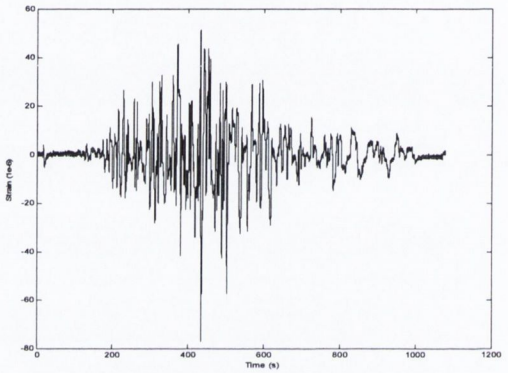

Figure D18.10: Strain Gauge 10

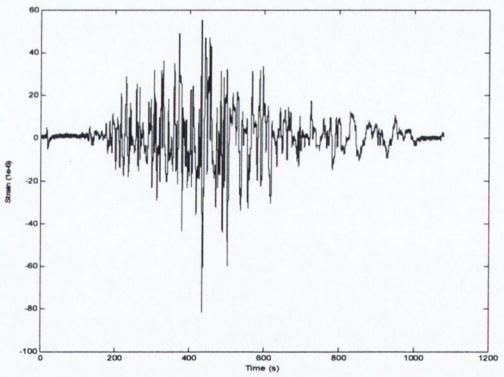

Figure D18.11: Strain Gauge 11

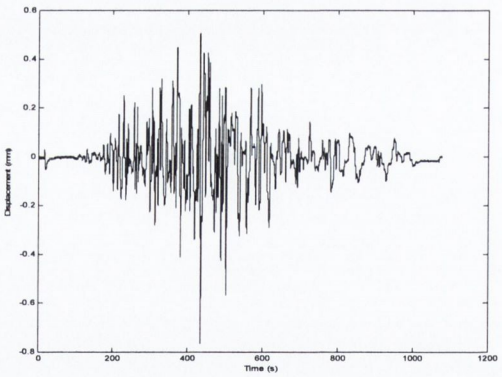

Figure D18.12: LVDT at Node 12

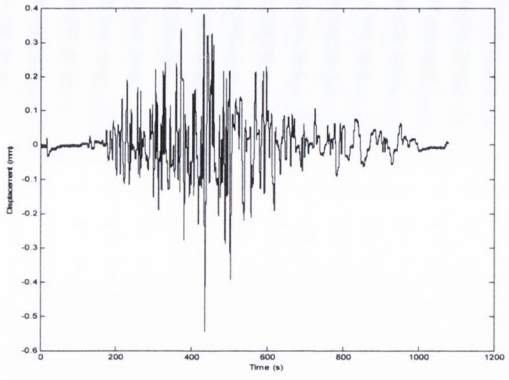

Figure D18.13: LVDT at Node 13

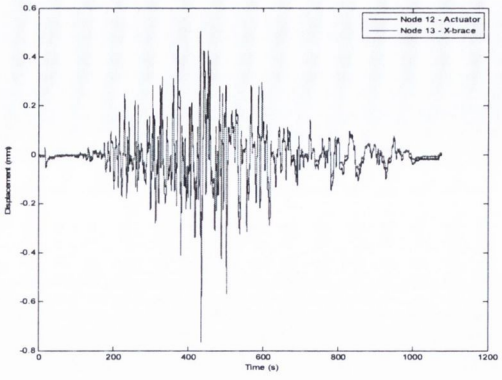

Figure D18.14: LVDT at Node 12 & 13

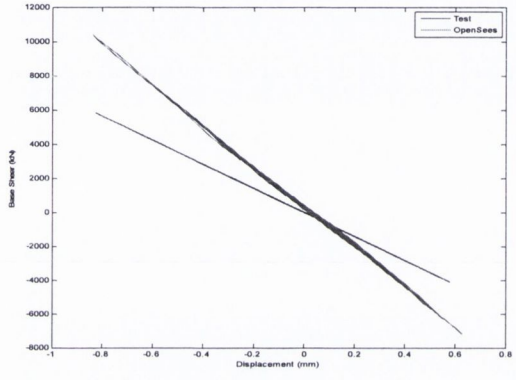

Figure D18.15: Base shear vs. displacement at Node 12

Appendix D19 – TEST 3E Results

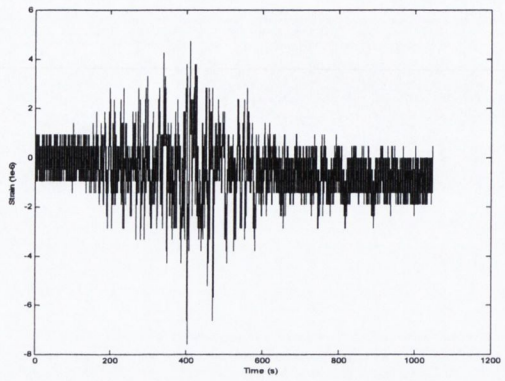

Figure D19.1: Strain Gauge 1

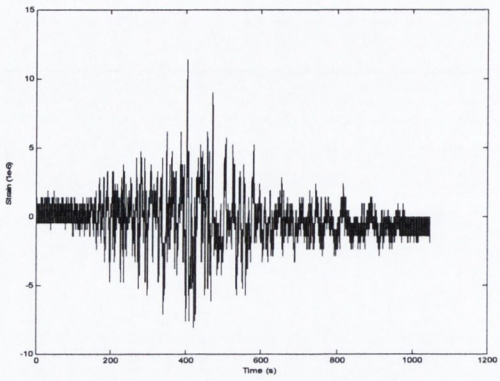

Figure D19.2: Strain Gauge 2

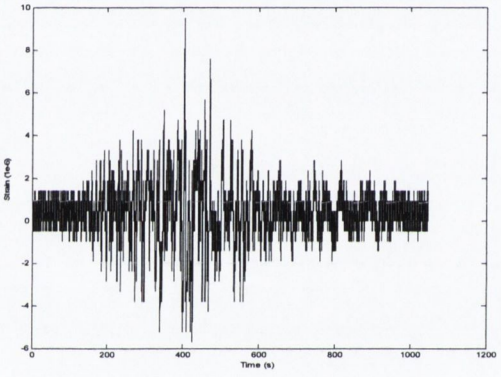

Figure D19.3: Strain Gauge 3

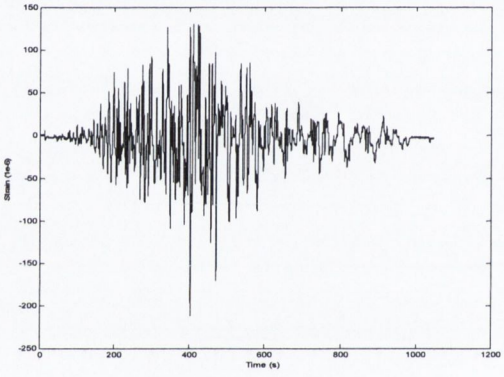

Figure D19.4: Strain Gauge 4

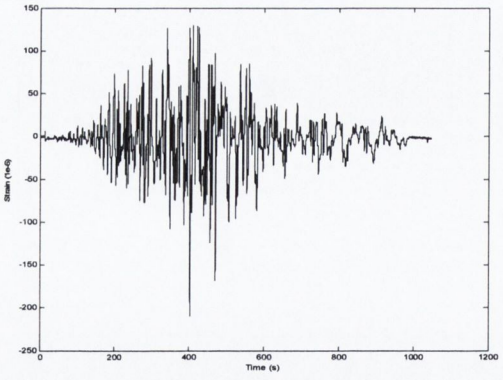

Figure D19.5: Strain Gauge 5

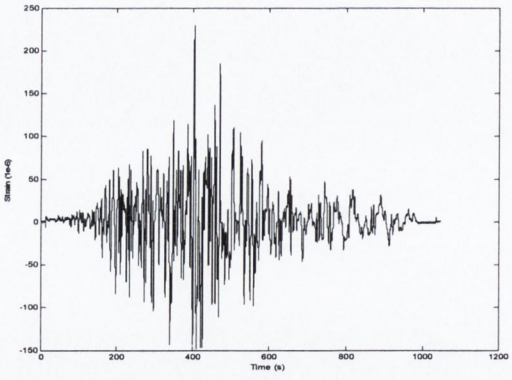

Figure D19.6: Strain Gauge 6

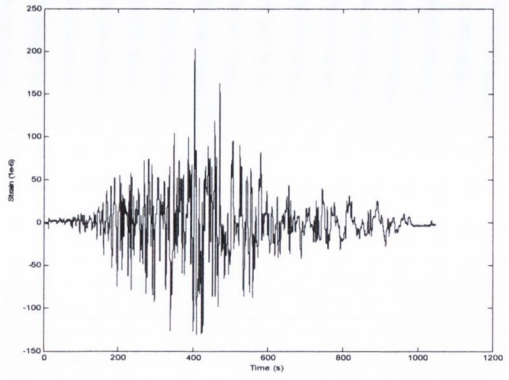

Figure D19.7: Strain Gauge 7

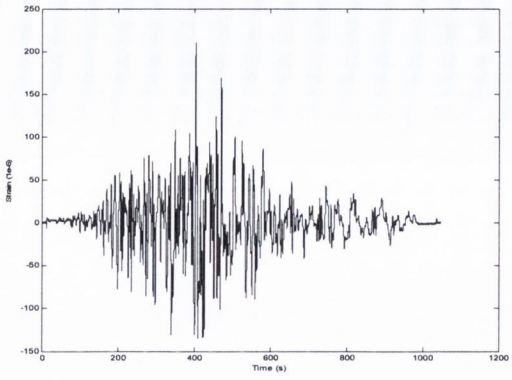

Figure D19.8: Strain Gauge 8

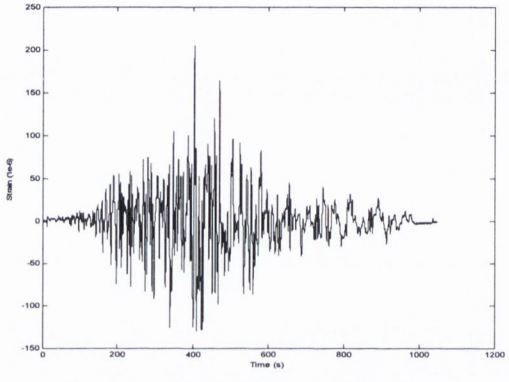

Figure D19.9: Strain Gauge 9

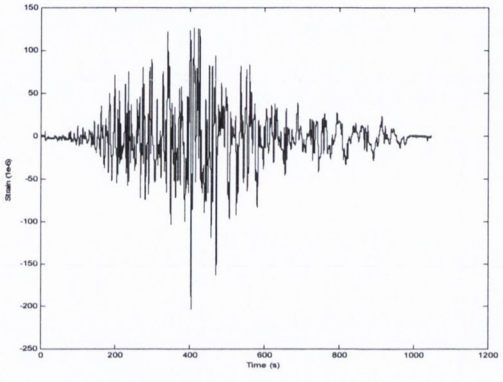

Figure D19.10: Strain Gauge 10

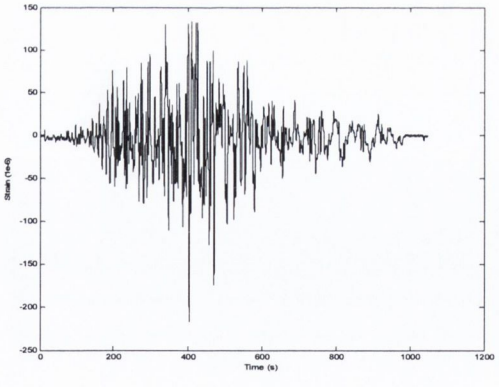

Figure D19.11: Strain Gauge 11

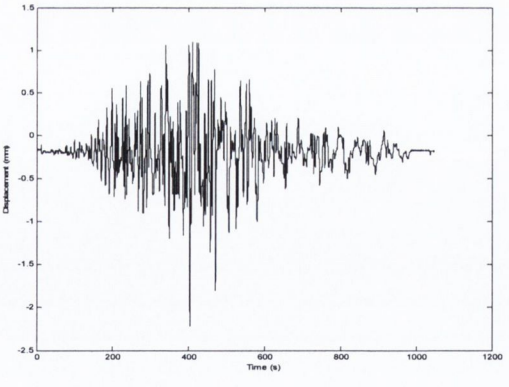

Figure D19.12: LVDT at Node 12

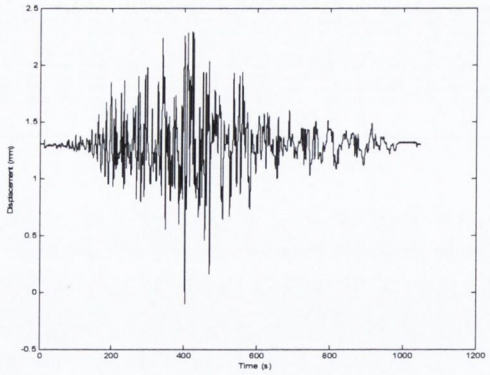

Figure D19.13: LVDT at Node 13

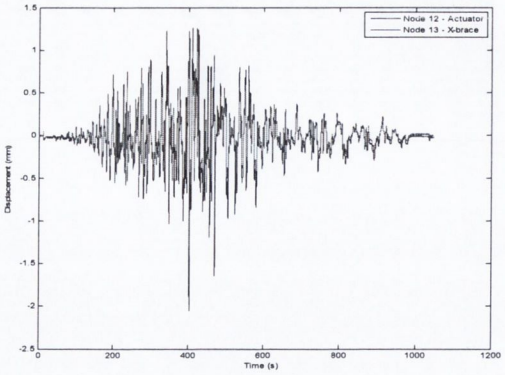

Figure D19.14: LVDT at Node 12 & 13

Appendix D20 – TEST 4F Results

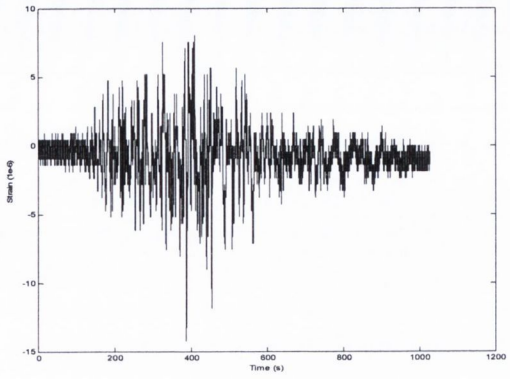

Figure D20.1: Strain Gauge 1

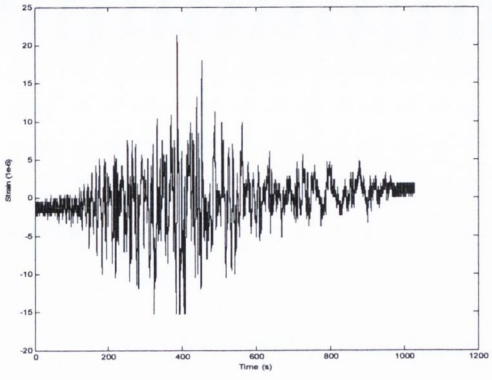

Figure D20.2: Strain Gauge 2

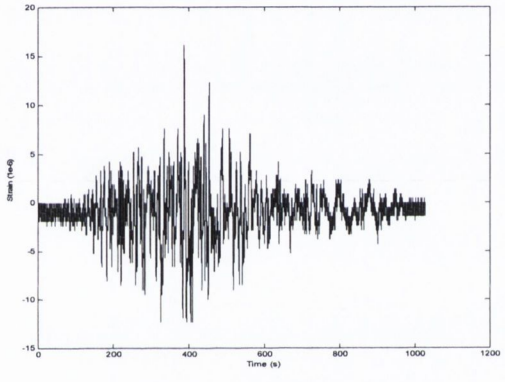

Figure D20.3: Strain Gauge 3

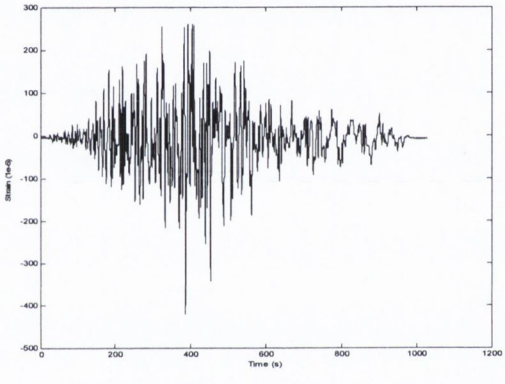

Figure D20.4: Strain Gauge 4

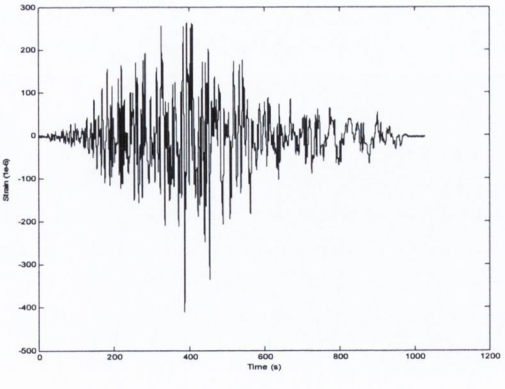

Figure D20.5: Strain Gauge 5

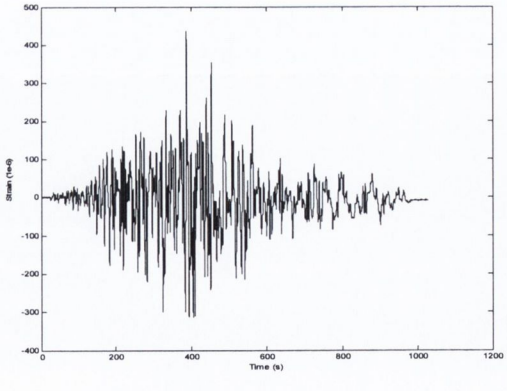

Figure D20.6: Strain Gauge 6

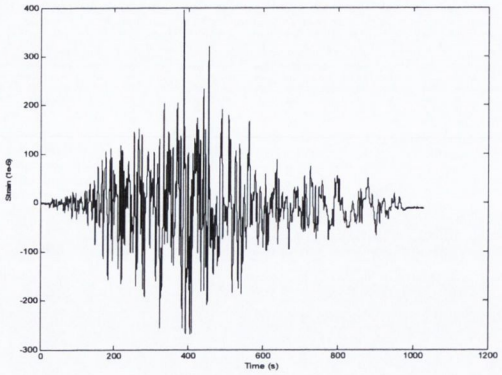

Figure D20.7: Strain Gauge 7

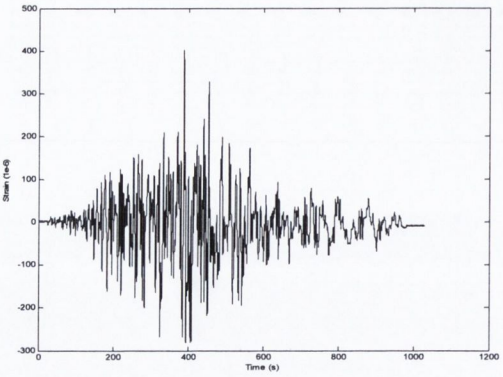

Figure D20.8: Strain Gauge 8

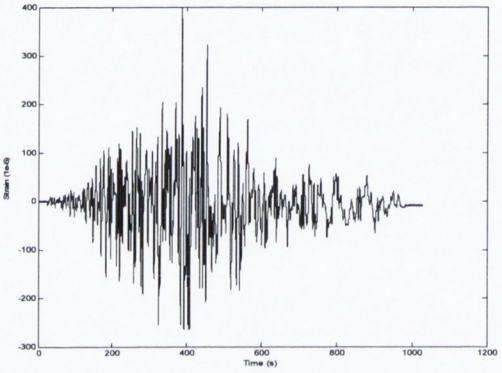

Figure D20.9: Strain Gauge 9

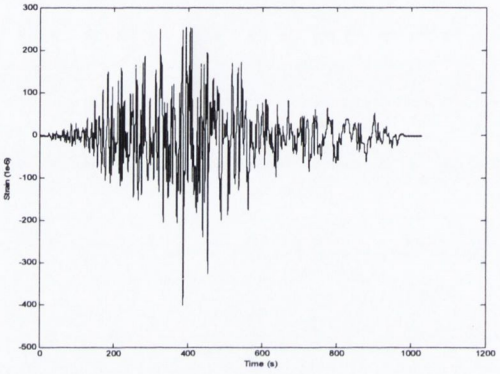

Figure D20.10: Strain Gauge 10

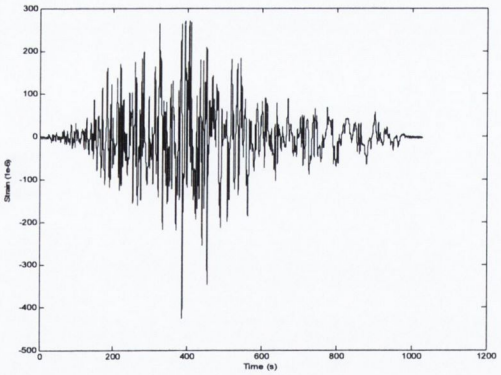

Figure D20.11: Strain Gauge 11

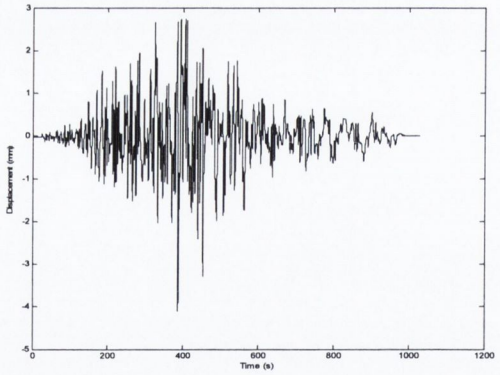

Figure D20.12: LVDT at Node 12

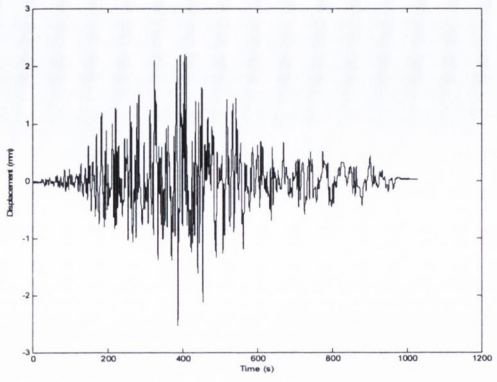

Figure D20.13: LVDT at Node 13

Appendix E - Three Dimensional Concentrically Braced Frame OpenSees Model

```
# FileName: TestFrame_Local_3D.tcl
# Author: Daniel McCrum
# Email: mccrumdp@tcd.ie
# Last Altered: May, 2011.

# Description:
# This file contains the final numerical model of the three-
# storey concentrically braced torsionally unbalanced structure
# with varying

# Model Information:
# PA RATIO:                          2.0
# SLENDERNESS:                       1.68
# LATERAL. TORS. FREQ.:              0.75
# MASS ECCENTRICITY:                 0.15L
#
#          _____________________
#         |                     |        ^
#         |                     |        |
#         |                     |        | 2200mm
#         |                     |        |
#         |_____________________|        v
#         |                     |        ^
#         |                     |        |
#         |                     |        | 2200mm
#         |                     |        |
#         |                     |        |
#          _____________________         v
#         |                     |        ^
#         |                     |        |
#         |                     |        | 2500mm
#         |                     |        |
#         |                     |        v
#       XXX                   XXX
#
#          <--------------------------------->
#             PA Ratio dependent

# Units: N mm sec Mg

wipe all;
file mkdir Data;        # Create directory for general data
file mkdir Data1;       # Create directory for first storey data
file mkdir Data2;       # Create directory for second storey data
source HEsection1.tcl;
source HSsection1.tcl;
source HSsection.tcl;

# ------------------------------------
# Start of model generation
# ------------------------------------
# create ModelBuilder (with two-dimensions and 3 DOF/node)
model BasicBuilder -ndm 3 -ndf 6
# ------------------------------------
# Define geometry for model
# ------------------------------------
set Lcol1 2500;
set Lcol2 2200;
set Lbeam1 3300;                # Change for Plan Aspect Ratio
set Lbeam2 3300;                # Change for Plan Aspect Ratio

# nodal coords.
#           X                     Y                     Z
node 1  0                       0                     0
node 2  0                       0                     $Lbeam2
```

```
node 3  0                       0                       [expr $Lbeam2*2]
node 4  [expr $Lbeam1]          0                       [expr $Lbeam2*2]
node 5  [expr $Lbeam1]          0                       $Lbeam2
node 6  [expr $Lbeam1]          0                       0

# FIRST FLOOR
node 7  0                       $Lcol1                  0
node 8  0                       $Lcol1                  $Lbeam2
node 9  0                       $Lcol1                  [expr $Lbeam2*2]
node 10 [expr $Lbeam1]          $Lcol1                  [expr $Lbeam2*2]
node 11 [expr $Lbeam1]          $Lcol1                  $Lbeam2
node 12 [expr $Lbeam1]          $Lcol1                  0


# SECOND FLOOR
node 27 0                       [expr $Lcol1+$Lcol2]    0
node 28 0                       [expr $Lcol1+$Lcol2]    $Lbeam2
node 29 0                       [expr $Lcol1+$Lcol2]    [expr $Lbeam2*2]
node 30 [expr $Lbeam1]          [expr $Lcol1+$Lcol2]    [expr $Lbeam2*2]
node 31 [expr $Lbeam1]          [expr $Lcol1+$Lcol2]    $Lbeam2
node 32 [expr $Lbeam1]          [expr $Lcol1+$Lcol2]    0

# THIRD FLOOR
node 47 0                       [expr $Lcol1+($Lcol2*2)] 0
node 48 0                       [expr $Lcol1+($Lcol2*2)] $Lbeam2
node 49 0                       [expr $Lcol1+($Lcol2*2)] [expr $Lbeam2*2]
node 50 [expr $Lbeam1]          [expr $Lcol1+($Lcol2*2)] [expr $Lbeam2*2]
node 51 [expr $Lbeam1]          [expr $Lcol1+($Lcol2*2)] $Lbeam2
node 52 [expr $Lbeam1]          [expr $Lcol1+($Lcol2*2)] 0

# Duplicate nodes for brace end zerolength sections
# FIRST STOREY
node 111 0                      0                       0
node 113 0                      0                       [expr $Lbeam2*2]
node 114 [expr $Lbeam1]         0                       [expr $Lbeam2*2]
node 116 $Lbeam1                0                       0

node 117 0                      $Lcol1                  0
node 119 0                      $Lcol1                  [expr $Lbeam2*2]
node 210 [expr $Lbeam1]         $Lcol1                  [expr $Lbeam2*2]
node 212 [expr $Lbeam1]         $Lcol1                  0

# SECOND STOREY
node 311 0                      $Lcol1                  0
node 313 0                      $Lcol1                  [expr $Lbeam2*2]
node 314 [expr $Lbeam1]         $Lcol1                  [expr $Lbeam2*2]
node 316 [expr $Lbeam1]         $Lcol1                  0
node 317 0                      [expr $Lcol1+$Lcol2]    0
node 319 0                      [expr $Lcol1+$Lcol2]    [expr $Lbeam2*2]
node 410 [expr $Lbeam1]         [expr $Lcol1+$Lcol2]    [expr $Lbeam2*2]
node 412 [expr $Lbeam1]         [expr $Lcol1+$Lcol2]    0

# THIRD STOREY
node 511 0                      [expr $Lcol1+$Lcol2]    0
node 513 0                      [expr $Lcol1+$Lcol2]    [expr $Lbeam2*2]
node 514 [expr $Lbeam1]         [expr $Lcol1+$Lcol2]    [expr $Lbeam2*2]
node 516 [expr $Lbeam1]         [expr $Lcol1+$Lcol2]    0

node 517 0                      [expr $Lcol1+($Lcol2*2)] 0
node 519 0                      [expr $Lcol1+($Lcol2*2)] [expr $Lbeam2*2]
node 610 [expr $Lbeam1]         [expr $Lcol1+($Lcol2*2)] [expr $Lbeam2*2]
node 612 [expr $Lbeam1]         [expr $Lcol1+($Lcol2*2)] 0

# Brace imperfection nodes 0.1% out-of-straight at mid-length
set delta1 4.14;
set delta2 6.0;
# FIRST STOREY
# LHS Brace Members
node 130 [expr ($Lbeam1/10)]            [expr ($Lcol1/10)]              0.0
node 131 [expr ($Lbeam1/10)+(((($Lbeam1/2)-($Lbeam1/10))/2)-$delta1]    [expr ($Lcol1/10)+(((($Lcol1/2)-($Lcol1/10))/2)+$delta1]
         [expr $delta2]
node 132 [expr (2*$Lbeam1/4)-$delta2]   [expr (2*$Lcol1/4)+$delta2]     0.0
node 133 [expr ($Lbeam1/2)+(((($Lbeam1/2)-($Lbeam1/10))/2)-$delta1][expr ($Lcol1/2)+(((($Lcol1/2)-($Lcol1/10))/2)+$delta1]
         [expr $delta2]
node 134 [expr $Lbeam1-($Lbeam1/10)]    [expr $Lcol1-($Lcol1/10)]       0.0
node 140 [expr $Lbeam1-($Lbeam1/10)]    [expr ($Lcol1/10)]              0.0
node 141 [expr ($Lbeam1/2)+(((($Lbeam1/2)-($Lbeam1/10))/2)-$delta1][expr ($Lcol1/10)+(((($Lcol1/2)-($Lcol1/10))/2)+$delta1]
         [expr $delta2]
```

```
node 142  [expr ($Lbeam1/10)+(((($Lbeam1/2)-($Lbeam1/10))/2)-$delta1] [expr ($Lcol1/2)+(((($Lcol1/2)-($Lcol1/10))/2)+$delta1]
[expr $delta2]
node 143  [expr ($Lbeam1/10)]          [expr $Lcol1-($Lcol1/10)]      0.0

# RHS Brace Members
node 150  [expr ($Lbeam1/10)]          [expr ($Lcol1/10)]             [expr $Lbeam2*2]
node 151  [expr ($Lbeam1/10)+(((($Lbeam1/2)-($Lbeam1/10))/2)-$delta1]  [expr ($Lcol1/10)+(((($Lcol1/2)-($Lcol1/10))/2)+$delta1]
[expr $delta1+$Lbeam2*2]
node 152  [expr (2*$Lbeam1/4)-$delta2]  [expr (2*$Lcol1/4)+$delta2]   [expr $delta2+$Lbeam2*2]
node 153  [expr ($Lbeam1/2)+(((($Lbeam1/2)-($Lbeam1/10))/2)-$delta1]  [expr ($Lcol1/2)+(((($Lcol1/2)-($Lcol1/10))/2)+$delta1]
[expr $delta1+$Lbeam2*2]
node 154  [expr $Lbeam1-($Lbeam1/10)]  [expr $Lcol1-($Lcol1/10)]      [expr $Lbeam2*2]
node 160  [expr $Lbeam1-($Lbeam1/10)]  [expr ($Lcol1/10)]             [expr $Lbeam2*2]
node 161  [expr ($Lbeam1/2)+(((($Lbeam1/2)-($Lbeam1/10))/2)-$delta1]  [expr ($Lcol1/10)+(((($Lcol1/2)-($Lcol1/10))/2)+$delta1]
          [expr $delta2+$Lbeam2*2]
node 162  [expr ($Lbeam1/10)+(((($Lbeam1/2)-($Lbeam1/10))/2)-$delta1]  [expr ($Lcol1/2)+(((($Lcol1/2)-($Lcol1/10))/2)+$delta1]
          [expr $delta2+$Lbeam2*2]
node 163  [expr ($Lbeam1/10)]          [expr $Lcol1-($Lcol1/10)]      [expr $Lbeam2*2]

# SECOND STOREY
# LHS Brace Members
node 230  [expr ($Lbeam1/10)]          [expr $Lcol1+($Lcol2/10)]              0.0
node 231  [expr ($Lbeam1/10)+(((($Lbeam1/2)-($Lbeam1/10))/2)-$delta1]  [expr $Lcol1+($Lcol2/10)+(((($Lcol2/2)-
($Lcol2/10))/2)+$delta1]       [expr $delta2]
node 232  [expr (2*$Lbeam1/4)-$delta2]  [expr $Lcol1+(2*$Lcol2/4)+$delta2]   0.0
node 233  [expr ($Lbeam1/2)+(((($Lbeam1/2)-($Lbeam1/10))/2)-$delta1]  [expr $Lcol1+($Lcol2/2)+(((($Lcol2/2)-
($Lcol2/10))/2)+$delta1]       [expr $delta2]
node 234  [expr $Lbeam1-($Lbeam1/10)]  [expr $Lcol1+$Lcol2-($Lcol2/10)]   0.0
node 240  [expr $Lbeam1-($Lbeam1/10)]  [expr $Lcol1+($Lcol2/10)]          0.0
node 241  [expr ($Lbeam1/2)+(((($Lbeam1/2)-($Lbeam1/10))/2)-$delta1]  [expr $Lcol1+($Lcol2/10)+(((($Lcol2/2)-
($Lcol2/10))/2)+$delta1]       [expr $delta2]
node 242  [expr ($Lbeam1/10)+(((($Lbeam1/2)-($Lbeam1/10))/2)-$delta1]  [expr $Lcol1+($Lcol2/2)+(((($Lcol2/2)-
($Lcol2/10))/2)+$delta1]       [expr $delta2]
node 243  [expr ($Lbeam1/10)]          [expr $Lcol1+$Lcol2-($Lcol2/10)]   0.0

# RHS Brace Members
node 250  [expr ($Lbeam1/10)]          [expr $Lcol1+($Lcol2/10)]      [expr $Lbeam2*2]
node 251  [expr ($Lbeam1/10)+(((($Lbeam1/2)-($Lbeam1/10))/2)-$delta1]  [expr $Lcol1+($Lcol2/10)+(((($Lcol2/2)-
($Lcol2/10))/2)+$delta1]       [expr $delta1+$Lbeam2*2]
node 252  [expr (2*$Lbeam1/4)-$delta2][expr $Lcol1+(2*$Lcol2/4)+$delta2]      [expr $delta2+$Lbeam2*2]
node 253  [expr ($Lbeam1/2)+(((($Lbeam1/2)-($Lbeam1/10))/2)-$delta1]          [expr $Lcol1+($Lcol2/2)+(((($Lcol2/2)-
($Lcol2/10))/2)+$delta1]       [expr $delta1+$Lbeam2*2]
node 254  [expr $Lbeam1-($Lbeam1/10)]  [expr $Lcol1+$Lcol2-($Lcol2/10)]   [expr $Lbeam2*2]

node 260  [expr $Lbeam1-($Lbeam1/10)] [expr $Lcol1+($Lcol2/10)]      [expr $Lbeam2*2]
node 261  [expr ($Lbeam1/2)+(((($Lbeam1/2)-($Lbeam1/10))/2)-$delta1]  [expr $Lcol1+($Lcol2/10)+(((($Lcol2/2)-
($Lcol2/10))/2)+$delta1]       [expr $delta2+$Lbeam2*2]
node 262  [expr ($Lbeam1/10)+(((($Lbeam1/2)-($Lbeam1/10))/2)-$delta1]  [expr $Lcol1+($Lcol2/2)+(((($Lcol2/2)-
($Lcol2/10))/2)+$delta1]       [expr $delta2+$Lbeam2*2]
node 263  [expr ($Lbeam1/10)] [expr $Lcol1+$Lcol2-($Lcol2/10)]       [expr $Lbeam2*2]

# THIRD STOREY
# LHS Brace Members
node 330  [expr ($Lbeam1/10)]          [expr ($Lcol1+$Lcol2)+($Lcol2/10)]      0.0
node 331  [expr ($Lbeam1/10)+(((($Lbeam1/2)-($Lbeam1/10))/2)-$delta1] [expr ($Lcol1+$Lcol2)+($Lcol2/10)+(((($Lcol2/2)-
($Lcol2/10))/2)+$delta1]       [expr $delta2]
node 332  [expr (2*$Lbeam1/4)-$delta2]
[expr ($Lcol1+$Lcol2)+(2*$Lcol2/4)+$delta2] 0.0
node 333  [expr ($Lbeam1/2)+(((($Lbeam1/2)-($Lbeam1/10))/2)-$delta1]  [expr ($Lcol1+$Lcol2)+($Lcol2/2)+(((($Lcol2/2)-
($Lcol2/10))/2)+$delta1]       [expr $delta2]
node 334  [expr $Lbeam1-($Lbeam1/10)]  [expr ($Lcol1+$Lcol2)+$Lcol2-($Lcol2/10)]   0.0

node 340  [expr $Lbeam1-($Lbeam1/10)]  [expr ($Lcol1+$Lcol2)+($Lcol2/10)]      0.0
node 341  [expr ($Lbeam1/2)+(((($Lbeam1/2)-($Lbeam1/10))/2)-$delta1][expr ($Lcol1+$Lcol2)+($Lcol2/10)+(((($Lcol2/2)-
($Lcol2/10))/2)+$delta1]       [expr $delta2]
node 342  [expr ($Lbeam1/10)+(((($Lbeam1/2)-($Lbeam1/10))/2)-$delta1] [expr ($Lcol1+$Lcol2)+($Lcol2/2)+(((($Lcol2/2)-
($Lcol2/10))/2)+$delta1]       [expr $delta2]
node 343  [expr ($Lbeam1/10)]          [expr ($Lcol1+$Lcol2)+$Lcol2-($Lcol2/10)]   0.0

# RHS Brace Members
node 350  [expr ($Lbeam1/10)]          [expr ($Lcol1+$Lcol2)+($Lcol2/10)]      [expr $Lbeam2*2]
node 351  [expr ($Lbeam1/10)+(((($Lbeam1/2)-($Lbeam1/10))/2)-$delta1] [expr ($Lcol1+$Lcol2)+($Lcol2/10)+(((($Lcol2/2)-
($Lcol2/10))/2)+$delta1]       [expr $delta1+$Lbeam2*2]
node 352  [expr (2*$Lbeam1/4)-$delta2]  [expr ($Lcol1+$Lcol2)+(2*$Lcol2/4)+$delta2]   [expr $delta2+$Lbeam2*2]
node 353  [expr ($Lbeam1/2)+(((($Lbeam1/2)-($Lbeam1/10))/2)-$delta1]  [expr ($Lcol1+$Lcol2)+($Lcol2/2)+(((($Lcol2/2)-
($Lcol2/10))/2)+$delta1]       [expr $delta1+$Lbeam2*2]
node 354  [expr $Lbeam1-($Lbeam1/10)]  [expr ($Lcol1+$Lcol2)+$Lcol2-($Lcol2/10)]   [expr $Lbeam2*2]
```

```
node 360  [expr $Lbeam1-($Lbeam1/10)]  [expr ($Lcol1+$Lcol2)+($Lcol2/10)]  [expr $Lbeam2*2]
node 361  [expr ($Lbeam1/2)+(((($Lbeam1/2)-($Lbeam1/10))/2)-$delta1][expr ($Lcol1+$Lcol2)+($Lcol2/10)+(((($Lcol2/2)-
($Lcol2/10))/2)+$delta1]  [expr $delta2+$Lbeam2*2]
node 362  [expr ($Lbeam1/10)+(((($Lbeam1/2)-($Lbeam1/10))/2)-$delta1]  [expr ($Lcol1+$Lcol2)+($Lcol2/2)+(((($Lcol2/2)-
($Lcol2/10))/2)+$delta1]  [expr $delta2+$Lbeam2*2]
node 363  [expr ($Lbeam1/10)]  [expr ($Lcol1+$Lcol2)+$Lcol2-($Lcol2/10)]  [expr $Lbeam2*2]

# ------------------------------------
# Define masses
# ------------------------------------
set massTotal1 86385;          # Mass in Mg
set massTotal2 43192;
set massTotal3 21596;

# Level of mass eccentricity
set eccmult1 0.53333333;       # Mass eccentricity factor for LHS Frame
set eccmult2 0.23333333;       # Mass eccentricity factor for Centre Frame
set eccmult3 0.23333333;       # Mass eccentricity factor for RHS Frame

# lateral torsional frequency ratio multiplier
set factor1 1.981;             # for lateral torsional frequency ratio of 0.75

# Nodal masses
# FIRST FLOOR
mass 7 [expr $massTotal1*0.5*$eccmult1*$factor1/9810] 0. [expr $massTotal1*0.5*$eccmult1*$factor1/9810] 1.0e-9 1.0e-9 1.0e-9;
mass 8 [expr $massTotal1*0.5*$eccmult2*$factor1/9810] 0. [expr $massTotal1*0.5*$eccmult2*$factor1/9810] 1.0e-9 1.0e-9 1.0e-9;
mass 9 [expr $massTotal1*0.5*$eccmult3*$factor1/9810] 0. [expr $massTotal1*0.5*$eccmult3*$factor1/9810] 1.0e-9 1.0e-9 1.0e-9;
mass 10 [expr $massTotal1*0.5*$eccmult3*$factor1/9810] 0. [expr $massTotal1*0.5*$eccmult3*$factor1/9810] 1.0e-9 1.0e-9 1.0e-9;
mass 11 [expr $massTotal1*0.5*$eccmult2*$factor1/9810] 0. [expr $massTotal1*0.5*$eccmult2*$factor1/9810] 1.0e-9 1.0e-9 1.0e-9;
mass 12 [expr $massTotal1*0.5*$eccmult1*$factor1/9810] 0. [expr $massTotal1*0.5*$eccmult1*$factor1/9810] 1.0e-9 1.0e-9 1.0e-9;

# SECOND FLOOR
mass 27 [expr $massTotal2*0.5*$eccmult1*$factor1/9810] 0. [expr $massTotal2*0.5*$eccmult1*$factor1/9810] 1.0e-9 1.0e-9 1.0e-9;
mass 28 [expr $massTotal2*0.5*$eccmult2*$factor1/9810] 0. [expr $massTotal2*0.5*$eccmult2*$factor1/9810] 1.0e-9 1.0e-9 1.0e-9;
mass 29 [expr $massTotal2*0.5*$eccmult3*$factor1/9810] 0. [expr $massTotal2*0.5*$eccmult3*$factor1/9810] 1.0e-9 1.0e-9 1.0e-9;
mass 30 [expr $massTotal2*0.5*$eccmult3*$factor1/9810] 0. [expr $massTotal2*0.5*$eccmult3*$factor1/9810] 1.0e-9 1.0e-9 1.0e-9;
mass 31 [expr $massTotal2*0.5*$eccmult2*$factor1/9810] 0. [expr $massTotal2*0.5*$eccmult2*$factor1/9810] 1.0e-9 1.0e-9 1.0e-9;
mass 32 [expr $massTotal2*0.5*$eccmult1*$factor1/9810] 0. [expr $massTotal2*0.5*$eccmult1*$factor1/9810] 1.0e-9 1.0e-9 1.0e-9;

# THIRD FLOOR
mass 47 [expr $massTotal3*0.5*$eccmult1*$factor1/9810] 0. [expr $massTotal3*0.5*$eccmult1*$factor1/9810] 1.0e-9 1.0e-9 1.0e-9;
mass 48 [expr $massTotal3*0.5*$eccmult2*$factor1/9810] 0. [expr $massTotal3*0.5*$eccmult2*$factor1/9810] 1.0e-9 1.0e-9 1.0e-9;
mass 49 [expr $massTotal3*0.5*$eccmult3*$factor1/9810] 0. [expr $massTotal3*0.5*$eccmult3*$factor1/9810] 1.0e-9 1.0e-9 1.0e-9;
mass 50 [expr $massTotal3*0.5*$eccmult3*$factor1/9810] 0. [expr $massTotal3*0.5*$eccmult3*$factor1/9810] 1.0e-9 1.0e-9 1.0e-9;
mass 51 [expr $massTotal3*0.5*$eccmult2*$factor1/9810] 0. [expr $massTotal3*0.5*$eccmult2*$factor1/9810] 1.0e-9 1.0e-9 1.0e-9;
mass 52 [expr $massTotal3*0.5*$eccmult1*$factor1/9810] 0. [expr $massTotal3*0.5*$eccmult1*$factor1/9810] 1.0e-9 1.0e-9 1.0e-9;

# ------------------------------------
# Define the boundary conditions
# ------------------------------------
# fix $tag $DX $DY $DZ $RX $RY $RZ
fix 1   1 1 1 0 1 0
fix 6   1 1 1 0 1 0

fix 2   1 1 1 0 1 0
fix 5   1 1 1 0 1 0

fix 3   1 1 1 0 1 0
fix 4   1 1 1 0 1 0

# Zero Length Elements
# Ground Floor
equalDOF 1 111 1 2 3 5
equalDOF 6 116 1 2 3 5
equalDOF 3 113 1 2 3 5
equalDOF 4 114 1 2 3 5

# First Floor Bottom
equalDOF 7 117 1 2 3 5
equalDOF 12 212 1 2 3 5
equalDOF 9 119 1 2 3 5
equalDOF 10 210 1 2 3 5

# First Floor Top
equalDOF 7 311 1 2 3 5
equalDOF 9 313 1 2 3 5
equalDOF 10 314 1 2 3 5
equalDOF 12 316 1 2 3 5
```

```
# Second Floor Bottom
equalDOF 27 317 1 2 3 5
equalDOF 29 319 1 2 3 5
equalDOF 30 410 1 2 3 5
equalDOF 32 412 1 2 3 5

# Second Floor Top
equalDOF 27 511 1 2 3 5
equalDOF 29 513 1 2 3 5
equalDOF 30 514 1 2 3 5
equalDOF 32 516 1 2 3 5

# Third Floor
equalDOF 47 517 1 2 3 5
equalDOF 49 519 1 2 3 5
equalDOF 50 610 1 2 3 5
equalDOF 52 612 1 2 3 5

# ------------------------------------
# Define materials
# ------------------------------------
set matID 1;
set steelTag 2;
set matStiff 3;
# uniaxialMaterial Steel02 $matTag $Fy $E $b $R0 $cR1 $cR2 $a1 $a2 $a3 $a4
uniaxialMaterial Steel02 $matID 235 210000 0.03 18.5 0.925 0.15 0.0 1.0 0.0 1.0
uniaxialMaterial Steel02 $steelTag 235 210000 0.03 18.5 0.925 0.15 -0.045 1.0 0.045 1.0
uniaxialMaterial Elastic $matStiff 1000000
set E 210e3;
set poisson 0.3;
set G [expr $E/([expr 2*(1+$poisson)])];      # Torsional Stiffness

# ------------------------------------
# Define section parameters
# ------------------------------------
# Column Parameters:
# 203 UC 46
set col2secID 20;
set col2FiberSecTag 21;
set d 203;                    # Overall section depth
set b 203;                    # Overall section width
set t 7.2;                    # Web thickness
set T 11;                     # Flange thickness
set dw [expr $d - 2*$T];      # Depth of web
set y [expr $d/2];
set subFLen 10;               # sub-division across flange length
set subFThk 5;                # sub-division across flange thickness
set subWLen 10;               # sub-division across web length
set subWThk 5;                # sub-division across web thickness
HEsection1 $col2FiberSecTag $matID $d $b $dw $t $subWLen $subWThk $subFLen $subFThk
puts "HESection1 defined";

# column torsional stiffness
set col2TorsTag 79;
set J9 8070000;
set GJ9 [expr $G*$J9];
uniaxialMaterial Elastic $col2TorsTag $GJ9; # Define column torsional stiffness
section Aggregator $col2secID $col2TorsTag T -section $col2FiberSecTag; # attach torsion and flexure

# Beam Parameters:
# 305x165x40UB Beam
set Ebeam 210000;
set Abeam 5130;
set Izbeam 6740e4;
set Iybeam 8503e4;
set Jbeam 47.2e4;

# Brace Parameters:
# 30 x 30 x 3 RHS
set bracesecID 7;
set braceFiberSecTag 8;
set d 30;                     # Overall section depth 30
set b 30;                     # Overall section width 30
set t 3;                      # Thickness 2.5
set subFLen 10;               # sub-division across flange length
set subFThk 5;                # sub-division across flange thickness
set subWLen 10;               # sub-division across web length
set subWThk 5;                # sub-division across web thickness
```

```
HSsection $braceFiberSecTag $matID $d $b $t $subWLen $subWThk $subFLen $subFThk
puts "HSSection defined";

# Brace torsional stiffness
set braceTorsTag 73;
set J4 6.15e8;
set GJ4 [expr $G*$J4];
uniaxialMaterial Elastic $braceTorsTag $GJ4;  # Define column torsional stiffness
section Aggregator $bracesecID $braceTorsTag T -section $braceFiberSecTag; # attach torsion and flexure

# Brace Parameters:
# 30 x 30 x 3 RHS
set bracesecID1 9;
set braceFiberSecTag1 10;
set d 30;                    # Overall section depth 30
set b 30;                    # Overall section width 30
set t 3;                     # Thickness 2.5
set subFLen 10;              # sub-division across flange length
set subFThk 5;               # sub-division across flange thickness
set subWLen 10;              # sub-division across web length
set subWThk 5;               # sub-division across web thickness
HSsection1 $braceFiberSecTag1 $matID $d $b $t $subWLen $subWThk $subFLen $subFThk
puts "HSSection1 defined";

# Brace torsional stiffness
set braceTorsTag1 75;
set J5 6.15e8;
set GJ5 [expr $G*$J5];
uniaxialMaterial Elastic $braceTorsTag1 $GJ5;  # Define column torsional stiffness
section Aggregator $bracesecID1 $braceTorsTag1 T -section $braceFiberSecTag1; # attach torsion and flexure

# ------------------------------------
# Define geometric transformation
# ------------------------------------
# Coordinate transformation
set ColTransfTag 10;
set Beam1TransfTag 20;
set BraceTransfTag 30;
geomTransf PDelta $ColTransfTag 0 0 1
geomTransf Linear $Beam1TransfTag 0 -1 0
geomTransf Corotational $BraceTransfTag 0 -1 0
set numintgrPtsCol 7;
set numintgrPtsBrace 7;

# ------------------------------------
# Define numerical elements
# ------------------------------------
# COLUMNS
# FIRST STOREY
# LHS
element nonlinearBeamColumn 1 1 7 $numintgrPtsCol $col2secID $ColTransfTag
element nonlinearBeamColumn 2 6 12 $numintgrPtsCol $col2secID $ColTransfTag

# Middle
element nonlinearBeamColumn 8 5 11 $numintgrPtsCol $col2secID $ColTransfTag
element nonlinearBeamColumn 9 2 8 $numintgrPtsCol $col2secID $ColTransfTag

# RHS
element nonlinearBeamColumn 10 3 9 $numintgrPtsCol $col2secID $ColTransfTag
element nonlinearBeamColumn 11 4 10 $numintgrPtsCol $col2secID $ColTransfTag

# SECOND STOREY
element nonlinearBeamColumn 21 7 27 $numintgrPtsCol $col2secID $ColTransfTag
element nonlinearBeamColumn 22 8 28 $numintgrPtsCol $col2secID $ColTransfTag
element nonlinearBeamColumn 23 9 29 $numintgrPtsCol $col2secID $ColTransfTag
element nonlinearBeamColumn 24 10 30 $numintgrPtsCol $col2secID $ColTransfTag
element nonlinearBeamColumn 25 11 31 $numintgrPtsCol $col2secID $ColTransfTag
element nonlinearBeamColumn 26 12 32 $numintgrPtsCol $col2secID $ColTransfTag

# THIRD STOREY
element nonlinearBeamColumn 31 27 47 $numintgrPtsCol $col2secID $ColTransfTag
element nonlinearBeamColumn 32 28 48 $numintgrPtsCol $col2secID $ColTransfTag
element nonlinearBeamColumn 33 29 49 $numintgrPtsCol $col2secID $ColTransfTag
element nonlinearBeamColumn 34 30 50 $numintgrPtsCol $col2secID $ColTransfTag
element nonlinearBeamColumn 35 31 51 $numintgrPtsCol $col2secID $ColTransfTag
element nonlinearBeamColumn 36 32 52 $numintgrPtsCol $col2secID $ColTransfTag
```

```
# BEAMS
# FIRST STOREY
element elasticBeamColumn 50 7 12 $Abeam $Ebeam $G $Jbeam $Iybeam $Izbeam $Beam1TransfTag
element elasticBeamColumn 51 8 11 $Abeam $Ebeam $G $Jbeam $Iybeam $Izbeam $Beam1TransfTag
element elasticBeamColumn 52 9 10 $Abeam $Ebeam $G $Jbeam $Iybeam $Izbeam $Beam1TransfTag
element elasticBeamColumn 53 7 8 $Abeam $Ebeam $G $Jbeam $Iybeam $Izbeam $Beam1TransfTag
element elasticBeamColumn 54 8 9 $Abeam $Ebeam $G $Jbeam $Iybeam $Izbeam $Beam1TransfTag
element elasticBeamColumn 55 10 11 $Abeam $Ebeam $G $Jbeam $Iybeam $Izbeam $Beam1TransfTag
element elasticBeamColumn 56 11 12 $Abeam $Ebeam $G $Jbeam $Iybeam $Izbeam $Beam1TransfTag

# SECOND STOREY
element elasticBeamColumn 60 27 32 $Abeam $Ebeam $G $Jbeam $Iybeam $Izbeam $Beam1TransfTag
element elasticBeamColumn 61 28 31 $Abeam $Ebeam $G $Jbeam $Iybeam $Izbeam $Beam1TransfTag
element elasticBeamColumn 62 29 30 $Abeam $Ebeam $G $Jbeam $Iybeam $Izbeam $Beam1TransfTag
element elasticBeamColumn 63 27 28 $Abeam $Ebeam $G $Jbeam $Iybeam $Izbeam $Beam1TransfTag
element elasticBeamColumn 64 28 29 $Abeam $Ebeam $G $Jbeam $Iybeam $Izbeam $Beam1TransfTag
element elasticBeamColumn 65 30 31 $Abeam $Ebeam $G $Jbeam $Iybeam $Izbeam $Beam1TransfTag
element elasticBeamColumn 66 31 32 $Abeam $Ebeam $G $Jbeam $Iybeam $Izbeam $Beam1TransfTag

# THIRD STOREY
element elasticBeamColumn 70 47 52 $Abeam $Ebeam $G $Jbeam $Iybeam $Izbeam $Beam1TransfTag
element elasticBeamColumn 71 48 51 $Abeam $Ebeam $G $Jbeam $Iybeam $Izbeam $Beam1TransfTag
element elasticBeamColumn 72 49 50 $Abeam $Ebeam $G $Jbeam $Iybeam $Izbeam $Beam1TransfTag
element elasticBeamColumn 73 47 48 $Abeam $Ebeam $G $Jbeam $Iybeam $Izbeam $Beam1TransfTag
element elasticBeamColumn 74 48 49 $Abeam $Ebeam $G $Jbeam $Iybeam $Izbeam $Beam1TransfTag
element elasticBeamColumn 75 50 51 $Abeam $Ebeam $G $Jbeam $Iybeam $Izbeam $Beam1TransfTag
element elasticBeamColumn 76 51 52 $Abeam $Ebeam $G $Jbeam $Iybeam $Izbeam $Beam1TransfTag

# Brace members
# Two element braces
# FIRST STOREY
# LHS Bay
element elasticBeamColumn 151 111 130 $Abeam 700000 $G $Jbeam $Iybeam $Izbeam $Beam1TransfTag
element nonlinearBeamColumn 152 130 131 $numintgrPtsBrace $bracesecID1 $BraceTransfTag
element nonlinearBeamColumn 153 131 132 $numintgrPtsBrace $bracesecID1 $BraceTransfTag
element nonlinearBeamColumn 154 132 133 $numintgrPtsBrace $bracesecID1 $BraceTransfTag
element nonlinearBeamColumn 155 133 134 $numintgrPtsBrace $bracesecID1 $BraceTransfTag
element elasticBeamColumn 156 134 212 $Abeam 700000 $G $Jbeam $Iybeam $Izbeam $Beam1TransfTag
element elasticBeamColumn 161 116 140 $Abeam 700000 $G $Jbeam $Iybeam $Izbeam $Beam1TransfTag
element nonlinearBeamColumn 162 140 141 $numintgrPtsBrace $bracesecID1 $BraceTransfTag
element nonlinearBeamColumn 163 141 132 $numintgrPtsBrace $bracesecID1 $BraceTransfTag
element nonlinearBeamColumn 164 132 142 $numintgrPtsBrace $bracesecID1 $BraceTransfTag
element nonlinearBeamColumn 165 142 143 $numintgrPtsBrace $bracesecID1 $BraceTransfTag
element elasticBeamColumn 166 143 117 $Abeam 700000 $G $Jbeam $Iybeam $Izbeam $Beam1TransfTag

# RHS Bay
element elasticBeamColumn 171 113 150 $Abeam 700000 $G $Jbeam $Iybeam $Izbeam $Beam1TransfTag
element nonlinearBeamColumn 172 150 151 $numintgrPtsBrace $bracesecID $BraceTransfTag
element nonlinearBeamColumn 173 151 152 $numintgrPtsBrace $bracesecID $BraceTransfTag
element nonlinearBeamColumn 174 152 153 $numintgrPtsBrace $bracesecID $BraceTransfTag
element nonlinearBeamColumn 175 153 154 $numintgrPtsBrace $bracesecID $BraceTransfTag
element elasticBeamColumn 176 154 210 $Abeam 700000 $G $Jbeam $Iybeam $Izbeam $Beam1TransfTag
element elasticBeamColumn 181 114 160 $Abeam 700000 $G $Jbeam $Iybeam $Izbeam $Beam1TransfTag
element nonlinearBeamColumn 182 160 161 $numintgrPtsBrace $bracesecID $BraceTransfTag
element nonlinearBeamColumn 183 161 152 $numintgrPtsBrace $bracesecID $BraceTransfTag
element nonlinearBeamColumn 184 152 162 $numintgrPtsBrace $bracesecID $BraceTransfTag
element nonlinearBeamColumn 185 162 163 $numintgrPtsBrace $bracesecID $BraceTransfTag
element elasticBeamColumn 186 163 119 $Abeam 700000 $G $Jbeam $Iybeam $Izbeam $Beam1TransfTag

# SECOND STOREY
# LHS Bay
element elasticBeamColumn 230 311 230 $Abeam 700000 $G $Jbeam $Iybeam $Izbeam $Beam1TransfTag
element nonlinearBeamColumn 231 230 231 $numintgrPtsBrace $bracesecID1 $BraceTransfTag
element nonlinearBeamColumn 232 231 232 $numintgrPtsBrace $bracesecID1 $BraceTransfTag
element nonlinearBeamColumn 233 232 233 $numintgrPtsBrace $bracesecID1 $BraceTransfTag
element nonlinearBeamColumn 234 233 234 $numintgrPtsBrace $bracesecID1 $BraceTransfTag
element elasticBeamColumn 235 234 412 $Abeam 700000 $G $Jbeam $Iybeam $Izbeam $Beam1TransfTag
element elasticBeamColumn 240 316 240 $Abeam 700000 $G $Jbeam $Iybeam $Izbeam $Beam1TransfTag
element nonlinearBeamColumn 241 240 241 $numintgrPtsBrace $bracesecID1 $BraceTransfTag
element nonlinearBeamColumn 242 241 232 $numintgrPtsBrace $bracesecID1 $BraceTransfTag
element nonlinearBeamColumn 243 232 242 $numintgrPtsBrace $bracesecID1 $BraceTransfTag
element nonlinearBeamColumn 244 242 243 $numintgrPtsBrace $bracesecID1 $BraceTransfTag
element elasticBeamColumn 245 243 317 $Abeam 700000 $G $Jbeam $Iybeam $Izbeam $Beam1TransfTag

# RHS Bay
element elasticBeamColumn 270 313 250 $Abeam 700000 $G $Jbeam $Iybeam $Izbeam $Beam1TransfTag
element nonlinearBeamColumn 271 250 251 $numintgrPtsBrace $bracesecID $BraceTransfTag
element nonlinearBeamColumn 272 251 252 $numintgrPtsBrace $bracesecID $BraceTransfTag
```

```
element nonlinearBeamColumn 273 252 253 $numintgrPtsBrace $bracesecID $BraceTransfTag
element nonlinearBeamColumn 274 253 254 $numintgrPtsBrace $bracesecID $BraceTransfTag
element elasticBeamColumn 275 254 410 $Abeam 700000 $G $Jbeam $Iybeam $Izbeam $Beam1TransfTag
element elasticBeamColumn 280 314 260 $Abeam 700000 $G $Jbeam $Iybeam $Izbeam $Beam1TransfTag
element nonlinearBeamColumn 281 260 261 $numintgrPtsBrace $bracesecID $BraceTransfTag
element nonlinearBeamColumn 282 261 252 $numintgrPtsBrace $bracesecID $BraceTransfTag
element nonlinearBeamColumn 283 252 262 $numintgrPtsBrace $bracesecID $BraceTransfTag
element nonlinearBeamColumn 284 262 263 $numintgrPtsBrace $bracesecID $BraceTransfTag
element elasticBeamColumn 285 263 319 $Abeam 700000 $G $Jbeam $Iybeam $Izbeam $Beam1TransfTag


# THIRD STOREY
# LHS Bay
element elasticBeamColumn 330 511 330 $Abeam 700000 $G $Jbeam $Iybeam $Izbeam $Beam1TransfTag
element nonlinearBeamColumn 331 330 331 $numintgrPtsBrace $bracesecID1 $BraceTransfTag
element nonlinearBeamColumn 332 331 332 $numintgrPtsBrace $bracesecID1 $BraceTransfTag
element nonlinearBeamColumn 333 332 333 $numintgrPtsBrace $bracesecID1 $BraceTransfTag
element nonlinearBeamColumn 334 333 334 $numintgrPtsBrace $bracesecID1 $BraceTransfTag
element elasticBeamColumn 335 334 612 $Abeam 700000 $G $Jbeam $Iybeam $Izbeam $Beam1TransfTag
element elasticBeamColumn 340 516 340 $Abeam 700000 $G $Jbeam $Iybeam $Izbeam $Beam1TransfTag
element nonlinearBeamColumn 341 340 341 $numintgrPtsBrace $bracesecID1 $BraceTransfTag
element nonlinearBeamColumn 342 341 332 $numintgrPtsBrace $bracesecID1 $BraceTransfTag
element nonlinearBeamColumn 343 332 342 $numintgrPtsBrace $bracesecID1 $BraceTransfTag
element nonlinearBeamColumn 344 342 343 $numintgrPtsBrace $bracesecID1 $BraceTransfTag
element elasticBeamColumn 345 343 517 $Abeam 700000 $G $Jbeam $Iybeam $Izbeam $Beam1TransfTag

# RHS Bay
element elasticBeamColumn 370 513 350 $Abeam 700000 $G $Jbeam $Iybeam $Izbeam $Beam1TransfTag
element nonlinearBeamColumn 371 350 351 $numintgrPtsBrace $bracesecID $BraceTransfTag
element nonlinearBeamColumn 372 351 352 $numintgrPtsBrace $bracesecID $BraceTransfTag
element nonlinearBeamColumn 373 352 353 $numintgrPtsBrace $bracesecID $BraceTransfTag
element nonlinearBeamColumn 374 353 354 $numintgrPtsBrace $bracesecID $BraceTransfTag
element elasticBeamColumn 375 354 610 $Abeam 700000 $G $Jbeam $Iybeam $Izbeam $Beam1TransfTag
element elasticBeamColumn 380 514 360 $Abeam 700000 $G $Jbeam $Iybeam $Izbeam $Beam1TransfTag
element nonlinearBeamColumn 381 360 361 $numintgrPtsBrace $bracesecID $BraceTransfTag
element nonlinearBeamColumn 382 361 352 $numintgrPtsBrace $bracesecID $BraceTransfTag
element nonlinearBeamColumn 383 352 362 $numintgrPtsBrace $bracesecID $BraceTransfTag
element nonlinearBeamColumn 384 362 363 $numintgrPtsBrace $bracesecID $BraceTransfTag
element elasticBeamColumn 385 363 519 $Abeam 700000 $G $Jbeam $Iybeam $Izbeam $Beam1TransfTag

# ------------------------------------
# Define Gravity load case
# ------------------------------------
set totalLoad7  [expr $massTotal1*0.5*$eccmult1*$factor1]
set totalLoad8 [expr $massTotal1*0.5*$eccmult2*$factor1]
set totalLoad9 [expr $massTotal1*0.5*$eccmult3*$factor1]
set totalLoad10 [expr $massTotal1*0.5*$eccmult3*$factor1]
set totalLoad11 [expr $massTotal1*0.5*$eccmult2*$factor1]
set totalLoad12 [expr $massTotal1*0.5*$eccmult1*$factor1]

set totalLoad27 [expr $massTotal2*0.5*$eccmult1*$factor1]
set totalLoad28 [expr $massTotal2*0.5*$eccmult2*$factor1]
set totalLoad29 [expr $massTotal2*0.5*$eccmult3*$factor1]
set totalLoad30 [expr $massTotal2*0.5*$eccmult3*$factor1]
set totalLoad31 [expr $massTotal2*0.5*$eccmult2*$factor1]
set totalLoad32 [expr $massTotal2*0.5*$eccmult1*$factor1]

set totalLoad47 [expr $massTotal3*0.5*$eccmult1*$factor1]
set totalLoad48 [expr $massTotal3*0.5*$eccmult2*$factor1]
set totalLoad49 [expr $massTotal3*0.5*$eccmult3*$factor1]
set totalLoad50 [expr $massTotal3*0.5*$eccmult3*$factor1]
set totalLoad51 [expr $massTotal3*0.5*$eccmult2*$factor1]
set totalLoad52 [expr $massTotal3*0.5*$eccmult1*$factor1]

pattern Plain 101 Linear {
        # FIRST STOREY
        load 7 0. $totalLoad7 0. 0. 0. 0.
        load 8 0. $totalLoad8 0. 0. 0. 0.
        load 9 0. $totalLoad9 0. 0. 0. 0.
        load 10 0. $totalLoad10 0. 0. 0. 0.
        load 11 0. $totalLoad11 0. 0. 0. 0.
        load 12 0. $totalLoad12 0. 0. 0. 0.
        # SECOND STOREY
        load 27 0. $totalLoad27 0. 0. 0. 0.
        load 28 0. $totalLoad28 0. 0. 0. 0.
        load 29 0. $totalLoad29 0. 0. 0. 0.
        load 30 0. $totalLoad30 0. 0. 0. 0.
        load 31 0. $totalLoad31 0. 0. 0. 0.
```

```
        load 32 0. $totalLoad32 0. 0. 0. 0.
        # THIRD STOREY
        load 47 0. $totalLoad47 0. 0. 0. 0.
        load 48 0. $totalLoad48 0. 0. 0. 0.
        load 49 0. $totalLoad49 0. 0. 0. 0.
        load 50 0. $totalLoad50 0. 0. 0. 0.
        load 51 0. $totalLoad51 0. 0. 0. 0.
        load 52 0. $totalLoad52 0. 0. 0. 0.
}

# ------------------------------------
# Start of gravity analysis
# ------------------------------------
set alphaSP 1e12;
set alphaMP 1e12;
constraints Penalty $alphaSP $alphaMP ;
set NumIter 10;                         # Set the number of iterations for convergence
set Tol 1.0e-6;
test NormDispIncr $Tol $NumIter;
numberer RCM ;
system BandGeneral ;
algorithm Newton ;
set LoadSteps 10;
set LoadIncr [expr 1.0/$LoadSteps];
integrator LoadControl $LoadIncr;
analysis Static ;

# ------------------------------------
# Define dynamic loads
# ------------------------------------
# set time series to be passed to uniform excitation
set dt 0.01
set scale 1.0
set accelSeries "Path -filePath Taiwan40.txt -dt $dt -factor [expr 9810*$scale]"
# create UniformExcitation load pattern for uni-directional excitation
# pattern UniformExcitation $tag $dir
pattern UniformExcitation  2 1 -accel $accelSeries

# ------------------------------------
# End of model generation
# ------------------------------------

# ------------------------------------
# Define Display
# ------------------------------------

source DisplayPlane.tcl;
source DisplayModel3D.tcl;
set xPixels 500;        # height of graphical window in pixels
set yPixels 500;        # height of graphical window in pixels
set xLoc 5;             # horizontal location of graphical window (0=upper left-most corner)
set yLoc 5;             # vertical location of graphical window (0=upper left-most corner)
set dAmp 10;            # Relative amplification factor for deformations
set ShapeType1 DeformedShape;
set windowTitle "2D Frame Deformed Shape";
set viewPlane ZY;
set nEigen 0;
recorder display $windowTitle $xLoc $yLoc $xPixels $yPixels  -wipe ; # display recorder

DisplayPlane $ShapeType1 $dAmp $viewPlane $nEigen 0;
recorder plot Data/RoofAccelSS.out Accel-Z 5 510 500 500 -columns 1 2; # Plot Load vs Disp
recorder plot Data/RoofDispSS.out FloorDrift-Z 515 510 500 500 -columns 1 2; # Plot Load vs Disp

set xLoc1 510;
set yLoc1 5;
set ShapeType DeformedShape;
DisplayModel3D $ShapeType $dAmp $xLoc1 $yLoc1 $xPixels $yPixels $nEigen

# ------------------------------------
# Start of analysis generation
# ------------------------------------
#constraints Transformation ;
set alphaSP 1e12;
set alphaMP 1e12;
constraints Penalty $alphaSP $alphaMP ;
#constraints Lagrange $alphaSP $alphaMP ;
numberer RCM ;
system UmfPack ;
```

```
set Tol 1.e-5;
set maxNumIter 1000;
test NormDispIncr $Tol $maxNumIter ;
#algorithm ModifiedNewton ;
algorithm KrylovNewton ;
set gamma 0.8;
integrator HHT $gamma ;
analysis Transient ;

# ------------------------------------
# End of analysis generation
# ------------------------------------

# ------------------------------------
# Define Dampnig
# ------------------------------------
set xDamp 0.1;                  # 10% damping ratio assumed
set MpropSwitch 1.0;
set KcurrSwitch 0.0;
set KcommSwitch 1.0;
set KinitSwitch 0.0;
set nEigenI 1;                  # mode 1
set nEigenJ 3;                  # mode 3
set type frequency;
set lambdaN [eigen $type [expr $nEigenJ]];          # eigenvalue analysis for nEigenJ modes
set lambdaI [lindex $lambdaN [expr $nEigenI-1]];    # eigenvalue mode i
set lambdaJ [lindex $lambdaN [expr $nEigenJ-1]];    # eigenvalue mode j
set omegaI [expr pow($lambdaI,0.5)];
set omegaJ [expr pow($lambdaJ,0.5)];
set alphaM [expr $MpropSwitch*$xDamp*(2*$omegaI*$omegaJ)/($omegaI+$omegaJ)];   # M-prop. damping; D = alphaM*M
set betaKcurr [expr $KcurrSwitch*2.*$xDamp/($omegaI+$omegaJ)];                 # current-K;+beatKcurr*KCurrent
set betaKcomm [expr $KcommSwitch*2.*$xDamp/($omegaI+$omegaJ)];                 # last-committed K;
set betaKinit [expr $KinitSwitch*2.*$xDamp/($omegaI+$omegaJ)];                 # initial-K;    +beatKinit*Kini
rayleigh $alphaM $betaKcurr $betaKinit $betaKcomm;                             # RAYLEIGH damping

set T1 [expr 2*3.141592654/$omegaI];
set Omega1 [expr $omegaI];
puts "The first period is: $T1";
puts "Omega 1 is: $Omega1";
puts "The first frequency is: [expr 1/$T1]";

set T3 [expr 2*3.141592654/$omegaJ];
set Omega3 [expr $omegaJ];
puts "The third period is: $T3";
puts "Omega 3 is: $Omega3";
puts "The third frequency is: [expr 1/$T3]";

# ------------------------------------
# Recorders
# ------------------------------------
# Record displacements at cantilever tip
recorder Node -file Data/RoofDispSS.out -time -node 47 -dof 1 disp;
recorder Node -file Data/RoofAccelSS.out -time -node 47 -dof 1 accel;
recorder Node -file Data/RoofDispFS.out -time -node 49 -dof 1 disp;
recorder Node -file Data/RoofAccelFS.out -time -node 49 -dof 1 accel;
recorder Node -file Data/RoofDispCentre8.out -time -node 48 -dof 1 2 3 disp;
recorder Node -file Data/RoofAccelCentre8.out -time -node 48 -dof 1 2 3 accel;
recorder Node -file Data/DBase.out -time -node 1 2 3 -dof 1 2 3 disp;

# Column Base Shear
recorder Node -file Data/RBase1.out -time -node 1 -dof 1 2 3 reaction;
recorder Node -file Data/RBase2.out -time -node 2 -dof 1 2 3 reaction;
recorder Node -file Data/RBase3.out -time -node 3 -dof 1 2 3 reaction;
recorder Node -file Data/RBase4.out -time -node 4 -dof 1 2 3 reaction;
recorder Node -file Data/RBase5.out -time -node 5 -dof 1 2 3 reaction;
recorder Node -file Data/RBase6.out -time -node 6 -dof 1 2 3 reaction;
recorder Node -file Data/ActuatorNodeF.out -time -node 7 -dof 1 2 3 4 5 6 reaction;
recorder Node -file Data/ActuatorNodeD.out -time -node 7 -dof 1 2 3 disp;

# Displacement for drift
recorder Node -file Data/DispSS1.out -time -node 7 -dof 1 2 3 disp;
recorder Node -file Data/DispFS1.out -time -node 12 -dof 1 2 3 disp;
recorder Node -file Data/DispSS2.out -time -node 27 -dof 1 2 3 disp;
recorder Node -file Data/DispFS2.out -time -node 32 -dof 1 2 3 disp;

# ------------------------------------
# Stiff Side Brace Data
# ------------------------------------
```

```
# Brace axial load
recorder Element -file Data/SSBrace2Ele1local.out -time -ele 152 localForce
recorder Element -file Data/SSBrace1Ele1local.out -time -ele 162 localForce
recorder Node -file Data/SSBrace1EndForce.out -time -node 162 -dof 1 2 3 reaction;
recorder Node -file Data/SSBrace2EndForce.out -time -node 152 -dof 1 2 3 reaction;
recorder Node -file Data/SSBrace1EndForce1.out -time -node 116 -dof 1 2 3 reaction;
recorder Node -file Data/SSBrace2EndForce1.out -time -node 111 -dof 1 2 3 reaction;

# Brace curvature
recorder Node -file Data/SSBrace1Curv.out -time -node 141 -dof 4 5 6 disp;
recorder Node -file Data/SSBrace2Curv.out -time -node 131 -dof 4 5 6 disp;
# Stress/Strain in braces
recorder Element -file Data/SSBr2sec7Top.out -time -ele 152 section $numintgrPtsBrace fiber 25 0 $matID stressStrain;
recorder Element -file Data/SSBr2sec1Top.out -time -ele 152 section 1 fiber 25 0 $matID  stressStrain;
recorder Element -file Data/SSBr2sec7Side.out -time -ele 152 section $numintgrPtsBrace fiber 0 25 $matID stressStrain;
recorder Element -file Data/SSBr2sec1Side.out -time -ele 152 section 1 fiber 0 25 $matID stressStrain;
recorder Element -file Data/SSBr1sec7Top.out -time -ele 162 section $numintgrPtsBrace fiber 25 0 $matID stressStrain;
recorder Element -file Data/SSBr1sec1Top.out -time -ele 162 section 1 fiber 25 0 $matID stressStrain;
recorder Element -file Data/SSBr1sec7Side.out -time -ele 162 section $numintgrPtsBrace fiber 0 25 $matID stressStrain;
recorder Element -file Data/SSBr1sec1Side.out -time -ele 162 section 1 fiber 0 25 $matID stressStrain;

# Gusset plate/brace end node
recorder Node -file Data/SSGussetNd.out -time -node 130 -dof 1 2 3 4 5 6 reaction;
recorder Node -file Data/SSGussetNd1.out -time -node 140 -dof 1 2 3 4 5 6 reaction;

# ------------------------------------
# Flexible Side Brace Data
# ------------------------------------
# Brace axial load
recorder Element -file Data/FSBrace2Ele1local.out -time -ele 172 localForce
recorder Element -file Data/FSBrace1Ele1local.out -time -ele 182 localForce
recorder Node -file Data/FSBrace1EndForce.out -time -node 113 -dof 1 2 3 reaction;
recorder Node -file Data/FSBrace2EndForce.out -time -node 114 -dof 1 2 3 reaction;

# Brace curvature
recorder Node -file Data/FSBrace1Curv.out -time -node 172 -dof 4 5 6 disp;
recorder Node -file Data/FSBrace2Curv.out -time -node 182 -dof 4 5 6 disp;

# Stress/Strain in Braces
recorder Element -file Data/FSBr2sec7Top.out -time -ele 172 section $numintgrPtsBrace fiber 25 0 $matID stressStrain; # Mid Brace
recorder Element -file Data/FSBr2sec1Top.out -time -ele 172 section 1 fiber 25 0 $matID stressStrain; # Brace End Stress
recorder Element -file Data/FSBr2sec7Side.out -time -ele 172 section $numintgrPtsBrace fiber 0 25 $matID stressStrain; # Mid Brace
recorder Element -file Data/FSBr2sec1Side.out -time -ele 172 section 1 fiber 0 25 $matID stressStrain; # Brace End Stress
recorder Element -file Data/FSBr1sec7Top.out -time -ele 182 section $numintgrPtsBrace fiber 25 0 $matID stressStrain; # Mid Brace
recorder Element -file Data/FSBr1sec1Top.out -time -ele 182 section 1 fiber 25 0 $matID stressStrain; # Brace End Stress
recorder Element -file Data/FSBr1sec7Side.out -time -ele 182 section $numintgrPtsBrace fiber 0 25 $matID stressStrain; # Mid Brace
recorder Element -file Data/FSBr1sec1Side.out -time -ele 182 section 1 fiber 0 25 $matID stressStrain; # Brace End Stress

puts "Regular recorders defined" ;

# ------------------------------------
# Stiff Side Brace Data 2nd Storey
# ------------------------------------
# Brace axial load
recorder Element -file Data1/SSBrace2Ele1local.out -time -ele 231 localForce
recorder Element -file Data1/SSBrace1Ele1local.out -time -ele 241 localForce

# Brace curvature
recorder Node -file Data1/SSBrace1Curv.out -time -node 241 -dof 4 5 6 disp;
recorder Node -file Data1/SSBrace2Curv.out -time -node 231 -dof 4 5 6 disp;

# Stress/Strain in braces
recorder Element -file Data1/SSBr2sec7Top.out -time -ele 231 section $numintgrPtsBrace fiber 25 0 $matID stressStrain;
recorder Element -file Data1/SSBr2sec1Top.out -time -ele 231 section 1 fiber 25 0 $matID stressStrain;
recorder Element -file Data1/SSBr2sec7Side.out -time -ele 231 section $numintgrPtsBrace fiber 0 25 $matID stressStrain;
recorder Element -file Data1/SSBr2sec1Side.out -time -ele 231 section 1 fiber 0 25 $matID stressStrain;
recorder Element -file Data1/SSBr1sec7Top.out -time -ele 241 section $numintgrPtsBrace fiber 25 0 $matID stressStrain;
recorder Element -file Data1/SSBr1sec1Top.out -time -ele 241 section 1 fiber 25 0 $matID stressStrain;
recorder Element -file Data1/SSBr1sec7Side.out -time -ele 241 section $numintgrPtsBrace fiber 0 25 $matID stressStrain;
recorder Element -file Data1/SSBr1sec1Side.out -time -ele 241 section 1 fiber 0 25 $matID stressStrain;

# ------------------------------------
# Flexible Side Brace Data 2nd Storey
# ------------------------------------
# Brace axial load
recorder Element -file Data1/FSBrace2Ele1local.out -time -ele 271 localForce
recorder Element -file Data1/FSBrace1Ele1local.out -time -ele 281 localForce
```

```
# Brace curvature
recorder Node -file Data1/FSBrace1Curv.out -time -node 261 -dof 4 5 6 disp;
recorder Node -file Data1/FSBrace2Curv.out -time -node 251 -dof 4 5 6 disp;

# Stress/Strain in Braces
recorder Element -file Data1/FSBr2sec7Top.out -time -ele 271 section $numintgrPtsBrace fiber 25 0 $matID stressStrain; # Mid Brace
recorder Element -file Data1/FSBr2sec1Top.out -time -ele 271 section 1 fiber 25 0 $matID stressStrain; # Brace End Stress
recorder Element -file Data1/FSBr2sec7Side.out -time -ele 271 section $numintgrPtsBrace fiber 0 25 $matID stressStrain; # Mid Brace
recorder Element -file Data1/FSBr2sec1Side.out -time -ele 271 section 1 fiber 0 25 $matID stressStrain; # Brace End Stress
recorder Element -file Data1/FSBr1sec7Top.out -time -ele 281 section $numintgrPtsBrace fiber 25 0 $matID stressStrain; # Mid Brace
recorder Element -file Data1/FSBr1sec1Top.out -time -ele 281 section 1 fiber 25 0 $matID stressStrain; # Brace End Stress
recorder Element -file Data1/FSBr1sec7Side.out -time -ele 281 section $numintgrPtsBrace fiber 0 25 $matID stressStrain; # Mid Brace
recorder Element -file Data1/FSBr1sec1Side.out -time -ele 281 section 1 fiber 0 25 $matID stressStrain; # Brace End Stress

# ------------------------------------
# Stiff Side Brace Data 3rd Storey
# ------------------------------------
# Brace axial load
recorder Element -file Data2/SSBrace2Ele1local.out -time -ele 331 localForce
recorder Element -file Data2/SSBrace1Ele1local.out -time -ele 341 localForce

# Brace curvature
recorder Node -file Data2/SSBrace1Curv.out -time -node 341 -dof 4 5 6 disp;
recorder Node -file Data2/SSBrace2Curv.out -time -node 331 -dof 4 5 6 disp;

# Stress/Strain in braces
recorder Element -file Data2/SSBr2sec7Top.out -time -ele 331 section $numintgrPtsBrace fiber 25 0 $matID stressStrain;
recorder Element -file Data2/SSBr2sec1Top.out -time -ele 331 section 1 fiber 25 0 $matID stressStrain;
recorder Element -file Data2/SSBr2sec7Side.out -time -ele 331 section $numintgrPtsBrace fiber 0 25 $matID stressStrain;
recorder Element -file Data2/SSBr2sec1Side.out -time -ele 331 section 1 fiber 0 25 $matID stressStrain;
recorder Element -file Data2/SSBr1sec7Top.out -time -ele 341 section $numintgrPtsBrace fiber 25 0 $matID stressStrain;
recorder Element -file Data2/SSBr1sec1Top.out -time -ele 341 section 1 fiber 25 0 $matID stressStrain;
recorder Element -file Data2/SSBr1sec7Side.out -time -ele 341 section $numintgrPtsBrace fiber 0 25 $matID stressStrain;
recorder Element -file Data2/SSBr1sec1Side.out -time -ele 341 section 1 fiber 0 25 $matID stressStrain;

# ------------------------------------
# Flexible Side Brace Data 3rd Storey
# ------------------------------------
# Brace axial load
recorder Element -file Data2/FSBrace2Ele1local.out -time -ele 371 localForce
recorder Element -file Data2/FSBrace1Ele1local.out -time -ele 381 localForce

# Brace curvature
recorder Node -file Data2/FSBrace1Curv.out -time -node 361 -dof 4 5 6 disp;
recorder Node -file Data2/FSBrace2Curv.out -time -node 351 -dof 4 5 6 disp;

# Stress/Strain in Braces
recorder Element -file Data2/FSBr2sec7Top.out -time -ele 371 section $numintgrPtsBrace fiber 25 0 $matID stressStrain; # Mid Brace
recorder Element -file Data2/FSBr2sec1Top.out -time -ele 371 section 1 fiber 25 0 $matID stressStrain; # Brace End Stress
recorder Element -file Data2/FSBr2sec7Side.out -time -ele 371 section $numintgrPtsBrace fiber 0 25 $matID stressStrain; # Mid Brace
recorder Element -file Data2/FSBr2sec1Side.out -time -ele 371 section 1 fiber 0 25 $matID stressStrain; # Brace End Stress
recorder Element -file Data2/FSBr1sec7Top.out -time -ele 381 section $numintgrPtsBrace fiber 25 0 $matID stressStrain; # Mid Brace
recorder Element -file Data2/FSBr1sec1Top.out -time -ele 381 section 1 fiber 25 0 $matID stressStrain; # Brace End Stress
recorder Element -file Data2/FSBr1sec7Side.out -time -ele 381 section $numintgrPtsBrace fiber 0 25 $matID stressStrain; # Mid Brace
recorder Element -file Data2/FSBr1sec1Side.out -time -ele 381 section 1 fiber 0 25 $matID stressStrain; # Brace End Stress

# ------------------------------
# Finally perform the analysis
# ------------------------------
# perform an eigenvalue analysis
set pi 3.14159265358979
set lambda [eigen -fullGenLapack 4]
puts "\nEigenvalues at start of transient:"
puts "lambda      omega      period"
foreach lambda $lambda {
   if {$lambda > 0.0} {
      set omega [expr pow($lambda,0.5)]
      set period [expr 2*$pi/pow($lambda,0.5)]
      puts "$lambda  $omega  $period"
   }
}

# open output file for writing
set outFileID [open Data/elapsedTime.txt w]
# perform the transient analysis
set tTot [time {
   for {set i 1} {$i < 4000} {incr i} {
      set t [time {analyze  1  [expr $dt/1.0]}]
```

```
    puts $outFileID $t
            #puts "step $i"
  }
}]
puts "\nElapsed Time = $tTot \n"
# close the output file
close $outFileID

set fmt1 "%s Analysis Result: CtrlNode %.2i, dof %.1i, Disp=%.4f %s";

# ------------------------------
# If Convergence Fails
# ------------------------------

set LunitTXT "m";
set IDctrlNode 48;
set IDctrlDOF 3;
if {$ok != 0 } {
        puts [format $fmt1 "PROBLEM WITH DYNAMIC ANALYSIS" $IDctrlNode $IDctrlDOF [nodeDisp $IDctrlNode
$IDctrlDOF] $LunitTXT]
} else {
        puts [format $fmt1 "DYNAMIC ANALYSIS COMPLETE:"  $IDctrlNode $IDctrlDOF [nodeDisp $IDctrlNode $IDctrlDOF]
$LunitTXT]
}

wipe
# ---------------------------------
# End of analysis
```